

Climate change and adaptive capacity building

Edited by

Wei Shui, Junyu Qi, Haijun Deng and Shaoquan Liu

Published in

Frontiers in Environmental Science

Frontiers in Ecology and Evolution



FRONTIERS EBOOK COPYRIGHT STATEMENT

The copyright in the text of individual articles in this ebook is the property of their respective authors or their respective institutions or funders. The copyright in graphics and images within each article may be subject to copyright of other parties. In both cases this is subject to a license granted to Frontiers.

The compilation of articles constituting this ebook is the property of Frontiers.

Each article within this ebook, and the ebook itself, are published under the most recent version of the Creative Commons CC-BY licence. The version current at the date of publication of this ebook is CC-BY 4.0. If the CC-BY licence is updated, the licence granted by Frontiers is automatically updated to the new version.

When exercising any right under the CC-BY licence, Frontiers must be attributed as the original publisher of the article or ebook, as applicable.

Authors have the responsibility of ensuring that any graphics or other materials which are the property of others may be included in the CC-BY licence, but this should be checked before relying on the CC-BY licence to reproduce those materials. Any copyright notices relating to those materials must be complied with.

Copyright and source acknowledgement notices may not be removed and must be displayed in any copy, derivative work or partial copy which includes the elements in question.

All copyright, and all rights therein, are protected by national and international copyright laws. The above represents a summary only. For further information please read Frontiers' Conditions for Website Use and Copyright Statement, and the applicable CC-BY licence.

ISSN 1664-8714
ISBN 978-2-83251-953-0
DOI 10.3389/978-2-83251-953-0

About Frontiers

Frontiers is more than just an open access publisher of scholarly articles: it is a pioneering approach to the world of academia, radically improving the way scholarly research is managed. The grand vision of Frontiers is a world where all people have an equal opportunity to seek, share and generate knowledge. Frontiers provides immediate and permanent online open access to all its publications, but this alone is not enough to realize our grand goals.

Frontiers journal series

The Frontiers journal series is a multi-tier and interdisciplinary set of open-access, online journals, promising a paradigm shift from the current review, selection and dissemination processes in academic publishing. All Frontiers journals are driven by researchers for researchers; therefore, they constitute a service to the scholarly community. At the same time, the *Frontiers journal series* operates on a revolutionary invention, the tiered publishing system, initially addressing specific communities of scholars, and gradually climbing up to broader public understanding, thus serving the interests of the lay society, too.

Dedication to quality

Each Frontiers article is a landmark of the highest quality, thanks to genuinely collaborative interactions between authors and review editors, who include some of the world's best academicians. Research must be certified by peers before entering a stream of knowledge that may eventually reach the public - and shape society; therefore, Frontiers only applies the most rigorous and unbiased reviews. Frontiers revolutionizes research publishing by freely delivering the most outstanding research, evaluated with no bias from both the academic and social point of view. By applying the most advanced information technologies, Frontiers is catapulting scholarly publishing into a new generation.

What are Frontiers Research Topics?

Frontiers Research Topics are very popular trademarks of the *Frontiers journals series*: they are collections of at least ten articles, all centered on a particular subject. With their unique mix of varied contributions from Original Research to Review Articles, Frontiers Research Topics unify the most influential researchers, the latest key findings and historical advances in a hot research area.

Find out more on how to host your own Frontiers Research Topic or contribute to one as an author by contacting the Frontiers editorial office: frontiersin.org/about/contact

Climate change and adaptive capacity building

Topic editors

Wei Shui — Fuzhou University, China

Junyu Qi — University of Maryland, College Park, United States

Haijun Deng — Fujian Normal University, China

Shaoquan Liu — Institute of Mountain Hazards and Environment, Chinese Academy of Sciences (CAS), China

Citation

Shui, W., Qi, J., Deng, H., Liu, S., eds. (2023). *Climate change and adaptive capacity building*. Lausanne: Frontiers Media SA. doi: 10.3389/978-2-83251-953-0

Table of contents

- 05 **Editorial: Climate change and adaptive capacity building**
Wei Shui, Wanyu Shui, Junyu Qi, Haijun Deng and Shaoquan Liu
- 08 **How do ecological vulnerability and disaster shocks affect livelihood resilience building of farmers and herdsman: An empirical study based on CNMASS data**
Yan Dongdong, Yang Xi and Sun Weihong
- 23 **Effect evaluation of ecological water conveyance in Tarim River Basin, China**
Ayong Jiao, Wenqi Wang, Hongbo Ling, Xiaoya Deng, Junjie Yan and Fulong Chen
- 39 **Land-use function evolution and eco-environmental effects in the tarim river basin from the perspective of production–living–ecological space**
Yang Wang, Yin Wang, Tingting Xia, Yang Li and Zhi Li
- 56 **Space-time perception and behavioral response of farmers to climate change: Evidence from Sichuan Province, China**
Junqiao Ma, Wenfeng Zhou, Shili Guo, Xin Deng, Jiahao Song and Dingde Xu
- 72 **Rio (1992) to Glasgow (2021): Three decades of inadequate mitigation of climate change and its slow onset effects**
Ilan Stavi
- 92 **Expansion of typical lakes in Xinjiang under the combined effects of climate change and human activities**
Wenqi Wang, Ayong Jiao, Qianjuan Shan, Zikang Wang, Zijie Kong, Hongbo Ling and Xiaoya Deng
- 110 **Extreme climate and crime: Empirical evidence based on 129 prefecture-level cities in China**
Jiquan Peng and Zhijun Zhan
- 124 **Bias correction of ERA-Interim reanalysis temperature for the Qilian Mountains of China**
Peng Zhao, Lu Gao, Miaomiao Ma and Jun Du
- 136 **Evaluation of coupled model intercomparison project phase 6 models in simulating precipitation and its possible relationship with sea surface temperature over Myanmar**
Zin Mie Mie Sein, Xiefei Zhi, Faustin Katchele Ogou, Isaac Kwesi Nooni and Khant Hmu Paing
- 156 **Isotope composition of daily precipitation from 2019 to 2020 in Sanming, southeastern China**
Jianrong Cai, Yunyue Yang, Zhijie Yang, Wanyin Qiu and Xiuyang Jiang

- 167 **Variations in precipitation and temperature in Xinjiang (Northwest China) and their connection to atmospheric circulation**
Guixiang Zhou, Yaning Chen and Junqiang Yao
- 181 **Spatiotemporal changes in temperature projections over Bangladesh using multi-model ensemble data**
H. M. Touhidul Islam, Mohammad Kamruzzaman, Shamsuddin Shahid, Mohammed Mainuddin, Edris Alam, Abu Reza Md. Towfiqul Islam, Jatish Chnadra Biswas and Md. Azharul Islam
- 203 **A 20-year vegetation cover change and its response to climate factors in the Guangdong-Hong Kong-Macao Greater Bay Area under the background of climate change**
Xianhui Feng, Zhilin Zeng and Mu He
- 216 **Microclimate effects and influential mechanisms of four urban tree species underneath the canopy in hot and humid areas**
Xianhui Feng, Huan Wen, Mu He and Yiqiang Xiao



OPEN ACCESS

EDITED AND REVIEWED BY

Hong Liao,
Nanjing University of Information Science
and Technology, China

*CORRESPONDENCE

Wei Shui,
✉ shuiweiman@163.com

SPECIALTY SECTION

This article was submitted to Atmosphere
and Climate,
a section of the journal
Frontiers in Environmental Science

RECEIVED 21 February 2023

ACCEPTED 23 February 2023

PUBLISHED 03 March 2023

CITATION

Shui W, Shui W, Qi J, Deng H and Liu S
(2023), Editorial: Climate change and
adaptive capacity building.
Front. Environ. Sci. 11:1171032.
doi: 10.3389/fenvs.2023.1171032

COPYRIGHT

© 2023 Shui, Shui, Qi, Deng and Liu. This
is an open-access article distributed
under the terms of the [Creative
Commons Attribution License \(CC BY\)](#).
The use, distribution or reproduction in
other forums is permitted, provided the
original author(s) and the copyright
owner(s) are credited and that the original
publication in this journal is cited, in
accordance with accepted academic
practice. No use, distribution or
reproduction is permitted which does not
comply with these terms.

Editorial: Climate change and adaptive capacity building

Wei Shui^{1*}, Wanyu Shui², Junyu Qi³, Haijun Deng⁴ and
Shaoquan Liu⁵

¹College of Environment and Safety Engineering, Fuzhou University, Fuzhou, China, ²Department of Geography and Resource Management, The Chinese University of Hong Kong, Shatin, Hong Kong SAR, China, ³CMNS-Earth System Science Interdisciplinary Center, University of Maryland, College Park, College Park, MD, United States, ⁴School of Geographical Sciences, Fujian Normal University, Fuzhou, China, ⁵Institute of Mountain Hazards and Environment, Chinese Academy of Sciences (CAS), Chengdu, China

KEYWORDS

climate change, socioeconomic vulnerabilities, risk assessment and prediction, adaptive capacity building, human-environment system, interdisciplinary approach, adaptation actions

Editorial on the Research Topic

Climate change and adaptive capacity building

The impacts of climate change that have been observed in recent years are significant and multifaceted, and climate change is having far-reaching effects on both natural and socio-economic systems. Climate change is a present and ongoing concern for humanity, and its adverse effects are driven by both critical infrastructure systems and increasing human activity, which pose risks that can be mitigated through appropriate adaptation measures. In order to better address the various challenges posed by long-term adaptation to climate change and to enhance human capacity for sustainable survival and development in the face of global climate risks, there is a need to strengthen regional case studies on climate change adaptation and to increase the assessment and prediction of climate change impacts on human economic and social activities.

This Research Topic, *Climate Change and Adaptive Capacity Building*, presents one review paper and 13 original research papers, from seven different countries (57 authors), and has papers that span the field of climate change, gives insight into ongoing Research Topic, and provides a basis for further study on reducing climate risk and strengthening adaptive capacity building. Here, we summarized some of the highlights derived from the 13 articles published in this Research Topic.

Air temperature is the primary indicator of climate change. Reanalysis temperature products play an important role in temperature estimates. However, some systematic biases exist between reanalysis data and observations affecting the accuracy of model prediction (Dyakonov et al., 2020; Rakhmatova et al., 2021). Therefore, bias correction of the ERA-Interim reanalysis data is essential, many methods have been constructed to correct bias like GPCP method and temperature lapse rate method (Szczypka et al., 2011; Gao et al., 2017). Zhao et al. used the temperature lapse-rate method to correct ERA-Interim reanalysis-temperature data in the Qilian Mountains of China from 1979 to 2017. The results of these researchers showed that correction methods based on ERA were reliable for bias correction, and will be especially applicable to mountainous areas with few observation stations. Islam et al. investigated probable temperature changes across Bangladesh using CMIP5 GCM temperature simulation, and is the first to use all available CMIP5 models to project temperature over the country. The dynamic assessment of

urban thermal vulnerability in the southeast coastal metropolis by (Shui et al., 2022), and reveals the main factors affecting the formation and spatial differentiation of UHV.

For a long time, there has been significant interest in understanding how climate change affects vegetation cover across various fields of study. A substantial amount of literature has been explored, indicating that the most significant phenomenon of climate change is that climate change affected the alteration of vegetation growth in the long time series and large spatial scale (Myneni et al., 1997; Tucker et al., 2001). The existing literature on vegetation cover change in China is very extensive, especially on NPP and its influencing mechanism, and there is little research on Evi (Shui et al., 2018). Feng et al. analysis the correlation between the vegetation cover change about 20 years and climate factors in the Guangdong-Hong Kong-Macao Greater Bay Area, their results indicated that the EVI changing trend in the future by R/S analysis method is affected by climate and human factors together and there are no significant factors. Besides, they found a significant positive correlation between the EVI trend and two climate factors (relative humidity and wind speed), which could make sense in the protection and establishment of the ecological environment in the GBA.

In order to reduce the risks associated with climate change, it is crucial to prioritize ecological protection and restoration efforts. Ecological water conveyance is an effective method for restoring the environment. Jiao et al. quantitatively assessed the impact of ecological water conveyance on ecological restoration in the Tarim River basin over the past 20 years, and concluded that ecological water conveyance has a positive effect on groundwater recharge and ecological restoration by constructing a basin ecological environment quality evaluation system. Wang et al. developed a production-living-ecological space (PLES) classification system which takes into account the land-use type and ecological environment in a comprehensive aspect. It serves as a crucial criterion for determining the appropriate combination of land-use functions and the current state of the ecological environment in the basin, preparing for future ecological restoration and other work.

Lakes can record the effects of climate change and human activities on regional hydrological processes at different time scales. Additionally, they play a crucial role in transmitting valuable data about global climate change and regional responses (Zhang et al., 2011; Tao et al., 2015). Wang et al. investigated the changes and attributions of typical lakes in Xinjiang from 1986 to 2020 using remote sensing big data cloud platform and mathematical and statistical methods. The results show that human activities and precipitation are the main factors affecting the changes of lakes.

Looking back at the past is also a crucial part of understanding climate change. Stable isotope signals in modern precipitation along with ancient isotope records preserved in natural archives can help reconstruct past climate and hydrological cycles (Yao et al., 2013). Cai et al. studied the isotopic variation characteristics of precipitation in different seasons (non-summer wind and summer wind) and proposed that the transfer of water vapor sources during water vapor transport

and the intensity of upstream atmospheric convection jointly affect the seasonal variation of precipitation isotopes.

In recent years, climate change has affected global ecological, economic and social systems in various ways. As we all know, trees in urban green spaces have positive effects and cool urban temperatures. Feng et al. studied the microclimate factors under the canopy of four evergreen trees in humid and hot regions and the relationship between microclimate factors and tree physiological parameters, which can optimize the selection of tree species for urban planning and improve the living environment of urban residents. Zhou et al. analyzed the climate and precipitation changes in Xinjiang in the past 60 years, explored the relationship between climate change and atmospheric circulation in Xinjiang at multiple scales. The results of the study can provide a reference for evaluating and predicting climate change in XJ (Sein et al.). The fluctuations in precipitation on both annual and seasonal scales, as well as the correlation between precipitation parameters and anomalies in sea surface temperatures (SST) in Myanmar from 1970 to 2014. An active response to climate change is necessary from an economic and social perspective. Ma et al. explores the effects of farmers' space-time perception of climate change. The results show that farmers' space-time perception of climate change significantly affects farmers' adaptive behavior. And Peng et al. points out that extreme climate has a significant positive effect on crime rates. All of the above can help the government to make decisions and maintain economic and social stability. Stavi et al. conducted a review of major climate change occurrences around the world and analyzed the efforts made by the international community to combat climate change from 1992 to 2021. The review suggests the need for increased policy development aimed at addressing climate and environmental concerns.

Author contributions

The authors make equal contributions to the editorial.

Conflict of interest

The authors declare that the research was conducted in the absence of any commercial or financial relationships that could be construed as a potential conflict of interest.

Publisher's note

All claims expressed in this article are solely those of the authors and do not necessarily represent those of their affiliated organizations, or those of the publisher, the editors and the reviewers. Any product that may be evaluated in this article, or claim that may be made by its manufacturer, is not guaranteed or endorsed by the publisher.

References

- Dyakonov, G. S., Ibrayev, R. A., and Shishkova, P. O. (2020). Assessment of ERA-interim reanalysis data quality for the caspian sea area. *Russ. Meteorology Hydrology* 45 (9), 650–657. doi:10.3103/S106837392009006X
- Gao, L., Bernhardt, M., Schulz, K., and Chen, X. (2017). Elevation correction of ERA-Interim temperature data in the Tibetan Plateau. *Int. J. Climatol.* 37 (9), 3540–3552. doi:10.1002/joc.4935
- Myneni, R. B., Keeling, C. D., Tucker, C. J., Asrar, G., and Nemani, R. R. (1997). Increased plant growth in the northern high latitudes from 1981 to 1991. *Nature* 386 (6626), 698–702. doi:10.1038/386698a0
- Rakhmatova, N., Arushanov, M., Shardakova, L., Nishonov, B., Taryannikova, R., Rakhmatova, V., et al. (2021). Evaluation of the perspective of ERA-interim and ERA5 reanalyses for calculation of drought indicators for Uzbekistan. *Atmosphere* 12 (5), 527. doi:10.3390/atmos12050527
- Szczypta, C., Calvet, J. C., Albergel, C., Balsamo, G., Boussetta, S., Carrer, D., et al. (2011). Verification of the new ECMWF ERA-Interim reanalysis over France. *Hydrol. Earth Syst. Sci.* 15 (2), 647–666. doi:10.5194/hess-15-647-2011
- Tao, S., Fang, J., Zhao, X., Zhao, S., Shen, H., Hu, H., et al. (2015). Rapid loss of lakes on the Mongolian Plateau. *Proc. Natl. Acad. Sci.* 112 (7), 2281–2286. doi:10.1073/pnas.1411748112
- Tucker, C. J., Slayback, D. A., Pinzon, J. E., Los, S. O., Myneni, R. B., and Taylor, M. G. (2001). Higher northern latitude normalized difference vegetation index and growing season trends from 1982 to 1999. *Int. J. Biometeorology* 45 (4), 184–190. doi:10.1007/s00484-001-0109-8
- Wang, Q. F., Zeng, J. Y., Shui, W., Fan, B., Tang, J., Jiang, C., et al. (2018). The effects of air temperature and precipitation on the net primary productivity in China during the early 21st century. *Front. Earth Sci.* 12, 818–833. doi:10.1007/s11707-018-0697-9
- Wu, C. W., Shui, W., Huang, Z. G., Wang, C., Wu, Y., Wu, Y., et al. (2022). Urban heat vulnerability: A dynamic assessment using multi-source data in coastal metropolis of southeast China. *Front. Public Health* 10, 989963. doi:10.3389/fpubh.2022.989963
- Yao, T., Masson-Delmotte, V., Gao, J., Yu, W., Yang, X., Risi, C., et al. (2013). A review of climatic controls on $\delta^{18}\text{O}$ in precipitation over the Tibetan Plateau: Observations and simulations. *Rev. Geophys.* 51 (4), 525–548. doi:10.1002/rog.20023
- Zhang, G., Xie, H., Kang, S., Yi, D., and Ackley, S. F. (2011). Monitoring lake level changes on the Tibetan Plateau using ICESat altimetry data (2003–2009). *Remote Sens. Environ.* 115 (7), 1733–1742. doi:10.1016/j.rse.2011.03.005



OPEN ACCESS

EDITED BY

Shaoquan Liu,
Institute of Mountain Hazards and
Environment (CAS), China

REVIEWED BY

Ziming Zhou,
Zhongnan University of Economics and
Law, China
Peng Jiquan,
Jiangxi University of Finance and
Economics, China

*CORRESPONDENCE

Sun Weihong,
sunwh@swufe.edu.cn

SPECIALTY SECTION

This article was submitted to
Interdisciplinary Climate Studies,
a section of the journal
Frontiers in Environmental Science

RECEIVED 20 July 2022

ACCEPTED 01 August 2022

PUBLISHED 25 August 2022

CITATION

Dongdong Y, Xi Y and Weihong S (2022),
How do ecological vulnerability and
disaster shocks affect livelihood
resilience building of farmers and
herdsmen: An empirical study based on
CNMASS data.
Front. Environ. Sci. 10:998527.
doi: 10.3389/fenvs.2022.998527

COPYRIGHT

© 2022 Dongdong, Xi and Weihong.
This is an open-access article
distributed under the terms of the
[Creative Commons Attribution License](#)
(CC BY). The use, distribution or
reproduction in other forums is
permitted, provided the original
author(s) and the copyright owner(s) are
credited and that the original
publication in this journal is cited, in
accordance with accepted academic
practice. No use, distribution or
reproduction is permitted which does
not comply with these terms.

How do ecological vulnerability and disaster shocks affect livelihood resilience building of farmers and herdsmen: An empirical study based on CNMASS data

Yan Dongdong¹, Yang Xi ² and Sun Weihong ^{3*}

¹Department of Sociology, School of Ethnology and Sociology, Inner Mongolia University, Hohhot, China, ²Institute of Population, School of Economics, Hebei University, Baoding, China, ³Population Research Institute, Research Institute of Social Development, Southwestern University of Finance and Economics, Chengdu, China

Based on the survey data on animal husbandry from 1,689 households in semi-agricultural and semi-pastoral counties in Inner Mongolia, this paper applied the “buffer capacity–organizational capacity–learning capacity” framework to analyze the current livelihood resilience of farmers and herdsmen, as well as the impact of ecological vulnerability and disaster shocks on this resilience. The results show that, first, due to the vicious ecological environment and natural disasters, livelihood resilience among farmers and herdsmen is generally low in the region, but that of herdsmen is significantly higher than that of farmers. There are clear differences between the dimensions of livelihood resilience in different households. Second, natural disasters, of which drought is the most obvious, have a great impact on livelihood resilience. However, there is a significant positive correlation between ecological vulnerability and the livelihood resilience of farmers and herdsmen; thus, we should reflect on the past development model of the region. Third, In addition to the impact of ecological vulnerability and disaster shocks, per capita income, human capital, policy support, social networks, and information access are the main obstacles to livelihood resilience. Combined with these research findings, this paper seeks to improve livelihood resilience through the strategies of avoiding disaster risk, changing the development mode, reducing path dependence, and identifying obstacles.

KEYWORDS

livelihood resilience, ecological vulnerability, disaster shocks, household type, farmers and herdsmen

Introduction

The livelihoods of farmers and herdsmen in the Inner Mongolia Autonomous Region are quite vulnerable due to the poor natural conditions and socio-economic environment. Due to the low annual rainfall (normally under 400 mm), high elevation (sometimes above 4,000 m), thin topsoil (at times less than 10 mm), and large area of desertification (accounting for 23.3% of China's desertification land area), the region has an extremely vulnerable ecological environment and low land productivity (Tan and Tan, 2017). Living conditions are characterized by the region's remoteness (it can take more than 3 h by car to reach the closest city), poor infrastructure (in some areas, there is no access to public transport and electricity), and the lack of access to public services (such as education, healthcare, and credit). This has led to relatively backward social and economic development in this region. Farmers and herdsmen are also often affected by natural disasters or environmental pressures, such as drought, hail, strong winds, snowstorms, and animal diseases, which pose great challenges to the livelihoods of local farmers and herdsmen (Fan et al., 2014).

With the development of sustainable livelihoods, research on rural livelihood resilience has attracted increasing attention. Many scholars have focused on the response of farmers' livelihood resilience to climate change and natural disasters (Tanner et al., 2014) and taken the ways to improve the livelihood resilience as the coping strategy (Adger et al., 2011; Gupta et al., 2020). What are the main factors affecting the farmers' and herdsmen's livelihood resilience, which have not been well understood in China. Especially in the farming-pastoral region just like Inner Mongolia Autonomous Region, research using comprehensive evaluation indicators to demonstrate how natural disasters and climate change affect livelihood resilience is also relatively limited. This study therefore seeks to accomplish the following: first, to understand the general level of livelihood resilience in the region and compare the differences between households and regions; second, to examine how natural disasters and the ecological environment affect the livelihood resilience of farmers and herdsmen; and third, to explore effective ways to improve the response of farmers and herdsmen to shocks and pressures.

Literature review and analysis framework

Livelihood resilience: Concept and measurement

The concept of resilience was first used in physics and engineering to describe the ability of a system to return to a normal state (Doorn et al., 2018). It was first introduced in

ecological science by Holling (1973) to measure the ability of a system to absorb changes and disturbances. In recent years, the concept of resilience has increasingly been used to explain dynamic changes in socio-economic status, but more emphasis has been placed on adaptability, transformability, social learning, and innovation (Folke, 2006). However, as livelihoods are increasingly being affected by changes in ecological, economic, and social systems, the concept of livelihood resilience is receiving increased attention (Quandt, 2018; Sina et al., 2019). The ability of residents to recover from external pressure events (Chambers and Conway, 1991), the adaptive strategies used to cope with the pressure and shocks (Liu et al., 2019), and the process of re-formulating livelihood strategies using livelihood capital and local resources (Sadik, 2009) are all regarded as elements of livelihood resilience. Although different scholars have put forward different concepts of livelihood resilience, they have reached a preliminary consensus that it refers to the ability of the livelihood system of a community or family to cope with environmental changes and to recover and transform in response to adverse impacts (Tanner et al., 2014; Li et al., 2019).

Measuring livelihood resilience is an arduous task. Because resilience is an evolving concept, a set of unified systems and methods for measuring it has not yet been developed. At present, the most comprehensive measurement is the household livelihood resilience model (HLRA) proposed by Quandt, (2018), which uses sustainable livelihoods and five kinds of capital to measure resilience. It not only provides a theoretical framework, measurement methods, and applicable tools for measuring resilience, but also includes subjective evaluation of resilience, emphasizing the heterogeneity of households and individuals. The other most widely used method is the three-dimensional measurement framework, which, represented by the work of Speranza et al. (2014), is an empirical application-oriented analysis and research method applicable to livelihood resilience. The framework contains buffer, self-organization, and learning capacities, and emphasizes the interaction between actors and social structure while laying a foundation for the empirical analysis of resilience from the perspective of groups and livelihoods.

Climate change, disaster shocks, and livelihood resilience

For farmers, when their livelihoods are directly or indirectly exposed to climate change, especially sudden disasters, it can have an adverse impact on family capacity, capital, or activities. Scholars have therefore explored the relationship between farmers' livelihood resilience and climate change or natural disasters (Adger et al., 2005; Forsyth, 2018). The impact of climate change on livelihoods mainly appears in the long-term change of climate elements and sudden meteorological disasters,

and it has a large impact on the resources, livelihood activities, and capacity of farmers (Wu and Li, 2009). Agriculture and animal husbandry are directly dependent on natural factors such as light, temperature, precipitation, and soil; thus, the livelihoods of farmers and herdsman are very sensitive to climate change, which can prolong the growth cycle of crops. Crops have also been affected by late frosts, resulting in reduced production (Zhu et al., 2013). Grassland climate warming and drying have reduced the quantity of grass production, which has an impact on animal husbandry (Zhang et al., 2007). Climate change has also led to meteorological disasters such as drought, flood, freezing, and hail, directly resulting in the decline of production and income (Zhang et al., 2018).

Numerous studies have assessed the impact of climate change and disasters on the vulnerability and sustainability of livelihoods. Hurricanes and storm surges have caused serious damage to the livelihoods and assets of coastal residents in Bangladesh, and even the careers of local residents will be changed due to the disasters (Msua et al., 2021). Long term drought, sudden rainstorms, high temperatures and frequent floods have brought long-term damage to agricultural production in northern Ghana, seriously reducing the livelihood resilience of local residents (Asante et al., 2021). In Wenchuan and Lushan earthquake-stricken areas, China, landslides and mudslides adversely affect on the livelihood of rural households (Yang et al., 2021). Severe climate change, including crop pests, disease outbreaks, droughts and floods, is the main reason for the vulnerability of families in South African (Mthethwa and Wale, 2022).

To mitigate the adverse impacts of climate change and disasters, the government and individual households have adopted different policies or measures to enhance livelihood resilience. The case of extreme drought events in rural Vietnam shows that livelihood resilience can be effectively improved by strengthening social participation, borrowing, saving, and choosing new economic activities (Aroui et al., 2015). Based on the research findings of Wenchuan and Lushan earthquake disaster areas, China, strengthening the communities' disaster prevention capacity and improving the residents' disaster preparedness capacity are gradually becoming an effective ways to cope with disaster risks and improve the well-being of residents (Ma et al., 2021). The vulnerability of climate change to food insecurity and poverty can be reduced through non-agricultural diversification, crop diversification, farm location changes and the application of agrochemicals (Asante et al., 2021). In addition, farmers can effectively improve their resilience to agricultural drought by participating in social networks and cooperatives more often. Diversification in on-farm enterprises, like livestock units, and off-farm income sources, play significant roles in increasing smallholder households' resilience to climatic risk (Kumar et al., 2020). At the same time, based on a survey of rural floods in Australia, it can be seen that livelihood resilience can be effectively improved

by obtaining loans and the help of local partnerships and relief organizations (Boon and Helen, 2014). There are also measures to cope with earthquake disasters, such as relocating settlements, improving social capital, and keeping away from dangerous environments (Despotaki et al., 2018). The impact of disasters such as sandstorms can be dealt with by using windbreak forests and planting disease-resistant plants (Licht et al., 2016).

Analysis framework

Before proposing the analysis framework, the key concepts of livelihood resilience, natural disaster risk, and ecological vulnerability must be clarified. In this study, livelihood resilience is measured according to the three-dimensional framework of buffer, organizational, and learning capacities proposed by Speranza et al. (2014).

Natural disaster risk refers to the probability of natural disasters occurring in a region. This indicator is a comprehensive evaluation of the level of risk of natural disasters, in combination with the various natural disasters occurring in a specific region (Yu et al., 2012). In the selection of evaluation indicators, disasters such as earthquakes, landslides, debris flows, floods, and droughts are considered, and a multi-index comprehensive evaluation model is designed (Liu et al., 2014). The specific evaluation method uses GIS technology and grid data to calculate the index weight and obtain a comprehensive value with a value ranging from 0 to 1.

Ecological vulnerability refers to the sensitive response and self-recovery ability of ecosystems relative to external disturbances at a specific scale of time and space. Related research looks at exposure, sensitivity, and adaptability (Wu and Zhang, 2014). Although ecological vulnerability is much talked about, it is not clearly defined vulnerability; it can, however, be measured (Jacquleen, 2013). Evaluation of the current situation is the most widely studied content in the measurement of ecological vulnerability, and the most commonly used method is index evaluation (Zhao et al., 2007).

According to the ecological landscape and production mode, the 54 counties in the Inner Mongolia Autonomous Region are divided into animal husbandry counties and semi-agricultural and semi-pastoral counties. Strictly speaking, there are no agricultural counties, but the actual situation is that in many semi-agricultural and semi-pastoral counties, farmers do not have grassland but are fully engaged in planting. Combined with the actual situation and research needs of the survey area, three types of households are defined: farmers refer to families who have no grassland but only cultivated land and are completely engaged in planting; herdsman are families that only have grassland and no arable land and are completely engaged in animal husbandry; and agro-pastoralists to families that have both grassland and cultivated land and engage in both planting and animal husbandry.

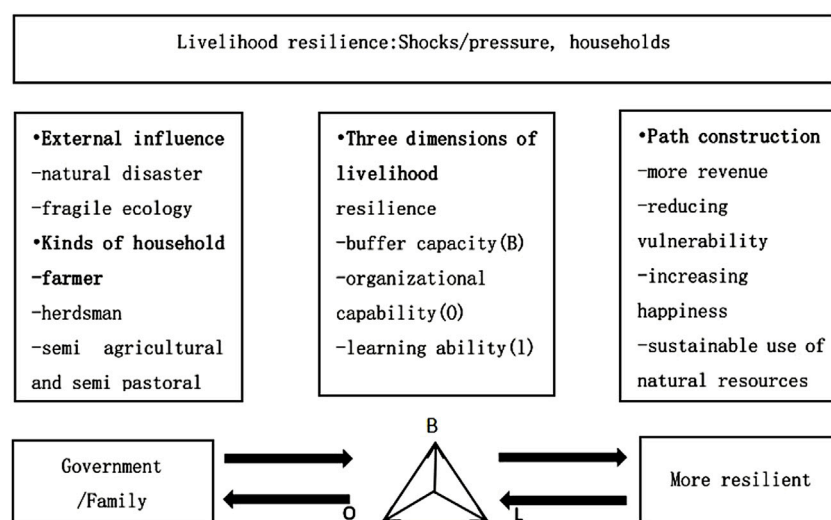


FIGURE 1
Organization of the article.

In this study, we first build an index evaluation system to measure the livelihood resilience of farmers and herdsmen in the study area. Second, we compare and analyze the livelihood resilience of farmers, herdsmen, and agro-pastoralists, as well as the differences in livelihood resilience between different households. Third, we build a hierarchical linear regression model and introduce two indicators of natural disaster risk and ecological vulnerability to study the impact of environmental differences and disaster shocks on household livelihood resilience. Finally, based on the research conclusions, this paper explores ways to improve the livelihood resilience of farmers in response to climate change and disasters. The organization of the article is shown in Figure 1.

grassland, desert grassland, and desert. Except for the eastern part of the region, the annual average precipitation in most areas is less than 400 mm, and the precipitation decreases from east to west. The overall climatic condition of the whole region is poor, and the vegetation coverage is low. The region is often affected by natural disasters or environmental pressure, such as drought, hail, strong winds, and snowstorms. In terms of industry, the whole region is dominated by agriculture and animal husbandry, with agriculture in the plains and hilly areas (e.g., the plains of Hetao and Tumechuan) and animal husbandry mainly distributed in the grassland areas of Hulunbuir, the Xing'an League, and the Xilin Gol League.

Data collection

In the summer of 2018, the Inner Mongolia University carried out a comprehensive social survey (CNMASS) of animal husbandry counties and semi-agricultural and semi-pastoral counties in Inner Mongolia. This survey investigated the livelihood mode, agricultural and animal husbandry production, infrastructure, population change, and relation between nationalities in the region. Specifically, questionnaires and semi-structured interviews were used to collect data covering the levels of counties, townships, villages, households, and individuals. The survey was conducted by multi-stage stratified sampling. In the first stage, 10 of the 54 counties in the region were randomly selected, taking into account the geographical distribution. In the second stage, from the above 10 counties, three townships were randomly selected for sampling, and from each township, four villages were then

Materials and methods

Study area

The study area is the Inner Mongolia Autonomous Region of China, which is located in the north of China, between 37° 24'–53° 23' N and 97° 12'–126° 04' E. The area spans more than 2,400 km from east to west and 1,700 km from north to south. Topographically, the Mongolian Plateau is the main feature, which has complex and diverse forms. Except for the southeast, the plateau accounts for about 50% of the total land area. The region primarily has a temperate continental monsoon climate. Precipitation is low and uneven, the wind is strong, and the variation between cold and heat are severe. From east to west, the region is composed of semi-humid, semi-arid, and arid areas, with, again from east to west, a vegetation landscape of forest,

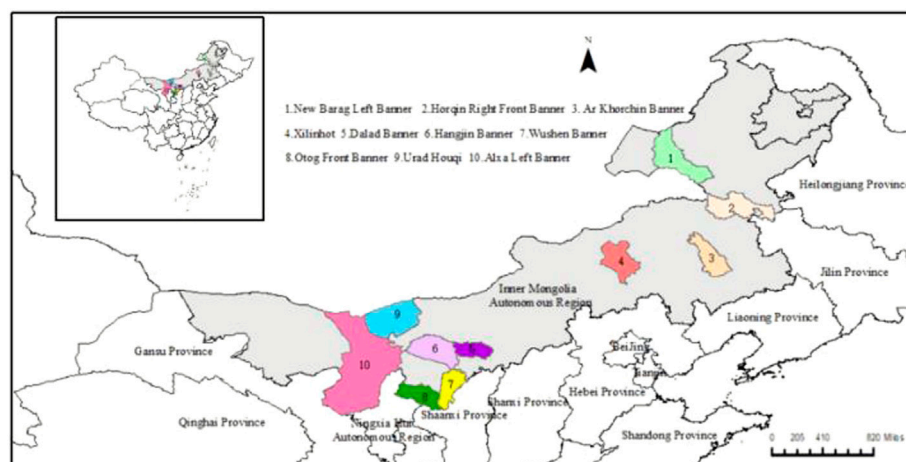


FIGURE 2
Survey area distribution¹.

selected for investigation based on convenience sampling (to ensure that there were at least 20 households in each village). In the third stage, among the selected villages, the respondents were selected according to indoor random sampling. The three-stage sampling yielded a total sample of 2,400 households and 120 villages. During the implementation of the project, roads in many villages were blocked due to heavy rain, and the random principle was not fully followed. We therefore selected the neighboring villages for investigation and finally investigated 2,412 households. The sampling distribution in the investigated area is shown in Figure 2.

Evaluation of ecological vulnerability and natural disaster risk

In June 2011, China officially released the “National Main Functional Area Planning.” This document requires the country to divide the land space into four categories according to the resource and environment carrying capacity, existing development density, and development potential: optimized development, key development¹,

Restricted development, and prohibited development.² The Inner Mongolia Autonomous Region undertook the planning task of the “Inner Mongolia Main Functional Area Planning,” studied the division of the main functional areas, and comprehensively evaluated the natural disaster risk and

ecological vulnerability of the whole region. Finally, according to the level of natural disaster risk, all counties in the region are divided into five levels from low to high;³ all counties in the region are also divided into five levels from low to high according to level of ecological vulnerability.⁴ The results of the two indicators in the “Inner Mongolia Main Functional Area Planning” document are used in this paper as the macro variables reflecting the ecological environment and natural disaster risk at the county level in the analysis model.

Measurement of livelihood resilience

The selection of indicators to measure the livelihood resilience of farmers and herdsman is based on an intensive review of the relevant literature and the data obtained from the field surveys. Table 1 shows the three components (buffer, organization, and learning) and composite indicators (Speranza et al., 2014).

Buffer capacity is a measure of the disturbance and change absorbed by a system while maintaining its structure, function, characteristics, and feedback unchanged. From the perspective of livelihood, buffer capacity refers to the ability of farmers to use their own resources and rights to resist livelihood risks (Kelly and Adger, 1999).

1 Banner is one of the administrative divisions at the same level as the county in China.

2 http://www.gov.cn/zhengce/content/2011-06/08/content_1441.htm.

3 The five assessment grades of natural disaster risk are areas of low risk, slight risk, medium risk, high risk, and extremely high risk.

4 The five assessment grades of ecological vulnerability are areas of low vulnerability, slight vulnerability, medium vulnerability, severe vulnerability, and extreme vulnerability.

TABLE 1 Indicator system to assess livelihood resilience.

Dimension	Indicator	Definition and description of indicators	Unit	Weight
Buffer capacity 0.540	Family labor (A1)	Total number of household labor force	Person	0.086
	Per capita education level (A2)	Ratio of total years of education to total population	Year/person	0.245
	House quality (A3)	Thatched cottage = 0.25, Adobe house = 0.5, Brick-concrete bungalow = 0.75, Building = 1	4 levels	0.040
	Per capita income of households (A4)	#0000FF; Ratio of annual total household income to total household population	%	0.385
	Cultivated land area (A5)	Land area actually cultivated by the family	Mu	0.122
	Grassland area (A6)	Grassland area actually grazed by the family	Mu	0.122
Organizational capability 0.297	Policy support (B1)	Government aid financially and subsidies obtained	Yuan	0.555
	Social network (B2)	Number of friends and relatives that can help	Household	0.235
	Trust between neighbors (B3)	The level of trust between neighbors	5 levels	0.068
	Traffic convenience (B4)	Where the main road leads: Townships = 1, Counties = 2, Prefecture level city = 3, Other prefecture level cities = 4, Other provinces = 5	5 levels	0.143
Learning capability 0.163	Education level of household head (C1)	Expressed by the length of schooling of the household head	Year	0.285
	Non-agricultural work experience (C2)	Ratio of the number of families with non-agricultural work experience to the total number of people	%	0.084
	Information acquisition capability (C3)	Ways and channels for families to obtain market, disaster, and employment information	5 levels	0.403
	Education investment (C4)	Amount of annual family education investment	Yuan	0.229

Mu is a measure of land in China. Per mu = 666.67 m².

The buffer capacity of a system or individual can be improved by improving the resource endowment, as reflected in livelihood capital and stability (Chen et al., 2016). The labor force and per capita education level represent the human capital of farming and herding families. The higher the population quantity and quality, the stronger the buffer capacity in the face of risk interference (Wen et al., 2018). The actual cultivated and grassland area represent the natural capital. Whether they have sufficient cultivated land and property is very important in resisting the shock of natural disasters (Liu et al., 2019). Housing quality represents the material capital of farming families. When farmers' livelihoods are hit, they can realize the material capital to improve their financial capital (per capita income) and enhance buffer capacity. The amount of financial capital directly affects whether farmers can maintain the function, structure, and feedback of their original basic livelihood when encountering shocks and also creates a certain potential resilience (Zheng et al., 2020). This dimension is represented by the A1 to A6 indicators.

Organizational capacity reflects how the family's self-management, institutional policies, and social connectivity shape resilience (Fuchs, 2014). Milestad and Darnhofer (2003) define the self-organization of the agricultural system as the ability of farmers or agricultural groups to establish flexible communication and mutual assistance networks, as well as to integrate into the local social, economic, and institutional

environment. Organizational capacity can be characterized by policy support, social network, neighborhood trust, and other indicators. Policy support represents the ability of farmers to obtain development opportunities and integrate their own resource advantages (Wen et al., 2018). Policy support is a powerful external force for families, and it is the main driving force for the improvement of family's organizational capacity when a disaster occurs. A social network indicates the degree of information sharing and mutual support among individual farmers. Lack of trust and communication isolates farmers and reduces their ability to self-organize (Wang et al., 2021). Social networks are the main source of informal loans and assistance. Accessibility reflects the ease with which an area is connected to the outside world, and reflects the efficiency of obtaining external assistance in an emergency (Wu et al., 2021). This dimension is represented by the B1 to B4 indicators.

Learning ability is the ability of individuals or organizations to create, acquire, transmit, and memorize knowledge and is of great significance to their rapid response and recovery after a shock (Kim, 1998). Four indicators, namely the education level of the household head, the ability to obtain information, the proportion of the population with non-agricultural experience, and the investment in family education, are selected. The education level of the household head directly affects a family's vision and planning for the future (Wen, 2018). The ability to obtain information reflects the ways and opportunities

TABLE 2 Variable descriptive statistics.

Variable name		Frequency	Ratio (%)	Maximum	Minimum
Livelihood resilience	Continuous variable	1689	100	0.016	0.357
	Herdsmen	834	49.38		
Kinds of household	(References group)			0	2
	Farmer	437	25.87		
Drought	Agro-pastoralists	418	24.75		
	Not affected (References group)	392	23.21	0	1
Freeze	Affected	1297	76.79		
	Not affected (References group)	1310	77.56	0	1
Natural disaster risk	Affected	397	22.44		
	Medium risk area	4	35.29		
Ecological vulnerability	High risk area	3	32.92	3	5
	Extremely high risk area	3	31.79		
	Low vulnerable area (References group)	1	6.45		
	(References group)				
	Slightly vulnerable area	1	9.59	1	4
	Moderately vulnerable area	4	44.76		
	Severe vulnerable area	4	39.19		

TABLE 3 t-test for mean differences in household livelihood resilience types.

	Kinds of household		Buffer capacity		Organizational capability		Learning capacity	
	Mean	T Value	Mean	T Value	Mean	T Value	Mean	T Value
Herdsmen	0.116		0.091		0.092		0.250	
Farmer	0.109	4.028***	0.075	8.702***	0.127	−9.345***	0.191	10.209***
Agro-pastoralists	0.122	−3.451***	0.090	−0.393	0.126	−9.975***	0.221	4.817***

* $p < 0.05$, ** $p < 0.01$, *** $p < 0.001$.

for farmers to obtain information, which can help them grasp market information and adjust their strategies in a timely way to cope with the impact of adverse changes (Wu et al., 2021). The proportion of the population with non-agricultural experience represents the vision and diverse production experience of different members of the family. Households may adopt diversified agriculture and off-farm employment as adaptive strategies to combine and transform their livelihood assets to be resilient to the disturbance (Li et al., 2016). The education level of household head will directly affect a family's vision and future livelihood planning, as well as the education investment of the whole family and the education of their children (Wen et al., 2018). It is in line with the concept of resilience that emphasizes the future and dynamics (Li et al., 2019). This is characterized by the C1 to C4 indicators.

As mentioned above, family livelihood resilience is measured by three dimensions: buffer, organization, and learning capacity.

Each dimension is represented by several indicators, and all indicators are integrated to form a comprehensive index (Table 1). Because each indicator is measured on a different scale, we adopt (Eq. 1) to standardize each indicator as an index (Wang et al., 2021):

$$index_{ij} = \frac{S_{ij} - S_{j,min}}{S_{j,max} - S_{j,min}}, \quad (1)$$

where S_{ij} and $index_{ij}$ are the original value and standardized value of index j of family i , respectively. $S_{j,min}$ and $S_{j,max}$ are the minimum and maximum values of index j , respectively. We use (Eq. 1) to adjust all indexes to 0–1. After each indicator is standardized, the analytic hierarchy process is used to determine the weights of specific indicators and dimension layers (Table 1). The livelihood resilience of different households can be obtained using standardized values for different indicator and dimension layer weights.

TABLE 4 Hierarchical linear regression of factors influencing livelihood resilience.

Variables		Null model (model 1)	Random-intercept model (model 2)	random-intercept model (including explanatory variables) (model 3)
		coef. (Std. Err.)	Coef. (Std. Err.)	Coef. (Std. Err.)
Level 1		Fixed effect		
Intercept (β_{0j})		0.116*** (0.003)	0.113*** (0.003)	0.105*** (0.006)
Household (β_{1j})	Farmer		−0.006*** (0.002)	−0.005** (0.002)
	Agro-pastoralists		0.001 (0.002)	0.001 (0.001)
Drought (β_{2j})			0.005** (0.002)	0.005** (0.002)
Freeze (β_{3j})			0.001 (0.002)	0.002 (0.002)
Level 2: Random-intercept model		Variance components		
Intercept (γ_{00})		0.008*** (0.002)	0.007*** (0.001)	0.004*** (0.001)
Level 2: Explanatory variables				
Ndi (γ_{01})	High risk			−0.015*** (0.005)
	Extremely high risk			−0.008* (0.001)
Ev (γ_{02})	Slight vulnerable			0.018** (0.009)
	Moderately vulnerable			0.015** (0.006)
	Highly vulnerable			0.017** (0.007)
Residual		0.029	0.028	0.028
ICC		0.071	0.065	0.027
AIC		−7153.195	−7164.528	−7162.495
BIC		−7136.899	−7126.505	−7097.312
Log likelihood		3579.5974	3589.264	3593.247
Individual observations		1689	1689	1689
Group observations		10	10	10

* $p < 0.05$, ** $p < 0.01$, *** $p < 0.001$; the values in brackets are standard errors.

Hierarchical linear regression model

A hierarchical linear regression model (HLM) is used to study the difference level and influencing factors of livelihood resilience among farmers, herdsmen, and agro-pastoralists. Different household types are thus taken as the main explanatory variables of livelihood resilience, and different types of disasters faced by households are introduced into the micro level of the model (Level 1) as individual factors affecting livelihood, similar to the ordinary OLS regression equation (Eq. 1). Natural disaster risk and ecological vulnerability are also included in the model (Level 2) as macro factors to explore the impact of ecological vulnerability and natural disasters on livelihood resilience. This level analyzes the variation of the intercept of the Level 1 (β_0 , representing the average livelihood resilience level of households) in different counties. The intercept of level 1 (random intercept) is divided into two parts in level 2, the intercept (γ_{00}) and the random component (u_{01}), through which the random intercept model is constructed.

At level 2, two indicators of natural disaster risk (*Nid*) and ecological vulnerability (*Ev*) are introduced to explain the variation of the random intercept. A random-intercept model with explanatory variables, is thus formed. It is worth noting that the slopes in level 1 does not change in level 2.

Level 1 (Eq. 1): $\ln(y_{ij}) = \beta_0 + \beta_1 \cdot \text{Household}_{ij} + \beta_2 \cdot \text{Drought}_{ij} + \beta_3 \cdot \text{Freeze}_{ij} + \varepsilon_{ij}$

Level 2 (Eq. 2): Adding two explanatory variables *nid* and *ev*, we obtain

$$\beta_0 = \gamma_{00} + \gamma_{01} \cdot \text{Ndi}_j + \gamma_{02} \cdot \text{Ev}_j + u_{0j}$$

In (Eq. 1), the β_0 represents the intercept, and β_1 to β_3 represents the regression coefficient related to the three explanatory variables of level 1. The subscript *i* represents the units in level 1—that is, each household—and *j* represents the units in level 2—that is, the county. In, β_0 is the intercept of level 1 related to the unit of level 2. γ_{00} is the intercept of level 2 and γ_{01} and γ_{02} are the regression coefficient corresponding to each explanatory variable of level 2. u_{0j} is the error term for level 2.

TABLE 5 Main obstacles of livelihood resilience indicators.

All households	Buffer capacity		Organizational capability		Learning ability	
Obstacle factor	A2	A4	B1	B2	C3	C4
Contribution (%)	8.71	14.71	21.23	8.54	15.40	7.68

Results

Descriptive analysis

Table 2 shows the family livelihood resilience and descriptive data for the main variables. A total of 1,689 effective samples were used after selection and processing. The maximum and minimum values of livelihood resilience are 0.357 and 0.016, respectively. The difference in livelihood resilience of different families is obvious. Drought and freezing are the main natural disasters affecting the agricultural and pastoral production in the region, and they have a great impact on livelihood resilience. According to the survey data, 76.79% of residents suffered from drought and 23.51% from freezing temperatures. For natural disaster risk, in the 10 counties in this survey, four are medium-risk areas, three are high-risk areas, and three are extremely high-risk areas.⁵ The overall natural disaster risk level of the surveyed areas is high. In terms of ecological vulnerability, eight of the 10 counties have medium or severe vulnerability.⁶ The overall ecological environment of the investigated area is very fragile.

Heterogeneity of livelihood resilience

From the results shown in Table 3, the resilience index of the surveyed residents' livelihood is not high as a whole, with an average of only 0.117. The resilience of farmers is the lowest, with an average of 0.109, followed by that of herdsmen (0.116) and then that of agro-pastoralists (0.122). The difference is quite clear. Although there is no significant difference in buffer capacity between herdsmen and agro-pastoralists, different dimensions of livelihood resilience differ significantly between household types.

The buffer and learning capacities of farmers are the lowest, with an average of 0.075 and 0.191, respectively, while the organizational capacity of herdsmen is the lowest, with an

average of 0.092. To a large extent, this is related to the special geographical location of the region and the tradition of agriculture and animal husbandry. Since ancient times, the region has been dominated by nomadism, and agriculture is limited by natural conditions. Except in a few plain areas (such as Hetao), the development of agriculture is relatively backward. The livelihood resilience of herdsmen is thus relatively high, and the buffer capacity of farmers is relatively low. Agro-pastoralists have relatively strong resistance to external shocks such as climate change and disasters due to their diversified production modes. Their buffer capacity is thus also relatively higher than that of farmers. Moreover, farmers' learning ability is relatively low. Farmers' income is far below that of herdsmen; so, their investment in education is relatively low. The organization capacity of herdsmen is relatively low, which may be related to their mode of production and living. The residential areas in the pastoral areas are relatively scattered, not concentrated, and pastoral areas are also relatively backward in transportation and other infrastructure. When herdsmen encounter external shocks, obtaining external assistance is inconvenient and the ability to organize self-recovery is relatively weak.

Factors influencing livelihood resilience

We use an HLM and consider natural disaster risk and ecological vulnerability as macro factors, incorporating them into level 2 of the model to explain the variation of livelihood resilience across counties (see Table 4).

According to the regression results, the variance (level 2) of the model1 is 0.008 ($p < 0.01$). From the variance results, the household belonging to different counties shows the differences in livelihood resilience due to different groups (different counties), indicating that the hierarchical linear model is applicable. Specifically, the total variance is $0.008 + 0.029 = 0.037$. The variance partition coefficient (VPC) is $0.008/0.037 = 0.2162$, which indicates that 21.62% of the variance in attainment can be attributed to differences between counties. the ICC value of model one is 0.071 and that of model two is 0.065. Compared with model 1, the decline of model two is not very obvious, but it still shows that there is indeed a variation in livelihood resilience at level 2, and the random effect has an impact. After introducing explanatory variables into level 2, the ICC value of model three is 0.027, which decreased significantly, indicating that the

⁵ Medium-risk areas: New Barag Left Banner, Wushen Banner, and Otog Front Banner, Xilinhot; High-risk areas: Ar Khorchin Banner, Hangjin Banner, and Horqin Right Front Banner; Extremely high-risk areas: Dalad Banner, Urad Houqi, and Alxa Left Banner.

⁶ Medium vulnerability areas: Ar Khorchin Banner, Ulat rear banner, Otog Front Banner, and Xilinhot; High vulnerability areas: Wushen Banner, Hangjin Banner, Dalat Banner, and Alxa Left Banner.

introduction of random effect item is reasonable. The random effect item has an explanatory force of $0.071 - 0.027 = 0.044$ (4.4%) on the county level (level 2). When the two indicators of natural disaster risk and ecological vulnerability are introduced, they can explain 42.85% of the variance in the average value of livelihood resilience across counties.

From the results of model 3, the fixed effect of the level 1 reflects the individual differences in livelihood resilience in different household types. Taking herdsmen as the reference group, the livelihood resilience of farmers is 0.005 units lower ($p < 0.05$), which indicates that, for the 10 counties in the survey area, the livelihood resilience of herdsmen is generally higher than that of farmers. However, the differences between herdsmen and agro-pastoralists did not reach the level of significance, which is in line with previous findings. In the Inner Mongolia Autonomous Region, herding is traditionally the main industry, and agriculture is restricted by the natural environment; so, its development is relatively weak. Drought is the main natural disaster affecting agriculture and animal husbandry. Compared with households affected by drought, the livelihood resilience of households not affected by drought was generally 0.005 units higher ($p < 0.01$). Drought not only reduces the yield of crops but also degrades the quality of grassland and harms animal husbandry. The impact of a freezing disaster is not obvious, but this may be related to the season during which we collected data. Before the period when the grassland is prone to frost in autumn and winter, the possibility of a frost disaster in the region is small.

Considering random effects, the intercept of level 1 (the average value of livelihood resilience of different household types) is significantly different from that of level 2 (between counties), and the variance component is 0.004 ($p < 0.01$). In terms of macro factors, the impact of natural disaster risk on livelihood resilience is negative and significant. The higher the level of natural disaster risk, the lower the overall level of livelihood resilience. Compared with medium-risk counties, the average livelihood resilience of farmers and herdsmen in counties with a high risk and an extremely high risk decreased by 0.015 ($p < 0.001$) and 0.008 ($p < 0.01$) units, respectively. The higher the level of risk of natural disasters, the greater the impact of disasters on livelihood resilience. Due to poor natural conditions, the living conditions of farmers and herdsmen are unstable, and the ability to cope with the pressure and shocks from natural disasters is significantly reduced (Tan and Tan, 2017). At this time, establishing a long-term risk early warning and risk management and control mechanism, promoting the diversification of livelihoods, and implementing active ecological policies have become effective ways to deal with livelihood vulnerability and improve livelihood resilience (Zhao, 2022). The government can improve access to land and water rights, thereby strengthening land governance to cope with drought (Bahta and Myeki, 2021). Residents and

communities can increase awareness of disaster risks and reduce the loss of livelihoods from disasters (Ma et al., 2022).

The higher the level of ecological vulnerability, the higher the livelihood resilience of farmers and herdsmen. This may appear counterintuitive, but after careful analysis of the study area, it became apparent that the counties with lower ecological vulnerability are often nature reserves and restricted development areas focused on ecological protection. There is no large-scale development of agriculture and animal husbandry in these counties. The overall livelihood resilience of the region is thus poor. For example, the livelihood resilience of New Barag Left Banner, Ar Khorchin Banner, and Horqin Right Front Banner is 0.110, 0.111, and 0.113, respectively. The higher the ecological vulnerability, the higher the livelihood resilience of farmers and herdsmen. This phenomenon is related to the development mode of treatment after pollution. For example, Ordos (0.122), which has the highest average livelihood elasticity, has suffered irreversible damage to the ecological environment, such as water resources, air, and grassland, due to extensive coal mining. Despite rapid economic and social development, ecological vulnerability is becoming increasingly serious (Wang and Zhang, 2015). Another example is Xilin Gol (0.014); from the 1990s to the beginning of the 21st century, overgrazing led to serious grassland degradation. The disordered mining of underground coal mines led to the exposure of a large area of grassland surface, which accelerated degradation and desertification (Wu et al., 2017). The previous extensive development led to the destruction of the ecological environment. With the rapid development of agriculture and animal husbandry, ecological damage has also become a new problem for the development of the region. It is thus clear that there is a significant positive correlation between ecological vulnerability and livelihood resilience. The best way to alleviate ecological vulnerability is to develop ecological agriculture and industrial diversification. How to achieve a “win-win” between ecological protection and sustainable livelihood development is the key to solve ecological problems in the future industrial development process (Qin et al., 2022). Eco agricultural projects can not only contribute to a significant increase in livelihood capital, but also increase the diversity of farmers’ livelihoods (Zhao et al., 2013). Encouraging farmers and herdsmen to develop characteristic farming, broadening income channels and reducing dependence on natural resources are important ways to achieve industrial transformation and sustainable development (Zhao, 2022).

Barriers to livelihood resilience

We further introduce factor contribution W_i (the weight of a single factor), indicator deviation V_i (the difference between the standardized value of a single indicator and 1), and obstacle O_i (indicating the impact of a single indicator on livelihood

resilience) to build an obstacle diagnosis model to identify the main obstacles affecting the livelihood resilience of farmers and herdsmen. Following Wen Tengfei et al. (2018)[33], the formula is as follows:

$$O_i = \frac{W_i \times V_i}{\sum_{i=1}^n (W_i \times V_i)} \times 100\% \quad (2)$$

In the identification of obstacles to the overall goal of livelihood resilience, the top six obstacles (the top two in each dimension) are selected. The evaluation of the livelihood resilience of farmers and herdsmen should not only judge the livelihood status in different research units but should also clarify the obstacles that affect the final results to put forward targeted policies and suggestions, which is of great significance to improve the adaptability and resilience of the study populations (see Table 5).

Once these barriers are alleviated, the livelihood resilience of farmers and herdsmen will rapidly improve. Among buffer capacity indicators, household per capita income (A4) is the most direct reflection of farmers' ability to buffer livelihood risks and adverse changes. During a crisis, this may be the last line of defense for households. Farmers can sell productive and non-productive assets to cushion the impact. The per capita education level (A2) is the main guarantee for the family labor force. The agricultural and pastoral production requires the input of labor from the start, and it also requires the labor force to have the ability and vision to organize future reconstruction. Family size and education attainment are key factors affecting farmers' livelihood resilience (Quandt, 2018). Human capital and financial capital have significant positive effects on livelihood strategies (Xu et al., 2019). Higher education per capita can significantly improve farmer livelihood resilience (Zhao et al., 2022). Among the organizational capacity indicators, policy support (B1), as the most direct external support system, can quickly and effectively help farmers and herdsmen improve their livelihood resilience after a shock. The social network (B2) represents power based on the relationship between blood and geography, which can organize a rescue force immediately after a shock, thus contributing to livelihood restoration. The ability of households to use their social capital through access to social networks and information has been shown to lead to better adaptive outcomes and enhance adaptive capacity (Bahta and Myeki 2021). At the same time, farmers are encouraged to become members of social networks and cooperatives to obtain agricultural credit, which can significantly improve the resilience and adaptability of families (Kumar et al., 2020). Among the learning capacity indicators, information acquisition (C3) reflects the timeliness of a family's access to relief information after a disaster, and it predicts future family development prospects. If families can obtain information about recovery and production on time, they can effectively restore the family livelihood. The level of investment in education (C4)

exacerbates the shortage of financial capital in the short term, but this long-term investment in the future has promising returns.

Discussion

The core of this study is to find methods to improve the livelihood resilience of farmers and herdsmen. The impact of natural disasters on livelihood resilience is negative, but there is a positive correlation between ecological vulnerability and resilience. Moreover, the variable resilience of different household types is also very obvious. Through the analysis of obstacle factors, we find that breaking through the main obstacle factors plays an important role in improving livelihood resilience; thus, we can focus on the aspects discussed below.

Avoiding disaster risk and expanding livelihood modes

From the analysis results of factors influencing livelihood resilience, natural disasters risk is the main factor restricting livelihood resilience. To cope with various risk environments, farmers and herdsmen should adopt a set of strategies, and both groups should pay attention to prior risk management. The eastern region can try to actively build a diversified industrial system on the basis of traditional animal husbandry to form an industrial chain to deal with the impact of disaster risks. More specifically, they can build the downstream industrial chain (including the production, processing, and sales of animal husbandry products) and create a business model combining chain operation with leading enterprises and family farms. Residents in the central and western regions are greatly affected by drought and freezing; so, the government should be committed to promoting land remediation, strengthening the construction of water conservancy projects such as reservoirs and irrigation canals, and promoting sprinkler and drip irrigation technologies (Wu et al., 2021). Farmers can reduce the impact of drought by adjusting the planting period and by building irrigation channels (Nwafor et al., 2014). Herdsmen can mitigate the adverse effects of climate change through artificial grass planting and adjustment of the livestock structure (Gongbuzeren and Li, 2018).

Farmers and herdsmen also need to deal with shocks afterward. Ideally, households can use risk-sharing tools, such as credit, crop and livestock insurance, and agricultural products options and futures, to transfer risks to the macro economy and operate more effectively (Zuo et al., 2007). However, tools such as agricultural insurance need the active support of the government, and most farmers and herdsmen do not have the specific skills required to make use of tools such as futures and options. Currently, saving, clearing assets, and borrowing in the short

term are the best methods for avoiding risk. The use of private lending based on social networks also plays a notable role.

Identifying resource advantages and changing the development mode

In addition to the negative impact of natural disaster risk, ecological vulnerability has a significant positive effect on the livelihood resilience. The conclusion reminds us that the relationship between ecological vulnerability and the livelihood resilience of farmers and herdsmen reveals that the development mode of treatment after pollution is not coordinated with resources and the environment. Identifying resource advantages and changing the development mode are the long-term pathways to enhance the future livelihood resilience of the region. We should seek to take the ecological industry as the leading factor and promote the combined development of traditional agriculture and animal husbandry and modern industrial transformation, as well as the coordination between industrial development and the existing resources and environment.

Eco-agriculture can help small-scale producers adapt to and mitigate climate change. There is growing evidence that this approach is beneficial to the environment, biodiversity, farmers' income, climate change adaptation, and resilience to multiple shocks and pressures (Mottet et al., 2020). Eco-agriculture is closely related to biological and economic diversity: the more developed the ecological farm is, the more diverse the crops, trees, animals, and economic activities are, and the greater the enhancement of economic and environmental resilience (FAO, 2019). With the increase in biodiversity, the soil is improved, which in turn helps to improve ecological resilience and strengthen the ecosystem (FAO, 2018).

Breaking path dependence and restructuring livelihoods

Restricted by the geographical environment, the livelihood resilience of farmers and herdsmen in the Inner Mongolia Autonomous Region has exhibited strong path dependence, which makes the family production mode too unitary, as the vast majority are focused on small-scale production and operation. Their ability to resist disasters and risks is very low. This path dependence must therefore be broken, which can be done in two ways: first, we should ensure the diversity of agricultural and animal husbandry development and break the original unitary production mode (Ingalls, 2020). For farmers and herdsmen, diversification includes the choice of agricultural and livestock products. In addition to traditional local crop varieties and livestock species, residents can try to grow economic or improved crops and introduce new livestock varieties.

Second, breaking path dependence can also advocate cooperation. Taking collective action to strengthen the network and cooperation between small-scale producers, producers' associations, cooperatives, and other participants is the cornerstone of building livelihood resilience (Li, 2018). In areas where conditions permit, with the help of cooperation and the industrial production chain, farmers and herdsmen can engage in large-scale production and improve their collective bargaining power and risk resistance.

Identifying obstacle factors and strengthening policy interventions

Obstacle analysis identifies the main obstacle factors of livelihood resilience. The conclusion reminds us that once these obstacles are alleviated, the livelihood elasticity of farmers and herdsmen will increase rapidly. Therefore, owning assets is the key to enabling families to recover from disasters. It is necessary to encourage families to consider their asset management and protection and to diversify their assets to avoid risk. Family members with a higher level of education are more valued in the labor market. When shocks have a negative impact on the family livelihood, if they can (temporarily or permanently) rely on another source of (non-agricultural or pastoral) income, they may be better able to adapt to those shocks. It is thus necessary for the government, families, and other different subjects to strengthen investment in education (including both infrastructure and financing), to expand educational opportunities, and to improve the overall level of human capital in the region (Wu et al., 2021).

The development of social protection policies (including public and private initiatives) can provide a certain degree of insurance and liquidity for production and help families seize economic opportunities to provide support and manage risks (Lowder et al., 2017). In the process of helping families recover their productivity, social protection policies can be adopted through social assistance (including cash or in kind subsidies), social insurance (including an insurance mechanism for disasters), labor market planning (to solve employment problems after a disaster), and other methods. Social networks are critical for the resilience of poor households and can provide access to opportunities, informal credit, and savings mechanisms to help cope with emergencies and shocks. We should encourage the normalization of social networks, and link them with productive enterprises and financial services to enhance their resilience.

Conclusion

Due to poor natural conditions and a fragile environment, the production and lifestyles of farmers and herdsmen in the

Inner Mongolia Autonomous Region are often affected by extreme weather and natural disasters, and their livelihood resilience is generally low. This threatens sustainability and social stability in the region. Improving the adaptability of farmers and herdsmen so that they can attain resilience in the face of external shocks would be the ideal condition for building a coordinated and sustainable society. For this, it is helpful to understand the main factors leading to low livelihood resilience and how these factors work. Among the many factors considered in this paper, we believe that ecological vulnerability and natural disaster risk are the most important external drivers affecting the livelihood resilience of farmers and herdsmen in the Inner Mongolia Autonomous Region.

Using CNMASS data from the survey conducted by the Inner Mongolia University in 2018, this paper studied the specific impact of the ecological environment and natural disasters on the livelihood resilience of farmers and herdsmen, focusing on the specific impact of drought and freezing. The main results show that natural disasters have a great impact on livelihood resilience. The higher the level of natural disaster risk, the lower the livelihood resilience of farmers and herdsmen, with drought being the most obvious disaster type. There is, however, a significant positive correlation between ecological vulnerability and the livelihood resilience of farmers and herdsmen, which indicates that there were great problems in the previous development mode of treatment after pollution. While various industries and the social economy are developing rapidly, the problems of the ecological environment cannot be avoided. It is thus necessary to adopt policies and measures to improve the sustainable livelihood of herdsmen. By clarifying the resource advantages and changing the development model, we can make development itself resilient. This can maintain and even improve the livelihood resilience of farmers and herdsmen in both the short term and long term.

In addition, this paper puts forward exploratory suggestions to improve the livelihood resilience of farmers and herdsmen, by identifying the obstacle factors of livelihood resilience. Strengthening policy support and guarantee, broadening social networks and improving social cooperation are the core contents of organizational capacity-building. Paying attention to education investment, improving the level of human capital, building an information network platform and enhancing the ability to obtain information are the long-term strategic choices

for farmers and herdsmen in realizing livelihood restoration and transformation.

Data availability statement

The datasets presented in this study can be found in online repositories. The names of the repository/repositories and accession number(s) can be found in the article/[Supplementary Material](#).

Author contributions

YD: data collection, investigation, methodology, software, and writing original draft. SW: investigation, methodology, and writing—review and editing. YX: writing—review and editing and investigation. All authors contributed to the article and approved the submitted version.

Conflict of interest

The authors declare that the research was conducted in the absence of any commercial or financial relationships that could be construed as a potential conflict of interest.

Publisher's note

All claims expressed in this article are solely those of the authors and do not necessarily represent those of their affiliated organizations, or those of the publisher, the editors and the reviewers. Any product that may be evaluated in this article, or claim that may be made by its manufacturer, is not guaranteed or endorsed by the publisher.

Supplementary material

The Supplementary Material for this article can be found online at: <https://www.frontiersin.org/articles/10.3389/fenvs.2022.998527/full#supplementary-material>

References

- Adger, P. M., and Kelly, W. N. (1999). Social vulnerability to climate change and the architecture of entitlements. *Mitig. Adapt. Strateg. Glob. Chang.* 4 (3-4), 253–266. doi:10.1023/A:1009601904210
- Adger, W. N., Brown, K., Nelson, D. R., Berkes, F., Eakin, H., Folke, C., et al. (2011). Resilience implications of policy responses to climate change. *WIREs. Clim. Change* 2 (5), 757–766. doi:10.1002/wcc.133
- Adger, W. N., Hughes, T. P., Folke, C., Carpenter, S. R., and Rockström, J. (2005). Social-ecological resilience to coastal disasters. *Science* 309 (5737), 1036–1039. doi:10.1126/science.1112122
- Arouri, M., Nguyen, A. B., and Youssef, C. (2015). Natural disasters, household welfare, and resilience: Evidence from rural Vietnam. *World Dev.* 70, 59–77. doi:10.1016/j.worlddev.2014.12.017

- Asante, F., Guodaar, L., and Arimiyaw, S. (2021). Climate change and variability awareness and livelihood adaptive strategies among smallholder farmers in semi-arid northern Ghana. *Environ. Dev.* 39, 100629. doi:10.1016/j.envdev.2021.100629
- Bahta, Y. T., and Myeki, V. A. (2021). Adaptation, coping strategies and resilience of agricultural drought in South Africa: Implication for the sustainability of livestock sector- sciencedirect. *Heliyon*. doi:10.1016/j.heliyon.2021.e08280
- Boon, H. J., and Helen, J. (2014). Disaster resilience in a flood-impacted rural Australian town. *Nat. Hazards* 71 (1), 683–701. doi:10.1007/s11069-013-0935-0
- Chambers, R., and Conway, G. R. (1991). *Sustainable rural livelihoods: Practical concepts for the 21st century*. UK (IDS): Institute of Development Studies.
- Chen, J., Xin, J. Y., and Sha, Y. (2016). Measures of the resilience, effect and countermeasures of household poverty: The perspective of household structure. *China Popul. Resour. Environ.* 26 (1), 150–157. doi:10.3969/j.issn.1002-2104.2016.01.020
- Cong, L. L., Lei, W. A. N. G., and Bo-wei, K. A. N. G. (2019). Measurement and influencing factors of livelihood resilience of relocated migrants. *J. Xi'an Jiaot. Univ. Soc. Sci.* 39 (4), 38–47. doi:10.15896/j.xjtuskxb.201904005
- Despotaki, V., Sousa, L., and Burton, C. G. (2018). Using resilience indicators in the prediction of earthquake recovery. *Earthq. spectra* 34 (1), 265–282. doi:10.1193/071316EQS107M
- Doorn, N., Gardoni, P., and Murphy, C. A. (2018). A multidisciplinary definition and evaluation of resilience: The role of social justice in defining resilience. *Sustain. Resilient Infrastructure* 4 (9), 112–123. doi:10.1080/23789689.2018.1428162
- Fan, S., Pandya-Lorch, R., and Yosef, S. (2014). *Resilience for food and nutrition security*. Washington, D.C: International Food Policy Reserch Institute (IFPRI): Washington, 9–13. doi:10.2499/9780896296787
- FAO (2018). *Livestock and agroecology: how they can support the transition towards sustainable food and agriculture*. Rome, Italy: Food and Agriculture Organization of the United Nations.
- FAO (2019). *Tool for agroecology performance evaluation (TAPE) – test version: Process of development and guidelines for application*. Egypt. Rome: Food and Agriculture Organization of the United Nations. Available at: <http://www.fao.org/3/ca7407en/ca7407en.pdf>.
- Folke, C. (2006). Resilience: The emergence of a perspective for social-ecological systems analyses. *Glob. Environ. change* 16 (3), 253–267. doi:10.1016/j.gloenvcha.2006.04.002
- Forsyth, T. (2018). Is resilience to climate change socially inclusive? Investigating theories of change processes in Myanmar. *World Dev.*, 111, 13–26. doi:10.1016/j.worlddev.2018.06.023
- Fuchs, C. (2004). The antagonistic self-organization of modern society. *Stud. Political Econ.* 73 (1), 183–209. doi:10.1080/19187033.2004.11675157
- Gongbuzeren, H. L., Huntsinger, W., and Li, W. (2018). Rebuilding pastoral social-ecological resilience on the Qinghai-Tibetan Plateau in response to changes in policy, economics, and climate. *E&S* 23 (2), 21. doi:10.5751/es-10096-230221
- Gupta, A. K., Negi, M., Nandy, S., Kumar, M., Singh, V., Valente, D., et al. (2020). Mapping socio-environmental vulnerability to climate change in different altitude zones in the indian himalayas. *Ecol. Indic.* 109, 105787. doi:10.1016/j.ecolind.2019.105787
- Holling, C. S. (1973). Resilience and stability of ecological systems. *Annu. Rev. Ecol. Syst.* 4 (1), 1–23. doi:10.1146/annurev.es.04.110173.000245
- Huan, Y. U., Kong, B., Tao, H. P., and Xuan-Qiong, L. I. (2012). Assessment and regionalization of natural hazard risk probability in sichuan province. *Earth Environ.* 40 (3), 397–404. doi:10.14050/j.cnki.1672-9250.2012.03.011
- Ifejika Speranza, C. I., Wiesmann, U., and Rist, S. (2014). An indicator framework for assessing livelihood resilience in the context of social-ecological dynamics. *Glob. Environ. Change* 28, 109–119. doi:10.1016/j.gloenvcha.2014.06.005
- Ingalls, M. L. (2020). Mountain agriculture: Opportunities for harnessing zero hunger in asia. Edited by Li xuan, mahmoud el solh, and kadambot H. M. Siddique. *Mt. Res. Dev.* 40 (4). doi:10.1659/mrd.mmm257.1
- Joseph, J. (2013). Measuring vulnerability to natural hazards: A macro framework. *Disasters* 37 (2), 185–200. doi:10.1111/j.1467-7717.2012.01299.x
- Kim, D. H. (2009). *The link between individual and organizational learning*. London: Routledge.
- Kumar, S., Mishra, A. K., Pramanik, S., Mamidanna, S., and Whitbread, A. M. (2020). Climate risk, vulnerability and resilience: Supporting livelihood of smallholders in semiarid India. *Land Use Policy* 97, 1–12. doi:10.1016/j.landusepol.2020.104729
- Li, Q., Amjath-Babu, T. S., and Zander, Pr. (2016). Role of capitals and capabilities in ensuring economic resilience of land conservation efforts: A case study of the grain for green project in China's loess hills. *Ecol. Indic.* 71, 636–644. doi:10.1016/j.ecolind.2016.07.027
- Licht, A., Dupont-Nivet, G., Pullen, A., Kapp, P., Abels, D., Lai, Z., et al. (2016). Resilience of the asian atmospheric circulation shown by paleogene dust provenance. *Nat. Commun.* 7, 12390–12396. doi:10.1038/ncomms12390
- Liu, B., Tao, H., Liu, S., and Hui, Y. (2014). Assessment and analysis of natural hazards danger degree in the Sichuan-Yunnan-Guizhou bordering area of Southwest China. *Geogr. Res.* 33 (2), 225–236. doi:10.11821/dlyj201402003
- Liu, W., Jie, L. L., and Jie, X. U. (2019). Evaluation of rural household's livelihood resilience of the Relocation and Settlement Project in contiguous poor areas. *Arid. Land Geogr.* 423, 673–680. doi:10.12118/j.issn1000-6060.2019.03.24
- Liu, W., Li, J., and Xu, J. (2020). Effects of disaster-related resettlement on the livelihood resilience of rural households in China. *Int. J. Disaster Risk Reduct.* 49, 101649. doi:10.1016/j.ijdrr.2020.101649
- Lowder, S. K., Bertini, R., and Croppenstedt, A. (2017). Poverty, social protection and agriculture: Levels and trends in data. *Glob. Food Secur.* 15, 94–107. doi:10.1016/j.gfs.2017.06.001
- Ma, Z., Guo, S., Deng, X., and Xu, D. (2021). Community resilience and resident's disaster preparedness: Evidence from China's earthquake-stricken areas. *Nat. Hazards* 108, 567–591. doi:10.1007/s11069-021-04695-9
- Ma, Z., Zhou, W., Deng, X., and Xu, D. (2022). Community disaster resilience and risk perception in earthquake-stricken areas of China. *Disaster Med. public health Prep.*, 1–11. doi:10.1017/dmp.2021.342
- Milestad, R., and Darnhofer, I. (2003). Building farm resilience: The prospects and challenges of organic farming. *J. Sustain. Agric.* 22 (3), 81–97. doi:10.1300/J064v22n03_09
- Mottet, A., Bicksler, A., Lucantoni, D., De Rosa, F. D., Scherf, P., Scopel, E., et al. (2020). Assessing transitions to sustainable agricultural and food systems: A tool for agroecology performance evaluation (tape). *Front. Sustain. Food Syst.* 4, 579154. doi:10.3389/fsufs.2020.579154
- Mthethwa, S., and Wale, E. (2022). Household vulnerability to climate change in South Africa: A multilevel regression model. *Dev. South. Afr.*, 1–16. doi:10.1080/0376835x.2022.2085667
- Nwafor, E. J., Umar, A., Muhammad, A., and Oloruntoba, O. (2014). Building resilience for adaptation to climate change among downstream communities in Nigeria through climate smart agriculture. *Int. J. Agric. Innovations Res.* 3 (1), 94–100. Available at: https://ijair.org/administrator/components/com_jresearch/files/publications/IJAIR_775_Final.pdf.
- Qin, Z., Haili, X., Xiao, L., Luwei, D., Bojie, W., Fengqi, C., et al. (2022). Livelihood vulnerability of pastoral households in the semiarid grasslands of northern China: Measurement and determinants. *Ecol. Indic.* 140, 109020. doi:10.1016/j.ecolind.2022.109020
- Quandt, Amy (2018). Measuring livelihood resilience: The household livelihood resilience approach (hlra). *World Dev.* 107, 253–263. doi:10.1016/j.worlddev.2018.02.024
- Sadik, M. S. (2009). "Indicator framework for assessing livelihood resilience to climate change for vulnerable communities dependent on Sundarban mangrove system," in *4th South Asia water research conference* (Kathmandu, 20–30).
- Sina, D., Chang-Richards, A. Y., Wilkinson, S., and Potangara, R. (2019). A conceptual framework for measuring livelihood resilience: Relocation experience from Aceh, Indonesia. *World Dev.* 117, 253–265. doi:10.1016/j.worlddev.2019.01.003
- Tan, S., and Tan, Z. (2017). Grassland tenure, livelihood assets and pastoralists' resilience: Evidence and empirical analyses from western China. *Econ. Political Stud.* 5 (4), 381–403. doi:10.1080/20954816.2017.1384605
- Tanner, T., Lewis, D., Wrathall, D., Bronen, R., Craddock-Henry, N., Huq, S., et al. (2014). Livelihood resilience in the face of climate change. *Nat. Clim. Change* 5 (1), 23–26. doi:10.1038/nclimate2431
- Uddin, C., Haque, A., Khan, B., Doberstein, D., and Cox, E. (2021). "Disasters threaten livelihoods, and people cope, adapt and make transformational changes": Community resilience and livelihoods reconstruction in coastal communities of Bangladesh. *Int. J. Disaster Risk Reduct.* 63, 102444. doi:10.1016/j.ijdrr.2021.102444
- Wang, Y. T., and Zhang, L. (2015). Coordinated development of mineral resources development and environmental protection—a case study of Ordos. *Econ. Forum* 5, 88–90. doi:10.3969/j.issn.1003-3580.2015.10.023
- Wang, Y., Zhang, Q., Li, Q., Wang, J., Sannigrahi, C., Bilsborrow, R., et al. (2021). Role of social networks in building household livelihood resilience under payments for ecosystem services programs in a poor rural community in China. *J. Rural Stud.* 86 (8), 208–225. doi:10.1016/j.jrurstud.2021.05.017
- Wen, T., Shi, Y., Yang, X., and Wang, T. (2018). The resilience of farmers' livelihoods and its influencing factors in semiarid region of the loess plateau—A case study of yuzhong county. *Chin. J. Agric. Resour. Regional Plan.* 39 (5), 172–182. doi:10.7621/cjarrp.1005-9121.20180523

- Wu, K. S., Yang, Q. Q., Ye, W. L., Yang, X. J., and He, Y., B. (2021). Farmers' livelihood resilience and livelihood construction path in the Loess Plateau. *J. Arid Land Resources Environ.* 35 (4), 24–30. doi:10.13448/j.cnki.jalre.2021.094
- Wu, Q., and Zhang, H. (2014). Review of ecological vulnerability research. *J. Cap. Normal Univ. Nat. Sci. Ed.* 35 (3), 61–66. doi:10.19789/j.1004-9398.2014.03.013
- Wu, Y. J., and Li, Y., E. (2009). Research progress on impacts of climate change on livelihood. *Chin. J. Agrometeorology* 30 (1), 1–8. doi:10.3969/j.issn.1000-6362.2009.01
- Xin, W., Kai, X., Zhang, J., Li, J., and Computer, S. O. (2018). Sand source of grassland desertification and its geological origin in xilin gol steppe of China. *J. Desert Res.* 38 (1), 92–100. doi:10.7522/j.issn.1000-694X.2016.00118
- Xu, D., Deng, X., Guo, S., and Liu, S. (2019). Sensitivity of livelihood strategy to livelihood capital: An empirical investigation using nationally representative survey data from rural China. *Soc. Indic. Res.* 144, 113–131. doi:10.1007/s11205-018-2037-6
- Yang, X., Guo, S., L., Deng, X., and Xu, D., D. (2021). Livelihood adaptation of rural households under livelihood stress: Evidence from sichuan province, China. *Agriculture* 11, 506. doi:10.3390/agriculture11060506
- Zhang, L., Zhang, Z., Chen, Y., Wei, X., and Song, X. (2018). Exposure, vulnerability, and adaptation of major maize-growing areas to extreme temperature. *Nat. Hazards* 91 (3), 1257–1272. doi:10.1007/s11069-018-3181-7
- Zhang, X. Y., Yao, Y. B., Deng, Z. Y., Yin, D., Wang, R. U., and Chen, C. P. (2007). Aimatic change over the grassland in the northeast border of Qinghai Tibetan Plateau and its influence on animal husbandry ewes raised in house. *Pratacultural Sci.* 24 (6), 66–73. doi:10.3969/j.issn.1001-0629.2007.06.015
- Zhao, X., Chen, H., Zhao, H., and Xue, B. (2022). Farmer households' livelihood resilience in ecological-function areas: Case of the yellow river water source area of China. *Environ. Dev. Sustain.* 24 (7), 9665–9686. doi:10.1007/s10668-021-01827-w
- Zhao, X., Zhang, L., Jiang, J. D., and Hou, C. (2013). The impact of ecological compensation on the farmers livelihood: A case study of huanghe river water supply areas of gannan. *Geogr. Res.* 32, 531–542. doi:10.11821/yj2013030014
- Zhao, Y. X., He, L., Liu, S. D., Liu, W. Q., and Zhang, J. P. (2007). Evaluation method of agro-ecosystem vulnerability. *Chin. J. Ecol.* 26 (5), 754–758. doi:10.1111/j.1467-7717.2012.01299.x
- Zhao-Nan, L. I. (2018). Influencing factors of grain yield and its dominance measurement in ecological vulnerable region based on the view of agricultural cooperatives: A case of gansu province. *J. North Minzu Univ. Soc. Sci.* 144 (6), 137–142. doi:10.7666/d.D01160351
- Zheng, D. Y., Hang, X. J., and Wang, C. (2020). Farmers' livelihood resilience and its optimization strategy in Loess Plateau of north Shaanxi province. *J. Arid Land Resour. Environ.* 34 (9), 9–16. doi:10.13448/j.cnki.jalre.2020.233
- Zhu, Z., Tao, F. L., Lou, Y. S., and Shi, W. J. (2013). Rice yield sensitivity to climate change in jiangsu province. *Resour. Sci.* 35 (5), 1035–1043.
- Zuo, T., Liu, Y. L., Qi, G. B., and Kuang, Z., R. (2007). The vulnerability of poor farmers and the risk mitigation effect of microfinance. *Rural. Econ.* 12, 52–56.



OPEN ACCESS

EDITED BY

Haijun Deng,
Fujian Normal University, China

REVIEWED BY

Huaiwei Sun,
Huazhong University of Science and
Technology, China
Bai Tao,
Xi'an University of Technology, China
Yong Liu,
Institute of Atmospheric Physics (CAS),
China

*CORRESPONDENCE

Hongbo Ling,
linghb@ms.xjb.ac.cn
Xiaoya Deng,
lily80876@163.com

SPECIALTY SECTION

This article was submitted to
Atmosphere and Climate,
a section of the journal
Frontiers in Environmental Science

RECEIVED 15 August 2022

ACCEPTED 26 August 2022

PUBLISHED 14 September 2022

CITATION

Jiao A, Wang W, Ling H, Deng X, Yan J
and Chen F (2022), Effect evaluation of
ecological water conveyance in Tarim
River Basin, China.
Front. Environ. Sci. 10:1019695.
doi: 10.3389/fenvs.2022.1019695

COPYRIGHT

© 2022 Jiao, Wang, Ling, Deng, Yan and
Chen. This is an open-access article
distributed under the terms of the
[Creative Commons Attribution License](#)
(CC BY). The use, distribution or
reproduction in other forums is
permitted, provided the original
author(s) and the copyright owner(s) are
credited and that the original
publication in this journal is cited, in
accordance with accepted academic
practice. No use, distribution or
reproduction is permitted which does
not comply with these terms.

Effect evaluation of ecological water conveyance in Tarim River Basin, China

Ayong Jiao¹, Wenqi Wang², Hongbo Ling^{2*}, Xiaoya Deng^{3*},
Junjie Yan⁴ and Fulong Chen¹

¹College of Water Conservancy & Architectural Engineering, Shihezi University, Shihezi, Xinjiang, China,

²Xinjiang Institute of Ecology and Geography, Chinese Academy of Sciences, Urumqi, Xinjiang, China,

³China Institute of Water Resources and Hydropower Research, Beijing, China, ⁴Institute of Resources and Ecology, Yili Normal University, Yining, Xinjiang, China

Ecological water conveyance is an important way to promote the restoration of degraded ecosystems in arid watersheds. However, there are few previous research results on how to quantitatively evaluate the effect of ecological water conveyance on ecological restoration. In this regard, this paper selects the Tarim River Basin as a typical area, analyzing the changes of desert riparian vegetation and hydrological elements, constructing a watershed ecological environment quality evaluation system, and comprehensively evaluating the ecological water conveyance effect of the damaged desert forest ecosystem. The conclusion showed that the proportion of the pixel area with an upward trend of Fractional Vegetation Cover (FVC) from 2000 to 2021 is as high as 84.3%. The plant diversity index in the ecological water conveyance area showed the characteristics of first obvious increase and then stable. The main body of groundwater depth showed an upward trend, and the Temperature Vegetation Dryness Index (TVDI) showed a downward trend of pixel area accounting for 57.0%, which indicated that ecological water conveyance had played a positive role in groundwater recharge and ecological restoration along the Tarim River. The ecological environment quality of the river basin showed a trend of transition from low-grade to high-grade, and the area with excellent ecological quality had increased from 4,635.50 km² in 2000 to 12,335.0 km² in 2021. The above research provides important scientific reference for the protection and restoration of vegetation degradation in arid watersheds.

KEYWORDS

ecological water conveyance, desert riparian vegetation, ecological environment quality, ecological restoration, Tarim River Basin

1 Introduction

Desert riparian forests are widely distributed on both sides of inland river basins in arid areas. It is a forest ecosystem with relatively single species in desert environment. They play an important role in wind prevention and sand fixation and maintaining the balance and stability of ecosystems in arid areas (Keyimu et al., 2018; Sun et al., 2022).

Water is the most important environmental factor to ensure the structural integrity and functional stability of ecosystem in arid areas. However, due to the disturbance of global climate change and human activities, the shortage of water resources has become an important factor affecting the ecosystem in arid areas, which directly restricts the development and evolution of the desert riparian forest ecosystem (Adam et al., 2009; Allen and Ingram, 2012; Deng and Chen, 2017; Wang and Qin, 2017; Ni et al., 2022). In addition, the ability of desert riparian forest ecosystems to resist external disturbances and self-repair is low, exacerbating various ecological problems such as land degradation, desertification, pests and diseases, and biodiversity damage. To this end, based on the purpose of ecological protection and restoration, in order to curb the degradation of natural vegetation, ecological water conveyance work has been carried out in many regions around the world (Chen et al., 2010; Zeng et al., 2016; Zhao et al., 2020). Therefore, after ecological water conveyance, understanding the restoration status of damaged desert forest ecosystems and the effect of ecological water conveyance has become a hot topic in the research on ecosystem restoration and protection in arid areas.

Desert riparian forests are mainly distributed in Central Asia, the Murray-Darling Basin in Australia, the Colorado River Basin in the western United States and northwestern China (Ding et al., 2017; Zhang et al., 2018). A large number of studies have shown that groundwater and soil moisture are the key factors to maintain the normal growth and development of desert riparian forests. The change of groundwater level directly affects the development of natural vegetation communities in desert riparian forests, and further affects the stability of desert ecosystems in arid areas. Drought stress will not only wilt plants, but also weaken the physiological functions and disease resistance of plants (Doble et al., 2006; Chui et al., 2011). The ecological water conveyance project can effectively raise the groundwater level and increase the soil water content. Therefore, it is very important to study the temporal and spatial variation of the groundwater level and soil drought for the protection and restoration of desert riparian forest vegetation (Halik et al., 2019; Ling et al., 2020). The species of desert riparian forest vegetation is relatively poor, the structure is relatively simple, the main feature is low species diversity, and ecological water conveyance can form a favorable environment for their survival. The study of species diversity in the process of vegetation restoration not only helps to correctly understand the process of vegetation restoration, but also helps to understand the dynamic succession process of the ecosystem (Runyan and D'Odorico, 2010; Kopec et al., 2013). The ecological water conveyance is mainly carried out along the river course. The farther away from the river course, the lower the fractional vegetation cover and the smaller the area of vegetation restoration. Therefore, the research on the degree of increase in fractional vegetation cover and the area of vegetation restoration is also an important indicator for evaluating the

degree of vegetation restoration (Guo et al., 2017; Huang F. et al., 2020). At present, with the implementation of the ecological water conveyance project, the ecological deterioration in the water conveyance area has been curbed. However, there are few previous research results on how to quantitatively evaluate the effect of ecological water conveyance. It is of great practical significance to comprehensively evaluate the overall ecological environment quality changes in the basin to promote the vegetation restoration in the arid area.

The Tarim River Basin, located in the Tarim Basin in northwestern China, is one of the most representative desert riparian forest distribution areas in China and even the world (Hao et al., 2010; Ling et al., 2017). In 2001, the Chinese government implemented an ecological water conveyance project in the lower reaches of the Tarim River. Therefore, this study selected the Tarim River Basin as a typical area. However, there are few long-term studies on the changes of vegetation belts in the Tarim River Basin, soil drought condition, and changes in the ecological quality of the whole basin after ecological water conveyance. Based on remote sensing data and field survey data, this study focuses on the changes of the desert riparian forest vegetation belt and hydrological conditions in the Tarim River Basin in the past 22 years. A quality evaluation system for the ecological environment of the Tarim River Basin was constructed to comprehensively evaluate the restoration of damaged desert forest ecosystems and the effectiveness of ecological water conveyance, in order to provide decision-making references for ecological conservation and sustainable development of inland river basins in arid regions.

2 Overview of the study area

The Tarim River Basin is located in the hinterland of Eurasia, and is located in the south of Xinjiang Uygur Autonomous Region (34°55'–43°08' N, 73°10'–94°05' E). It is the largest inland river in China. It is connected with Pakistan in South Asia and India, Afghanistan in West Asia, Tajikistan in Central Asia and Kyrgyzstan, and the basin area reaches 1.027 million km². The study area has a hot, dry climate, and water resources are scarce. The climate is classified as warm temperate extreme arid. The annual average precipitation is less than 50 mm and the annual average evaporation is more than 2,500 mm. The Tarim River Basin is one of the most fragile regions in China, and even the world. Among them, the main stream of Tarim River is composed of Aksu River, Hotan River, Yarkant River and other rivers, starting from Xiaojiake, and finally into Taitema Lake. Arbor-shrub-grass vegetation belts mainly comprising *Populus euphratica*, *Tamarix ramosissima*, *Lycium ruthenicum*, *Phragmites communis*, and *Apocynum venetum* are present on both sides of the river. After the completion of the Daxihaizi Reservoir in 1972, the incoming water in the middle and upper reaches was completely intercepted, resulting in the complete

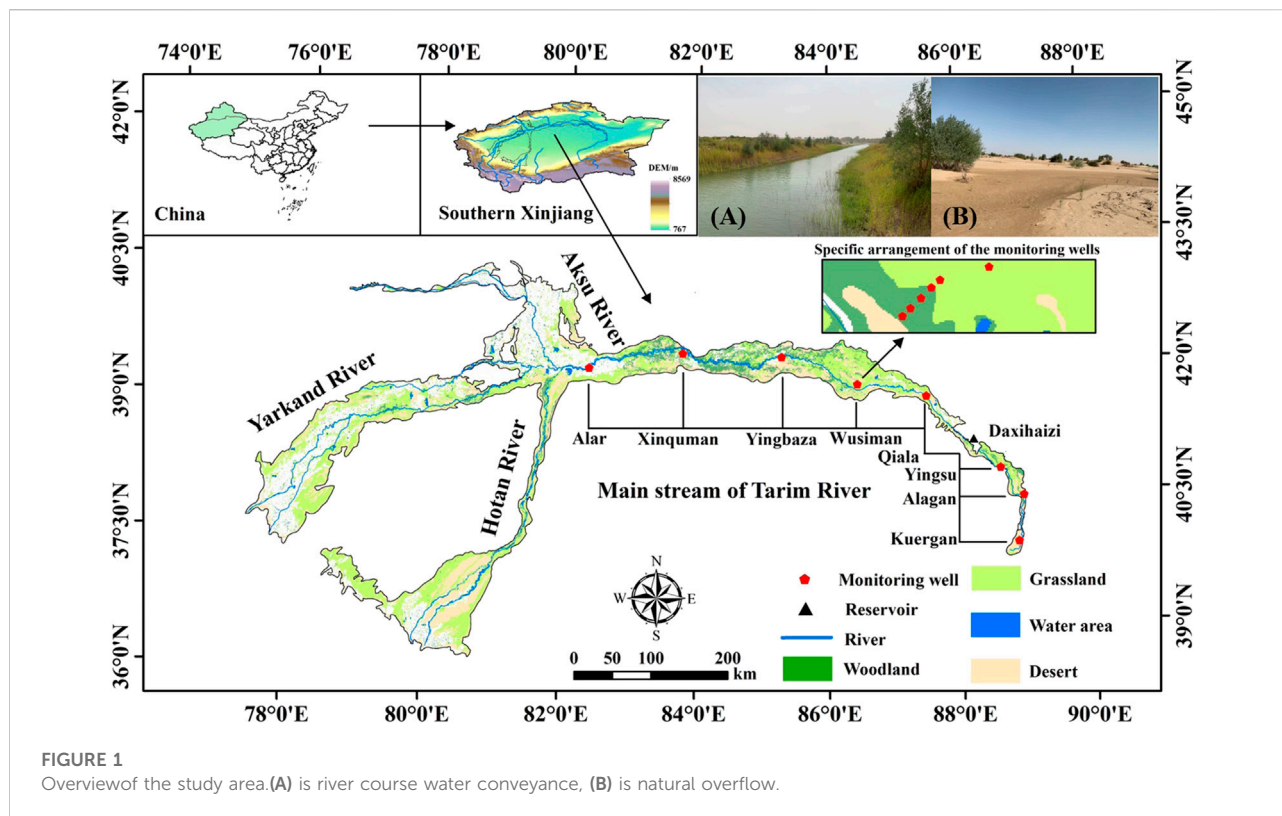


FIGURE 1

Overview of the study area. (A) is river course water conveyance, (B) is natural overflow.

disconnection of the lower reaches of the Tarim River and the drying up of the Taitema Lake. Large areas of natural vegetation have been degraded and the groundwater level has decreased, and thus, the ecological environment has been severely damaged. In 2001, the Chinese government invested 10.7 billion yuan to implement comprehensive management of the Tarim River Basin with the fundamental aim of restoring the downstream ecosystems. In order to further improve the effect of comprehensive management, since 2016, the autonomous region government launched a special action for ecological protection of *Populus euphratica* forest in the Tarim River Basin, using ecological sluices and water conveyance channels to introduce water into forest areas (see Figures 1A,B), and promote the recovery of *Populus euphratica* forest ecosystem through overflow interference. At present, the special action for ecological protection of *Populus euphratica* has been carried out for 6 years, and the comprehensive management of the Tarim River Basin has been carried out for 22 years. The accumulated ecological water conveyance in the lower reaches of Tarim River is 8.793 billion m³, and the average annual water conveyance is 400 million m³. The degradation of the ecological environment in the Tarim River Basin has been effectively halted. The long-term disconnection of the downstream river has improved and the green vegetation in the riparian zone is characterized by positive physiological and ecological responses. Therefore, the Tarim River is not only the area with the most serious damage to

the ecological environment caused by artificial interference, but also the most successful typical case of human intervention in promoting ecological restoration.

3 Data sources and research methods

3.1 Data sources

Table 1 lists the all the data sets used in our study. Images of Normalized Difference Vegetation Index (NDVI) were used to calculate the Fractional Vegetation Cover (FVC) and the Temperature Vegetation Dryness Index (TVDI). There are now more 100 vegetation indexes. NDVI, the Ratio Vegetation Index (RVI), Enhanced Vegetation Index (EVI) and the Soil Adjusted Vegetation Index (SAVI) are widely mentioned or used. Yet each vegetation index has strength and weakness. RVI does not perform well when the FVC is <50% (Jackson, 1983), which rules RVI out when quantifying the vegetation in the desert ecosystems. Defect of NDVI comes from its saturation when measuring dense vegetation. SAVI and EVI are both modified NDVI with adjustment from the effects of soil brightness in the background and improved sensitivity to dense vegetation (Huete, 1988; Matsushita et al., 2007). Despite the adjustment and improvement of SAVI and EVI, NDVI is

TABLE 1 Data and sources used by the institute.

Ecological indicators	Time period	Time resolution	Spatial resolution	Data source
TVDI	2000–2021	16 days/8 days	250 m/1000 m	MOD13Q1/MOD11A2
NDVI	2000–2021	16 days	250 m	MOD13Q1
Measured groundwater level	2003–2020	—	—	Field investigation
RSEI	2000–2021	8 days/8 days/16 days	500 m/1000 m/500 m	MOD09A1/MOD11A2/MOD13A1

the one that is most widely used. And it is also generally agreed that NDVI is sensitive in low to moderate dense vegetation such as semi-arid areas (Tucker, 1986; Diallo et al., 1991; Xue and Su, 2017). In addition, high-quality time series NDVI are readily available from data sets of MODIS NDVI, SPOT NDVI and GIMMS NDVI. That's why NDVI was selected in this study. 16-day composited NDVI images were derived from the MODIS MOD13Q1 product, Savitzky-Golay filtering was performed to the NDVI time series to smooth out noise caused by poor atmospheric conditions (Chen et al., 2004). And The MVC was applied to produce yearly NDVI, which would further improve the quality of the NDVI images by reducing noise caused by poor atmospheric conditions (Holben, 1986).

16-day composited images of Land Surface Temperature (LST) of daytime, together with NDVI, were used to calculate TVDI. The time series LST images were derived from MODIS MOD11A2 product. LST images were averaged to get yearly LST.

The groundwater depth data were proved by the Tarim River Basin Administration bureau. And the date set were collected from six typical monitoring sections set along the main stream of Tarim River, namely, Alar, Wusiman, Qiala, Yingsu, Alagan and Kuergan (see Figure 1).

Quadrat sampling method was used to collect the number of vegetation species and plants. From 2015 to 2021, sampling was carried out in the Shaya *Populus euphratica* Forest Park in the upper reaches of the main stream of Tarim River and the Luntai *Populus euphratica* Forest Park in the middle reaches of the main stream of Tarim River. Three 25 m × 25 m fixed monitoring quadrats were set at each sampling point.

3.2 Calculation method

3.2.1 TVDI calculation method

The TVDI was used to characterize the soil moisture, and it was calculated based on the NDVI and LST with the following formula:

$$TVDI = (LST - LST_{min}) / (LST_{max} - LST_{min}) \quad (1)$$

$$LST_{max} = a_1 + b_1 \times NDVI \quad (2)$$

$$LST_{min} = a_2 + b_2 \times NDVI, \quad (3)$$

where LST is the surface temperature of any pixel, LST_{min} is the minimum surface temperature corresponding to a certain NDVI value, which is called the wet edge, (LST_{max} is the maximum surface temperature corresponding to a certain NDVI value, which is called the dry edge, and a_1 , a_2 , b_1 , and b_2 are the coefficients in the dry-wet boundary equation. The value of TVDI ranges among (0, 1). A pixel is more arid when the value is closer to 1 and more humid when the value is closer to 0. According to previous drought monitoring studies conducted in Tarim River Basin (Huang J. et al., 2020), the TVDI values were classified as follows: TVDI ≤ 0.46 representing drought free, 0.46 < TVDI ≤ 0.57 for light drought, 0.57 < TVDI ≤ 0.76 for moderate drought, 0.76 < TVDI ≤ 0.86 for severe drought, and TVDI > 0.86 for extreme drought.

3.2.2 Calculation method of vegetation data

The Fractional Vegetation Cover (FVC) is an important indicator for measuring the surface fractional vegetation cover in a region, and it has a strong positive correlation with NDVI. Based on the pixel dichotomy model and NDVI data, the fractional vegetation cover was calculated using the inversion model with the following formula:

$$FVC = \frac{NDVI - NDVI_{min}}{NDVI_{max} - NDVI_{min}}, \quad (4)$$

where FVC is the fractional vegetation cover, and $NDVI_{min}$ and $NDVI_{max}$ are the minimum and maximum NDVI values of all pixels in the area, respectively. $NDVI_{min}$ and $NDVI_{max}$ were optimized with 5–95% as the confidence interval for the NDVI values. According to the vegetation distribution characteristics, the fractional vegetation cover values were classified as follows: FVC ≤ 5% for extremely low fractional vegetation cover, 5% < FVC ≤ 10% for low fractional vegetation cover, 10% < FVC ≤ 20% for medium fractional vegetation cover, and FVC ≥ 20% for high fractional vegetation cover.

In order to analyze the changes in the diversity indices for vegetation after ecological water conveyance, the Simpson and Shannon–Wiener indices were calculated for vegetation in the samples as follows.

$$\text{Simpson Index: } D = 1 - \sum_{i=1}^s P_i^2 \quad (i = 1, 2, 3, \dots, S) \quad (5)$$

$$\text{Shannon-Wiener Index: } H = \sum_{i=1}^S (P_i \ln P_i), \quad (6)$$

where P_i is the frequency of occurrence for the i -th species, $P_i = N_i/N$, N is the total number of individuals in the quadrat, and N_i is the number of individuals for the i -th species.

3.2.3 Comprehensive effect evaluation of ecological water conveyance

The Google Earth Engine platform can rapidly screen out the images with the best quality by directly accessing the data set and using the cloud mask algorithm, thereby avoiding the inefficiency of local download, storage, and preprocessing. In this study, based on the Google Earth Engine platform, MOD09A1, MOD13A1, and MOD11A2 data were used to calculate the humidity, greenness, dryness and heat indices for each year. Principal component analysis was then conducted to construct the remote sensing ecological index. It should be noted that each index has different units and numerical ranges, so the four indices were normalized with the following formula (Chen et al., 2019; Zhang et al., 2021):

$$NI_i = \frac{I_i - I_{\min}}{I_{\max} - I_{\min}}, \quad (7)$$

where NI_i is the index normalization result, I_i is the i -th pixel value, I_{\min} is the minimum value, and I_{\max} is the maximum value.

Principal component analysis was performed with ENVI software, where the four normalized index bands were combined into new images to obtain relevant statistical results. After positive and negative values for principal component 1 (PC1) were transferred and normalized, the remote sensing-based ecological index (RSEI) was obtained as:

$$RSEI_0 = 1 - PC1 \quad (8)$$

$$RSEI = \frac{RSEI_0 - RSEI_{0\min}}{RSEI_{0\max} - RSEI_{0\min}}, \quad (9)$$

where RSEI is the remote sensing ecological index value and the ecological quality is better when the value is closer to 1, and $RSEI_{0\min}$ and $RSEI_{0\max}$ denote the minimum and maximum $RSEI_0$ values, respectively. According to the ecological environment quality status in the study area and the ecological environment classification standard in "Technical Criterion for Ecosystem Status Evaluation" (HJ192-2015), the RSEI indices were classified into four habitat conditions as follows: $RSEI \leq 0.2$ for poor, $0.2 < RSEI \leq 0.4$ for moderate, $0.4 < RSEI \leq 0.6$ for good, and $RSEI > 0.6$ for excellent.

3.2.4 Mann-Kendall trend test

The Mann-Kendall statistical test obtained the trends of TVDI, FVC and RSEI and test the significance of the changes. The Mann-Kendall statistical test is a non-parametric test

method. The time series $X_1, X_2, X_3, \dots, X_n$ are successively compared, and the results are represented by $sgn(\theta)$:

$$sgn(\theta) = \begin{cases} 1, & \theta > 0 \\ 0, & \theta = 0 \\ -1, & \theta < 0 \end{cases} \quad (10)$$

The calculated result of the Mann-Kendall statistic is:

$$S = \sum_{i=1}^{n-1} \sum_{k=i+1}^n sgn(x_k - x_i) \quad (11)$$

where x_k and x_i are random variables and n is the length of the selected data series. The test statistic Z_c is:

$$Z_c = \begin{cases} \frac{s-1}{\sqrt{\text{var}(s)}}, & s > 0 \\ 0, & s = 0 \\ \frac{s+1}{\sqrt{\text{var}(s)}}, & s < 0 \end{cases} \quad (12)$$

where $|Z_c| \geq 1.96$ indicates that at the 0.05 significance level, the sample sequence has a significant trend. Positive Z_c indicates an upward trend, and negative Z_c indicates a downward trend.

4 Results

4.1 Temporal and spatial variation of hydrological factors

The annual average TVDI in the Tarim River Basin mostly ranges from 0.69 to 0.76, with obvious spatial differences (see Figure 2A). The areas with relatively high degree of soil drought were mainly distributed in the lower reaches of the main stream of Tarim River, and in Moyu County and Luopu County in the Hotan River Basin. The areas with relatively low soil aridity are mainly distributed near Alar in the Aksu River Basin, the Hotan River, and the upper reaches of the Yarkand River. The proportion of moderate drought in the whole basin is as high as 31.7%, followed by severe drought, reaching 27.7%. The proportion of light drought and extreme drought is equivalent, which are 18.4% and 20.5% respectively, and the proportion of drought free is the lowest, only 1.6%. From the results, the Tarim River Basin was still moderate drought.

From 2000 to 2021, the area of pixels with a downward trend in TVDI in the Tarim River Basin ($Z_c < 0$) accounted for 57.0%, which was higher than that of TVDI with increasing trend ($Z_c > 0$), indicating that the soil in the Tarim River Basin has a stronger trend of humidification than that of aridity (see Figure 2B). Among them, the areas with a downward trend in TVDI ($Z_c < 0$) are mainly located in most areas of the Aksu River Basin, the upper reaches of the main stream of Tarim River, and the middle and lower reaches of the Yarkand River Basin. The areas with an upward trend in TVDI ($Z_c > 0$) are mainly located in Moyu

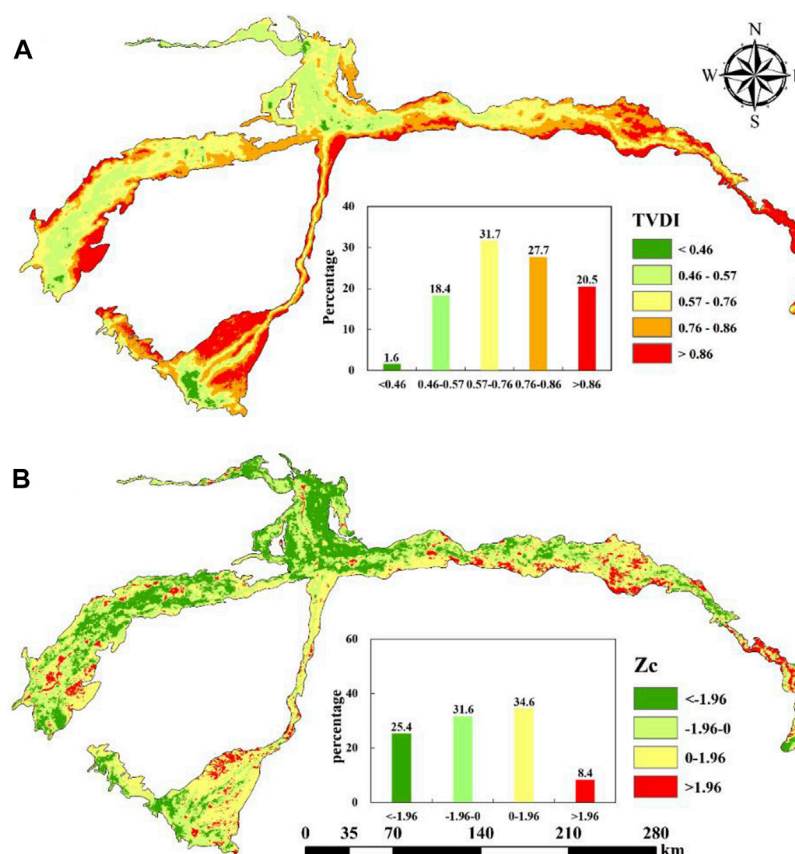


FIGURE 2

Spatial distribution (A) of annual average TVDI and spatial distribution (B) of TVDI variation trend in Tarim River Basin from 2000 to 2021.

County and Luopu County in the Hotan River Basin. In the whole basin, TVDI showed a significant decreasing trend ($Z_c < -1.96$), and the pixel area accounted for 25.4%, mainly distributed in most areas of Aksu River Basin and the middle reaches of Yarkand River Basin. The proportion of pixel area of TVDI with non-significant increasing trend ($0 < Z_c < 1.96$) and non-significant decreasing trend ($-1.96 < Z_c < 0$) is equivalent, which is 34.6% and 31.6%, respectively. The proportion of pixel area with significant increasing trend of TVDI ($Z_c > 1.96$) is the lowest, which is only 8.4%. It shows that the soil in Tarim River Basin has a tendency of wetting after ecological water conveyance.

According to Figure 3, From 2003 to 2020, the groundwater depth of the main stream of the Tarim River showed a trend of gradual uplift. Among the monitoring sections where the buried depth of groundwater is showed uplifted, the groundwater section in the lower reaches of the main stream of Tarim River has a significant rising trend, with the highest lifting rate of 0.0348 m/month in Kuergan, 0.0148 m/month in Yingsu and 0.0142 m/month in Alagan. In addition, the monthly average uplift values of groundwater depth in Alar

and Qiala are 0.0040 m/month, 0.0007 m/month, and 0.0118 m/month respectively. In recent 20 years, the lower reaches of the main stream of Tarim River as a key ecological water conveyance area, groundwater uplift significantly, indicating that ecological water conveyance along the Tarim River has played a positive role in groundwater recharge and ecological restoration, and created good hydrological conditions for vegetation growth.

4.2 Temporal and spatial variation of fractional vegetation cover

It can be seen from Figure 4A that the annual average FVC in the Tarim River Basin is mostly between 20% and 30%, and the spatial differences are also obvious. The areas with higher fractional vegetation cover are mainly distributed in the upper and middle reaches of the Yarkand River Basin, the Aksu River Basin, the upper reaches of the Hotan River Basin and the upper reaches of the main stream of Tarim River, and the areas with lower fractional vegetation cover are mainly distributed in the

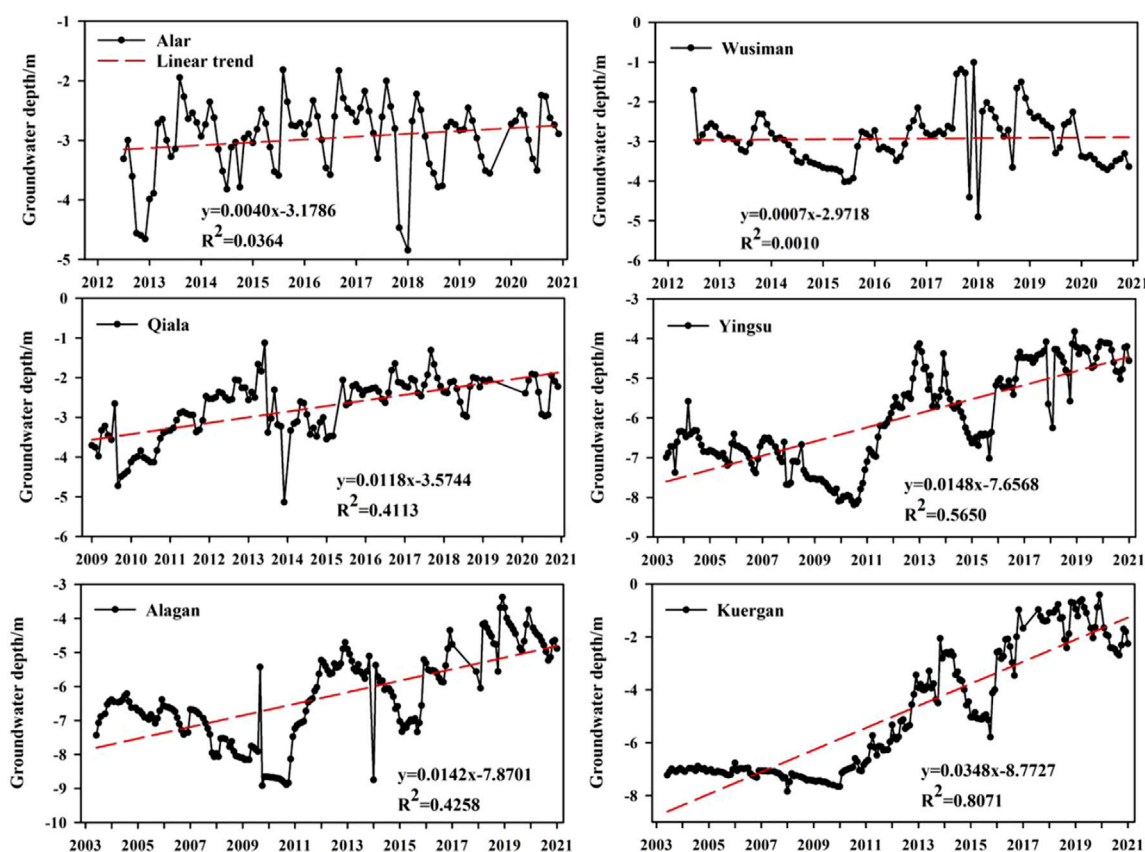


FIGURE 3

The variation process of groundwater depth in each section of the main stream of Tarim River month by month.

middle and lower reaches of the Hotan River Basin and the lower reaches of the main stream of Tarim River. In the space, high fractional vegetation cover ($FVC > 20\%$) accounted for up to 42.0% in the whole basin, followed by extremely low fractional vegetation cover ($FVC \leq 5\%$), reaching 30.9%. The proportions of low fractional vegetation cover ($5\% < FVC \leq 10\%$) and medium fractional vegetation cover ($10\% < FVC \leq 20\%$) were equivalent, which were 13.4% and 13.7%, respectively.

It can be seen from Figure 4B that the area of pixels with an upward trend in FVC ($Z_c > 0$) in the Tarim River Basin from 2000 to 2021 accounted for 84.3%, which is much higher than the area of pixels with a downward trend in FVC ($Z_c < 0$), indicating that after the ecological water conveyance, the fractional vegetation cover showed an obvious improvement trend. Among them, the area with an upward trend of FVC ($Z_c > 0$) is widely distributed in the whole basin, and the area of pixels with a downward trend ($Z_c < 0$) only accounts for 15.7%, which is scattered in the main stream of Tarim River and part of the Hotan River Basin. The pixel area with a significant upward trend in FVC ($Z_c > 1.96$) in the whole basin accounted for 63.5%, and

the pixel area with a non-significant upward trend in FVC ($0 < Z_c < 1.96$) accounted for 20.8%. The proportions of non-significant decreasing trend ($-1.96 < Z_c < 0$) and significant decreasing trend ($Z_c < -1.96$) were very small, accounting for 11.3% and 4.4% respectively.

According to the sample plot monitoring results, the average diversity index values in the vegetation survey plots were used to measure the species diversity. It can be seen from Figure 5, in the Shaya *Populus euphratica* Forest Park, the Simpson index and Shannon-Wiener index (Shannon index) values were significantly lower in 2015 than 2017, 2018, and 2021, and thus the riparian vegetation was gradually restored after ecological water conveyance. The Simpson index of Luntai *Populus Euphratica* Forest Park in the middle reaches of the Tarim River increased significantly and then decreased slightly. The Shannon-Wiener index of Luntai *Populus Euphratica* Forest Park in 2015 was significantly lower than that in 2017, 2018 and 2021, which indicated that the community species diversity level increased significantly after the water conveyance was more than 2 years, but with the increase of water conveyance frequency, the diversity level began to decline and then stabilized. On the whole,

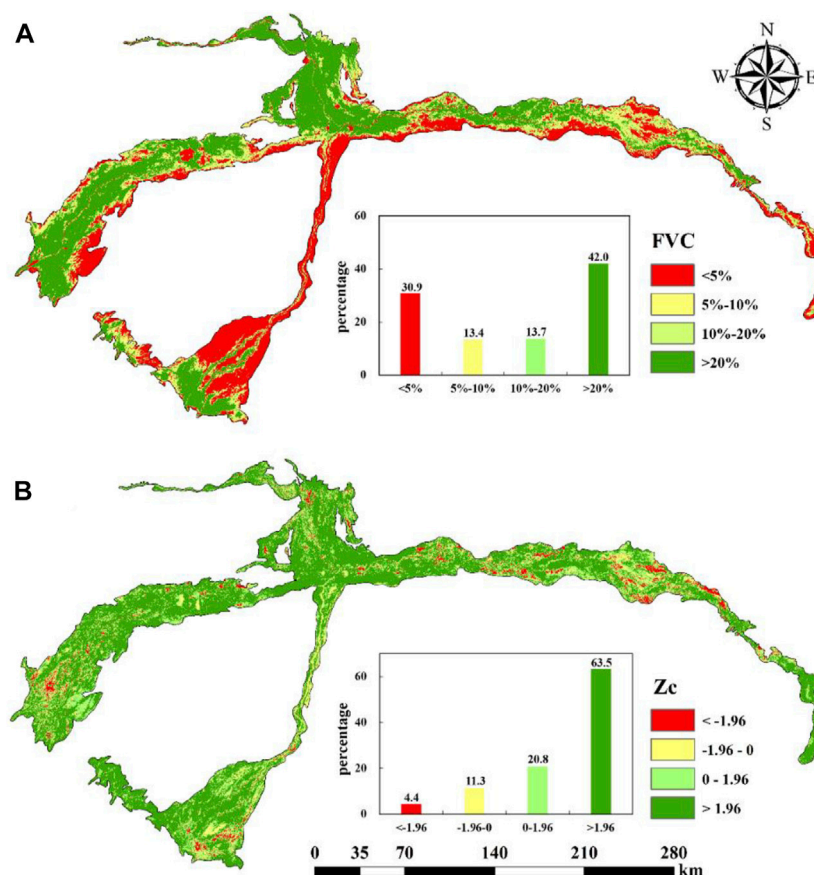


FIGURE 4

Spatial distribution (A) of annual average FVC and spatial distribution (B) of FVC variation trend in Tarim River Basin from 2000 to 2021.

under the current normalized water conveyance mode, the ecological environment of the study area has been improved, and the level of species diversity tends to be stable during changes.

4.3 Temporal and spatial variation of ecological quality

It can be seen from Figure 6A, the annual average RSEI in the Tarim River Basin is mostly between 0.33 and 0.39, with significant spatial differences. The areas with good ecological quality are mainly distributed in parts of the Aksu River Basin, the main stream of the Tarim River, the Hotan River Basin and the upper reaches of the Yarkand River Basin, while the areas with poor ecological quality are mainly distributed in the middle and lower reaches of the main stream of the Tarim River and the lower reaches of the Hotan River Basin. The pixel area with excellent ecological quality ($RSEI > 0.6$) in the whole basin accounted for the lowest proportion, only 8.1%, and the pixel

area with good ecological quality ($0.4 < RSEI \leq 0.6$) accounted for 31.2%. The pixel area with moderate ecological quality ($0.2 < RSEI \leq 0.4$) accounted for the highest proportion, reaching 37.3%, and the pixel area with poor ecological quality ($RSEI \leq 0.2$) accounted for 23.4%. From the results, the ecological environment quality of Tarim River Basin is moderate.

It can be seen from Figure 6B that the area of pixels with an upward trend in RSEI ($Z_c > 0$) in the Tarim River Basin from 2000 to 2021 accounted for 58.9%, which is higher than the area of pixels with a downward trend in RSEI ($Z_c < 0$). It indicated that the ecological quality of the Tarim River Basin showed a trend of improvement after ecological water conveyance. Among them, the areas with an upward trend in RSEI ($Z_c > 0$) are mainly distributed in the Aksu River Basin, the upper and lower reaches of the main stream of the Tarim River, the upper and middle reaches of the Yarkand River Basin and the upper reaches of the Hotan River Basin. The areas with decreasing trend ($Z_c < 0$) are mainly distributed in the middle and lower reaches of the Hotan River Basin. The pixel area of RSEI in the whole basin showed a significant upward trend ($Z_c > 1.96$), accounting for up to 34.0%.

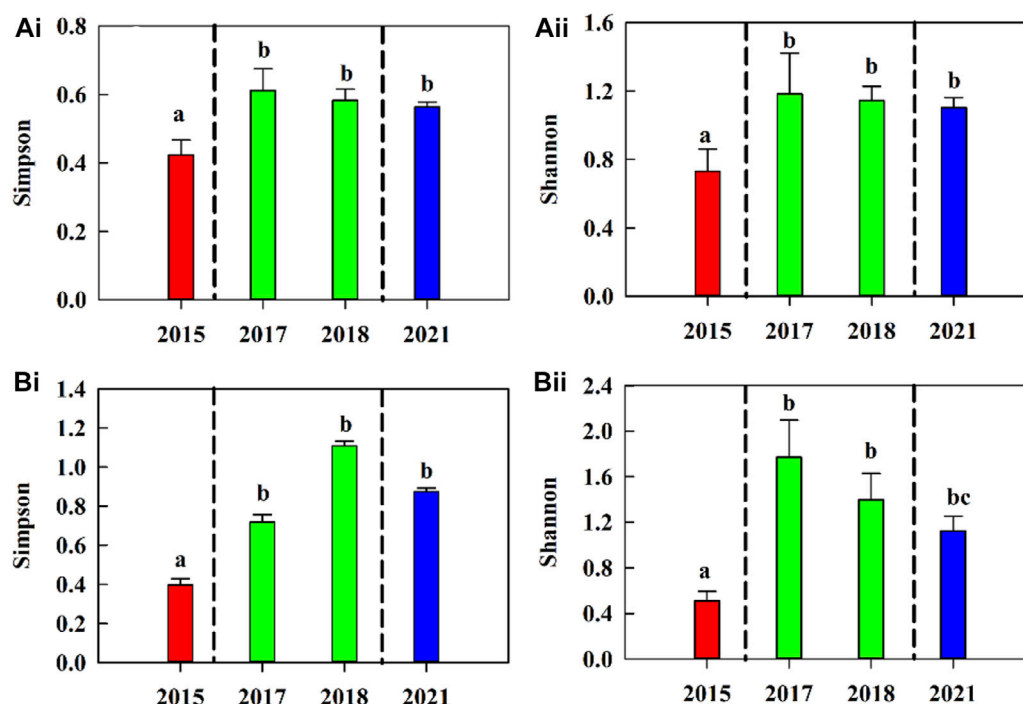


FIGURE 5

Temporal and spatial variation characteristics of species diversity in the upper and middle reaches of the main stream of the Tarim River. (Ai, Aii) is Shaya *Populus euphratica* Forest Park, (Bi, Bii) is Luntai *Populus euphratica* Forest Park.

The pixel area of RSEI showed a non-significant upward trend ($0 < Zc < 1.96$) and a non-significant downward trend ($-1.96 < Zc < 0$), which were 24.9 % and 31.4%, respectively. The pixel area of RSEI showed a significant downward trend ($Zc < -1.96$), which was the smallest, accounting for only 9.7%.

In order to further explore the changes in the ecological quality level of the Tarim River Basin over the past 22 years, the RSEI data of the Tarim River Basin in 2000 and 2021 were analyzed with the help of ArcGIS 10.7 spatial analysis function. It can be seen from Table 2 that the ecological environment quality level of the Tarim River Basin shows a trend of transition from low grade to high grade, and the area with excellent ecological quality has increased from 4,635.50 km² in 2000 to 12,335.00 km² in 2021, mainly concentrated in the upper reaches of the main stream of the Tarim River, the upper reaches of the Hotan River Basin, the Aksu River Basin and the Yarkand River Basin, the area with moderate ecological quality decreased from 41,307.00 km² in 2000 to 30,075.25 km² in 2021, while the area with poor and good ecological quality did not change much. In general, after more than 20 years of ecological water conveyance project implementation, the ecological condition of the study area has been improved, and the effect is relatively obvious.

It can be seen from Figure 7, during the period of ecological water conveyance from 2000 to 2021, the

drought degree of the Tarim River basin gradually decreased, while the fractional vegetation cover increased year by year, and the ecological quality of the Tarim River basin gradually improved. The ecological water conveyance provided a positive role for the ecological restoration of the Tarim River Basin.

5 Discussion

5.1 Correlation of vegetation with hydrological factors and ecological environment quality

It can be seen from Figure 8 that the FVC and TVDI of the main stream of the Tarim River, Aksu River, Yarkang River and Hotan River were all significantly negatively correlated at the $p = 0.01$ level. The correlation coefficients were -0.725 , -0.587 , -0.758 and -0.689 , respectively. In general, the higher the degree of soil drought, the more the vegetation growth would be inhibited, and the smaller the FVC would be. With the progress of ecological water conveyance, the soil drought of the main stream of Tarim River, Aksu River, Yarkand River and Hotan River had been alleviated, creating favorable conditions for the growth of natural vegetation.

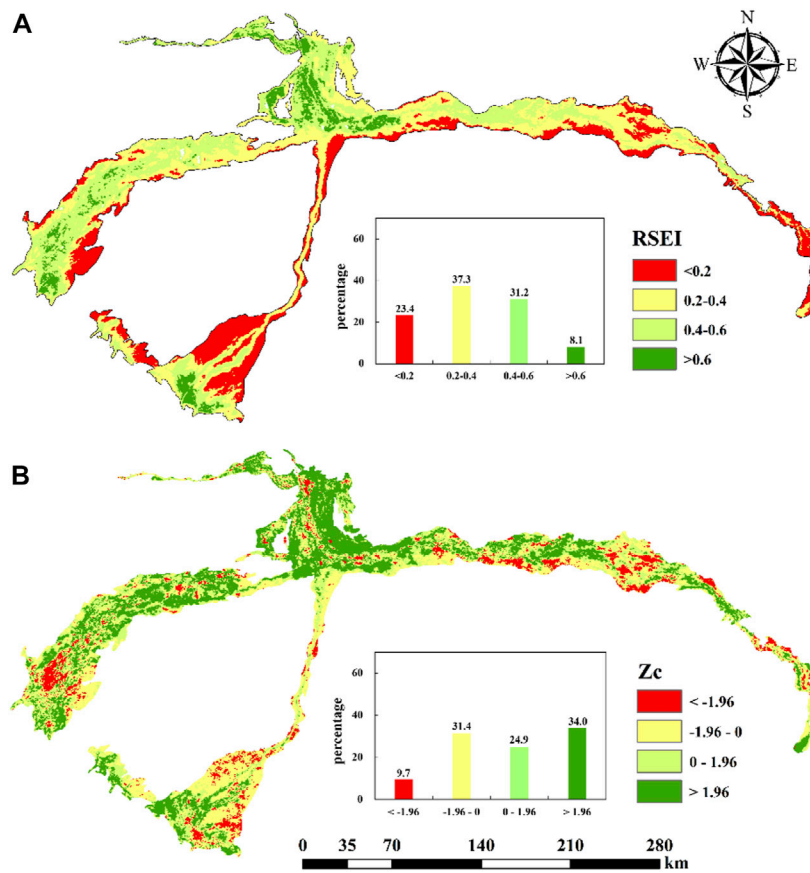


FIGURE 6 Spatial distribution (A) of annual average RSEI and spatial distribution (B) of RSEI variation trend in Tarim River Basin from 2000 to 2021.

TABLE 2 Area transfer matrix of different ecological quality grades in Tarim River Basin from 2000 to 2021 Unit/km².

Ecological quality level		2021				
		Poor	Middle	Good	Excellent	Total
2000	Poor	15,195.75	3,041.25	136.75		18,373.75
	Middle	6,527.25	25,687.00	7,935.75	1,157.00	41,307.00
	Good		1,342.75	18,572.75	7,700.50	27,616.00
	Excellent		4.25	1,153.75	3,477.50	4,635.50
	Total	21,723.00	30,075.25	27,799.00	12,335.00	91,932.25

It can be seen from Figure 9 that the annual average value of groundwater depth in the Qiala-Yingsu and Yingsu-Taitema Lake reaches from 2003 to 2020 was significantly positively correlated with FVC at the $p = 0.01$ level. The correlation coefficients were 0.942 and 0.957, respectively. In arid and semi-arid regions, the groundwater level was a key limiting factor affecting vegetation growth in the Tarim River Basin

due to the hot and dry climate and scarce precipitation. Ecological water conveyance greatly raised the groundwater level and provided good hydrological conditions for vegetation growth. From the results, the shallower the groundwater depth, the greater the FVC value, the better the growth of vegetation.

It can be seen from Figure 10 that the FVC of the main stream of the Tarim River, the Aksu River, the Yarkang River

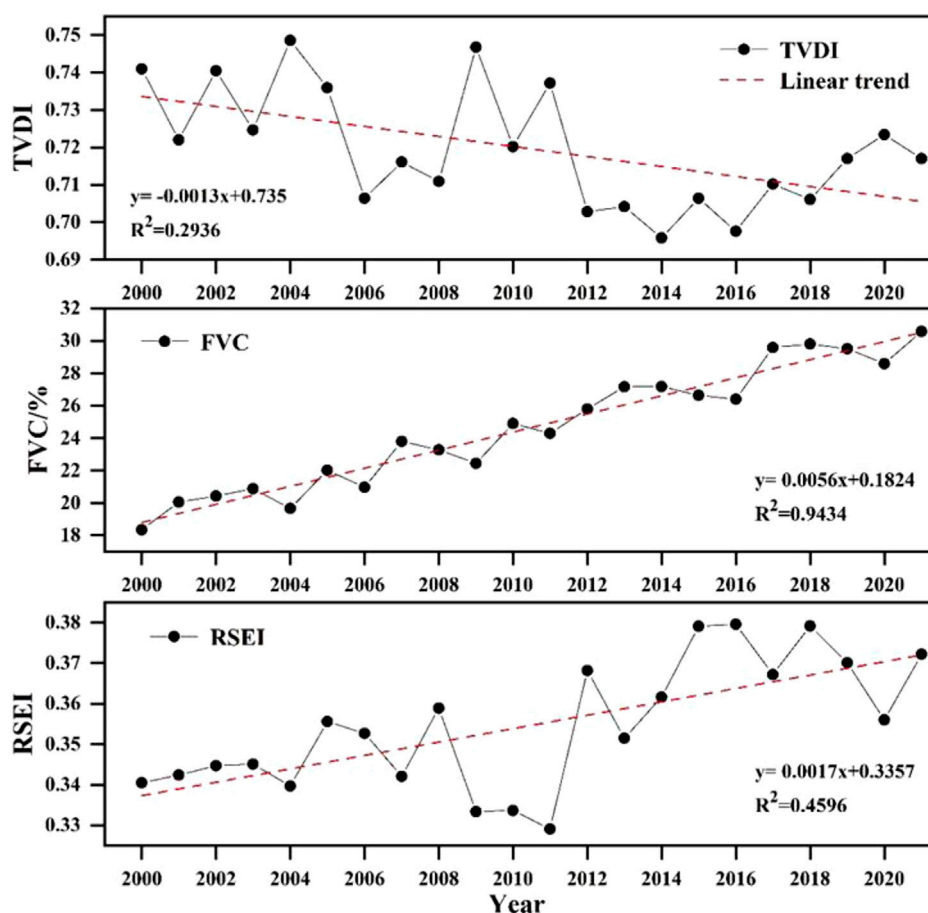


FIGURE 7

Variation trends of annual average TVDI, annual average FVC, and annual average RSEI in the Tarim River Basin from 2000 to 2021.

and the Hotan River were significantly positively correlated with the RSEI at the $p = 0.01$ level, and the correlation coefficients were 0.658, 0.877, 0.738 and 0.573, respectively. After ecological water conveyance, the groundwater level in the water conveyance area increased significantly, the soil drought was alleviated, the ecological quality of the whole basin was improved, and the limiting factors for vegetation growth were also weakened. Therefore, in general, the higher the ecological quality of the region, the better the vegetation growth, FVC would be greater.

This study discussed the correlation between vegetation factors and soil drought status, annual variation process of groundwater depth, and overall ecological quality status in the Tarim River Basin from 2000 to 2021. Compared with other studies, this study had a longer period, more indexes were selected, and was more representative and dynamic. However, there were still many shortcomings. For the change of vegetation factors after ecological water conveyance, the

influence of climate factors and human activities was not taken into account. For the change of soil drought, although the rainfall of Tarim River Basin was less than 50 mm, the effect of meteorological factors was small, but still could not be ignored (Deng et al., 2022a).

5.2 Suggestions on expanding the effect of ecological water conveyance

Ecological water conveyance is an important way to promote the restoration of degraded ecosystems in arid areas. From 1972 to 2000, the integrity of the surface hydrological process was lost due to the cutoff of the lower reaches of the Tarim River. During this period, the overall plant community showed extreme decline in growth and lack of species. After ecological water conveyance, this situation had changed significantly, and the flooding disturbance had a

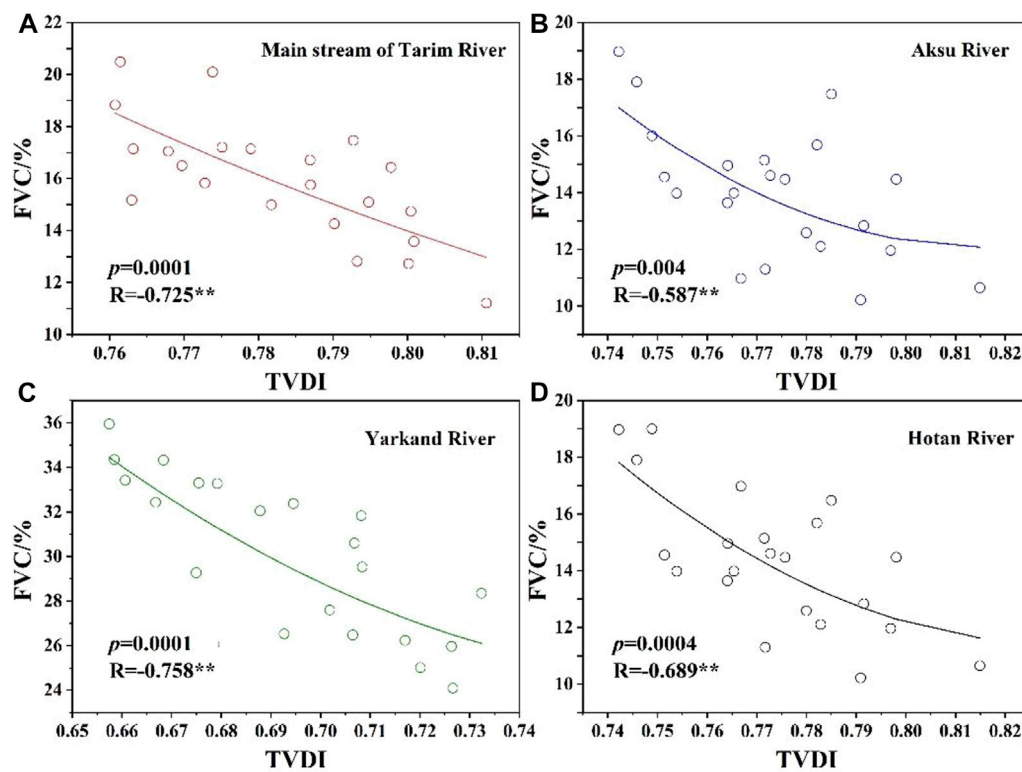


FIGURE 8

Correlation analysis of FVC and TVDI. (A) is main stream of Tarim River, (B) is Aksu River, (C) is Yarkand River, (D) is Hotan River.

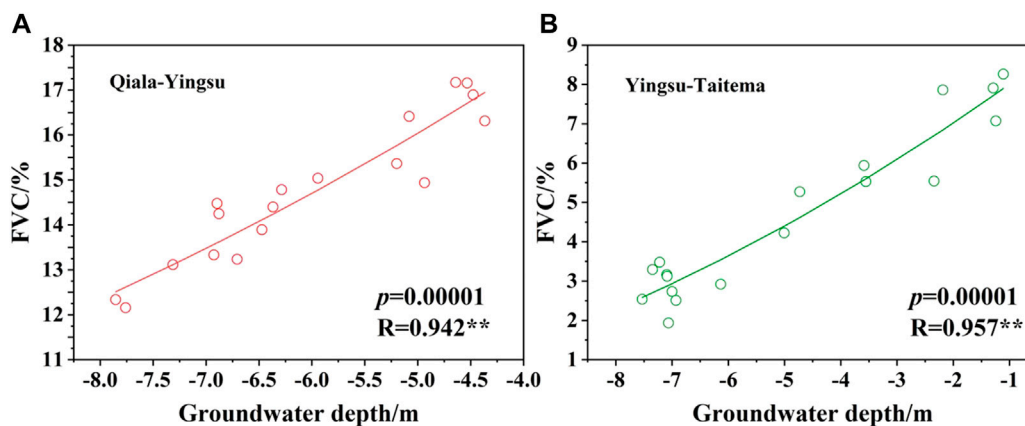


FIGURE 9

Correlation analysis of FVC and groundwater depth. (A) is Qiala-Yingsu, (B) is Yingsu-Taitema.

very significant effect on the increase of biodiversity in the water conveyance area (Keram et al., 2019; Ling et al., 2019; Bai et al., 2021; Deng et al., 2022b). In arid and semi-arid regions, some of the seeds produced by vegetation are characterized by dormancy and strong resistance to

drought and high temperatures, and thus they could survive for a long time. Ecological water conveyance can create conditions for germination and growth of plant seeds by changing the surface soil water content through the action of surface water (Casanova and Brock, 2000; Cavin et al.,

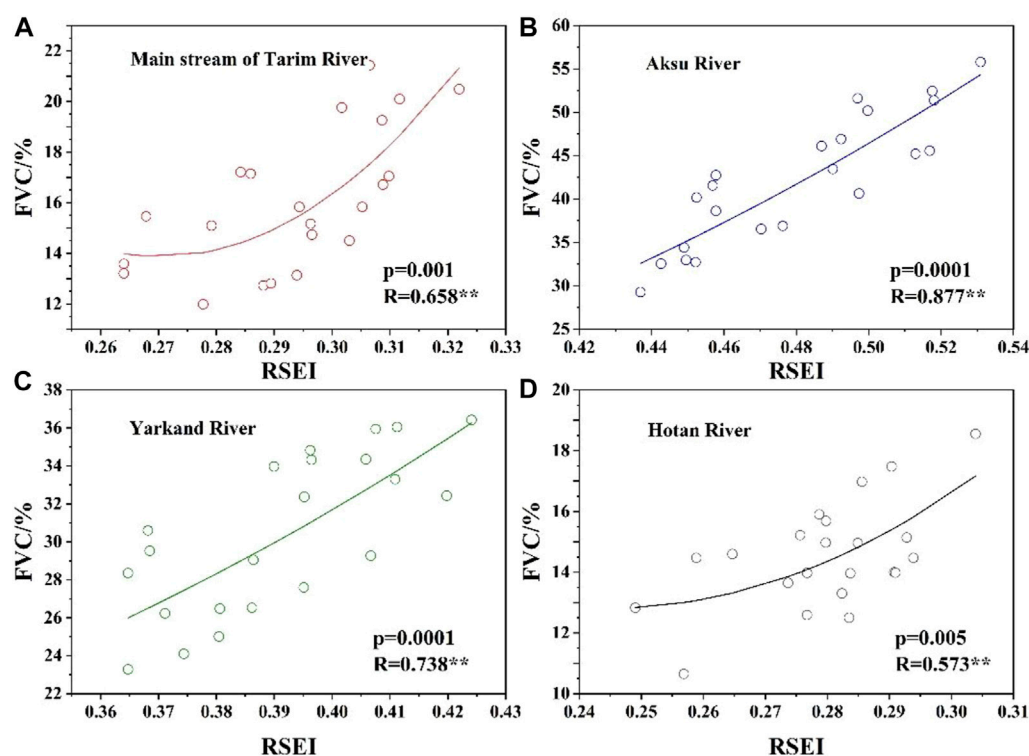


FIGURE 10

Correlation analysis of FVC and RSEI. (A) is main stream of Tarim River, (B) is Aksu River, (C) is Yarkand River, (D) is Hotan River.

2013). At the same time, some seeds were spread along the direction of water flow to other areas, where they could reproduce and grow quickly when they meet the suitable environmental conditions. The surface runoff formed by ecological water conveyance could effectively reduce the groundwater salinity in the water conveyance area. The groundwater salinity within 1 km along the two sides of the river decreases from about 4 to 11 g L⁻¹ before water conveyance to 1–5 g L⁻¹ on average, and the osmotic stress of vegetation was alleviated. The ecological water conveyance project had been carried out for 22 years, providing a suitable ecological water level for the natural vegetation. The desert riparian forest with *Populus euphratica*, *Tamarix ramosissima*, *Alhagi sparsifolia* and *Phragmites australis* as the main groups had been rejuvenated in the ecological water conveyance area (Deng et al., 2015; Garssen et al., 2015). The ecological environment of the whole study area began to improve, and the low and extremely low fractional vegetation cover in the study area gradually changed to medium and high fractional vegetation cover, indicating that the fractional vegetation cover showed an improvement trend after the ecological water conveyance.

In the past 20 years, the ecological water conveyance in the Tarim River Basin had been mainly through four ways:

River course water conveyance, Ecological sluice water conveyance, Natural overflow and Agricultural sluice diversion (Chen et al., 2008; Piao et al., 2011). At present, river course water conveyance is the main way, which can effectively raise the groundwater level on both sides of the river, and has a significant effect on the growth and rejuvenation of the existing natural vegetation near the river. However, at present, the water conveyance mode along the natural river only affects the natural vegetation near the river bank, and the restoration scope is very limited, making it difficult to restore the herbaceous plants on both sides of the river bank in a large area (Xu et al., 2008; Sims and Colloff, 2012). In terms of the groundwater uplift amplitude on both sides of the river, the groundwater uplift amplitude of the main stream of the Tarim River has slowed down in recent years. The groundwater level of the Qiala, Yingsu, Alagan and Kurgan sections gradually tended to balance. As for how to expand the effect of ecological restoration, according to the water requirements of desert riparian forest ecosystem, through the regulation of ecological water conservancy projects, we can build a planar water conveyance mode and expand the scope of the water receiving area of ecological water conveyance. We need to ensure that the groundwater level within 2 km away from the river is

maintained at a depth of 4–6 m, which can not only meet the water requirements for *Poplar* floating, germination and growth, but also prevent soil secondary salinization (Zalewski, 2002). Ecological water conveyance is mainly carried out from June to September when the water inflow of the Tarim River is relatively large. The use of planar water conveyance can greatly improve the vegetation habitat conditions and improve the stability and sustainability of the ecological protection and restoration system (Ling et al., 2015).

6 Conclusion

This study discussed the temporal and spatial changes of soil drought, the monthly change process of groundwater depth, the change of fractional vegetation cover and the change of overall ecological quality in the Tarim River Basin from 2000 to 2021, and comprehensively evaluated the restoration of damaged desert forest ecosystem and the effectiveness of ecological water conveyance. The following conclusions are obtained:

From 2000 to 2021, the pixel area with a downward trend of TVDI ($Z_c < 0$) in the Tarim River Basin accounted for 57.0%, which was higher than the pixel area with an upward trend of TVDI ($Z_c > 0$). The soil in the study area showed a wetting development trend. Among the monitoring sections with rising groundwater depth, the groundwater section in the lower reaches of the Tarim River has a significant lifting trend, and the Kurgan has the largest lifting rate of 0.0348 m/month. From 2000 to 2021, the pixel area of FVC in Tarim River Basin with an upward trend ($Z_c > 0$) accounted for 84.3%, which was much higher than the pixel area of FVC with a downward trend ($Z_c < 0$). Among them, FVC with a no significant downward trend ($-1.96 < Z_c < 0$) and a significant downward trend ($Z_c < -1.96$) accounted for a small proportion, which were 11.3% and 4.4% respectively. From 2000 to 2021, the pixel area with an upward trend ($Z_c > 0$) of RSEI in the Tarim River Basin accounted for 58.9%, of which the pixel area with a significant upward trend ($Z_c > 1.96$) accounted for as much as 34.0%, which was mainly distributed in the Aksu River Basin, the upper reaches of the mainstream of the Tarim River, the upper and middle reaches of the Yarkand River Basin and the upper reaches of the Hotan River Basin. In the past 20 years, the ecological quality of the Tarim River Basin has improved to a certain extent. From 2000 to 2021, the FVC of the main stream of the Tarim River, the Aksu River, the Yarkand River and the Hotan River had a significant correlation with TVDI and

RSEI at the $p = 0.01$ level. From 2003 to 2020, the FVC of the Qiala-Yingsu and Yingsu-Taitema Lake reaches was significantly positively correlated with groundwater depth at the $p = 0.01$ level.

Data availability statement

The original contributions presented in the study are included in the article/Supplementary Material, further inquiries can be directed to the corresponding author.

Author contributions

The authors undertook different tasks for this article. AJ. Data processing and wrote the paper. AJ, WW and XD. Analyzed the data. HL, JY and FC provided direction for the research work. HL. Designed the research and revised the article. All authors have read and agreed to the published version of the manuscript.

Funding

This research was funded by the National Natural Science Foundation of China (52179028), the West Light Foundation of Chinese Academy of Sciences (2019-XBQNXZ-A-001), and the Xinjiang Water Conservancy Science and Technology Special Fund Project (XSKJ-2022-10).

Conflict of interest

The authors declare that the research was conducted in the absence of any commercial or financial relationships that could be construed as a potential conflict of interest.

Publisher's note

All claims expressed in this article are solely those of the authors and do not necessarily represent those of their affiliated organizations, or those of the publisher, the editors and the reviewers. Any product that may be evaluated in this article, or claim that may be made by its manufacturer, is not guaranteed or endorsed by the publisher.

References

- Adam, J. C., Hamlet, A. F., and Lettenmaier, D. P. (2009). Implications of global climate change for snowmelt hydrology in the twenty-first century. *Hydrol. Process.* 23, 962–972. doi:10.1002/hyp.7201
- Allen, M. R., and Ingram, W. J. (2012). Erratum: Corrigendum: Constraints on future changes in climate and the hydrologic cycle. *Nature* 489, 590. doi:10.1038/nature11456

- Bai, Y., Liu, Y., Kueppers, L. M., Feng, X., Yu, K., Yang, X., et al. (2021). The coupled effect of soil and atmospheric constraints on the vulnerability and water use of two desert riparian ecosystems. *Agric. For. Meteorol.* 311, 108701. doi:10.1016/j.agrformet.2021.108701
- Casanova, M. T., and Brock, M. A. (2000). How do depth, duration and frequency of flooding influence the establishment of wetland plant communities? *Plant Ecol.* 147 (2), 237–250. doi:10.1023/A:1009875226637
- Cavin, L., Mountford, E. P., Peterken, G. F., and Jump, A. S. (2013). Extreme drought alters competitive dominance within and between tree species in a mixed forest stand. *Funct. Ecol.* 27 (6), 1424–1435. doi:10.1111/1365-2435.12126
- Chen, J., Jonsson, P., Tamura, M., Gu, Z. H., Matsushita, B., and Eklundh, L. (2004). A simple method for reconstructing a high-quality NDVI time-series data set based on the Savitzky-Golay filter. *Remote Sens. Environ.* 91, 332–344. doi:10.1016/j.rse.2004.03.014
- Chen, W., Huang, H. P., Tian, Y. C., and Du, Y. Y. (2019). Monitoring and assessment of the eco-environment quality in the sanjiangyuan region based on Google Earth engine. *J. Geo-information Sci.* 21 (09), 1382–1391. doi:10.12082/dqxkx.2019.190095
- Chen, Y., Chen, Y., Xu, C., Ye, Z., Li, Z., Zhu, C., et al. (2010). Effects of ecological water conveyance on groundwater dynamics and riparian vegetation in the lower reaches of Tarim River, China. *Hydrol. Process.* 24, 170–177. doi:10.1002/hyp.7429
- Chen, Y. J., Li, W. H., Liu, J. Z., and Li, J. Q. (2008). Analysis on the effects of water conveyance embankments on the ecological conservation in the middle reaches of the Tarim River. *Arid. Zone Res.* 25 (4), 550–555. doi:10.13866/j.azr.2008.04.017
- Chui, T. F. M., Low, S. Y., and Liong, S. Y. (2011). An ecohydrological model for studying groundwater-vegetation interactions in wetlands. *J. Hydrol. X.* 409, 291–304. doi:10.1016/j.jhydrol.2011.08.039
- Deng, H., Chen, Y., and Chen, X. (2022b). Driving factors and changes in components of terrestrial water storage in the endorheic Tibetan Plateau. *J. Hydrol. X.* 612, 128225. doi:10.1016/j.jhydrol.2022.128225
- Deng, H. J., and Chen, Y. J. (2017). Influences of recent climate change and human activities on water storage variations in Central Asia. *J. Hydrol. X.* 544, 46–57. doi:10.1016/j.jhydrol.2016.11.006
- Deng, H., Pepin, N. C., Chen, Y., Guo, B., Zhang, S., Zhang, Y., et al. (2022a). Dynamics of diurnal precipitation differences and their spatial variations in China. *J. Appl. Meteorol. Climatol.* 61 (8), 1015–1027. doi:10.1175/jamc-d-21-0232.1
- Deng, X. Y., Xu, H., Ye, M., Li, B., Fu, J., Li, B., et al. (2015). Impact of long-term zero-flow and ecological water conveyance on the radial increment of *Populus euphratica* in the lower reaches of the Tarim River, Xinjiang, China. *Reg. Environ. Change* 15 (1), 13–23. doi:10.1007/s10113-014-0603-2
- Diallo, O., Diouf, A., Hanan, N. P., Ndiaye, A., and Prévost, Y. (1991). AVHRR monitoring of savanna primary production in Senegal, west africa: 1987–1988. *Int. J. Remote Sens.* 12 (6), 1259–1279. doi:10.1080/01431169108929725
- Ding, J., Zhao, W., Daryanto, S., Wang, L., Fan, H., Feng, Q., et al. (2017). The spatial distribution and temporal variation of desert riparian forests and their influencing factors in the downstream Heihe River basin, China. *Hydrol. Earth Syst. Sci.* 21, 2405–2419. doi:10.5194/hess-21-2405-2017
- Doble, R., Simmons, C., Jolly, I., and Walker, G. (2006). Spatial relationships between vegetation cover and irrigation-induced groundwater discharge on a semi-arid floodplain, Australia. *J. Hydrol. X.* 329, 75–97. doi:10.1016/j.jhydrol.2006.02.007
- Garssen, A. G., Baattrup-Pedersen, A., Voesenek, L., Verhoeven, J. T. A., and Soons, M. B. (2015). Riparian plant community responses to increased flooding: A meta-analysis. *Glob. Chang. Biol.* 21 (8), 2881–2890. doi:10.1111/gcb.12921
- Guo, H., Jiapaer, G., Bao, A., Li, X., Huang, Y., Ndayisaba, F., et al. (2017). Effects of the Tarim River's middle stream water transport dike on the fractional cover of desert riparian vegetation. *Ecol. Eng.* 99, 333–342. doi:10.1016/j.ecoleng.2016.10.074
- Halik, U., Aishan, T., Betz, F., Kurban, A., and Rouzi, A. (2019). Effectiveness and challenges of ecological engineering for desert riparian forest restoration along China's largest inland river. *Ecol. Eng.* 127, 11–22. doi:10.1016/j.ecoleng.2018.11.004
- Hao, X. M., Li, W. H., Huang, X., Zhu, C. G., and Ma, J. X. (2010). Assessment of the groundwater threshold of desert riparian forest vegetation along the middle and lower reaches of the Tarim River, China. *Hydrol. Process.* 24 (2), 178–186. doi:10.1002/hyp.7432
- Holben, B. N. (1986). Characteristics of maximum-value composite images from temporal AVHRR data. *Int. J. Remote Sens.* 7, 1417–1434. doi:10.1080/01431168608948945
- Huang, F., Ochoa, C. G., Chen, X., Cheng, Q., and Zhang, D. (2020). An entropy-based investigation into the impact of ecological water diversion on land cover complexity of restored oasis in arid inland river basins. *Ecol. Eng.* 151, 105865. doi:10.1016/j.ecoleng.2020.105865
- Huang, J., Zhang, Y., Wang, M. X., Wang, F., Tang, Z., and He, H. (2020). Spatial and temporal distribution characteristics of drought and its relationship with meteorological factors in Xinjiang in last 17 years. *Acta eco. Sin.* 40 (03), 1077–1088. doi:10.5846/stxb201810302341
- Huete, A. R. (1988). A soil-adjusted vegetation index (SAVI). *Remote Sens. Environ.* 25 (3), 295–309. doi:10.1016/0034-4257(88)90106-X
- Jackson, R. D. (1983). Spectral indices in N-Space. *Remote Sens. Environ.* 13 (5), 409–421. doi:10.1016/0034-4257(83)90010-x
- Keram, A., Halik, U., Keyimu, M., Aishan, T., Mamat, Z., and Rouzi, A. (2019). Gap dynamics of natural *Populus euphratica* floodplain forests affected by hydrological alteration along the Tarim River: Implications for restoration of the riparian forests. *For. Ecol. Manage.* 438, 103–113. doi:10.1016/j.foreco.2019.02.009
- Keyimu, M., Halik, U., Betz, F., and Dulamsuren, C. (2018). Vitality variation and population structure of a riparian forest in the lower reaches of the Tarim River, NW China. *J. For. Res. (Harbin)*. 29, 749–760. doi:10.1007/s11676-017-0478-4
- Kopeck, D., Michalska-Hejduk, D., and Krogulec, E. (2013). The relationship between vegetation and groundwater levels as an indicator of spontaneous wetland restoration. *Ecol. Eng.* 57, 242–251. doi:10.1016/j.ecoleng.2013.04.028
- Ling, H. B., Zhang, P., Xu, H. L., and Zhao, X. F. (2015). How to regenerate and protect desert riparian *Populus euphratica* forest in arid areas. *Sci. Rep.* 5, 15418. doi:10.1038/srep15418
- Ling, H., Guo, B., Yan, J., Deng, X., Xu, H., and Zhang, G. (2020). Enhancing the positive effects of ecological water conservancy engineering on desert riparian forest growth in an arid basin. *Ecol. Indic.* 118, 106797. doi:10.1016/j.ecolind.2020.106797
- Ling, H., Xu, H., Guo, B., Deng, X., Zhang, P., and Wang, X. (2019). Regulating water disturbance for mitigating drought stress to conserve and restore a desert riparian forest ecosystem. *J. Hydrol. X.* 572, 659–670. doi:10.1016/j.jhydrol.2019.03.049
- Ling, H., Zhang, P., Guo, B., Xu, H., Ye, M., and Deng, X. (2017). Negative feedback adjustment challenges reconstruction study from tree rings: A study case of response of *Populus euphratica* to river discontinuous flow and ecological water conveyance. *Sci. Total Environ.* 574, 109–119. doi:10.1016/j.scitotenv.2016.09.043
- Matsushita, B., Yang, W., Chen, J., Onda, Y., and Qiu, G. (2007). Sensitivity of the enhanced vegetation index (EVI) and normalized difference vegetation index (NDVI) to topographic effects: A case study in high-density cypress forest. *Sensors (Basel)*. 7, 2636–2651. doi:10.3390/s7112636
- Ni, Z., Zhang, E., Sun, W., Meng, X., Ning, D., Jiang, Q., et al. (2022). Response of the chironomid community to late Holocene climate change and anthropogenic impacts at Lake Ulungur, arid Central Asia. *Quat. Int.* 613, 91–100. doi:10.1016/j.quaint.2021.08.007
- Piao, S. L., Wang, X. H., Ciais, P., Zhu, B., Wang, T., and Liu, J. (2011). Changes in satellite-derived vegetation growth trend in temperate and boreal Eurasia from 1982 to 2006. *Glob. Chang. Biol.* 17, 3228–3239. doi:10.1111/j.1365-2486.2011.02419.x
- Runyan, C. W., and D'Odorico, P. (2010). Ecohydrological feedbacks between salt accumulation and vegetation dynamics: Role of vegetation-groundwater interactions. *Water Resour. Res.* 46, W11561. doi:10.1029/2010wr009464
- Sims, N. C., and Colloff, M. J. (2012). Remote sensing of vegetation responses to flooding of a semi-arid floodplain: Implications for monitoring ecological effects of environmental flows. *Ecol. Indic.* 18, 387–391. doi:10.1016/j.ecolind.2011.12.007
- Sun, H., Wang, P., Chen, Q., Zhang, D., and Xing, Y. (2022). Coupling the water use of *Populus euphratica* and *Tamarix ramosissima* and evapotranspiration partitioning in a desert riparian forest ecosystem. *Agric. For. Meteorol.* 323, 109064. doi:10.1016/j.agrformet.2022.109064
- Tucker, C. J. (1986). Cover Maximum normalized difference vegetation index images for sub-Saharan Africa for 1983–1985. *Int. J. Remote Sens.* 7 (11), 1383–1384. doi:10.1080/01431168608948941
- Wang, Y.-J., and Qin, D.-H. (2017). Influence of climate change and human activity on water resources in arid region of Northwest China: An overview. *Adv. Clim. Change Res.* 8, 268–278. doi:10.1016/j.jaccr.2017.08.004
- Xu, H. L., Ye, M., and Li, J. M. (2008). The water transfer effects on agricultural development in the lower Tarim River. Xinjiang of China. *Agric. Water Manag.* 95 (1), 59–68. doi:10.1016/j.agwat.2007.09.004

Xue, J., and Su, B. (2017). Significant remote sensing vegetation indices: A review of developments and applications. *J. Sens.* 2017, 1–17. doi:10.1155/2017/1353691

Zalewski, M. (2002). Ecohydrology—The use of ecological and hydrological processes for sustainable management of water resources / ecohydrologie—La prise en compte de processus écologiques et hydrologiques pour la gestion durable des ressources en eau. *Hydrological Sci. J.* 47 (5), 823–832. doi:10.1080/02626660209492986

Zeng, Y., Xie, Z., Yu, Y., Liu, S., Wang, L., Jia, B., et al. (2016). Ecohydrological effects of stream-aquifer water interaction: A case study of the heihe river Basin, northwestern China. *Hydrol. Earth Syst. Sci.* 20, 2333–2352. doi:10.5194/hess-20-2333-2016

Zhang, H., Song, J. Y., Li, M., and Han, W. H. (2021). Eco-environmental quality assessment and cause analysis of Qilian Mountain National Park based on GEE. *Chin. J. Ecol.* 40 (06), 1883–1894. doi:10.13292/j.1000-4890.202106.034

Zhang, M., Wang, S., Fu, B., Gao, G., and Shen, Q. (2018). Ecological effects and potential risks of the water diversion project in the Heihe River Basin. *Sci. Total Environ.* 619, 794–803. doi:10.1016/j.scitotenv.2017.11.037

Zhao, W., Ding, J., Wang, Y., Jia, L., Cao, W., and Tarolli, P. (2020). Ecological water conveyance drives human-water system evolution in the Heihe watershed, China. *Environ. Res.* 182, 109009. doi:10.1016/j.envres.2019.109009



OPEN ACCESS

EDITED BY
Wei Shui,
Fuzhou University, China

REVIEWED BY
Dingde Xu,
Sichuan Agricultural University, China
Xinchen Gu,
Tianjin University, China
Zhixun Huang,
Michigan State University, United States
Qiang Yu,
Beijing Forestry University, China
Shanshan Wang,
Xinjiang Institute of Ecology and
Geography (CAS), China

*CORRESPONDENCE
Yang Li,
ly_mly@126.com

[†]These authors have contributed equally
to this work and share first authorship

SPECIALTY SECTION
This article was submitted to
Interdisciplinary Climate Studies,
a section of the journal
Frontiers in Environmental Science

RECEIVED 27 July 2022
ACCEPTED 25 August 2022
PUBLISHED 16 September 2022

CITATION
Wang Y, Wang Y, Xia T, Li Y and Li Z
(2022), Land-use function evolution and
eco-environmental effects in the tarim
river basin from the perspective of
production–living–ecological space.
Front. Environ. Sci. 10:1004274.
doi: 10.3389/fenvs.2022.1004274

COPYRIGHT
© 2022 Wang, Wang, Xia, Li and Li. This
is an open-access article distributed
under the terms of the [Creative
Commons Attribution License \(CC BY\)](#).
The use, distribution or reproduction in
other forums is permitted, provided the
original author(s) and the copyright
owner(s) are credited and that the
original publication in this journal is
cited, in accordance with accepted
academic practice. No use, distribution
or reproduction is permitted which does
not comply with these terms.

Land-use function evolution and eco-environmental effects in the tarim river basin from the perspective of production–living–ecological space

Yang Wang^{1†}, Yin Wang^{1†}, Tingting Xia¹, Yang Li^{2*} and Zhi Li³

¹Xinjiang Key Laboratory of Grassland Resources and Ecology, College of Grassland Science, Xinjiang Agricultural University, Urumqi, China, ²Nuclear and Radiation Safety Center of the Ministry of Ecological Environment, Nuclear and Radiation Emergency Department, Beijing, China, ³State Key Laboratory of Desert and Oasis Ecology, Xinjiang Institute of Ecology and Geography, Chinese Academy of Sciences, Urumqi, China

The identification of land type multi-functionality is a basic tool for the organization, coordination, and configuration of basin land, and provides a key criterion for determining the combination of land-use functions and the status quo of the ecological environment in the basin. However, a feasible identification method system for this purpose has not yet been established. Therefore, in this study, we construct a production–living–ecological space (PLES) classification system from the comprehensive perspective of land-use type and ecological environment. Based on remote sensing of PLES and statistical land-use status data for 2000, 2005, 2010, 2015, and 2020, we analyze the evolutionary characteristics of land-use function using the transfer matrix and center of gravity transfer methods. These are combined with the eco-environmental quality index to reveal the driving factors of eco-environmental quality spatial differentiation using the geographic detector model. The results indicate that the overall ecological environment quality index of the Tarim River Basin presents a downward trend, with a spatial differentiation pattern of high in the northwest and low in the southeast. Over the past 20 years, the ecological environment quality index has dropped by 0.852. The structural evolution and regional differentiation of PLES areas are remarkable, all of which expanded over the study period (except for the key ecological land). The center of gravity of production land presented the most obvious migration, with a total migration of 10,601.76 m to the northeast. Eco-environmental effects are found to be mainly driven by socio-economic factors, of which population density growth is the most important. The implementation of some ecological restoration projects has played a role in slowing down the degradation trend of the ecological environment quality in the Tarim River Basin; however, due to population increases and socio-economic development, the ecological environment degradation has overall been exacerbated.

KEYWORDS

production-living-ecological space (PLES), eco-environmental effect, geographic detector model, driving factors, tarim river basin

1 Introduction

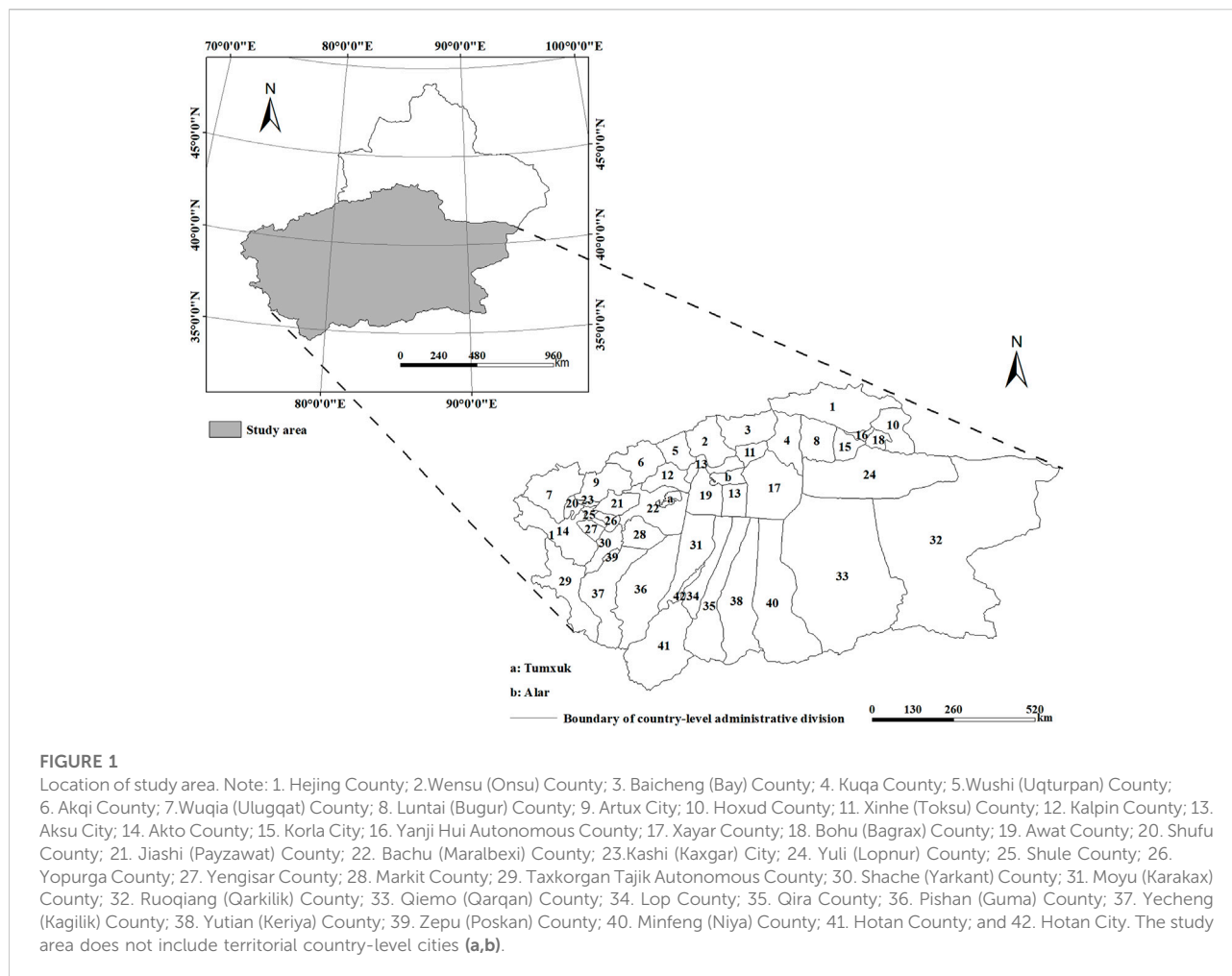
Rapid socio-economic development and human activities have led to land-use changes globally, which have thus become a popular research topic (Tesfaw et al., 2018; Jia et al., 2022). Soil erosion in China is mainly concentrated in ecologically fragile areas, such as the Tarim River Basin (Wang et al., 2016a; Li et al., 2021), located in the south of Xinjiang. With the intensification of human activities (Song et al., 2018) and the continuous development of the economy, the changes in land-use in the Tarim River Basin have become more and more obvious (Zhao et al., 2013), and important natural resources, such as grassland, forest land, and terrestrial water reserves, have changed accordingly (Deng and Chen, 2017). Due to the continuous degradation of the ecological environment and hydrological environment in the Tarim River Basin, the land desertification in the basin has directly intensified (Feng et al., 2001). Land-use change affects nearly one-third of the global land area (Winkler et al., 2021), and changes in land area will inevitably have different impacts on different ecological and environmental indicators. In particular, land-use change may negatively affect carbon pools (Padbhushan et al., 2022) and soil erosion (Gong et al., 2022), and it can also cooperate with climate change to promote net primary productivity (Xiao et al., 2019). It is worth mentioning that surface runoff (Daneshi et al., 2020), the spatial pattern of water quality (Zhang et al., 2018), and landscape complexity (Galpern and Gavin, 2020) have all been shown to be strongly correlated with land-use change.

Land-use change refers to the evolution process of land-use structure and function, corresponding to social and economic development in both temporal and spatial dimensions. As an important carrier of human survival, land can provide a wide range of products and services, collectively referred to as land-use function, which refers to the attributes and states of different land-use types in directly or indirectly providing various products and services to human beings (Liu, 2018; Zou et al., 2021). Land-use change is an important part and driving factor of global ecological environment change (Eziz et al., 2010), and ecological protection and restoration work needs to be based on quantitative ecological monitoring results, in order to provide targeted and scientific implementation plans. Therefore, ecological monitoring and evaluation have attracted extensive research attention (Zhang and Zhang, 2018). Research on evaluation methods has shown that some scholars evaluate changes in ecosystem quality based on land-use change (Lambin and Meyfroidt, 2011), while a large number of researchers have utilized modeling methods (e.g., sampling) to evaluate ecological simulations. However, these methods require a significant amount of statistical data in the ecological

evaluation, are affected by human activities, and it may be difficult to evaluate an area with sufficient accuracy when only considering fuzzy evaluation (Chase and Knight, 2013).

The concept of land-use function originated from agricultural research, mainly referring to agricultural production functions (Andersen et al., 2013) and paying attention to the multi-functional uses of land. According to the Organization for Economic Co-operation and Development (OECD), the Food and Agriculture Organization (FAO), and the Common Agricultural Policy (CAP), agricultural functions can be divided into productive, economic and social, ecological and environmental, and cultural and recreational functions (Andersen et al., 2013). Production-living-ecological space (PLES) is a theory, proposed by the Chinese government in the ecological civilization construction strategy, with the goal of achieving sustainable utilization and focusing on the perspective of multi-functional land use (Fu et al., 2021). According to the functional attributes of land, China's land is divided into production, living, and ecological space, the consideration of which allows us to more intuitively observe the evolution of land-use. Determining land-use area is a critical step in better identifying the land-use functional structure and dynamic trade-offs (Wiggering et al., 2006). Therefore, quantification of land-use functions is critical to understand the complexity of interactions between multiple different land-use types.

The Tarim River Basin is a fragile ecological environment. In recent years, many scholars have carried out a series of studies on the Tarim River Basin. Although there exist many studies on land-use change in the Tarim River Basin (Wang et al., 2022), research on the ecological environment quality of the Tarim River Basin combined with PLES is scarce. Although the driving factors of the ecological environment have been analyzed, the selected factors are not yet comprehensive enough. Based on the perspective of production-living-ecological space (PLES), we systematically study the evolution of land-use functions and eco-environmental effects in the Tarim River Basin by using the transfer matrix, the center of gravity transfer model, and the eco-environmental quality index in this paper. Combined with the result regarding the decrease in the eco-environmental quality index, the current situation of the eco-environmental decline in the Tarim River Basin is revealed. Through analysis of the driving factors of the eco-environmental effect in the Tarim River Basin using the geographic detector, we find that social and economic factors are the main driving force affecting the eco-environmental effect of the Tarim River Basin. This study details a comprehensive evaluation of the eco-environmental state of the Tarim River Basin, thus providing relevant government agencies with a scientific basis for eco-environmental protection.



2 Data and materials

2.1 Description of the study area

The Tarim River Basin is the largest inland river basin in China. It is located in southern Xinjiang, at the geographical coordinates of $73^{\circ}10' - 94^{\circ}05'E$, $34^{\circ}55' - 43^{\circ}08'N$. The basin includes nine major water systems, covering an area of $103 \times 10^4 \text{ km}^2$ and accounting for 61.82% of the total area of Xinjiang. Situated between Tianshan and the Kunlun Mountains, the Tarim River Basin is entirely inland and has a continental arid climate with little monsoon influence. There are 42 counties (cities) and two construction corps in five prefectures in the basin; namely, Bayangol Mongol Autonomous Prefecture, Aksu Administrative Offices, Kashgar Administrative Prefecture, Kizilsu Kirgiz Autonomous Prefecture, and Hotan Administrative Offices. Therefore, in order to better study the Tarim River Basin, we divided the Tarim River Basin according to county-level administrative

boundaries. The boundaries and division of the Tarim River Basin are shown in Figure 1.

As of 2020, the total population of the basin had reached 11.951718 million, accounting for 46.23% of the total population of Xinjiang, with a GDP of 41.2712 million yuan. The total value of the primary industry was 91.131 billion yuan, accounting for 46.00% of the total value of the primary industry in Xinjiang; the value of the secondary industry was 125.941 billion yuan, accounting for 26.54% of the total value of the secondary industry in Xinjiang; and the total value of the tertiary industry was 195.640 billion yuan, accounting for 27.66% of the total value of the tertiary industry in Xinjiang. It can be seen, from these figures, that the primary industries in the Tarim River Basin occupy a relatively large proportion of the total value of the primary industry in Xinjiang, while secondary and tertiary industries are still relatively backward, compared with the areas north of the Tianshan Mountains, mainly due to the relatively large area of the basin. The cost of transportation is higher than that in the north of the Tianshan Mountains and, so, the

development of the processing, manufacturing, and service industries in this basin has relatively lagged behind.

2.2 Methods

2.2.1 Data collection and processing

Land-use data for the Tarim River Basin in 2000, 2005, 2010, 2015, and 2020 were obtained from the Resources and Environmental Science and Data Center of the Chinese Academy of Sciences (<http://www.resdc.cn/>; accessed on 20 March 2022), comprising TM land-use data with 30 m spatial resolution. PLES data included production space, living space, and ecological space. Production space refers to the territorial space that provides services for production and business activities, living space refers to the places that people use in their daily activities, and ecological space refers to the territorial space that has ecological protection, which is of great significance for sustainable development. According to the existing PLES classification basis, and fully considering the characteristics of the unused land in the Tarim River Basin, we classified the unused land as ecological accommodation land separately, and conducted research together with production land, living land, and key ecological land as first-level land types. The socio-economic and demographic data for the study area were obtained from the Xinjiang Statistical Yearbook and Xinjiang Production and Construction Corps Statistical Yearbook. The meteorological data (precipitation and air temperature) were obtained from the China Meteorological Data website (<http://cdc.cma.gov.cn>). The monthly average values of 16 meteorological stations with complete data were selected, and Inverse Distance Weight spatial interpolation of the meteorological data was carried out, according to the longitude and latitude of each meteorological station.

2.2.2 Classification system of PLES and calculation of eco-environmental quality index

Land is a multi-functional complex, integrating production, living, and ecological functions. However, due to differences in land-use mode and intensity, the leading functions of different land-use types vary greatly. Therefore, scientific identification of regional PLES is an important consideration in this study.

We used the land classification system adopted by the Chinese Academy of Sciences (Liu et al., 2002). By combining the land-use characteristics of the study area, the PLES classification system was constructed based on the principle of combining the dominant and secondary functions of the land. The eco-environmental quality values of different secondary land types were formulated referring to the research results of domestic and foreign experts on the calculation of the values for land-use functional ecosystem services; especially the eco-environmental quality values of land-use types formulated by

Zhai et al. (2022). Based on the PLES classification, we used an ecological environment quality index considering 26 different land-use types, and calculated the eco-environmental quality index of production land, key ecological land, living land, and ecological accommodation land using the area weighting method. In order to improve the data accuracy and reduce errors, we calculated the ecological environment quality index in the basin for every year (Table 1).

2.2.3 Land-use transfer matrix

Land-use function evolution refers to the mutual conversion and spatial distribution of the three dominant functions of land use: Production, living, and ecology. The evolution of the land-use functional structure can be realized through the land-use type transfer matrix model. The transfer matrix is not an index but, instead, arranges transfer areas of various land-use changes in the form of a matrix. Through this matrix, land-use structural and directional changes can be analyzed, which comprises the basis for analyzing land-use.

By comparing the area of the land-use transfer matrix in 2000, 2005, 2010, 2015, and 2020, we could intuitively determine the structural characteristics and land-use types of land-use change in the Tarim River Basin. For the land-use data in 2000, 2005, 2010, 2015, and 2020, according to the PLES classification standard, the ArcGIS10.2 reclassification function was used to obtain the PLES status distribution map. ArcGIS 10.2 was used to re-classify and process the land-use distribution maps for any two periods, and the PivotTable function of Excel was used to construct the land-use function transfer matrix, expressed as:

$$S_{ij} = \begin{bmatrix} S_{11} & S_{12} & \cdots & S_{1n} \\ S_{21} & S_{22} & \cdots & S_{2n} \\ \vdots & \vdots & \ddots & \vdots \\ S_{n1} & S_{n2} & \cdots & S_{nn} \end{bmatrix} \quad (1)$$

where S denotes the area, i and j index the land-use types at the beginning and end of the research period, respectively, and n is the number of land-use types. Based on the cross-analysis of land-use type data for different periods, land-use type transfer matrices for four periods (2000–2005, 2005–2010, 2010–2015, and 2015–2020) were established.

2.2.4 Shift in the land-use function center of gravity transfer model

The land-use function center of gravity transfer model was constructed based on the principle of the population distribution center of gravity in population geography. The basic method is as follows: The research area is first divided into k evaluation units, after which the coordinates of the geometric center of each assessment unit (latitude and longitude) are determined. The center coordinates are then multiplied by the evaluation unit types of land area and divided by the total area of that land-use type in the study area. This gives the barycentric coordinates of a certain function of land in the area (Li and Huang, 2022), expressed as:

TABLE 1 Land use function classification system and eco-environmental quality index of the Tarim River Basin.

Land use function classification of production-living-ecological space		Corresponding to land use type	Eco-environmental quality index of each year				
First class	Second class		2000	2005	2010	2015	2020
Production Land	Agricultural production land	Paddy fields, dry land	0.2507	0.2506	0.2507	0.2505	0.2500
	Industrial production land	Other construction land	0.1500	0.1500	0.1500	0.1500	0.1500
Key ecological land	Forestry ecological land	Woodland, shrub land, sparse woodland, other woodland	0.6598	0.6596	0.6592	0.6595	0.6288
	Water ecological land	Canals, lakes, reservoirs, permanent glaciers and snow, beaches	0.8404	0.8408	0.8434	0.8435	0.7782
	Meadow ecological land	High coverage grassland, medium coverage grassland, low coverage grassland	0.3541	0.3537	0.3540	0.3544	0.3734
Living land	Urban living land	Urban land	0.0161	0.0157	0.0158	0.0156	0.0150
	Rural living land	Rural settlements	0.2000	0.2000	0.2000	0.2000	0.2000
Ecological accommodation land	Other ecological land	Sandy land, gobi, saline-alkali land, marsh land, bare land, bare rock and stony land, other	0.2000	0.2000	0.2000	0.2000	0.2000

$$X_t = \sum_{i=1}^n (S_{ki} \times X_k) / \sum_{i=1}^n S_{ki} \quad (2)$$

$$Y_t = \sum_{i=1}^n (S_{ki} \times Y_k) / \sum_{i=1}^n S_{ki} \quad (3)$$

where X_t and Y_t are the latitude and longitude coordinates of the center of gravity of a certain land resource distribution in year t , respectively; X_k and Y_k are the latitude and longitude coordinates of the geometric center of the k th evaluation unit, respectively; S_{ki} is the area of a certain land type in the k th evaluation unit; and n is the number of land resource types based on PLES. The barycenter shift distance refers to the straight-line distance between the barycenter in a certain year and that in subsequent years. If t and $(t+1)$ are associated to $P_t (X_t, Y_t)$ and $P_{t+1} (X_{t+1}, Y_{t+1})$, respectively, then the barycenter shift distance of adjacent years is calculated as:

$$L = \sqrt{(X_{t+1} - X_t)^2 + (Y_{t+1} - Y_t)^2} \quad (4)$$

2.2.5 Eco-environmental effects of land-use function evolution

2.2.5.1 Eco-environmental quality index

The classification of land functions can be carried out from an eco-environmental perspective. Different factors, such as human activities, will have an impact on the structure and function of the environment and ecosystems, which we call eco-environmental effects.

The ecological environment quality index was used to quantitatively represent the overall ecological environmental quality for five different periods in the Tarim River Basin (Pang et al., 2022). The calculation formula is as follows:

$$EV_k = \sum_{i=1}^n \left(\frac{S_{ki}}{S_k} \times V_i \right) \quad (5)$$

where EV_k is the ecological environment quality index of evaluation unit k , S_{ki} is the area of functional land type i in the k th evaluation unit, and S_k is the total land area of the k th evaluation unit. Additionally, V_i is the eco-environmental quality index of functional land class i , and n is the number of land resource types, based on PLES.

2.2.5.2 Ecological contribution rate

The ecological contribution rate of land-use function evolution refers to the function of land-use conversion in regional ecological environmental quality of change. This index quantifies the various functions of regional land-use conversion and its impact on the ecological environment. Additionally, it separates the dynamics of the main land-use types, in order to explore changes in the regional ecological environment. A positive value means that the transformation improves the regional ecological environment quality, while a negative value indicates that the transformation reduces the quality (Hou et al., 2022; Li and Wu, 2022). It is calculated as follows:

$$LEI = (LE_j - LE_i) \times \Delta S_k / S_k \quad (6)$$

where LEI is the ecological contribution degree of land-use function evolution, LE_i and LE_j are the eco-environmental quality indices of land-use function change in types reflected in the early and late stages, respectively, ΔS_k is the area of changed land-use type, and S_k is the total land area of the k th evaluation unit.

2.2.6 Geographic detector model

The geographical detector model is a statistical method which can be used to detect spatial differentiation and explain its driving forces without imposing too many constraints. This approach overcomes the shortcomings of traditional statistical methods, in terms of dealing with variables (Wang et al., 2016b). Factor detection is carried out to detect the spatial differentiation of an attribute Y and the extent to which a factor X explains the spatial differentiation of Y.

Combined with the characteristics of the study area and the availability of data, the driving factors of eco-environmental effects were selected from the aspects of natural environment and social economy, including the natural environment factors elevation (X1), slope (X2), aspect (X3), air temperature (X4), and precipitation (X5), as well as the socio-economic factors distance to water (X6), distance to roads at the township level and above (X7), primary industry (X8), secondary industry (X9), tertiary industry (X10), and population density (X11). The eco-environmental quality index and the driving factors were spatially matched, and the dependent and independent variables at each discrete point were then extracted. The calculation formula is (Yang et al., 2020; Xiong et al., 2022):

$$q = 1 - \frac{\sum_{h=1}^L N_h \sigma_h^2}{N \sigma^2} \quad (7)$$

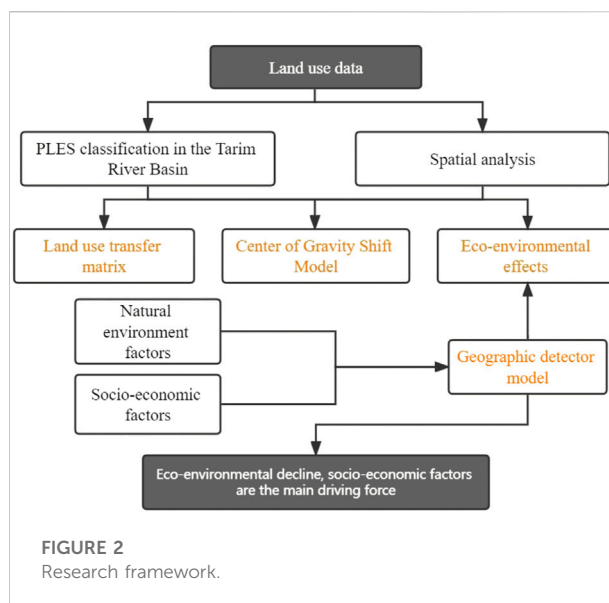
where q denotes the explanatory power of the driving factors, which has values in the range of [0, 1]. If $q = 0$, the ecological environment quality is randomly distributed. The larger the q value, the stronger the explanatory power of the driving factors. In the equation, N_h and N are the number of sub-level sample units and entire research units, respectively, and σ_h^2 and σ^2 describe the variance of the ecological environment index at the sub-level and whole research unit level, respectively.

Interaction detection is mainly carried out to determine whether each factor has an impact on the dependent variable independently or post-interaction, and whether the influencing force is weakened or enhanced. The relationships between the two factors can be divided into five categories:

- 1) $q(X1 \cap X2) < \min(q(X1), q(X2))$, non-linear weakening;
- 2) $\min(q(X1), q(X2)) < q(X1 \cap X2) < \max(q(X1), q(X2))$, single-factor non-linear attenuation;
- 3) $q(X1 \cap X2) > \max(q(X1), q(X2))$, double factor enhancement;
- 4) $q(X1 \cap X2) = q(X1) + q(X2)$, independent;
- 5) $q(X1 \cap X2) > q(X1) + q(X2)$, non-linear enhancement.

2.3 Research framework

In order to better study the evolution of land-use function and the influencing factors of the ecological environment effect in

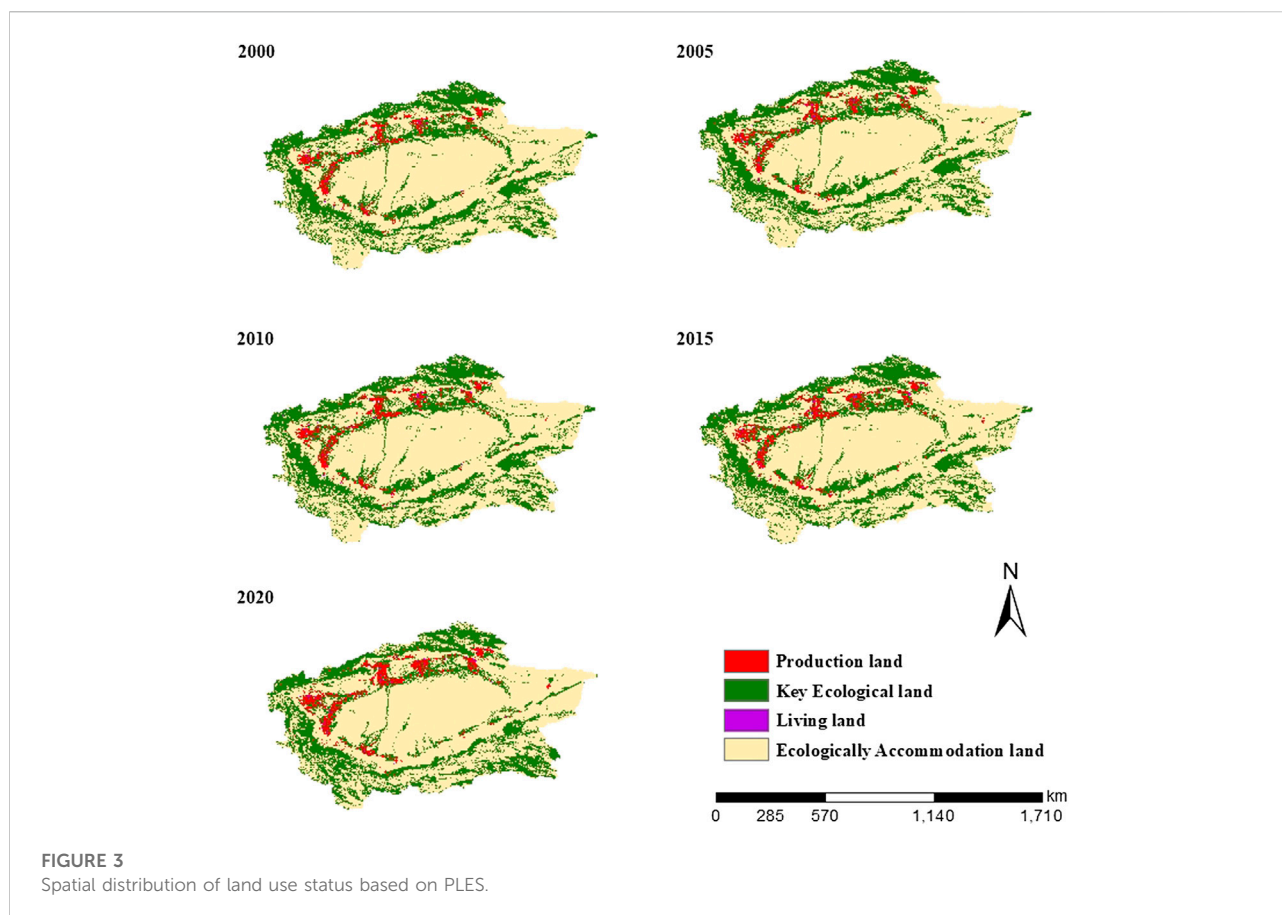


the Tarim River Basin, we carried out four key steps (Figure 2). First, the land-use data were processed and classified by PLES. Then, combined with the transfer matrix, the center of gravity transfer model was used to analyze the evolution of land-use functions. Third, we used the ecological environment index and ecological contribution rate to study the ecological environment effect in the Tarim River Basin. Finally, we used the five natural environment factors and six socio-economic factors to explore the driving force of the ecological environment effect with the geographic detector model. Through these steps, the land-use function evolution characteristics in the Tarim River Basin and the driving factors for the spatial differentiation of ecological environment effects could be clarified.

3 Results and analysis

3.1 Evolution characteristics of land-use function

We used ArcGIS 10.2 to re-classify the five-phase land-use remote sensing data in 2000, 2005, 2010, 2015, and 2020; the results are shown in Figure 3. As can be seen from the figure, the production land, living land, and ecological accommodation land areas in the Tarim River Basin expanded in the period 2000–2020. In particular, the area of production land grew by 16,650.55 km², representing a 62.16% increase over the 20-year period. The key ecological land area decreased by 24,716.87 km² (or 7.3%). Residential land expanded by 718.36 km², with the largest increase (348.13 km²) occurring in 2015–2020; this expansion accounted for 48.46% of the increase during the study period, while 39.61% occurred between 2010 and 2015.



The ecological accommodation area increased by 6839.63 km² (or 1.02%).

The land-use pattern in the Tarim River Basin changed significantly from 2000 to 2020. In order to more intuitively observe the internal conversion of land-use types in the basin, the land-use transfer matrix was adopted to define both the transformation direction and quantity of land function transformation (Table 2). The analysis results indicated that the biggest change occurred in production land, which increased by 16,650.55 km², accounting for 68.49% of the total area transferred. Of the transferred land, most came from key ecological land (70.52%) and ecological accommodation land (25.58%). A total of 6941.59 km² was transferred to ecological accommodation land and 718.36 km² was transferred to living land, accounting for 28.55% and 2.95% of the total transfer area, respectively.

In terms of land-use function transfer area, only key ecological land was transferred, totaling 24,310.50 km². Most of this land was converted to ecological accommodation (96.96%), with the rest being converted to production land and living land. The encroachment of ecological accommodation land on key ecological land reduced its area, thus having a major impact on the quality of the surrounding ecological environment.

3.2 Shift in land-use gravity center

The gravity center formula was used to calculate the gravity center coordinates of PLES in the study area in 2000, 2005, 2010, 2015, and 2020. The formula was also used to determine the position and shifting direction of the center of gravity. Figure 4 shows the shifting distance of the center between each year.

The production space center of gravity was located in Aksu Administrative Offices throughout the study period. It can be seen, from Figure 3, that the production land was mainly concentrated in the west and northwest of the Tarim River Basin. Due to its remote geographical location and inconvenience of transportation in the Tarim River Basin, the economy is relatively backward. At present, agriculture is still the mainstay in the basin. Some areas with relatively developed agriculture, such as Korla City, Aksu City, and Shache County, rank higher in the basin, from the perspective of primary industries. Therefore, the center of gravity of production land mainly fell in the Aksu region, located in the northwest direction of the Tarim River Basin. The center of gravity of key ecological land was mainly in the Hotan Administrative Offices, which is relatively rich in hydropower resources. The center of living land was situated in the Aksu

TABLE 2 Transition matrix of production-living-ecological space (PLES) for different periods in the Tarim River Basin during 2000–2020.

Year	Production-living-ecological space (PLES)	Production land	Living land	Key ecological land	Ecological accommodation land	Transfer out
2000–2005	Production Land	26391.27	97.18	239.21	57.72	394.11
	Living land	51.27	1401.29	6.12	1.95	1409.36
	Key ecological land	3571.60	17.65	330045.85	1337.51	331401.01
	Ecological accommodation land	749.56	85	1798.04	666019.89	667832.77
	Transfer in	4372.43	1433.80	331850.00	667359.35	
2005–2010	Production Land	30289.82	63.88	352.22	57.79	473.89
	Living land	50.67	1471.52	6.89	1.90	1480.30
	Key ecological land	1084.24	6.53	329657.43	1341.02	331004.98
	Ecological accommodation land	511.07	4.38	1343.79	665557.83	666906.00
	Transfer in	1645.97	1482.43	331008.11	666900.74	
2010–2015	Production Land	31712.58	149.77	70.35	3.13	223.25
	Living land	11.52	1534.51	0.28	—	1534.79
	Key ecological land	3959.52	68.84	327298.96	45.00	327412.80
	Ecological accommodation land	2047.63	77.75	346.66	664498.42	664922.83
	Transfer in	6018.67	1681.09	327645.91	664543.42	
2015–2020	Production Land	32360.05	1135.03	3514.02	722.16	5371.20
	Living land	834.12	804.90	160.32	31.53	996.74
	Key ecological land	7807.93	160.53	216275.75	103316.06	319752.34
	Ecological accommodation land	2433.86	78.55	90568.02	571248.95	661895.52
	Transfer in	11075.91	1043.97	307004.09	674596.55	

Administrative Offices. In 2017, Xinjiang vigorously promoted the construction of new urban areas, providing Aksu Administrative Offices with a facilitative platform for urbanization. During the study period, the center of ecological accommodation was mainly in northern Hotan Administrative Offices, the center of the Tarim River Basin. Although Hotan Administrative Offices possesses some water resource carrying capacity and vegetation coverage, sandy land is the main land type there, and it is one of the driest areas in China. Moreover, the center of the Tarim Basin is a vast desert, such that the center of ecological accommodation is mainly located in this area.

From the perspective of the transfer direction and distance of the center of gravity, migration to the northeast was the main trend regarding the transfer of the center of gravity of production land. The shift in the center of gravity of production land moved 10,601.76 m in a northeastern direction over the past 20 years, from Awat County to Aksu City. Due to the remote geographical location of the Tarim River Basin, transportation is inconvenient and its economy is relatively backward. At present, agriculture remains the backbone in the watershed. It can be seen, from [Figure 3](#), that the production land was mainly concentrated in the west and northwest of the Tarim River Basin, such as Aksu City and Shache County. However, some areas with relatively developed agriculture, such as Korla City located in the northeast of the basin, experienced rapid expansion of

production land during the study period. Therefore, the center of gravity of production land in the Tarim River Basin mainly moved to the northeast. During the same period, the center of gravity of key ecological land transferred 48,199.56 m to the southeast. Due to the rapid economic development in the northwest of the basin and the further expansion of production land, key ecological land has been occupied. Coupled with global warming in recent years, the melting of glaciers has led to an increase in vegetation in the southeast of the basin, causing the center of gravity of key ecological land to move to the southeast. The center of gravity of living land moved first 9,211.67 m to the northwest, then 31,658.08 m to the northeast, and finally 40,809.96 m to the northwest. Overall, the center of gravity of living land has moved 49,796.42 m to the northwest. The Tarim River Basin has a wide area and a lot of unused land. The population is mainly distributed in the northwest area of the Tarim River Basin, including Aksu City, Korla City, and other cities. These cities have large populations and a rapid urbanization process, causing the center of gravity of living land to mainly move towards the northwest. The center of gravity migration of ecological accommodation area was the smallest, migrating only 20,242.04 m to the south. With rapid economic development in the northwest region of the study area, problems such as over-exploitation of land have appeared. Therefore, the center of gravity of ecological accommodation

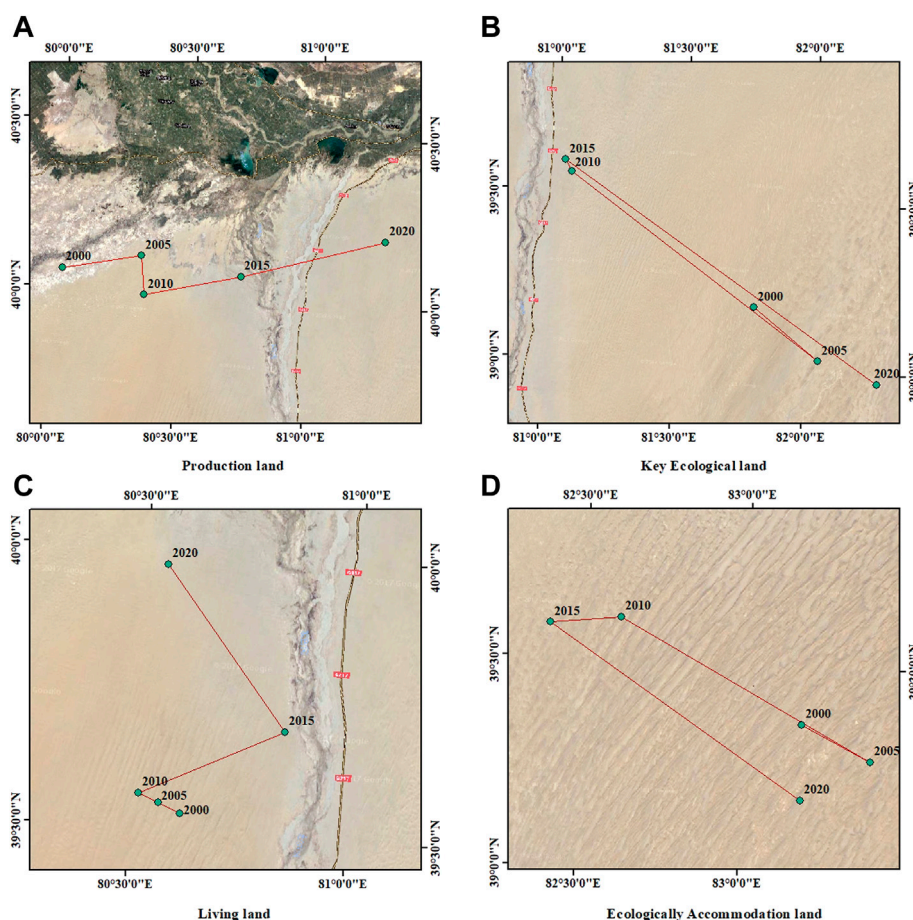


FIGURE 4
Location, shifting direction, and distance of gravity center of PLES during 2000–2020.

moved to the northwest region as a whole from 2000 to 2015. Later, due to global warming and high evapotranspiration, the ecological accommodation land encroached on the waters and grasslands in the southern part of the Tarim River Basin, causing the center of gravity of the ecological accommodation to move to the southeast from 2015 to 2020.

3.3 Eco-environmental effects of land-use function evolution

3.3.1 Evolution of eco-environmental quality

The calculation results for the eco-environmental quality index of the study area indicated that the index dropped from 0.1568 to 0.1480 between 2000 and 2020 (Table 3), indicating an annual decrease in quality. This was mainly due to the intensification of human activities, acceleration of the urbanization process, and the gradual increase in land exploitation. Between 2015 and 2020 in particular, the

TABLE 3 Eco-environmental quality index for the study period.

Year	2000	2005	2010	2015	2020
Eco-environmental quality index	0.1568	0.1563	0.1562	0.1563	0.1480

permanent glacier area was greatly reduced, due to climate warming (Deng et al., 2019). Melting glaciers caused an increase in lakes and canals (Deng et al., 2022), but the environmental quality indices of lakes and canals are lower than that of permanent glaciers and, so, the overall eco-environmental quality of the Tarim River Basin presented a downward trend. The amount of forestland also decreased.

Figure 5 shows that the counties in the north and southwest of the Tarim River Basin presented higher ecological environment quality indices. Combined with Figure 3, it can be seen that these counties and cities had more grassland ecological land, forest ecological land, and water area at each

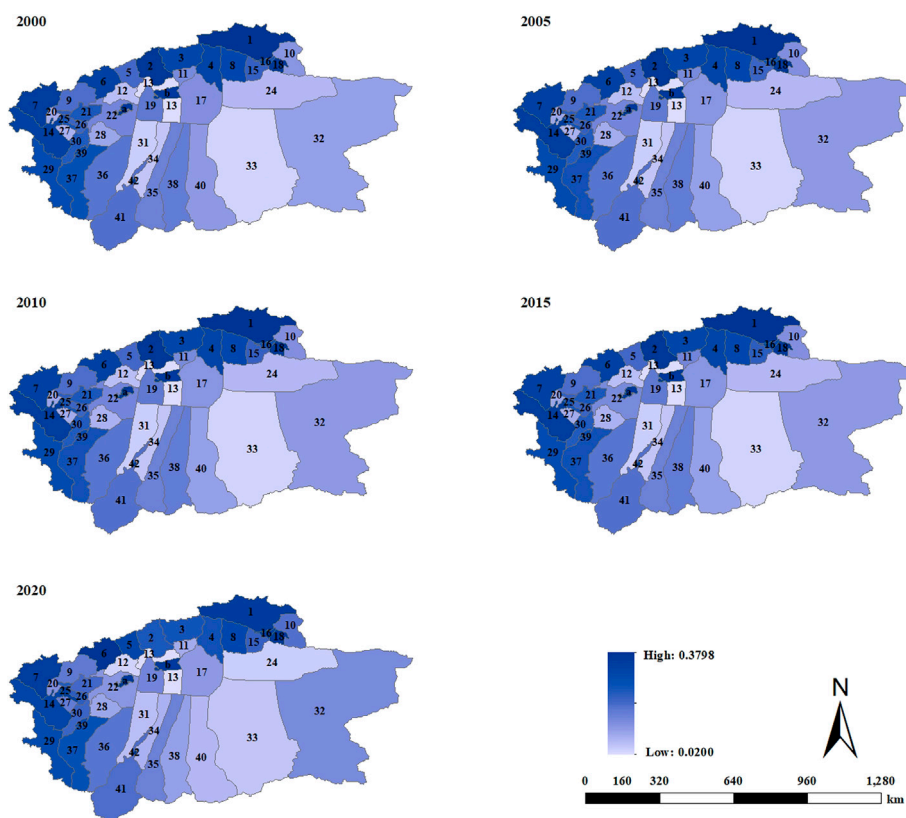


FIGURE 5
Spatial distribution of eco-environmental quality in different years.

evaluation time point; such as Hejing County, Kuqa County, Akto County, and so on.

3.3.2 Differences in ecological contribution rate

There were two opposing effects (i.e., positive and negative impacts) on eco-environmental quality in the study area. These can mitigate each other, to some extent, thus maintaining the index within a stable range.

According to the analysis in Table 4, the conversion of low ecological quality land (e.g., sandy land) into grassland (ecological land) was the leading factor for the improvement of ecological environment quality, accounting for 75.11% of the positive effects. The conversion of other ecological land types into water ecological land, such as grassland ecological land into water ecological land and forest ecological land, also improved the ecological environment quality of the Tarim River Basin, accounting for nearly one-fifth of the positive contribution rate to the ecological environment. In addition, the conversions of land-use function for ecological environment improvement in the Tarim River Basin were relatively concentrated; for example, ecological land was converted into grassland ecological land and water ecological land, and

grassland ecological land was converted into water and forest ecological land. These conversions resulted in a higher ecological environment quality index, accounting for more than 90% of the positive effects on the ecological environment.

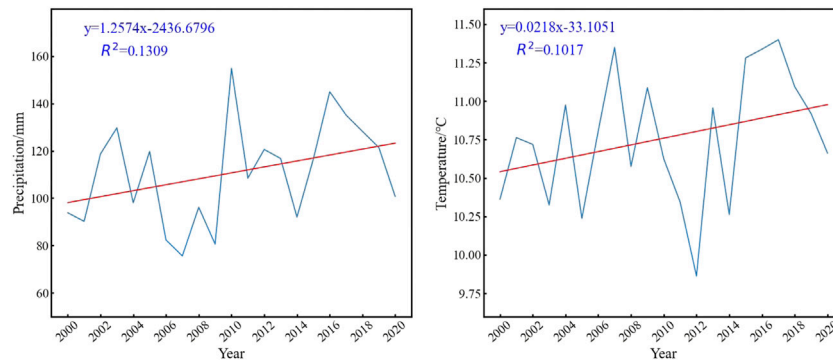
Conversely, the occupation of grassland ecological land and woodland ecological land by agricultural production land and other ecological land, as well as the occupation of water ecological land and woodland ecological land by grassland ecological land, were important factors leading to the deterioration of ecological environment quality in the Tarim River Basin. In particular, the conversion of grassland and forestland into other ecological land accounted for more than 80% of the negative effects on the ecological environment.

3.3.3 Characteristics of climate change

The trend changes for precipitation and average annual temperature in the study area from 2000 to 2020 are illustrated in Figure 6. As can be seen from the figure, the average annual precipitation and temperature both showed gradually increasing trends, which differed slightly. The trend change rates for precipitation and temperature were 1.257 and 0.022, respectively. Although the increase in air temperature was

TABLE 4 Land type transformation and contribution rate to PLES in the Tarim River Basin in 2000–2020.

Eco-environmental effect	Major land use transformation types	Transition area/km ²	Ecological contribution rate	Percentage of contribution/%
Positive effect of ecological environment	Other ecological land -Agricultural production land	4813.0623	0.001092	2.80
	Meadow ecological land -Water ecological land	3624.4386	0.001490	3.83
	Other ecological land -Water ecological land	5580.3654	0.004122	10.59
	Agricultural production land -Forestry ecological land	1102.5081	0.000404	1.04
	Meadow ecological land -Forestry ecological land	6018.1092	0.001602	4.12
	Other ecological land -Forestry ecological land	1371.6504	0.000815	2.09
	Agricultural production land -Meadow ecological land	1394.8848	0.000166	0.43
	Other ecological land-Meadow ecological land	84403.8639	0.029239	75.11
Subtotal			0.038929	100
Negative effect of ecological environment	Forestry ecological land - Agricultural production land	2095.1055	−0.000832	2.28
	Meadow ecological land -Agricultural production land	12204.7812	−0.001232	3.37
	Forestry ecological land - Meadow ecological land	5702.4378	−0.001583	4.34
	Water ecological land - Meadow ecological land	7282.2114	−0.003296	9.03
	Agricultural production land - Urban and rural residential land	1253.5596	−0.000062	0.17
	Forestry ecological land -Other ecological land	1807.7238	−0.001130	3.09
	Meadow ecological land -Other ecological land	86305.6134	−0.028373	77.72
Subtotal			−0.036507	100

FIGURE 6
Linear trend change.

only minor, precipitation showed a more significant increasing trend. Specifically, air temperature showed an obvious decline from 2009 to 2012, followed by an increasing trend from 2012 to 2020, such that the overall change trend is not obvious. On the

other hand, precipitation decreased up to 2009, then began to rise. This trend reversal reveals that, under the influence of global warming, the temperature in the Tarim River Basin is on an upward trajectory. The study region is an extremely arid area,

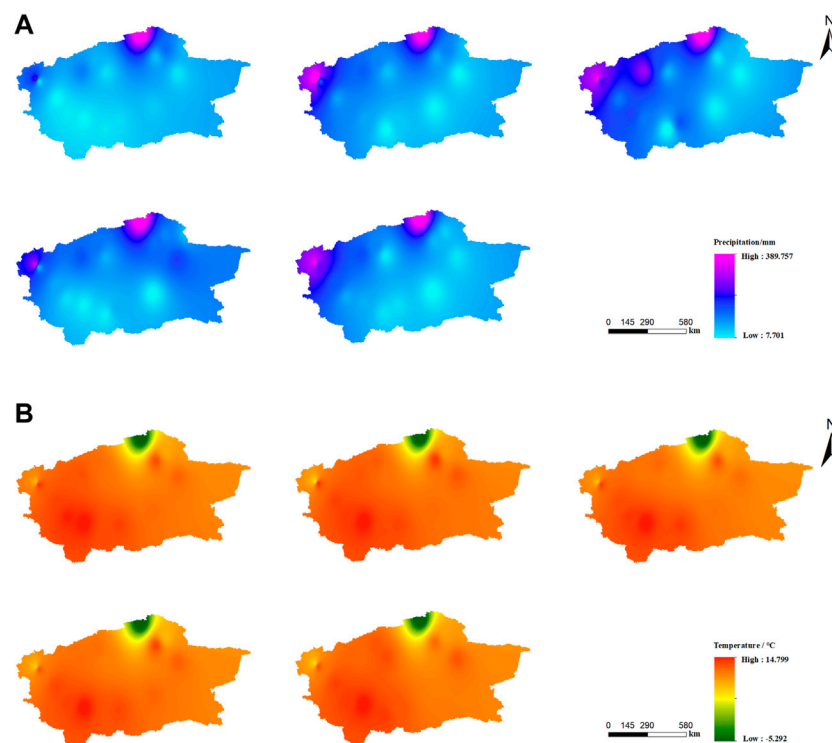


FIGURE 7

(A) Spatial distribution characteristics of precipitation (mm) in the Tarim River Basin from 2000 to 2020. (B) Spatial distribution of air temperature (°C) in the Tarim River Basin from 2000 to 2020.

thus lacking water, an increase in temperature will accelerate the melting of glaciers and usually result in increases in evaporation from the underlying surface. Therefore, the increase in precipitation in the Tarim River Basin is significant.

Our results revealed that the ecological environment quality of the Tarim River Basin has changed. The natural environmental and socio-economic factors appeared to have a substantial impact on the ecological environment quality of the basin. In terms of the natural environment, we further analyzed the impact of climate on eco-environmental quality through spatial correlation analysis; the results are shown in Figures 7A,B. The spatial distribution of eco-environmental quality was positively correlated with precipitation from 2000 to 2020. Figure 5 illustrates that the points of high regional ecological environment quality were mainly concentrated in the northwest and southwest of the Tarim River Basin; for example, Hejing County, Wuqa County, and Akto County were representative of high-quality local precipitation. Accordingly, due to relatively abundant precipitation, the grassland, forestland, and so on had a positive impact on the ecological environment quality of the land area. The proportion of high-coverage grassland and woodland was also higher there than in other areas.

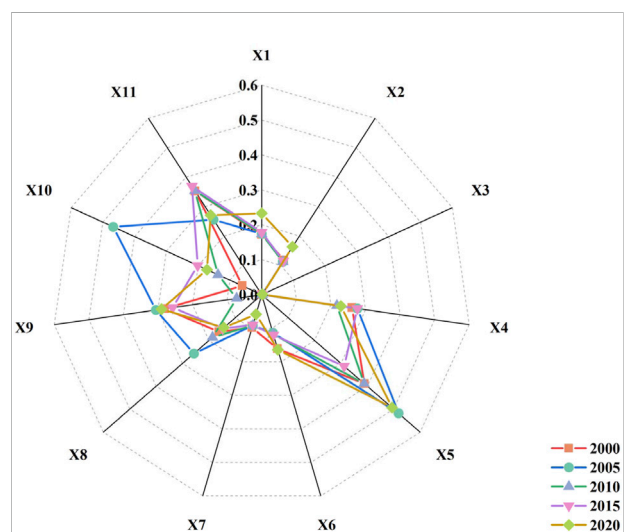
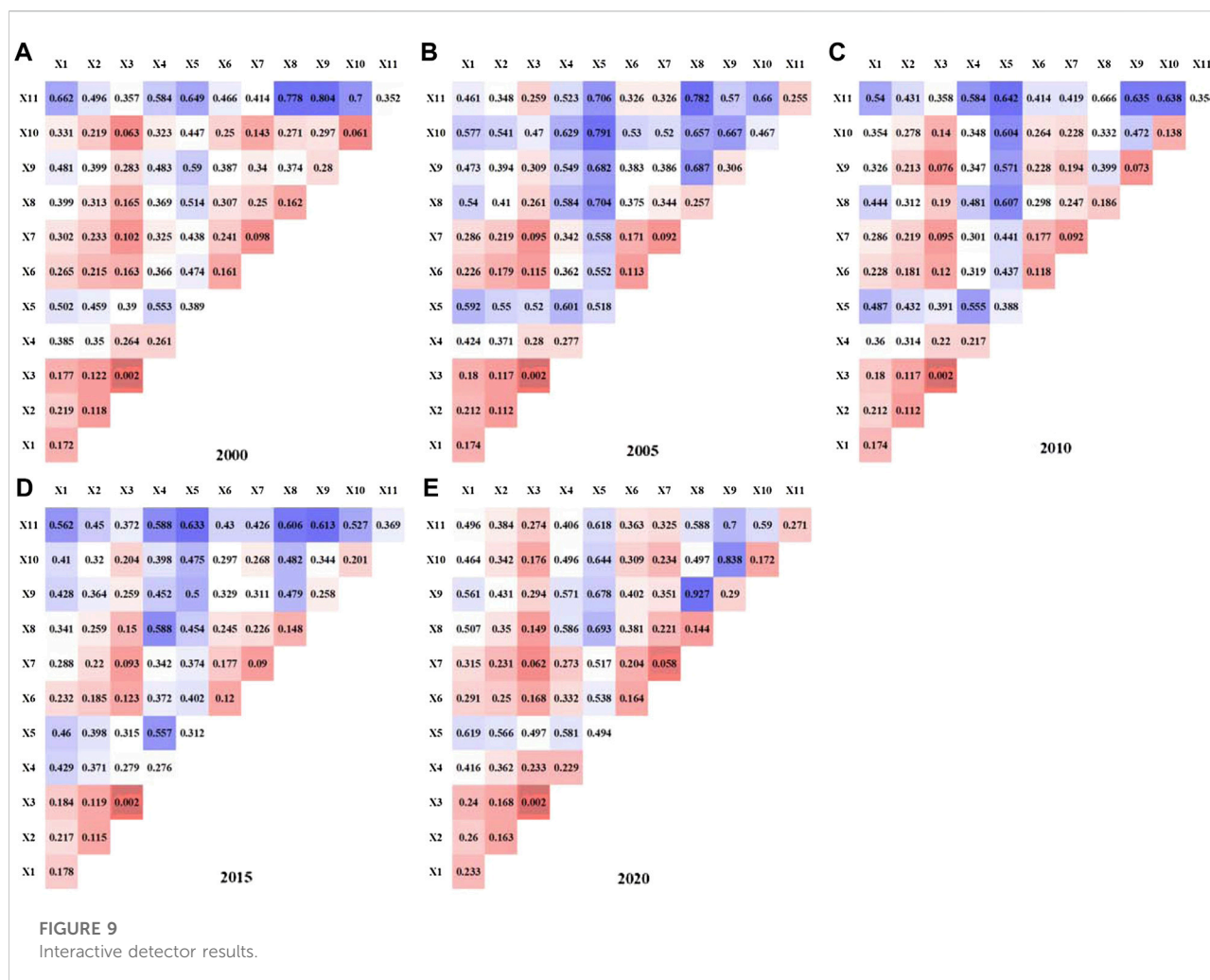


FIGURE 8

Contribution rate of impact factors.

However, there was a negative correlation between ecological environment quality and temperature in the study area, and the increase in evapotranspiration due to



higher temperatures was quite prominent, making the water area smaller than that in other areas.

3.3.4 Analysis of the formation mechanism of ecological environmental quality

As shown in Figure 8, the spatial differentiation of the eco-environmental quality index was the result of multiple factors. We considered five natural environmental factors and six socio-economic factors, with the natural environmental factors including elevation, gradient, slope direction, air temperature, and precipitation, while the socio-economic factors included distance to water, distance to roads at the township level, primary, secondary, and tertiary industries, as well as population density. Detection of the influence of the ecological environment quality index in the Tarim River Basin was carried out by using the geographic detector. The q value in the factor detection result represents the explanatory power of a factor, with respect to spatial differentiation.

Precipitation was found to play a major role among the natural environmental factors, while population density was highly influential among the socio-economic factors, indicating that the ecological environment quality of the study area was significantly affected by precipitation and population density. From the point of view of the natural environment and socio-economic factors, the overall explanatory power of socio-economic factors was stronger than that of the natural environment factors. Therefore, while natural environmental factors are important, socio-economic factors were the main ones affecting the ecological environmental quality during the study period.

Different factors have different impacts on ecological environmental quality. At the same time, there exist complex interactions between and among factors, which lead to differences in the magnitude, intensity, and direction of the impact factors. Furthermore, interactions between the factors may increase their impact on ecological environmental quality. Considering the eleven different influencing factors listed above,

interaction detection analysis was conducted. The results (Figure 9) demonstrated that the interaction modes between any two factors mainly included non-linear enhancement and double factor enhancement, and there were no mutual independent or weakening relationships. The impact strength of interactions on ecological environment quality was significantly higher than that of any single factor; in other words, the spatial evolution of the ecological environmental quality in the Tarim River Basin is primarily the result of the joint action of multiple factors. The higher the interaction q value, the greater the impact of the interaction between the corresponding two factors on the ecological environmental quality.

From 2000 to 2020, the factors with the strongest interaction impact on eco-environmental quality were population density \cap secondary industry (0.804), tertiary industry \cap precipitation (0.791), population density \cap primary industry (0.666), population density \cap precipitation (0.633), and secondary industry \cap primary industry (0.927). The q values of the interactions between population density and precipitation and other factors were high ($q > 0.5$), related to the high explanatory power of these single factors. Among the natural environmental factors, the interaction between precipitation and temperature was the strongest, followed by precipitation and elevation, which showed significant double-factor enhancement effects. For socio-economic factors, the strongest interactions were population density \cap secondary industry (0.804), population density \cap primary industry (0.782), population density \cap primary industry (0.666), population density \cap secondary industry (0.613), and secondary industry \cap primary industry (0.927). The interaction between population density and production value was the strongest, showing a significant non-linear enhancement effect. The strongest interactions between socio-economic and natural environmental factors were population density \cap elevation (0.662), tertiary industry \cap precipitation (0.791), population density \cap precipitation (0.642), population density \cap precipitation (0.633), and primary industry \cap precipitation (0.693).

Although the interaction between population density and precipitation was the most prominent, interactions within socio-economic factors were significantly stronger than interactions between natural environmental factors or between natural environmental factors and socio-economic factors. The study area is vast and the climate type is relatively simple, but socio-economic development and human activities are complex. These features exerted a significant impact on living space and production space area, leading to the strong observed interaction between socio-economic factors.

4 Discussion

Based on analysis of the spatial and temporal distribution characteristics of PLES and eco-environmental quality, we determined the driving mechanism of eco-environmental

quality in the Tarim River Basin by considering both natural environmental and socio-economic factors. The calculation results of the ecological environment quality index indicated that the ecological environment of the Tarim River Basin has gradually declined (Wang et al., 2020), as the ecological environment index decreased from 0.1568 in 2000 to 0.1480 in 2020. As the future will likely bring increased global climate warming, along with more frequent human activities in the Tarim River Basin region, the basin's ecological environment quality index is anticipated to continue to decline. This trend reflects the expansion of production, living, and ecological accommodation land along with a decrease in key ecological land; over the study period, the key ecological land decreased by 24,716.8692 km². Continued and rapid changes in land-use are thought to lead to the severe ecological degradation of natural ecosystems, such as forest ecosystems (Endress and Chine, 2001) and river ecosystems (Yunus et al., 2003). At the beginning of the 21st century, Xinjiang Uygur Autonomous Region began to vigorously develop its social economy. With the expansion of cultivated land and construction land, the development and utilization of water resources have been strengthened; consequently, the water volume of the main stream of the Tarim River has been greatly reduced. Precipitation has been unable to meet water demand, resulting in a significant reduction in ecological land water areas (Wang et al., 2021), comprising a total reduction of 13,665.5622 km² during the study period. Moreover, industrialization, agricultural production, and other human activities require extensive water resources, which means that construction land is mostly distributed in areas close to roads and water bodies. Therefore, the more developed the social economy, the more obvious the changes in PLES will be. These changes will, in turn, affect the eco-environmental quality index.

Over the past 20 years, the areas of cultivated land, construction land, and other production land in the Tarim River Basin have continued to increase, while the area of key ecological land (e.g., grassland and forest land) has continued to decline. In order to vigorously develop the economy, the ecological land area has been continuously encroached upon. This phenomenon is widespread in developing countries (Abdullah and Nakagoshi, 2006). During the study period, the population of the Tarim River Basin continued to grow and the population density continued to increase, thus increasing the area of urban and rural land, as well as other living land. In addition, agriculture is the main economic activity in the Tarim River Basin. Since 2000, grain and cotton prices have continued to rise, and a large number of woodlands and grasslands have been reclaimed into cultivated land, resulting in a sharp increase in the area of cultivated land. Population growth leads to an increase in food demand, which indirectly leads to an increase in the area of cultivated land. The area of unused land in the Tarim River Basin presented a trend of first decreasing and then increasing. The decrease in the area of unused land from

2000 to 2015 was due to the start of the comprehensive treatment project in the Tarim River Basin, which reduced the area of unused land, to a certain extent. Then, due to the rapid population growth in the past 5 years, the forest and grassland have been over-cultivated, and the forest and grassland have been degraded into unused land, thus aggravating the degradation of the ecological environment in the Tarim River Basin.

This paper demonstrates that socio-economic factors have a greater impact on the quality of the ecological environment than natural environment factors. The Tarim River Basin is an ecologically fragile zone in the extremely arid region of Northwest China (Zhang et al., 2020) and, so, that natural environment factors (e.g., precipitation) have a significant impact on the cultivated land, grassland, and forest land in the region. However, due to the small changes in elevation, slope, and aspect in a short period of time, the impact on the ecological environment is limited, and did not play an obvious leading role in this study. The Tarim River Basin is an important part of the “One Belt, One Road” initiative, and the regional development of national engineering construction projects accelerated the urbanization process of the Tarim River Basin during the study period. While the government has vigorously promoted the economic development of the region, this also makes the ecological environment quality of the study area vulnerable to the influence of population increase and economic development. Socio-economic factors have gradually been identified as key factors affecting ecological environment changes (Nagendra et al., 2004).

In view of the current situation, regarding the deterioration of the ecological environment in the Tarim River Basin, we believe that relevant government departments should implement a comprehensive planning plan for the Tarim River Basin as soon as possible, based on the “Water Law of the People’s Republic of China” and other relevant laws and regulations, clarifying important ideas for the sustainable development of the ecological environment of the basin. This may involve increasing the amount of water flowing into the Tarim River from various sources through measures such as the management of the main stream, or protection of the unified management and dispatch of water resources in the basin. In addition, in order to reconcile the contradiction between economic development and ecosystem protection, government departments should increase supervision, strictly prohibit the destruction of forests, return farmland to uncultivated land, and speed up ecological construction projects. The previous ecological water transfer project in the Tarim River Basin produced positive ecological, economic, and social benefits (Ye et al., 2009). At the same time, based on the advantages of local resources, characteristic pillar ecological industries should be created, ecological agriculture and key ecological industries should be vigorously enhanced, tourism and cultural industries should be deeply developed, sustainable economic and trade development should be promoted, and

unnecessary reclamation of woodland and grassland should be reduced.

There is a lot of unused land in the Tarim River Basin, which we classified as ecological accommodation land separately, and studied it together with production land, living land, and key ecological land as first-level land types. Through research on the evolution of land-use function and the effect on the ecological environment, we further clarified the status quo regarding the overall decline of the ecological environment in the Tarim River Basin. This study provides new ideas and methodological references for the analysis of land-use change in arid and semi-arid regions.

In addition, it is worth noting that we only selected factors affecting ecological environmental quality with respect to the impact of different natural environment and socio-economic factors. There was no further research on the intensity of land-use and human activity, and there remains a lack of research and discussion on the influencing factors at the micro-level, such as soil quality and soil type. In the future, the driving mechanisms of eco-environmental effects should be explored more comprehensively; for example, through combination with spatial analysis methods, such as kernel density estimation, in order to further reveal the spatial pattern of eco-environmental quality.

5 Conclusion

Based on the perspective of PLES, we analyzed the evolution characteristics of land-use functions, ecological environment effects, and driving factors in the Tarim River Basin from 2000 to 2020. Our key conclusions are as follows:

- 1) The areas of production land, living land, and ecological accommodation land in the study area increased continuously over the study period, increasing by 16,650.55 km², 718.36 km², and 6839.63 km², respectively; notably, they were all expanding outwards. Meanwhile, the area of key ecological land decreased (by 24,716.87 km²). These change trends and spatial distributions were consistent with the ecological environment quality index results.
- 2) From 2000 to 2020, the ecological environment of the Tarim River Basin was degraded as a whole, and there was obvious spatial heterogeneity. The eco-environmental quality index dropped from 0.1568 in 2000 to 0.1480 in 2020 overall; however, the eco-environmental quality index in the northwest region remained relatively high.
- 3) There were differences in the factors driving the spatial differentiation of eco-environmental effects in the Tarim River Basin. The evolution of the ecological environment quality in the Tarim River Basin was primarily the result of the combined effects of multiple influencing factors. The

explanatory power of socio-economic factors on the ecological environment effect was generally higher than that of other factors (i.e., natural environment factors).

Data availability statement

The datasets presented in this study can be found in online repositories. The names of the repository/repositories and accession number(s) can be found below: <http://www.gscloud.cn/search>.

Author contributions

YGW and YNW conceived the study design and implemented the field research, YNW and TX. collected and analyzed the field data; YL and ZL applied statistics, mathematics, or other forms of technology to analyze or research data. YNW wrote the paper with the help of YGW. All authors have read and agreed to the published version of the manuscript.

References

- Abdullah, S. A., and Nakagoshi, N. (2006). Changes in landscape spatial pattern in the highly developing state of Selangor, peninsular Malaysia. *Landsc. Urban Plan.* 77 (3), 263–275. doi:10.1016/j.landurbplan.2005.03.003
- Andersen, P. S., Vejre, H., Dalgaard, T., and Brandt, J. (2013). An indicator-based method for quantifying farm multifunctionality. *Ecol. Indic.* 25, 166–179. doi:10.1016/j.ecolind.2012.09.025
- Chase, J. M., and Knight, T. M. (2013). Scale-dependent effect sizes of ecological drivers on biodiversity: Why standardised sampling is not enough. *Ecol. Lett.* 16 (1), 17–26. doi:10.1111/ele.12112
- Daneshi, A., Brouwer, R., Najafinejad, A., Panahi, M., Zarandian, A., and Fadia, M. F. (2020). Modelling the impacts of climate and land use change on water security in a semi-arid forested watershed using InVEST. *J. Hydrology* 593, 125621. doi:10.1016/j.jhydrol.2020.125621
- Deng, H. J., Chen, Y. N., and Chen, X. W. (2022). Driving factors and changes in components of terrestrial water storage in the endorheic Tibetan Plateau. *J. Hydrology* 612, 128225. doi:10.1016/j.jhydrol.2022.128225
- Deng, H. J., and Chen, Y. N. (2017). Influences of recent climate change and human activities on water storage variations in Central Asia. *J. Hydrology* 544, 46–57. doi:10.1016/j.jhydrol.2016.11.006
- Deng, H. J., Chen, Y. N., and Li, Y. (2019). Glacier and snow variations and their impacts on regional water resources in mountains. *J. Geogr. Sci.* 29 (1), 84–100. doi:10.1007/s11442-019-1585-2
- Endress, B. A., and China, J. D. (2001). Landscape patterns of tropical forest recovery in the Republic of Palau. *Biotropica* 33 (4), 555–565. doi:10.1646/0006-3606(2001)033
- Eziz, M., Yimit, H., Mohammad, A., and Huang, Z. F. (2010). Oasis land-use change and its effects on the oasis eco-environment in Keriya Oasis, China. *Int. J. Sustain. Dev. World Ecol.* 17 (3), 244–252. doi:10.1080/13504500903211871
- Feng, Q., Endo, K. N., and Cheng, G. D. (2001). Towards sustainable development of the environmentally degraded arid rivers of China—a case study from Tarim River. *Environ. Geol.* 41 (1–2), 229–238. doi:10.1007/s002540100387
- Fu, C., Tu, X. Q., and Huang, A. (2021). Identification and characterization of production–living–ecological space in a central urban area based on POI data: A case study for wuhan, China. *Sustainability* 13 (14), 7691. doi:10.3390/SU13147691
- Galpern, P., and Gavin, M. P. (2020). Assessing the potential to increase landscape complexity in Canadian prairie croplands: A multi-scale Analysis of land use pattern. *Front. Environ. Sci.* 8, 31. doi:10.3389/fenvs.2020.00031
- Gong, W. F., Liu, T. D., Duan, X. Y., Sun, Y. X., Zhang, Y. Y., Tong, X. Y., et al. (2022). Estimating the soil erosion response to land-use land-cover change using GIS-based rusle and remote sensing: A case study of miyun reservoir, north China. *Water* 1, 742. doi:10.3390/w14050742
- Hou, Y. F., Chen, Y. N., Ding, J. L., Li, Z., Li, Y. P., and Sun, F. (2022). Ecological impacts of land use change in the arid Tarim River basin of China. *Remote Sens.* 14 (8), 1894. doi:10.3390/rs14081894
- Jia, S. S., Yang, C. Y., Wang, M. X., and Failler, P. (2022). Heterogeneous impact of land-use on climate change: Study from a spatial perspective. *Front. Environ. Sci.* 10, 840603. doi:10.3389/fenvs.2022.840603
- Lambin, E. F., and Meyfroidt, P. (2011). Global land use change, economic globalization, and the looming land scarcity. *Proc. Natl. Acad. Sci. U. S. A.* 108 (9), 3465–3472. doi:10.1073/pnas.1100480108
- Li, C. X., and Wu, J. Y. (2022). Land use transformation and eco-environmental effects based on production–living–ecological spatial synergy: Evidence from shaanxi province, China. *Environ. Sci. Pollut. Res.* 29 (27), 41492–41504. doi:10.1007/s11356-022-18777-z
- Li, H. X., Wan, H. W., Sun, L., Liu, Y. P., Li, L. P., and Wang, Y. C. (2021). Remote sensing assessment and key driving factors of ecosystem health in Xinjiang. *Arid. Land Geogr.* 44 (02), 460–470. doi:10.12118/j.issn.1000-6060.2021.02.17
- Li, J. X., and Huang, W. (2022). Research on evolution of population and economy spatial distribution pattern in ecologically fragile areas: A case study of ningxia, China. *Front. Environ. Sci.* 10, 814569. doi:10.3389/fenvs.2022.814569
- Liu, J. Y., Liu, M. L., Deng, X. Z., Zhuang, D. F., Zhang, Z. X., and Luo, D. (2002). The land use and land cover change database and its relative studies in China. *J. Geogr. Sci.* 12 (3), 275–282. doi:10.1007/BF02837545
- Liu, Y. S. (2018). Introduction to land use and rural sustainability in China. *Land Use Policy* 74, 1–4. doi:10.1016/j.landusepol.2018.01.032
- Nagendra, H., Munroe, D. K., and Southworth, J. (2004). From pattern to process: Landscape fragmentation and the analysis of land use/land cover change. *Agric. Ecosyst. Environ.* 101 (2–3), 111–115. doi:10.1016/j.agee.2003.09.003
- Padbhushan, R., Kumar, U., Sharma, S., Rana, D. S., Kumar, R., Kohli, A., et al. (2022). Impact of land-use changes on soil properties and carbon pools in India: A meta-analysis. *Front. Environ. Sci.* 9, 794866. doi:10.3389/fenvs.2021.794866
- Pang, R. Q., Hu, N., Zhou, J. R., Sun, D. Q., and Ye, H. Y. (2022). Study on eco-environmental effects of land-use transitions and their influencing factors in the central and southern liaoning urban agglomeration: A production–living–ecological perspective. *Land* 11 (6), 937. doi:10.3390/land11060937

Funding

This research was funded by the Natural Science Foundation of Xinjiang Uygur Autonomous Region (2021D01E02).

Conflict of interest

The authors declare that the research was conducted in the absence of any commercial or financial relationships that could be construed as a potential conflict of interest.

Publisher's note

All claims expressed in this article are solely those of the authors and do not necessarily represent those of their affiliated organizations, or those of the publisher, the editors and the reviewers. Any product that may be evaluated in this article, or claim that may be made by its manufacturer, is not guaranteed or endorsed by the publisher.

- Song, X. P., Hansen, M. C., Stehman, S. V., Potapov, P. V., Tyukavina, A., Vermote, E. F., et al. (2018). Global land change from 1982 to 2016. *Nature* 560, 639–643. doi:10.1038/s41586-018-0411-9
- Tesfaw, A. T., Pfaff, A., Golden Kroner, R. E., Qin, S., Medeiros, R., and Mascia, M. B. (2018). Land-use and land-cover change shape the sustainability and impacts of protected areas. *Proc. Natl. Acad. Sci. U. S. A.* 115, 2084–2089. doi:10.1073/pnas.1716462115
- Wang, J. F., Zhang, T. L., and Fu, B. J. (2016). A measure of spatial stratified heterogeneity. *Ecol. Indic.* 67, 250–256. doi:10.1016/j.ecolind.2016.02.052
- Wang, L. Y., Zhang, S. Y., Liu, Y. F., and Liu, Y. L. (2022). Interaction between construction land expansion and cropland expansion and its socioeconomic determinants: Evidence from urban agglomeration in the middle reaches of the yangtze river, China. *Front. Environ. Sci.* 10, 882582. doi:10.3389/fenvs.2022.882582
- Wang, X., Zhao, X. L., Zhang, Z. X., Yi, L., Zuo, L. J., Wen, Q. K., et al. (2016). Assessment of soil erosion change and its relationships with land use/cover change in China from the end of the 1980s to 2010. *Catena* 137, 256–268. doi:10.1016/j.catena.2015.10.004
- Wang, Y., Xia, T. T., Shataer, R., Zhang, S., and Li, Z. (2021). Analysis of characteristics and driving factors of land-use changes in the Tarim River Basin from 1990 to 2018. *Sustainability* 13, 10263. doi:10.3390/SU131810263
- Wang, Y., Zhang, S., Zhen, H., Chang, X. E., Shataer, R., and Li, Z. (2020). Spatiotemporal evolution characteristics in ecosystem service values based on land use/cover change in the Tarim River basin, China. *Sustainability* 12 (18), 7759. doi:10.3390/su12187759
- Wiggering, H., Dalchow, C., Glemnitz, M., Helming, K., Müller, K., Schultz, A., et al. (2006). Indicators for multifunctional land use-linking socio-economic requirements with landscape potentials. *Ecol. Indic.* 6 (1), 238–249. doi:10.1016/j.ecolind.2005.08.014
- Winkler, K., Fuchs, R., Rounsevell, M., and Herold, M. (2021). Global land use changes are four times greater than previously estimated. *Nat. Commun.* 12 (1), 2501. doi:10.1038/s41467-021-22702-2
- Xiao, X. Y., Li, X. B., Jiang, T., Tan, M. H., Hu, M. Y., Liu, Y. Q., et al. (2019). Response of net primary production to land use and climate changes in the middle-reaches of the Heihe River Basin. *Ecol. Evol.* 9 (8), 4651–4666. doi:10.1002/ece3.5068
- Xiong, L. W., Li, S. X., Zou, B., Peng, F., Fang, X., and Xue, Y. (2022). Long time-series urban heat island monitoring and driving factors analysis using remote sensing and geodetector. *Front. Environ. Sci.* 9, 828230. doi:10.3389/fenvs.2021.828230
- Yang, L. J., Yang, X. R., Wei, W., and Pan, J. H. (2020). Spatio-temporal evolution and influencing factors of water resource carrying capacity in shiyang river basin: Based on the geographical detector method. *Water Supply* 20 (4), 1409–1424. doi:10.2166/ws.2020.057
- Ye, Z. X., Chen, Y. N., Li, W. H., and Yan, Y. (2009). Effect of the ecological water conveyance project on environment in the Lower Tarim River, Xinjiang, China. *Environ. Monit. Assess.* 149 (1–4), 9–17. doi:10.1007/s10661-008-0178-9
- Yunus, A. J. M., Nakagoshi, N., and Lbrahim, A. L. (2003). Application of GIS and remote sensing for measuring and evaluating land-use change and its impact on water quality in the Pinang River watershed. *Ecol. Civ. Eng.* 6 (1), 97–110. doi:10.3825/ece.6.97
- Zhai, Y. X., Zhang, F. Y., and Ma, L. N. (2022). Changes of production-living-ecology land transformation and eco-environmental effects in Xinjiang in last 40 years. *Chin. J. Soil Sci.* 53 (03), 514–523. doi:10.19336/j.cnki.trtb.2021073102
- Zhang, F., Wang, J., and Wang, X. P. (2018). Recognizing the relationship between spatial patterns in water quality and land-use/cover types: A case study of the jinghe oasis in Xinjiang, China. *Water* 10, 646. doi:10.3390/w10050646
- Zhang, H., Xue, L. Q., Wei, G. H., Dong, Z. C., and Meng, X. Y. (2020). Assessing vegetation dynamics and landscape ecological risk on the mainstream of Tarim River, China. *Water* 12 (8), 2156. doi:10.3390/w12082156
- Zhang, Q. Q., and Zhang, T. Z. (2018). Land consolidation design based on an evaluation of ecological sensitivity. *Sustainability* 10 (10), 3736. doi:10.3390/su10103736
- Zhao, R. F., Chen, Y. N., Shi, P. J., Zhang, L. H., Pan, J. H., and Zhao, H. L. (2013). Land use and land cover change and driving mechanism in the arid inland river basin: A case study of Tarim River, Xinjiang, China. *Environ. Earth Sci.* 68 (2), 591–604. doi:10.1007/s12665-012-1763-3
- Zou, L. L., Liu, Y. S., Wang, J. Y., and Yang, Y. Y. (2021). An analysis of land use conflict potentials based on ecological-production-living function in the southeast coastal area of China. *Ecol. Indic.* 122, 107297. doi:10.1016/j.ecolind.2020.107297



OPEN ACCESS

EDITED BY
Wei Shui,
Fuzhou University, China

REVIEWED BY
Hua Lu,
Jiangxi University of Finance
and Economics, China
Yingnan Zhang,
Zhejiang University, China

*CORRESPONDENCE
Dingde Xu
dingdexu@sicau.edu.cn

SPECIALTY SECTION
This article was submitted to
Interdisciplinary Climate Studies,
a section of the journal
Frontiers in Ecology and Evolution

RECEIVED 20 July 2022
ACCEPTED 08 August 2022
PUBLISHED 21 September 2022

CITATION
Ma J, Zhou W, Guo S, Deng X, Song J
and Xu D (2022) Space-time
perception and behavioral response
of farmers to climate change: Evidence
from Sichuan Province, China.
Front. Ecol. Evol. 10:998945.
doi: 10.3389/fevo.2022.998945

COPYRIGHT
© 2022 Ma, Zhou, Guo, Deng, Song
and Xu. This is an open-access article
distributed under the terms of the
[Creative Commons Attribution License](#)
(CC BY). The use, distribution or
reproduction in other forums is
permitted, provided the original
author(s) and the copyright owner(s)
are credited and that the original
publication in this journal is cited, in
accordance with accepted academic
practice. No use, distribution or
reproduction is permitted which does
not comply with these terms.

Space-time perception and behavioral response of farmers to climate change: Evidence from Sichuan Province, China

Junqiao Ma¹, Wenfeng Zhou¹, Shili Guo², Xin Deng³,
Jiahao Song¹ and Dingde Xu^{4*}

¹College of Management, Sichuan Agricultural University, Chengdu, China, ²College of Economics, Southwestern University of Finance and Economics, Chengdu, China, ³College of Economics, Sichuan Agricultural University, Chengdu, China, ⁴Sichuan Center for Rural Development Research, College of Management, Sichuan Agricultural University, Chengdu, China

It is of great significance for global environmental governance to guide farmers to effectively perceive climate change. Based on the survey data of 540 farmers in Sichuan Province, China, this study used binary Logit model and Multinomial Logistic Regression model to explore the effects of farmers' space-time perception of climate change and their interaction effects on farmers' adaptation behavior to climate change. The results showed that: (1) 88.51% of farmers took adaptation measures to climate change, and 61.11% of them took both passive and active adaptation measures. Among the 7 measures, the highest rate of "Increase irrigation" is 23%, and the lowest rate of "Migrant work" is only 5%. (2) The scale difference of farmers' time perception of climate change has a significant positive impact on their adaptive behavior of climate change. In terms of time: climate change perception in the next 5 years > in the next 10 years > in the next 15 years. (3) The scale difference of farmers' space perception of climate change has a significant positive impact on their adaptation behavior to climate change. In other words, spatially, farmers' perception of climate change is global > national > local village (the perception of local province is not significant). (4) Farmers' space-time perception of climate change significantly affects farmers' adaptive behavior. Among them, "farmers' perception of climate change in the next 5 years" and their own "village's perception of climate change" play an important role. This study will help deepen the understanding of farmers' perception of climate change and their adaptive behavior, and provide reference for national policy making.

KEYWORDS

space-time perception of climate change, adaptive behavior, scale effect, farmers, China

Introduction

Global climate change has become a human consensus (Waldman et al., 2017). Since 1850–1900, the global average surface temperature has risen by about 1°C, while the average surface temperature in China has risen by about 1.46°C in the past 60 years (Wang et al., 2016). It is predicted by IPCC that the global temperature will increase by at least 1.5°C in the next 20 years (Pielke et al., 2022), and the annual mean temperature change rate in China will further increase by 2030 (Chao et al., 2020), rising from 0.32°C/ (10 a) to 0.48°C/ (10 a). The intensification of climate change has a severe impact on the global ecological, economic and social systems (Feng and Xu, 2014; Clayton, 2020; Malhi et al., 2020). For example, in 2016, Canada was affected by high temperatures and strong winds, leading to the largest forest fire in history, causing economic losses of 3 billion US dollars (Sun et al., 2017). From 2001 to 2020, floods in China caused over 100 million people to be affected annually, with direct economic losses up to 167.86 billion Yuan (Li and Zhao, 2022). Increasingly prominent meteorological problems have attracted extensive attention of the international community (Dietz et al., 2020). In this context, the 2016 Paris Agreement sets forth goals such as “achieving carbon neutrality by the second half of the century between anthropoid emissions and removal of greenhouse gases,” marking a new stage in global climate governance (Li and Chai, 2017).

China has been adhering to the concept of green development and has attached great importance to climate change response (Chai et al., 2020). As early as 1990, China formulated policies to address climate change, calling for better understanding and management of climate change. In 2020, China proposed its first “dual carbon target,” aiming to peak carbon dioxide emissions by 2030 and achieve carbon neutrality by 2060, demonstrating the country’s determination to tackle climate change (Bo and Zhuang, 2018). However, China’s total carbon dioxide emissions currently rank first in the world and its carbon intensity is 130% of the global average (Zhang et al., 2021). Climate change mitigation is a great challenge and cannot be separated from the broad support of subjects at all levels of society (Liu et al., 2021). As the main unit of agricultural production, farmers’ response to climate change will have an important impact on national climate governance. On the one hand, the agricultural production activities of farmers are the main emission sources of carbon dioxide (Zhang et al., 2021). On the other hand, due to the limitations of income, education level and other conditions, farmers have insufficient understanding of climate change and limited emission reduction ability (Lv and Chen, 2010). Therefore, how to effectively improve farmers’ ability to perceive and cope with climate change will become the only way to achieve the “dual carbon goal” and mitigate climate change.

Adaptation to climate change refers to the process in which people attempt to mitigate the hazards of climate change while taking advantage of the positive benefits of climate change (Ogunbode et al., 2019; Gao et al., 2021). At present, the academic circle has conducted extensive studies on farmers’ adaptive behavior to climate change, mainly involving farmers’ perception of climate change (Rayamajhee et al., 2021), adaptive behavior of climate change (Phuong et al., 2018a,b), willingness to respond to climate change (Hossain et al., 2022). Among them, adaptive behavior of climate change has always been the focus of academic attention. According to the existing research, the factors affecting farmers’ adaptive behavior decisions on climate change mainly focus on the following aspects: First, basic personal characteristics, such as farmer’s gender (Jin et al., 2015), age (Islam et al., 2013) and education level (Fosu-Mensah et al., 2012), have been proved to significantly affect farmer’s adaptation to climate change. Second, basic family characteristics, for example, Abid et al. (2016), Thinda et al. (2020) found that household income, arable land area and agricultural product disaster experience were important factors affecting farmers’ response to climate change.

To sum up, although many existing literatures focus on the core factors that affect farmers’ adaptive behavior to climate change, most of these factors focus on the basic characteristics of individual farmers and families. From the perspective of temporal and spatial perception of climate change, few studies have focused on the impact of temporal and spatial perception and interaction effects of climate change on farmers’ adaptive behaviors. In the only studies, they either focused only on the climate change trend at the macro level, adopted more qualitative analysis methods, or only analyzed farmers’ perception of climate change in time or space (Pahl et al., 2014; Shi, 2016), lack of multi-dimensional analysis of micro-subject climate change perception. In the vast rural areas, limited information channels result in farmers’ perception of climate change can only be judged by their own experience. The deviation between climate change perception experience and reality will have a negative effect on farmers’ response to climate change. For example, when farmers’ perception of small regional climate change threat is not obvious, it may cause farmers’ enthusiasm to deal with it is insufficient. Poor understanding of long-term climate change risks may lead farmers to choose short-term measures and ignore long-term effects and environmental hazards. At present, it has been confirmed by quantitative methods that differences in individual climate change risk perception in a certain period will significantly affect adaptive behaviors (Wheeler et al., 2021). However, in the context of increasingly obvious climate change, the impacts of temporal and spatial perception and interaction effects of climate change on farmers’ adaptive behaviors are still relatively neglected. So in the process of farmers coping with climate change, can they perceive climate change in different time and space? If so, will the temporal and spatial scales of

climate change perception and their interaction affect farmers' adaptation to climate change differently? This is the problem to be solved in this paper.

Theoretical analysis and research hypotheses

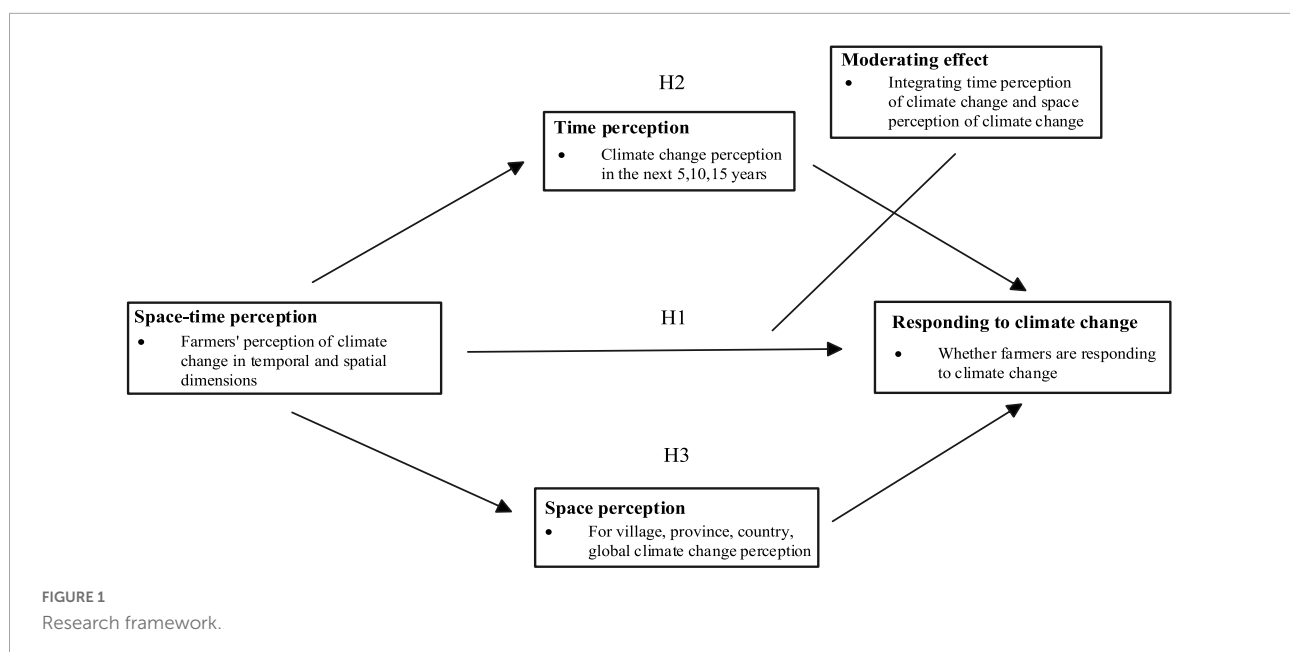
Climate change adaptation refers to people's attempt to avoid the damage of climate change to personal life and property, while taking advantage of the positive effects of climate change. At present, some scholars believe that farmers' adaptation measures to climate change can be divided into engineering and non-engineering, the former including Wells and channels, etc., and the latter including agricultural adjustment and agricultural insurance purchase, etc. (Chen et al., 2014). According to the sequence of drought and coping behaviors, some scholars divided climate change adaptation into pre-event and post-event remedial behaviors. Among them, ex ante remedial actions include mulching film, while ex post remedial actions include increasing irrigation and fertilizer application, etc. (Feng et al., 2016). Based on the research of Lv and Chen (2010) and Chen et al. (2014), this paper divided farmers' climate change adaptation measures into active adaptation and passive adaptation. In the process of farmers' response to climate change, climate change perception is the key factor affecting their decision-making. When the perceived risk of climate change is high, the possibility of adapting to climate change will increase (Zhao, 2014).

Scale features refer to the temporal and spatial representation of geographical phenomena and processes. Since scale features are internal features of things, they often

need observation to identify them, thus forming the observation scale. That is, the changes revealed by observations at different time and spatial scales. The change of observation scale will change the spatial and temporal observation resolution, which will lead to the change of geographical phenomena and process information characteristics, and finally show a certain scale effect (Fu, 2014).

According to the "multi-scale conceptual framework" in spatial scale theory, spatial scale can be divided into global scale, regional scale and local scale (Li, 2014). Among them, global scale refers to the global scope; Regional scale refers to countries, provinces, towns, economic zones, etc. Local scale refers to municipalities, villages, etc. (Zhang et al., 2020). Different spatial scales have significant differences in agricultural production, regional environment, economic level and other aspects (Kobayashi et al., 2014; Zorrilla-Miras et al., 2014). In the local, the impact of population, land and other factors changes will be transmitted locally to the region and the world. At present, spatial scale theory is mostly applied in the field of ecosystem and administrative management, mainly focusing on landscape layout (Fan et al., 2018), urban planning (Liu and Zhang, 2015), and regional economy (Guan et al., 2015).

With the deepening of research, scale effect has also been developed in the field of time. Construal Level Theory holds that object events and self-time, space, social distance are closely related to individual psychological distance cognition, which has an important influence on the psychological construction of object events. People will adopt high-level construction for things with a psychological distance, that is, their perception is more abstract, generalized and context-removed. For things with close psychological distance, they will adopt low level construction, that is, the perception is more specific, clear



and contextual. Different levels of construction will affect individuals' cognitive and emotional experience and influence their behavioral choices (Bar-Anan et al., 2006; Trope and Liberman, 2010). Based on the constructional level theory, some scholars found that the expansion of psychological distance in time would reduce people's concern about climate change and thus reduce their willingness to take measures against climate change (Spence et al., 2012). Vivid and accurate cognition of the future will enhance people's perception of climate change risk and thus enhance their willingness to cope with climate change (D'Argembeau et al., 2011; Lee et al., 2020). Nowadays, constructively-related theories have been preliminarily applied in the fields of pro-environmental behavior and climate change (Lin et al., 2020).

However, space-time scale theory also seems to have more general applicability. For example, Zhang et al. (2019, 2020) discussed the impact of land use change on regional ecosystem services based on spatial and temporal differences. Therefore, there may also be time and space scale effects in the process of climate change perception on farmers' adaptive behaviors. However, the existing literature often takes climate change perception as a whole, which covers the difference of the impact of climate change perception on farmers' coping behavior in different time and space. Therefore, farmers' perception of climate change can be divided into two categories in this paper: first, space perception of climate change, that is, perception of climate change in the global, national, provincial and village. Time perception of climate change refers to the degree of perception of climate change in the next 5, 10 and 15 years. Compared with the long time distance, the short time distance people's prediction is more specific and accurate, and has a greater direct impact on farmers' adaptation behavior to climate change. Compared with far-space distance, near-space distance is more difficult to detect climate change and has less impact on farmers' response to climate change. Based on this, the following hypotheses are made in this study (Figure 1).

H1: Farmers' space-time perception and interaction effects of climate change will positively affect their adaptive behaviors.

H2: Compared with the perception of climate change over a long time distance, the perception of climate change over a short time distance has a greater impact on farmers' adaptation behavior decisions to climate change.

H3: Compared with far-space distance climate change perception, near-space distance climate change perception has less impact on farmers' adaptive behavior decisions of climate change.

Materials and methods

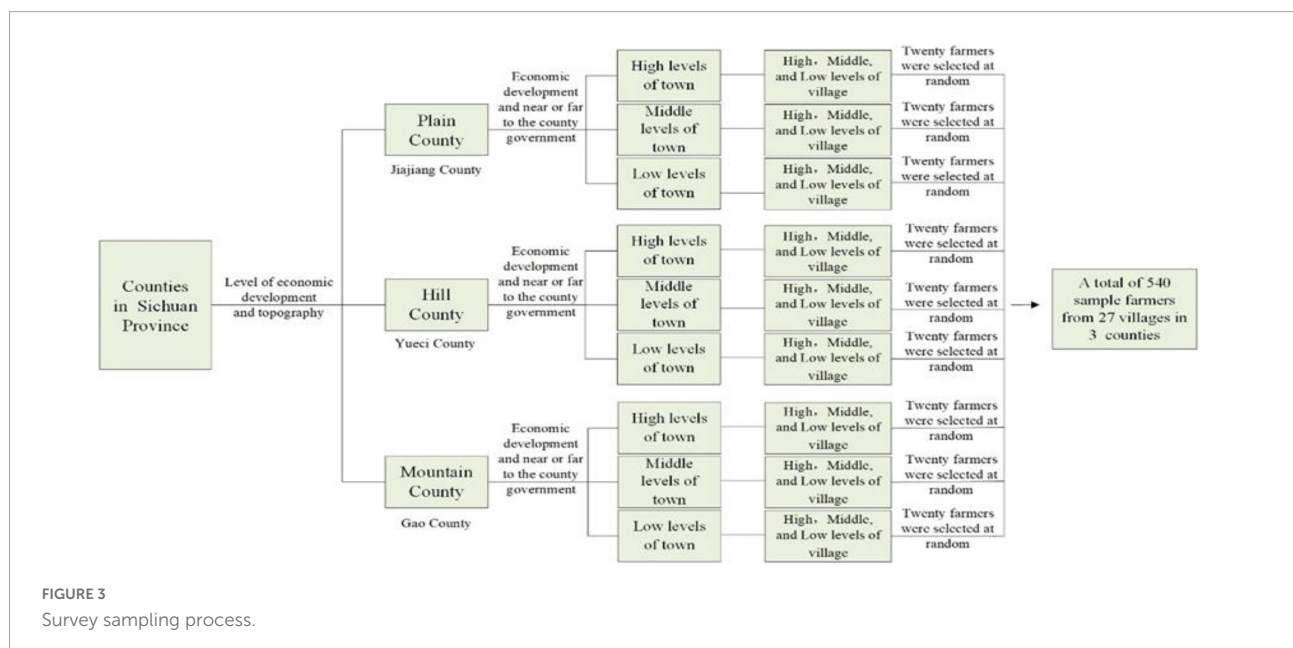
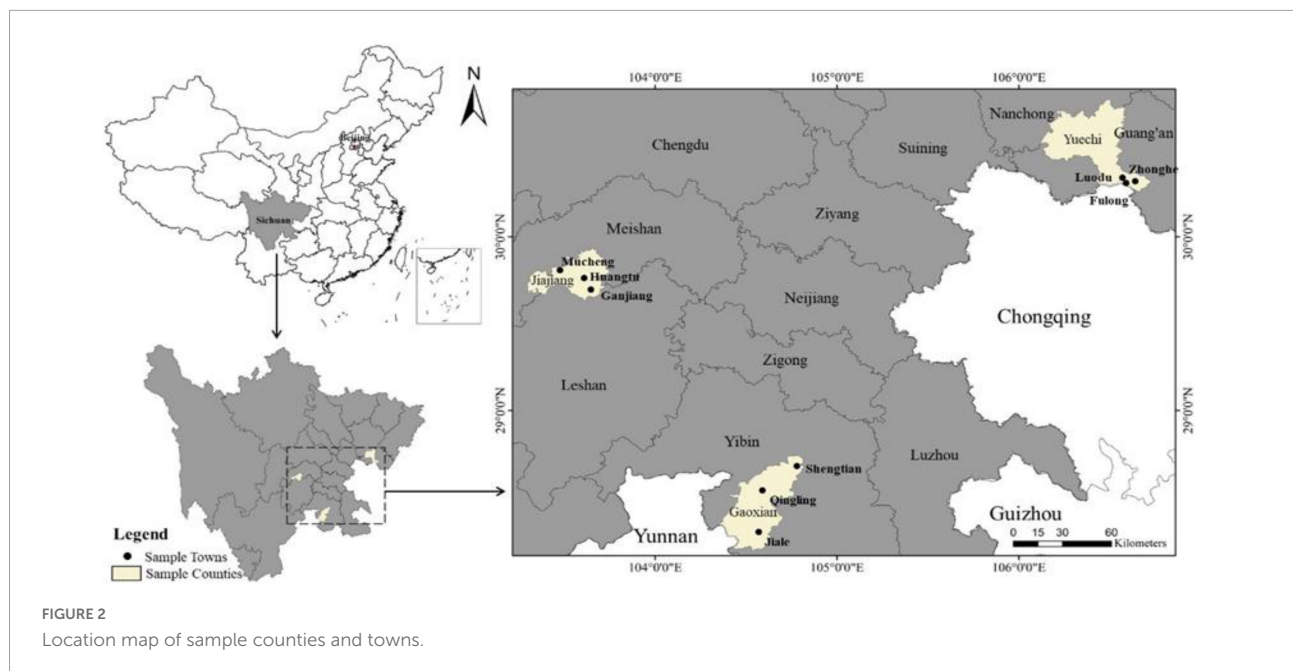
Sample and data sources

Sichuan is one of China's major grain-producing areas, forming subtropical humid monsoon climate, subtropical monsoon climate and other climates. According to statistics, the farmland with perennial drought and water shortage in Sichuan Province accounts for more than 60% of the province's cultivated land area (Xu et al., 2019). As a typical climate vulnerable area, Sichuan Province is also common with meteorological disasters such as rainstorm, flood and high temperature. The data used in this study are from the research group's survey and statistics of 27 villages in 3 districts and counties, 9 towns and 27 villages in Sichuan Province, China in July 2021. The survey method is one-to-one interview, and each questionnaire lasts about 1–1.5 h. The respondents are the family members who know more about family agricultural production, and 61.30% of them are household heads. The research content mainly includes the basic characteristics of individual farmers and families, the perception of time and space of climate change, and the response measures to climate change. In order to ensure the representativeness of samples, stratified equal probability sampling is adopted in this study, with specific procedures as follows.

First of all, according to the topography (plain, mountain and hill) and other indicators, the 183 districts and counties in Sichuan province were divided into three categories: good, medium and poor, and one district were randomly selected. Secondly, according to the three districts and counties in the distance from the county government, the level of economic development and other indicators, each district and county randomly selected three sample towns, good, medium and poor, a total of 9 sample towns. Thirdly, according to the distance of villages to the town government and the level of economic development, each sample village was randomly selected as good, medium and poor villages, totaling 27 sample villages. Then, 20 farmers were selected from the village roster according to the preset random number table as the investigation object. After the village cadres determined the time with the interviewed farmers in advance, 16 researchers with strict training went to the farmers' homes for one-to-one investigation. Finally, a total of 540 effective peasant household questionnaires were obtained from 9 townships and 27 villages in 3 districts and counties, and the questionnaire recovery rate was 100% (Figures 2, 3).

Definition of variables

The purpose of this paper is to investigate the impact of space-time perception of climate change on farmers' adaptive behavior to climate change. Based on the research of Deressa et al. (2009), Lv and Chen (2010) and Chen et al. (2014) and



combined with field research experience, this paper divides the adaptation measures of farmers to climate change into active adaptation and passive adaptation. The former includes adjusting crop type/variety, building infrastructure, learning about climate change technology, and going out to work because of climate change. The latter includes increasing pesticide/fertilizer, increasing irrigation, and adjusting crop time. If the farmer does not take active and passive adaptation measures, the value of “are you taking action on climate change” is 0, otherwise the value is 1. Among the 540 data of farmers, 478 households have adopted measures to cope with climate change,

accounting for 88.51% of the total. According to [Wheeler et al. \(2021\)](#), farmers’ perception of climate change may differ at space-time scales. The core variable of this paper is time perception: “Do you think climate change will intensify in the next 5 years,” “Do you think climate change will intensify in the next 10 years,” and “Do you think climate change will intensify in the next 15 years.” Second, space perception: “How serious do you think the current global climate change impact is,” “How serious do you think the current global climate change impact on China,” “How serious do you think the current global climate change impact on Sichuan Province,” “How serious do

you think the current global climate change impact on your village.”

In addition, considering that farmers’ decision-making on coping with climate change may be affected by a variety of other factors, this paper included the individual characteristics of respondents, family characteristics and meteorological disaster experience into the model as control variables. Among them, the personal characteristics of interviewees include gender, age, education level and other indicators of interviewees, which are generally considered to be related to farmers’ response to climate change (Wang et al., 2010; Habtemariam et al., 2016; Harvey et al., 2018). Household characteristics include household gross income per capita (Obayelu et al., 2014), arable land per capita (Abid et al., 2015) and other indicators. In addition, crop disaster experience may directly affect farmers’ adaptation behavior decisions to climate change (Rozaki et al., 2021). Therefore, “Have crops been damaged by the weather” is included in the model assessment as family experience. Finally, considering that regional differences may affect farmers’ responses to climate change, dummy variables of districts and counties are set to control the regression errors caused by regional differences. Variable definitions and basic statistics are shown in Table 1.

Model construction

The above descriptive statistical analysis of farmers’ spatio-temporal perception of climate change and its adaptive behavior measures is difficult to distinguish the impact of climate change perception on farmers’ adaptive behavior at different time and spatial scales. In addition, farmers’ personal characteristics, family characteristics and regional factors may also influence their adaptive behaviors (Niles et al., 2013; Wood et al., 2014). Therefore, in order to better quantify the impact of various factors on farmers’ adaptation measures, this paper intends to adopt the following measurement model:

$$P_{ij} = \beta_0 + \beta_1 X_1 + \dots + \beta_i X_i + \varepsilon \quad (1)$$

$$Q_{ij} = \gamma_0 + \gamma_1 X_1 + \dots + \gamma_i X_i + \sigma_1 H_1 + \sigma_i H_i + k \quad (2)$$

$$M_{ij} = \partial_0 + \partial_1 X_1 + \partial_i X_i + \tau \quad (3)$$

Equation 1 is a binary Logit model, where P_{ij} is the probability of household i in village j taking measures to cope with climate change. If the farmers adopts adaptation measures (active adaptation or passive adaptation), the value is assigned to 1; otherwise, it is 0. β_0 is a constant term; $X_1 \dots X_i$ is the core independent variable, control variable and regional dummy variable; $\beta_1 \dots \beta_i$ is the regression coefficient; ε is the residual term. Among them, there are 7 core independent variables, namely, farmers’ perception of climate change in the next 5,

10, and 15 years from time perception of climate change; Farmers’ perception of global, national, Sichuan province and their own village climate change in their perception of climate spatial change.

On the basis of Equations 1, 2 adds the product item H_i of the interaction term between time perception and space perception of climate change. Thus, the impacts of farmers’ perception of climate change at different time and spatial scales on their adaptive behaviors can be measured. In the formula, Q_{ij} is the probability of farmers i in village j taking measures against climate change. γ_0 is a constant term; $X_1 \dots X_i$ is the core independent variable, control variable and regional dummy variable; $\gamma_1 \gamma_i, \sigma_1 \sigma_i$ is the regression coefficient; k is the residual term. In order to avoid possible multicollinearity problems, Hayes (2013) is referred to in this paper for centralized processing of Equation 2 to improve the accuracy of the model.

Equation 3 is similar to Equation 1. M_{ij} is the probability of farmers i in village j taking measures to cope with climate change, and its values are 1, 2, 3 and 4, respectively, indicating that household does not take measures to climate change, only adopts active adaptive measures, only adopts passive measures, and both measures are adopted. ∂_0 is a constant term; $X_1 \dots X_i$ is the core independent variable, control variable and regional dummy variable; $\partial_1 \partial_i$ is regression coefficient; τ is the residual term.

Estimation approach

Considering the difference of dependent variables in the equation, different estimation methods are adopted in this paper. Since the dependent variable in Equations 1, 2, namely whether farmers take countermeasures against climate change is a dichotomous variable, binary Logit model was used for regression in this study. In Equation 2, $V_1 V_i$ represents farmers’ perception of global, national, provincial and village climate change. Time perception of climate change $H_1 H_i$ is set to three dummy variables dum1 (farmers think climate change will intensify in the next 5 years is 1; otherwise, it is 0), dum2 (farmers think climate change will intensify in the next 10 years is 1; otherwise, it is 0), and dum3 (farmers think climate change will intensify in the next 15 years is 1; otherwise, it is 0). The three dummy variables were, respectively, multiplied with the four variables of spatial perception of climate change, and the interaction terms $H_i V_i$ were included in Equation 1. In Equation 3, the types of coping measures of farmers are composed of four discrete values (1, 2, 3 and 4), which are independent of each other. Therefore, the MNL model (disordered multi-classification Logit model) is used for analysis in this paper. Firstly, the utility function of the decision maker is constructed, and it is assumed that the farmers choose to realize the principle of utility maximization. Then the maximum likelihood was used to estimate the model

TABLE 1 Variable definition and descriptive statistic.

Variable	Definitions	Mean	SD
Climate	Are you taking action on climate change? (0 = no, 1 = yes)	0.89	0.32
Time perception			
Further 5 years	Do you think climate change will intensify in the next 5 years? (1–5) ^b	3.57	1.05
Further 10 years	Do you think climate change will intensify in the next 10 years? (1–5) ^b	3.55	1.05
Further 15 years	Do you think climate change will intensify in the next 15 years? (1–5) ^b	3.54	1.08
Space perception			
Earth	How serious do you think the current global climate change impact is? (1–5) ^b	3.96	1.01
China	How serious do you think the current global climate change impact on China? (1–5) ^b	3.79	1.01
Sichuan	How serious do you think the current global climate change impact on Sichuan Province? (1–5) ^b	3.69	1.05
Village	How serious do you think the current global climate change impact on your village? (1–5) ^b	3.46	1.26
Individual features			
Gender	Gender of head of household (0 = male, 1 = female)	0.40	0.49
Age	Age of head of household (year)	58.48	11.84
Education	Years of education of household head (year)	6.55	3.44
Family features			
Income	Annual cash income per capita in 2020 (Yuan/person) ^a	19,462.51	33,420.40
Land	Per capita arable land area in 2020 (land/person)	1.43	4.26
Disaster experience	Have crops been damaged by the weather? (0 = no, 1 = yes)	0.70	0.46
Other control variables			
County	Dummy variable of county (Yuechi = 0)		

^aDuring the survey period, 1 \$ = 6.74 Yuan; ^b1–5 are indicators measured using the 5-point Likert scale, which means from weakly disagree to strongly agree.

parameters, and the influence of different factors on different choices of farmers' adaptive behavior was calculated. In order to reflect the influence of independent variables on dependent variables, Tables 2–4, report the marginal coefficients of the model and the standard errors of cluster at the county level.

Results

Descriptive statistical analysis

Adaptation measures against climate change by farmers

What adaptation measures will farmers adopt in the context of climate change? Table 5 shows farmers' choice of adaptation measures to climate change. The results showed that about 88.51% of the 540 peasant households had adopted measures to cope with climate change. Among them, 61.11% farmers adopted both passive adaptation and active adaptation measures. 7.59% of farmers only used active measures and 19.81% only used passive measures. This may be because the active measures require higher economic and cultural levels of farmers and are difficult to implement.

Among the farmers taking measures to cope with climate change (Figure 4), the highest rate of increase irrigation adoption is 23% in the passive adaptive measures, and the similar rate of increase fertilizer/pesticide application and

adjusted crop time adoption is 17%. Among the active adaptation measures, the adoption rate of adjusting crop type/variety was the highest at 17%, while the number of people who chose to cope with climate change by out-migrating for work accounted for only 5%. In general, whether in active adaptation or passive adaptation, farmers tend to choose the measures with low economic and time costs. Increasing irrigation measures are the most frequently used response measures by farmers. This reflects that in the context of climate change, how to reduce the behavioral cost of farmers coping with climate change and improve the stability of irrigation water are important directions to improve farmers' ability to cope with climate change.

Farmers' perception of climate change in time and space

In this paper, farmers' perception of climate change can be divided into three categories: obvious perception, uncertain perception and not obvious perception. Specifically, when farmers' perception score is 4/5, they are classified as "obvious perception" (type I), 3 as "uncertain" (type II), and 1/2 as "not obvious perception" (type III). Table 6 shows the descriptive statistical table of farmers' perception of climate change in time and space. The results show that farmers' perception of climate change in space is more obvious than their perception of climate change in time.

TABLE 2 Logit regression results of climate change time and space perception of farmers.

	Model 1	Model 2	Model 3	Model 4	Model 5	Model 6	Model 7
Time perception							
Further 5 years	0.028*** (0.005)						
Further 10 years		0.024*** (0.006)					
Further 15 years			0.023*** (0.005)				
Space perception							
Earth				0.036** (0.016)			
China					0.035** (0.015)		
Sichuan						0.027 (0.017)	
Village							0.024*** (0.004)
Individual and family features							
Gender	0.015 (0.013)	0.016 (0.014)	0.015 (0.014)	0.019 (0.016)	0.018 (0.017)	0.017 (0.014)	0.014* (0.008)
Age	−0.003** (0.001)	−0.003** (0.001)	−0.003** (0.001)	−0.003** (0.001)	−0.003** (0.001)	−0.003** (0.001)	−0.003** (0.001)
Education	0.001 (0.002)	0.001 (0.002)	0.001 (0.002)	−0.000 (0.002)	0.000 (0.002)	0.000 (0.002)	0.001 (0.002)
Ln (Person income)	0.029** (0.012)	0.027** (0.012)	0.026** (0.012)	0.030*** (0.010)	0.031*** (0.010)	0.032*** (0.011)	0.031** (0.013)
Ln (Person land)	0.144*** (0.030)	0.139*** (0.028)	0.137*** (0.029)	0.144*** (0.029)	0.141*** (0.028)	0.139*** (0.027)	0.140*** (0.033)
Climate reduce	−0.026 (0.053)	−0.023 (0.050)	−0.020 (0.052)	−0.020 (0.042)	−0.022 (0.045)	−0.021 (0.048)	−0.021 (0.055)
County	Yes	Yes	Yes	Yes	Yes	Yes	Yes
N	540	540	540	540	540	540	540

The standard errors of cluster at the county in parentheses; the report result is marginal effect; * $p < 0.1$, ** $p < 0.05$, *** $p < 0.01$.

(1) Time perception of climate change: in type I, farmers' time perception of climate change in the next 5 years is the most obvious, accounting for 50.19%, which is higher than 47.96 and 46.11% in the next 10 and 15 years. In type II, 42.78% of farmers are most difficult to determine their perception of climate change in the next 15 years, which is larger than 40.37 and 38.89% in the next 10 and 5 years. In type III, farmers' perception of climate change in the next 5, 10, and 15 years has little difference. Comparatively speaking, farmers' perception of climate change in the next 10 years is the least obvious, accounting for 11.67%, which is higher than that of 11.11 and 10.93% in the next 15 and 5 years. In conclusion, farmers' perception of the time of short-range climate change is more obvious, and its perception degree decreases with time extension. The possible explanation for this is that farmers are more concerned about the recent situation and have higher cognitive accuracy than identifying long-term risks.

(2) Spatial perception of climate change: In type I, farmers' spatial perception of global climate change is most obvious, accounting for 66.85%, which is higher than 61.85, 56.11, and 50.93% in China, Sichuan province and this village. In type II, the uncertainty of farmers' spatial perception of climate change in Sichuan province accounts for the highest 31.30%, which is higher than 28.52, 25.56, and 24.07% in China, the world and the village. In type III, farmers' perception of climate change varies greatly, especially their perception of climate change in their own village accounts for 25.00%, which is larger than 12.59% in Sichuan Province, 9.63% in China and 7.59% in the world. In conclusion, farmers' spatial perception of long-distance climate change is more obvious, and their perception degree increases with the expansion of space. The possible explanation is that the phenomenon of climate change is more obvious in a larger region, and it is easier for farmers to obtain information related to this region through the Internet, TV and other channels.

TABLE 3 Logit regression results of space-time perception and moderating effect of farmers' climate change.

	Model 1		Model 2		Model 3		Model 4	
	Marginal coefficient	Standard error	Marginal coefficient	Standard error	Marginal coefficient	Standard error	Marginal coefficient	Standard error
Time perception								
Further 5 years	0.033***	(0.006)			0.028***	(0.010)	0.037***	(0.016)
Further 10 years	−0.016	(0.027)			−0.014	(0.022)	−0.023	(0.032)
Further 15 years	0.011	(0.019)			0.002	(0.017)	−0.003	(0.024)
Space perception								
Earth			0.025	(0.024)	0.024	(0.023)	0.025	(0.022)
China			0.021	(0.026)	0.019	(0.026)	0.006	(0.017)
Sichuan			−0.023	(0.024)	−0.026	(0.024)	−0.015	(0.018)
Village			0.020	(0.016)	0.019	(0.016)	0.018*	(0.010)
Individual and family features								
Gender	0.015	(0.014)	0.018	(0.015)	0.017	(0.016)	0.024	(0.022)
Age	−0.003**	(0.001)	−0.003**	(0.001)	−0.003**	(0.001)	−0.003**	(0.001)
Education	0.001	(0.002)	0.001	(0.003)	0.001	(0.003)	0.003	(0.003)
Ln (Person income)	0.029**	(0.012)	0.031***	(0.010)	0.032***	(0.010)	0.029**	(0.012)
Ln (Person land)	0.144***	(0.031)	0.147***	(0.032)	0.152***	(0.035)	0.148***	(0.033)
Climate reduce	−0.025	(0.053)	−0.024	(0.048)	−0.030	(0.051)	−0.025	(0.049)
Earth * F5							−0.038***	(0.006)
Earth * F10							0.023	(0.023)
Earth * F15							0.001	(0.043)
China * F5							−0.072**	(0.029)
China * F10							0.066	(0.077)
China * F15							−0.007	(0.072)
Sichuan * F5							0.012	(0.042)
Sichuan * F10							0.040	(0.063)
Sichuan * F15							−0.028	(0.031)
Village * F5							0.029***	(0.008)
Village * F10							−0.046***	(0.014)
Village * F15							0.027***	(0.009)
County	Yes	Yes	Yes	Yes	Yes	Yes	Yes	Yes
N	540	540	540	540	540	540	540	540

The standard errors of cluster at the county in parentheses; the report result is marginal effect; F5, F10, and F15 represent farmers' perception of climate change in the next 5, 10, and 15 years; * $p < 0.1$, ** $p < 0.05$, *** $p < 0.01$.

Binary logistic model estimation

Table 2 shows the regression results of time and space perception of climate change on farmers' climate change response behaviors. Model 1–7 takes into account the influence of control variables and regional dummy variables on the premise that the core variables time perception and space perception of climate change are included. To better explain the results, we tested the marginal effect of each variable in Model 1–7.

In terms of time perception of climate change, the regression results of Model 1, 2 and 3 show that farmers' time perception of climate change has a positive significance on their adaptive behavior decisions at 1% level, and there is a scale difference, that is, the next 5 years > the next 10 years > the next 15 years. When farmers' perception of climate change increases by 1% in the next 5, 10, and 15 years, their probability of coping with climate change increases by 2.8, 2.4, and 2.3%, respectively. This may be because, influenced by factors such as knowledge level, personal experience and preference, farmers care more about

immediate interests and neglect long-term situations (Ou, 2003; Peng, 2012). In terms of space perception of climate change, the regression results of Model 4, 5, 6 and 7 showed that farmers' spatial perception of climate change had a positive impact on their adaptive behavior of climate change, and there was a scale difference, that is, global > China > local village. Among them, the climate change perception of global, Chinese and local villages has a positive impact on farmers' adaptive behaviors at the levels of 5, 5, and 1%, respectively. Only the climate change perception of Sichuan province has no significant impact on farmers' adaptive behaviors. When the farmers' perception of global, Chinese and local climate change increased by 1%, the probability of taking response measures increased by 3.6, 3.5, and 2.4%, respectively. The explanation is that farmers are less sensitive to climate change in smaller regions because they have lived longer in their own villages and provinces than in large regions such as China and the world. In addition, farmers' perception of regional climate change may also be affected by the difficulty in observing small-scale regional climate change and obtaining relevant information (Xu et al., 2015; Mei et al., 2019).

TABLE 4 Impacts of time-space perception of climate change on farmers' adaptive behavior selection.

	I only take passive measures		II only take active measures		III take both measures	
	Marginal coefficient	Standard error	Marginal coefficient	Standard error	Marginal coefficient	Standard error
Time perception						
Further 5 years	−0.011	(0.033)	−0.030	(0.022)	0.022	(0.037)
Further 10 years	0.132**	(0.060)	0.096***	(0.035)	−0.166**	(0.070)
Further 15 years	−0.135***	(0.050)	−0.069**	(0.028)	0.174***	(0.058)
Space perception						
Earth	−0.013	(0.034)	−0.055***	(0.021)	0.120***	(0.037)
China	−0.035	(0.044)	0.025	(0.026)	0.009	(0.049)
Sichuan	0.003	(0.037)	0.018	(0.020)	−0.055	(0.041)
Village	0.059***	(0.021)	−0.010	(0.012)	−0.033	(0.023)
Individual and family features						
Gender	0.017	(0.037)	−0.007	(0.024)	0.020	(0.044)
Age	0.002	(0.002)	0.000	(0.001)	−0.004*	(0.002)
Education	−0.013**	(0.005)	0.000	(0.004)	0.017***	(0.007)
Ln (person income)	−0.002	(0.020)	0.012	(0.014)	−0.010	(0.024)
Ln (person land)	0.089***	(0.034)	−0.070**	(0.033)	0.121***	(0.047)
Climate reduce	−0.049	(0.038)	−0.060**	(0.024)	0.123***	(0.044)
County	Yes	Yes	Yes	Yes	Yes	Yes
N	540	540	540	540	540	540

The report result is marginal effect; the standard errors in parentheses; * $p < 0.1$, ** $p < 0.05$, *** $p < 0.01$.

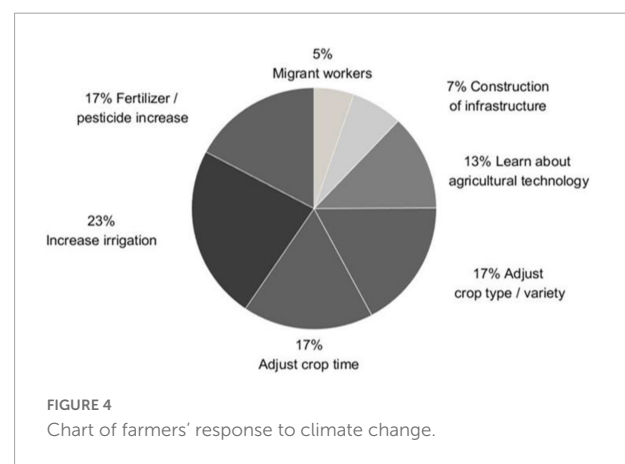
In terms of control variables, gender, household per capita income, and household per capita arable land area have positive effects on the adaptation behavior of farmers to climate change. The possible reason is that the higher the household income of farmers, the less restrictive effect the economic cost of coping measures has on farmers (Hisali et al., 2011; Akter et al., 2016). Age has negative and significant effect on farmers' response to climate change at 5% level. This may be because the older the farmers are, the less able they are to acquire information and receive information, and the lower their sensitivity to climate change. Education level and disaster experience had no significant effect on farmers' adaptation to climate change. This may be due to the limitation of sample characteristics.

TABLE 5 Statistical table of farmers' adaptation measures to climate change.

	Family number	Proportion (%)
The total sample	540	100
No countermeasures were taken	62	11.48
Take countermeasures		
(1) Take both measures	330	61.11
(2) Only take active measures	41	7.59
(3) Only take passive measures	107	19.81

Interaction term regression model estimation

The impact of each core independent variable on farmers' adaptation to climate change has been verified above. Next, this paper discusses the impact difference of climate change perception on farmers' adaptive behavior of climate change from three dimensions of climate change temporal perception, climate change spatial perception, and climate change temporal and spatial perception (Table 3).



Model 1 shows the results of only including climate change time perception and control variables and regional variables. Compared with Table 2, when the three core variables of climate change time perception are included in the regression, the estimation effect of the model is weakened. Only the climate change perception in the next 5 years has a positive impact on farmers' adaptive behavior at 1% level. This may be because the perception of the time of climate change will significantly affect farmers' adaptation to climate change, but farmers' perception of future climate change is only a general cognition, and it is difficult to clearly distinguish the changes in different time periods. At the same time, because farmers pay more attention to the recent situation and are easier to identify, their perception of climate change in the next 5 years is more obvious, and even their perception may be confused with the perception of longer-term climate change. Model 2 shows the results of only including spatial perception and control variables and regional variables of climate change. Compared with Table 2, when the four core variables of spatial perception of climate change are included in the regression, the estimation effect of the model is not obvious. This may be because the spatial awareness of climate change will be obvious when farmers adapt to climate change behavior. However, when the global, China, Sichuan province and local village spatial perception variables of climate change are included in the model, they may influence each other and thus reduce the role of farmers in coping with climate change. For example, when farmers' perception of climate change in their village or province is not obvious, and their information channels and cognition level are limited, they may think that changes in China and the world are not obvious either.

Model 3 shows the regression results of integrating temporal perception of climate change, spatial perception of climate change, control variables and regional variables. Compared with Model 1 and 2, when the seven core variables of climate change perception were included in the regression, the estimated effect of the Model changed little. Only the temporal perception of climate change in the next 5 years has a positive significant effect on farmers' adaptive behavior decisions at 1% level. This indicates that farmers are more sensitive to the short-term

risk perception under the temporal and spatial dimensions of climate change.

Based on Model 3, Model 4 shows the result after the interaction product and centralization of three time-sensing variables of climate change and four spatial variables. The results show that only the time perception of climate change in the next 5 years and the perception of climate change in the village have positive significance on the behavior decision of farmers' adaptation to climate change at 5 and 10% levels. Among the interaction items, "Earth * F5," "China * F5," and "Village * F10" have significant negative impacts on farmers' climate change response behaviors at 1, 5, and 1% levels, respectively. The impacts of "Village * F5" and "Village * F15" on farmers' climate change response behaviors are significantly positive at 1% level, respectively. This indicates that farmers have a low perception of climate change in short time distance and short time distance, and may even have a negative response to climate change due to their underestimation of risks. However, in the case of farmers' perception of near-spatial climate change, the fuzziness of their perception of far-temporal climate change has little impact on farmers, and farmers are still actively responding to climate change.

In terms of control variables, farmers' age has a significant negative impact on their adaptation behavior to climate change, and per capita income and arable land area have a significant positive impact on farmers' adaptation to climate change. Gender, disaster experience and education level have no significant impact on farmers' adaptation to climate change. Therefore, more training should be given to farmers on climate change to improve their awareness and coping ability. At the same time, reduce the economic and time costs of farmers to cope with climate change.

Multinomial logit model estimation

It has been discussed above that farmers' perception of time and space of climate change at different scales will affect their adaptive behaviors. In this context, what is the difference

TABLE 6 Statistical table of farmers' perception of climate change in time and space.

	I obvious perception		II uncertain perception		III not obvious perception	
	N	Proportion (%)	N	Proportion (%)	N	Proportion (%)
Time perception						
Further 5 years	271	50.19	210	38.89	59	10.93
Further 10 years	259	47.96	218	40.37	63	11.67
Further 15 years	249	46.11	231	42.78	60	11.11
Space perception						
Earth	361	66.85	138	25.56	41	7.59
China	334	61.85	154	28.52	52	9.63
Sichuan	303	56.11	169	31.30	68	12.59
Village	275	50.93	130	24.07	135	25.00

between farmers' choice of measures to cope with climate change? To answer this question, this section uses the MNL model to take the initiative to adaptive, passive adaptive to the control group is not used, to discuss climate change awareness of time and space to I use only passive adaptive measures, II only with active adaptive measures and type III both measures adopted three to adapt to the effects of policy decision, Such as [Table 4](#). The results show that the time perception of remote climate change has a more significant impact on farmers' specific adaptation measures, while the national and provincial climate change perception has no significant impact on farmers. Specifically:

(1) In terms of climate change time perception, the impact of climate change perception on farmers' adaptation measures in the next 5 years is not obvious. In the next 10 years, the perception of climate change for farmers to adopt passive measures and active measures is positively significant at 5 and 1% level, respectively, but the perception of climate change for farmers to adopt both measures is negatively significant at 5% level. When farmers' perception of climate change in the next 10 years increases by 1%, the probability of adopting passive adaptation measures and active adaptation measures increases by 13.2 and 9.6%, respectively, and the probability of adopting both measures decreases by 16.6%. What's interesting is that the perception of climate change over the next 10 and 15 years is the opposite. In the next 15 years, farmers' perception of climate change is negatively significant at the level of 1% for passive measures and 5% for active measures, but positively significant at the level of 1% for both measures. For each 1% increase in farmers' perception of climate change in the next 15 years, the probability of adopting passive adaptation measures and active adaptation measures will decrease by 13.5 and 6.9%, respectively, and the probability of adopting both measures will increase by 17.4%. This may indicate that when specific measures are taken to cope with climate change, farmers have no obvious preference to cope with short-term climate change. However, when dealing with the risk of medium-term climate change in the future (the next 10 years), farmers choose to adopt certain targeted measures because they have a certain level of awareness of the risk. When dealing with the long-term threat of climate change (the next 15 years), the difficulty of predicting the risk leads them to prefer both measures, thus reducing the potential damage.

(2) In terms of spatial perception of climate change, the impact of climate change perception in China and Sichuan province on farmers' adaptation measures is not obvious. The perception of global climate change for farmers only adopting active adaptation measures and adopting both measures is significantly negative and positive at 1% level, respectively. When the farmers' perception of global climate change increased by 1%, the probability of adopting active adaptation measures decreased by 5.5%, and the probability of adopting both measures increased by 12.0%. The climate change perception

of the village is positively significant to the passive adaptation measures adopted by farmers at 1% level. When farmers' perception of climate change increased by 1%, the probability of adopting passive adaptation measures increased by 5.9%. This may indicate that in response to the large-scale climate change crisis (global), farmers' willingness to adopt both active and passive adaptation measures for personal life and property, production and operation has been greatly enhanced. However, when farmers perceive only small scale climate change (their village), they tend to choose only passive adaptation measures. This may be because farmers underestimate the threat of small-scale climate change or the effectiveness of individual coping behaviors, and tend to choose only passive adaptation measures with low time and economic cost.

In terms of control variables, age of individual characteristics was negatively significant to both measures at the level of 10%. Education level is only passive adaptive measure, and both measures are negative significant at 5% level and positive significant at 1% level, respectively. The per capita arable land area and crop disaster experience of households were negatively significant at the level of 5% and positively significant at the level of 1%. In addition, the per capita arable land has a significant positive impact on the passive adaptation measures adopted by farmers. This may indicate that households with larger per capita land area and disaster experience have higher awareness of climate change risk prevention and higher willingness to adopt active and passive adaptation measures.

Discussion

Based on the survey data of 540 farmers in Sichuan Province, China, this study used binary Logit model and Multinomial Logistic Regression model (MNL) to explore the effects of farmers' space-time perception of climate change and their interaction effects on their adaptation behavior to climate change. Compared with previous studies, the marginal contribution of this paper is as follows: First, from the perspective of farmers' space-time perception of climate change, the impact of climate change on farmers' response to climate change is analyzed based on scale effect. Secondly, Logit model were used to quantify the space-time scale differences of farmers' perception of climate change. In addition, MNL model was used to discuss the impact of different spatial and temporal climate change perceptions on farmers' adaptive measures. Thirdly, representative micro-individual data were used to focus on the behavior of farmers in rural areas of China in response to climate change, so as to provide reference for the formulation of climate change policies in China and other developing countries.

Global climate change is an indisputable fact ([Hase et al., 2021](#)), which will have a huge impact on human production and life. [Horowitz \(2009\)](#) showed that there was a strong

negative correlation between national per capita GDP and temperature, and global GDP would decrease by 3.8% for every 1°C increase in national temperature. Climate change also threatens global environmental governance, national food security, and children's nutritional health (McMahon and Gray, 2021; Baste and Watson, 2022). In response to the threat of climate change, 153 countries and the European Community signed the United Nations Framework Convention on Climate Change (UNFCCC) in 1992, hoping to control the rate of global warming by reducing greenhouse gas emissions. Since then, the international community has held many meetings calling on countries to actively change climate and discharge carbon dioxide within the agreed limits. However, the climate change crisis appears to be more severe than predicted. According to the latest assessment report from the Intergovernmental Panel on Climate Change, global surface temperatures in the 21st century will exceed 1.5 and 2°C without deep controls on emissions of greenhouse gases such as carbon dioxide. Climate change is a matter of human welfare and equity, and the efforts of governments at all levels, the private sector and the public are indispensable.

China has always played an important role in promoting global climate governance. From 1998, when China officially promulgated the Energy Conservation Law of the People's Republic of China, to 2007, when China explicitly proposed to “strengthen capacity building to cope with climate change and make contribution to global climate protection,” to 2020, when China proposed the “dual carbon target,” China's participation in the global cause of climate change mitigation has been on the rise (Hu, 2012). Although all sectors of society attach great importance to the response to climate change, residents, especially small farmers, as the main body of adaptation to climate change, are not optimistic about the perception and response to climate change. Low awareness of climate change, high cost of adaptation measures and poor response effect restrict the implementation of relevant policies at the micro individual level. Therefore, how to help farmers out of the plight of climate change will have far-reaching significance for global climate governance.

In the context of intensified climate change, the academic community has conducted extensive research on the adaptation behavior of farmers to climate change. However, in general, these factors are mostly concentrated in the gender, age, economic income and other aspects of farmers, and few studies have explored from the perspective of space-time perception of climate change. In the only studies, either only focus on the trend of climate change at the macro level, or mostly adopt qualitative analysis methods, or only analyze the perception of farmers' climate change in single dimension of time or space. For example, Yu et al. (2011) used descriptive statistics to study the perception intensity of local precipitation and temperature changes in the past 50 years by residents of different age groups in Shaanxi. Wang and Yu (2015) used the perception intensity

formula to show that there were differences in the accuracy of residents' climate perception in different small areas in southern Shaanxi. In Hanzhong, Ankang, and Shangluo, the consistency rates between the perceived precipitation change and the measured precipitation change were 100, 44.4 and 66.7%, respectively. In general, the existing research still lacks the quantitative analysis of micro-subject climate change perception in multiple dimensions. Therefore, this paper used binary Logit model and MNL model to explore the impact of farmers' spatio-temporal climate change perception and their interaction effects on farmers' climate change adaptive behavior.

There are still some shortcomings in this study, which can be further expanded in future research. For example, differences in the impact of spatio-temporal perception of farmers' climate change on farmers' response to climate change under different climate types and meteorological natural disasters and the reasons can be discussed. Secondly, the spatial and temporal perception intensity of climate change and its impact on the adoption of specific measures can be further studied in different dimensions. Thirdly, from the perspective of farmers' perception of climate change in time and space in the past, it can be discussed whether it will affect their current climate change adaptive behavior and the difference in impact. Finally, there may be a “perception-behavior” cycle affecting the temporal and spatial perception of climate change among farmers. For example, farmers have a strong perception of climate change risks in the past 5 years and may take active measures to deal with them. The guarantee of corresponding measures may reduce the current perception of climate change risk and the enthusiasm of farmers to cope with it. The mechanism and characteristics of “perception-behavior” in the space-time perception of climate change of farmers can be further studied.

Conclusion

Based on the survey data of 540 farmers in Sichuan Province, China, this study used binary Logit model and MNL model to explore the effects of farmers' space-time perception of climate change and their interaction effects on farmers' adaptation behavior to climate change. The results showed that: (1) 88.51% of farmers took adaptation measures to climate change, and 61.11% of them took both passive and active adaptation measures. (2) The scale difference of farmers' time and space perception of climate change has a significant positive impact on their adaptive behavior of climate change. In terms of time: climate change perception in the next 5 years > in the next 10 years > in the next 15 years. In terms of space: farmers' perception of climate change is global > national > local village (the perception of local province is not obvious). (3) Farmers' space-time perception of climate change significantly affects farmers' adaptive behavior. Among them, “farmers' perception of climate change in the next

5 years” and their own “village’s perception of climate change” play an important role.

This paper has important implications for guiding farmers to effectively adapt to climate change, and its conclusions are also applicable to other developing countries. (1) The state should improve policies related to climate change and issue regulations to support farmers in coping with climate change. The study shows that farmers may make blind choices when making decisions on climate change response measures due to the influence of time and economic cost. The state should attach importance to the construction and maintenance of rural infrastructure and strengthen the funding support for infrastructure construction of grassroots governments. We will formulate overall reference standards for rural infrastructure construction, urge local governments to implement them in light of local conditions, and supervise them by setting up responsibility mechanisms and supervision groups. At the same time, the state also should increase investment in rural infrastructure and provide certain economic subsidies to farmers responding to climate change, so as to enhance their willingness to cope with climate change. (2) Local governments should combine local characteristics to develop green and low-carbon agricultural products and reduce greenhouse gas emissions from production, logistics and packaging of agricultural products while implementing orders from higher authorities. The study found that the excessive use of chemical fertilizers in the adaptation process of farmers to climate change will increase carbon dioxide emissions and deteriorate soil properties. In addition, at present, farmers mostly adopt passive adaptive measures such as increasing irrigation and adjusting farming time. By buying agricultural insurance and planting subsidies, the local government can guide them to take measures to deal with climate change. In addition, the government should give play to the demonstration and guidance role of community-level agricultural technology departments and major farmers in villages, strengthen training and services in agricultural technology for farmers, reduce their blind application of chemical fertilizers and pesticides, and improve their ability to adapt to climate change in a scientific way. (3) Village collectives should actively implement the instructions of their superiors and expand climate change-related knowledge training for farmers. In our survey, farmers paid more attention to the immediate situation and had no obvious perception of long-term threat of climate change and surrounding environment. In this regard, the village’s collectives should use radio, mobile phones, brochures and other media to strengthen publicity on the long-term potential risks of climate change and surrounding environmental changes. Keep a close eye on climate change information. For example, when disasters such as flood and drought are likely to occur in the local area, inform households in time and assist farmers to take preventive measures. (4) Farmers should actively respond to the call of the government, actively participate in village

collective climate change related training sessions. They are supposed to close and village cadres, neighbors and other groups of communication and other ways, effectively expand the family information channels. Thus, they can strengthen their own green production awareness and take appropriate measures to deal with climate change.

Data availability statement

The original contributions presented in this study are included in the article/supplementary material, further inquiries can be directed to the corresponding author.

Ethics statement

The studies involving human participants were reviewed and approved by School of Management, Sichuan Agricultural University. The patients/participants provided their written informed consent to participate in this study. Written informed consent was obtained from the individual(s) for the publication of any potentially identifiable images or data included in this article.

Author contributions

JM and DX: conceptualization, writing—original draft preparation, and writing—review and editing. JM, WZ, and DX: methodology. JM, SG, and JS: formal analysis. XD, JS, and DX: investigation. DX: supervision and funding acquisition. All authors read and agreed to the published version of the manuscript.

Conflict of interest

The authors declare that the research was conducted in the absence of any commercial or financial relationships that could be construed as a potential conflict of interest.

Publisher’s note

All claims expressed in this article are solely those of the authors and do not necessarily represent those of their affiliated organizations, or those of the publisher, the editors and the reviewers. Any product that may be evaluated in this article, or claim that may be made by its manufacturer, is not guaranteed or endorsed by the publisher.

References

- Abid, M., Scheffran, J., Schneider, U. A., and Ashfaq, M. J. E. S. D. (2015). Farmers' perceptions of and adaptation strategies to climate change and their determinants: the case of Punjab province, Pakistan. *Earth Syst. Dyn.* 6, 225–243. doi: 10.5194/esd-6-225-2015
- Abid, M., Schneider, U. A., and Scheffran, J. (2016). Adaptation to climate change and its impacts on food productivity and crop income: perspectives of farmers in rural Pakistan. *J. Rural Stud.* 47, 254–266. doi: 10.1016/j.jrurstud.2016.08.005
- Akter, S., Krupnik, T. J., Rossi, F., and Khanam, F. (2016). The influence of gender and product design on farmers' preferences for weather-indexed crop insurance. *Glob. Environ. Change* 38, 217–229. doi: 10.1016/j.gloenvcha.2016.03.010
- Bar-Anan, Y., Liberman, N., and Trope, Y. (2006). The association between psychological distance and construal level: evidence from an implicit association test. *J. Exp. Psychol. Gen.* 135:609. doi: 10.1037/0096-3445.135.4.609
- Baste, I. A., and Watson, R. T. (2022). Tackling the climate, biodiversity and pollution emergencies by making peace with nature 50 years after the Stockholm Conference. *Glob. Environ. Change* 73:102466. doi: 10.1016/j.gloenvcha.2022.102466
- Bo, F., and Zhuang, G. Y. (2018). Evolution and phased characteristics of China's climate change policy. *Collect* 6:24.
- Chai, Q. M., Guo, H. Y., Liu, C. Y., Dong, L., Ju, L. X., Liu, C. S., et al. (2020). Global Climate Change and China's Action Plan – China's Climate Governance during the 14th Five-Year Plan period (In writing). *J. Yuejiang Univ.* 12, 36–58.
- Chao, Q. C., Yan, Z. W., Sun, Y., Jiang, Z. H., Liao, H., Jia, G. S., et al. (2020). New scientific understanding of climate change in China. *China Popul. Resour. Environ.* 30, 1–9.
- Chen, H., Wang, J., and Huang, J. (2014). Policy support, social capital, and farmers' adaptation to drought in China. *Glob. Environ. Change* 4, 193–202. doi: 10.1016/j.gloenvcha.2013.11.010
- Clayton, S. (2020). Climate anxiety: psychological responses to climate change. *J. Anxiety Disord.* 74:102263. doi: 10.1016/j.janxdis.2020.102263
- D'Argembeau, A., Renaud, O., and Van der Linden, M. (2011). Frequency, characteristics and functions of future-oriented thoughts in daily life. *Appl. Cogn. Psychol.* 25, 96–103. doi: 10.1002/acp.1647
- Deressa, T. T., Hassan, R. M., Ringler, C., Alemu, T., and Yesuf, M. (2009). Determinants of farmers' choice of adaptation methods to climate change in the Nile Basin of Ethiopia. *Glob. Environ. Change* 19, 248–255. doi: 10.1016/j.gloenvcha.2009.01.002
- Dietz, T., Shwom, R. L., and Whitley, C. T. (2020). Climate change and society. *Annu. Rev. Sociol.* 46, 135–158. doi: 10.1146/annurev-soc-121919-054614
- Fan, M., Peng, Y., Wang, Q. H., Mi, K., and Qing, F. T. (2018). Relationship between landscape pattern and plant diversity and its spatial scale effect: a case study of otindag Sandy Land. *Acta Ecol. Sin.* 8, 2450–2461.
- Feng, S., and Xu, C. L. (2014). Review of global climate change and its impact on human society and economy. *Popul. Resour. Environ. China* 24, 6–10.
- Feng, X. L., Chen, Z. X., and Huo, X. X. (2016). An empirical study on farmers' adaptive behavior under drought conditions: data from 1079 apple farmers. *J. Arid Land Resour. Environ.* 3, 43–49.
- Fosu-Mensah, B. Y., Vlek, P. L., and MacCarthy, D. S. (2012). Farmers' perception and adaptation to climate change: a case study of Sekyedumase district in Ghana. *Environ. Dev. Sustain.* 14, 495–505. doi: 10.1007/s10668-012-9339-7
- Fu, B. J. (2014). Approaches and methods of integrated geographical research: coupling of pattern and process. *Acta Geogr. Sin.* 69:578.
- Gao, X., Li, G. C., and Yin, C. J. (2021). Household adaptive behavior and its impact on grain yield per unit area under climate change. *J. China Agric. Univ.* 26, 240–248.
- Guan, W. H., Peng, X., Zhang, H., and Wei, Y. H. (2015). Regional economic disparities in Jiangsu Province at different spatial scales. *Resour. Environ. Yangtze Basin* 24:2003R2011. doi: 10.1016/j.jenvman.2020.110901
- Habtemariam, L. T., Gandorfer, M., Kassa, G. A., and Heissenhuber, A. (2016). Factors influencing smallholder farmers' climate change perceptions: a study from farmers in Ethiopia. *Environ. Manag.* 58, 343–358. doi: 10.1007/s00267-016-0708-0
- Harvey, C. A., Saborio-Rodríguez, M., Martínez-Rodríguez, M. R., Viguera, B., Chain-Guadarrama, A., Vignola, R., et al. (2018). Climate change impacts and adaptation among smallholder farmers in Central America. *Agric. Food Security* 7, 1–20. doi: 10.1186/s40066-018-0209-x
- Hase, V., Mahl, D., Schäfer, M. S., and Keller, T. R. (2021). Climate change in news media across the globe: an automated analysis of issue attention and themes in climate change coverage in 10 countries (2006–2018). *Glob. Environ. Change* 70:102353. doi: 10.1016/j.gloenvcha.2021.102353
- Hayes, A. F. (2013). Introduction to mediation, moderation, and conditional process analysis: a regression-based approach. New York, ny: the guilford press. *J. Educ. Meas.* 51, 335–337. doi: 10.1111/jedm.12050
- Hisali, E., Birungi, P., and Buyinza, F. (2011). Adaptation to climate change in Uganda: evidence from micro level data. *Glob. Environ. Change* 21, 1245–1261. doi: 10.1016/j.gloenvcha.2011.07.005
- Horowitz, J. K. (2009). The income-temperature relationship in a cross-section of countries and its implications for global warming. *Environ. Resour. Econ.* 44, 475–493. doi: 10.1007/s10640-009-9296-2
- Hossain, M. S., Alam, G. M., Fahad, S., Sarker, T., Moniruzzaman, M., and Rabbany, M. G. (2022). Farmers' willingness to pay for flood insurance as climate change adaptation strategy in northern Bangladesh. *J. Clean. Product.* 2022:130584. doi: 10.1016/j.jclepro.2022.130584
- Hu, A. G. (2012). China's climate change policies: background, goals and debates. *Country Rep.* 12:2009.
- Islam, M. M., Barnes, A., and Toma, L. (2013). An investigation into climate change scepticism among farmers. *J. Environ. Psychol.* 34, 137–150. doi: 10.1016/j.jenvp.2013.02.002
- Jin, J., Wang, X., and Gao, Y. (2015). Gender differences in farmers' responses to climate change adaptation in Yongqiao District, China. *Sci. Total Environ.* 538, 942–948. doi: 10.1016/j.scitotenv.2015.07.027
- Kobayashi, H., Watando, H., and Kakimoto, M. (2014). A global extent site-level analysis of land cover and protected area overlap with mining activities as an indicator of biodiversity pressure. *J. Clean. Product.* 84, 459–468. doi: 10.1016/j.jclepro.2014.04.049
- Lee, P. S., Sung, Y. H., Wu, C. C., Ho, L. C., and Chiou, W. B. (2020). Using episodic future thinking to pre-experience climate change increases pro-environmental behavior. *Environ. Behav.* 52, 60–81. doi: 10.1177/0013916518790590
- Li, J. F., and Chai, Q. M. (2017). The significance of the entry into force of the paris agreement. *World Environ.* 1, 16–18.
- Li, S. C. (2014). *Geography of Ecosystem Services*. Beijing: Science Press.
- Li, Y., and Zhao, S. S. (2022). Flood disaster loss and disaster risk in China from 2001 to 2020. *Adv. Clim. Change Res.* 18:12
- Lin, F., Chen, X. W., Yao, W. Y., Fang, Y. H., Deng, H. J., Wu, J. F., et al. (2020). Multi-time scale analysis of water conservation in forest discontinuous watershed based on swat model. *Acta Geogr. Sin.* 75:14.
- Liu, Q., and Zhang, Z. Y. (2015). The significance of Spatial scale – Reflections on the planning of residential public facilities in Zhuhai under the neighborhood Center model. *Urban Plann. Rev.* 9, 45–52.
- Liu, Y. H., Li, Y. H., and Wang, W. T. (2021). Challenges, opportunities and actions for China to achieve “dual carbon” goals. *China Popul. Resour. Environ.* 9:57.
- Ly, Y. R., and Chen, S. F. (2010). Farmers' perception of climate change and analysis of adaptive behaviors. *China Rural Econ.* 07, 75–86. doi: 10.1007/s00267-016-0742-y
- Malhi, Y., Franklin, J., Seddon, N., Solan, M., Turner, M. G., Field, C. B., et al. (2020). Climate change and ecosystems: Threats, opportunities and solutions. *Philos. Trans. R. Soc. B* 375:20190104. doi: 10.1098/rstb.2019.0104
- McMahon, K., and Gray, C. (2021). Climate change, social vulnerability and child nutrition in South Asia. *Glob. Environ. Change* 71:102414. doi: 10.1016/j.gloenvcha.2021.102414
- Mei, J. M., Huang, X. H., Zhou, R. Z., Ren, Y. H., Hou, L., and Hao, W. Y. (2019). Perception and adaptation of farmers and herdsmen to climate change at different altitudes. *Acta Ecol. Sin.* 39:7805R7814.
- Niles, M. T., Lubell, M., and Haden, V. R. (2013). Perceptions and responses to climate policy risks among California farmers. *Glob. Environ. Change* 23, 1752–1760. doi: 10.1016/j.gloenvcha.2013.08.005
- Obayelu, O. A., Adepoju, A. O., and Idowu, T. (2014). Factors influencing farmers' choices of adaptation to climate change in Ekiti State, Nigeria. *J. Agric. Environ. Int. Dev.* 108, 3–16. doi: 10.12895/jaied.20141.140

- Ogunbode, C. A., Demski, C., Capstick, S. B., and Sposato, R. G. (2019). Attribution matters: revisiting the link between extreme weather experience and climate change mitigation responses. *Glob. Environ. Change* 54, 31–39. doi: 10.1016/j.gloenvcha.2018.11.005
- Ou, X. O. (2003). *Research on Agricultural Land Use and Land Conversion in Huaihua City*. Dissertation. Changsha: Hunan Normal University.
- Pahl, S., Sheppard, S., Boomsma, C., and Groves, C. (2014). Perceptions of time in relation to climate change. *Wiley Interdiscip. Rev. Clim. Change* 5, 375–388. doi: 10.1002/wcc.272
- Peng, D. Y. (2012). The cooperative nature of Chinese farmers – with comments on Professor Cao Jinqing's opinion. *Rural Discov. China* 3:5.
- Phuong, L. T. H., Biesbroek, G. R., Sen, L. T. H., and Wals, A. E. (2018a). Understanding smallholder farmers' capacity to respond to climate change in a coastal community in Central Vietnam. *Clim. Dev.* 10, 701–716. doi: 10.1080/17565529.2017.1411240
- Phuong, L. T. H., Wals, A., Sen, L. T. H., Hoa, N. Q., Van Lu, P., and Biesbroek, R. (2018b). Using a social learning configuration to increase Vietnamese smallholder farmers' adaptive capacity to respond to climate change. *Local Environ.* 23, 879–897. doi: 10.1080/13549839.2018.1482859
- Pielke, R. Jr., Burgess, M. G., and Ritchie, J. (2022). Plausible 2005–2050 emissions scenarios project between 2° C and 3° C of warming by 2100. *Environ. Res. Lett.* 17:024027. doi: 10.1088/1748-9326/ac4ebf
- Rayamajhee, V., Guo, W., and Bohara, A. K. (2021). The perception of climate change and the demand for weather-index microinsurance: evidence from a contingent valuation survey in Nepal. *Clim. Dev.* 14, 557–570. doi: 10.1080/17565529.2021.1949574
- Rozaki, Z., Wijaya, O., Rahmawati, N., and Rahayu, L. (2021). Farmers' disaster mitigation strategies in Indonesia. *Rev. Agric. Sci.* 9, 178–194. doi: 10.7831/ras.9.0_178
- Shi, X. M. (2016). Research progress on public perception of climate change and adaptive behavior. *Bull. Soil Water Conserv.* 36:8.
- Spence, A., Poortinga, W., and Pidgeon, N. (2012). The psychological distance of climate change. *Risk Anal. Int. J.* 32, 957–972. doi: 10.1111/j.1539-6924.2011.01695.x
- Sun, S., Li, D., Liu, L. L., Wang, Z. Y., and Yin, Y. Z. (2017). Global major synoptic and climatic events in 2016 and their causes. *Meteorol. Mthly* 43, 477–485.
- Thinda, K. T., Ogundeji, A. A., Belle, J. A., and Ojo, T. O. (2020). Understanding the adoption of climate change adaptation strategies among smallholder farmers: evidence from land reform beneficiaries in South Africa. *Land Use Policy* 99:104858. doi: 10.1016/j.landusepol.2020.104858
- Trope, Y., and Liberman, N. (2010). Construal-level theory of psychological distance. *Psychol. Rev.* 117, 440–463. doi: 10.1037/a0020319
- Waldman, K. B., Blekking, J. P., Attari, S. Z., and Evans, T. P. (2017). Maize seed choice and perceptions of climate variability among smallholder farmers. *Glob. Environ. Change* 47, 51–63. doi: 10.1016/j.gloenvcha.2017.09.007
- Wang, C. Y., and Yu, Y. C. (2015). Spatial-temporal variation of people's perception of climate change in southern Shaanxi. *Chinese Agric. Sci. Bull.* 31, 244–251.
- Wang, J., Mendelsohn, R., Dinar, A., and Huang, J. (2010). How Chinese farmers change crop choice to adapt to climate change. *Clim. Change Econ.* 1, 167–185. doi: 10.1142/S2010007810000133
- Wang, Y. J., Zhou, B. T., Ren, Y. Y., and Sun, C. H. (2016). Impacts of global climate change on China's climate security. *J. Appl. Meteorol.* 27, 750–758.
- Wheeler, S. A., Nauges, C., and Zuo, A. (2021). How stable are Australian farmers' climate change risk perceptions? New evidence of the feedback loop between risk perceptions and behaviour. *Glob. Environ. Change* 68:102274. doi: 10.1016/j.gloenvcha.2021.102274
- Wood, S. A., Jina, A. S., Jain, M., Kristjanson, P., and DeFries, R. S. (2014). Smallholder farmer cropping decisions related to climate variability across multiple regions. *Glob. Environ. Change* 25, 163–172. doi: 10.1016/j.gloenvcha.2013.12.011
- Xu, B., Li, X. H., and Xue, Y. T. (2019). Drought disaster risk analysis and zoning in Sichuan Province. *Climate Change Res. Lett.* 8:571.
- Xu, X. X., Yu, J., and Lei, X. (2015). Cognitive processing components of imagining the future and their brain networks. *Adv. Psychol. Sci.* 23:394.
- Yu, Y. C., Zhou, Q., and Wang, C. Y. (2011). Spatial-temporal variation of public perception of climate change in Northern Shaanxi Province. *J. Northwest Univ.* 41, 134–138.
- Zhang, F., Yushanjiang, A., and Jing, Y. (2019). Assessing and predicting changes of the ecosystem service values based on land use/cover change in Ebinur Lake Wetland National Nature Reserve, Xinjiang, China. *Sci. Total Environ.* 656, 1133–1144. doi: 10.1016/j.scitotenv.2018.11.444
- Zhang, W. J., Yan, S. J., Zhang, J., Jiang, Y., and Deng, A. X. (2021). Win-win strategy of national food security and agricultural dual carbon goals. *Sci. Agric. Sin.* 54, 3892–3902.
- Zhang, Y. S., Wu, D. T., and Lv, X. (2020). Effects of land use/cover change on ecosystem services: a review from a spatial perspective. *J. Nat. Resour.* 35, 1172–1189.
- Zhao, X. Y. (2014). Review of research on farmers' perception and adaptation to climate change. *Chinese J. Appl. Ecol.* 25, 2440–2448.
- Zorrilla-Miras, P., Palomo, I., Gómez-Baggethun, E., Martín-López, B., Lomas, P. L., and Montes, C. (2014). Effects of land-use change on wetland ecosystem services: a case study in the Doñana marshes (SW Spain). *Landsc. Urban Plann.* 122, 160–174. doi: 10.1016/j.landurbplan.2013.09.013



OPEN ACCESS

EDITED BY

Haijun Deng,
Fujian Normal University, China

REVIEWED BY

Shuhua Zhang,
Xi'an University of Science and
Technology, China
Andrea Santos,
Federal University of Rio de Janeiro,
Brazil

*CORRESPONDENCE

Ilan Stavi,
istavi@adssc.org

SPECIALTY SECTION

This article was submitted to
Interdisciplinary Climate Studies,
a section of the journal
Frontiers in Environmental Science

RECEIVED 21 July 2022

ACCEPTED 06 September 2022

PUBLISHED 26 September 2022

CITATION

Stavi I (2022), Rio (1992) to Glasgow
(2021): Three decades of inadequate
mitigation of climate change and its
slow onset effects.
Front. Environ. Sci. 10:999788.
doi: 10.3389/fenvs.2022.999788

COPYRIGHT

© 2022 Stavi. This is an open-access
article distributed under the terms of the
[Creative Commons Attribution License](#)
(CC BY). The use, distribution or
reproduction in other forums is
permitted, provided the original
author(s) and the copyright owner(s) are
credited and that the original
publication in this journal is cited, in
accordance with accepted academic
practice. No use, distribution or
reproduction is permitted which does
not comply with these terms.

Rio (1992) to Glasgow (2021): Three decades of inadequate mitigation of climate change and its slow onset effects

Ilan Stavi^{1,2*}

¹Dead Sea and Arava Science Center, Yotvata, Israel, ²Eilat Campus, Ben-Gurion University of the
Negev, Eilat, Israel

This study reviews the global increase in atmospheric greenhouse gas (GHG) concentrations, including carbon dioxide (CO₂), methane (CH₄), and nitrous oxide (N₂O), alongside the accelerated climatic change and its slow onset effects (or events) between 1992 and 2021. The establishment of the United Nations Framework Convention on Climate Change (UNFCCC) in 1992, and the simultaneous UN Earth Summit in Rio de Janeiro, generated the international efforts to tackle climatic change. Over the years, the UNFCCC-Conference of the Parties (COP) has led the efforts in climate change mitigation and adaptation, with many sequential meetings across the world. Three decades later, at the COP26 meeting in Glasgow in 2021, it is evident that climate change impacts have substantially worsened. Despite some uncertainties, it seems that over the last three decades, the climate change slow onset events, including 1) increasing temperatures, 2) glacial retreat, 3) sea level rise, 4) ocean acidification, 5) soil salinization, 6) land and forest degradation, 7) loss of biodiversity, and 8) desertification, have substantially exacerbated. Simultaneously, other (non-GHGs related) anthropogenic impacts, including habitat fragmentation, land-use and sea-use change and misuse, species overexploitation, environmental pollution, infrastructure constructions, and urbanization, have considerably increased. With the aim of achieving the Shared Socio-Economic Pathways 1.9 (SSP1-1.9) or SSP1-2.6 ultimate goals—keeping global warming in 2,100 below 1.5°C or 2.0°C, respectively, compared to preindustrial levels—it may still be possible to avoid climate change's irreversible tipping points. To reach this target, policymaking must become more decisive and proactive, with continuous risks assessment, frequent monitoring of outcomes and their compatibility to goals, implementing practical legislation tools, and assigning specific financial instruments, aimed at effectively tackling climate change slow onset events and related environmental issues. Substantial efforts should be invested in boosting climate change mitigation, while simultaneously targeting effective climatic change adaptation measures and promoting environmental conservation and restoration. Relying on tools such as the UN Sustainable Development Goals (SDGs) will sustain provisioning, supporting, regulating, and cultural ecosystem services, thus improving water-, food-, environmental-, energy-, economic-, health-, and governance-security, while lessening the

risks of social unrest, violent conflicts, mass migration, and other humanitarian catastrophes.

KEYWORDS

climatic change feedbacks, coral bleaching, deforestation, global warming, mountain glacier, rainstorms and floods, Representative concentration pathway (RCP), Small island developing states (SIDS)

Introduction

The United Nations Framework Convention on Climate Change (UNFCCC)—predesigned in the late 1980s, and officially established in 1992—provided the foundation for intergovernmental efforts to address the responsibility of humankind for the increased emission of greenhouse gases (GHGs) (Climate Change Secretariat, 2002). Specifically, the Convention was aimed at promoting an international environmental treaty for combating climate change and its worldwide adverse impacts on natural and managed ecosystems, as well as on human health and welfare. The Convention acknowledged that per capita emissions are substantially greater in developed countries than in developing ones, but that the share of emissions from the developing countries is expected to grow to meet their social, economic, and developmental needs. Thus, the Convention called for ‘cooperation by all countries and their participation in effective international response, in accordance with their common but differentiated responsibilities and respective capabilities, as well as with their social and economic conditions’ (UNFCCC, 1992).

The simultaneous establishment of Conference of the Parties (COP) as the supreme body of the UNFCCC provided the Convention with administrative instruments for stabilizing atmospheric GHG concentrations, and with the timeframe for its implementation (Climate Change Secretariat, 2002). It was declared that ‘the Parties should protect the climate system for the benefit of present and future generations, and on the basis of equity. Accordingly, the developed country Parties should take the lead in combating climate change and its adverse impacts’. Further, in terms of adaptation actions, it was declared that priority should be given to developing country Parties that are particularly vulnerable to adverse impacts of climate change, such as small island countries, low-lying coastal countries, dryland countries, etc. Article seven in the treaty details the COP’s responsibilities, among which is the periodic examination of ‘obligations of the Parties and the institutional arrangements under the Convention ... review reports submitted by its subsidiary bodies and provide guidance to them’, and set up ‘ordinary sessions of the COP every year’ (UNFCCC, 1992).

Although the first COP meeting (COP1) was held in 1995 (in Berlin) (UNFCCC, 1995), it is a direct outcome of the UN Earth Summit (also known as the UN Conference on Environment and Development) held in 1992 in Rio de Janeiro, which addressed

climatic change and related challenges, including increasing temperatures and decreasing precipitations, sea level rise, ocean acidification, soil salinization, land degradation and desertification, forest and biodiversity loss, and other environmental issues (UN, 1993). Since then, and over three decades, many additional COP meetings were held (Table 1). Among the earlier meetings, the Kyoto Conference 1997 is particularly remarkable as it led to the publishing of the Kyoto Protocol, which states specific and measurable actions to be taken by the Parties. Among these actions, the requirement to reduce global GHG emissions by at least 5% in the commitment period between 2008 and 2012, is probably the most ambitious (UN, 1998). Among the later meetings, the Paris Conference (2015) is a prominent landmark due to the resulting Paris Agreement, with the specific call for limiting global warming to 1.5–2.0°C compared to pre-industrial levels. Four years later, in 2019, a voluntary initiative of the COP26 Universities Network—a group of over 80 United Kingdom universities and research centers—was established, aimed at promoting the goal of ‘net zero emissions’ (also named as ‘carbon neutrality’) by 2050 (Reid and Wood, 2021).

However, despite these meetings, decisions, and recommendations, global GHG emissions have continued to rise over time, continuously breaking records of atmospheric concentrations of the major GHGs—including carbon dioxide (CO₂; Figure 1A), methane (CH₄; Figure 1B), and nitrous oxide (N₂O; Figure 1C). Among the GHGs, CO₂ is the most widespread, and its main anthropogenic sources are related to land-use change, deforestation, and burning of fossil fuels (Harper et al., 2018). The main anthropogenic sources of CH₄ are enteric fermentation by ruminant livestock animals, as well as rice paddies and landfills. The global warming potential (GWP) of CH₄ is 28 times greater than that of CO₂ (Lin et al., 2021). The main anthropogenic source of N₂O is the excess use of nitrogen (N) fertilizer in agricultural lands. The GWP of N₂O is ~300 times greater than that of CO₂ (Wang et al., 2021).

Concordant with the soaring atmospheric GHG concentrations, climate change, expressed by extreme weather events and abrupt interruptions of climatic patterns, including severe and consecutive droughts on the one hand, and harsh rainstorms and devastating floods on the other hand, have become the new ‘normal’ weather regime (Bowen, 2015). The biophysical effects of climate change are various, and occur over a wide range of temporal scales. Among these, eight effects that

TABLE 1 The United Nations Framework Convention on Climate Change (UNFCCC) Conference of the Parties (COPs)' meeting history.

Meeting name/#	Year	Location	Extraordinary outcomes
The Earth Summit	1992	Rio de Janeiro	First official addressing of climate change
COP1	1995	Berlin	
COP2	1996	Geneva	Kyoto Protocol
COP3	1997	Kyoto	
COP4	1998	Buenos Aires	
COP5	1999	Bonn	
COP6	2000	Hague	
COP6-2	2001	Bonn	
COP7	2001	Marrakesh	
COP8	2002	New Delhi	
COP9	2003	Milan	
COP10	2004	Buenos Aires	
COP11	2005	Montreal	Paris Agreement
COP12	2006	Nairobi	
COP13	2007	Bali	
COP14	2008	Poznań	
COP15	2009	Copenhagen	
COP16	2010	Cancún	
COP17	2011	Durban	
COP18	2012	Doha	
COP19	2013	Warsaw	
COP20	2014	Lima	
COP21	2015	Paris	
COP22	2016	Marrakesh	
COP23	2017	Bonn	
COP24	2018	Katowice	
COP25	2019	Madrid	
COP26	2021	Glasgow	
COP27 ^a	2022	Sharm El-Sheikh	
COP28 ^a	2023	Abu Dhabi	

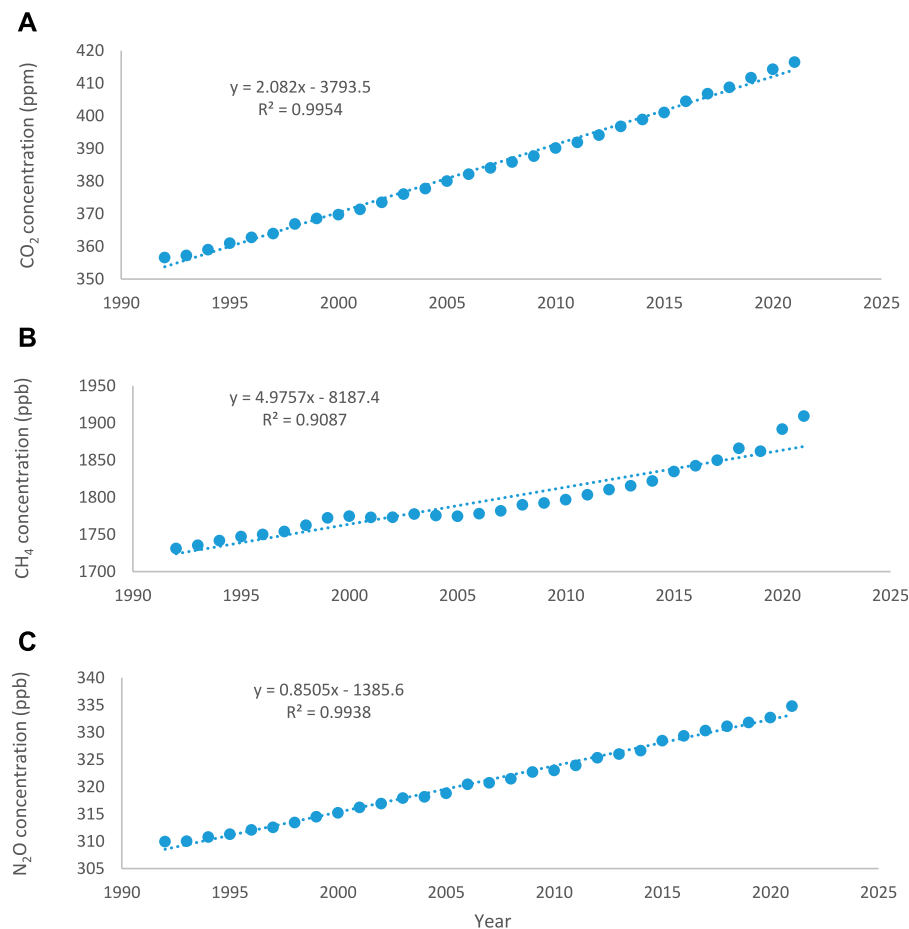
^aplanned.

take place over relatively long timeframes have been termed by the UNFCCC as 'slow onset effects' (or 'slow onset events'). These events include 1) increasing temperatures, 2) glacial retreat, 3) sea level rise, 4) ocean acidification, 5) soil salinization, 6) land and forest degradation, 7) loss of biodiversity, and 8) desertification (UNFCCC, 2012). The objective of this synthesis study is to concisely review the sequential trends caused by the slow onset events over the last three decades (1992–2021), as well as some of the most influential consequences for future life on Earth. As shown throughout this synthesis, failure to halt the accelerating increase in atmospheric GHG concentrations and the consequent abrupt climatic change over this timeframe have exacerbated the slow onset events, risking biophysical quality of terrestrial and marine ecosystems, and jeopardizing ecosystem services. However, beyond the climate change related slow onset events, other (non-GHGs related), direct anthropogenic

impacts—including habitat fragmentation, land- (and sea-) use change and misuse, environmental pollution, and species overexploitation, alongside mineral mining and quarrying, infrastructure construction, and urbanization—have amplified some of these events throughout the last three decades. Further, the net effect of some of these direct anthropogenic impacts may exceed the effects of climate change, substantially modifying the Earth's biophysical environment and degrading ecosystem services. These direct anthropogenic impacts are concisely discussed, emphasizing their potential consequences for global sustainability.

Increasing temperatures

Radiative forcing, in which the mix of gases in the atmosphere retains some of the solar energy from reflection

**FIGURE 1**

Changes in atmospheric concentrations of carbon dioxide (CO₂: **(A)**), methane (CH₄: **(B)**), and nitrous oxide (N₂O: **(C)**) between 1992 and 2021. Data source: <https://www.statista.com/statistics/1091926/atmospheric-concentration-of-co2-historic/> (**(A)**); [https://www.eea.europa.eu/data-and-maps/s/daviz/atmospheric-concentration-of-carbon-dioxide-5#tab-chart_5_filters=%7B%22rowFilters%22%3A%7B%7D%3B%22columnFilters%22%3A%7B%22pre_config_polutant%22%3A%5B%22CH4%20\(ppb\)%22%5D%7D%7D](https://www.eea.europa.eu/data-and-maps/s/daviz/atmospheric-concentration-of-carbon-dioxide-5#tab-chart_5_filters=%7B%22rowFilters%22%3A%7B%7D%3B%22columnFilters%22%3A%7B%22pre_config_polutant%22%3A%5B%22CH4%20(ppb)%22%5D%7D%7D) (**(B)**); [https://www.eea.europa.eu/data-and-maps/s/daviz/atmospheric-concentration-of-carbon-dioxide-5#tab-chart_5_filters=%7B%22rowFilters%22%3A%7B%7D%3B%22columnFilters%22%3A%7B%22pre_config_polutant%22%3A%5B%22N2O%20\(ppb\)%22%5D%7D%7D](https://www.eea.europa.eu/data-and-maps/s/daviz/atmospheric-concentration-of-carbon-dioxide-5#tab-chart_5_filters=%7B%22rowFilters%22%3A%7B%7D%3B%22columnFilters%22%3A%7B%22pre_config_polutant%22%3A%5B%22N2O%20(ppb)%22%5D%7D%7D) (**(C)**).

on Earth, is a natural process that enables life on Earth. However, elevated GHG concentrations in the atmosphere causes the energy imbalance (Wigley, 2021). Sequential data obtained by the National Oceanic and Atmospheric Administration (NOAA) clearly demonstrate the increased radiative forcing by CO₂, CH₄, N₂O, as well as their total radiative forcing between 1992 and 2019 (Figure 2A). The term Equilibrium Climate Sensitivity was coined to assist in estimating the climatic response to radiative forcing, aimed at avoiding climatic irreversible tipping points, and particularly negating temperature rise beyond a certain level (IPCC, 2014; IPCC 2021).

Specifically, compared to preindustrial level (the 1850–1900 baseline), the global surface temperature average over 2081–2,100 is projected to be higher by 1.0–1.8°C (1.5°C on average) under the very low GHG emissions scenario (“Taking

the green road 1st: coded as the Shared Socioeconomic Pathways (SSP)1–1.9, or as the Representative Concentration Pathway (RCP)1.9 (where the 1.9 represents the end-of-century radiative forcing of 1.9 W m^{−2}). At the same time, the low GHG emissions scenario (“Taking the green road 2nd: SSP1–2.6, or RCP2.6) will cause global warming of up to 2.0°C. Further, the intermediate GHG emissions scenario (“Middle of the road”: SSP2–4.5, or RCP4.5) is anticipated to cause temperature increase by 2.1–3.5°C, whereas the high GHG emissions scenario (“A road divided”: SSP3–7.0, or RCP7.0) is expected to increase temperature by 2.8–4.6°C, and the very high GHG emissions scenario (“Taking the highway”: SSP5–8.5, or RCP8.5) is forecasted to increase temperature by 3.3–5.7°C (IPCC, 2021). Regardless, it is acknowledged that global warming highly varies across the globe. For example, the average temperature of the

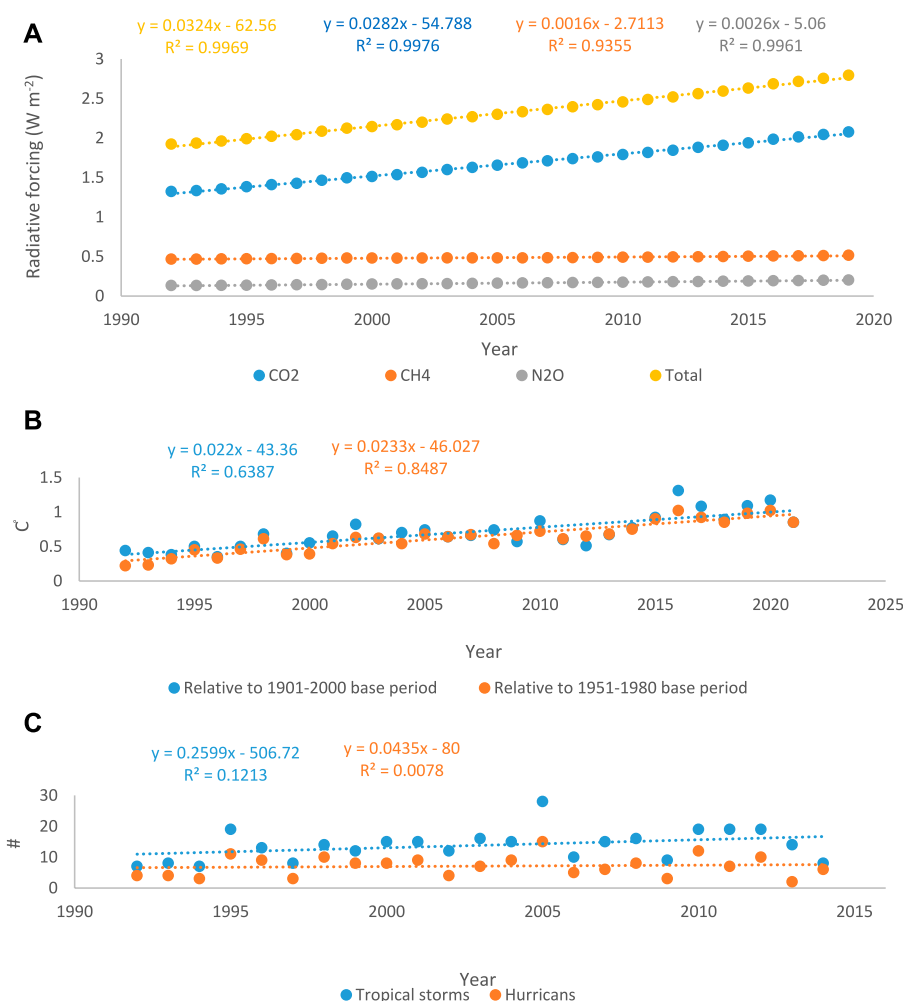


FIGURE 2

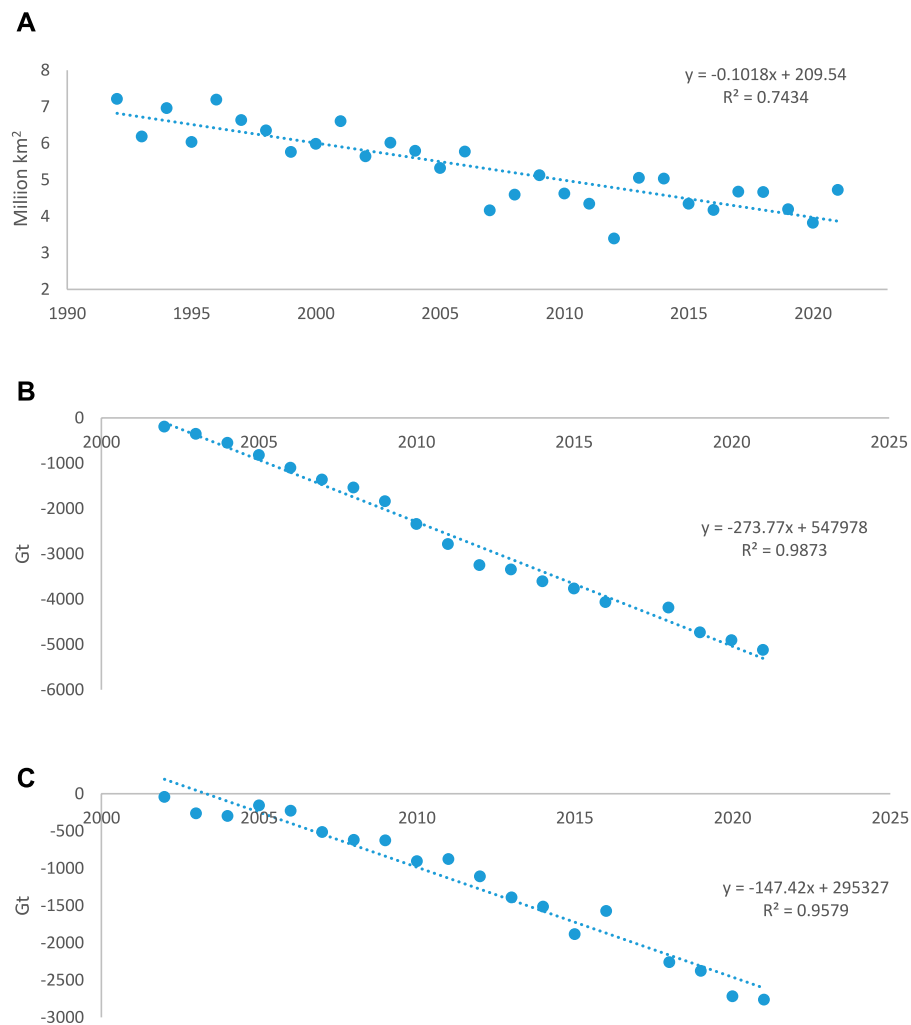
Changes in radiative forcing imposed by carbon dioxide (CO₂), methane (CH₄), and nitrous oxide (N₂O), as well as total radiative forcing, between 1992 and 2019 (A); global temperature anomalies relative to the 1901–2000 and 1951–1980 base periods (B); the number of tropical storms and hurricanes per year, at a global scale, between 1992 and 2014 (C). Data source: NOAA (National Oceanic and Atmospheric Administration). 2020. The NOAA Annual Greenhouse Gas Index. www.esrl.noaa.gov/gmd/aggi (A); Data source for the 1901–2000 base period: <https://www.ncdc.noaa.gov/cag/global/time-series>; data source for the 1951–1980 base period: <https://climate.nasa.gov/vital-signs/global-temperature/> (B); <https://www.nhc.noaa.gov/climo/images/AtlanticStormTotalsTable.pdf> (C).

coldest days in the Arctic region is projected to increase by about three times the global average increase (IPCC, 2021), while in the Mediterranean, mean temperatures in the coming decades are forecasted to be 20% warmer than the global average (Lionello and Scarascia, 2018).

Overall, global warming during the last three decades is evident when addressing temperature anomalies. Data obtained by NOAA and the National Aeronautics and Space Administration (NASA) show an increasing trend of global temperature between 1992 and 2021 relative to baselines of both 1901–2000 and 1951–1980 (Figure 2B). Further, of the 10 warmest years between 1880 and 2020, eight were in the second decade of the 21st century. The other two warmest years

were 2005 and 2010 (<https://www.ncei.noaa.gov/access/monitoring/monthly-report/global/202013>).

Specifically, increasing global temperatures warm ocean water and elevate oceanic evaporation, therefore interrupting the natural water cycle (Collins et al., 2013), and increasing the frequency and magnitude of extreme climatic events, such as major (category 3–5) tropical cyclones (IPCC, 2021; Bloemendaal et al., 2022). At the same time, there is uncertainty regarding long-term trends of all (including both ‘normal’ and major) Atlantic hurricanes and tropical cyclones (IPCC, 2021). To some extent, this concurs with data obtained by NOAA, demonstrating a slight and non-significant increase in total number of tropical storms and

**FIGURE 3**

Change in Arctic sea ice cover (in September) between 1992 and 2021 (A); Greenland ice sheet cumulative mass variation between 2002 and 2021 (B); Antarctica ice sheet cumulative mass variation between 2002 and 2021 (C). Data source: <https://climate.nasa.gov/vital-signs/arctic-sea-ice/> (A); <https://climate.nasa.gov/vital-signs/ice-sheets/> (B,C).

hurricanes per year between 1992 and 2014 (Figure 2C). It was suggested that the long-term trend toward more high-end rapid intensification (24-h intensification events of ≥ 50 kt day⁻¹) of tropical cyclones is somewhat muted by the simultaneous trend toward La Niña-like climatic conditions, increasing cyclone activity over the north Atlantic while decreasing it over the north and south Pacific (Klotzbach et al., 2022). One way or another, rising global temperatures have caused monsoon activity to increase since the 1980s over West Africa (IPCC, 2021).

Increased water-loss from terrestrial water bodies by evaporation is an additional important direct effect of elevated temperatures on the biophysical environment (Xia et al., 2022). Another prominent direct effect is higher soil-water evaporation,

which has resulted in long-term and severe ecological and agricultural stress, reducing the soil's capacity to support primary productivity (Dolschak et al., 2019; IPCC, 2021). The resulting mass mortality of vegetation, and the consequent decreased plant cover, is expected to cause the aggravation of sand- and dust-storms (ESCAP, 2018). Overall, the increased evaporation losses impact natural biogeochemical cycles and adversely affect a wide range of ecosystem services and functions (Mooney et al., 2009). Further, the increasing temperatures are projected to accelerate permafrost thawing in high latitudes (IPCC, 2021). Due to the massive stores of organic carbon locked in permafrost, thawing triggers extensive microbial breakdown of carbon into CO₂ and CH₄ that are released to the atmosphere, generating a positive feedback

with climate change (Schuur et al., 2015). The combined effect of the increasing temperatures degrades ecological and environmental quality, deteriorating water-, food-, economic-, and health-security for extensive human populations, resulting in generation and exacerbation of humanitarian catastrophes across the globe (Stavi et al., 2021a).

Glacial retreat

Net loss of glacier cover has been mostly substantial for the northern hemisphere. Across the Arctic sea ice region, glacier cover has substantially decreased. Between 2011 and 2020, annual average cover of Arctic sea ice reached its lowest level since at least 1850. Compared to the 1979–1988 timeframe, glacier cover in 2010–2019 across this region has decreased by 40% in September (when Arctic sea ice reaches its minimum) and by 10% in March (IPCC, 2021). September Arctic sea ice is declining at a rate of 13% per decade relative to the 1981–2010 average (Figure 3A). Over the past two decades, a substantial decrease in ice sheet mass was also observed for Greenland (Figure 3B). According to a recently published long-term study, the loss of Greenland's ice sheet increased from $41 \pm 17 \text{ Gt yr}^{-1}$ in 1990–2000 to $187 \pm 17 \text{ Gt yr}^{-1}$ in 2000–2010 and to $286 \pm 20 \text{ Gt yr}^{-1}$ in 2010–2018. However, due to a series of cold summers, the acceleration trend in ice sheet loss shifted from positive in 2000–2010 to negative in 2010–2018 (Mouginot et al., 2019).

While there is a consensus regarding the tremendous decline in northern glaciers and ice sheets, it seems that glacier and ice trends in the southern polar region are somewhat controversial. In a recent summary for policymakers by the Intergovernmental Panel on Climate Change (IPCC), it was stated that due to opposing impacts and substantial variability across the Antarctic sea ice over the past decades, the trend in ice sheet and glacier cover is not clear (IPCC, 2021). At the same time, NASA shows a clear decrease in Antarctica's ice sheet mass over the last two decades (Figure 3C). This trend is consistent with a recent long-term study, which revealed that Antarctica's ice sheet mass loss increased from $50 \pm 14 \text{ Gt yr}^{-1}$ in 1989–2000 to $166 \pm 18 \text{ Gt yr}^{-1}$ in 1999–2009 and to $252 \pm 26 \text{ Gt yr}^{-1}$ in 2009–2017. To some extent, this controversy could be attributed to local variability in surficial conditions and the resulting glacial processes (Rignot et al., 2019). At a finer resolution, this controversy is exemplified by Zhang et al. (2020), who recorded that the ice sheet volume of west Antarctica declined while it increased in east Antarctica during the years 2002–2019. For the very same timeframe, Zhang and others found a net loss of $68.7 \pm 8.1 \text{ km}^3 \text{ yr}^{-1}$ of Antarctic ice sheet volume, and an acceleration loss rate of $5.5 \pm 0.9 \text{ km}^3 \text{ yr}^{-2}$.

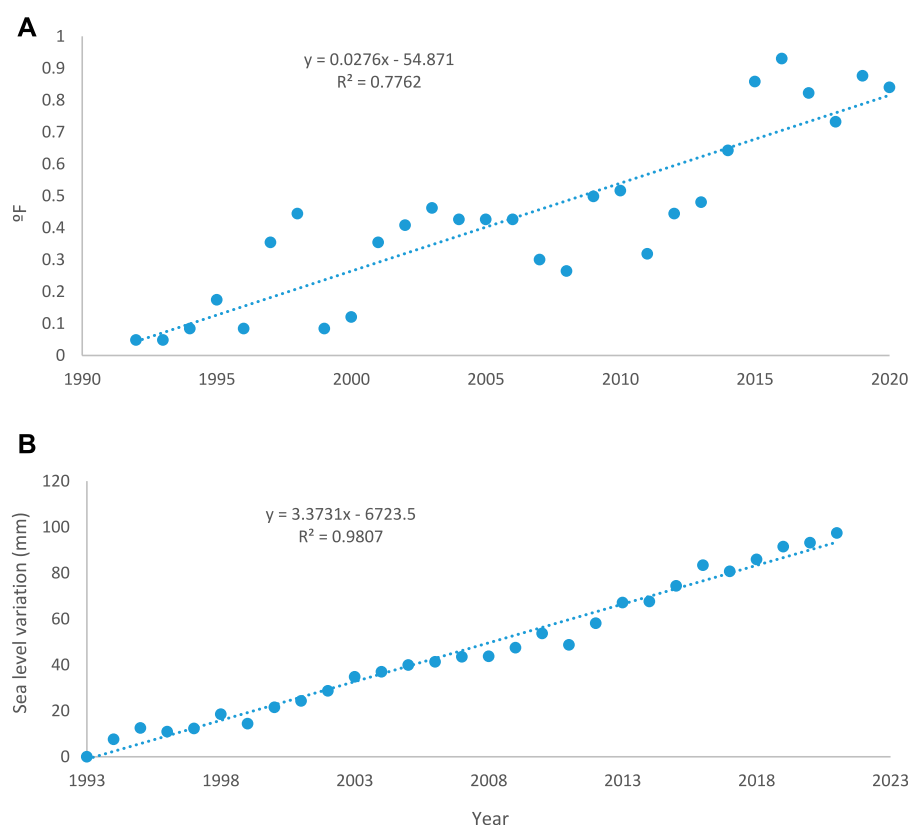
A recent review study showed that between 1994 and 2017, Earth lost 28 trillion tonnes of ice, including 7.6 trillion tonnes

from the Arctic sea ice, 6.5 trillion tonnes from Antarctic ice shelves, 6.1 trillion tonnes from mountain glaciers, 3.8 trillion tonnes from the Greenland ice sheet, 2.5 trillion tonnes from the Antarctic ice sheet, and 0.9 trillion tonnes from the Southern Ocean sea ice. Of these, 58% of the ice loss was from the Northern Hemisphere, and 42% from the Southern Hemisphere. According to the same study, since the 1990s, the rate of ice loss has increased by 50%—from 0.8 to 1.2 trillion tonnes per year (Slater et al., 2021).

Among the mountain glaciers, those in the Central Asian corridors—such as the Tien Shan, Pamir, Karakoram, and Himalaya—are of specific interest. Substantial changes in these glaciers' mass have been reported for the last decades and are also forecasted for the coming decades. These changes are attributed to latitudinal, altitudinal, topographic, and geologic conditions, as well as to glacier type and properties (Chen et al., 2016; Li et al., 2016; Shahgedanova et al., 2020). Yet, an overall negative mass balance—both for the past and future—has been reported/forecasted for most Central Asian glaciers (Chen et al., 2016; Li et al., 2016; Pohl et al., 2017; Bolch et al., 2022). In humanitarian terms, the receding Central Asian glaciers directly impact the living conditions of large rural populations, which are already vulnerable and often impoverished, and generally lack the financial or political capacity to overcome the changing environmental conditions (USAID, 2018). The most direct forecasted effect is the decrease in glacier-fed streamflow, reducing the availability of fresh water for domestic use and agricultural irrigation by local populations, adversely affecting their water-, food-, and economic-security (Stavi et al., 2021a). In addition, hydropower generation, which relies on glacial water flow, is also expected to substantially decrease, adversely impacting energy security for these populations (USAID, 2018).

Sea level rise

Global sea level rise is attributed to the simultaneous impacts of melting glaciers and ice sheets, and the thermal expansion of the oceans' water. Globally, thermal expansion was responsible for 50% of sea level rise between 1971 and 2018, while the remainder is attributed to melting glaciers and ice sheets (IPCC, 2021). Oceans' water thermal expansion is attributed to the increase in water temperature. Data obtained by NASA shows an increasing trend in global sea surface temperature anomaly (between 1992 and 2020: Figure 4A), and a corresponding sea level rise (between 1993 and 2021: Figure 4B). Relative to the 1995–2014 baseline, the likely global mean sea level rise by 2100 is 0.28–0.55 m under the very low GHG emissions scenario (SSP1-1.9/RCP1.9), 0.32–0.62 m under the low GHG emissions scenario (SSP1-2.6/RCP2.6), 0.44–0.76 m under the intermediate GHG emissions scenario (SSP2-4.5/RCP4.5), and 0.63–1.01 m under

**FIGURE 4**

Mean global sea surface temperature anomaly between 1992 and 2020, relative to the 1971–2000 baseline (A); mean change in sea level between 1993 and 2021 (B). Data source: https://www.epa.gov/sites/default/files/2021-04/sea-surface-temp_fig-1.csv; <https://www.epa.gov/climate-indicators/climate-change-indicators-sea-surface-temperature> (A); <https://climate.nasa.gov/vital-signs/sea-level/> (B).

the very high GHG emissions scenario (SSP5-8.5/RCP8.5) (IPCC, 2021).

Specifically, sea level rise risks coastal aquifers, increasing the probability of groundwater salinization and adversely affecting water security of extensive human populations around the world (Jasechko et al., 2020; IPCC, 2022a). Also, sea level rise is expected to increase the frequency and severity of coastal flooding in low-lying areas, and to intensify shoreline erosion along sandy coasts (IPCC, 2021). A particular adverse impact is the projected damages to shoreline infrastructures (IPCC, 2022a), and specifically to coastal cities that have expanded into areas previously uninhabited due to flood risk. Low-lying cities exist in some of the most populated countries, such as China, India, Bangladesh, several Southeastern Asian countries, as well as in some other parts of the world, and are expected to experience substantial inundation already in the mid-21st century (Jevrejeva et al., 2016).

Overall, it seems that flooding risks affect global populations disproportionately, as the relative contribution of developed countries to sea level rise is 64–69% greater than that of developing countries (updated data to 2005: Hardy and Nuse,

2016). Within the latter group of countries, a special focus on inequality should be put on Small Island Developing States (SIDS: Thomas et al., 2020), which encompass a total of 58 states across the Caribbean Sea, Atlantic Ocean, Indian Ocean, South China Sea, and the Pacific Ocean (UN-OHRLS, 2015). Altogether, the SIDS inhabit approximately 65 million people (approximately 0.8% of the ~8.0 billion global human population: Mead, 2021), while contributing less than 1% of global GHG emissions, and yet, suffer the most from sea level rise (Thomas et al., 2020). The inherent physical features of SIDS—small size and remoteness—make them highly susceptible to the influence of large-scale ocean-atmosphere interactions, such as trade winds, El Niño, monsoons, tropical cyclones, and hurricanes. In addition, many SIDS—among which are nine least developed countries (LDCs)—experience particular socio-economic hardships, which further aggravate their vulnerability. This includes small population size, high dependence on traditional economic sectors such as agriculture and fishery, and high public debt level (UN-OHRLS, 2015), as well as the concentration of large populations (of which one-third live on land less than 5 m

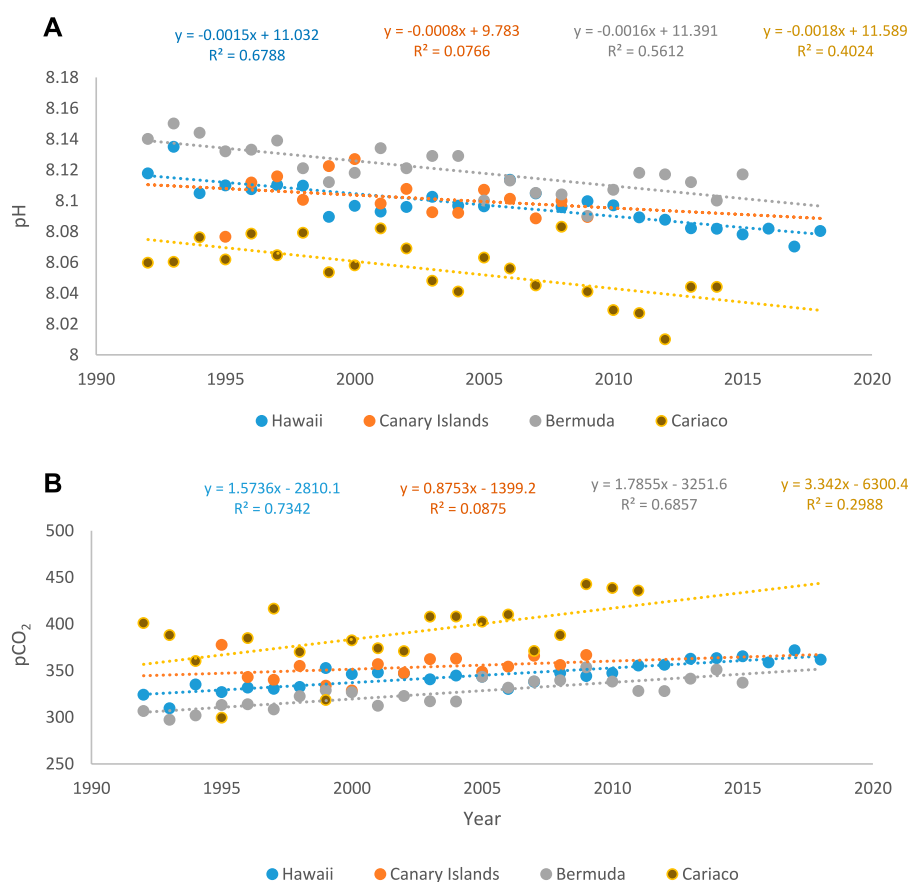


FIGURE 5

Mean change in ocean pH between 1992 and 2018 (A); mean change in ocean CO₂ partial pressure (pCO₂) between 1992 and 2018 (B). Data source: Bates, 2016; González-Dávila, 2012; University of South Florida, 2021; University of Hawaii, 2021; EPA's Climate Change Indicators in the United States: www.epa.gov/climate-indicators; <https://www.epa.gov/climate-indicators/climate-change-indicators-ocean-acidity>

above sea level), agricultural lands, and infrastructures in coastal zones. Altogether, these conditions exacerbate the susceptibility of SIDS to climate change, and worsen the water-, food-, environmental-, and economic-insecurity of their populations (Mead, 2021). In economic terms, the annual climate change-related loss of gross domestic product (GDP) in SIDS ranges between ~1.0 and 6.5%, as opposed to a world average of ~0.5% (UN-OHRLLS, 2015).

Sea level rise has already displaced people in a number of SIDS including Kiribati, Solomon Islands, the Marshall Islands, and the Federated States of Micronesia. Displacement of people from SIDS is expected to surge over the 21st century, as extensive lands in these islands will become inhabitable as a result of sea level rise (UN-OHRLLS, 2015). Indeed, SIDS are recognized as the most immediately vulnerable area to mass outmigration (Handmer and Nalau, 2019). The migrated and resettled SIDS' populations are likely to experience substantial changes in their social fabric, traditional culture, and lifestyle, with the

probable significant degradation in their economic security (UN-OHRLLS, 2015; Handmer and Nalau, 2019).

Ocean acidification

Acidification of oceans is a complex phenomenon in which several contributing factors together lower the pH of seawater. This phenomenon is predominated by atmospheric CO₂ incorporation in the seawater-pools of dissolved inorganic carbon, which originate from several oceanic biogeochemical cycles and sources (Mostofa et al., 2016). It is evident that during the last three decades ocean acidification has been substantial. Data obtained from the United States Environmental Protection Agency (EPA: www.epa.gov/climate-indicators/climate-change-indicators-ocean-acidity) for Hawaii (1992–2018), Bermuda (1992–2015), Cariaco (NE Venezuela: 1992–2014), and the Canary Islands (1995–2009), shows a trend of decreasing seawater pH for all sites (though not significantly so for the

latter) (Figure 5A). While the increase in acidification of oceans has been primarily attributed to the continuously rising atmospheric concentration of CO₂, the contribution of natural factors—including plant litter decomposition, volcanic eruptions, CO₂ emissions from freshwater sources, etc.—is also acknowledged (Mostofa et al., 2016). Regardless, oceans' elevated CO₂ (alongside higher seawater temperature) may increase primary productivity (a process known as the 'CO₂ fertilization effect') of specific marine species, partially offsetting the atmospheric concentration of this GHG (Holding et al., 2015). Yet, data obtained from the EPA's website demonstrate the increase in ocean CO₂ partial pressure (pCO₂) for each of the four sites over time (though not significantly so for the Canary Islands) (Figure 5B). Assessing the Pearson product-moment correlation coefficient between the ocean pCO₂ level and seawater pH reveals a negative and very strong correlation for Hawaii ($r = -0.9913$), the Canary Islands ($r = -0.9991$), and Bermuda ($r = -0.9800$), whilst a negative but only intermediately-strong correlation for Cariaco ($r = -0.4767$) (data for calculation of r values was obtained from: www.epa.gov/climate-indicators/climate-change-indicators-ocean-acidity).

In addition, anthropogenic emissions of nitrogen oxides (NO_x) and sulfur dioxide (SO₂) by industrial, transportation, and agricultural sectors, increase the acidity of aerosols that are then deposited in oceans, further elevating ocean acidity (Baker et al., 2021). Overall, ocean acidification causes substantial modifications in the seawater carbonate (CO₃²⁻) system, with simultaneous, complex impacts on its components. Calcifying organisms are specifically impacted, as the lower pH of seawater decreases calcification and growth rates of corals and other marine organisms (Mostofa et al., 2016), and dissolves their calcium carbonate (CaCO₃) structure. Specifically, in warm water, symbiosis between corals and the unicellular microalgae *Symbiodinium* genus may be interrupted, resulting in the loss of the characterizing brown symbionts and a subsequent paling of the coral host, a process known as bleaching. Coral bleaching at the scale of colonies or groups of colonies has been documented since the early 20th century. Yet, regional-scale mass bleaching was first reported in the early 1980s. It was suggested that oceans' rising temperature combined with increasing acidification accelerate coral mass bleaching (Hoegh-Guldberg et al., 2017).

Coral reefs support biodiversity and encompass habitats for rich wildlife. Once mass bleaching takes place, it degrades the resilience of reef ecosystems, eventually causing their collapse. Beyond the adverse effects on this supporting ecosystem service, mass bleaching is expected to adversely affect other services. Among the provisioning ecosystem services, fishery is the most obvious, providing vital nutrition to many coastal communities. Also, in some communities, such as the Solomon Islands, corals are harvested and used as a construction material. In terms of regulating services, the reefs protect shoreline areas from waves and extreme storms, thus lessen coastal erosion. Simultaneously, the reefs store carbon and enable the cycling of nutrients and

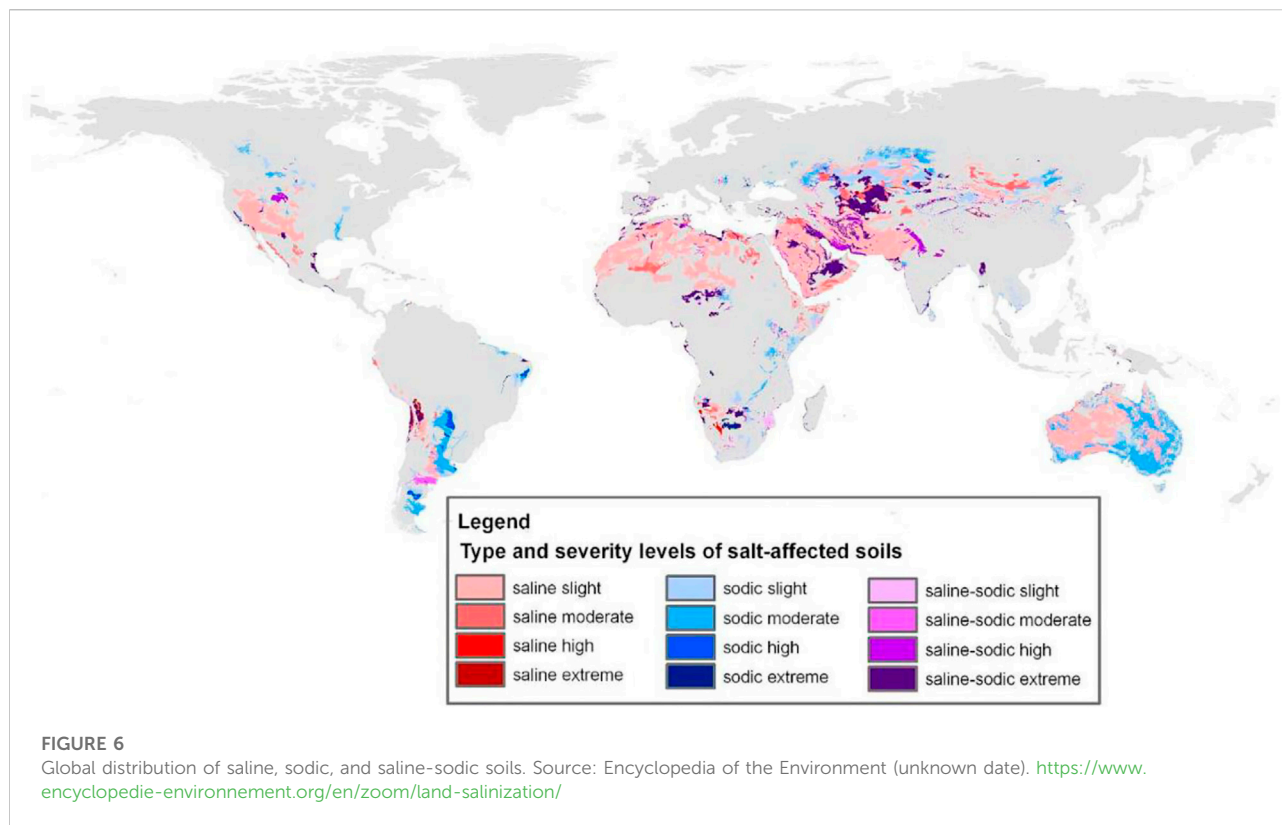
other elements. The most prominent cultural service is probably reef tourism, which has grown substantially over recent decades (UN-OHRLS, 2015; Woodhead et al., 2019). Obviously, the most adversely impacted human communities are those who reside in SIDS, where coral reefs encompass an important source for subsistence, fisheries, tourism, and shoreline protection. This risk seems to be particularly relevant for SIDS in the Pacific and Indian Oceans, where some of the SIDS have already lost 80% of their corals (UN-OHRLS, 2015). Under the SSP1-2.6/RCP2.6 GHG emissions scenario, global SIDS are projected to lose 70–90% of reef-building corals, while under the SSP2-4.5/RCP4.5 scenario and beyond, global SIDS may lose up to 99% of corals (IPCC, 2022b).

Soil salinization

Natural soil salinity is attributed to the prevailing geophysical conditions, and is known as primary salinization. These geophysical conditions include the parent material mineralogy, topography, and the water table properties. One of the major causes of primary salinization is chemical weathering of parent material, and the resulted release of cations (such as calcium (Ca²⁺), potassium (K⁺), magnesium (Mg²⁺), and sodium (Na⁺)) and anions (such as bicarbonates (HCO₃⁻), chloride (Cl⁻), and sulphate (SO₄²⁻)) to the soil solution. In saline soils, the salt content reduces the plants' water uptake capacity, decreases the availability of nutrients for vegetation, and imposes plant toxicity (Litalien and Zeeb, 2020; Stavi et al., 2021b). Salinity, measured in electrical conductivity (EC) of the soil solution, ranges from 0 to 2 dS m⁻¹ for non-saline, 2–4 dS m⁻¹ for slightly saline, 4–8 dS m⁻¹ for moderately saline, 8–16 dS m⁻¹ for strongly saline, and >16 dS m⁻¹ for very strongly saline soil (Salt Farm Foundation, 2018).

In humid regions, the dissolved ions are prone to leaching and transportation to surface or belowground waterbodies. However, in drylands, the soluble ions remain in the soil exchangeable complex, or precipitate as secondary minerals. This precipitation can occur when the ionic concentration in the soil solution reaches the saturation of a certain salt. Under certain conditions, Na⁺ ions may replace the precipitated less soluble salts in the exchange complex, a process known as primary sodification, which imposes high toxicity conditions for plants. Depending on the salt composition in the soil solution, primary salinization-sodification processes may also take place, characterized by EC value > 4 dS m⁻¹ (compared to EC < 4 in sodic soils) and pH value being usually <8.5 (compared to pH > 8.5 in sodic soils) (Stavi et al., 2021b). A specific type of soil salinization, termed as 'saline seep', occurs in recharge alluvial plains laying over shallow, salt-rich underground waterbodies (SDSU Extension, 2019).

Like in warm dryland regions, where high evaporation rates increase the salt concentration of the water solution (Stavi et al.,



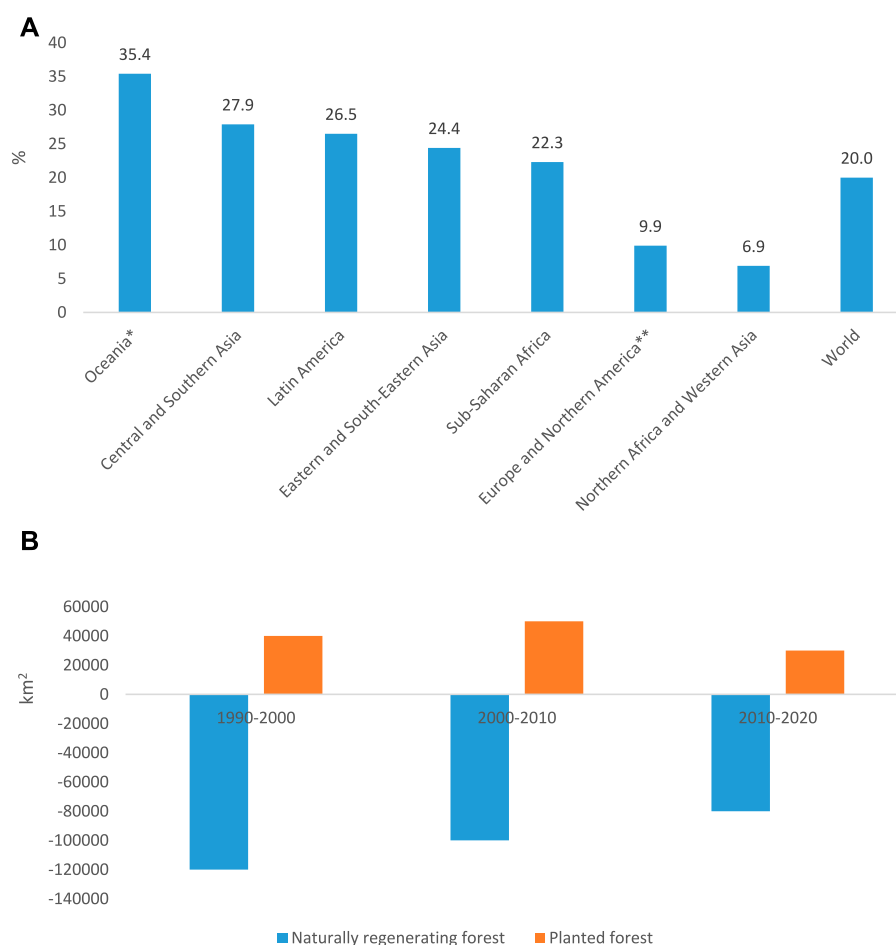
2021b), the global rising temperatures elevate evaporation rates, increasing the extent and severity of soil salinization. Additionally, the increase in frequency and magnitude of droughts across extensive parts of the world is further expected to accelerate the extent and severity of soil salinity (Bannari and Al-Ali, 2020). An additional primary salinity mechanism is related to aeolian salt deposition, in which salts originating in seawater are deposited—either by rainfall (wet deposition) or without rainfall (dry deposition)—up to several kilometres inland, causing salinization across extensive areas (Hassani et al., 2021). A specific primary salinity process in coastal areas that are prone to tides is caused by the intrusion of seawater into inland's surface- or underground-water bodies. For surface water bodies, this process is specifically prominent in river deltas. The extent and severity of this process are exacerbated by the rising sea level (Eslami et al., 2021).

Sometimes, it is not easy to distinguish between the site-specific share of anthropogenic vs natural causes of salinization. Yet, soil salinity, sodicity, and salinity-sodicity processes in non-agricultural lands are usually attributed to droughts and increasing temperatures, and therefore, are more related to 'natural' causes. At the same time, such processes taking place in agricultural lands, and specifically in irrigated croplands, are generally attributed to direct anthropogenic impacts, and are termed secondary salinization, secondary sodification, or secondary salinization-sodification (Stavi et al., 2021b). Time-

series databanks or exclusive maps for dynamics over time of naturally-vs anthropogenic-caused saline and sodic soils do not exist. Nevertheless, a recent study shows that global saline land area increased from slightly over 9 M km² in 1986 to over 10.5 M km² in 2016 (Ivushkin et al., 2019). Figure 6 demonstrates the global distribution of saline, sodic, and saline-sodic lands. A recent modeling study of future soil salinization dynamics until 2,100 identifies the drylands of Southwest United States, Central and South America, South Africa, and Australia as salinity hotspots, whilst forecasting a decrease in soil salinity in Northwest United States, Eastern Europe, western Central Asia, and the Horn of Africa (Hassani et al., 2021).

Land and forest degradation

Land degradation encompasses several processes that can take place separately, or in conjunction with others. The main processes of land (or soil) degradation are structure deformation, depleted organic carbon pool, biochemical deterioration (including nutrient depletion and acidification), salinization (and the related processes of sodification and combined salinization-sodification), and erosion by wind or water (Olsson et al., 2019). Climatic change is a major cause of land and soil degradation, with prominent impacts on each of the involved processes (Talukder et al., 2021). Further, oxidation of

**FIGURE 7**

Proportion of degraded land between 2000 and 2015 (%) **(A)**; global annual net change in area of naturally regenerating- and planted-forests, by decade, between 1990 and 2020 **(B)**. Notes: *Including Australia, New Zealand and Papua New Guinea, and excluding the islands of Oceania; **Excluding Switzerland and the United States; modified from: <https://unstats.un.org/sdgs/report/2019/goal-15/> **(A)**; modified from: <https://www.fao.org/forest-resources-assessment/2020/en/> **(B)**

soil organic carbon emits CO₂ to the atmosphere, turning soils from carbon-sinks to carbon-sources, and exacerbating climatic change feedbacks (Lal, 2010). Yet, it seems that the complex nature of land and soil degradation, as well as the difficulty in monitoring its spatiotemporal dynamics (including the degree of degradation—ranging between light, moderate, strong, and extreme), have negated the generation of time-series, globally inclusive database of this issue. Specifically, distinguishing between ‘natural’ causes of land and soil degradation processes vs anthropogenic ones—such as habitat fragmentation, vegetation clearing, land-use change, agricultural malpractices, irrational grazing management, the expansion of infrastructures, urbanization, and environmental pollution—is often impossible. One way or another, climatic change aggravates anthropogenic-driven processes of land and soil degradation (Olsson et al., 2019; Talukder et al., 2021).

Taking these limitations into account, and considering the substantial uncertainties, no conclusive insights can be achieved regarding global extents and trends of naturally-driven land and soil degradation over the period of focus of this study (1992–2021).

Yet, a global assessment for 1997–2003 estimated that land degradation processes occur in 15–63% of total land area (Safriel, 2007). According to the United Nations, between 2000 and 2015, global proportion of degraded land encompassed 20% of the total land area (<https://unstats.un.org/sdgs/report/2019/goal-15/>; Figure 7A). A proxy global assessment of land degradation, determined according to changes in remotely sensed Normalized Difference Vegetation Index (NDVI) data for 1981–2003, revealed degradation of a total area of over 35 M km² throughout this period, encompassing ~23% of the globe’s terrestrial area (Bai et al., 2008). A somewhat more recent global

assessment of NDVI changes—for 1998–2013—reveals net declined or stressed productivity in 19% of grasslands and 26% of shrublands and other open lands (European Environment Agency, 2019). Recently, the United Nations Convention to Combat Desertification (UNCCD) estimated the global extent of land degradation to encompass over 18 M km² (UNCCD, 2021). The decreased productive capacity of the degraded lands substantially deteriorates a wide range of ecosystem services and functions, namely reduced food, feed, and fiber production, hence risking food- and economic-security (GEF, 2019).

In terms of forest degradation, one of its main indicators is tree dehydration, which is attributed to increasing temperatures and long-term droughts (Earles et al., 2018). Drought-stressed trees become more susceptible to pest infestations, resulting in mass tree mortality. Regardless of drought-stress, increasing temperatures accelerate the spread of some tree pathogens and diseases throughout the world's forests (Anderegg et al., 2015). One way or another, the stressed or desiccated trees become an available fuel, elevating the frequency and magnitude of high-severity wildfires. Forest wildfires turn biomass-assimilated carbon into CO₂, emitting this GHG to the atmosphere and aggravating climatic change feedbacks (Berenguer et al., 2021). Regardless, the extent of anthropogenic deforestation for the logging industry and/or for the establishment of croplands and grazing lands, as well as for urbanization and the construction of infrastructures, has been enormous, accelerating the rates of forest loss. Yet, the global rate of forest area loss is under debate. For example, according to the Global Forest Watch, out of ~40 M km² of global forests, deforestation for logging, agriculture, and urbanization between 2001 and 2021 encompassed ~1.17 M km², 0.88 M km², and 31 k km², respectively (<https://www.globalforestwatch.org/>). However, according the World Bank, total (including both natural- and anthropogenic-driven) loss of forest area across the globe is considerably less, encompassing a total of 1.3 M km² between 1990 and 2016 (<https://data.worldbank.org/indicator/AG.LND.FRST.K2>). According to the Food and Agriculture Organization (FAO) of the United Nations, between 1990 and 2020, the rate of annual loss of naturally regenerating forests has decreased, and moreover, faced some mitigation by forest planting (Figure 7B). Yet, in addition to negating the important regulating ecosystem service of carbon sequestration, the combination of natural- and anthropogenic-driven forest degradation adversely affects many other ecosystem services. Among the other regulating services, flood and soil erosion control are probably the most prominent. The major provisioning services are forest-derived food (such as fruits, nuts, edible bulbs, and mushrooms) and wood (including logs, poles, and fuelwood) products. Among the supporting services, biodiversity is most important. Forests

also fulfil cultural and spiritual services, such as heritage sites and communal identity (Stavi et al., 2022).

Nevertheless, despite the generally adverse impacts of climatic change on the world forests, higher atmospheric CO₂ concentrations are acknowledged to increase tree photosynthesis through the CO₂ fertilization effect. With this effect, forests' increasing productivity offsets some of the CO₂ emissions, potentially mitigating climate change to some extent. However, while this effect seems to be prominent for young trees, its potential impact on mature trees is still questionable, a fact that is related to the tree's carbon-use efficiency, which is higher in young individuals than in mature ones (Luo and Niu, 2020).

Loss of biodeversity

Biodiversity loss has been widely attributed to the degradation or extinction of ecosystems and habitats. Climatic change, specifically rising temperatures, has caused extensive destruction of terrestrial, marine, and freshwater ecosystems, with the consequent adverse impact on biodiversity's supporting ecosystem service. Specifically, temperatures exceed levels that species can cope with, causing the mass mortality of plants and animals. The rising temperatures also accelerate infestation of diseases and pathogens, further threatening many species in diverse biomes. If global warming is to exceed 2.1°C in 2,100 (SSP2-4.5/RCP4.5 and beyond), risks of habitat collapse and ecosystems extinction are to escalate rapidly, with biodiversity hotspots suffering the most (IPCC, 2022c). According to the United Nations, over the last decades, the Red List Index of species survival—which represents the changing state of global biodiversity—has declined by ~10%, from 0.821 in 1993 to 0.735 in 2019 (<https://unstats.un.org/sdgs/report/2019/goal-15/>; Figure 8).

However, a plethora of studies have shown that climate change impact on biodiversity is not that clear. Regarding plant diversity, global extinctions have generally not been directly related to climatic change. At the same time, local extinctions have taken place in the climatic margins of a species' range. Overall, the major threats (in descending importance) to plant diversity were identified as habitat loss-fragmentation-degradation > species overexploitation > species invasion > air pollution > climate change (Corlett, 2016). A global meta-analysis of local-scale plant biodiversity changes over time—comprised of information provided in published studies and of data obtained from reports on vegetation monitoring plots around the world—revealed no clear adverse effect on species richness and diversity. The timeframe for these studies and reports varied highly, and ranged between five and 261 years. While some of the studies and reports showed an increase in species richness and/or diversity, others showed a decline in these vegetation parameters. Specifically, despite the

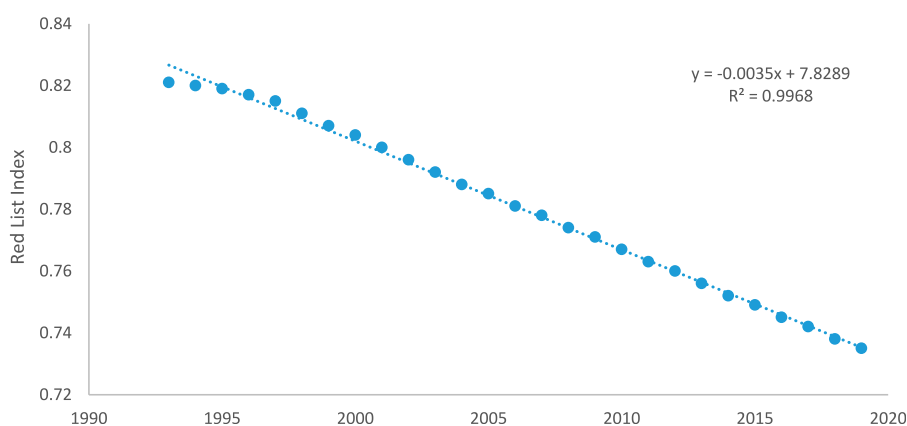


FIGURE 8

Red List Index of species (including >20,000 species of mammals, birds, amphibians, corals, and cycads) survival, between 1993 and 2019. Source: UN Stats. <https://unstats.un.org/sdgs/report/2019/goal-15/>

possible decline in plant diversity at a local scale—for example due to species outmigration—global-scale plant biodiversity is not necessarily adversely affected by climatic change (Vellend et al., 2013).

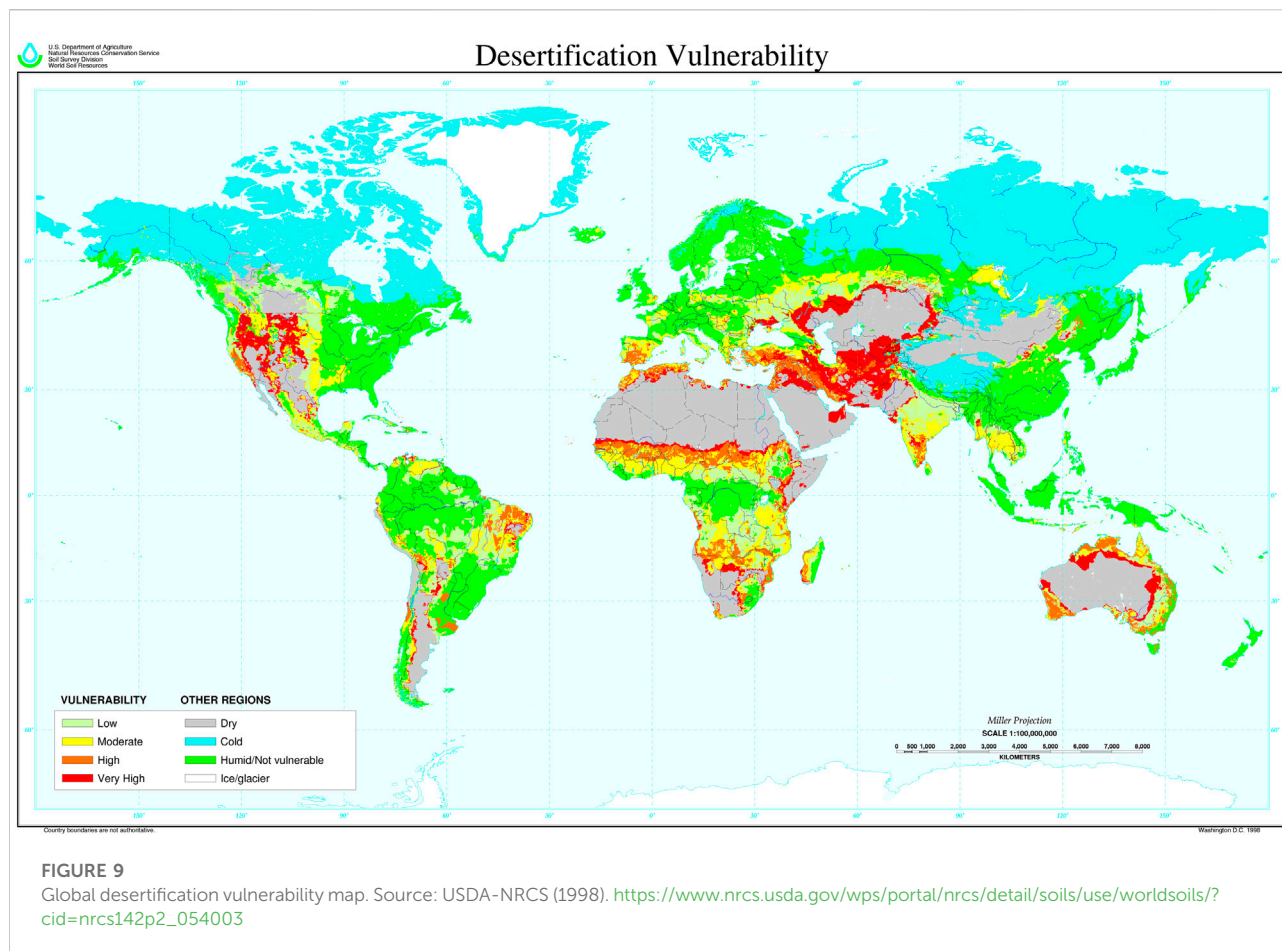
A recent report by the World Wildlife Fund (WWF, 2020) assessed the risk imposed on animal (including mammals, birds, fish, reptiles, and amphibians) biodiversity by climate change between 1970 and 2016, alongside the threats imposed by four other main factors, including land- (and sea-) use change and misuse, species overexploitation, invasive species and diseases, and environmental pollution. The assessment was separately conducted for five regions, including North America; Latin America and Caribbean; Europe and Central Asia; Africa; and Asia-Pacific. Altogether, these five factors reduced the global abundance of 20,811 populations—representing 4,392 animal species—by 68% along this period. However, calculating the average risk imposed on biodiversity by each of the five factors revealed that climate change is of least importance. Namely, the impact imposed by these factors followed the order of land- (and sea-) use change and misuse ($50.1 \pm 2.3\%$) > species overexploitation ($24.4 \pm 2.8\%$) > invasive species and diseases ($12.6 \pm 0.6\%$) > environmental pollution ($6.8 \pm 1.6\%$) > climate change ($6.1 \pm 1.4\%$) (means and SE calculation is based on data obtained from WWF, 2020).

Nevertheless, in the context of biodiversity loss, separating between the impacts of climate change and other dominating factors is not always straightforward. For example, climatic changes are expected to stimulate vegetation invasion. A broadly accepted viewpoint is that climatic changes increase the capacity of alien plant species to invade new territories, while simultaneously decreasing the resistance of natural ecosystems to invasions by interrupting their dynamic equilibrium (Thuiller et al., 2007). Yet, the impact of climate change on vegetation invasiveness seems to be rather complex,

and moreover, scale-dependent. A systematic review of many modeling case studies showed high variability in the effects of climatic change on vegetation invasion in terrestrial systems. Specifically, in regional-to global-scale models, a reduction in species range size was predicted more often than an increase. Conversely, in local-to small-scale models, an increase in species range size was forecasted more frequently than a reduction (Bellard et al., 2018).

Desertification

Desertification is defined as land degradation in dry sub-humid, semi-arid, and arid regions, whereas land degradation in hyper-arid regions is excluded from the definition of desertification (UNCCD, 1994; see Figure 9 for global desertification vulnerability map (USDA-NRCS, 1998)). This process causes the deterioration of productive capacity, ecological integrity, and ecosystem services of the affected land. Desertification derives from either natural or anthropogenic causes, with often the two act simultaneously. Among the ‘natural’ causes, climate change is predominant (Mirzabaev et al., 2019; Fan et al., 2020). A recent assessment of climatic trends across the world’s drylands between 1979 and 2018 revealed a general increase in temperatures and decrease in precipitations, with the most notable changes recorded during the last decade. During this entire period, the rate of temperature increase has been $0.032^{\circ}\text{C yr}^{-1}$, and the rate of precipitation decrease has been $0.074 \text{ mm month}^{-1} \text{ yr}^{-1}$ (Daramola and Xu, 2022). Yet, at the regional scale, variations are more dramatic. For example, warming of the Saharan Belt and the surrounding oceans during recent decades has led to substantial modifications in the nature of the Hadley Cell system, causing convective rainstorms to become more intense and intermittent

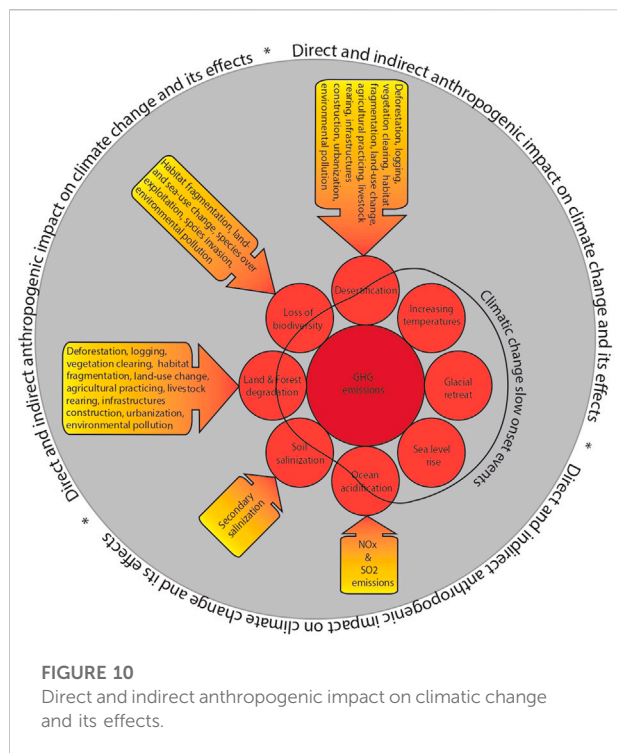


(Biasutti, 2019). In the China–Mongolia–Russia Economic Corridor, between 2000 and 2015, the areal cover of slight desertification has faced ~32% increase (from ~720,000 km² to ~950,000 km²), while that of severe desertification has faced ~13% decrease (from ~82,000 km² to ~71,000 km²). Overall, while the total desertified area along this period increased by ~10%, the degree of desertification showed a decreasing trend (Fan et al., 2020). At the same time, another study implemented in Central Asia revealed regional increasing temperatures since the 1980s, coupled with northward and eastward areal expansion of the arid-cold (BWk) climatic region into the semi-arid-cold (BSk) climatic region (Hu and Han, 2022).

One way or another, increasing temperatures and severe droughts across extensive drylands elevate evaporation loss and reduce soil-water content, causing the mass mortality of vegetation (Stavi et al., 2018). The resulted increase in frequency and severity of dust- and sand-storms further exaggerate drylands' environmental degradation. The simultaneous rarer but stronger rainstorms cause extensive flooding and large-scale soil erosion processes, alongside depletion of soil organic carbon pools. The combined effect of these processes causes the expansion and aggravation of

drylands. However, because different sets of indicators, approaches, and methodologies are used, the global assessment of extent and severity of desertification is rather complicated, and suffers substantial uncertainties. Further, these uncertainties complicate the quantification of past desertification, as well as the prediction of future desertification (Mirzabaev et al., 2019). Yet, a recent study showed that between 1982 and 2015, climate change has caused the degradation and desertification of almost 5.5 M km² (encompassing almost 13%) of the world drylands (Burrell et al., 2020). A recently developed index—the Global Desertification Vulnerability Index (GDVI)—revealed that the present combined impact of climatic change and direct anthropogenic activities impose moderate, high, and very high desertification risk in 13, 7, and 9%, respectively, of the global terrestrial area. Compared to the 2000–2014 baseline, the GDVI projects that in 2,100, the areal coverage of low desertification risk will decline from 47 to 35% under the SSP2-4.5/RCP4.5, and to 24% under the SSP5-8.5/RCP8.5 (Huang et al., 2020).

Yet, in addition to modern climatic changes that are attributed to anthropogenic emissions of GHGs,



desertification processes can also be generated by natural meteorological conditions. For example, changes in regional wind patterns that modify dust deposition, possibly decreasing the input of mineral material to the system. The simultaneous increase in extent and severity of soil erosion processes results in the net loss of mineral materials from the system (Stavi et al., 2010). Overall, the major anthropogenic drivers of desertification are land-use change and unsustainable land management practices, including intensified agriculture, overgrazing by livestock, and clearing of woody vegetation, alongside extensive infrastructure construction, mineral mining and quarrying, urban expansion, and environmental pollution. These practices and land-uses increase the pressures imposed on the already fragile drylands, exacerbating the degradation in their productivity and functioning (Mirzabaev et al., 2019). Across the world, desertification adversely affects the livelihood of over 200 million people, most of whom live in developing countries (Burrell et al., 2020) in South, Central, and East Asia, the Middle East, the Saharan Belt, and North and West Africa (Mirzabaev et al., 2019). The combined effect of 'natural' and anthropogenic driven desertification is expected to deteriorate the water-, food-, environmental-, energy-, economic-, health-, and governance-security of human populations across the world's drylands. Further, these impacts are expected to exaggerate the potential for social unrest, violent conflicts, and mass migration, aggravating humanitarian disasters across the globe (Stavi et al., 2021a).

Boosting climate change mitigation and adaptation, and enhancing environmental conservation and restoration: A wakeup call

Despite some uncertainties, it seems that climatic change slow onset events have significantly exacerbated during the last three decades (between 1992 and 2021). Simultaneously, many other direct anthropogenic-driven causes have further aggravated the slow onset events and adversely affected environmental quality (Figure 10). Over time, the combined impacts of the slow onset events and other anthropogenic causes have substantially degraded provisioning, supporting, regulating, and cultural ecosystem services. The global human population growth—forecasted to reach 9.8 billion in 2050 and 11.2 billion in 2100 (<https://www.un.org/en/desa/world-population-projected-reach-98-billion-2050-and-112-billion-2100>)—is expected to substantially exaggerate environmental stressors. This state calls for the implementation of urgent measures in climate change mitigation and adaptation, as well as in environmental conservation and restoration.

Fore and foremost, proactive decision making at all levels—ranging between the local to international scales—should become more decisive, including continuous risk assessment, frequent monitoring of outcomes and their compatibility to goals, implementing practical legislation tools, and assigning specific financial instruments, aimed at enhancing the mitigation of climatic change slow onset events and related environmental aspects (Jones et al., 2014). Shifting to more nature-based solutions and environmentally-friendly modes of operation should be encouraged by subsidizing the relevant economic sectors. Another potential mechanism is by paying for accomplishing ecosystem services (Capodaglio and Callegari, 2018). Policy makers may benefit from following the United Nations Sustainable Development Goals (UN SDGs: <https://sdgs.un.org/>), while allowing flexibility and adjustments of its principles according to emerging environmental issues. Alongside these measures, decision makers should promote climate- and environmental-justice policies, particularly supporting the most vulnerable communities and countries, which are often deprived of governance power at the local, national, regional, and international levels (Thomas et al., 2020).

In the energy sector, fossil fuels should be replaced by renewable energy sources, such as solar, wind, geothermal, marine energies, biomass conversion-based energies, and others (Demirbaş, 2006). Deforestation should be heavily controlled, and offset by extensive climate-smart afforestation and reforestation projects (Verkerk et al., 2020). Also, mass tree planting in croplands and grazing lands should be promoted, by applying agroforestry and silvopastoral practices (Raskin and Osborn, 2019). In relevant coastal areas, conservation and restoration of mangrove systems should be promoted, to control inundation and minimize coastline erosion (Kumano et al., 2021). Further, tree-planting in densely populated

areas such as towns and municipalities should be maximized, to reduce the 'urban heat island' effect (Schwaab et al., 2021). Overall, land degradation should be minimized by adopting conservation practices, coupled with the use of offsetting mechanisms such as the Zero Net Land Degradation (ZNLD, also known as the Land Degradation Neutrality (LDN): Tal, 2015). Regardless, promoting a change in human diet from animal-protein based to alternative sources of protein—through extensive investments in the food-tech sector—is expected to substantially cut the stressors imposed on global agricultural and grazing lands, while simultaneously conserving water resources, reducing GHG emissions, and lessening environmental pollution (Mbow et al., 2019).

Regardless, environmental contamination should be minimized through the control and treatment of pollution sources, alongside the implementation of environmentally-friendly waste management, and the recovery of polluted air, water, and soil resources. A promising strategy in this context is the multiple-R concept, such as the Reduce-Reuse-Recycle (3R), Reduce-Reuse-Recycle-Recovery (4R), etc. (Yu et al., 2021). Simultaneously, the mass development of alternative eco-friendly and biodegradable materials, as well as of clean technologies (green technologies), should be of top priority (Ko, 2020). Altogether, judicious implementation of these measures is expected to assist in the reviving of global environmental health.

Conclusion

The rising atmospheric concentrations of GHGs over the past three decades (1992–2021) has caused the substantial exacerbation of climatic change. Despite some uncertainties, it seems that this caused the aggravation of slow onset effects, including increasing temperatures, glacial retreat, sea level rise, ocean acidification, soil salinization, land and forest degradation, loss of biodiversity, and desertification. Yet, as shown throughout this review study, other (non-GHGs related) anthropogenic impacts, such as habitat fragmentation, land- (and sea-) use change and misuse, environmental pollution, and urbanization, have also intensified along this period, considerably increasing the stressors imposed on environmental quality and ecosystem services. Therefore, proactive policymaking and legislation of climate change

mitigation measures, alongside effective adaptation means and inclusive environmental conservation and restoration practices, should be of top priority, potentially alleviating the damages to environmental health and global sustainability, and avoiding climatic irreversible tipping points.

Author contributions

IS has designed, wrote, and finalized the manuscript.

Funding

The Dead Sea and Arava Science Center is supported by the Israel Ministry of Science and Technology.

Acknowledgments

The author is grateful to Michelle Finzi for proofreading of the manuscript. The author much appreciates the helpful and constructive comments made by two reviewers on the original submission.

Conflict of interest

The author declares that the research was conducted in the absence of any commercial or financial relationships that could be construed as a potential conflict of interest.

Publisher's note

All claims expressed in this article are solely those of the authors and do not necessarily represent those of their affiliated organizations, or those of the publisher, the editors and the reviewers. Any product that may be evaluated in this article, or claim that may be made by its manufacturer, is not guaranteed or endorsed by the publisher.

References

- Anderegg, W. R. L., Hicke, J. A., Fisher, R. A., Allen, C. D., Aukema, J., Bentz, B., et al. (2015). Tree mortality from drought, insects, and their interactions in a changing climate. *New Phytol.* 208, 674–683. doi:10.1111/nph.13477
- Bai, Z. G., Dent, D. L., Olsson, L., and Schaepman, M. E. (2008). Proxy global assessment of land degradation. *Soil Use Manag* 24, 223–234. doi:10.1111/j.1475-2743.2008.00169.x
- Baker, A. R., Kanakidou, M., Nenes, A., Myriokefalitakis, S., Croot, P. L., Duce, R. A., et al. (2021). Changing atmospheric acidity as a modulator of nutrient deposition and ocean biogeochemistry. *Sci. Adv.* 7, eabd8800. doi:10.1126/sciadv.abd8800
- Bannari, A., and Al-Ali, Z. M. (2020). Assessing climate change impact on soil salinity dynamics between 1987–2017 in arid landscape using landsat TM, ETM+ and OLI data. *Remote Sens.* 12, 2794. doi:10.3390/rs12172794
- Bellard, C., Jeschke, J. M., Leroy, B., and Mace, G. M. (2018). Insights from modeling studies on how climate change affects invasive alien species geography. *Ecol. Evol.* 8, 5688–5700. doi:10.1002/ece3.4098
- Berenguer, E., Lennox, G. D., Ferreira, J., Malhi, Y., Aragão, L. E. O. C., Barreto, J. R., et al. (2021). Tracking the impacts of El Niño drought and fire in human-modified Amazonian forests. *Proc. Natl. Acad. Sci. U. S. A.* 118, 30. doi:10.1073/pnas.2019377118

- Biasutti, M. (2019). Rainfall trends in the african sahel: Characteristics, processes, and causes. *Wiley Interdiscip. Rev. Clim. Change* 10, e591. doi:10.1002/wcc.591
- Bloemendaal, N., de Moel, H., Martinez, A. B., Muis, S., Haigh, I. D., van der Wiel, K., et al. (2022). A globally consistent local-scale assessment of future tropical cyclone risk. *Sci. Adv.* 8, eabm8438. doi:10.1126/sciadv.abm8438
- Bolch, T., Duethmann, D., Wortmann, M., Liu, S., and Disse, M. (2022). Declining glaciers endanger sustainable development of the oases along the Aksu-Tarim River (Central Asia). *Int. J. Sustain. Dev. World Ecol.* 29, 209–218. doi:10.1080/13504509.2021.1943723
- Bowen, V. (2015). Extreme weather: Is 'abnormal' becoming the new 'normal'? *Weather* 70, S15–S16. doi:10.1002/wea.2528
- Burrell, A. L., Evans, J. P., and De Kauwe, M. G. (2020). Anthropogenic climate change has driven over 5 million km² of drylands towards desertification. *Nat. Commun.* 11, 3853. doi:10.1038/s41467-020-17710-7
- Capodaglio, A. G., and Callegari, A. (2018). Can payment for ecosystem services schemes be an alternative solution to achieve sustainable environmental development? A critical comparison of implementation between Europe and China. *Resources* 7, 40. doi:10.3390/resources7030040
- Chen, Y., Li, W., Deng, H., Fang, G., and Li, Z. (2016). Changes in central asia's water tower: Past, present and future. *Sci. Rep.* 6, 35458. doi:10.1038/srep35458
- Climate Change Secretariat (2002). A guide to the climate change convention process, preliminary 2nd edition. AvailableAt: <https://unfccc.int/resource/process/guideprocess-p.pdf>.
- Collins, M., Knutti, R., Arblaster, J., Dufresne, J. L., Fichetef, T., Friedlingstein, P., et al. (2013). "Long-term climate change: Projections, commitments and irreversibility", in *The physical science basis. Contribution of working group I to the fifth assessment report of the intergovernmental Panel on climate change*. Editors T. F. Stocker, D. Qin, G. K. Plattner, M. Tignor, S. K. Allen, J. Boschung, et al. (Cambridge: Cambridge University Press). AvailableAt: https://www.ipcc.ch/site/assets/uploads/2018/02/WG1AR5_Chapter12_FINAL.pdf.
- Corlett, R. T. (2016). Plant diversity in a changing world: Status, trends, and conservation needs. *Plant Divers.* 38, 10–16. doi:10.1016/j.pld.2016.01.001
- Daramola, M. T., and Xu, M. (2022). Recent changes in global dryland temperature and precipitation. *Int'l J. Climatol.* 42, 1267–1282. doi:10.1002/joc.7301
- Demirbas, A. (2006). Global renewable energy resources. *Energy Sources Part A Recovery Util. Environ. Eff.* 28, 779–792. doi:10.1080/009083190910488
- Dolschak, K., Gartner, K., and Berger, T. W. (2019). The impact of rising temperatures on water balance and phenology of European beech (*Fagus sylvatica* L.) stands. *Model. Earth Syst. Environ.* 5, 1347–1363. doi:10.1007/s40808-019-00602-1
- Earles, J. M., Stevens, J. T., Sperling, O., Orozco, J., North, M. P., and Zwieniecki, M. A. (2018). Extreme mid-winter drought weakens tree hydraulic-carbohydrate systems and slows growth. *New Phytol.* 219, 89–97. doi:10.1111/nph.15136
- ESCAP (2018). Sand and dust storms in Asia and the pacific: Opportunities for regional cooperation and action. The economic and social commission for Asia and the pacific. AvailableAt: https://www.unescap.org/sites/default/files/UNESCAP%20SDS%20Report_1.pdf.
- Eslami, S., Hoekstra, P., Minderhoud, P. S. J., Trung, N. N., Hoch, J. M., Sutanudjaja, E. H., et al. (2021). Projections of salt intrusion in a mega-delta under climatic and anthropogenic stressors. *Commun. Earth Environ.* 2, 142. doi:10.1038/s43247-021-00208-5
- European Environment Agency (2019). Land degradation knowledge base: Policy, concepts and data. AvailableAt: <https://www.eionet.europa.eu/etcs/etc-uls/products/etc-uls-reports/etc-uls-report-2019-1-land-degradation-knowledge-base-policy-concepts-and-data>.
- Fan, Z., Li, S., and Fang, H. (2020). Explicitly identifying the desertification change in CMREC area based on multisource remote data. *Remote Sens.* 12, 3170. doi:10.3390/rs12193170
- GEF (2019). Global environmental facility land degradation. AvailableAt: https://www.thegef.org/sites/default/files/publications/gef_land_degradation_bifold_august_2019_0.pdf.
- Handmer, J., and Nalau, J. (2019). "Understanding loss and damage in pacific small island developing states," in *Loss and damage from climate change – concepts, methods and policy options*. Editors R. Mechler, M. Bouwer, T. Schinko, S. Surminski, and J. A. Linnerooth-Bayer (Berlin: Springer), 365–381. doi:10.1007/978-3-319-72026-5_15
- Hardy, R. D., and Nuse, B. L. (2016). global sea-Level rise: Weighing country responsibility and risk. *Clim. Change* 137, 333–345. doi:10.1007/s10584-016-1703-4
- Harper, A. B., Powell, T., Cox, P. M., House, J., Huntingford, C., Lenton, T. M., et al. (2018). Land-use emissions play a critical role in land-based mitigation for Paris climate targets. *Nat. Commun.* 9, 2938. doi:10.1038/s41467-018-05340-z
- Hassani, A., Azapagic, A., and Shokri, N. (2021). Global predictions of primary soil salinization under changing climate in the 21st century. *Nat. Commun.* 12, 6663. doi:10.1038/s41467-021-26907-3
- Hoegh-Guldberg, O., Poloczanska, E. S., Skirving, W., and Dove, S. (2017). Coral reef ecosystems under climate change and ocean acidification. *Front. Mar. Sci.* 4, 158. doi:10.3389/fmars.2017.00158
- Holding, J. M., Duarte, C. M., Sanz-Martin, M., Mesa, E., Arrieta, J. M., Chierici, M., et al. (2015). Temperature dependence of CO₂-enhanced primary production in the European Arctic Ocean. *Nat. Clim. Change* 5, 1079–1082. doi:10.1038/nclimate2768
- Hu, Q., and Han, Z. (2022). Northward expansion of desert climate in Central Asia in recent decades. *Geophys. Res. Lett.* 49, e2022GL098895. doi:10.1029/2022gl098895
- Huang, J., Zhang, G., Zhang, Y., Guan, X., Wei, Y., and Guo, G. (2020). Global desertification vulnerability to climate change and human activities. *Land Degrad. Dev.* 31, 1380–1391. doi:10.1002/ldr.3556
- IPCC (2014). Climate change 2014: Synthesis Report *Contribution of working groups I, II and III to the fifth assessment report of the intergovernmental Panel on climate change*. Geneva, Switzerland: IPCC, 151. AvailableAt: https://www.ipcc.ch/site/assets/uploads/2018/02/SYR_AR5_FINAL_full.pdf.
- IPCC (2022a). Climate change 2022: Impacts, adaptation and vulnerability – summary for policymakers. The Working Group II contribution to the Sixth Assessment Report. AvailableAt: <https://www.ipcc.ch/report/sixth-assessment-report-working-group-ii/>.
- IPCC (2022c). Fact sheet - biodiversity: Climate change impacts and risks. Contribution of Working Group II to the Sixth Assessment Report of the Intergovernmental Panel on Climate Change. AvailableAt: https://report.ipcc.ch/ar6wg2/pdf/IPCC_AR6_WGII_FactSheet_Biodiversity.pdf.
- IPCC (2022b). Fact sheet - small Islands: Climate change impacts and risks. Contribution of Working Group II to the Sixth Assessment Report of the Intergovernmental Panel on Climate Change. AvailableAt: https://www.ipcc.ch/report/ar6/wg2/downloads/outreach/IPCC_AR6_WGII_FactSheet_SmallIslands.pdf.
- IPCC (2021). "Summary for policymakers", in climate change 2021: The physical science basis," in *Contribution of working group I to the sixth assessment report of the intergovernmental Panel on climate change* (Geneva: IPCC Press). AvailableAt: https://www.ipcc.ch/report/ar6/wg1/downloads/report/IPCC_AR6_WGI_SPM_final.pdf.
- Ivushkin, K., Bartholomeus, H., Bregt, A. K., Pulatov, A., Kempen, B., and de Sousa, L. (2019). Global mapping of soil salinity change. *Remote Sens. Environ.* 231, 111260. doi:10.1016/j.rse.2019.111260
- Jasechko, S., Perrone, D., Seybold, H., Fan, Y., and Kirchner, J. W. (2020). Groundwater level observations in 250,000 coastal US wells reveal scope of potential seawater intrusion. *Nat. Commun.* 11, 3229. doi:10.1038/s41467-020-17038-2
- Jevrejeva, S., Jackson, L. P., Riva, R. E. M., Grinsted, A., and Moore, J. C. (2016). Coastal sea level rise with warming above 2 °C. *Proc. Natl. Acad. Sci. U.S.A.* 113, 13342–13347. doi:10.1073/pnas.1605312113
- Jones, R. N., Patwardhan, A., Cohen, S. J., Dessai, S., Lammel, A., Lempert, R. J., et al. (2014). "Foundations for decision making", in Climate change 2014: Impacts, adaptation, and vulnerability. Part A: Global and sectoral aspects," in *Contribution of working group II to the fifth assessment report of the intergovernmental Panel on climate change*. Editors C. B. Field, V. R. Barros, D. J. Dokken, K. J. Mach, M. D. Mastrandrea, T. E. Bilir, et al. (Cambridge: Cambridge University Press). AvailableAt: https://www.ipcc.ch/site/assets/uploads/2018/02/WGIIAR5-Chap2_FINAL.pdf.
- Klotzbach, P. J., Wood, K. M., Schreck, C. J., III, Bowen, S. G., Patricola, C. M., and Bell, M. M. (2022). Trends in global tropical cyclone activity: 1990–2021. *Geophys. Res. Lett.* 49, e2021GL095774. doi:10.1029/2021gl095774
- Ko, Y. T. (2020). Modeling an innovative green design method for sustainable products. *Sustainability* 12, 3351. doi:10.3390/su12083351
- Kumano, N., Tamura, M., Inoue, T., and Yokoki, H. (2021). Estimating the cost of coastal adaptation using mangrove forests against sea level rise. *Coast. Eng. J.* 63, 263–274. doi:10.1080/21664250.2021.1892968
- Lal, R. (2010). Managing soils and ecosystems for mitigating anthropogenic carbon emissions and advancing global food security. *BioScience* 60, 707–721. doi:10.1525/bio.2010.60.9.8
- Li, Z., Tian, L., Wu, H., Wang, W., Zhang, S., Zhang, J., et al. (2016). Changes in glacier extent and surface elevations in the Depuchangdake region of northwestern Tibet, China. *Quat. Res.* 85, 25–33. doi:10.1016/j.yqres.2015.12.005
- Lin, X., Zhang, W., Crippa, M., Peng, S., Han, P., Zeng, N., et al. (2021). A comparative study of anthropogenic CH₄ emissions over China based on the

ensembles of bottom-up inventories. *Earth Syst. Sci. Data* 13, 1037–1088. doi:10.5194/essd-13-1073-2021

Lionello, P., and Scarascia, L. (2018). The relation between climate change in the Mediterranean region and global warming. *Reg. Environ. Change* 18, 1481–1493. doi:10.1007/s10113-018-1290-1

Litalien, A., and Zeeb, B. (2020). Curing the Earth: A review of anthropogenic soil salinization and plant-based strategies for sustainable mitigation. *Sci. Total Environ.* 698, 134235. doi:10.1016/j.scitotenv.2019.134235

Luo, Y., and Niu, S. (2020). Mature forest shows little increase in carbon uptake in a CO₂-enriched atmosphere. *Nature* 580, 191–192. doi:10.1038/d41586-020-00962-0

Mbow, C., Rosenzweig, C., Barioni, L. G., Benton, T. G., Herrero, M., Krishnapillai, M., et al. (2019). “Food security,” in *Climate change and land: An IPCC special report on climate change, desertification, land degradation, sustainable land management, food security, and greenhouse gas fluxes in terrestrial ecosystems* (Geneva: IPCC Press). AvailableAt: https://www.ipcc.ch/site/assets/uploads/sites/4/2021/02/08_Chapter-5_3.pdf.

Mead, L. (2021). Small islands, large oceans: Voices on the frontlines of climate change. AvailableAt: <https://www.iisd.org/system/files/2021-03/still-one-earth-SIDS.pdf>.

Mirzabaev, A., Wu, J., Evans, J., García-Oliva, F., Hussein, I. A. G., Iqbal, M. H., et al. (2019). “Desertification,” in *Climate change and land: An IPCC special report on climate change, desertification, land degradation, sustainable land management, food security, and greenhouse gas fluxes in terrestrial ecosystems* (Geneva: IPCC Press). AvailableAt: https://www.ipcc.ch/site/assets/uploads/sites/4/2019/11/06_Chapter-3.pdf.

Mooney, H., Larigauderie, A., Cesario, M., Elmquist, T., Hoegh-Guldberg, O., Lavorel, S., et al. (2009). Biodiversity, climate change, and ecosystem services. *Curr. Opin. Environ. Sustain.* 1, 46–54. doi:10.1016/j.cosust.2009.07.006

Mostofa, K. M. G., Liu, C. Q., Zhai, W. D., Minella, M., Vione, D., Gao, K., et al. (2016). Reviews and syntheses: Ocean acidification and its potential impacts on marine ecosystems. *Biogeosciences* 13, 1767–1786. doi:10.5194/bg-13-1767-2016

Mouginot, J., Rignot, E., Björk, A. A., van den Broeke, M., Millan, R., Morlighem, M., et al. (2019). Forty-six years of Greenland ice sheet mass balance from 1972 to 2018. *Proc. Natl. Acad. Sci. U.S.A.* 116, 9239–9244. doi:10.1073/pnas.1904242116

Olsson, L., Barbosa, H., Bhadwal, S., Cowie, A., Delusca, K., Flores-Renteria, D., et al. (2019). “Land degradation,” in *Climate change and land: An IPCC special report on climate change, desertification, land degradation, sustainable land management, food security, and greenhouse gas fluxes in terrestrial ecosystems* (Geneva: IPCC Press). AvailableAt: https://www.ipcc.ch/site/assets/uploads/sites/4/2019/11/07_Chapter-4.pdf.

Pohl, E., Gloaguen, R., Andermann, C., and Knoche, M. (2017). Glacier melt buffers river runoff in the Pamir Mountains. *Water Resour. Res.* 53, 2467–2489. doi:10.1002/2016wr019431

Raskin, B., and Osborn, S. (2019). *The agroforestry handbook – agroforestry for the UK*. Bristol: Soil Association Ltd. AvailableAt: <https://www.soilassociation.org/media/19141/the-agroforestry-handbook.pdf>.

Reid, A., and Wood, E. (2021). COP26-An introduction to the UN conference of the Parties. The scottish parliament information center (SPICe). AvailableAt: <https://sp-bpr-en-prod-cdnep.azureedge.net/published/2021/6/2/65344c5f-7066-4f46-aad8-92a91a4033e5/SB%2021-28.pdf>.

Rignot, E., Mouginot, J., Scheuchl, B., van den Broeke, M., van Wessem, M. J., and Morlighem, M. (2019). Four decades of antarctic ice sheet mass balance from 1979–2017. *Proc. Natl. Acad. Sci. U.S.A.* 116, 1095–1103. doi:10.1073/pnas.1812883116

Safriel, U. N. (2007). “The Assessment of global trends in land degradation,” in *Climate and land degradation*. Editors M. V. K. Sivakumar and N. Ndiang’ui (Berlin: Springer), 1–38.

Salt Farm Foundation (2018). Further reading on salinization, Hoornderweg. AvailableAt: [https://www.salineagricultureworldwide.com/uploads/file_uploads/files/More%20info%20on%20Salinization-%20Salt%20Farm%20Foundation%202018\(1\).pdf](https://www.salineagricultureworldwide.com/uploads/file_uploads/files/More%20info%20on%20Salinization-%20Salt%20Farm%20Foundation%202018(1).pdf).

Schuur, E. A. G., McGuire, A. D., Schadel, C., Grosse, G., Harden, J. W., Hayes, D. J., et al. (2015). Climate change and the permafrost carbon feedback. *Nature* 520, 171–179. doi:10.1038/nature14338

Schwaab, J., Meier, R., Mussetti, G., Seneviratne, S., Bürgi, C., and Davin, E. L. D. (2021). The role of urban trees in reducing land surface temperatures in European cities. *Nat. Commun.* 12, 6763. doi:10.1038/s41467-021-26768-w

SDSU Extension (2019). *Soybean best management practices – chapter 47: Managing high water tables and saline seeps in soybean production*. Brookings: South Dakota State University Press. AvailableAt: <https://extension.sdstate.edu/sites/default/files/2020-03/S-0004-47-Soybean.pdf>.

Shahgedanova, M., Afzal, M., Hagg, W., Kapitsa, V., Kasatkin, N., Mayr, E., et al. (2020). Emptying water towers? Impacts of future climate and glacier change on

river discharge in the northern tien Shan, central Asia. *Water* 12, 627. doi:10.3390/w12030627

Slater, T., Lawrence, I. R., Otsuka, I. N., Shepherd, A., Gourmelen, N., Jakob, L., et al. (2021). Review article: Earth’s ice imbalance. *Cryosphere* 15, 233–246. doi:10.5194/tc-15-233-2021

Stavi, I., Paschalidou, A., Kyriazopoulos, A. P., Halbac-Cotoara-Zamfir, R., Siad, S. M., Suska-Malawska, M., et al. (2021a). Multidimensional food security nexus in drylands under the slow onset effects of climate change. *Land* 10, 1350. doi:10.3390/land10121350

Stavi, I., Perevolotsky, A., and Avni, Y. (2010). Effects of gully formation and headcut retreat on primary production in an arid rangeland: Natural desertification in action. *J. Arid Environ.* 74, 221–228. doi:10.1016/j.jaridenv.2009.08.007

Stavi, I., Rachmilevitch, S., Hjazin, A., and Yizhaq, H. (2018). Geodiversity decreases shrub mortality and increases ecosystem tolerance to droughts and climate change. *Earth Surf. Process. Landforms* 43, 2808–2817. doi:10.1002/esp.4412

Stavi, I., Thevs, N., and Priori, S. (2021b). Soil salinity and sodicity in drylands: A review of causes, effects, monitoring, and restoration measures. *Front. Environ. Sci.* 9, 712831. doi:10.3389/fenvs.2021.712831

Stavi, I., Thevs, N., Welp, M., and Zdruli, P. (2022). Provisioning ecosystem services related with oak (*Quercus*) systems: A review of challenges and opportunities. *Agroforest Syst.* 96, 293–313. doi:10.1007/s10457-021-00718-3

Tal, A. (2015). The implications of environmental trading mechanisms on a future Zero Net Land Degradation protocol. *J. Arid Environ.* 112, 25–32. doi:10.1016/j.jaridenv.2014.05.013

Talukder, B., Ganguli, N., Matthew, R., vanLoon, G. W., Hipel, K. W., and Orbinski, J. (2021). Climate change-triggered land degradation and planetary health: A review. *Land Degrad. Dev.* 32, 4509–4522. doi:10.1002/ldr.4056

Thomas, A., Baptiste, A., Martyr-Koller, R., Pringle, P., and Rhiney, K. (2020). Climate change and small island developing states. *Ann. Rev. Environ. Resour.* 45, 6–27. doi:10.1146/annurev-environ-012320-083355

Thuiller, W., Richardson, D. M., and Midgley, G. F. (2007). “Will climate change promote alien plant invasions?” in *Ecological studies* (Berlin: Biological Invasions. Springer), 197–211.

UN (1998). Kyoto protocol to the united Nations Framework convention on climate change. AvailableAt: <https://unfccc.int/resource/docs/convkp/kpeng.pdf>.

UN (1993). Report of the united Nations conference on environment and development, volume I resolutions adopted by the conference. AvailableAt: <https://www.un.org/esa/dsd/agenda21/Agenda%2021.pdf>.

UN-OHRLS (2015). *Small island developing states in numbers – climate change edition 2015*. New York, NY: The United Nations Office of the High Representative for the Least Developed Countries. AvailableAt: https://sustainabledevelopment.un.org/content/documents/2189SIDS-IN-NUMBERS-CLIMATE-CHANGE-EDITION_2015.pdf.

UNCCD (1994). Elaboration of an international convention to combat desertification in countries experiencing serious drought and/or desertification, particularly in Africa. United Nations Convention to Combat Desertification. AvailableAt: https://wedocs.unep.org/bitstream/handle/20.500.11822/27569/UNCCD_English.pdf?sequence=1&isAllowed=y.

UNCCD (2021). Proportion of land that is degraded over total land area – SDG indicator 15.3.1, united Nations convention to combat desertification. AvailableAt: https://unece.org/sites/default/files/2021-05/2.2_UNCCD_SDGIndicator1531_merged.pdf.

UNFCCC (1995). Provisional agenda and annotations, including suggestions for the organization of work – note by the Executive Secretary. AvailableAt: <https://unfccc.int/cop5/resource/docs/cop1/01.pdf>.

UNFCCC (2012). Slow onset events – technical paper. AvailableAt: <https://unfccc.int/resource/docs/2012/tp/07.pdf>.

UNFCCC (1992). United Nations Framework convention on climate change. AvailableAt: https://unfccc.int/files/essential_background/background_publications_htmlpdf/application/pdf/conveng.pdf.

USAID (2018). *Climate risk profile – central Asia fact sheet*. Washington, D.C.2 United States Agency for International Development. AvailableAt: https://reliefweb.int/sites/reliefweb.int/files/resources/2018-April-30_USAID_CadmusCISF_Climate-Risk-Profile-Central-Asia.pdf.

Vellend, M., Baeten, L., Myers-Smith, I. S., Elmendorf, S. C., Beauséjour, R., Brown, C. D., et al. (2013). Global meta-analysis reveals no net change in local-scale plant biodiversity over time. *Proc. Natl. Acad. Sci. U.S.A.* 110, 19456–19459. doi:10.1073/pnas.1312779110

Verkerk, P. J., Costanza, R., Hetemäki, L., Kubiszewski, I., Leskinen, P., Nabuurs, G. J., et al. (2020). Climate-smart forestry: The missing link. *For. Policy Econ.* 115, 102164. doi:10.1016/j.forpol.2020.102164

Wang, C., Amon, B., Schulz, K., and Mehdi, B. (2021). Factors that influence nitrous oxide emissions from agricultural soils as well as their representation in simulation models: A review. *Agronomy* 11, 770. doi:10.3390/agronomy11040770

Wigley, T. M. L. (2021). The relationship between net GHG emissions and radiative forcing with an application to Article 4.1 of the Paris Agreement. *Clim. Change* 169, 13. doi:10.1007/s10584-021-03249-z

Woodhead, A. J., Hicks, C. C., Norström, A. V., Williams, G. J., and Graham, N. A. J. (2019). Coral reef ecosystem services in the Anthropocene. *Funct. Ecol.* 33, 1023–1034. doi:10.1111/1365-2435.13331

WWF (2020). *Living planet report 2020*. Gland: World Wildlife Fund. Available At: <https://www.zsl.org/sites/default/files/LPR%202020%20Full%20report.pdf>.

Xia, Q. Q., Chen, Y. N., Zhang, X. Q., Ding, J. L., and Lv, G. H. (2022). Identifying reservoirs and estimating evaporation losses in a large arid inland basin in northwestern China. *Remote Sens.* 14, 1105. doi:10.3390/rs14051105

Yu, K. H., Zhang, Y., Li, D. N., Montenegro-Marin, C. E., and Kumar, P. M. (2021). Environmental planning based on reduce, reuse, recycle and recover using artificial intelligence. *Environ. Impact Assess. Rev.* 86, 106492. doi:10.1016/j.eiar.2020.106492

Zhang, B., Wang, Z., Yang, Q., Liu, J., An, J., Li, F., et al. (2020). Elevation changes of the Antarctic ice sheet from joint Envisat and CryoSat-2 radar altimetry. *Remote Sens.* 12, 3746. doi:10.3390/rs12223746



OPEN ACCESS

EDITED BY

Haijun Deng,
Fujian Normal University, China

REVIEWED BY

Baofu Li,
Qufu Normal University, China
Yi He,
Northwest University, China
Junqiang Yao,
China Meteorological Administration,
China

*CORRESPONDENCE

Hongbo Ling,
linghb@ms.xjb.ac.cn
Xiaoya Deng,
lily80876@163.com

SPECIALTY SECTION

This article was submitted to
Atmosphere and Climate,
a section of the journal
Frontiers in Environmental Science

RECEIVED 09 August 2022

ACCEPTED 23 August 2022

PUBLISHED 28 September 2022

CITATION

Wang W, Jiao A, Shan Q, Wang Z,
Kong Z, Ling H and Deng X (2022),
Expansion of typical lakes in Xinjiang
under the combined effects of climate
change and human activities.
Front. Environ. Sci. 10:1015543.
doi: 10.3389/fenvs.2022.1015543

COPYRIGHT

© 2022 Wang, Jiao, Shan, Wang, Kong,
Ling and Deng. This is an open-access
article distributed under the terms of the
Creative Commons Attribution License
(CC BY). The use, distribution or
reproduction in other forums is
permitted, provided the original
author(s) and the copyright owner(s) are
credited and that the original
publication in this journal is cited, in
accordance with accepted academic
practice. No use, distribution or
reproduction is permitted which does
not comply with these terms.

Expansion of typical lakes in Xinjiang under the combined effects of climate change and human activities

Wenqi Wang¹, Ayong Jiao², Qianjuan Shan¹, Zikang Wang¹,
Zijie Kong^{3,4}, Hongbo Ling^{1*} and Xiaoya Deng^{5*}

¹Xinjiang Institute of Ecology and Geography, Chinese Academy of Sciences, Ürümqi, China, ²College of Water Conservancy & Architectural Engineering, Shihezi University, Shihezi, China, ³State Key Laboratory of Hydraulic Engineering Simulation and Safety, Tianjin University, Tianjin, China, ⁴School of Civil Engineering, Tianjin University, Tianjin, China, ⁵China Institute of Water Resources and Hydropower Research, Beijing, China

Lakes are important guarantees of regional economic development and ecological security. Previous studies focused on trends of surface area and water level of lakes in Xinjiang, but paid less attention to nonlinear change and driving mechanisms of lake areas at annual and monthly scales. To address this issue, this study used a remote-sensing Big Data cloud platform and mathematical statistical methods to investigate the change in typical lakes and its attribution in Xinjiang during 1986–2020. The results showed that: 1) there was a significant linear trend in Xinjiang lakes: except for Jili Lake, the plains lakes showed an insignificant ($p > 0.1$) expansion trend, while the mountain lakes showed an significant expansion trend ($p < 0.01$). 2) There was a significant nonlinear trend in Xinjiang lakes: most of the plains lakes showed periodicity at 14 and 21 years, however most of the mountain lakes showed periodicity at 17 and 21 years. Most of the mutation trends of plains lakes were not significant, yet the mutation trends of mountain lakes showed significant expansion. 3) Human activities were the dominant factor leading to changes in the plains lakes: among the anthropogenic factors, farmland area, GDP, and population had significant effects on lake area ($p < 0.1$), and lake expansion was closely related to population and farmland area. Among climatic elements, precipitation mainly affected the changes in plains lakes. 4) Climate change was the dominant factor leading to changes in mountain lakes. The effects of temperature change on mountain lakes were all significantly positive ($p < 0.05$). In the future, it will be necessary to build lake protection schemes that adapt to climate change and human disturbances. This study can provide an important scientific basis for the rational development and utilization of lakes in Xinjiang.

KEYWORDS

xinjiang lakes, plains lakes, mountain lakes, climate change, human activities

1 Introduction

Lakes are an important part of the terrestrial hydrosphere and are particularly sensitive to climate and environmental change. They can record the impact of climate change and human activities on regional hydrological processes at different time scales, especially for inland areas with less precipitation. They are important information carriers to reveal global climate change and regional responses (Zhang et al., 2011; Tao et al., 2015). Lakes are important reservoirs of water resources in arid areas and an important part of the water cycle in arid areas (Song et al., 2013; Song et al., 2013; Kaplan and Avdan, 2017). They are among the most sensitive geographical units in response to global climate change and are also affected by human activities (Jing et al., 2018). In recent decades, inland lakes have undergone drastic changes due to natural environmental changes and human activities (Feng et al., 2016; Deng and Chen, 2017; Deng et al., 2022). However, on a global scale, no consistent trend of lake water level has been found (Wu et al., 2008). In the mountain regions of Asia, mountain glaciers have been shrinking due to rising temperature and increasing precipitation, which has accelerated the expansion of glacial lakes in recent decades (Song et al., 2016; Liu et al., 2019; Huang et al., 2021). Although lakes at high latitudes are expanding, most lakes in arid subtropical regions are shrinking due to the multiple effects of climate warming, population increase, irrigation area expansion and water demand increase caused by economic development (Chaudhari et al., 2018; Wang et al., 2020). There is high vulnerability of water resources in Northwest China. With global warming, increased glacial meltwater have led to rapid increases in lake area on the Tibetan Plateau and Xinjiang (Yao et al., 2022). In addition, the role of lake water resources as a key strategic resource should not be ignored (Qin et al., 2020; Yu et al., 2020). The natural climate characteristics of drought, little rainfall, and strong evaporation has made Xinjiang a restricted water-short environment for a long time. As a natural reservoir and ecological barrier, lakes play an important role in coordinating the space-time balance of water resources, maintaining regional ecological health, and optimizing the human living environment in Xinjiang. Therefore, monitoring and analyzing dynamic changes in lakes, exploring the temporal and spatial evolution of lakes, and implementing lake protection and restoration are hotspots of current ecological environment research (Yu et al., 2020).

Xinjiang is an extremely arid region in China, located in the center of Eurasia and far from the sea (Li et al., 2011). At the same time, Xinjiang is also one of the important distribution areas of lakes in China, with diverse types and wide distribution. However, since the mid-20th Century, due to climate change and unsustainable human economic activities (Zhang et al., 2013), lakes in Xinjiang have changed, which has attracted the attention of many experts and researchers. Remote-sensing

images, such as those from Landsat series satellites (MSS, TM, ETM+), SPOT, PlanetScope, and hyperspectral data, have frequently been used to study dynamic changes in lakes (Riaza and Müller, 2010; Song et al., 2013; Revelles and Van Geel, 2016; Cooley et al., 2017). Methods of lake water extraction include the single-band threshold method, the water quality index method, the spectral classification method (Lira, 2006; Ouma and Tateishi, 2006; Gautam et al., 2015), and others. However, most of these studies focused only on linear changes in water area and water volume. Changes in the number and area of lakes are a major problem in the field of lake research. In addition, the interaction between lakes and climate factors may be uneven in altitude zones, basins, and landscapes. So far, the dynamic response of lakes to different altitude gradients and different basin climatic factors has been unclear, which limits our understanding of the interaction between water resources and climate and affects the rational utilization of regional water resources (Zheng et al., 2021). In addition, there are still few detailed analyses of changes in different lakes and the quantitative impact of local climate and human activities (Yu et al., 2020). The lakes in Xinjiang show different change trends at different altitudes (Jing et al., 2018); with the influence of complex topographic and geomorphic conditions, the types of lakes in the region are diverse. Lakes are distributed in different geomorphic types such as plains (altitude <1,500 m), mountains (1,500 m <altitude <3,500 m), and plateaus (altitude >3,500 m). For example, the water supply of plains Lake Ebinur is provided by seasonal snowmelt water and rainfall, which is affected by climate change (Jing et al., 2018). Its shrinkage is also related to rapid land reclamation and ecological environment deterioration (Zhang et al., 2015a). Therefore, further research is needed to determine the changes in different types of lakes and their influencing factors. Water resources are the key to social and economic development and river basin construction in Xinjiang, but research on changes in water resources in Xinjiang is limited, especially in terms of long-term sequences and large spatial scale (Wufu et al., 2020).

Previous studies only focused on the linear changes of lake area, and ignored the nonlinear changes. In addition, previous studies only considered the possible influencing factors of lake area change, and the impact degree of different influencing factors was rarely explored. Therefore, using remote-sensing images, this study investigated three important issues through discussion of the linear and nonlinear variation of lake area at annual and monthly scales, construction of structural equation models, and analysis of the driving mechanism of lake area changes. The three issues are as follows: 1) to summarize the linear change rules of the interannual trend of lake area in Xinjiang based on remote-sensing images; 2) to explore periodic change rules and abrupt-change event diagnosis of lakes in Xinjiang and the intra-year non-linear change rules; and 3) attribution and problems of the evolution of typical lakes in Xinjiang. The overall research process is shown in Figure 1.

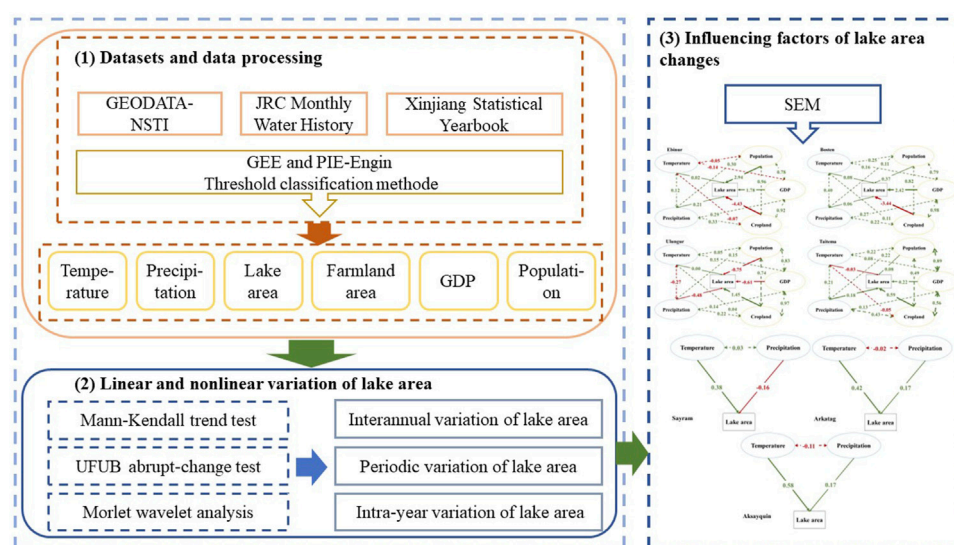


FIGURE 1
The overall framework of the study.

2 Materials and methods

2.1 Study area

Xinjiang is located in the arid area of northwest China ($73^{\circ}20' \sim 96^{\circ}25'E$, $34^{\circ}15' \sim 49^{\circ}10'N$) and is one of the most important places of lake distribution in China. The areas of 110 natural lakes are more than 1 km^2 , and the water area is about $6,236.44 \text{ km}^2$ (Yang et al., 2019). Some of the lakes are terminal lakes and legacies of the ancient Mediterranean Sea. Because Xinjiang is located at a middle latitude in the center of Eurasia, moist water vapor from the ocean has difficulty reaching it. Annual precipitation in Xinjiang is less than 200 mm (Wang et al., 2012), and the spatial distribution is uneven. At the same time, the Tarim Basin, the largest basin in China, and numerous mountains are distributed in Xinjiang, including the Altai Mountains in the north, the Kunlun Mountains in the south, and the Tianshan Mountains that span the whole province. Xinjiang has complex topographic and geomorphic conditions and various types of lakes, including 53 plateau lakes (altitude $>3500 \text{ m}$), 23 alpine lakes ($1,500 \text{ m} < \text{altitude} < 3,500 \text{ m}$), and 45 plains lakes ($<1,500 \text{ m}$) (Bai et al., 2011). The spatial distribution of lakes in Xinjiang is extremely uneven, which is an important reason for spatial differences in regional water resources. From a quantitative standpoint, about 40% of the lakes are concentrated in the surrounding Tianshan Mountains, about 30% in the southern Qiangtang Plateau, about 21% in the southern foothills of the Altai Mountains, and relatively few in the Tarim and Junggar Basins.

The total number of lakes in Xinjiang has been increasing at an average rate of five per year, and the number of large lakes (over 50 km^2) has increased significantly (Zheng et al., 2021). Therefore, ten large lakes (over 100 km^2) in Xinjiang (Li et al., 2015) were selected in this study and divided into two types: plains lakes (altitude $<1,500 \text{ m}$) and mountain lakes (altitude $>1,500 \text{ m}$) to analyze the evolution of and protection strategies for major lakes in Xinjiang (Figure 2). Among these, Lakes Ebinur, Bosten, Ulungur, Jili, and Taitema are plains lakes (altitude $<1,500 \text{ m}$), and Lakes Sayram, Aqqikkol, Ayakkum, Arkatag, and Aksayquin are mountain lakes (altitude $>1,500 \text{ m}$). The plains Lakes Ebinur, Bosten, Ulungur, Jili, and Taitema are all located in the basin area and belong to a temperate continental arid climate with little precipitation and large evaporation. Rivers within the basin are the main source of replenishment for lakes. The largest area of lakes generally occurs in spring, and the smallest area generally occurs in summer and autumn. The mountain Lake Sayram is located in the Junggar Basin, and Lakes Aqqikkol, Ayakkum, Arkatag, and Aksayquin are located in the Kunlun Mountains, which belong to a continental arid climate, where the lakes are mainly replenished by precipitation and meltwater ice and snow. The largest area of lakes generally occurs in autumn, and the smallest area generally occurs in winter and spring.

2.2 Datasets

To study the influence of climatic factors on the number and area changes of lakes, this study used a monthly average

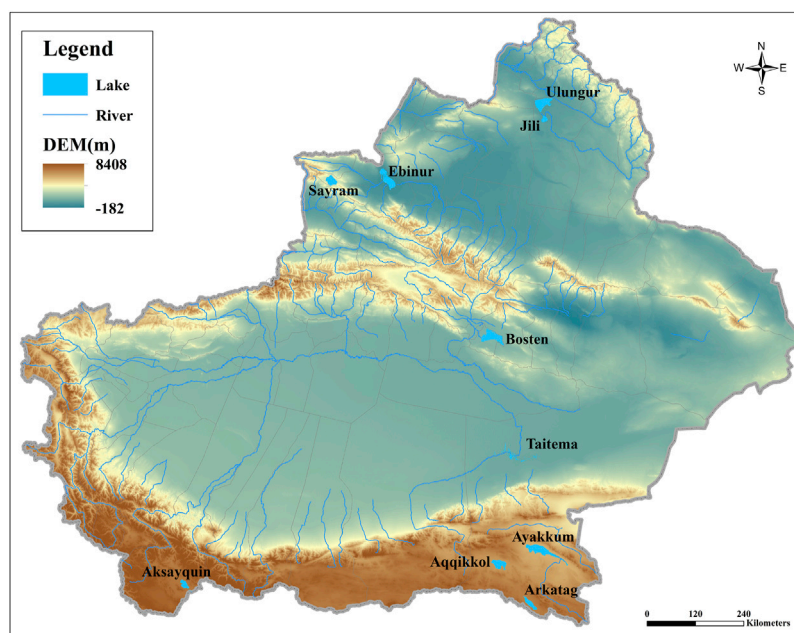


FIGURE 2
Distribution of typical lakes in Xinjiang.

temperature and precipitation dataset (<http://www.geodata.cn/>) for China with a spatial resolution of 1 km from January 1901 to December 2020. The data are based on global climate data with a spatial resolution of 0.5° released by CRU (Climatic Research Unit) and on global high-resolution climate data released by WorldClim through the Delta spatial downscaling scheme in the region of China. The temperature unit is 0.1°C , and the precipitation unit is 0.1 mm. To study the influence of human factors on lake volume and area changes, this study used the farmland area (km^2), GDP (ten thousand yuan) and population (ten thousand) of each lake basin from 1988 to 2020 as obtained from the Xinjiang Statistical Yearbook (xinhjiang.gov.cn) from 1988 to 2020.

2.3 Methods

2.3.1 The Big Data cloud platform

To improve the efficiency and accuracy of lake water extraction, this study was based on the Google Earth Engine (GEE) (<https://code.earthengine.google.com>) and the Pixel Information Expert Engine (PIE-Engine), which are two remote-sensing Big Data and cloud computing platforms, to efficiently process massive remote-sensing images.

The JRC Monthly Water History (V1.3) dataset contains maps of the spatial and temporal distribution of surface water from 1984 to 2020 and provides statistics on the extent and variation of water bodies at a spatial resolution of 30 m (Pekel

et al., 2016). This dataset has only one band and three values: 0, 1, and 2, where 0 means no data; 1 means that there are data, but not for water; and 2 means that there are data for a water body.

The threshold classification method is a classical image segmentation algorithm. It uses the difference between the target object of interest and the non-target object of a certain image feature of a remote-sensing image to divide the image into several classes by setting the threshold, which achieves the separation of target and non-target objects. This study evaluated each raster point in the image and determined whether the raster point belonged to the water body based on the band characteristics of the JRC Monthly Water History dataset, which can be expressed by a mathematical formula as follows:

$$g(x, y) = \begin{cases} \text{no data} & , f(x, y) = 0 \\ \text{non-water} & , f(x, y) = 1 \\ \text{water} & , f(x, y) = 2 \end{cases} \quad (1)$$

where $f(x, y)$ is the original image and $g(x, y)$ is the segmented image. By counting the number of grid cells within the study area and multiplying by the area of each grid cell, the water area within the study region can be obtained.

2.3.2 Mann-Kendall trend test

Based on long-time-series lake area data, linear regression and nonparametric tests were performed using the Mann-Kendall trend test (Mann, 1945; Kendall, 1948) to calculate the rate of change in lake area from 1986 to 2020 and to test

its significance. The Mann-Whitney mutation test (Odeh, 1972; Whitney, 1997) obtained the year of abrupt lake area change in the study region and determined the time period causing the abrupt change in lake area. The influence of climate change and human activities on lake area change was clarified by correlation analysis, and the main research method to clarify the cause of lake area change was the Mann-Kendall trend test.

The Mann-Kendall statistical test is a non-parametric test method. The time series $X_1, X_2, X_3, \dots, X_n$ are successively compared, and the results are represented by $\text{sgn}(\theta)$:

$$\text{sgn}(\theta) = \begin{cases} 1, \theta > 0 \\ 0, \theta = 0 \\ -1, \theta < 0 \end{cases} \quad (2)$$

The calculated result of the Mann-Kendall statistic is:

$$s = \sum_{i=1}^{n-1} \sum_{k=i+1}^n \text{sgn}(x_k - x_i), \quad (3)$$

where x_k and x_i are random variables and n is the length of the selected data series. The test statistic Z_c is:

$$Z_c = \begin{cases} \frac{s-1}{\sqrt{\text{Var}(s)}}, & s > 0 \\ 0, & s = 0 \\ \frac{s+1}{\sqrt{\text{Var}(s)}}, & s < 0 \end{cases} \quad (4)$$

where $|Z_c| \geq 1.96$ indicates that at the 0.05 significance level, the sample sequence has a significant trend, and $|Z_c| > 2.58$ indicates that at the 0.01 significance level, the sample sequence has a significant trend. Positive Z_c indicates an upward trend, and negative Z_c indicates a downward trend.

For the time series X_i ($i = 1, 2, \dots, n$), an order S_k , which represents the cumulative number of $X_i > X_j$ ($1 \leq j \leq i$) in the i th sample, is then constructed. The expression is:

$$S_k = \sum_{i=1}^k r_i \quad (k = 1, 2, \dots, n) \quad (5)$$

Under the assumption that the time series are independent and random,

$$E_{(S_k)} = \frac{k(k-1)}{4} \text{Var}_{(S_k)} = \frac{k(k-1)(2k+5)}{72} \quad (6)$$

Then the statistic UF_k is defined as

$$UF_k = \frac{|S_k - E(S_k)|}{\sqrt{\text{Var}(S_k)}} \quad (k = 1, 2, \dots, n) \quad (7)$$

UF is the standard normal distribution, given the level of significance. If $|UF_k| > U_\alpha$, this indicates an obvious trend in the time series. UF greater than zero indicates an upward trend, whereas UF less than zero indicates a downward trend. The next step is to plot UF as a curve on the time axis and then inversely arrange the time series into a series x_n, x_{n-1}, \dots, x_1 according to

the above method to make a reverse statistic UB_k curve. Then the U_k series is tested, given the significance level $\alpha = 0.05$. If there is an intersection of two curves in the confidence interval $|U| \leq 1.96$, the time corresponding to that point is the point in time when the sequence suddenly changed.

2.3.3 Periodicity analysis

In this study, the Morlet wavelet analysis method was used to study the periodic changes of temperature and precipitation in the lake area. For the time series function $f(t)$, the wavelet variation is defined as

$$W_f(a, b) = \frac{1}{\sqrt{a}} \int_{-\infty}^{\infty} f(t) \psi^*\left(\frac{t-b}{a}\right) dt, \quad (8)$$

where $W_f(a, b)$ is the wavelet coefficients; a is the scale factor, which determines the width of the wavelet; and b is the translation factor, which is the parameter reflecting the moving wavelet position. ψ is the conjugate of ψ^* :

$$\psi(x) = Ce^{-\frac{x^2}{2}} \cos(5x) \quad (9)$$

The wavelet squared difference is

$$W_p(a) = W_f(a, b)^2 \quad (10)$$

Wavelet variance represents the intensity of periodic fluctuations of time series within this scale (Gao and Li, 1993). The scale of the corresponding peak is the main period of the sequence. The wavelet coherence spectrum is used to measure the strength of local correlation between two time series in time-frequency space. The wavelet coherence spectra of two time series X and Y are defined as follows:

$$R_n^2(s) = \frac{|S(s^{-1} W_n^{XY}(s))|^2}{S(s^{-1} |W_n^X(s)|^2) \cdot S(s^{-1} |W_n^Y(s)|^2)} \quad (11)$$

$$S(W) = S_{scale}(S_{time}(W_n(s))) \quad (12)$$

where S_{scale} and S_{time} are smoothed along the scaling and translation axes of wavelet time respectively:

$$S_{time}(W)|_s = (W_n(s) * c_1^{-t^2/2s^2})|_s \quad (13)$$

$$S_{scale}(W)|_n = (W_n(s) * c_2 \Pi(0.6s))|_n \quad (14)$$

where c_1 and c_2 are normalization constants, Π is a rectangular function, and the parameter 0.6 is an empirically determined scale that is decorrelated with the Morlet wavelength.

2.3.4 Structural equation model

A structural equation model (SEM) is a comprehensive data statistical and analysis method based on the variable covariance matrix to analyze the relationship between multivariate data (Garrido et al., 2022). According to the prior knowledge of researchers, the dependence relationship between factors in the system is preset. This information can distinguish the

relationship strength of each factor. The variables selected in this study include temperature and precipitation at plains and mountain lakes, basin farmland area, GDP, and population. In SEM, the “dependence” relationship between variables is used to replace the “causality” relationship. In the SEM graphical framework, this “dependence” relationship is usually represented by a one-way arrow pointing to the response variable, with the starting point of the arrow indicating the predictor variable. When the “cause” and “effect” relationship between variables cannot be accurately judged according to current cognition, or when the variables are causal to each other, two-way arrows are used to link related variables. Green, red, and dashed arrows indicate significant positive, significant negative, and insignificant path relationships respectively. The value is the normalized path coefficient, and the arrow thickness represents the relative magnitude of the normalized path coefficient. A structural equation model is then fitted by the Lavaan package in the R language.

3 Results

3.1 Interannual variation of lake area

3.1.1 Plains lakes

Except for Lake Jili, all plains lakes showed an insignificant ($p > 0.1$) expansion trend. Lake Jili showed a significant expansion trend ($p < 0.05$). The areal expansion of Lake Taitema was significant ($p < 0.01$), and the annual growth rate of Lake Taitema was the highest (8.17 km^2), followed by Lake Ebinur.

From 1986 to 2020, the areas of Lakes Ebinur and Bosten both showed an “expansion-shrinkage-expansion” trend (as shown in Figure 3). Before 2000, the area of Lake Ebinur was relatively stable, and Lake Bosten showed a steady increasing trend. From 2002 to 2008 and from 1996 to 2006, the area of these two lakes both exceeded the multi-year average area (593.61 km^2 and 976.11 km^2). The largest areas of Lakes Ebinur and Bosten appeared at the beginning of the 21st Century, at 810.38 km^2 and $1,071.32 \text{ km}^2$ respectively. The smallest areas appeared after 2010, at 417.30 km^2 and 904.93 km^2 respectively. The main area where Lake Ebinur changed was the northwest entrance to the lake; the expansion area of Lake Bosten in 2002 was mainly in the north and southeast parts of the lake. In 2013, the lake contracted inward as a whole, after which the lake began to expand (as shown in Figure 3). Lake Ulungur was connected with Lake Jili, but the water storage capacity of Lake Jili was much smaller than that of Lake Ulungur. Under the inflow conditions of the same period, the changes in Lake Jili were more complex. From 1988 to 2020, the multi-year average area of Lake Ulungur was 849.14 km^2 , which was 680.08 km^2 larger than that of Lake Jili. Lake Jili showed a significant expansion trend ($p < 0.05$),

whereas Lake Ulungur showed an insignificant expansion trend ($p > 0.1$). From the perspective of spatial distribution, the area of Lake Ulungur was relatively stable, but the entrance to Lake Jili and the southeast part changed significantly (as shown in Figure 3). Due to the great impact of ecological water conveyance, the area of Lake Taitema changed significantly from 1988 to 2020. The multi-year average lake area was 84.82 km^2 , and the annual growth rate was $8.17 \text{ km}^2 \text{ a}^{-1}$. The expansion trend was significant ($p < 0.01$). From 1986 to 2020, the largest area was 402.12 km^2 in 2017, whereas the smallest area was almost zero because the lake dried up. Lake Taitema expanded from the center of the lake to the surrounding areas, and the lake area increased as a whole (as shown in Figure 3).

3.1.2 Mountain lakes

The mountain lakes showed a significant expansion trend ($p < 0.01$), among which the growth rate of Lake Sayram was the lowest, only $0.2 \text{ km}^2 \text{ a}^{-1}$, and the growth rate of Lake Ayakkum was the highest, at $17.32 \text{ km}^2 \text{ a}^{-1}$.

Before 2000, the annual growth rate of Lake Sayram was $0.20 \text{ km}^2 \text{ a}^{-1}$, and the area was smaller than its multi-year average area of 461.52 km^2 , with the smallest area of 459.86 km^2 occurring in 1998. After 2000, the areal growth rate was $0.14 \text{ km}^2 \text{ a}^{-1}$, which was less than before 2000, and the area became larger than the multi-year average area. From 2004 to 2020, the area stably changed between 463 km^2 and 465 km^2 , and the lake area was 464.77 km^2 in 2020. From a spatial point of view, the changes to this water body happened mainly at the peripheral boundary (as shown in the figure). The areas of Lakes Aqqikkol, Ayakkum, and Arkatag increased significantly ($p < 0.01$), and their areas in 2020 were 1.78, 1.91, and 2.59 times those before 2000. The multi-year average area of Lake Aqqikkol was 444.91 km^2 . After 2005, the area was larger than the multi-year average area. The minimum area was 331.43 km^2 , and the maximum was 588.5 km^2 . From 1986 to 2020, the area of Lake Ayakkum expanded from 556.82 km^2 to $1,062.62 \text{ km}^2$. The expansion rate of its lake area was the fastest among all mountain lakes, with a growth rate of $17.32 \text{ km}^2 \text{ a}^{-1}$. The multi-year average area of Lake Arkatag was 218.94 km^2 . In 1987 and 1988, the area of Lake Arkatag was 228.47 km^2 and 252.6 km^2 respectively. It then plummeted to 166.05 km^2 in 1989 and continued to decline to 112.46 km^2 in 1990, after which it gradually increased in a fluctuating pattern. From 1989 to 2004, the lake area was smaller than its multi-year average. In 2005 and later, the area of Lake Arkatag showed a significant upward trend. In 2020, the largest lake area was 290.90 km^2 . Before 2005, the area of Lake Aksayquin was 198.10 km^2 , which was smaller than its multi-year average, and the smallest area (160.27 km^2) appeared in 2002. Before 2005, the annual growth rate of Lake Aksayquin was $0.96 \text{ km}^2 \text{ a}^{-1}$, but after 2005, the annual growth rate became $2.32 \text{ km}^2 \text{ a}^{-1}$. The lake area has exceeded 200 km^2 since 2006 and has been on the rise,

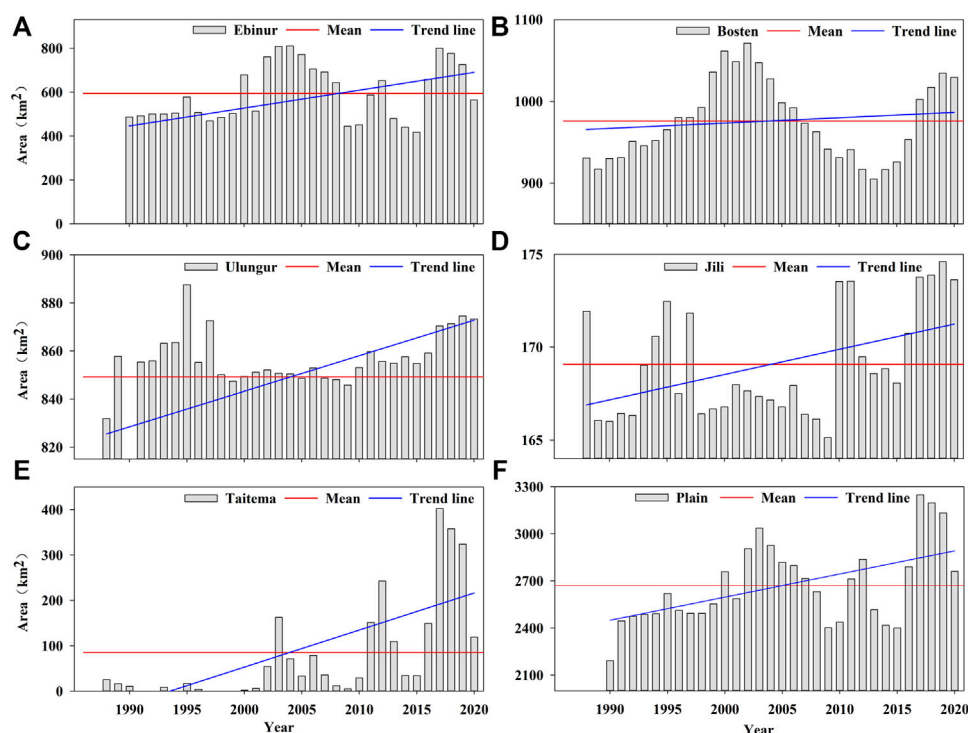


FIGURE 3

Area changes of typical plains lakes in Xinjiang from 1986 to 2020 (A) Lake Ebinur; (B) Lake Bosten; (C) Lake Ulungur; (D) Lake Jili; (E) Lake Taitema; (F) the plains lakes.

reaching a maximum in 2020. From the perspective of spatial changes in the lake, the East and west parts of Lake Aqqikkol, the entrance to Lake Ayakkum, and the southeast part of Lake Arkatag increased significantly. The water body of Lake Aksayquin expanded significantly at the southeast entrance, and the lake size increased as a whole (as shown in Figure 4).

3.2 The periodic variation of lake area

3.2.1 Plains lakes

The abrupt-change test results showed that (as shown in Figure 5), except for Lakes Jili and Taitema that had only one mutation year, there were two mutation years in plains lake area from 1986 to 2020, and the abrupt-change trends were mostly insignificant. Lake Ebinur showed abrupt shrinkage in 2008 and 2017; the former was a significant change ($p < 0.05$), but the latter was insignificant. The average lake area increased by 4.2% after the transition year 2017. There was an significant expansion mutation in 1991 in Lake Bosten ($p < 0.01$), in which the average area increased by 7.4%. In 2009, an insignificant shrinkage mutation occurred, and the average area decreased by 3.5%. The area of Lake Ebinur showed periodicity at 7, 12, and 21 years, and that of Lake Bosten

showed periodicity at 9, 14, and 21 years (Figure 6). In these cases, the wavelet variance at 13 and 14 years was the largest respectively (Figure 6), indicating that the main periodicity of area change for Lakes Ebinur and Bosten was 13 and 14 years respectively. The 12-years cyclic oscillation of Lake Ebinur after 2007 was significantly greater than before 2007, whereas the 12-years cyclic oscillation of Lake Bosten was relatively stable. Lake Ulungur had a significant shrinkage mutation in 1995 ($p < 0.05$) and an insignificant expansion mutation in 2018, in which the average area increased by 3.4%. Lake Jili had an significant expansion mutation in 2016 ($p < 0.01$), in which the average area increased by 3.4%. The area of Lake Ulungur showed periodicity at 9, 17, and 21 years and that of Lake Jili at 11, 14 and 21 years (Figure 6), with a main period of 21 years. For the 21-years cycle, the negative-positive phase change of Lakes Ulungur and Jili occurred in 2001, indicating that Lakes Ulungur and Jili showed a shrinking trend before 2001 and an expanding trend after 2001. This was consistent with the analysis results of the mutation test. After 2000, the 11-years and 14-year periodic oscillations of Lake Ulungur were significantly smaller than before 2000, whereas the periodic oscillations of Lake Bosten were relatively stable. Lake Taitema showed an significant expansion mutation in 2009 ($p < 0.01$), in which the average area increased by 6.2%.

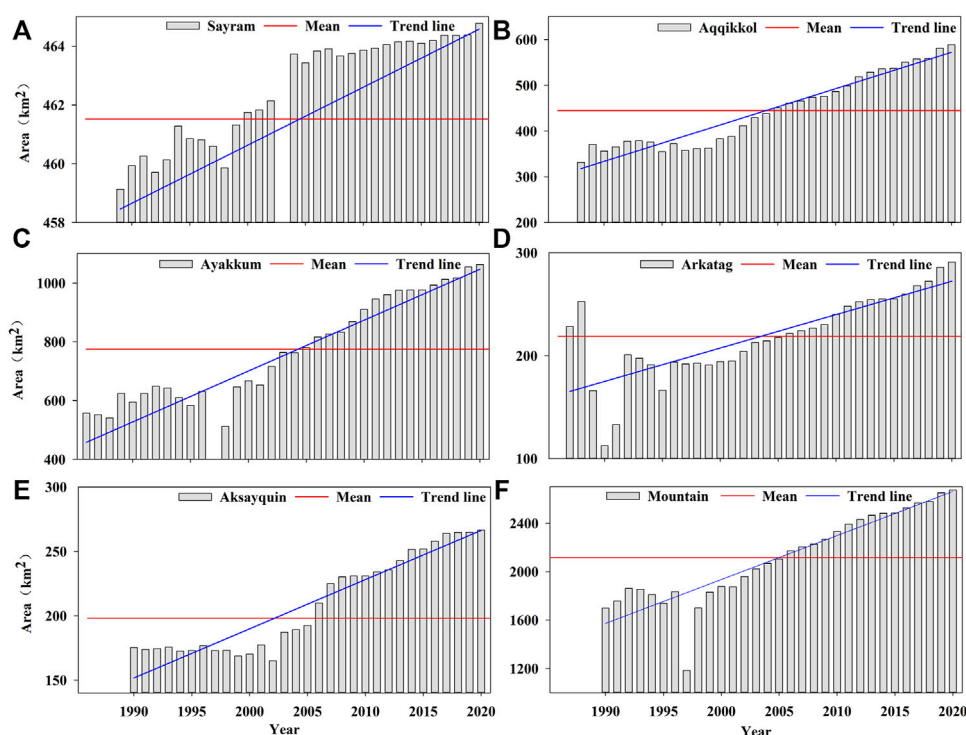


FIGURE 4

Area changes of typical mountain lakes in Xinjiang from 1986 to 2020 (A) Lake Sayram; (B) Lake Aqqikkol; (C) Lake Ayakkum; (D) Lake Arkatag; (E) Lake Aksayquin; (F) the mountain lakes.

The lake area showed periodicity at 8, 17, and 21 years, with a main period of 21 years.

3.2.2 Mountain lakes

Compared with plains lakes, the periodic change rule of mountain lakes was relatively simple. The abrupt-change test results showed that (as shown in Figure 7) significant mutations had occurred in mountain lakes ($p < 0.01$), and the mutation years were mainly concentrated around 2009. Lakes Sayram, Aqqikkol, Ayakkum, Arkatag, and Aksayquin had significant expansion mutations in 2009, 2008, 2008, 2011, and 2012 respectively. From 2009 to 2020, the areas of Lakes Ayakkum and Aqqikkol increased by 46.3% and 35.9% respectively, whereas the area of Lake Sayram increased by only 0.9% from 2010 to 2020. The main periodicity of lake area change in mountain lakes was 21 years (Figure 8). The area of Lake Sayram showed periodicity at 7, 17, and 21 years. Lakes Aqqikkol and Arkatag showed periodicity at 13, 17, and 21 years. Lakes Ayakkum and Aksayquin showed periodicity at 17 and 21 years. The 7-years cycle oscillation (Figure 8) of Lake Sayram showed an increasing trend before 2003 and a weakening trend after 2003. The decadal changes showed that the area of mountain lakes showed a downward trend

before 2003–2006 and an upward trend afterwards. This was consistent with the analysis results of the mutation test.

3.3 Intra-year variation of lake area

3.3.1 Plains lakes

Due to the influence of winter snow cover, this study selected the change in lake area from May to October to analyze changing lake area at a monthly scale. The change in plains lake area had obvious seasonality (as shown in Figure 9). The multi-year average area of Lake Ebinur shrank from May to October, with a maximum of 493.24 km² in May and a minimum of 423.41 km² in October. On the contrary, Lake Bosten showed an overall expansion trend, with a smaller lake area from May to August and a larger lake area in September and October. The variation trend of the monthly-scale standard deviation of the areas of Lakes Ebinur and Bosten was also opposite: the standard deviation of the area of Lake Ebinur increased from May to October (a minimum of 21.86 km² in May, a maximum of 61.77 km² in July), whereas the standard deviation of the area of Lake Bosten showed a decreasing trend (a maximum of 99.10 km² in May, a minimum of 54.24 km² in October). This showed that from May to October, the area of Lake Ebinur

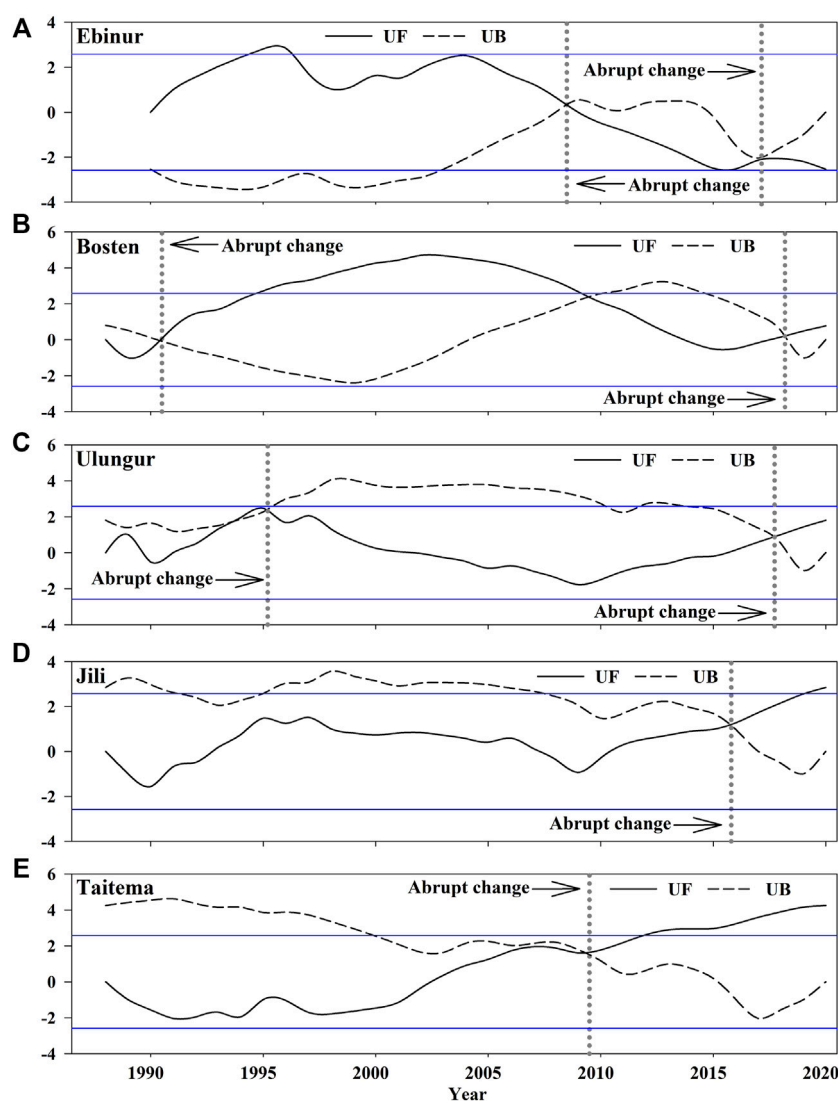


FIGURE 5

Results of the abrupt-change test of typical plains lakes area in Xinjiang from 1986 to 2020 (A) Lake Ebinur; (B) Lake Bosten; (C) Lake Ulungur; (D) Lake Jili; (E) Lake Taitema.

shrank and fluctuated greatly, whereas the area of Lake Bosten expanded and stabilized. The areas of Lakes Ulungur and Jili reached a maximum in May (860.78 km^2 and 167.67 km^2 respectively), and the overall lake area decreased sequentially through spring, summer, and autumn. In addition, the standard deviation of the area of Lake Ulungur increased from May to October, showing a trend of first increasing, then decreasing, and then increasing again. The standard deviation fluctuated between 11.03 km^2 and 86.86 km^2 . The standard deviation was the largest and the average area was the smallest (821.40 km^2) in July. Abnormally small areas occurred mostly in July. The standard deviation of Lake Jili's area was small from May to October, with a maximum in May (9.40 km^2) and a minimum in October, only

3.61 km^2 . Therefore, the area of Lake Ulungur was larger, and the monthly-scale variation fluctuated greatly, whereas the area of Lake Jili was one-fifth that of Lake Ulungur, and the monthly-scale variation in lake area was stable. The overall area of Lake Taitema shrank from May to June, with a minimum (110.53 km^2) in June, and then expanded month by month, reaching a maximum (181.47 km^2) in October. The multi-year average monthly area of Lake Taitema was 47.08 km^2 smaller than that of Lake Jili, but the area change in Lake Taitema was greatly affected by runoff and human disturbances. Therefore, the average standard deviation of Lake Taitema was 135.94 km^2 larger than that of Lake Jili and was the largest among the plains lakes.

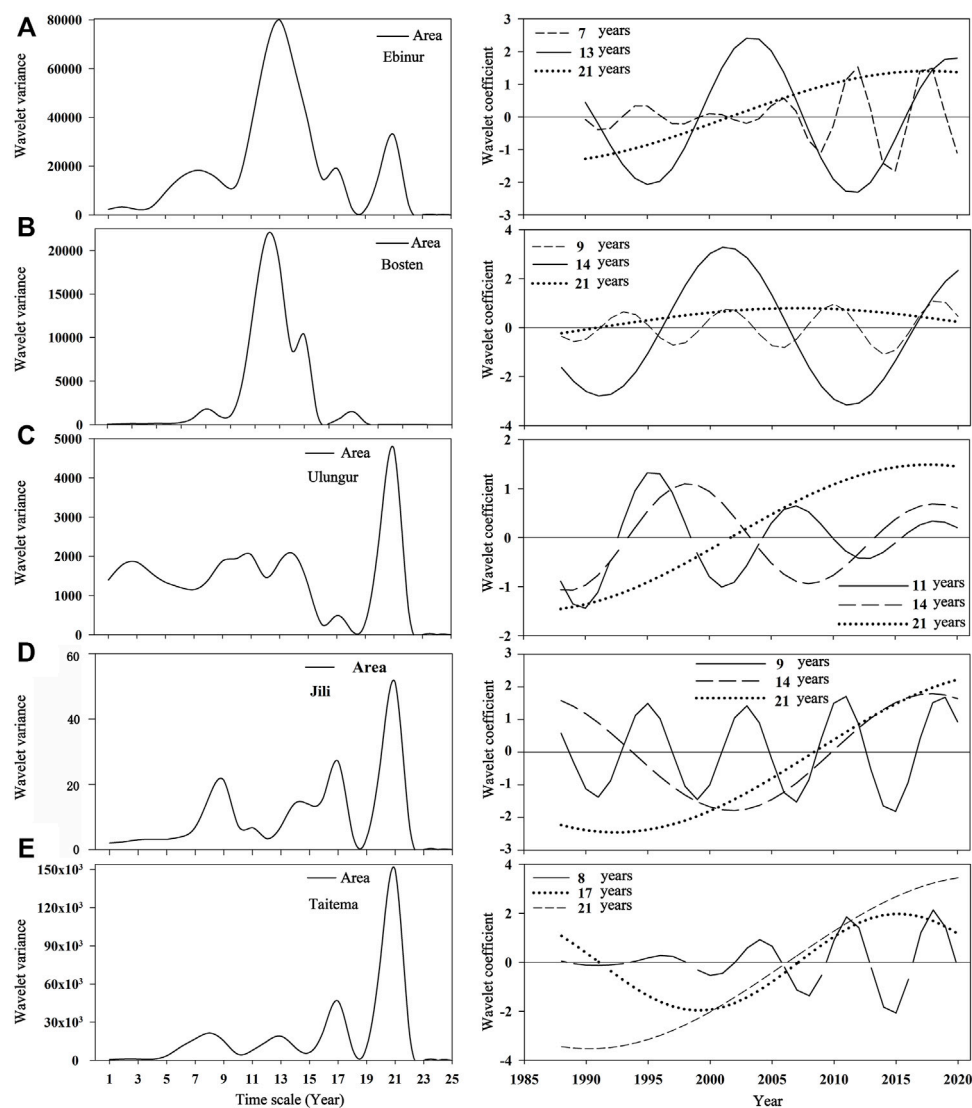


FIGURE 6

Results of wavelet analysis of typical plains lakes area in Xinjiang from 1986 to 2020 (A) Lake Ebinur; (B) Lake Bosten; (C) Lake Ulungur; (D) Lake Jili; (E) Lake Taitema.

3.3.2 Mountain lakes

Compared with plains lakes, mountain lakes had less obvious seasonality and smaller monthly-scale standard deviations. The multi-year average area of Lake Sayram showed a trend of decreasing, increasing, and then decreasing again: the multi-year annual average area reached a maximum in September (462.64 km^2), and the standard deviation was the smallest, only 1.72 km^2 ; the area in June was the smallest (453.02 km^2), with the largest standard deviation (18.92 km^2). Excluding factors such as ice and snow coverage and lake freezing, the change in Lake Sayram area was relatively stable. The

multi-year average area and standard deviation of Lakes Aqqikkol and Ayakkum showed a trend of first decreasing, then increasing, and then decreasing again. In summer, ice and snow melt water made the lake expand, the area fluctuated greatly, and the lake area and standard deviation reached their maximum values (the area was 456.12 km^2 and 825.33 km^2 respectively; the standard deviation was 94.42 km^2 and 180.80 km^2 respectively). From May to October, the rates of change in the areas of Lakes Aqqikkol and Ayakkum were 7.60% and -1.20% respectively. It is clear that the area of Lake Aqqikkol fluctuated more obviously. The overall area of Lake

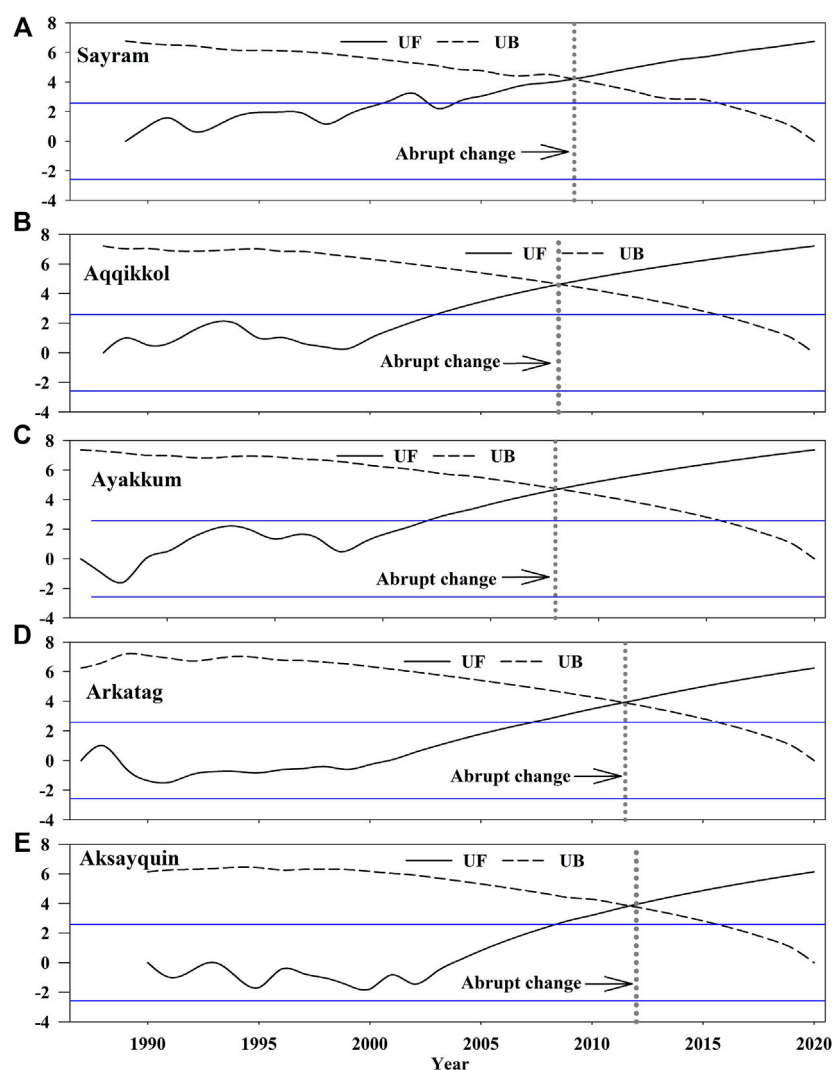


FIGURE 7

Results of the abrupt-change test of typical mountain lake areas in Xinjiang from 1986 to 2020 (A) Lake Sayram; (B) Lake Aqqikkol; (C) Lake Ayakkum; (D), Lake Arkatag; (E) Lake Aksayquin.

Arkatag increased from spring to autumn, with the smallest area in May (159.26 km^2), the largest area in September (229.94 km^2), and an area rate of change of 24.92%. The standard deviation of the area of Lake Arkatag reached a minimum of 30.7994 km^2 (May) and a maximum of 36.8794 km^2 (September). Among Lakes Aqqikkol, Ayakkum, and Arkatag, Lake Arkatag had the smallest area and was most affected by meltwater, and hence the area fluctuated greatly. The multi-year average area of Lake Aksayquin increased month by month. The lake area was the smallest in May (181.04 km^2) and the largest in September (229.94 km^2). The rate of change in lake area was 11.54%, with the standard deviation showing a decreasing trend and the area fluctuating greatly.

4 Discussion

4.1 Influencing factors of plains lake area changes

4.1.1 Effects of human activities on lake area

Human activities were frequent in the plains lake basins. Domestic water and agricultural irrigation affected the changes in lake water volume and area (Chai et al., 2013; Wufu et al., 2020). Therefore, this study mainly analyzed the relationship between lake area change and human activities in the plains area. By identifying changes in population, farmland area, and GDP in the plains lake basins, the influence of human activities on changes in lake area was elucidated.

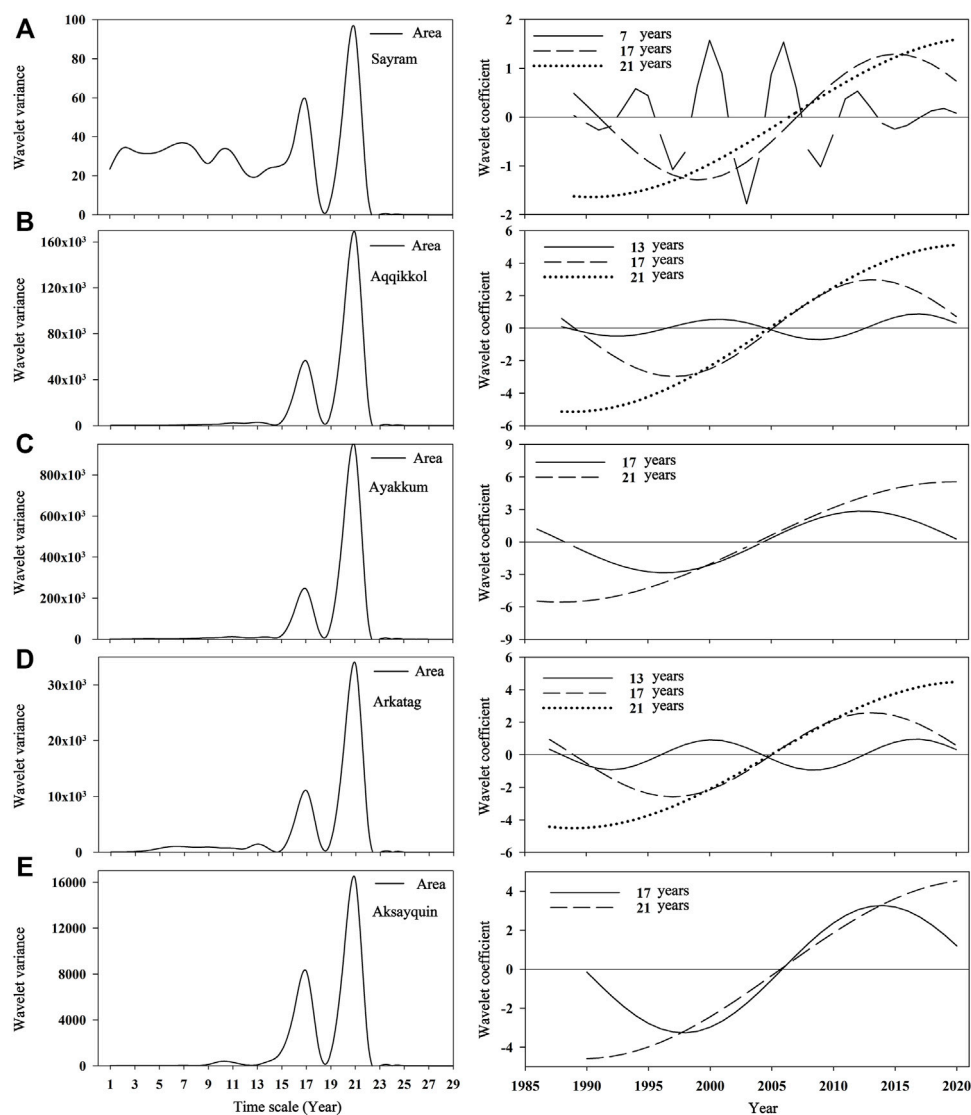
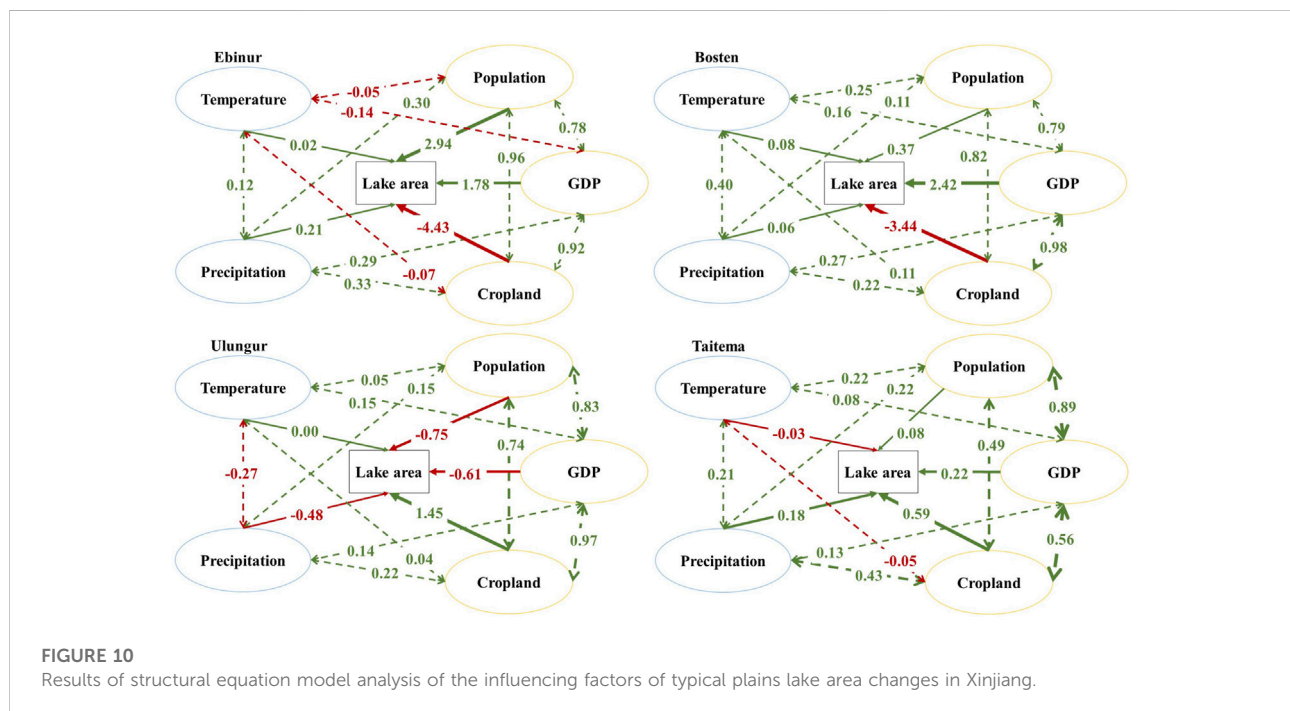
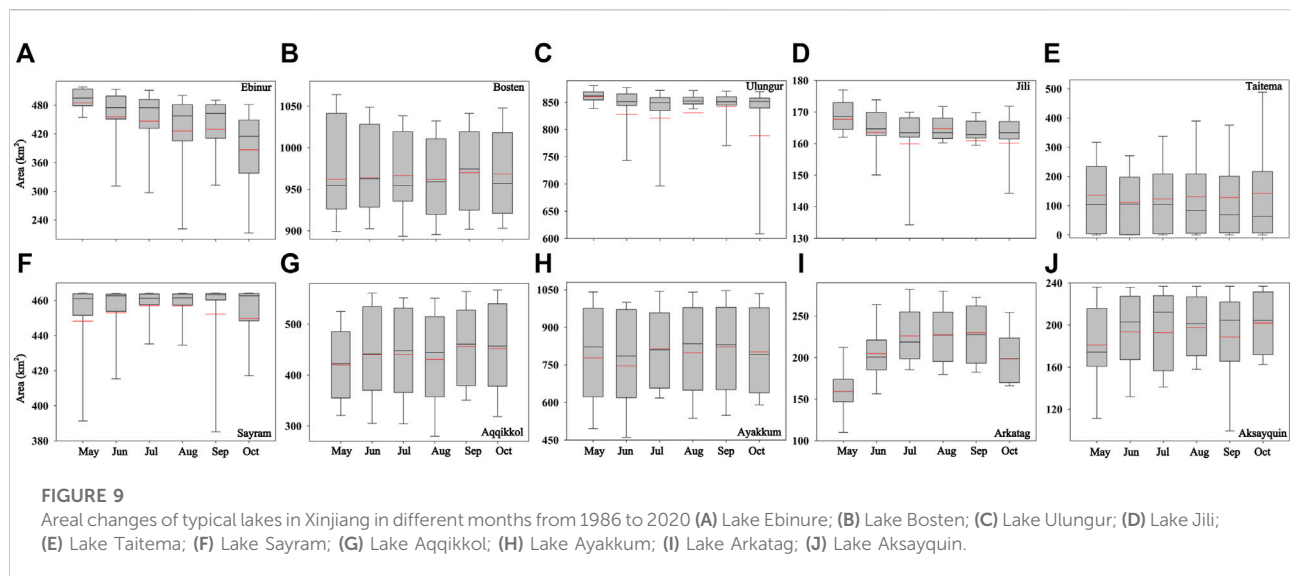


FIGURE 8

Results of the wavelet analysis of typical mountain lake areas in Xinjiang from 1986 to 2020 (A) Lake Sayram; (B) Lake Aqqikkol; (C) Lake Ayakkum; (D) Lake Arkatag; (E) Lake Aksayquin.

From the analysis results of the structural equation model (Figure 10), among the human activity factors, the farmland area and population of the Lake Ebinur basin had significant ($p < 0.1$) negative and positive effects on lake area respectively (path coefficients of -4.43 and 2.94 respectively). Compared with the impact of climatic factors, the main reason for the reduction in Lake Ebinur area was interception of surface runoff. Since the early 1950s, the area of Lake Ebinur had changed with the population and farmland area of the basin (Zhang et al., 2015b; Zhang et al., 2017; Zhang et al., 2021): from the early 1970s to the mid-1990s, population and farmland growth was slow, the lake area changed slightly, and the lake area was basically maintained at about 600 km^2 except for dry

years. At the beginning of the 21st Century, the population and farmland area increased significantly, resulting in a continuous degradation trend of the lake area, which reached its lowest value of 417.29 km^2 in 2015. In recent years, the farmland area and population stabilized, and the lake area began to revert and remained at about 600 km^2 . The changes in farmland area, GDP, and population in the Lake Bosten basin had significant negative, positive, and positive effects on lake area ($p < 0.01$) respectively (path coefficients of -3.44 , 2.42 , and 0.37 respectively). Since 1993, the farmland area, GDP, and population of Bortala Mongol Autonomous Prefecture have shown an increasing trend. This was inconsistent with the overall trend of changes in lake area, which was mainly due to direct correlation between the inflow



and outflow of Lake Bosten. For example, from 2000 to 2017, the water storage capacity of Lake Bosten and the changes in lake area showed obvious consistency changes. Since 2015, the slowdown in the growth rates of population and farmland in this region contributed to lake expansion. Population changes in the Lake Ulungur basin had a significant ($p < 0.1$) negative effect on lake area (path coefficient of -0.75). Population and farmland in this region had been increasing for a long time. The shrinkage

in lake area after the 1990s was mainly due to increasing farmland area, extensive agricultural water use, and a population surge. After 2009, even though the area of farmland and the population continued to increase, the lake area gradually reverted under the influence of water-saving irrigation practices and ecological water diversion in recent years. Lake Jili is replenished by the Ulungur River, which belongs to the freshwater lake with water intake and output.

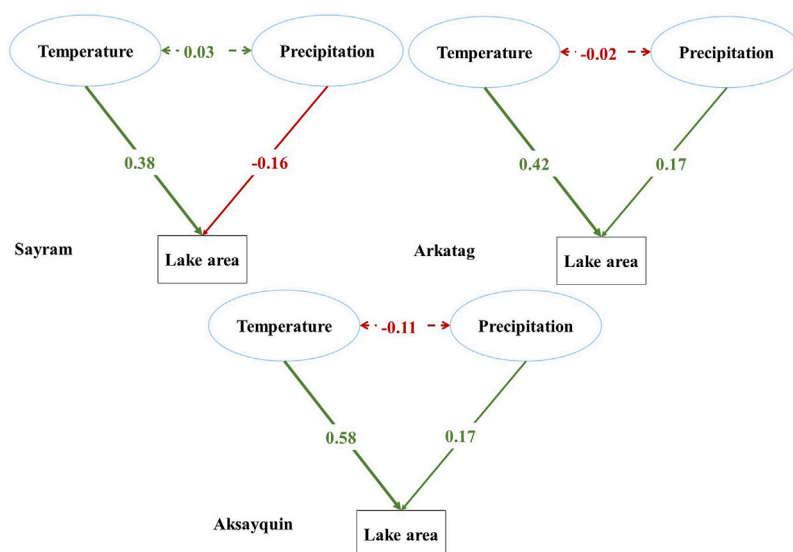


FIGURE 11

Results of structural equation model analysis of the influencing factors of typical mountain lake area changes in Xinjiang.

Its change pattern was basically the same as that of the Lake Ulungur area. Human activities amplified the fluctuations in lake area caused by climate change. We want to emphasize that the findings that the unbalanced changes might be attributed to different reasons (i.e., climate change and human activities) are based on limited evidence and therefore preliminary. Indeed, human activities such as agricultural irrigation also played a role in affecting the lakes (Ma et al., 2010). In view of changes in farmland area, GDP, and population, strengthening research into the carrying capacity of water resources in plains lake basins, strictly controlling population, and strengthening comprehensive management of water resources are the fundamental components of ecological protection of plains lakes. The main amount of water in Lake Taitema came from the discharge of the Daxihaizi Reservoir and the replenishment of the Cherchen River. In the 1970s, Lake Taitema was once dried up by human activities. Since 2000, the ecological environment downstream of the Tarim River and Lake Taitema has been restored through ecological water conveyance. The area of Lake Taitema from 2000 to 2020 was affected by the inflow and outflow of the Tarim River. The cumulative water inflow of the Tarim River was 2.081 billion cubic meters, with an average annual water inflow of 94 million cubic meters. The lake area reached its maximum in 2017 and had been decreasing in recent years with a decrease in the amount of water discharged. For Lake Taitema, in the case of a high flow year, the current complete ecological reservoir (Daxihaizi Reservoir) control system and the ecological gates of each section had to be manually regulated and operated to avoid all the ecological water flowing into Lake Taitema at one time. It is necessary to formulate a further

and more reasonable water resource regulation plan according to the relationship between the discharge volume and the lake area and to use the ecological gates of the sections below and at the Daxihaizi Reservoir to regulate the inflow to the lake during flood periods. The intent is to avoid large wastage of water under local high-intensity evaporation conditions.

4.1.2 Effects of climatic factors on lake area

The variation characteristics of temperature and precipitation of lake basins in Xinjiang were tested by Mann-Kendall trends. Because Lakes Ulungur and Jili operate as a unit, this subsection discusses them as the Ulungur River Basin as a whole.

Rising temperatures must be compensated for by precipitation to maintain lake area. The temperature and precipitation of plains lakes were generally increasing during the study period. If precipitation did not compensate for the loss of lake area, the temperature rise would lead to a decrease in lake area. From 1985 to 2020, the annual average temperature of the plains lake basins showed a significant upward trend ($p < 0.01$), with growth rates of 0.03, 0.05, 0.04, and 0.03, respectively, and mutation years of 1996, 1994, 1994, and 1997, respectively. The temperature of plains lakes showed periodicity at 9, 17, and 21 years, with the main period being 21 years. For the 21-years cycle, the negative-positive phase change in temperature occurred in 1999, 1998, 2001, and 2000, indicating that the temperature of the plains lakes was declining before 2000 and rising after 2000. This was consistent with the mutation years around 2000 and the significant upward mutation trends. The basins of Lakes Ebinur and Bosten had less precipitation and

stronger evaporation, which was mainly supplied from river flow. Rising temperature caused evaporation and had an impact on lake area (Jing et al., 2020). The structural equation model results (Figure 10) showed that the effect of temperature change on the areas of Lakes Ebinur and Bosten constituted an insignificant ($p > 0.1$) positive effect (path coefficients of 0.02 and 0.08 respectively), the effect of temperature change on the area of Lake Ulungur was almost zero, and the effect of temperature change on the area of Lake Taitema was insignificant ($p > 0.1$) (path coefficient of -0.03). These results showed that the effect of temperature change on the area of plains lakes was largely insignificant ($p > 0.1$).

Annual precipitation at plains lakes showed an insignificant increase ($p > 0.1$), with rates of change of 0.25, 0.85, 0.11, and 0.48, respectively. The mutation years were 1998, 1992, 1992, and 2018, and the mutation trends were insignificant ($p > 0.1$). The effect of very low precipitation at Lake Taitema on lake area was negligible. Therefore, the correlation between climate and the area of Lake Taitema was not further analyzed in this section. The precipitation at plains lakes mostly showed periodicities at 17 and 21 years, with main periods of 7, 6, 11, and 21 years respectively. The precipitation at Lake Ebinur decreased before 2002 and increased after 2002. Before 1998 and before 2010, precipitation at Lakes Bosten and Ulungur showed an increasing trend, but a decreasing trend after 1998 and after 2010. Precipitation at Lake Taitema showed a decreasing trend before 2011 and an increasing trend after 2011. The periodicity of precipitation changes at Lakes Ebinur and Taitema was relatively consistent with the mutation years and the significant mutation upward trend, whereas Lakes Bosten and Ulungur gave the opposite result. The effects of precipitation on the areas of Lakes Ebinur and Taitema were both insignificant ($p > 0.1$) positive effects (path coefficients of 0.21 and 0.18 respectively), whereas Lake Bosten had an insignificant positive effect (path coefficient of 0.06), and Lake Ulungur had an significant negative effect (path coefficient of -0.48). The results of the structural equation model showed that the precipitation increase for Lakes Ebinur and Taitema promoted the expansion of the lakes, but that the precipitation changes for Lakes Bosten and Ulungur had less impact on lake expansion and even led to shrinkage of the lakes under the influence of human activities (Jing et al., 2018).

At an intra-year scale, changes in temperature and precipitation led to a strong seasonality in plains lake areas. The problem of water resource development and distribution should be solved, and agricultural water consumption in plains lake basins should be adjusted in spring and summer to ensure ecological water utilization (Zheng et al., 2021).

4.2 Influencing factors of mountain lake area changes

Due to their geographical location, mountain lakes have been less affected by human activities, and therefore this study analyzed

climate change as the main factor for changes in mountain lake area (Wufu et al., 2020). The Central Kunlun mountain lakes are composed of Lakes Arkatag, Ayakkumu, and Aqqikkol, and hence this study discussed all three as the Middle Kunlun Mountain Lakes.

From 1985 to 2020, the annual average temperature of mountain lake basins showed an significant increase ($p < 0.001$), with growth rates of 0.04, 0.03 and 0.06, respectively, and the significant mutation increase years were 1994, 2000, and 1998, respectively. The temperature of mountain lakes showed periodicity at 17 and 21 years, with a main period of 21 years. For the 21-years cycle, negative-positive phase changes in temperature occurred in 2001, 2001, and 2005, indicating that plains lakes temperature declined before the early 21st Century and then rose. This was consistent with the mutation years around 2000 and the significant upward mutation trend. The effects of temperature changes on mountain lake area were all significantly positive ($p < 0.05$) (path coefficients of 0.38, 0.42, and 0.58 respectively), of which the Middle Kunlun Mountain Lakes and Lake Aksayquin showed significant positive effects ($p < 0.001$) (Figure 11). This showed that the increase in temperature was closely related to increases in lake area in mountain basins (Yang et al., 2020; Liu et al., 2022). The temperature of mountainous areas increased significantly around 2000. The increase in lake inflow due to melting of ice and snow contributed to an increase in lake area around 2010, which also indicated that lake area has a certain lag phase for temperature changes.

From 1985 to 2020, annual precipitation in the mountain lake basins showed an insignificant increase ($p > 0.1$) with growth rates of 0.98, 0.05, and 0.05, and the significant mutation increase years were 2001, 2001, and 1988 respectively. The precipitation at Lake Sayram showed periodicity at 6 and 21 years, the Middle Kunlun Mountain Lakes at 13 and 21 years, and Lake Aksayquin at 5, 17, and 21 years. The main periods were 6, 13, and 5 years, respectively. Precipitation in the Lake Sayram basin and the Middle Kunlun Mountain Lakes basin showed a decreasing trend before the beginning of the 21st Century and then an increasing trend; precipitation in the Lake Aksayquin Basin showed an increasing trend before 1992, decreased from 1992 to 2008, and has increased since then. The effect of precipitation changes on mountain lake area was insignificant ($p > 0.1$), and there was even a negative effect (precipitation at Lake Sayram had a negative effect on lake area, with a path coefficient of -0.16), which was mainly caused by rainfall weakening the positive effect of temperature.

In mountain and plateau areas, which have been less affected by human activities, lake area changes were more closely related to climate change. Although both temperature and precipitation showed an overall upward trend from 1986 to 2020, the increase in temperature was more significant ($p < 0.001$), and lake expansion and contraction trends were more closely related to changes in temperature. This illustrated the sensitivity of mountain lakes to climate change. However, the impact of climate change on mountain lakes was also becoming more and more significant. In recent years,

rising water level has brought about serious collapse of the lakeshore, causing harm to roads around the lake. The increase in precipitation has increased erosion of grasslands and the Earth's surface, reducing the erosion resistance of soil, and large amounts of nitrogen, phosphorus, and organic nutrients have been integrated into the lake with rainwater, exacerbating lake eutrophication. Therefore, strengthening local ecological restoration and grassland recovery and comprehensively controlling sources of lake pollution are important tasks for ecological environmental protection in mountain lake basins.

5 Conclusion

Taking the top ten lakes in Xinjiang as examples, this study analyzed the temporal and spatial dynamics of lakes in Xinjiang from 1986 to 2020 by using lake area, climatic factors, and ecological and environmental factors. The main conclusions of the study are as follows:

- 1) Except for Lakes Jili and Taitema, the plains lakes showed an insignificant ($p > 0.1$) expansion trend. Lake Jili showed a significant expansion trend ($p < 0.05$), and Lake Taitema showed an significant expansion trend ($p < 0.01$). Most of the plains lakes showed periodicity at 14 or 21 years. Except for the area changes in Lakes Jili and Taitema, which had only one mutation year, the plains lakes had two mutation years of area change between 1986 and 2020, but the mutation trends were mostly insignificant.
- 2) The mountain lakes showed significant expansion trends ($p < 0.01$) and significant expansion mutations occurring in 2009, 2008, 2008, 2011, and 2012, respectively. Most mountain lakes showed periodicity at 17 or 21 years. The decadal change pattern revealed that the area of mountain lakes showed a downward trend before 2003–2006 and then an upward trend. This was in line with the results of the abrupt-change test.
- 3) Human activities were the leading factor influencing lake area changes in plains lake basins. Changes in temperature and precipitation did not have a significant effect on area changes in plains lake basins ($p > 0.1$). Among anthropogenic factors, farmland area, GDP, and population change had significant ($p < 0.1$) effects on lake area, and the slowing growth rates of population and farmland area contributed to lake expansion. Therefore, the protection strategy for plains lakes must adjust the development and allocation of water resources according to the dominant influencing factors of different lakes.
- 4) Due to their geographical location, mountain lakes have been less affected by human activities. Climate change was the dominant factor in changes in mountain lakes. The effects of temperature change on mountain lakes were all significantly positive ($p < 0.05$). When the temperature increased significantly, melting of ice and snow led to increasing inflow into the lake and increasing lake area. Rainfall weakened the positive effect of temperature.

Therefore, for mountain lakes, ecological and environmental protection measures are needed against damage caused by rising water level and erosion of shores and soils by precipitation.

Data availability statement

The original contributions presented in the study are included in the article/[Supplementary Material](#), further inquiries can be directed to the corresponding author.

Author contributions

The authors undertook different tasks for this paper. WW performed data processing and wrote the paper. WW, AJ, ZW, and ZK analyzed the data. HL and XD provided direction for the research work, designed the research and revised the paper. All authors have read and agreed to the published version of the manuscript.

Funding

This research was funded by the National Natural Science Foundation of China (52179028), the West Light Foundation of Chinese Academy of Sciences (2019-XBQNXX-A-001), and the Xinjiang Water Conservancy Science and Technology Special Fund Project (XSKJ-2022-10).

Conflict of interest

The authors declare that the research was conducted in the absence of any commercial or financial relationships that could be construed as a potential conflict of interest.

Publisher's note

All claims expressed in this article are solely those of the authors and do not necessarily represent those of their affiliated organizations, or those of the publisher, the editors and the reviewers. Any product that may be evaluated in this article, or claim that may be made by its manufacturer, is not guaranteed or endorsed by the publisher.

Supplementary material

The Supplementary Material for this article can be found online at: <https://www.frontiersin.org/articles/10.3389/fenvs.2022.1015543/full#supplementary-material>

SUPPLEMENTARY FIGURE S1

Spatial distribution of area changes in typical years at typical lakes in Xinjiang from 1986 to 2020.

SUPPLEMENTARY FIGURE S2

Variation of temperature and precipitation at typical lakes in Xinjiang from 1985 to 2020 (A) Lake Ebinure; (B) Lake Bosten; (C) Lake Ulungur; (D) Lake Taitema; (E) Lake Sayram; (F) Lake Arkatag; (J) Lake Aksayquin.

SUPPLEMENTARY FIGURE S3

Results of wavelet analysis of temperature in typical plains lake basins in Xinjiang from 1985 to 2020 (A) Lake Ebinure; (B) Lake Bosten; (C) Lake Ulungur; (D) Lake Taitema.

SUPPLEMENTARY FIGURE S4

Results of wavelet analysis of precipitation in typical plains lake basins in Xinjiang from 1985 to 2020 (A) Lake Ebinure; (B) Lake Bosten; (C) Lake Ulungur; (D) Lake Taitema.

SUPPLEMENTARY FIGURE S5

Results of wavelet analysis of temperature in typical mountain lake basins in Xinjiang from 1985 to 2020 (A) Lake Sayram; (B) Lake Arkatag; (C) Lake Aksayquin.

SUPPLEMENTARY FIGURE S6

Results of wavelet analysis of precipitation in typical mountain lake basins in Xinjiang from 1985 to 2020 (A) Lake Sayram; (B) Lake Arkatag; (C) Lake Aksayquin.

References

- Bai, J., Chen, X., Li, J., Yang, L., and Fang, H. (2011). Changes in the area of inland lakes in arid regions of central Asia during the past 30 years. *Environ. Monit. Assess.* 178 (1), 247–256. doi:10.1007/s10661-010-1686-y
- Chai, H., Cheng, W., Zhou, C., Zhao, S., and Liu, H. (2013). Climate effects on an inland alpine lake in Xinjiang, China over the past 40 years. *J. Arid. Land* 5 (2), 188–198. doi:10.1007/s40333-013-0156-0
- Chaudhari, S., Felfelani, F., Shin, S., and Pokhrel, Y. (2018). Climate and anthropogenic contributions to the desiccation of the second largest saline lake in the twentieth century. *J. Hydrol. X.* 560, 342–353. doi:10.1016/j.jhydrol.2018.03.034
- Cooley, S. W., Smith, L. C., Stepan, L., and Mascaro, J. (2017). Tracking dynamic northern surface water changes with high-frequency planet CubeSat imagery. *Remote Sens. (Basel)* 9 (12), 1306. doi:10.3390/rs9121306
- Deng, H., Chen, Y., and Chen, X. (2022). Driving factors and changes in components of terrestrial water storage in the endorheic Tibetan Plateau. *J. Hydrol. X.* 612, 128225. doi:10.1016/j.jhydrol.2022.128225
- Deng, H., and Chen, Y. (2017). Influences of recent climate change and human activities on water storage variations in Central Asia. *J. Hydrol. X.* 544, 46–57. doi:10.1016/j.jhydrol.2016.11.006
- Feng, L., Han, X., Hu, C., and Chen, X. (2016). Four decades of wetland changes of the largest freshwater lake in China: Possible linkage to the Three Gorges Dam? *Remote Sens. Environ.* 176, 43–55. doi:10.1016/j.rse.2016.01.011
- Gao, W., and Li, B. L. (1993). Wavelet analysis of coherent structures at the atmosphere-forest interface. *J. Appl. Meteorol. Clim.* 32 (11), 1717–1725. doi:10.1175/1520-0450(1993)032<1717:WAOCSA>2.0.CO;2
- Garrido, M., Hansen, S. K., Yaari, R., and Hawlena, H. (2022). A model selection approach to structural equation modelling: A critical evaluation and a road map for ecologists. *Methods Ecol. Evol.* 13 (1), 42–53. doi:10.1111/2041-210X.13742
- Gautam, V. K., Gaurav, P. K., Murugan, P., and Annadurai, M. J. A. P. (2015). Assessment of surface water Dynamics in Bangalore using WRI, NDWI, MNDWI, supervised classification and KT transformation. *Aquat. Procedia* 4, 739–746. doi:10.1016/j.aqpro.2015.02.095
- Huang, W., Duan, W., and Chen, Y. (2021). Rapidly declining surface and terrestrial water resources in Central Asia driven by socio-economic and climatic changes. *Sci. Total Environ.* 784, 147193. doi:10.1016/j.scitotenv.2021.147193
- Jing, Y., Zhang, F., He, Y., Johnson, V. C., and Arikana, M. (2020). Assessment of spatial and temporal variation of ecological environment quality in Ebinur lake wetland national nature reserve, Xinjiang, China. *Ecol. Indic.* 110, 105874. doi:10.1016/j.ecolind.2019.105874
- Jing, Y., Zhang, F., and Wang, X. (2018). Monitoring dynamics and driving forces of lake changes in different seasons in Xinjiang using multi-source remote sensing. *Eur. J. Remote Sens.* 51 (1), 150–165. doi:10.1080/22797254.2017.1413955
- Kaplan, G., and Avdan, U. (2017). Object-based water body extraction model using Sentinel-2 satellite imagery. *Eur. J. Remote Sens.* 50 (1), 137–143. doi:10.1080/22797254.2017.1297540
- Kendall, M. G. (1948). Rank correlation methods. *Am. Math. Mon.* 57, 6–7. doi:10.2307/2307656
- Li, Q., Lu, L., Wang, C., Li, Y., Sui, Y., and Guo, H. (2015). MODIS-derived spatiotemporal changes of major lake surface areas in arid Xinjiang, China, 2000–2014. *Water* 7 (10), 5731–5751. doi:10.3390/w7105731
- Li, X., Jiang, F., Li, L., and Wang, G. (2011). Spatial and temporal variability of precipitation concentration index, concentration degree and concentration period in Xinjiang, China. *Int. J. Climatol.* 31 (11), 1679–1693. doi:10.1002/joc.2181
- Lira, J. (2006). Segmentation and morphology of open water bodies from multispectral images. *Int. J. Remote Sens.* 27 (18), 4015–4038. doi:10.1080/01431160600702384
- Liu, H., Chen, Y., Ye, Z., Li, Y., and Zhang, Q. (2019). Recent lake area changes in Central Asia. *Sci. Rep.* 9 (1), 1–11. doi:10.1038/s41598-019-52396-y
- Liu, Y., Ye, Z., Jia, Q., Mamat, A., and Guan, H. (2022). Multi-source remote sensing data for Lake change detection in Xinjiang, China. *Atmos. (Basel)* 13 (5), 713. doi:10.3390/atmos13050713
- Ma, R., Duan, H., Hu, C., Feng, X., Li, A., Ju, W., et al. (2010). A half-century of changes in China's lakes: Global warming or human influence? *Geophys. Res. Lett.* 37 (24). doi:10.1029/2010GL045514
- Mann, H. (1945). Non-parametric tests against trend. *Econometrica* 13, 245. doi:10.2307/1907187
- Odeh, R. E. (1972). Algorithm AS 55: The generalized mann-whitney U-statistic. *Appl. Stat.* 21 (3), 348–351. doi:10.2307/2346292
- Ouma, Y. O., and Tateishi, R. (2006). A water index for rapid mapping of shoreline changes of five east african rift valley lakes: An empirical analysis using Landsat TM and ETM+ data. *Int. J. Remote Sens.* 27 (15), 3153–3181. doi:10.1080/01431160500309934
- Pekel, J. F., Cottam, A., Gorelick, N., and Belward, A. S. (2016). High-resolution mapping of global surface water and its long-term changes. *Nature* 540 (7633), 418–422. doi:10.1038/nature20584
- Qin, J., Ding, Y. J., Zhao, Q. D., Wang, S. P., and Chang, Y. P. (2020). Assessments on surface water resources and their vulnerability and adaptability in China. *Adv. Clim. Change Res.* 11 (4), 381–391. doi:10.1016/j.accre.2020.11.002
- Revelles, J., and Van Geel, B. (2016). Human impact and ecological changes in lakeshore environments. The contribution of non-pollen palynomorphs in Lake Banyoles (NE Iberia). *Rev. Palaeobot. Palynol.* 232, 81–97. doi:10.1016/j.revpalbo.2016.05.004
- Riaza, A., and Müller, A. (2010). Hyperspectral remote sensing monitoring of pyrite mine wastes: A record of climate variability (pyrite belt, Spain). *Environ. Earth Sci.* 61 (3), 575–594. doi:10.1007/s12665-009-0368-y
- Song, C., Huang, B., and Ke, L. (2013). Modeling and analysis of lake water storage changes on the Tibetan Plateau using multi-mission satellite data. *Remote Sens. Environ.* 135, 25–35. doi:10.1016/j.rse.2013.03.013
- Song, C., Sheng, Y., Ke, L., Nie, Y., and Wang, J. (2016). Glacial lake evolution in the southeastern Tibetan Plateau and the cause of rapid expansion of proglacial lakes linked to glacial-hydrogeomorphic processes. *J. Hydrol. X.* 540, 504–514. doi:10.1016/j.jhydrol.2016.06.054
- Tao, S., Fang, J., Zhao, X., Zhao, S., Shen, H., Hu, H., et al. (2015). Rapid loss of lakes on the Mongolian Plateau. *Proc. Natl. Acad. Sci. U. S. A.* 112 (7), 2281–2286. doi:10.1073/pnas.1411748112
- Wang, J., Cai, X., Chen, F., Zhang, Z., Zhang, Y., Sun, K., et al. (2020). Hundred-year spatial trajectory of lake coverage changes in response to human activities over Wuhan. *Environ. Res. Lett.* 15 (9), 094022. doi:10.1088/1748-9326/ab9db0
- Wang, T., Yan, C. Z., Song, X., and Xie, J. L. (2012). Monitoring recent trends in the area of aeolian desertified land using Landsat images in China's Xinjiang region. *ISPRS J. Photogramm. Remote Sens.* 68, 184–190. doi:10.1016/j.isprsjprs.2012.01.001
- Whitney, J. (1997). Notes on methodology-Testing for differences with the nonparametric mann-whitney U test. *J. WOCN* 1 (24), 12–18. doi:10.1016/S1071-5754(97)90044-9

Wu, S., Bates, B., Zbigniew Kundzewicz, A. W., and Palutikof, J. (2008). *Climate change and water*. Geneva: Technical Paper of the Intergovernmental Panel on Climate Change.

Wufu, A., Wang, H., Chen, Y., Rusuli, Y., Ma, L., Yang, S., et al. (2020). Lake water volume fluctuations in response to climate change in Xinjiang, China from 2002 to 2018. *PeerJ* 8, e9683. doi:10.7717/peerj.9683

Yang, J., Ma, L., Li, C., Liu, Y., Ding, J., and Yang, S. (2019). Temporal-spatial variations and influencing factors of lakes in inland arid areas from 2000 to 2017: A case study in Xinjiang. *Geomat. Nat. Hazards Risk* 10 (1), 519–543. doi:10.1080/19475705.2018.1531942

Yang, L., Feng, Q., Yin, Z., Deo, R. C., Wen, X., Si, J., et al. (2020). Regional hydrology heterogeneity and the response to climate and land surface changes in arid alpine basin, northwest China. *Catena* 187, 104345. doi:10.1016/j.catena.2019.104345

Yao, J., Chen, Y., Guan, X., Zhao, Y., Chen, J., and Mao, W. (2022). Recent climate and hydrological changes in a mountain-basin system in Xinjiang, China. *Earth. Sci. Rev.* 226, 103957. doi:10.1016/j.earscirev.2022.103957

Yu, H., Tu, Z., Yu, G., Xu, L., Wang, H., and Yang, Y. (2020). Shrinkage and protection of inland lakes on the regional scale: A case study of hubei province, China. *Reg. Environ. Change* 20 (1), 4–14. doi:10.1007/s10113-020-01594-w

Zhang, F., Kung, H. T., and Johnson, V. C. (2017). Assessment of land-cover/land-use change and landscape patterns in the two national nature reserves of

Ebinur Lake Watershed, Xinjiang, China. *Sustainability* 9 (5), 724. doi:10.3390/su9050724

Zhang, F., Tiyp, T., Johnson, V. C., Kung, H., Ding, J., Zhou, M., et al. (2015b). Evaluation of land desertification from 1990 to 2010 and its causes in Ebinur Lake region, Xinjiang China. *Environ. Earth Sci.* 73 (9), 5731–5745. doi:10.1007/s12665-014-3830-4

Zhang, F., Tiyp, T., Johnson, V. C., Kung, H. T., Ding, J. L., Sun, Q., et al. (2015a). The influence of natural and human factors in the shrinking of the Ebinur Lake, Xinjiang, China, during the 1972–2013 period. *Environ. Monit. Assess.* 187 (1), 1–14. doi:10.1007/s10661-014-4128-4

Zhang, G., Xie, H., Kang, S., Yi, D., and Ackley, S. F. (2011). Monitoring lake level changes on the Tibetan Plateau using ICESat altimetry data (2003–2009). *Remote Sens. Environ.* 115 (7), 1733–1742. doi:10.1016/j.rse.2011.03.005

Zhang, G., Xie, H., Yao, T., and Kang, S. (2013). Water balance estimates of ten greatest lakes in China using ICESat and Landsat data. *Chin. Sci. Bull.* 58 (31), 3815–3829. doi:10.1007/s11434-013-5818-y

Zhang, J., Zhou, J., Zhang, G., Ji, Y., Zeng, Y., Fan, W., et al. (2021). Climate-and human-driven variations in lake area and number in North Xinjiang, China. *Int. J. Remote Sens.* 42 (2), 469–485. doi:10.1080/01431161.2020.1809740

Zheng, L., Xia, Z., Xu, J., Chen, Y., Yang, H., and Li, D. (2021). Exploring annual lake dynamics in Xinjiang (China): Spatiotemporal features and driving climate factors from 2000 to 2019. *Clim. Change* 166 (3), 36–20. doi:10.1007/s10584-021-03136-7



OPEN ACCESS

EDITED BY

Shaoquan Liu,
Institute of Mountain Hazards
and Environment (CAS), China

REVIEWED BY

Shili Guo,
Southwestern University of Finance
and Economics, China
Gao Xue,
Northeastern University, China

*CORRESPONDENCE

Zhijun Zhan
2201903077@stu.jxufe.edu.cn

SPECIALTY SECTION

This article was submitted to
Interdisciplinary Climate Studies,
a section of the journal
Frontiers in Ecology and Evolution

RECEIVED 26 August 2022

ACCEPTED 12 September 2022

PUBLISHED 06 October 2022

CITATION

Peng J and Zhan Z (2022) Extreme
climate and crime: Empirical evidence
based on 129 prefecture-level cities
in China.
Front. Ecol. Evol. 10:1028485.
doi: 10.3389/fevo.2022.1028485

COPYRIGHT

© 2022 Peng and Zhan. This is an
open-access article distributed under
the terms of the [Creative Commons
Attribution License \(CC BY\)](#). The use,
distribution or reproduction in other
forums is permitted, provided the
original author(s) and the copyright
owner(s) are credited and that the
original publication in this journal is
cited, in accordance with accepted
academic practice. No use, distribution
or reproduction is permitted which
does not comply with these terms.

Extreme climate and crime: Empirical evidence based on 129 prefecture-level cities in China

Jiquan Peng and Zhijun Zhan*

School of Economics, Jiangxi University of Finance and Economics, Nanchang, China

Climate change is having profound effects on natural and socio-economic systems, especially *via* extreme climate events. Using panel data from 129 prefectural-level cities in China from 2013 to 2019, this paper explores the effects of extreme climate on crime rates based on a climate index and manual collection of crime data. The results showed that extreme climate has a significant positive effect on crime rates, increasing by 0.035% for every 1% increase in the extreme climate index. This occurs through two mechanistic pathways: reduced agricultural output and lower employment income. The heterogeneity analysis shows that extreme climate has a greater impact on crime rates in eastern areas which are economically developed and have high levels of immigration. This study provides new perspectives on the impact of extreme climate on the economy and society, in which governments can actively participate in climate governance through environmental protection, energy conservation and emission reduction, and technological innovation to reduce crime rates by reducing the occurrence of extreme climate.

KEYWORDS

climate change, global warming, crime rates, quantile regression model, mechanisms of effect

Introduction

Crime is considered a major factor affecting social stability. At the Third Plenary Session of the 18th CPC Central Committee, it was stressed that comprehensive management of social security should be strengthened, and all types of criminal activities should be prevented and punished strictly following existing laws. In January 2018, the CPC Central Committee and the State Council issued the Notice on the Special Struggle against Darkness and Evil, to ensure that people live and work in peace, society is stable and orderly, and the country enjoys long-term peace and stability. China's crime rate is growing at a much faster rate than that of other developed countries (Hu et al., 2005). The arrest rate increased from 3.64 per 10,000 people in 1998 to 7.78 per 10,000 people in 2017, and the prosecution rate increased from 3.34 per 10,000 people to 12.28 per 10,000 people for the same period. Historically, scholars have studied the causes of crime by focusing on traditional social factors such as age, gender, race, education, and social and

economic status (Hindelang, 1981; Devine et al., 1988; Kolvin et al., 1988). However, as the economy and society continue to develop, the legal system improves, and the standard of living increases, the rate of criminal offenses continues to increase. This suggests that crime rates are no longer influenced by these social factors alone, but that unknown factors may also influence the occurrence of crime (Cohn, 1990).

The Sixth Assessment Report (AR6) of the United Nations Intergovernmental Panel on Climate Change (IPCC) points out that climate change and the frequency of extreme climate events pose a growing threat to the economy, health, and security, and their impact is increasing in magnitude. In particular, the government may aim to reduce the extremes through policies such as restructuring industries and strengthening environmental management. This may have an impact on social stability, and people's behavior may become more extreme due to the stimulus from extreme climate events. According to the China Blue Book on Climate Change (2021), China is a sensitive impact area for global climate change, with a warming rate significantly higher than the global average. With the second largest economy in the world, the negative ecological, social, and economic impacts of climate change faced by China should not be ignored (Duan et al., 2019). In this context, considering that factors other than social factors indirectly influence crime rates, climate extremes, which have a profound negative impact on socioeconomic stability, may be one of the important reasons for influencing crime. While extreme climates bring about macroscopic damage, they may also influence people's propensity to commit crimes at the microscopic level. So, does climate extremes affect crime rates? What is the mechanism of action of extreme climate affecting crime rates? Answering these questions is the main purpose of this paper.

Literature review and theoretical analysis

Literature review

The effects of high temperatures on people have been a long-standing concern in the field of psychology. Several experimental psychological studies have found a direct positive relationship between temperature and aggression—high temperatures enhance aggression and criminal tendencies (Anderson, 1989; DeWall and Bushman, 2009). Being randomly assigned to a hot room rather than a suitably warm room makes subjects more likely to be hostile and to behave more aggressively toward others (DeWall et al., 2011); presenting words or pictures associated with high temperatures also makes subjects more irritable (Wilkowski et al., 2009). In addition to studies based on experimental paradigms, many scholars have also studied the relationship between temperature and crime based on correlational data. Crime has been found to show a

clear seasonal pattern: violent crime (Stevens et al., 2019) and property crime (Linning et al., 2017) increase significantly in the summer months.

However, the correlation between temperature and violent crime can be overestimated, and the correlation between violent crime and temperature disappears when social variables are excluded (Rotton, 1986). This suggests that the relationship between climate and criminal behavior cannot be explained by a single factor and that seasonal fluctuations in crime rates are determined by a combination of environmental and social factors (McDowall et al., 2012). Moreover, because there is a negative correlation between crime rates in the short term in region: where crime rates are high in 1 week, they are lower in subsequent weeks (Jacob et al., 2007), studies using daily or weekly data cannot accurately estimate the long-term effects of climate change on crime (Ranson, 2014). Yet, other studies, using hourly or daily data, have shown a correlation between temperature and crime rates (Brunsdon et al., 2009; Mares, 2013a; Baryshnikova et al., 2021). However, when annual data are used for estimation, studies show that the correlation between temperature and crime rates is not significant (Lynch et al., 2020, 2022).

Some scholars have also studied the impact of meteorological factors, such as sunlight, heat, and rainfall on crime. The theory of daily activities suggests that the three elements of criminally motivated offenders, suitable criminal targets, and lack of effective protection are important conditions for crime to occur (Miró, 2014). Weather conditions can influence crime by altering people's daily activities and social behavior (Hipp et al., 2004; Miles-Novelo and Anderson, 2019). Specifically, warmer temperatures increase the frequency of interpersonal interactions, thereby increasing the likelihood of interpersonal violence or crime (Rotton and Cohn, 2003; Berman et al., 2020). As people go on holiday more often in summer, they are more likely to be burgled (Cohn and Rotton, 2000). Frequent rainfall makes it easier for offenders to avoid surveillance, leading to higher rates of crime on rainy days (Shen et al., 2020). Reduced daylight also makes it easier for crimes to be concealed, increasing the frequency of offenders committing crimes on cloudy days (Doleac and Sanders, 2015). In addition to weather conditions, recent literature has also discussed the impact of factors such as air pollution (Burkhardt et al., 2019; Bondy et al., 2020) and environmental damage (Mbonane et al., 2019) on crime rates, finding that unsuitable environments can contribute to crime.

The impact of extreme climate on social stability and economic development has been documented in many areas, including agricultural production (Deschênes and Greenstone, 2007), industrial output or economic growth (Dell et al., 2012; Chen and Yang, 2019), international trade (Jones and Olken, 2010), labor productivity (Zhang et al., 2018; Letta and Tol, 2019), and population mortality (Deschênes and Greenstone, 2011). Extreme weather events often lead to reduced crop yields

(Rehman et al., 2022), rangeland degradation (Holechek et al., 2020; Nanzad et al., 2021), and wildfires and floods that cause property damage (Irish et al., 2010; Rossiello and Szema, 2019). These lead to widening income disparities, increased individual discontent, reduced opportunity costs of violence, countries political conflict, and even war (Burke et al., 2009; Hsiang et al., 2011; Koubi, 2017; Roche et al., 2020). Particularly for countries already facing severe economic problems, extreme climate can further exacerbate stress and induce more violence (Mares, 2013b). Extreme climate shocks can lead to large-scale group migrations and the cultural and socio-economic pressures of a migrating population can indirectly increase conflict (Ghimire et al., 2015; Burrows and Kinney, 2016; Koubi et al., 2018). Studies have also found a significant contribution to crime rates from hurricane disasters (Spencer and Strobl, 2019).

In summary, past studies on the impact of climate on crime rates have focused on the relationship between the mean climate distribution, such as mean temperature and mean precipitation, with crime rates, without emphasizing the impact of climate extremes on crime rates; although some literature has explored the impact of climate extremes on conflict and violence at the national level, fewer studies have directly analyzed the impact of climate extremes on crime rates at the regional level within a country; finally, most of the existing literature simply regresses crime rates on climate variables, which lacks precision in identification strategies and lacks the analysis of causal mechanisms between the variables. To remedy the shortcomings of the existing literature, this paper manually collected crime and climate data from 129 prefectural-level cities in China, and explored the influence of extreme climate on regional crime rates and its mechanism of action based on the construction of an extreme climate index using daily temperature data.

Theoretical analysis

Extreme climate does not directly contribute to regional crime rates—there must be intermediate mechanisms at work. From an economic point of view, crime is a risky choice in which the expected benefits to the individual are higher than the opportunity costs, and lower incomes are the main way in which the opportunity costs to the individual are reduced. The main income of rural and urban residents is derived from agricultural business income and wage income, respectively. When the income of rural and urban residents is insufficient to support their household expenses, individuals may take the risk of increasing their household income by committing crimes.

First, is the agricultural output reduction effect. Agriculture in rural China plays a role in social stabilization, yet it is agricultural production that is most vulnerable to climate change (Castellano and Moroney, 2018). Traditional agriculture cannot effectively offset severe weather (Piontek et al., 2014), and extreme weather events such as high-temperature periods

(Burke et al., 2015), drops or increases in rainfall (Barrios et al., 2010; Zhang and Huang, 2012), or snow (Boehm et al., 2016) can severely affect normal agricultural production (Chen et al., 2016; Yang et al., 2017; Pickson et al., 2022). Specifically, high temperatures can affect photosynthesis in crops (Shah and Paulsen, 2003), droughts can affect irrigation (Lesk et al., 2016), and heavy rainfall can lead to large-scale loss of soil fertility (Li and Fang, 2016). Natural disasters, such as floods (Qin et al., 2022), hurricanes (Martinez, 2020), and hail storms (Raihan et al., 2020), can directly damage crops. As a result, the range of negative impacts of extreme climate on agricultural output can reduce farming incomes, forcing some farming populations into economic hardship, inducing criminal behavior. Extreme climate may also drive farmers to towns and cities, thereby increasing urban crime rates.

Second, is the employment income reduction effect. Agriculture is a component of the regional economy, but extreme climate can also affect the non-farm sector of the economy (Hsiang, 2010). Extreme climates generally reduce employment income for urban dwellers through both lower labor productivity and higher production costs. High temperatures can prevent workers from concentrating on their work (Qiu and Zhao, 2022) and increase worker fatigue, thereby reducing overall worker productivity (Flouris and Schlader, 2015). Although increased mechanization can offset the negative effects of high temperatures on industrial labor productivity to some extent (Day et al., 2019), high temperatures are more disruptive to brain-intensive complex labor than physically intensive simple labor (Zander and Mathew, 2019), such that the negative effects of extreme heat on individual labor productivity in urban environments are pervasive and persistent (Cai et al., 2018; Lee et al., 2018). Furthermore, in addition to reducing labor productivity, extreme heat can also lead to an overall reduction in working hours (Caldeira and Brown, 2019), which can increase life stress and lower life expectations, further reducing the opportunity cost of criminal behavior (White, 2016). Natural disasters caused by extreme climate can lead to a global surge in energy prices (Lee et al., 2021), pushing up the cost of raw materials, as well as increasing the cost of labor for businesses, ultimately leading to a reduction in demand for labor. This results in increased unemployment and lower incomes, thereby triggering crime. The theoretical mechanism by which climate change affects crime rates is shown in Figure 1. Based on the above theoretical analysis, the following research hypotheses are proposed:

Hypothesis 1: There may be a significant positive effect of extreme climate on crime rates.

Hypothesis 2: The extreme climate may affect crime rates in two ways: by reducing agricultural output and by lowering employment income.

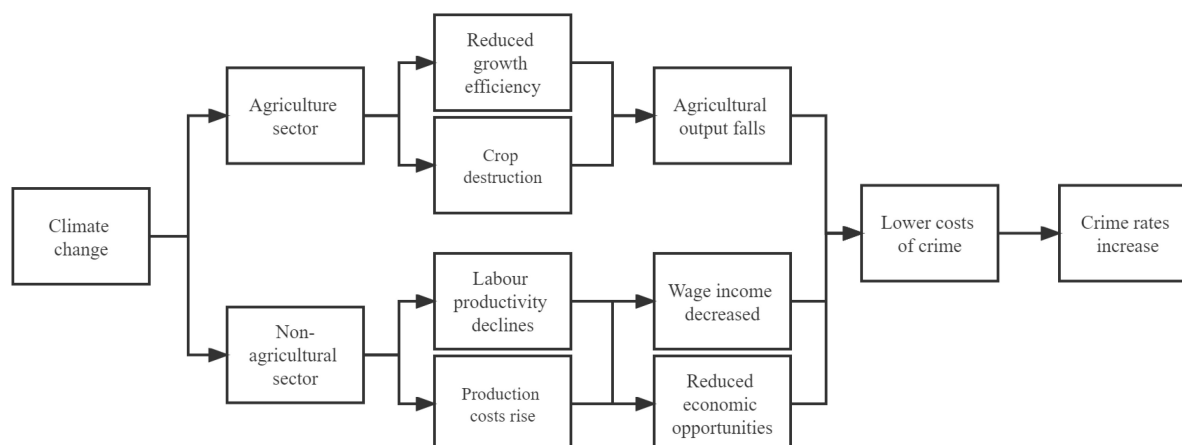


FIGURE 1
Mechanisms of climate change increasing crime rates.

Data and methods

Data source

This paper compiles panel data for 129 prefecture-level cities in China from 2013 to 2019. Among them, the crime rate data were obtained from the annual work reports of local procuratorates in each region, the daily temperature data were obtained from the National Meteorological Science Data Center, and the control data were obtained from the China Urban Statistical Yearbook, provincial statistical yearbooks, and regional statistical bulletins. Since some regions did not publish crime rates for some years, this paper uses linear interpolation to fill in the missing values.

Variable definition and descriptive statistics

Extreme climate

The independent variable in this paper is extreme climate. Extreme climate is a phenomenon in which the weather and climate of a place deviate significantly from its average state, and it can be expressed in terms of anomalous records of climate elements or the number of days exceeding a specific threshold value (Ren et al., 2010). The World Meteorological Organization (WMO) has proposed a set of index systems to measure an extreme climate index, which consists of 27 variables, including daily temperature and precipitation. The concept of the index is to count the number of days in a year that exceed a defined absolute or relative threshold (Chen et al., 2013). In this paper, three temperature variables were selected to measure the extreme climate index: “summer days (the number of days

with daily maximum temperature > 25°C),” “hot night days (the number of days with daily minimum temperature > 20°C),” “warm day days (days with daily maximum temperature > 90% quantile).” These three variables are brought into RCLimDex software for the calculation to derive the extreme climate index values. RCLimDex was developed by Zhang and Yang (2004) of the Canadian Meteorological Research Center and has been promoted by the World Meteorological Organization’s Climate Commission (Peterson et al., 2008; Choi et al., 2009; Xu et al., 2013). The greater the calculated extreme climate index, the greater the number of days of extreme climate in the year in that region.

Crime rate

The dependent variable in this paper is the crime rate, which is measured as the number of criminal arrests per 10,000 people, referring to the definition of crime by Edlund et al. (2013). The robustness of the model was analyzed using the criminal prosecution rate per 10,000 people as a second measure of crime. The criminal arrest rate and criminal prosecution rate may underestimate the true level of crime, but as long as they are consistent over time and location, they will provide a robust relative measure of trends (Li et al., 2019). To exclude the effect of extreme values on the regression results, the crime rate variables were winsorized at 1% and 99% percentiles.

Control variables

To control for factors other than extreme climate that affect crime rates, population density, household registration rate, per capita GDP, urban–rural income ratio, urban employee unemployment insurance rate, higher education rate, and the unemployment rate were added to the regression model, drawing on previous studies (Cheong and Wu, 2015; Chang et al., 2019). In addition, climate variables including annual

TABLE 1 Descriptive statistics of all variables.

Type	Variable	Abbreviation	Definitions	Mean	SD	Min	Max
Dependent variables	The arrest rate	Arrest	Criminal arrests per 10,000 people	6.24	3.15	1.86	33.85
	The prosecution rate	Prose	Criminal prosecutions per 10,000 people	10.46	4.49	2.37	38.43
Independent variables	The extreme climate index	Climdex	extreme climate indices	77.43	32.95	4.93	159.41
	Warm days	tx90p	Sum of the number of days with daily maximum temperature (90% quantile (days)	2.21	0.77	0.48	5.11
	Tropical nights	tr	The sum of the number of days in a year when the daily minimum temperature is (20 (C (days)	88.86	55.48	0	229
	Summer days	su25	Sum of the number of days in a year with a daily maximum temperature (25°C (days)	141.22	45.8	14	274
	Above 35°C		Sum of the number of days in a year with a daily maximum temperature (35°C (days)	11.19	12	0	64
Control variables	Population density	PD	Population density (persons / km ²)	519.36	565.72	5.52	4, 250
	Household registration rate	HRR	Household population / resident population (%)	1.04	0.21	0.19	1.56
	Per capita GDP	lnPCG	The logarithm of per capita GDP (yuan)	10.82	0.56	9.22	12.58
	Unemployment insurance rate	UIR	Number of urban unemployment insurance participants/number of urban workers (%)	0.87	0.34	0.05	2.3
	Urban–rural income ratio	UER	Disposable income of urban residents / disposable income of rural residents (%)	2.31	0.41	1	3.57
	Higher education rate	HER	Number of people with a Bachelor's Degree or above per 10,000 people	172.86	188.75	0.74	1, 064.77
	Unemployment rate	UR	Number of urban registered unemployed / number of urban workers (%)	0.06	0.03	0	0.24
	Average annual temperature	AAT	Annual average temperature (°C)	16.21	4.43	− 0.16	24.41
	Relative humidity	RH	Annual average relative humidity (%)	70.32	10.01	40	88
	Precipitation	Prec	Annual accumulated precipitation (mm)	1, 195.33	1, 774.92	41.8	50, 223.55
Mechanistic variables	Hours of sunshine	HS	Annual accumulated sunshine hours (h)	1, 862.73	540.72	754.1	3, 376.1
	Percentage of agriculture output	PAO	The ratio of agricultural output to regional GDP (%)	10.98	0.26	10.26	12.06
	Per capita wage income	lnPWI	The logarithm of per capita wage income (yuan)	10.95	6.45	0.3	37.19
	Area		1 (east; 2 (mid; 3 (west	10.98	0.26	10.26	12.06
	Degree of regional development	DRD	0 (developed; 1 (under-developed	1.91	0.77	1	3
	Population flow	PF	Resident population minus household population (10,000 persons)	0.5	0.5	0	1

Population flow greater than 0 indicates an inflow of population and less than 0 indicates an outflow of population. Number of observations is 903.

average temperature, precipitation, sunshine duration, and relative humidity, were controlled (Li et al., 2015; Auffhammer et al., 2020). The descriptive statistics for all variables as shown in Table 1.

Model

Based on the above hypotheses, this paper will construct a panel data of 129 prefecture-level cities in China from 2013–2019 for further empirical analysis. In order to better identify the

effect of extreme climate on crime rate, this paper will control the region fixed effect and the time trend in the panel model, which can also greatly reduce the risk of omitted variable bias in the model and further improve the accuracy of the model estimation by constructing a time-region double fixed panel model, and the specific regression model is shown in Equation 1.

$$CR_{it} = \beta_0 + \beta_1 Climdex_{it} + \beta_2 X_{it} + \mu_i + \nu_t + \varepsilon_{it} \quad (1)$$

where i denotes the region, t denotes the year, CR_{it} indicates the crime rate, $Climdex_{it}$ indicates extreme climate index, X_{it} is a

set of control variables, μ_i is the region fixed effect, v_t is the year fixed effect, and ε_{it} is the random error. β_1 is our main coefficient of interest, and if it is significantly positive, this indicates that extreme climate increases regional crime rates.

Panel OLS (ordinary least squares) estimation can only obtain the average effect of extreme climate on crime rates, and cannot portray the dynamic effect of extreme climate at different quartiles of the crime rate. To further investigate the effect of extreme climate at different levels of crime rates, the panel quantile method is applied to the regression model (2) to portray the dynamic trajectory of the marginal effect of extreme climate on the change in crime rates. The basic idea of panel quantile regression is to treat the independent variable as a functional distribution, sum the absolute values of the minimization-weighted residuals, and estimate the effect of the independent variable at the conditional quantile point of the independent variable. Since the fixed effects in the traditional panel quantile model decompose the random perturbation term into different components, it is difficult to explain the estimation results for each quantile. Powell (2022) proposed a non-additive fixed effects panel quantile model (QRPD), which introduces the panel quantile estimation into the framework of the instrumental variable approach so that the random perturbation term contains fixed effects and ensures the inseparability of the random perturbation term. The estimated coefficients are more accurate and the estimation results are more robust than the traditional panel quantile model. In this paper, five quartiles (5%, 25%, 50%, 75%, and 95%) are selected to construct the panel quantile function.

$$Q_{CR_{it}} = \theta(\tau)Climdex_{it} + \beta(\tau)X_{it} \quad (2)$$

where τ indicates the corresponding quantile, $Q_{CR_{it}}$ indicates the crime rate at the corresponding quantile, $Climdex_{it}$ indicates the extreme climate index at the corresponding quantile, and X_{it} is a set of control variables, the same as in model (1).

Results and discussion

Baseline regression results of climate extremes on crime rates

Using model (1), the effect of extreme climate on crime rates was examined using a fixed panel OLS model. Column (1) of Table 2 shows the regression results without the inclusion of control variables, column (2) shows the regression results with the gradual inclusion of regional characteristic variables to control for the effects of factors other than climate on crime rates, and column (3) shows the regression results with the inclusion of all control variables. It can be seen that there is a significant positive relationship between extreme climate and crime rate regardless of the number of control variables added, and the regression coefficients increase with the

TABLE 2 Baseline regression results of climate extremes on crime rates.

Variable	(1)	(2)	(3)
Climdex	0.023*** (0.006)	0.028*** (0.005)	0.035*** (0.005)
PD		−0.002 (0.003)	−0.002 (0.003)
HRR		4.393 (2.971)	4.698 (3.015)
lnPCG		0.509** (0.256)	0.494** (0.246)
UIR		−1.063** (0.461)	−1.028** (0.473)
UER		−0.318 (0.312)	−0.255 (0.278)
HER		0.008* (0.004)	0.008* (0.004)
UR		2.555 (2.142)	2.584 (2.045)
AAT			−0.309*** (0.110)
RH			−0.015 (0.021)
Prec			−0.000*** (0.000)
HS			0.000 (0.001)
Cons	4.387*** (0.517)	−4.800 (5.186)	−0.436 (5.496)
Year FE	Yes	Yes	Yes
City FE	Yes	Yes	Yes
N	903	903	903
r ²	0.119	0.218	0.231

***, **, and * denote significance at the 1, 5, and 10% levels, respectively.

gradual addition of regional characteristics variables and climate variables, indicating that the accuracy of the model estimation is improving. The regression coefficient of the extreme climate index on the crime rate in column (3) is 0.035 and is significant at the 1% level, indicating that extreme climate significantly increases the crime rate. Specifically, each 1% increase in the extreme climate index increases the crime rate by 0.035%, or 3.5 additional arrests per 10,000 persons authorized.

In terms of control variables, per capita GDP is significantly positively correlated with crime rate, suggesting that areas with higher economic levels have higher crime rates. The unemployment insurance rate is significantly negatively correlated with the crime rate, suggesting that better social security can reduce crime rates. Educational attainment is significantly positively correlated with the crime rate, possibly due to the presence of more new high-tech crimes with higher education. The significant negative association between annual mean temperature and crime rate seems to be

contrary to our expectation, probably because the annual mean temperature does not reflect the economic and social impact of temperature extremes, which is around 16°C in the sample data, a temperature range that is favorable for economic production.

Moreover, the direct estimation of the effect of annual mean temperature on crime rates is not complete (Mares, 2013a), and the relationship between the two may be the result of aggregation bias (Hsiang et al., 2011). Such estimates are meaningful only if the elevating effect on crime rates occurs when temperatures exceed a certain threshold or reach extremes. In addition, the expected regression coefficient of the unemployment rate, as an important indicator of the degree of social instability, should be significantly positive, but the actual regression coefficient is not significant. This may be because the ratio of the number of urban registered unemployed to the number of urban workers does not reflect the real unemployment situation. Some studies show that the effect of unemployment on crime is not certain, the relationship between the two depends on the arrest rate (Lee, 2018), and that unemployment insurance benefits may mitigate the impact of unemployment on crime (NoghaniBehambari and Maden, 2021).

Endogeneity test results of regression models

Extreme climate, as an exogenous variable, is not influenced by crime rates and the existence of reverse causality is not likely. However, it may still lead to endogeneity due to the omission of other key variables, so the instrumental variable approach is applied. In this paper, “Volume of industrial soot (dust) emission” and “Greenery coverage” are selected as the instrumental variables of the extreme climate index. Smoke and dust particles can reduce the amount of solar radiation reaching the ground by blocking sunlight (Wang et al., 2009), which in turn reduces the atmospheric temperature; while urban greening plays an important role in reducing urban temperature due to photosynthesis and transpiration of plants (Zhu et al., 2017). Smoke (dust) emission and greening coverage of built-up areas are related to regional air temperature, but cannot directly affect crime rate, satisfying the assumption of instrumental variables. Column (1) in Table 3 shows the regression results of the first stage of the two-stage least-squares method. There are significant correlations between soot emissions and green coverage with an extreme climate, and the F-value of the first stage is larger than 10, indicating that the instrumental variables are reasonably chosen. Column (2) shows the IV estimation results, and the results of the over-identification test support the original hypothesis that all instrumental variables are exogenous, indicating that there is no over-identification problem in the model. The results show that after considering the endogeneity problem, there is still a significant positive effect

TABLE 3 Endogeneity test results of regression models.

Variable	(1)	(2)
	Climdex	Arrest
Climdex		0.095*** (2.630)
lnEmission	-2.432*** (0.564)	
Green	-0.105** (0.050)	
PD	-0.004 (0.004)	-0.002 (0.002)
HRR	-9.884** (4.818)	5.229*** (1.685)
lnPCG	-2.819*** (1.038)	0.670*** (0.242)
UIR	2.472 (2.265)	-1.128*** (0.360)
UER	-4.483*** (1.424)	-0.008 (0.281)
HER	-0.008 (0.008)	0.009*** (0.003)
UR	-12.435 (10.170)	3.064* (1.744)
AAT	4.414*** (0.826)	-0.577*** (0.185)
RH	-0.175 (0.123)	-0.004 (0.019)
Prec	0.000*** (0.000)	-0.000** (0.000)
HS	-0.002 (0.002)	0.001 (0.001)
_Cons	92.789*** (16.736)	-7.488* (-1.906)
Year effect	Yes	Yes
City effect	Yes	Yes
F value	440.13	
Hansen J statistic		0.484
P value		0.487
N	903	903
r ²	0.972	0.889

***, **, and * denote significance at the 1, 5, and 10% levels, respectively.

of the extreme climate index on the crime rate, indicating that the regression results are robust.

Quantile regression results of extreme climate on crime rate

To more intuitively examine the marginal effects of extreme climate at different levels of crime rates, model (2) was applied

TABLE 4 Quantile regression results of extreme climate on crime rate.

Variable	(1)	(2)	(3)	(4)	(5)
	5%	25%	50%	75%	95%
Climdex	0.005*** (0.001)	0.008*** (0.001)	0.013*** (0.002)	0.024*** (0.007)	0.026*** (0.002)
PD	0.000*** (0.000)	0.001*** (0.000)	0.001 (0.001)	−0.000*** (0.000)	−0.000 (0.000)
HRR	−0.909*** (0.156)	−1.996*** (0.086)	−5.980*** (0.186)	−4.088*** (0.640)	−8.166*** (0.173)
lnPCG	1.299*** (0.084)	0.570*** (0.041)	0.457*** (0.097)	1.031*** (0.088)	1.599*** (0.175)
UIR	0.752*** (0.111)	0.591*** (0.078)	−0.944 (0.915)	1.243*** (0.071)	1.009*** (0.139)
UER	0.634*** (0.040)	−0.186*** (0.053)	−0.016 (0.0590)	0.508*** (0.0530)	1.355*** (0.178)
HER	0.001*** (0.000)	0.002*** (0.000)	0.002*** (0.001)	0.004*** (0.001)	0.002*** (0.000)
UR	1.648* (0.925)	−1.618*** (0.355)	2.228 (3.703)	−2.356 (1.680)	−14.794*** (1.299)
AAT	0.1410*** (0.009)	0.058*** (0.007)	0.032 (0.040)	0.006 (0.047)	−0.166*** (0.033)
RH	−0.0270*** (0.002)	−0.007 (0.004)	0.002 (0.012)	0.068*** (0.010)	0.035*** (0.012)
Prec	0.000*** (0.000)	0.000*** (0.000)	0.000*** (0.000)	0.000*** (0.000)	0.001*** (0.000)
HS	−0.000*** (0.000)	0.000*** (0.000)	0.001 (0.000)	0.001*** (0.000)	−0.000** (0.000)
Year FE	Yes	Yes	Yes	Yes	Yes
City FE	Yes	Yes	Yes	Yes	Yes
N	903	903	903	903	903

***, **, and * denote significance at the 1, 5, and 10% levels, respectively.

using panel quartiles, and the standard errors of the regression coefficients were obtained using the adaptive Monte Carlo (MCMC) method with 1,000 samples. From the estimated results (Table 4), the regression coefficients of the extreme climate index at each quantile are all positive and significant at the 1% level, which again verifies the finding that extreme climate significantly increases the crime rate in the baseline regression. The trend of the regression coefficients of the extreme climate index at each quartile shows that as the crime rate quartile increases, the regression coefficients of the extreme climate at the corresponding quartile also increase. The effect of extreme climate on areas with lower crime rates is weaker and the effect of extreme climate on areas with higher crime rates is stronger. The possible reason for this result is that areas with higher crime rates are more vulnerable to negative external shocks due to social instability. Extreme climate can be more damaging to these areas, and thus crime rates in high crime areas are more affected by extreme climate than in low crime areas.

Robustness test

To ensure the reliability of the previous estimation results, robustness tests were conducted using substitution variables and adjusting for standard errors. Since there are multiple measures of the crime rate and extreme climate, we conducted regressions after replacing the independent variables. First, the number of criminal offenses prosecuted per 10,000 people is used as a proxy for the crime rate. Second, as defined by the China Meteorological Administration, the sum of the number of extreme temperature days ($> 35^{\circ}\text{C}$) in a year is used as a proxy indicator of extreme climate. The robust standard errors in the baseline model have been clustered to the regional level and, considering that the standard errors of regions within the same province may still be correlated, the standard errors are further clustered to province–year interactions as a way to test the robustness of regression models. Column (1) in Table 5 shows the regression results after replacing the dependent variables, column (2) shows the regression results after replacing the

TABLE 5 Robustness test results of regression models.

Variable	(1)	(2)	(3)
	Prose	Arrest	Arrest
Climdex	0.047*** (0.011)		0.027*** (0.004)
Above 35°C		0.024*** (0.006)	
PD	-0.001 (0.003)	-0.002 (0.003)	-0.002 (0.002)
HRR	7.117* (3.819)	4.195 (3.068)	1.461 (2.234)
lnPCG	0.429 (0.359)	0.398 (0.252)	0.341 (0.329)
UIR	-1.135* (0.636)	-0.920** (0.448)	0.186 (0.556)
UER	-0.936* (0.558)	-0.386 (0.280)	0.000 (0.226)
HER	0.011** (0.005)	0.007 (0.005)	0.006 (0.004)
UR	-0.624 (3.936)	1.697 (2.110)	-0.029 (1.857)
AAT	-0.192 (0.1650)	-0.184 (0.126)	0.126 (0.099)
RH	0.0150 (0.032)	-0.016 (0.023)	0.019 (0.028)
Prec	-0.000*** (0.000)	-0.000*** (0.000)	-0.000*** (0.000)
HS	0.001 (0.001)	-0.000 (0.001)	0.000 (0.001)
_Cons	-3.396 (8.1280)	3.015 (5.773)	-4.410 (4.343)
Year FE	Yes	Yes	Yes
City FE	Yes	Yes	Yes
Year × Prov Effect	No	No	Yes
N	903	903	903
r2	0.272	0.213	0.510

***, **, and * denote significance at the 1, 5, and 10% levels, respectively.

independent variables, and column (3) shows the regression results for clustering to province- and year-level standard errors. The results show that the robustness tests are significant at the 1% level and the sign of the regression coefficients is positive, as expected.

Mechanism of the effect of climate extremes on crime rates

In this paper, agricultural output is the key variable for rural areas and the per capita wage income is chosen to measure

TABLE 6 Mechanism of the effect of climate extremes on crime rates.

Variable	(1)	(2)	(3)
	Arrest	PAO	PWI
Climdex	0.035*** (0.005)	-0.041*** (0.009)	-0.001* (0.000)
PD	-0.002 (0.003)	-0.001 (0.001)	0.000*** (0.000)
HRR	4.698 (3.015)	1.837 (1.610)	0.089 (0.081)
lnPCG	0.494** (0.246)	-2.058*** (0.372)	0.036*** (0.009)
UIR	-1.028** (0.473)	1.0590 (0.701)	0.051** (0.022)
UER	-0.255 (0.278)	0.664 (0.549)	-0.064*** (0.016)
HER	0.008* (0.004)	-0.005** (0.003)	-0.000 (0.000)
UR	2.584 (2.045)	7.841** (3.457)	0.072 (0.138)
AAT	-0.309*** (0.110)	0.196 (0.118)	0.001 (0.006)
RH	-0.015 (0.021)	-0.073** (0.028)	0.001 (0.001)
Prec	-0.000*** (0.000)	0.000*** (0.000)	0.000 (0.000)
HS	0.000 (0.001)	-0.001** (0.001)	-0.000 (0.000)
_Cons	-0.436 (5.496)	36.989*** (6.396)	10.281*** (0.205)
Year FE	Yes	Yes	Yes
City FE	Yes	Yes	Yes
N	903	903	903
r2	0.231	0.398	0.921

***, **, and * denote significance at the 1, 5, and 10% levels, respectively.

employment income in urban areas. In Table 6, the dependent variable in column (1) is the number of arrests per 10,000 people; the dependent variable in column (2) is the agricultural output, and the dependent variable in column (3) is employment income. Extreme climate reduces agricultural output, which weakens the role of agriculture as a “stabilizer.” The results in column (3) show that the regression coefficient of the extreme temperature index is significantly negative at the 10% level, indicating that it reduces the income of non-agricultural workers. By reducing labor productivity and increasing the production costs of enterprises, the extreme climate may lead to a decrease in the demand for labor and an increase in unemployment in enterprises. This leads to a decrease in the income of workers and the opportunity cost of crime, thus inducing more criminal activity.

TABLE 7 Heterogeneous effects of climate extremes on crime rates.

Variable	(1)	(2)	(3)	(4)	(5)	(6)	(7)
	Eastern	Middle	Western	Backward	Developed	Outflow	Inflow
Climdex	0.051*** (0.016)	0.013 (0.010)	0.028*** (0.007)	0.032*** (0.008)	0.047*** (0.014)	0.031*** (0.008)	0.062*** (0.014)
PD	−0.006 (0.004)	0.006*** (0.001)	−0.0077 (0.005)	0.007*** (0.002)	−0.005 (0.004)	0.003 (0.003)	−0.006 (0.005)
HRR	12.404** (5.402)	8.717*** (1.642)	2.704 (5.794)	10.790*** (1.979)	6.482 (4.222)	10.802*** (1.560)	6.687 (8.253)
lnPCG	−0.051 (0.518)	0.736** (0.341)	−0.299 (0.358)	0.423 (0.328)	0.359 (0.389)	0.615** (0.248)	0.426 (0.529)
UIR	−0.800 (0.908)	0.248 (0.619)	0.779 (0.476)	−0.008 (0.369)	−1.915** (0.877)	−0.255 (0.426)	−1.230 (0.928)
UER	−0.857 (0.590)	−1.296 (0.802)	0.098 (0.166)	−0.672 (0.461)	0.201 (0.317)	−0.259 (0.389)	0.065 (0.599)
HER	0.013 (0.011)	0.004 (0.003)	−0.001 (0.004)	0.004 (0.003)	0.009 (0.007)	0.004 (0.003)	0.010 (0.010)
UR	8.279 (7.457)	2.759 (2.329)	0.454 (2.355)	2.286 (2.181)	−0.234 (3.288)	0.892 (2.042)	6.551 (7.242)
AAT	−0.371** (0.184)	−0.101 (0.134)	0.028 (0.134)	−0.184 (0.116)	−0.457** (0.188)	−0.279** (0.127)	−0.238 (0.187)
RH	−0.031 (0.046)	−0.016 (0.024)	−0.008 (0.025)	0.010 (0.020)	−0.015 (0.037)	−0.018 (0.020)	0.070 (0.073)
Prec	−0.000** (0.000)	−0.000* (0.000)	0.000 (0.000)	−0.000* (0.000)	−0.000* (0.000)	−0.000*** (0.000)	−0.000 (0.001)
HS	0.001 (0.002)	0.000 (0.001)	0.000 (0.001)	−0.000 (0.000)	0.001 (0.001)	0.000 (0.000)	0.001 (0.002)
_Cons	3.611 (9.135)	−10.569* (6.132)	3.999 (9.486)	−11.051* (6.325)	2.741 (7.295)	−11.248** (4.780)	−5.480 (11.325)
Year FE	Yes	Yes	Yes	Yes	Yes	Yes	Yes
City FE	Yes	Yes	Yes	Yes	Yes	Yes	Yes
N	315	357	231	455	448	609	294
r ²	0.274	0.536	0.351	0.438	0.216	0.383	0.216

***, **, and * denote significance at the 1, 5, and 10% levels, respectively.

Heterogeneous effects of climate extremes on crime rates

Geographic heterogeneity

China is a vast country with distinctly different geographic conditions and regional climates. To further examine the geographical heterogeneity of extreme climate on crime rates, the sample was divided into eastern, middle, and western areas for regression according to the criteria of the National Bureau of Statistics, and the regression results are presented in columns (1) to (3) in [Table 7](#). The regression results show that extreme climate has a significant positive effect on crime rates in the eastern and western areas, and the contribution to crime rates in the eastern area is more pronounced. This is because eastern China has a long coastline and is often subject to extreme natural disasters, such as typhoons and tsunamis. Western China has

low levels of economic development and the effects of extreme climate on agricultural production are severe, both of which lead to a high crime rate.

Heterogeneity of economic levels

There may be differential effects of extreme climate on crime rates in regions with different levels of economic development. Referring to [Kumar and Khanna \(2019\)](#), the sample is divided into economically under-developed and economically developed regions according to the median regional GDP, and estimation results are presented in columns (4) and (5) in [Table 7](#). Extreme climate contributes more significantly to the crime rate in economically developed regions, which may be because the extreme climate is more likely to increase the cost of energy consumption and pollution emissions ([Li et al., 2015](#)). This leads to an increase in raw material costs and

labor costs for enterprises, which will reduce labor demand and employee wages, resulting in increased unemployment. More unemployed people increase the inequality of development (Yang and Tang, 2022), and endangers the social stability and sustainable livelihood of residents, leading to more crime.

Population mobility heterogeneity

The mobile populations generated by urbanization usually have an impact on regional crime rates (Chen et al., 2017). This paper divides the sample into population inflow and population outflow regions based on the difference between the resident and registered populations (columns 6 and 7 in Table 7). The estimation results show that extreme climate contributes more to the crime rate in the inbound areas, which may be because mobile populations tend to lack stable social relationships and social security, and have lower risk tolerance than residents when exposed to extreme climate shocks (Zhong et al., 2017). This makes them more vulnerable to the negative economic impact of extreme climate, thus driving higher crime rates in the inbound areas.

Conclusion and policy insight

Using crime data from 129 prefectural-level cities in China from 2013–2019, this paper analyzed the impact of extreme climate on crime rates and its mechanism of action based on the construction and measurement of the extreme climate index. It is found that extreme climate has a significant positive effect on crime rate, with crime rate increasing by 0.035% for every 1% increase in the extreme climate index. The results based on the panel quantile model showed that the effect of extreme climate on crime rate increased continuously with the increase of regional crime rate, which means that extreme climate has a greater effect on the areas with high quantile crime rate. The action mechanism test showed that extreme climate can increase crime rates *via* the agricultural output path and the employment income path. From the heterogeneity analysis, it is clear that the differences in the effects of climate extremes on crime rates are related to geographic characteristics, economic level and population movement, and specifically, the climate extremes has a greater impact on crime rates in eastern regions, economically developed regions and population inflow regions.

The findings of this paper confirm that climate extremes are an important factor influencing criminal offending behavior. This study provides a new perspective for understanding the impact of climate change on the economy and society, and has policy implications for promoting climate governance and social stability. In the context of climate change, to reduce the impact of climate extremes on social stability, the government should pay attention to the following aspects: First, strengthen environmental protection. Atmospheric environmental pollution from fossil fuel combustion is the

main source of climate change, and the emission of atmospheric pollutants should be reduced and the quality of atmospheric environment should be improved to cope with climate change. In addition to the atmospheric environment, ecological environmental protection also needs attention. Strengthening ecological protection and restoration of ecologically fragile areas can enhance the regional climate coping capacity and use the cyclic function of the natural ecosystem to achieve sustainable carbon reduction. Second, adjust the industrial structure. We should firmly follow the green and low-carbon development path and actively respond to the negative impact of global warming on social stability in the medium and long term. Specifically, we should vigorously develop green and low-carbon industries and strictly control greenhouse gas emissions in key industries in key cities to promote and force a green transformation of the economic structure, which will mitigate the adverse effects of climate change while also helping to promote high-quality sustainable economic development and improve the region's resilience in the face of extreme climate shocks. Third, pay attention to technological innovation. Technological innovation is an important way to address climate change, and the government should call on the whole society to attach importance to low-carbon technological innovation and application, actively support the R&D and industrialization demonstration and promotion of various low-carbon technologies, and build a clean, low-carbon, safe and efficient energy system. Climate change is a common challenge for all countries in the world, and countries should increase exchanges and cooperation to enable the research and development, deployment and large-scale promotion and application of climate change technologies on a global scale. China is the largest developing country in the world, and the conclusion of this paper that climate extremes significantly contribute to regional crime rates has important implications for climate governance and social governance issues in other developing countries. In the context of global warming, developing countries should pay attention to the exogenous impact of extreme climate events on social stability and regional crime and actively participate in global climate governance. There are some limitations to this paper. Climate is dynamic and its impact on society and the economy occurs in the long term. As such, panel data over longer periods than in this study would be useful for further analysis. Second, there are many types of crime, and the impact and mechanisms of extreme climate on different types of crimes will vary. However, due to the availability of data, in this paper, a more general rate is used—the types of crimes should be further subdivided and examined in the future. Third, this paper uses the analysis concept of “extreme climate–economy–crime,” but the mechanisms of extreme temperature influencing crime are more complicated, and areas such as psychology, society, and ecology should be studied further.

Data availability statement

The original contributions presented in this study are included in the article/**Supplementary material**, further inquiries can be directed to the corresponding author/s.

Author contributions

JP conceived of the study. JP and ZZ conducted the experiments and acquired and analyzed the data. ZZ conducted the statistical analysis and drafted the manuscript. Both authors contributed to the final version of the manuscript.

Funding

This research was funded by the National Natural Science Foundation of China (No. 72063012); MOE (Ministry of Education in China) Humanities and Social Sciences Youth Foundation (No. 20YJC790103); General Project of Science and Technology Research of Jiangxi Provincial Department of Education (No. GJJ210526); Jiangxi Province Postdoctoral Research Routine Funding Project (No. 2020RC23); and 2020 Jiangxi Provincial Social Science Planning Fund Project (20YJ33).

References

- Anderson, C. A. (1989). Temperature and aggression: Ubiquitous effects of heat on occurrence of human violence. *Psychol. Bull.* 106, 74–96. doi: 10.1037/0033-2909.106.1.74
- Auffhammer, M., Hsiang, S. M., Schlenker, W., and Sobel, A. (2020). Using weather data and climate model output in economic analyses of climate change. *Rev. Environ. Econ. Policy* 7, 181–198. doi: 10.1093/reep/ret016
- Barrios, S., Bertinelli, L., and Strobl, E. (2010). Trends in rainfall and economic growth in Africa: A neglected cause of the African growth tragedy. *Rev. Econ. Stat.* 92, 350–366. doi: 10.1162/rest.2010.11212
- Baryshnikova, N., Davidson, S., and Wesselbaum, D. (2021). Do you feel the heat around the corner? The effect of weather on crime. *Empir. Econ.* 63, 179–199. doi: 10.1007/s00181-021-02130-3
- Berman, J., Bayham, J., and Burkhardt, J. (2020). Hot under the collar: A 14-year association between temperature and violent behavior across 436 US counties. *Environ. Res.* 191:110181. doi: 10.1016/j.envres.2020.110181
- Boehm, R., Cash, S. B., Anderson, B. T., Ahmed, S., Griffin, T. S., Robbat, A. Jr., et al. (2016). Association between empirically estimated monsoon dynamics and other weather factors and historical tea yields in China: Results from a yield response model. *Climate* 4:20. doi: 10.3390/cli4020020
- Bondy, M., Roth, S., and Sager, L. (2020). Crime is in the air: The contemporaneous relationship between air pollution and crime. *J. Assoc. Environ. Resour. Econ.* 7, 555–585. doi: 10.1086/707127
- Brunsdon, C., Corcoran, J., Higgs, G., and Ware, A. (2009). The influence of weather on local geographical patterns of police calls for service. *Environ. Plan. B Plan. Des.* 36, 906–926. doi: 10.1068/b32133
- Burke, M., Hsiang, S. M., and Miguel, E. (2015). Global non-linear effect of temperature on economic production. *Nature* 527, 235–239. doi: 10.1038/nature15725
- Burke, M. B., Miguel, E., Satyanath, S., Dykema, J. A., and Lobell, D. B. (2009). Warming increases the risk of civil war in Africa. *Proc. Natl. Acad. Sci. U.S.A.* 106, 20670–20674. doi: 10.1073/pnas.0907998106
- Burkhardt, J., Bayham, J., Wilson, A., Carter, E., Berman, J. D., O'Dell, K., et al. (2019). The effect of pollution on crime: Evidence from data on particulate matter and ozone. *J. Environ. Econ. Manage.* 98:102267. doi: 10.1016/j.jeem.2019.102267
- Burrows, K., and Kinney, P. L. (2016). Exploring the climate change, migration and conflict nexus. *Int. J. Environ. Res. Public Health* 13:443. doi: 10.3390/ijerph13040443
- Cai, X., Lu, Y., and Wang, J. (2018). The impact of temperature on manufacturing worker productivity: Evidence from personnel data. *J. Comp. Econ.* 46, 889–905. doi: 10.1016/j.jce.2018.06.003
- Caldeira, K., and Brown, P. T. (2019). Reduced emissions through climate damage to the economy. *Proc. Natl. Acad. Sci. U.S.A.* 116, 714–716. doi: 10.1073/pnas.1819605116
- Castellano, R. L. S., and Moroney, J. (2018). Farming adaptations in the face of climate change. *Renew. Agric. Food Syst.* 33, 206–211. doi: 10.1017/s174217051700076x
- Chang, Y. S., Kim, H. E., and Jeon, S. (2019). Do larger cities experience lower crime rates? A scaling analysis of 758 cities in the US. *Sustainability* 11:3111. doi: 10.3390/su11113111

Acknowledgments

The valuable comments and suggestions of editors and reviewers are gratefully acknowledged.

Conflict of interest

The authors declare that the research was conducted in the absence of any commercial or financial relationships that could be construed as a potential conflict of interest.

Publisher's note

All claims expressed in this article are solely those of the authors and do not necessarily represent those of their affiliated organizations, or those of the publisher, the editors and the reviewers. Any product that may be evaluated in this article, or claim that may be made by its manufacturer, is not guaranteed or endorsed by the publisher.

Supplementary material

The Supplementary Material for this article can be found online at: <https://www.frontiersin.org/articles/10.3389/fevo.2022.1028485/full#supplementary-material>

- Chen, C., Zhang, Y., Wang, L., Yan, T., and Song, J. (2013). Research on the change of extreme precipitation in Jiangxi province based on RCLIMDEX model. *China Rural Water Hydropower* 11, 41–45. doi: 10.3969/j.issn.1007-2284.2013.11.011
- Chen, J., Liu, L., Zhou, S., Xiao, L., and Jiang, C. (2017). Spatial variation relationship between floating population and residential burglary: A case study from ZG, China. *ISPRS Int. J. Geo Inf.* 6:246. doi: 10.3390/ijgi6080246
- Chen, S., Chen, X., and Xu, J. (2016). Assessing the impacts of temperature variations on rice yield in China. *Clim. Change* 138, 191–205. doi: 10.1007/s10584-016-1707-0
- Chen, X., and Yang, L. (2019). Temperature and industrial output: Firm-level evidence from China. *J. Environ. Econ. Manage.* 95, 257–274. doi: 10.1016/j.jeem.2017.07.009
- Cheong, T. S., and Wu, Y. (2015). Crime rates and inequality: A study of crime in contemporary China. *J. Asia Pac. Econ.* 20, 202–223. doi: 10.1080/13547860.2014.964961
- Choi, G., Collins, D., Ren, G., Trewin, B., Baldi, M., Fukuda, Y., et al. (2009). Changes in means and extreme events of temperature and precipitation in the Asia-Pacific Network region, 1955–2007. *Int. J. Climatol.* 29, 1906–1925. doi: 10.1002/joc.1979
- Cohn, E. G. (1990). Weather and crime. *Br. J. Criminol.* 30, 51–64. doi: 10.1093/oxfordjournals.bjc.a047980
- Cohn, E. G., and Rotton, J. (2000). Weather, seasonal trends and property crimes in Minneapolis, 1987–1988. A moderator-variable time-series analysis of routine activities. *J. Environ. Psychol.* 20, 257–272. doi: 10.1006/jevp.1999.0157
- Day, E., Fankhauser, S., Kingsmill, N., Costa, H., and Mavrogiani, A. (2019). Upholding labour productivity under climate change: An assessment of adaptation options. *Clim. Policy* 19, 367–385. doi: 10.1080/14693062.2018.1517640
- Dell, M., Jones, B. F., and Olken, B. A. (2012). Temperature shocks and economic growth: Evidence from the last half century. *Am. Econ. J. Macroecon.* 4, 66–95. doi: 10.1257/mac.4.3.66
- Deschênes, O., and Greenstone, M. (2007). The economic impacts of climate change: Evidence from agricultural output and random fluctuations in weather. *Am. Econ. Rev.* 97, 354–385. doi: 10.1257/aer.102.7.3749
- Deschênes, O., and Greenstone, M. (2011). Climate change, mortality, and adaptation: Evidence from annual fluctuations in weather in the US. *Am. Econ. J. Appl. Econ.* 3, 152–185. doi: 10.1257/app.3.4.152
- Devine, J. A., Sheley, J. F., and Smith, M. D. (1988). Macroeconomic and social-control policy influences on crime rate changes, 1948–1985. *Am. Sociol. Rev.* 53, 407–420. doi: 10.2307/2095648
- DeWall, C., and Bushman, B. (2009). Hot under the collar in a lukewarm environment: Hot temperature primes increase aggressive cognition and biases. *J. Exp. Soc. Psychol.* 45, 1045–1047. doi: 10.1016/j.jesp.2009.05.003
- DeWall, C. N., Anderson, C. A., and Bushman, B. J. (2011). The general aggression model: Theoretical extensions to violence. *Psychol. Violence* 1, 245–258. doi: 10.1037/a0023842
- Doleac, J. L., and Sanders, N. J. (2015). Under the cover of darkness: How ambient light influences criminal activity. *Rev. Econ. Stat.* 97, 1093–1103. doi: 10.1162/rest_a_00547
- Duan, H., Zhang, G., Wang, S., and Fan, Y. (2019). Robust climate change research: A review on multi-model analysis. *Environ. Res. Lett.* 14:033001. doi: 10.1088/1748-9326/aaf8f9
- Edlund, L., Li, H., Yi, J., and Zhang, J. (2013). Sex ratios and crime: Evidence from China. *Rev. Econ. Stat.* 95, 1520–1534. doi: 10.1162/REST_a_00356
- Flouris, A., and Schlader, Z. (2015). Human behavioral thermoregulation during exercise in the heat. *Scand. J. Med. Sci. Sports* 25, 52–64. doi: 10.1111/sms.12349
- Ghimire, R., Ferreira, S., and Dorfman, J. H. (2015). Flood-induced displacement and civil conflict. *World Dev.* 66, 614–628. doi: 10.1016/j.worlddev.2014.09.021
- Hindelang, M. J. (1981). Variations in sex-race-age-specific incidence rates of offending. *Am. Sociol. Rev.* 46, 461–474. doi: 10.2307/2095265
- Hipp, J. R., Curran, P. J., Bollen, K. A., and Bauer, D. J. (2004). Crimes of opportunity or crimes of emotion? Testing two explanations of seasonal change in crime. *Soc. Forces* 82, 1333–1372. doi: 10.1353/sof.2004.0074
- Holeczek, J. L., Geli, H. M., Cibils, A. F., and Sawalrah, M. N. (2020). Climate change, rangelands, and sustainability of ranching in the Western United States. *Sustainability* 12:4942. doi: 10.3390/su12124942
- Hsiang, S. M. (2010). Temperatures and cyclones strongly associated with economic production in the Caribbean and Central America. *Proc. Natl. Acad. Sci. U.S.A.* 107, 15367–15372.
- Hsiang, S. M., Meng, K. C., and Cane, M. A. (2011). Civil conflicts are associated with the global climate. *Nature* 476, 438–441. doi: 10.1038/nature10311
- Hu, L., Hu, A., and Xu, S. (2005). A case study of the impact of the disparity between the rich and the poor upon criminal offences. *J. Manage. World* 6, 34–44+171–172. doi: 10.19744/j.cnki.11-1235/f.2005.06.005
- Irish, J. L., Frey, A. E., Rosati, J. D., Olivera, F., Dunkin, L. M., Kaihatu, J. M., et al. (2010). Potential implications of global warming and barrier island degradation on future hurricane inundation, property damages, and population impacted. *Ocean Coast. Manage.* 53, 645–657. doi: 10.1016/j.ocecoaman.2010.08.001
- Jacob, B., Lefgren, L., and Moretti, E. (2007). The dynamics of criminal behavior evidence from weather shocks. *J. Hum. Resour.* 42, 489–527. doi: 10.2139/ssrn.647644
- Jones, B. F., and Olken, B. A. (2010). Climate shocks and exports. *Am. Econ. Rev.* 100, 454–459. doi: 10.1257/aer.100.2.454
- Kolvin, I., Miller, F. J., Fleeting, M., and Kolvin, P. A. (1988). Social and parenting factors affecting criminal-offence rates: Findings from the Newcastle Thousand family study (1947–1980). *Br. J. Psychiatry* 152, 80–90. doi: 10.1192/bjp.152.1.80
- Koubi, V. (2017). Climate change, the economy, and conflict. *Curr. Clim. Change Rep.* 3, 200–209. doi: 10.1007/s40641-017-0074-x
- Koubi, V., Böhmelt, T., Spilker, G., and Schaffer, L. (2018). The determinants of environmental migrants' conflict perception. *Int. Organ.* 72, 905–936. doi: 10.1017/s0020818318000231
- Kumar, S., and Khanna, M. (2019). Temperature and production efficiency growth: Empirical evidence. *Clim. Change* 156, 209–229. doi: 10.1007/s10584-019-02515-5
- Lee, C.-C., Wang, C.-W., Ho, S.-J., and Wu, T.-P. (2021). The impact of natural disaster on energy consumption: International evidence. *Energy Econ.* 97:105021. doi: 10.1016/j.eneco.2020.105021
- Lee, K. (2018). Unemployment and crime: The role of apprehension. *Eur. J. Law Econ.* 45, 59–80. doi: 10.1007/s10657-016-9526-3
- Lee, S.-W., Lee, K., and Lim, B. (2018). Effects of climate change-related heat stress on labor productivity in South Korea. *Int. J. Biometeorol.* 62, 2119–2129. doi: 10.1007/s00484-018-1611-6
- Lesk, C., Rowhani, P., and Ramankutty, N. (2016). Influence of extreme weather disasters on global crop production. *Nature* 529, 84–87. doi: 10.1038/nature16467
- Letta, M., and Tol, R. S. (2019). Weather, climate and total factor productivity. *Environ. Resour. Econ.* 73, 283–305. doi: 10.1007/s10640-018-0262-8
- Li, C., Xiang, X., and Gu, H. (2015). Climate shocks and international trade: Evidence from China. *Econ. Lett.* 135, 55–57. doi: 10.1016/j.econlet.2015.07.032
- Li, J., Wan, G., Wang, C., and Zhang, X. (2019). Which indicator of income distribution explains crime better? Evidence from China. *China Econ. Rev.* 54, 51–72. doi: 10.1016/j.chieco.2018.10.008
- Li, Z., and Fang, H. (2016). Impacts of climate change on water erosion: A review. *Earth Sci. Rev.* 163, 94–117. doi: 10.1016/j.earscirev.2016.10.004
- Linning, S. J., Andresen, M. A., and Brantingham, P. J. (2017). Crime seasonality: Examining the temporal fluctuations of property crime in cities with varying climates. *Int. J. Offender Ther. Comp. Criminol.* 61, 1866–1891. doi: 10.1177/0306624x16632259
- Lynch, M. J., Stretesky, P. B., and Long, M. A. (2020). Climate change, temperature, and homicide: A tale of two cities, 1895–2015. *Weather Clim. Soc.* 12, 171–181. doi: 10.1175/WCAS-D-19-0068.1
- Lynch, M. J., Stretesky, P. B., Long, M. A., and Barrett, K. L. (2022). The climate change-temperature-crime hypothesis: Evidence from a sample of 15 large US cities, 2002 to 2015. *Int. J. Offender Ther. Comp. Criminol.* 66, 430–450. doi: 10.1177/0306624x20969934
- Mares, D. (2013a). Climate change and crime: Monthly temperature and precipitation anomalies and crime rates in St. Louis, MO 1990–2009. *Crime Law Soc. Change* 59, 185–208.
- Mares, D. (2013b). Climate change and levels of violence in socially disadvantaged neighborhood groups. *J. Urban Health* 90, 768–783. doi: 10.1007/s11524-013-9791-1
- Martinez, A. B. (2020). Improving normalized hurricane damages. *Nat. Sustain.* 3, 517–518. doi: 10.1038/s41893-020-0550-5
- Mbonane, T. P., Mathee, A., Swart, A., and Naicker, N. (2019). A study protocol to determine the association between lifetime lead exposure and violent criminal behaviour in young males in conflict with the law. *BMC Public Health* 19:932. doi: 10.1186/s12889-019-7025-5

- McDowall, D., Loftin, C., and Pate, M. (2012). Seasonal cycles in crime, and their variability. *J. Quant. Criminol.* 28, 389–410. doi: 10.1007/s10940-011-9145-7
- Miles-Novelo, A., and Anderson, C. A. (2019). Climate change and psychology: Effects of rapid global warming on violence and aggression. *Curr. Clim. Change Rep.* 5, 36–46. doi: 10.1007/s40641-019-00121-2
- Miró, F. (2014). "Routine activity theory," in *The encyclopedia of theoretical criminology*, ed. J. M. Miller (Chichester: John Wiley & Sons), 1–7. doi: 10.1002/9781118517390.wbctc198
- Nanzad, L., Zhang, J., Tuvdendorj, B., Yang, S., Rinzin, S., Prodhon, F. A., et al. (2021). Assessment of drought impact on net primary productivity in the terrestrial ecosystems of Mongolia from 2003 to 2018. *Remote Sens.* 13:2522. doi: 10.3390/rs13132522
- NoghaniBehambari, H., and Maden, B. (2021). Unemployment insurance generosity and crime. *Appl. Econ. Lett.* 28, 1076–1081. doi: 10.1080/13504851.2020.1798337
- Peterson, T. C., Zhang, X., Brunet-India, M., and Vázquez-Aguirre, J. L. (2008). Changes in North American extremes derived from daily weather data. *J. Geophys. Res. Atmos.* 113:D07113. doi: 10.1029/2007jd009453
- Pickson, R. B., He, G., and Boateng, E. (2022). Impacts of climate change on rice production: Evidence from 30 Chinese Provinces. *Environ. Dev. Sustain.* 24, 3907–3925. doi: 10.1007/s10668-021-01594-8
- Piontek, F., Müller, C., Pugh, T. A., Clark, D. B., Deryng, D., Elliott, J., et al. (2014). Multisectoral climate impact hotspots in a warming world. *Proc. Natl. Acad. Sci. U.S.A.* 111, 3233–3238. doi: 10.1073/pnas.1222471110
- Powell, D. (2022). Quantile regression with nonadditive fixed effects. *Empir. Econ.* 63, 1–17. doi: 10.1007/s00181-022-02216-6
- Qin, X., Shi, Q., Wang, D., and Su, X. (2022). Inundation impact on croplands of 2020 flood event in three Provinces of China. *IEEE J. Sel. Topics Appl. Earth Obs. Remote Sens.* 15, 3179–3189. doi: 10.1109/jstars.2022.3161320
- Qiu, Y., and Zhao, J. (2022). Adaptation and the distributional effects of heat: Evidence from professional archery competitions. *South. Econ. J.* 88, 1149–1177. doi: 10.1002/soej.12553
- Raihan, M. L., Onitsuka, K., Basu, M., Shimizu, N., and Hoshino, S. (2020). Rapid emergence and increasing risks of hailstorms: A potential threat to sustainable agriculture in Northern Bangladesh. *Sustainability* 12:5011. doi: 10.3390/su12125011
- Ranson, M. (2014). Crime, weather, and climate change. *J. Environ. Econ. Manage.* 67, 274–302. doi: 10.1016/j.jeem.2013.11.008
- Rehman, T. H., Shah, A. K., and Hussain, S. J. (2022). Effect of climate change on agricultural productivity in Japan. *J. Agric.* 6, 13–23. doi: 10.53819/81018102t5075
- Ren, G., Feng, G., and Yan, Z. (2010). Progresses in observation studies of climate extremes and changes in mainland China. *Clim. Environ. Res.* 15, 337–353. doi: 10.3878/j.issn.1006-9585.2010.04.01
- Roche, K. R., Müller-Itten, M., Dralle, D. N., Bolster, D., and Müller, M. F. (2020). Climate change and the opportunity cost of conflict. *Proc. Natl. Acad. Sci. U.S.A.* 117, 1935–1940. doi: 10.1073/pnas.1914829117
- Rossiello, M. R., and Szema, A. (2019). Health effects of climate change-induced wildfires and heatwaves. *Cureus* 11, e4771. doi: 10.7759/cureus.4771
- Rotton, J. (1986). Determinism redux: Climate and cultural correlates of violence. *Environ. Behav.* 18, 346–368. doi: 10.1177/0013916586183003
- Rotton, J., and Cohn, E. G. (2003). Global warming and US crime rates: An application of routine activity theory. *Environ. Behav.* 35, 802–825. doi: 10.4324/9781315095301-9
- Shah, N., and Paulsen, G. (2003). Interaction of drought and high temperature on photosynthesis and grain-filling of wheat. *Plant Soil* 257, 219–226. doi: 10.1023/a:1026237816578
- Shen, B., Hu, X., and Wu, H. (2020). Impacts of climate variations on crime rates in Beijing, China. *Sci. Total Environ.* 725:138190. doi: 10.1016/j.scitotenv.2020.138190
- Spencer, N., and Strobl, E. (2019). Crime watch: Hurricanes and illegal activities. *South. Econ. J.* 86, 318–338. doi: 10.1002/soej.12376
- Stevens, H. R., Beggs, P. J., Graham, P. L., and Chang, H.-C. (2019). Hot and bothered? Associations between temperature and crime in Australia. *Int. J. Biometeorol.* 63, 747–762. doi: 10.1007/s00484-019-01689-y
- Wang, C., Jeong, G.-R., and Mahowald, N. (2009). Particulate absorption of solar radiation: Anthropogenic aerosols vs. dust. *Atmos. Chem. Phys.* 9, 3935–3945. doi: 10.5194/acp-9-3935-2009
- White, R. (2016). Criminality and climate change. *Nat. Clim. Change* 6, 737–739. doi: 10.1038/nclimate3052
- Wilkowski, B. M., Meier, B. P., Robinson, M. D., Carter, M. S., and Feltman, R. (2009). "Hot-headed" is more than an expression: The embodied representation of anger in terms of heat. *Emotion* 9, 464–477. doi: 10.1037/a0015764
- Xu, W., Li, Q., Wang, X. L., Yang, S., Cao, L., and Feng, Y. (2013). Homogenization of Chinese daily surface air temperatures and analysis of trends in the extreme temperature indices. *J. Geophys. Res. Atmos.* 118, 9708–9720. doi: 10.1002/jgrd.50791
- Yang, X., and Tang, W. (2022). Climate change and regional inequality: The effect of high temperatures on fiscal stress. *Urban Clim.* 43:101167. doi: 10.1016/j.uclim.2022.101167
- Yang, X., Tian, Z., Sun, L., Chen, B., Tubiello, F. N., and Xu, Y. (2017). The impacts of increased heat stress events on wheat yield under climate change in China. *Clim. Change* 140, 605–620. doi: 10.1007/s10584-016-1866-z
- Zander, K. K., and Mathew, S. (2019). Estimating economic losses from perceived heat stress in urban Malaysia. *Ecol. Econ.* 159, 84–90. doi: 10.1016/j.ecolecon.2019.01.023
- Zhang, P., Deschenes, O., Meng, K., and Zhang, J. (2018). Temperature effects on productivity and factor reallocation: Evidence from a half million Chinese manufacturing plants. *J. Environ. Econ. Manage.* 88, 1–17. doi: 10.1016/j.jeem.2017.11.001
- Zhang, T., and Huang, Y. (2012). Impacts of climate change and inter-annual variability on cereal crops in China from 1980 to 2008. *J. Sci. Food Agric.* 92, 1643–1652. doi: 10.1002/jsfa.5523
- Zhang, X., and Yang, F. (2004). RCLimDex (1.0) user manual. *Clim. Res. Branch Environ. Can.* 22, 1–23. doi: 10.1007/springerreference_28001
- Zhong, H., Xu, J., and Piquero, A. R. (2017). Internal migration, social exclusion, and victimization: An analysis of Chinese rural-to-urban migrants. *J. Res. Crime Delinq.* 54, 479–514. doi: 10.1177/0022427816676861
- Zhu, C., Ji, P., and Li, S. (2017). Effects of urban green belts on the air temperature, humidity and air quality. *J. Environ. Eng. Landsc. Manage.* 25, 39–55. doi: 10.3846/16486897.2016.1194276



OPEN ACCESS

EDITED BY

Shaoquan Liu,
Institute of Mountain Hazards and
Environment (CAS), China

REVIEWED BY

Xiaotong Zhang,
Beijing Normal University, China
Jianping Tang,
Nanjing University, China
Narendra Singh,
Aryabhata Research Institute of
Observational Sciences, India

*CORRESPONDENCE

Lu Gao,
l.gao@foxmail.com

SPECIALTY SECTION

This article was submitted to
Atmosphere and Climate,
a section of the journal
Frontiers in Environmental Science

RECEIVED 31 August 2022

ACCEPTED 02 November 2022

PUBLISHED 15 November 2022

CITATION

Zhao P, Gao L, Ma M and Du J (2022),
Bias correction of ERA-Interim
reanalysis temperature for the Qilian
Mountains of China.
Front. Environ. Sci. 10:1033202.
doi: 10.3389/fenvs.2022.1033202

COPYRIGHT

© 2022 Zhao, Gao, Ma and Du. This is an
open-access article distributed under
the terms of the [Creative Commons
Attribution License \(CC BY\)](#). The use,
distribution or reproduction in other
forums is permitted, provided the
original author(s) and the copyright
owner(s) are credited and that the
original publication in this journal is
cited, in accordance with accepted
academic practice. No use, distribution
or reproduction is permitted which does
not comply with these terms.

Bias correction of ERA-Interim reanalysis temperature for the Qilian Mountains of China

Peng Zhao^{1,2}, Lu Gao^{3,4,5*}, Miaomiao Ma⁶ and Jun Du¹

¹Linze Inland River Basin Research Station, Key Laboratory of Inland River Basin Science, Northwest Institute of Eco-Environment and Resource, Chinese Academy of Sciences, Lanzhou, China, ²University of Chinese Academy of Sciences, Beijing, China, ³Institute of Geography, Fujian Normal University, Fuzhou, China, ⁴Fujian Provincial Engineering Research Center for Monitoring and Accessing Terrestrial Disasters, Fujian Normal University, Fuzhou, China, ⁵Key Laboratory for Humid Subtropical Eco-Geographical Processes of the Ministry of Education, Fujian Normal University, Fuzhou, China, ⁶China Institute of Water Resources and Hydropower Research, Beijing, China

Air temperature is the primary indicator of climate change. Reanalysis temperature products are important datasets for temperature estimates over high-elevation areas with few meteorological stations. However, they contain biases in observations, so a bias correction is required to enhance the accuracy of modeling predictions. In this study, we used the temperature lapse-rate method to correct ERA-Interim reanalysis-temperature data in the Qilian Mountains of China from 1979 to 2017. These temperature lapse rates were based on observations (Γ_{Obs}) and on model internal vertical lapse rates derived from different ERA-Interim pressure levels (Γ_{ERA}). The results showed that the temperature lapse rates in warm periods were larger than those in cold periods. Both the original and corrected ERA-Interim temperature can significantly capture the warming trend exhibited by observations. In general, the temperature lapse rate method was reliable for correcting ERA-interim reanalysis-temperature data. Although Γ_{Obs} performed best in bias correction, it depends heavily on the density of ground observation stations and is not appropriate for remote areas with a low data coverage. Correction methods based on Γ_{ERA} were shown to be reliable for bias correction, and will be especially applicable to mountainous areas with few observation stations. Our results contribute to the improvement of quality of data products and enhance the accuracy of modeling of climate change effects and risks to the environment and human health.

KEYWORDS

bias correction, ERA-interim reanalysis, temperature lapse rates, Qilian Mountains, climate change

1 Introduction

The Qilian Mountains (QLM), located on the northeast margin of the Tibetan Plateau (TP), serve as an important ecological security barrier for northwestern China and an important water source for the Heihe River basin (Sun and Liu, 2013; Yang et al., 2020). However, the ecological environment of the QLM has been impacted by human activities,

including deforestation, overgrazing, overexploitation of water and energy resources (Yang et al., 2017; Wang X. et al., 2019; Zhou et al., 2019). Ground observations are the most widely used source of data for climate change studies in the QLM. However, surface meteorological stations are sparse in the QLM, especially in high-elevation areas (>2500 m) with complex terrain (Lv et al., 2019), decreasing the prediction value of data (Lin et al., 2017; Wang et al., 2018; Liu et al., 2020a; Liu et al., 2020b; Cheng et al., 2020). Moreover, observation data acquired by surface meteorological stations are inherently limited due to uneven spatiotemporal distribution, especially in mountain areas, and such data may not be sufficient to replicate true variability in the climatic characteristics in the QLM.

Spatial interpolation methods, such as inverse distance weights (IDW) and Kriging interpolation, are generally applied to obtain data in areas lacking observational data (Gao et al., 2018). However, interpolation methods often lead to large errors resulting from inadequate density and uneven spatial distribution of observational stations. Reanalysis data have been widely verified and used because they have higher temporal resolution and longer time series than observation data, and they can substitute for observation data (Gao et al., 2016; Zhang et al., 2019; Zhao et al., 2019; Makama and Lim, 2020; Demchev et al., 2021; Politi et al., 2021; Rakhmatova et al., 2021; Xu et al., 2021; Zhao and He, 2022b). However, some systematic biases exist between reanalysis and observations (Dyakonov et al., 2020; Rakhmatova et al., 2021), necessitating a bias correction of reanalysis.

Bias corrections of ERA-Interim reanalysis data have been studied in previous studies (Di Giuseppe et al., 2013; Kryza et al., 2016; Jones et al., 2017). For example, Bieniek et al. (2016) constructed a downscaling method that effectively reduced biases between reanalysis and observation data, especially for those errors that were caused by elevation differences. Szczypka et al. (2011) constructed a GPCP (product of the Global Precipitation Climatology Project) correction method to correct ERA-Interim data and showed that this method can reduce biases between ERA-Interim and observation data. Gao et al. (2014) constructed a LASSO (least absolute shrinkage and selection operator) algorithm and found that this method performed well in predicting the occurrence of a precipitation event, and reduced biases for some observational stations more than other downscaling methods. Paredes et al. (2018) used a regression correction method to correct ERA-Interim data and showed that it could significantly reduce root-mean-square-error (RMSE) between ERA-Interim and observations.

Previous studies have shown that this bias can be significantly corrected and reduced by an elevation correction method. Temperature lapse rates, representing the empirical relationship between elevation and temperature, are often applied to interpolate observations or to scale model results of near surface air temperature with respect to elevation as well as for generating the required small-scale information of near

surface air temperature (Gao et al., 2012; Gao et al., 2017). The most common used value for temperature lapse rate is -6.0 and -6.5°C to more complex approaches, which use varied numbers for the month of the year or at least different values for different seasons. However, a fixed lapse rate can be problematic because temperature gradients can vary significantly over short time periods and short distances, especially in complex terrain. The variability of lapse rate may be affected by many factors (Jiang et al., 2016; Qing et al., 2018). This lapse rate variability can just be monitored by dense meteorological station networks or by using alternative methods that can cover the temporal and spatial change of air temperature.

A solution is to use reanalysis data for different pressure levels that can also be used for a characterization of lapse rates and a subsequent downscaling of modeled temperatures that are independent with observations (Gao et al., 2012; Gao et al., 2017). For example, Gao et al. (2017) used the temperature lapse rate method to correct ERA-Interim reanalysis temperature data and showed that this method could correct ERA-Interim temperature data and improve the quality of downscaling. Gao et al. (2012) constructed a temperature-correction model by using ERA-Interim temperature and geopotential height at 925 hPa, 850 hPa and 700 hPa levels, independent of meteorological stations; subsequent tests showed that the model could successfully correct ERA-Interim. Previous studies about the correction of reanalysis temperature in the Chinese Qilian Mountains remained unclear. Our studies can provide a reference when using and correcting reanalysis temperature in the Qilian Mountains.

Here, we used ERA-Interim temperature and geopotential height at 600 hPa, 700 hPa, 850 hPa, and 925 hPa to calculate temperature lapse rates and combine lapse rates derived from observations to correct ERA-Interim reanalysis temperature data, with the purpose of revealing climatic trends based on optimally corrected ERA-Interim data. The ERA-Interim reanalysis data, observational temperature data and correction methods are introduced in Section 2. The correction results were shown in Section 3. The discussion is analyzed in Section 4. Finally, the conclusions in this study are summarized in Section 5.

2 Data and methods

2.1 ERA-Interim data (T_e)

ERA-Interim reanalysis data were downloaded from the European Centre for Medium Range Weather Forecasts (ECMWF); the data had a time step of 6 h (00.00, 06.00, 12.00, and 18.00 UTC), spatial resolution of $0.25 \times 0.25^{\circ}$, and covered a time period from 1 January 1979 to 31 December 2017. Geographical locations of the ERA-Interim grid points spanned $35.5\text{--}40.75^{\circ}\text{N}$ and $93.0\text{--}104.5^{\circ}\text{E}$, sufficient to cover the entire

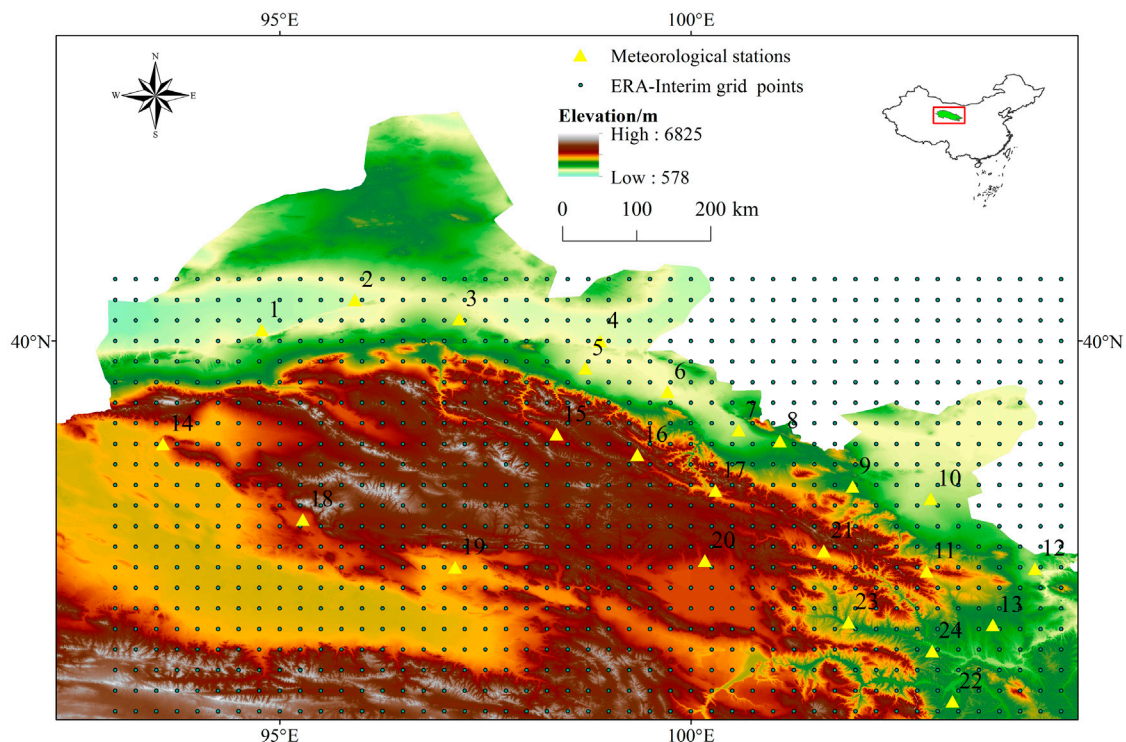


FIGURE 1
Distribution of the ERA-Interim grid points and meteorological stations in the QLM.

QLM (Figure 1). A time difference conversion method was applied to match the ERA-Interim temperature data in UTC time zone and observation data in local time. The used output variables are 2 m temperature, surface geopotential as well as temperature and geopotential height at 600, 700, 850, and 925 hPa levels. The ERA-Interim surface geopotential height (H_{ERA}) was obtained by dividing geopotential by gravity at each grid point. Altitudes corresponding to the four pressure layers (600, 700, 850, and 925 hPa) were approximately 4,000, 3,000, 1,500, and 500 m, respectively. It should be noted that the main reason for the selection of these pressure layers was that the geopotential heights of these pressure layers can reflect true characteristics of mountain climate (Gao et al., 2018), and can cover the altitude range of most stations in the QLM, which is convenient for subsequent correction and comparison.

2.2 Observations (T_o)

Observational temperature data and altitude information recorded by meteorological stations were downloaded from the China Meteorological Data Sharing Service System of the National Meteorological Information Center (<http://cdc.cma.gov.cn/index.jsp>).

The quality of observed temperature data was strictly controlled and verified by the data provider. The quality and completeness of observed temperature data are significantly improved after controlling, so it can be applied directly in climate change research. Twenty-four meteorological stations located in the QLM were selected. Observations from these stations included altitude, latitude, longitude, daily mean temperature, daily maximum temperature, and daily minimum temperature. Detailed information on the 24 meteorological stations can be found in Table 1. Briefly, these stations are located at different altitudes ranging from approximately 1,000–3,500 m. The highest station is Station No.15 with an altitude of 3,460 m, and the lowest station is Station No.1 with an altitude of 1,100 m. The geographical distribution of the 24 meteorological stations and ERA-Interim grid points are shown in Figure 1 and Table 1. There are positive elevation differences at 23 stations, only Station No.11 has a negative elevation difference between T_e and T_o . ERA-Interim grid points nearest to each meteorological station were selected for comparison based on the longitude and latitude coordinates of 24 meteorological stations, which can avoid the error caused by multigrid spatial interpolation (Zhao et al., 2020). Four seasons were defined as: spring (March to May), summer

TABLE 1 Meteorological stations information.

No	Site name	Latitude (°)	Longitude (°)	Elevation (m)	H _{ERA} (m)	H _{ERA} -H _{Obs} (m)
1	Dun Huang	40.13	94.78	1100	1508	408
2	An Xi	40.50	95.92	1182	1668	486
3	Yu Menzhen	40.27	97.18	1580	1869	289
4	Jin Ta	40.00	98.90	1270	1631	360
5	Jiu Quan	39.67	98.72	1470	1981	511
6	Gao Tai	39.38	99.72	1357	2225	868
7	Zhang Ye	38.92	100.58	1550	2074	524
8	Shan Dan	38.78	101.08	1760	2168	409
9	Yong Chang	38.23	101.97	1987	2277	291
10	Wu Wei	38.08	102.92	1525	1940	415
11	Wu Shaoling	37.20	102.87	3045	2604	-441
12	Jing Tai	37.23	104.18	1620	1761	141
13	Gao Lan	36.55	103.67	2032	2146	114
14	Leng Hu	38.75	93.58	2762	2941	179
15	Tuo Le	38.87	98.37	3460	3936	476
16	Ye Niugou	38.62	99.35	3200	3649	449
17	Qi Lian	38.18	100.30	2800	3346	546
18	Da Chaidan	37.83	95.28	3000	3364	364
19	De Lingha	37.25	97.13	2762	3469	708
20	Gang Cha	37.33	100.17	3100	3556	456
21	Men Yuan	37.45	101.62	2800	3309	509
22	Lin Xia	35.62	103.18	1900	2579	679
23	Xi Ning	36.58	101.92	2231	2916	685
24	Min He	36.23	102.93	1900	2412	512

Note: H_{ERA}, is the ERA-Interim grid point height (m).

TABLE 2 Summary of Γ and T_{ref} used in five correction methods for 24 test stations.

Methods	Γ	T_{ref}
Method I	$\Gamma_{600-700}$	T_{ERA_2m}
Method II	$\Gamma_{600-850}$	T_{ERA_2m}
Method III	$\Gamma_{700-850}$	T_{ERA_2m}
Method IV	$\Gamma_{700-925}$	T_{ERA_2m}
Method V	Γ_{Obs}	T_{ERA_2m}

(June to August), autumn (September to November), and winter (December to February).

2.3 Correction methods

ERA-Interim reanalysis temperature data were corrected using Equation 1:

$$T_t = T_{ref} + \Gamma \times \Delta h \quad (1)$$

$$\Gamma_{600-700} = (T_{600} - T_{700}) / (H_{600} - H_{700}) \quad (2)$$

$$\Gamma_{600-850} = (T_{600} - T_{850}) / (H_{600} - H_{850}) \quad (3)$$

$$\Gamma_{700-850} = (T_{700} - T_{850}) / (H_{700} - H_{850}) \quad (4)$$

$$\Gamma_{700-925} = (T_{700} - T_{925}) / (H_{700} - H_{925}) \quad (5)$$

$$\Gamma_{Obs} = T_{Obs} / H_{Obs} \quad (6)$$

where T_t is the corrected temperature, and T_{ref} is the temperature to be corrected. Δh is the elevation difference between meteorological stations and ERA-Interim grid points. Γ represents temperature lapse rates calculated from observations and ERA-Interim temperatures as well as geopotential heights at different pressures. Γ can be calculated from Equations 2–6. These calculations were repeated to obtain temperature lapse rates for five different sets of pressures, here referred to as Methods I–V (Table 2). ERA-Interim internal lapse rates are fully independent of observations (Gao et al., 2017). $\Gamma_{600-700}$, $\Gamma_{600-850}$, $\Gamma_{700-850}$, $\Gamma_{700-925}$ represent the temperature lapse rates at four pressure levels. T_{600} , T_{700} , T_{850} and T_{925} represent the temperature at 600, 700, 850 and 925 hPa pressure level, respectively. H_{600} , H_{700} , H_{850} and H_{925} represent the height at 600, 700, 850 and 925 hPa pressure level, respectively. Γ_{Obs} is the

TABLE 3 Monthly lapse rates ($^{\circ}\text{C}/\text{km}$) based on observations (Γ_{Obs}) and ERA-Interim (Γ_{600_700} , Γ_{600_850} , Γ_{700_850} , and Γ_{700_925}) during the period 1979–2017.

Month	Γ_{600_700}	Γ_{600_850}	Γ_{700_850}	Γ_{700_925}	Γ_{Obs}
January	-5.59	-5.19	-4.88	-5.32	-3.13
February	-5.66	-5.64	-5.62	-5.88	-3.68
March	-6.11	-6.29	-6.42	-6.43	-4.75
April	-6.66	-6.76	-6.84	-6.69	-5.77
May	-6.88	-6.80	-6.74	-6.53	-6.30
June	-6.93	-6.67	-6.46	-6.22	-6.54
July	-6.61	-6.31	-6.09	-5.87	-6.22
August	-6.32	-6.15	-6.01	-5.83	-5.78
September	-6.23	-6.25	-6.27	-6.14	-5.16
October	-6.13	-6.23	-6.31	-6.31	-4.64
November	-6.02	-5.74	-5.52	-5.79	-4.25
December	-5.68	-5.16	-4.76	-5.22	-3.32
Average	-6.24	-6.10	-5.99	-6.02	-4.96

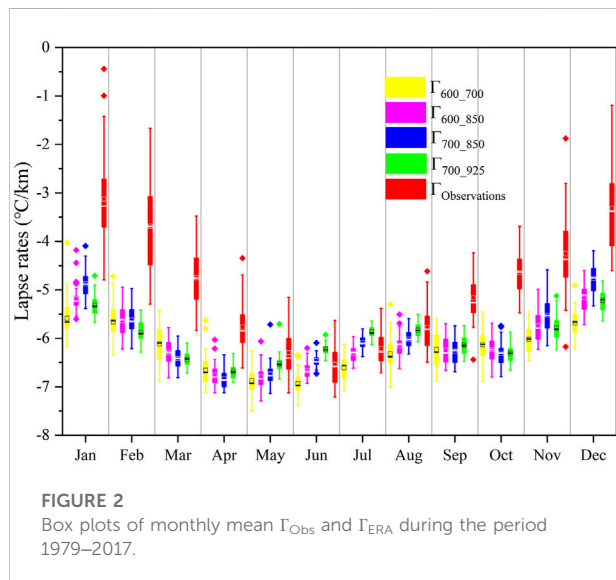


FIGURE 2
Box plots of monthly mean Γ_{Obs} and Γ_{ERA} during the period 1979–2017.

temperature lapse rate calculated from observations. T_{Obs} and H_{Obs} are the temperature and elevation of meteorological stations, respectively.

3 Results

3.1 Variability in temperature lapse rates

Table 3 and Figure 2 show the variability in five temperature lapse rates over a 12-month period across the QLM; these lapse rates are Γ_{600_700} , Γ_{600_850} , Γ_{700_850} , Γ_{700_925} , and Γ_{Obs} . The four ERA-Interim temperature lapse rates

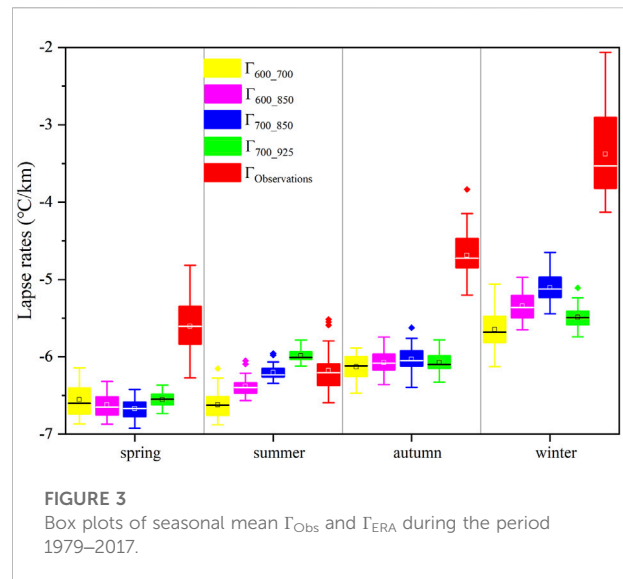


FIGURE 3
Box plots of seasonal mean Γ_{Obs} and Γ_{ERA} during the period 1979–2017.

(Γ_{ERA}) were different from the temperature lapse rate based on observations (Γ_{Obs}) with Γ_{Obs} was lower than Γ_{ERA} across the whole period in general. The five temperature lapse rates initially increased, and then decreased across the 12-month period, with the largest values in May and June (Figure 3). The lowest temperature lapse rates were found in winter.

3.2 Evaluation of correction methods

Table 4 shows the biases between observed and original ERA-Interim temperature as well as corrected ERA-Interim temperature for 24 meteorological stations during the period 1979–2017. The bias between observed and original ERA-Interim temperature at Station No.11 was positive (2.83°C), which indicated that ERA-Interim data were higher than observation data at Station No.11. Biases at Station No.11 remained positive after correction, but biases were smaller than the uncorrected ERA-Interim; the smallest bias for corrected ERA-Interim was found using Method I (0.08°C). Biases between the original ERA-Interim temperature and observed temperature at Stations No.12, 13, and 15 were negative (-1.33 , -1.05 , and -3.86°C , respectively), which indicated that ERA-Interim data were lower than observation data. There were also clear biases for the five sets of corrected ERA-Interim temperature at these stations, and these biases were also negative. The largest reductions in bias were obtained with Method I, in which they were reduced to -0.45 , -0.34 , and -0.90°C at Stations No.12, 13 and 15, respectively. Biases between original ERA-Interim and observed temperatures were also negative at Stations No.8, 20, 21 and 24 (-2.06 , -2.54 , -2.57 and -3.02°C , respectively), which again indicated that ERA-Interim data were lower than

TABLE 4 Biases (°C) between daily observed and original ERA-Interim temperature, and between observed and corrected ERA-Interim temperature (Methods I–V) for 24 meteorological stations during the period 1979–2017.

No	Site name	Original ERA-Interim	Method I	Method II	Method III	Method IV	Method V
1	Dun Huang	−0.40	2.14	2.08	2.04	2.05	1.62
2	An Xi	−1.16	1.87	1.80	1.75	1.76	1.25
3	Yu Menzhen	−0.66	1.15	1.11	1.08	1.08	0.78
4	Jin Ta	−0.73	1.52	1.47	1.43	1.44	1.06
5	Jiu Quan	−1.83	1.35	1.28	1.23	1.24	0.70
6	Gao Tai	−3.50	1.92	1.80	1.71	1.73	0.81
7	Zhang Ye	−2.31	0.96	0.89	0.83	0.84	0.29
8	Shan Dan	−2.06	0.49	0.43	0.39	0.40	−0.03
9	Yong Chang	−1.01	0.81	0.77	0.74	0.75	0.44
10	Wu Wei	−1.78	0.81	0.75	0.71	0.72	0.28
11	Wu Shaoling	2.83	0.08	0.14	0.18	0.17	0.64
12	Jing Tai	−1.33	−0.45	−0.47	−0.49	−0.48	−0.63
13	Gao Lan	−1.05	−0.34	−0.36	−0.37	−0.37	−0.49
14	Leng Hu	−1.05	0.07	0.04	0.02	0.03	−0.16
15	Tuo Le	−3.86	−0.90	−0.96	−1.01	−1.00	−1.50
16	Ye Niugou	−1.51	1.29	1.23	1.18	1.19	0.72
17	Qi Lian	−3.32	0.09	0.01	−0.04	−0.03	−0.61
18	Da Chaidan	−1.26	1.01	0.96	0.92	0.93	0.54
19	De Lingha	−3.37	1.04	0.94	0.87	0.89	0.14
20	Gang Cha	−2.54	0.31	0.25	0.20	0.21	−0.27
21	Men Yuan	−2.57	0.60	0.53	0.48	0.49	−0.05
22	Lin Xia	−2.93	1.30	1.21	1.14	1.15	0.44
23	Xi Ning	−3.18	1.10	1.00	0.93	0.95	0.22
24	Min He	−3.02	0.17	0.10	0.05	0.06	−0.48

TABLE 5 Mean seasonal bias (°C) of original ERA-Interim temperature and corrected temperature data compared with observed temperature for 24 meteorological stations during the period 1979–2017.

Seasons	Original ERA-Interim	Method I	Method II	Method III	Method IV	Method V
Spring	−2.29	0.42	0.45	0.47	0.42	0.03
Summer	−2.00	0.74	0.64	0.56	0.47	0.55
Autumn	−1.87	0.67	0.65	0.63	0.65	0.07
Winter	−1.10	1.23	1.10	1.00	1.16	0.30
Average	−1.82	0.77	0.71	0.67	0.68	0.24

observation data. The largest reductions in bias for these four stations were found by correcting ERA-Interim using Method V, and biases were reduced to −0.03, −0.27, −0.05, and −0.48°C, respectively. Biases for corrected ERA-Interim at these four stations using Methods I–IV were larger and remained negative. For all other stations, biases for uncorrected ERA-Interim were negative, but those for corrected ERA-Interim (using all five methods) were positive. Generally, the corrected results obtained *via* Method V were better than those obtained

with the other four methods, which was mainly because the temperature lapse rates of Method V were calculated using observation data, while those of the other four methods were calculated using ERA-Interim data. Biases for corrected ERA-Interim using Method I were generally smaller than when using Methods II–IV; this may be because the temperature lapse rates of Method I were calculated with ERA-Interim height and temperature in the 600–700 hPa range, and the geopotential height in this range is higher than that at the other three

TABLE 6 Correlation coefficients (*r*) between daily observed and original ERA-Interim temperature, and between observed temperature and data obtained from five correction methods for 24 meteorological stations during the period 1979–2017.

No	Site name	Original ERA-Interim	Method I	Method II	Method III	Method IV	Method V
1	Dun Huang	0.987	0.986	0.986	0.987	0.987	0.988
2	An Xi	0.979	0.976	0.978	0.978	0.978	0.975
3	Yu Menzhen	0.972	0.974	0.975	0.974	0.974	0.976
4	Jin Ta	0.971	0.967	0.968	0.968	0.969	0.968
5	Jiu Quan	0.949	0.951	0.952	0.953	0.952	0.960
6	Gao Tai	0.917	0.898	0.904	0.907	0.910	0.908
7	Zhang Ye	0.911	0.892	0.895	0.897	0.901	0.897
8	Shan Dan	0.932	0.920	0.925	0.929	0.930	0.926
9	Yong Chang	0.924	0.922	0.922	0.922	0.923	0.921
10	Wu Wei	0.907	0.899	0.902	0.904	0.904	0.902
11	Wu Shaoling	0.933	0.933	0.932	0.931	0.932	0.914
12	Jing Tai	0.910	0.907	0.908	0.908	0.908	0.911
13	Gao Lan	0.960	0.959	0.960	0.960	0.960	0.961
14	Leng Hu	0.944	0.943	0.943	0.943	0.943	0.940
15	Tuo Le	0.947	0.943	0.944	0.943	0.944	0.929
16	Ye Niugou	0.897	0.892	0.894	0.894	0.895	0.870
17	Qi Lian	0.886	0.875	0.879	0.881	0.882	0.874
18	Da Chaidan	0.949	0.947	0.946	0.946	0.947	0.940
19	De Lingha	0.952	0.950	0.952	0.952	0.952	0.932
20	Gang Cha	0.887	0.880	0.881	0.882	0.883	0.876
21	Men Yuan	0.835	0.814	0.819	0.821	0.825	0.806
22	Lin Xia	0.936	0.940	0.937	0.934	0.934	0.948
23	Xi Ning	0.386	0.409	0.390	0.374	0.380	0.373
24	Min He	0.929	0.926	0.928	0.929	0.930	0.934

pressure levels used. Meteorological stations in the QLM are mainly at elevations above 2,000 m; therefore, temperature lapse rates may be not applicable to the correction of ERA-Interim temperature data for those areas where elevations are below 1,500 m.

Table 5 shows seasonal biases between observed temperature and original ERA-Interim temperature, and for the corrected ERA-Interim temperature data for the QLM. In general, all five correction methods showed significantly reduced biases compared to those between observed and original ERA-Interim temperature. Biases for corrected ERA-Interim temperature data with four methods, and the correction result obtained using Method IV were markedly lower. The mean seasonal biases of the original ERA-Interim and the four correction methods based on the Γ_{ERA} were 0.77, 0.71, 0.67, 0.68, and 0.24°C, respectively. Corrected biases for spring and autumn were generally smaller than for summer and winter. For example, with Method V, biases in spring, summer, autumn, and winter were 0.03, 0.55, 0.07, and 0.30°C, respectively. Correlation coefficients (*r*) between observations and original ERA-Interim as well as corrected ERA-Interim were all above 0.9 (Table 6).

RMSE improved (decreased) for the corrected ERA-Interim temperature data (Table 7). RMSE for corrected ERA-Interim temperature data decreased for Stations No. 5–24 indicating that temperature lapse rates effectively corrected ERA-Interim temperature at these stations. Method I performed best at Station 11, reducing RMSE by 91%. Methods II, III, and IV performed best at Station No.17, reducing RMSE by 90.3, 90.2, and 90.3%, respectively. Method V performed best at Station No.19, reducing RMSE by 91.6%. However, RMSE increased for corrected ERA-Interim temperature data at Stations No. 1-4 compared to those for non-corrected ERA-Interim temperature data. This may be due to low elevations of these four stations, which were below 1600 m. Therefore, temperature lapse rates may be unsuitable for correcting ERA-Interim temperature data at these stations. The average RMSE for corrected ERA-Interim temperature data across the 24 meteorological stations using our correction methods were 0.98, 0.94, 0.91, 0.92, and 0.70, respectively for Methods I to V, representing reductions in the mean RMSE of 50.2%, 52.2%, 53.9%, 53.5%, and 65.3%, respectively, compared to the uncorrected ERA-Interim data. In general, Method V performed best. Correction Methods I–IV

TABLE 7 RMSE (°C) between daily observed and original ERA-Interim temperature, and between observed temperature and data obtained from five correction methods for 24 meteorological stations during the period 1979–2017.

No	Site name	Original ERA-Interim	Method I	Method II	Method III	Method IV	Method V
1	Dun Huang	0.42	2.14	2.09	2.04	2.05	1.62
2	An Xi	1.17	1.87	1.81	1.76	1.77	1.26
3	Yu Menzhen	0.67	1.16	1.12	1.09	1.09	0.79
4	Jin Ta	0.75	1.53	1.48	1.44	1.45	1.07
5	Jiu Quan	1.85	1.37	1.30	1.24	1.26	0.73
6	Gao Tai	3.51	1.94	1.83	1.74	1.76	0.87
7	Zhang Ye	2.33	1.01	0.95	0.89	0.90	0.43
8	Shan Dan	2.09	0.60	0.55	0.51	0.52	0.32
9	Yong Chang	1.04	0.85	0.81	0.78	0.79	0.51
10	Wu Wei	1.85	0.96	0.91	0.88	0.89	0.57
11	Wu Shaoling	2.84	0.25	0.28	0.30	0.29	0.69
12	Jing Tai	1.38	0.57	0.59	0.60	0.59	0.72
13	Gao Lan	1.07	0.38	0.40	0.41	0.40	0.51
14	Leng Hu	1.07	0.21	0.21	0.20	0.20	0.26
15	Tuo Le	3.87	0.93	0.99	1.04	1.03	1.53
16	Ye Niugou	1.54	1.32	1.26	1.22	1.23	0.79
17	Qi Lian	3.33	0.34	0.32	0.32	0.32	0.69
18	Da Chaidan	1.29	1.04	0.99	0.96	0.96	0.61
19	De Lingha	3.38	1.06	0.97	0.89	0.91	0.28
20	Gang Cha	2.55	0.42	0.38	0.35	0.36	0.40
21	Men Yuan	2.62	0.78	0.72	0.68	0.69	0.49
22	Lin Xia	2.94	1.32	1.23	1.16	1.17	0.48
23	Xi Ning	3.22	1.22	1.14	1.08	1.09	0.61
24	Min He	3.03	0.34	0.31	0.30	0.30	0.55

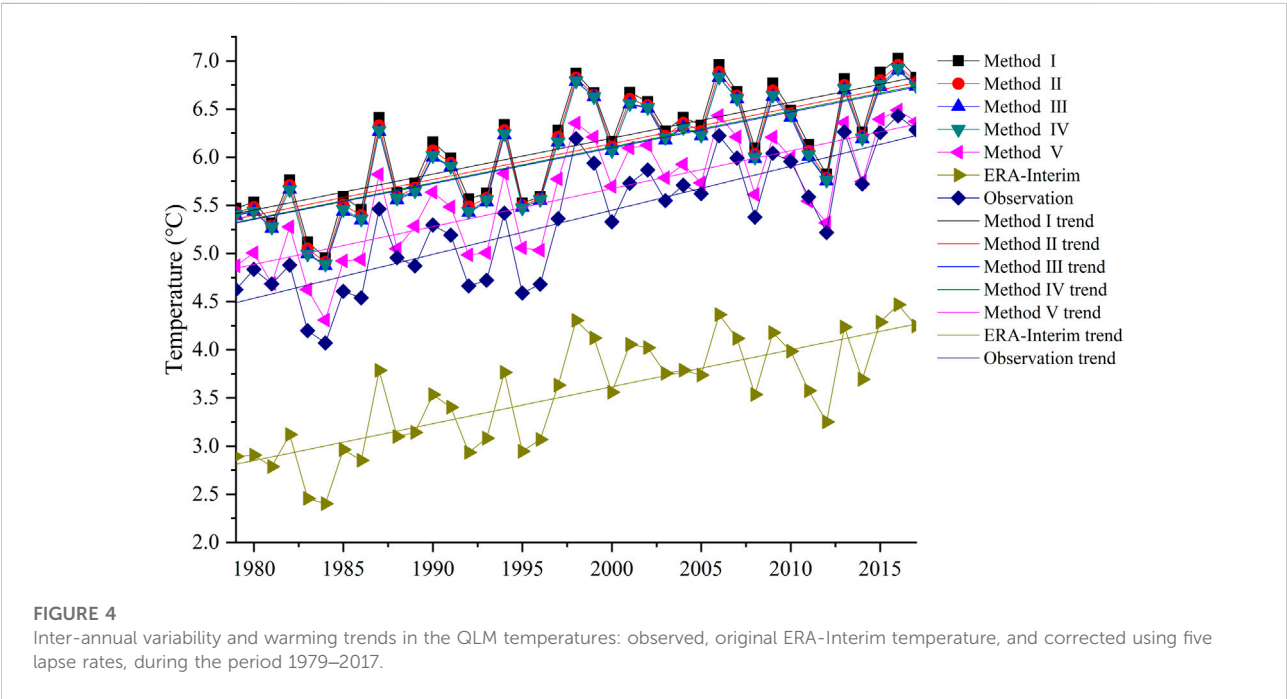


TABLE 8 Seasonal warming trends ($^{\circ}\text{C}/\text{decade}$) observed, original ERA-Interim temperature, and temperatures corrected with five methods for the period 1979–2017 in the QLM.

Temperature	Spring	Summer	Autumn	Winter	Annual
Observations	0.54	0.55	0.40	0.34	0.46
ERA-Interim	0.46	0.48	0.35	0.24	0.38
Method I	0.46	0.46	0.34	0.23	0.37
Method II	0.46	0.46	0.34	0.22	0.37
Method III	0.46	0.46	0.34	0.22	0.37
Method IV	0.46	0.46	0.34	0.22	0.37
Method V	0.51	0.51	0.36	0.20	0.39

performed better than Method V at Stations No. 11, 12, 13, 14, 15, 17, 20, and 24. These eight stations were at high elevations; stations No. 11, 15, and 20 were located at altitude above 3,000 m; 13, 14, and 17 were at were located at altitude above 2,000 m, and 12 and 24 were at were located at altitude above 1500 m. Methods I–IV may therefore be more suitable for correcting ERA-Interim temperature data at high-elevation meteorological stations.

3.3 Plateau-wide temperature climatology and trends

Figure 4 shows the inter-annual variations and warming trends over the QLM from 1979 to 2017. The ERA-Interim and corrected temperature can successfully capture trends in the observations, including an increasing trend in observed temperature, original ERA-Interim temperature, and corrected temperature during the period 1979–2017 (Table 8). The largest increasing rate was found in summer ($0.55^{\circ}\text{C}/\text{decade}$), and the smallest increasing rate was found in winter ($0.34^{\circ}\text{C}/\text{decade}$). The increasing trends shown by both the original ERA-Interim temperature and corrected temperature data underestimated the warming trend exhibited by observation data. The internal variability and increasing trends were similar for Methods I–IV, while Method V most closely matched the warming trend of the observed temperatures. In general, Method V reflected the best correction results, showing the smallest biases at a seasonal scale, and the best reflection of warming rates in the QLM.

4 Discussion

4.1 Analysis of temperature lapse rates

Our results indicated that temperature lapse rates exhibited bigger values in warm periods and smallest values in cold periods, which is mainly because the cold

air invasion in winter has a more dramatic effect on the temperature at low altitudes than at high altitudes. (Jiang et al., 2016). Qing et al. (2018) also found that temperature lapse rates during warmer months are bigger than that in colder months in the QLM, which is consistent with this study. In this study, the absolute value of Γ_{Obs} was lower than that of Γ_{ERA} , and the lowest temperature lapse rates were detected in winter, which is consistent with previous research (Jiang et al., 2016).

4.2 Analysis of correction results

The corrected temperatures obtained in this study using Method V were better than those obtained using the other four correction methods in terms of the increasing trend in observed temperature, which was similar with previous studies (Gao et al., 2012; Gao et al., 2017). The temperature lapse rates in Method V were calculated using observed temperature data, the correction results were tested with observation data, and the method depends critically on the density of ground observation stations; therefore, Method V may outperform the other methods. However, although Method V performed well, mountainous areas have few meteorological stations, therefore this method cannot be widely promoted. Gao et al. (2012) also found that temperature lapse rates calculated from observations were not reliable when observations contained outliers. Methods I–IV, which were based on Γ_{ERA} , were more flexible and independent of meteorological stations, may be applicable to correcting temperature data specifically for high-elevation stations. Furthermore, this method should be easy to extend, and will be particularly useful in mountainous areas with few observation stations. The most important advantage is that the method based on Γ_{ERA} is fully independent from the observed data. Thus, it provides a tool for correcting ERA-Interim temperature data for any high mountainous areas where no observations exist (Gao et al., 2018; Luo et al., 2019; Fan et al., 2021). Gao et al. (2017) indicates that the correction

TABLE 9 Comparison of four correction methods based on Γ_{ERA} .

Evaluation index	Method I	Method II	Method III	Method IV
Seasonal bias (°C)	0.77	0.71	0.67	0.68
Daily RMSE (°C)	0.98	0.94	0.91	0.92
Daily r	0.904	0.905	0.905	0.906
Daily bias (°C)	0.77	0.71	0.67	0.68

method using ERA-Interim internal vertical lapse rates can capture the inter-annual variations for the plateau-wide climatology very well, which is similar with this study. The bias reflects the specific difference of temperature before and after the correction, while the correlation coefficient mainly reflects the similarity between the site observations and the ERA-Interim temperature changes. The correction method based on temperature lapse rate mainly corrects the ERA-Interim temperature according to the height difference between meteorological stations and reanalysis grid points. Therefore, it mainly corrects the systematic errors between ERA-Interim temperature and observed values, which has little influence on the temperature trend. This is the reason why the bias of some sites decreased after correction, but the correlation coefficient did not change much. The correction skills are weak in winter except for Method V (Table 5, Table 8). In addition to the altitude difference, the snow cover and glaciers may also be the main reasons for the bias in winter (Zhao and He, 2022a), so the elevation correction method may not be suitable for the bias correction in winter. In addition, after comparing biases, RMSE, and r of Methods I–IV based on Γ_{ERA} , we concluded that the corrected results using Method III were superior to those using Methods I, II, and IV. The seasonal bias, RMSE, r , and mean station biases of Method III were 0.67°C, 0.91°C, 0.905, and 0.67°C, respectively (Table 9). Hence, Method III should be the most suitable for the correction of ERA-Interim temperature data in the Qilian Mountains. Gao et al. (2012) found that using (global climate) model showed a convincing performance when compared to measured data of the twelve stations, again especially for those in higher elevations, which is similar with this study.

4.3 Analysis of potential uncertainties

Although the five correction methods can improve the accuracy of ERA-Interim temperature data, they do not consider the characteristics of terrain or geographical location. Errors between the observed and ERA-Interim temperature data were not only caused by the differences between the station and ERA-Interim grid cell elevation, but also by other factors, such as the large-scale error of ERA-Interim, glacier, and errors introduced by the assimilation

system and the interpolation method (Dee, 2005; Dee and Uppala, 2009). Therefore, it may not be sufficient to correct ERA-Interim temperature using only the temperature lapse rate; additional influencing factors need to be considered in future research. The 24 meteorological stations considered in this study were situated at different altitudes and were widely spaced geographically. Discrepancies exist in direct comparisons of temperature lapse rates established using observation data and those established using ERA-Interim data. The 2881 ERA-interim grid points shown in Figure 1 span a large area, covering not only the QLM, but also areas adjacent to the QLM. Some of these grid points were located in the interior of the Tibetan Plateau, which increased terrain complexity and may lead to different temperature lapse rates. Moreover, due to the spatial location and altitude of the 24 meteorological stations are different, the calculated temperature lapse rates cannot represent a single station, but instead, represent a generalized area. Whether the representativeness is significant or not is worthy of a further study. Finally, in the formula $T_i = T_{\text{ref}} + \Gamma \times \Delta h$, the T_{ref} uses the ERA-Interim 2 m temperature values corresponding to the 24 stations, and the system error for T_{ref} is transferred, contributing to the final correction error. In addition, temperature lapse rate changes could be more variable from surface to within boundary layer and in the presence of clouds, which may affect the overall bias correction.

4.4 Future research

The aims of the error corrections performed in this study were to verify the reliability of the method and to establish a foundation for future downscaling research. For example, with DEM data for the entire QLM, we can correct all 2881 ERA-Interim grid points using Method III, and obtain temperature data from all grid points. ERA-Interim temperature data can be downscaled to higher resolution, contributing to a high-resolution data set for climate change research in this region (Gao et al., 2018; Fan et al., 2021). We focused on ERA-Interim data in this study, which is the third-generation reanalysis product of the ECMWF. However, future studies can extend the methods used here to other reanalysis products such as ERA5 and ERA5-Land (Wang C. et al., 2019; Liu et al., 2021; Zhao and He., 2022a). In addition, it would be worth trying to use

radiosonde vertical profiles to calculate lapse rates and to verify the same in this study. Moreover, temperature lapse rate may vary in different atmospheric conditions and slightly from one geographical location, especially in the boundary layer and in the presence of cloud.

5 Conclusions

In this study, ERA-Interim temperature data were corrected using temperature lapse rate methods, with the corrected results were verified using bias, r , and RMSE. Four ERA-Interim temperature lapse rates (Γ_{ERA}) were different from the temperature lapse rate based on observations (Γ_{Obs}). The Γ_{ERA} and Γ_{Obs} in warm periods were larger than those in cold periods. Biases indicated that the corrected results using Method V were more accurate than those using the other four methods. Among the four ERA-Interim temperature lapse rates (i.e., Methods I–IV), Method III generally performed best. For seasonal biases, Method V performed best. The mean seasonal biases of the original ERA-Interim and the four correction methods based on the Γ_{ERA} were 0.77, 0.71, 0.67, 0.68, and 0.24°C, respectively, with significant correlation coefficients ($r > 0.9$). In general, the corrected results for spring and autumn were more accurate than those for summer and winter. For the correction coefficient (r), the corrected r was above 0.9 for the majority of meteorological stations. The RMSE for corrected ERA-Interim improved compared to RMSE for uncorrected ERA-Interim for 19 stations, indicating that the temperature lapse rate method was suitable for correcting ERA-Interim temperature data. The mean RMSE of the five correction methods used here for data from 24 stations were 0.98°C, 0.94°C, 0.91°C, 0.92°C, and 0.70°C, respectively. The ERA-Interim and five sets of corrected temperature data successfully captured the trend of increasing observed temperatures in the QLM for the period 1979–2017. In general, temperature lapse rate method is reliable for correcting reanalysis temperature data. Although Γ_{Obs} performed best in bias correction, it critically depends on the density of ground observation stations. Correction methods based on Γ_{ERA} were shown to be reliable for bias correction and are applicable in mountainous areas with few observation stations.

References

- Bieniek, P. A., Bhatt, U. S., Walsh, J. E., Rupp, T. S., Zhang, J., Krieger, J. R., et al. (2016). Dynamical downscaling of ERA-interim temperature and precipitation for Alaska. *J. Appl. Meteorol. Climatol.* 55, 635–654. doi:10.1175/jamc-d-15-0153.1
- Cheng, P., Kong, X., Luo, H., and Wang, Y. (2020). Climate change and its runoff response in the middle section of the Qilian Mountains in the past 60 years. *Arid. land Geogr.* 43, 1192–1201.
- Dee, D. P., and Uppala, S. (2009). Variational bias correction of satellite radiance data in the ERA-Interim reanalysis. *Q. J. R. Meteorol. Soc.* 135, 1830–1841. doi:10.1002/qj.493
- Dee, D. P. (2005). Bias and data assimilation. *Q. J. R. Meteorol. Soc.* 131, 3323–3343. doi:10.1256/qj.05.137
- Demchev, D. M., Kulakov, M. Y., Makshtas, A. P., Makhotina, I. A., Fil'chuk, K. V., and Frolov, I. E. (2021). Verification of ERA-interim and ERA5 reanalyses data on surface air temperature in the arctic. *Russ. Meteorol. Hydrol.* 45, 771–777. doi:10.3103/s1068373920110035
- Di Giuseppe, F., Molteni, F., and Dutra, E. (2013). Real-time correction of ERA-Interim monthly rainfall. *Geophys. Res. Lett.* 40, 3750–3755. doi:10.1002/grl.50670

Data availability statement

Publicly available datasets were analyzed in this study. This data can be found here: <https://apps.ecmwf.int/datasets/data/interim-full-daily/levtype=sfc/>.

Author contributions

PZ: Designed study, collected meteorological data and write article. LG, MM and JD: Final edit and provide fund support.

Funding

This study was supported by the National Key Research and Development Program of China, No. 2019YFC0507403, the National Key Program for Developing Basic Science, Grant No. 2018YFC1505805, the Scientific Project from Fujian Provincial Department of Science and Technology, No. 2019R1002-3, and the Scientific Project from Fujian Key Laboratory of Severe Weather, No. 2020KFKT01.

Conflict of interest

The authors declare that the research was conducted in the absence of any commercial or financial relationships that could be construed as a potential conflict of interest.

Publisher's note

All claims expressed in this article are solely those of the authors and do not necessarily represent those of their affiliated organizations, or those of the publisher, the editors and the reviewers. Any product that may be evaluated in this article, or claim that may be made by its manufacturer, is not guaranteed or endorsed by the publisher.

- Dyakonov, G. S., Ibrayev, R. A., and Shishkova, P. O. (2020). Assessment of ERA-interim reanalysis data quality for the caspian sea area. *Russ. Meteorol. Hydrol.* 45, 650–657. doi:10.3103/s106837392009006x
- Fan, M., Xu, J., Chen, Y., and Li, W. (2021). Reconstructing high-resolution temperature for the past 40 years in the Tianshan Mountains, China based on the Earth system data products. *Atmos. Res.* 253, 105493. doi:10.1016/j.atmosres.2021.105493
- Gao, L., Bernhardt, M., and Schulz, K. (2012). Elevation correction of ERA-Interim temperature data in complex terrain. *Hydrol. Earth Syst. Sci.* 16, 4661–4673. doi:10.5194/hess-16-4661-2012
- Gao, L., Bernhardt, M., Schulz, K., and Chen, X. (2017). Elevation correction of ERA-Interim temperature data in the Tibetan Plateau. *Int. J. Climatol.* 37, 3540–3552. doi:10.1002/joc.4935
- Gao, L., Bernhardt, M., Schulz, K., Chen, X., Chen, Y., and Liu, M. (2016). A first evaluation of ERA-20cm over China. *Mon. Weather Rev.* 144, 45–57. doi:10.1175/mwr-d-15-0195.1
- Gao, L., Schulz, K., and Bernhardt, M. (2014). Statistical downscaling of ERA-interim forecast precipitation data in complex terrain using LASSO algorithm. *Adv. Meteorology* 2014, 1–16. doi:10.1155/2014/472741
- Gao, L., Wei, J., Wang, L., Bernhardt, M., Schulz, K., and Chen, X. (2018). A high-resolution air temperature data set for the Chinese Tian Shan in 1979–2016. *Earth Syst. Sci. Data* 10, 2097–2114. doi:10.5194/essd-10-2097-2018
- Jiang, J. C., Liu, J. Z., Qin, C. Z., Miao, Y. M., and Zhu, A. X. (2016). Near-surface air temperature lapse rates and seasonal and type differences in China. *Prog. Geogr.* 35, 1538–1548.
- Jones, P. D., Harpham, C., Troccoli, A., Gschwind, B., Ranchin, T., Wald, L., et al. (2017). Using ERA-Interim reanalysis for creating datasets of energy-relevant climate variables. *Earth Syst. Sci. Data* 9, 471–495. doi:10.5194/essd-9-471-2017
- Kryza, M., Walaszek, K., Ojrzyska, H., Szymanowski, M., Werner, M., and Dore, A. J. (2016). High-resolution dynamical downscaling of ERA-interim using the WRF regional climate model for the area of Poland. Part 1: Model configuration and statistical evaluation for the 1981–2010 period. *Pure Appl. Geophys.* 174, 511–526. doi:10.1007/s00024-016-1272-5
- Lin, P., He, Z., Du, J., Chen, L., Zhu, X., and Li, J. (2017). Recent changes in daily climate extremes in an arid mountain region, a case study in northwestern China's Qilian Mountains. *Sci. Rep.* 7, 2245. doi:10.1038/s41598-017-02345-4
- Liu, H., Li, Y., Zhang, X., and Xu, M. L. (2021). Climate differences in different time scales in the east and west sections of the Qilian Mountains. *J. Lanzhou Univ. Nat. Sci.* 56, 724–732. doi:10.13885/j.issn.0455-2059.2020.06.003
- Liu, J., Hagan, D. F. T., and Liu, Y. (2020a). Global land surface temperature change (2003–2017) and its relationship with climate drivers: AIRS, MODIS, and ERA5-land based analysis. *Remote Sens.* 13, 44. doi:10.3390/rs13010044
- Liu, J., Jiang, G., Wu, Q., Zhang, T., and Gao, S. (2020b). Regional climate change signals inferred from a borehole temperature profile in Muli, Qilian Mountain, using the Tikhonov method. *Arct. Antarct. Alp. Res.* 52, 450–460. doi:10.1080/15230430.2020.1801149
- Luo, H., Ge, F., Yang, K., Zhu, S., Peng, T., Cai, W., et al. (2019). Assessment of ECMWF reanalysis data in complex terrain: Can the CERA-20C and ERA-Interim data sets replicate the variation in surface air temperatures over Sichuan, China? *Int. J. Climatol.* 39, 5619–5634. doi:10.1002/joc.6175
- Lv, Y., Li, Z., Feng, Q., Li, Y. G., Yuan, R. F., Gui, J., et al. (2019). Analysis of extreme temperature changes in Qilian Mountains in the past 60years. *Plateau meteorol.* 38, 959–970.
- Makama, E. K., and Lim, H. S. (2020). Variability and trend in integrated water vapour from ERA-interim and IGRA2 observations over peninsular Malaysia. *Atmosphere* 11, 1012. doi:10.3390/atmos11091012
- Paredes, P., Martins, D. S., Pereira, L. S., Cadima, J., and Pires, C. (2018). Accuracy of daily estimation of grass reference evapotranspiration using ERA-Interim reanalysis products with assessment of alternative bias correction schemes. *Agric. Water Manag.* 210, 340–353. doi:10.1016/j.agwat.2018.08.003
- Politi, N., Vlachogiannis, D., Sfetsos, A., and Nastos, P. T. (2021). High-resolution dynamical downscaling of ERA-Interim temperature and precipitation using WRF model for Greece. *Clim. Dyn.* 57, 799–825. doi:10.1007/s00382-021-05741-9
- Qing, W. W., Han, C. T., and Liu, J. F. (2018). A study on temperature lapse rate in Hulugou watershed, Qilian Mountains. *J. Lanzhou Univ. Nat. Sci.* 54, 44–50+58. doi:10.13885/j.issn.0455-2059.2018.01.008
- Rakhmatova, N., Arushanov, M., Shadakova, L., Nishonov, B., Taryannikova, R., Rakhmatova, V., et al. (2021). Evaluation of the perspective of ERA-interim and ERA5 reanalyses for calculation of drought indicators for Uzbekistan. *Atmosphere* 12, 527. doi:10.3390/atmos12050527
- Sun, J., and Liu, Y. (2013). Drought variations in the middle Qilian Mountains, northeast Tibetan Plateau, over the last 450 years as reconstructed from tree rings. *Dendrochronologia* 31, 279–285. doi:10.1016/j.dendro.2012.07.004
- Szczypta, C., Calvet, J. C., Albergel, C., Balsamo, G., Boussetta, S., Carrer, D., et al. (2011). Verification of the new ECMWF ERA-Interim reanalysis over France. *Hydrol. Earth Syst. Sci.* 15, 647–666. doi:10.5194/hess-15-647-2011
- Wang, C., Graham, R. M., Wang, K., Gerland, S., and Granskog, M. A. (2019a). Comparison of ERA5 and ERA-interim near-surface air temperature, snowfall and precipitation over arctic sea ice: Effects on sea ice thermodynamics and evolution. *Cryosphere* 13, 1661–1679. doi:10.5194/tc-13-1661-2019
- Wang, Q., Yang, Q., Guo, H., Xiao, X., Jin, H., Li, L., et al. (2018). Hydrothermal variations in soils resulting from the freezing and thawing processes in the active layer of an alpine grassland in the Qilian Mountains, northeastern Tibetan Plateau. *Theor. Appl. Climatol.* 136, 929–941. doi:10.1007/s00704-018-2529-y
- Wang, X., Chen, R., Han, C., Yang, Y., Liu, J., Liu, Z., et al. (2019b). Response of frozen ground under climate change in the Qilian Mountains, China. *Quat. Int.* 523, 10–15. doi:10.1016/j.quaint.2019.06.006
- Xu, J., Tian, R., and Feng, S. (2021). Comparison of atmospheric vertical motion over China in ERA-interim, JRA-55, and NCEP/NCAR reanalysis datasets. *Asia. Pac. J. Atmos. Sci.* 57, 773–786. doi:10.1007/s13143-021-00226-5
- Yang, W., Wang, Y., Wang, S., Webb, A. A., Yu, P., Liu, X., et al. (2017). Spatial distribution of Qinghai spruce forests and the thresholds of influencing factors in a small catchment, Qilian Mountains, northwest China. *Sci. Rep.* 7, 5561. doi:10.1038/s41598-017-05701-6
- Yang, Y., Chen, R.-s., Song, Y.-x., Han, C.-t., Liu, Z.-w., and Liu, J.-f. (2020). Spatial variability of soil hydraulic conductivity and runoff generation types in a small mountainous catchment. *J. Mt. Sci.* 17, 2724–2741. doi:10.1007/s11629-020-6258-1
- Zhang, B., Zhang, R., Wu, L., and Nie, C. (2019). Changes of precipitation and moisture extremes in ERA-interim reanalysis viewed from a new space. *Environ. Res. Commun.* 2, 011004. doi:10.1088/2515-7620/ab59c7
- Zhao, P., and He, Z. (2022a). A first evaluation of ERA5-land reanalysis temperature product over the Chinese qilian mountains. *Front. Earth Sci.* 10, 907730. doi:10.3389/feart.2022.907730
- Zhao, P., and He, Z. (2022b). Temperature change characteristics in gansu province of China. *Atmosphere* 13, 728. doi:10.3390/atmos13050728
- Zhao, P., Gao, L., Wei, J., Ma, M., Deng, H., Gao, J., et al. (2020). Evaluation of ERA-interim air temperature data over the qilian mountains of China. *Adv. Meteorology* 2020, 1–11. doi:10.1155/2020/7353482
- Zhao, S., Zhang, S., Cheng, W., and Zhou, C. (2019). Model simulation and prediction of decadal mountain permafrost distribution based on remote sensing data in the qilian mountains from the 1990s to the 2040s. *Remote Sens.* 11, 183. doi:10.3390/rs11020183
- Zhou, J., Li, Q., Wang, L., Lei, L., Huang, M., Xiang, J., et al. (2019). Impact of climate change and land-use on the propagation from meteorological drought to hydrological drought in the eastern qilian mountains. *Water* 11, 1602. doi:10.3390/w11081602



OPEN ACCESS

EDITED BY
Wei Shui,
Fuzhou University, China

REVIEWED BY
Jianqi Zhang,
National University of Defense
Technology, China
Haijun Deng,
Fujian Normal University, China

*CORRESPONDENCE

Xiefei Zhi,
zhi@nuist.edu.cn

SPECIALTY SECTION

This article was submitted to
Atmosphere and Climate,
a section of the journal
Frontiers in Environmental Science

RECEIVED 14 July 2022

ACCEPTED 25 October 2022

PUBLISHED 15 November 2022

CITATION

Sein ZMM, Zhi X, Ogou FK, Nooni IK and
Paing KH (2022), Evaluation of coupled
model intercomparison project phase
6 models in simulating precipitation and
its possible relationship with sea surface
temperature over Myanmar.
Front. Environ. Sci. 10:993802.
doi: 10.3389/fenvs.2022.993802

COPYRIGHT

© 2022 Sein, Zhi, Ogou, Nooni and
Paing. This is an open-access article
distributed under the terms of the
[Creative Commons Attribution License](#)
(CC BY). The use, distribution or
reproduction in other forums is
permitted, provided the original
author(s) and the copyright owner(s) are
credited and that the original
publication in this journal is cited, in
accordance with accepted academic
practice. No use, distribution or
reproduction is permitted which does
not comply with these terms.

Evaluation of coupled model intercomparison project phase 6 models in simulating precipitation and its possible relationship with sea surface temperature over Myanmar

Zin Mie Mie Sein¹, Xiefei Zhi^{1,2*}, Faustin Katchele Ogou^{3,4},
Isaac Kwesi Nooni^{5,6} and Khant Hmu Paing⁷

¹Collaborative Innovation Centre on Forecast and Evaluation of Meteorology Disaster, Key Laboratory of Meteorological Disasters, Ministry of Education, Nanjing University of Information Science and Technology, Nanjing, China, ²Weather Online Institute of Meteorological Applications, Wuxi, China, ³Laboratory of Atmospheric Physics, Department of Physics, University of Abomey-Calavi, Cotonou, Benin, ⁴College of Earth Science, University of Chinese Academy of Sciences, Beijing, China, ⁵School of Atmospheric Science and Remote Sensing, Wuxi University, Wuxi, China, ⁶School of Geographical Sciences, Nanjing University of Information Science and Technology, Nanjing, China, ⁷School of Computer and Software, Nanjing University of Information Science and Technology, Nanjing, China

The study investigated the precipitation variability over Myanmar at the annual and seasonal scales by comparing 12 model outputs from the Coupled Model Intercomparison Project Phase 6 (CMIP6) with gridded observational data provided by the Global Precipitation Climatology Centre (GPCC) from 1970 to 2014. Using Mann–Kendall and Sen's slope estimator, the trend analysis was assessed. Correlation analysis was also used to investigate the relationship of observational and Ensemble means precipitation with sea surface temperature (SST) anomalies. Results show a better correlation pattern of ENS with observation precipitation than that of individual selected models during the May–October season than that of the annual scale. Meanwhile, UKESM1-0-LL, NESM3, and HadGEM3-CC31-LL show high correlation with a relatively low root-mean-square difference. A few models roughly capture the spatiotemporal patterns of precipitation during MJJASO over Myanmar. The root mean square errors (RMSEs) of MIROC6, CNRM-ESM2-1, CNRM-CM6, and NESM3 are lower than that of ENS, whereas the RMSEs of CESM2, GFDL-CM4, HadGEM3-CC31-LL, GFDL-ESM4, UKESM1-0-LL, MPI-ESM1-2-HR, MRI-ESM2-0, and IPSL-CM6A-LR are higher than that of ENS, for annual precipitation. Heterogeneous correlation coefficients and slope changes are evident within the country at both annual and seasonal periods. Overall, the ENS showed a long-term increasing annual trend. Most of the model exhibited increasing annual trends while some showed decreasing annual trends. The correlation between the annual series and SST anomalies shows stronger correlation coefficient than that of seasonal. Overall, the correlation analysis of the SST anomalies reveals significant positive and negative relationships with the ENS precipitation. We recommend considering future projections of precipitation changes over Myanmar in future work.

KEYWORDS

CMIP6, Taylor diagram, correlational analysis, GPCC, climate change, precipitation, Myanmar

1 Introduction

In many modelling studies, global warming has been linked to extreme events. These extreme events have intensified across many regions around the globe (IPCC 2021) and led to several natural disasters that have resulted in losses of lives and property (Amato et al., 2019; Iqbal et al., 2019; IPCC 2021). One such region is Myanmar, where the spatiotemporal variability of the changes in precipitation means that understanding the performance of models in simulating precipitation over this country is an important line of research (Kitoh et al., 2013). Myanmar is a country in Southeast Asia that experiences harsh consequences of climate change, mainly in the form of flooding and drought over whole or part of the country.

To study historical extreme events, observational data and global climate model (GCM) outputs are used (Taylor et al., 2012; O'Neill et al., 2016). The Coupled Model Intercomparison Project (CMIP) is a project framework that compares GCMs in an attempt to help further our understanding of the reaction of the climate system to different scenarios of anthropogenic warming. The ability of climate models to simulate precipitation variations in the globe and some regions that showed obvious warming and wetting trends result from different levels of anthropogenic warming (Taylor et al., 2012; Meehl et al., 2014; Eyring et al., 2016; O'Neill et al., 2016), with past studies having revealed these findings on the basis of the Coupled Model Intercomparison Project Phase 5 (CMIP5) and older versions (Babar et al., 2014; Alexander 2016; Ge et al., 2019; Ge et al., 2021). Despite these findings from global and regional climate models, there is no consensus on the historical change in precipitation. Several reasons have been proposed for this lack of consensus, but data quality and limitations to the coverage of data are viewed as the major obstacles (Alexander 2016).

Additionally, there were reports that argued the limitations in CMIP data are due to their respective configurations, CMIP5 models and their older versions find it difficult to detect historical trends at time scales long enough to overcome the natural variability of the climate. However, in the latest release of CMIP namely the CMIP6, new radiative forcings used by authors and the improved quality and resolution of the models provide a better representation of the responses of the climate system, which is of great interest for vulnerability impact assessment studies (Stouffer et al., 2017). In addition, specific to the present study, this is particularly important in addressing the variability of precipitation in different climate regions. For instance, the skill of CMIP6 GCMs in simulating the variability of precipitation over Asia has been demonstrated (Wang et al., 2018; Fremme and Sodemann 2019).

Several studies on evaluating CMIP6 GCMs over Asia have been conducted (Jiang et al., 2007; Jiang et al., 2012; Dong et al., 2018; He

and Zhao, 2018; Iqbal et al., 2021). For example, Iqbal et al. (2021) found that CMIP6 models reproduce the spatial patterns of precipitation well over mainland Southeast Asia. However, a study that considers as large a region as this may with the same approach fail to depict the features of a relatively smaller region that are needed for the development of appropriate local governance policies. Horton et al. (2017) assessed the climate risk using NASA NEX baseline data and the results revealed that the wet season will become wetter, with precipitation projected to increase in the future. Changes in extreme precipitation are likely to increase the level of flooding in many parts of Myanmar during the wet season. Indeed, in 2021, the monsoon floods during the peak monsoon season (July–August) in Myanmar affected more than 125,000 people across the country, resulting in crop losses and food insecurity (OCHA 2021). Similarly, in early of the year 2020, more than 2000 deaths were observed during the monsoon season in India, Myanmar, Pakistan, Nepal, Bangladesh, and Afghanistan, with 166 of those deaths resulting from a landslide caused by heavy rain at a mine in Upper Myanmar in early July of the same year (WMO 2021). Myanmar is a country located in the monsoonal belt of Asia with a large dependence on agricultural rain-fed, making the precipitation variability and its subsequent impacts an issue of considerable economic significance. Extreme weather is a perennial occurrence in Myanmar, as demonstrated by (Eckstein et al., 2020) in their study during 1970–2014. Flooding usually occurs in June–October (the summer monsoon), with the biggest threat in August (the mid-monsoon season) (Department of Disaster Management 2020). Nonetheless, despite numerous studies having been carried out over the Southeast Asian region, including Myanmar, our level of understanding at the local scale in this country remains insufficient. Moreover, precipitation varies substantially at such a local scale. The interaction between precipitation variability and its common drivers are certainly worthy of exploration. The most common factors are the atmospheric circulation and its indices, decadal and interdecadal variabilities, periodicities and oscillations, and the sea surface temperature (SST) anomalies over key regions, including El Niño. Previous studies have investigated the influence of local change in SST including the El Niño, the Pacific decadal Oscillation, India Ocean index and Atlantic Multi-Decadal Oscillation (Sein et al., 2015; Sein et al., 2022); henceforth the global SST is considered in the present study.

The overall goal of this study is to provide basic information of the precipitation variability at the local scale in Myanmar, which, to the best of our knowledge, is the first of its kind. It also compares the performance of model at annual and seasonal scales. In this current era of climate change, erratic patterns and trends of precipitation often occur. In this work, we use CMIP6-modeled precipitation, which is evaluated against

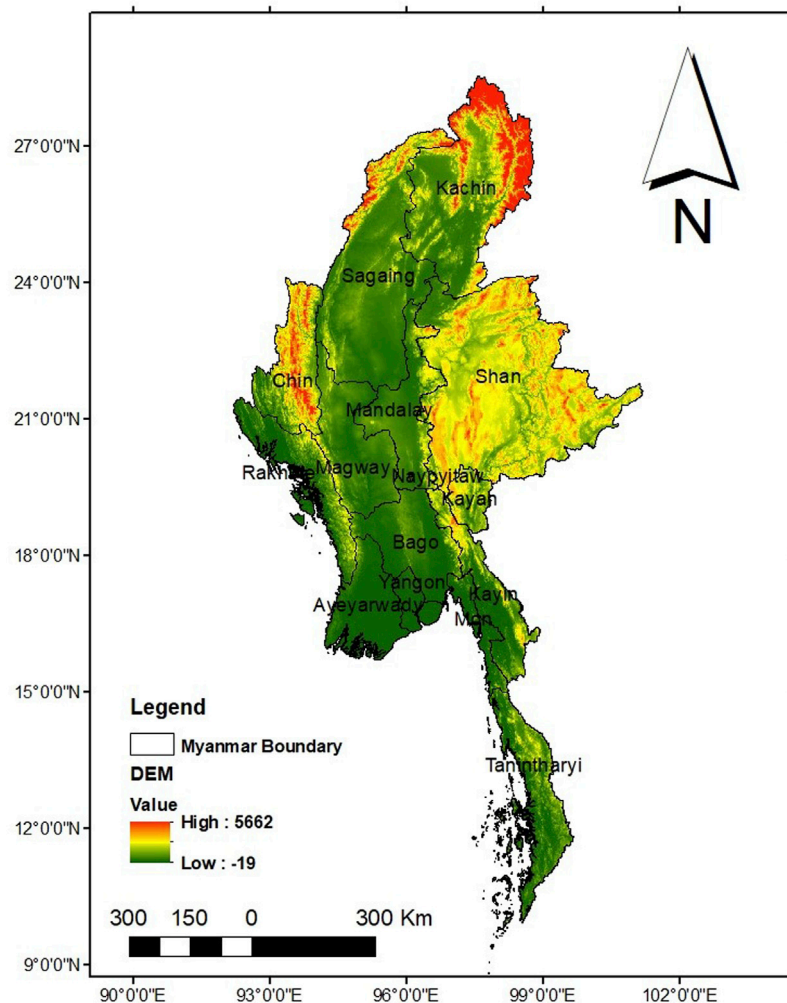


FIGURE 1
Elevation map of Myanmar (mm).

gridded observational precipitation and the SST data, to analyze the relationship between precipitation and SST over Myanmar. The outcome of this study is important for policymaking in different departments of Myanmar's government involved in disaster risk management, such as the Department of Meteorology and Hydrology.

2 Study area, data and methods

2.1 Study area

The latitude-longitude coordinates of Myanmar range from 9°32' to 28°31'N in latitude and 92°10' to 101°11'E in longitude. The country covers 676,578 km² (Figure 1). The study area is characterized by tropical to subtropical monsoon climate (NECC

2012). Myanmar is influenced by the Indian monsoon with three main seasons: summer (March–April), rainy (May–October), and winter (December–February). For further details, see (Ren et al., 2017; Oo et al., 2020; Sein et al., 2021a). The country has large rivers that cross the country (Sein et al., 2022). The rainfall variability in the region has adverse socioeconomic impacts. For example, in July 2019, torrential rain, flooding and landslides in Mon state caused the deaths of 75 people, with 40 remaining missing under the mud (Department of Disaster Management 2020). In August 2020, widespread flooding occurred in the Ayeyarwady and Thanlyin river basins, which affected at least 21,500 people. More recently, in 2021, continuous monsoon rains caused flooding in the west coastal area (Rakhine state) and in southeastern and southern Myanmar (i.e., the states of Mon and Kayin and the region of Tanintharyi), impacting 3,000 people (OCHA 2021).

TABLE 1 Details of the CMIP6 GCMs used in this study.

No.	Model	Institution	Approximate grid spacing
1	CNRM-ESM2-1	National Centre for Meteorological Research and European Centre for Research and Advanced Training in Scientific Computation, France	1.40625 × 1.40625
2	GFDL-CM4	National Oceanic and Atmospheric Administration Geophysical Fluid Dynamics Laboratory, United States	1.25 × 1
3	CNRM-CM6-1	National Centre for Meteorological Research and European Centre for Research and Advanced Training in Scientific Computation, France	1.40625 × 1.40625
4	GFDL-ESM4	National Oceanic and Atmospheric Administration Geophysical Fluid Dynamics Laboratory, United States	1.25 × 1
5	HadGEM3-GC31-LL	Met Office Hadley Centre, United Kingdom	1.875 × 1.25
6	IPSL-CM6A-LR	Institute Pierre Simon Laplace, France	2.5 × 1.25874
7	MIROC6	University of Tokyo, National Institute for Environmental Studies and Japan Agency for MarineEarth Science and Technology, Japan	1.40625 × 1.40625
8	CESM2	National Center for Atmospheric Research	1.25 × 0.94
9	MPI-ESM1-2-HR	Max Planck Institute for Meteorology, Germany	0.9375 × 0.9375
10	MRI-ESM2-0	Meteorological Research Institute, Japan	1.125 × 1.125
11	NESM3	Nanjing University of Information Science and Technology, China	1.875 × 1.875
12	UKESM1-0-LL	Met Office Hadley Centre, United Kingdom	1.875 × 1.25

2.2. Datasets

2.2.1 Observed precipitation

Monthly precipitation data at a 0.5 grid resolution (Schneider et al., 2015) from the Global Precipitation Climatology Centre (GPCC) dataset, version 7 (GPCC 2021), are used in this work. The data are available from <https://psl.noaa.gov/data/gridded/data.gpcc.htm> and have been used and verified with the region's observed precipitation (Sein et al., 2015; Sein et al., 2021a).

2.2.2 CMIP6 models

The historical experiments of 12 CMIP6 models (Eyring et al., 2016) were obtained from <https://esgf-node.llnl.gov/search/cmip6> for the period 1950–2014 (Table 1). All models were resampled to a common grid of 0.5 × 0.5 using bilinear interpolation. Prior to computation, the daily data were aggregated to a monthly basis. The ensemble mean (ENS) of the 12 CMIP6 models has been computed. Details of all the CMIP6 models used in the present work, including the name of the modelling center, their institution's identity, and horizontal resolution (longitude × latitude), are given in Table 1.

2.2.3 SST

This study investigates the relationship of the SST with each model and the ENS of precipitation at annual and seasonal scales following (Ashok et al., 2007; Vinayachandran et al., 2009). The Extended Reconstructed SST dataset, version 5 [ERSST.v5; Huang et al. (2017)], for the period from 1854 to the present day, is used for this purpose,

obtained from the National Oceanic and Atmospheric Administration (NOAA) via <https://climatedataguide.ucar.edu/climate-data/sst-data-noaa-extended-reconstruction-ssts-version-5-ersstv5>. The horizontal resolution of the data is 2 × 2. The atmospheric circulation pattern is shown using the reanalysis u and v winds that are retrieved from NCEP-NCAR website.

2.1 Materials and methods

2.3.1 Mann–Kendall test

To analyze the trends, this study uses the Mann–Kendall (MK) test (Mann 1945), calculated as follows:

$$S = \sum_{i=1}^{n-1} \sum_{j=i+1}^n \text{sgn}(x_i - x_j) \quad (1)$$

where S is the rating score (called the MK sum), x is the data value, i and j are counters, and n represents the number of data points. Then,

$$\text{Var}(S) = \frac{n(n-1)(2n+5)}{18} \quad (2)$$

where $\text{Var}(S)$ is the standardized variance, and

$$Z_s = \begin{cases} \frac{S-1}{\sqrt{\text{Var}(S)}}, & \text{if } S > 0 \\ 0, & \text{if } S = 0 \\ \frac{S+1}{\sqrt{\text{Var}(S)}}, & \text{if } S < 0 \end{cases} \quad (3)$$

in which $|Z| > Z_{\alpha/2}$ represents the time series of the data. The significance level is shown by $\alpha = 0.05$, or $Z_{\alpha/2} = 1.96$, and $|Z| > 1.96$ means a significant trend.

To compute the linear trend rate, the Theil-Sen's estimator was used based on Eq. 4. Here, note that trend rate values greater than zero (i.e., $\Delta\sigma > 0$) denotes a positive value (or increasing rate) and trend rate values less than zero (i.e., $\Delta\sigma < 0$), denotes a negative value (or means decreasing rate).

$$\beta = \text{median}\left(\frac{x_j - x_k}{j - k}\right) \quad (4)$$

where the slope between two points is shown as β ; medium represents a function; x_j and x_k correspond to data values for time points j and k ($j > k$), respectively.

2.3.2 Bilinear interpolation

The bilinear interpolation method uses four 4) known neighboring image coordinates located diagonally from each other to compute the final interpolated value based on the weight of each pixel values from samples. The study followed the general bilinear procedures explained in Bayen et al. (2015). This method was implemented in Climate Data Operators (CDO).

Let assume, the final interpolated value is a function (f) at a location $V(x, y)$.

$$\begin{aligned} (x, y) = & U_{00} \frac{(x_1 - x_0)(y_1 - y_0)}{(x_1 - x_0)(y_1 - y_0)} + U_{10} \frac{(x - x_1)(y_1 - y_0)}{(x_1 - x_0)(y_1 - y_0)} \\ & + U_{01} \frac{(x_1 - x_0)(y - y_1)}{(x_1 - x_0)(y_1 - y_0)} + U_{11} \frac{(x - x_0)(y - y_0)}{(x_1 - x_0)(y_1 - y_0)} \end{aligned} \quad (5)$$

where $V(x_i, y_j) = U_{ij}$, $i, j = 0, 1$. $U_{00}(x, t)$, $U_{01}(x, t)$, $U_{10}(x, y)$ and $U_{11}(x, y)$ denotes four (4) known neighboring image coordinates.

2.3.3 Taylor diagram

A Taylor diagram (Taylor et al., 2012) provides a graphical summary of how closely a pattern or set of patterns resembles observations. For more details on the nomenclature of the Taylor diagram, we refer readers to (Taylor et al., 2012). The correlation (r), root mean square error (RMSE), and relative bias (RBIAS) were computed as follows:

$$r = \frac{\sum_{i=1}^n (X_i - \bar{X})(Y_i - \bar{Y})}{\sqrt{\sum_{i=1}^n (X_i - \bar{X})^2} \sqrt{\sum_{i=1}^n (Y_i - \bar{Y})^2}} \quad (6)$$

where n , X_i and Y_i represent the number of years and the CMIP6 and GPCC series, for example, at time i ; and \bar{X} and \bar{Y} represent the average of X_i and Y_i for the study period, respectively.

The RMSD stands for root mean square deviation between two variables mainly the predicted (simulated models) and reference (GPCC), which is defined as follows:

$$RMSD^2 = \sum_{i=1}^N \frac{(x_i - x'_i)^2}{N} \quad (7)$$

The RMSE gives the magnitude of the forecast errors. The RMSE is defined as the root mean square error with giving formula:

$$RMSE = \sqrt{\sum_{i=1}^N \frac{(x_i - x'_i)^2}{N}} \quad (8)$$

Where x_i and x'_i represent the predicted and reference values, respectively. N is the total number of values in x_i and x'_i with x_i and x'_i having the same size.

The RBIAS is computed as follows:

$$RBIAS = \frac{\bar{X}_i - \bar{Y}_i}{\bar{Y}_i} \times 100\% \quad (9)$$

where X_i is the simulated precipitation and Y_i is the observed precipitation; \bar{X} and \bar{Y} are the long-term means of precipitation, respectively.

3 Results

3.1 Precipitation variations in GPCP

3.1.1 Annual and seasonal mean climatology

Figure 2 presents the spatial pattern of annual and seasonal precipitation from observation (GPCP) over the period 1970–2014. Figure 2A presents the spatial variations of annual precipitation from GPCP observations over the study area. The annual precipitation results showed a distribution in the range of <100 to >600 mm (Figure 2A). The study observed highest precipitation amount of 450 mm yr^{-1} (range 300–600 mm yr^{-1}) occurred the southern region of Mon province and western portions of Rakhine province. In addition, the study observed that the lowest precipitation amount ranges from <50 mm yr^{-1} in the Mandalay province (in the central region) to 100 mm yr^{-1} in the Shan province located in the eastern part of the country. We observed distinct spatial patterns in the north (i.e., Kachin and Sagaing province) and southmost (Yangon and Ayeyarwady) part of the study area with values of 150–200 mm year^{-1} .

Figure 2B shows the seasonal (MJJASO) variations in GPCP precipitation observations. The Rakhine (i.e., western region), Yangon Ayeyarwady, Mon, Kayin and Tanintharyi (southmost region), and Kachin (northern region) presented a distinct spatial variation with mean seasonal values ranges from 400 to 600 mm. We observed a distinct decreasing amount from <200 mm in Shan province (eastern region), Naybityaw, Magwa, Chin to <100 mm in south of Sagaing and Mandalay region.

3.1.2 Trends in annual and seasonal precipitation

Figure 3 presents the trends of the annual and seasonal precipitation over Myanmar during 1970–2014 based on the

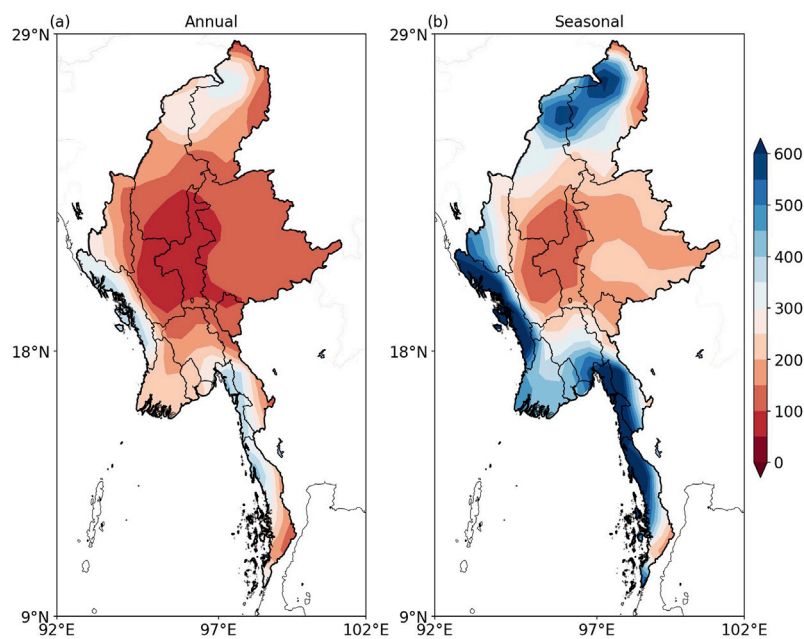


FIGURE 2
Spatial distribution of GPCP precipitation observations for (A) annual (B) seasonal during 1970–2014 (mm).

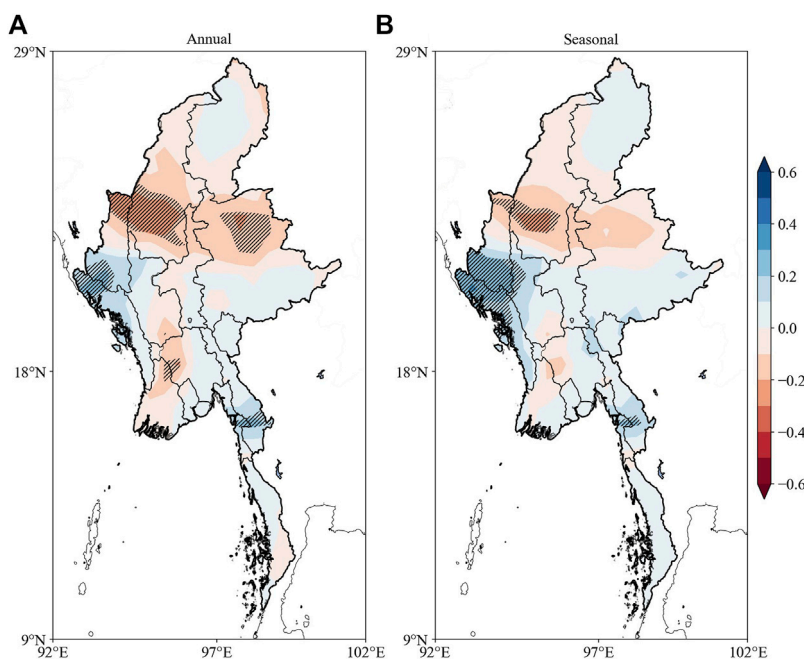


FIGURE 3
MK trend test of GPCP PRE observation for (A) annual and (B) seasonal precipitation. Hatches indicate significance at the 90% confidence level.

MK test at the 90% confidence level for the observation (GPCP). The central and eastern parts of the country underwent weakly positive change, whereas the rest of the country shows a negative

variation (Figure 3A). The GPCP results show a significant decrease in precipitation over the northwest and east but a significant increase over the Gulf of Martaban. Figure 3B

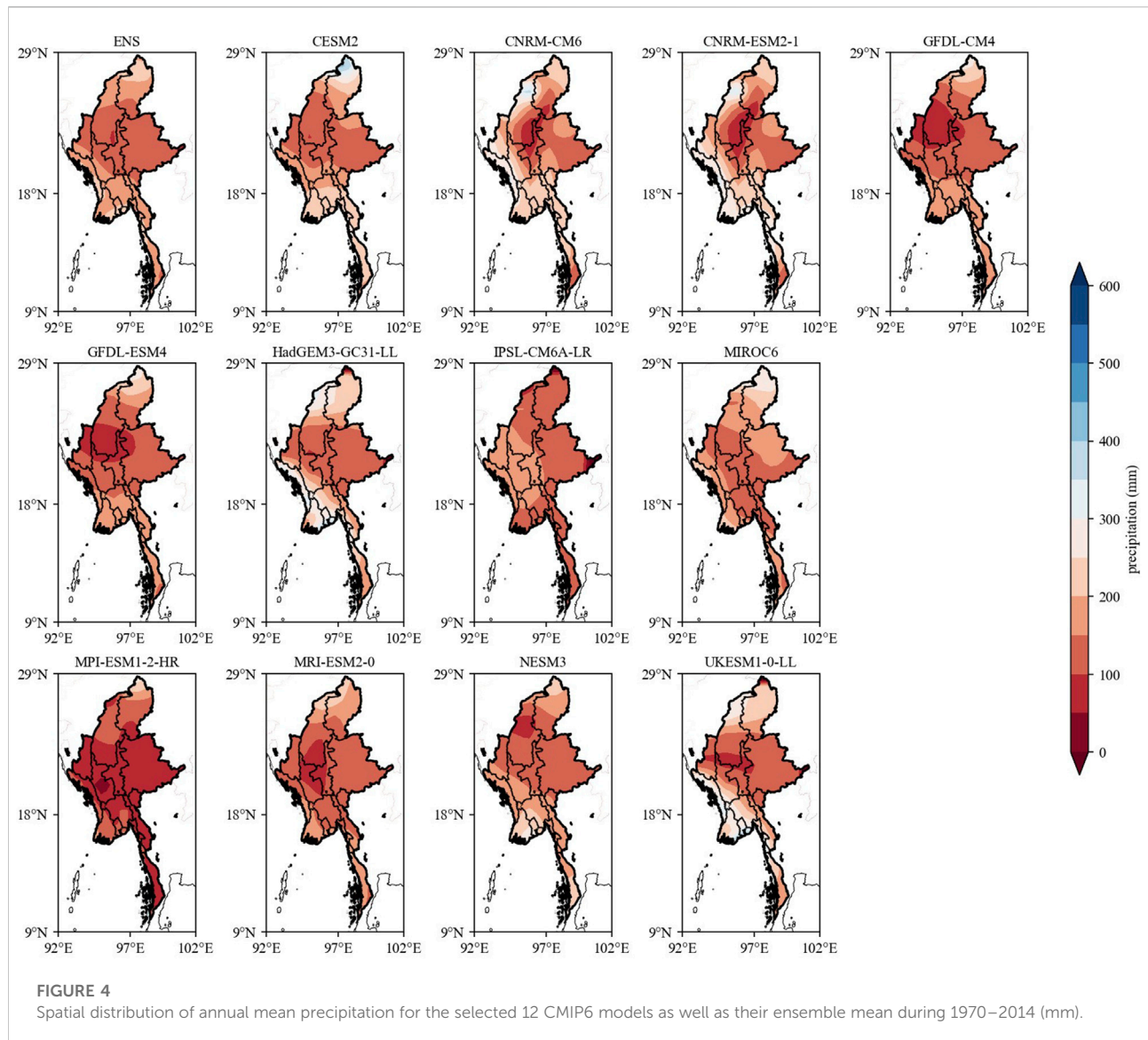
show the MK test is also applied to investigate the linear trends in the seasonal (MJJASO) variation of precipitation. Overall, the GPCP results show a positive (negative) trend in the west and Gulf of Martaban (northwest).

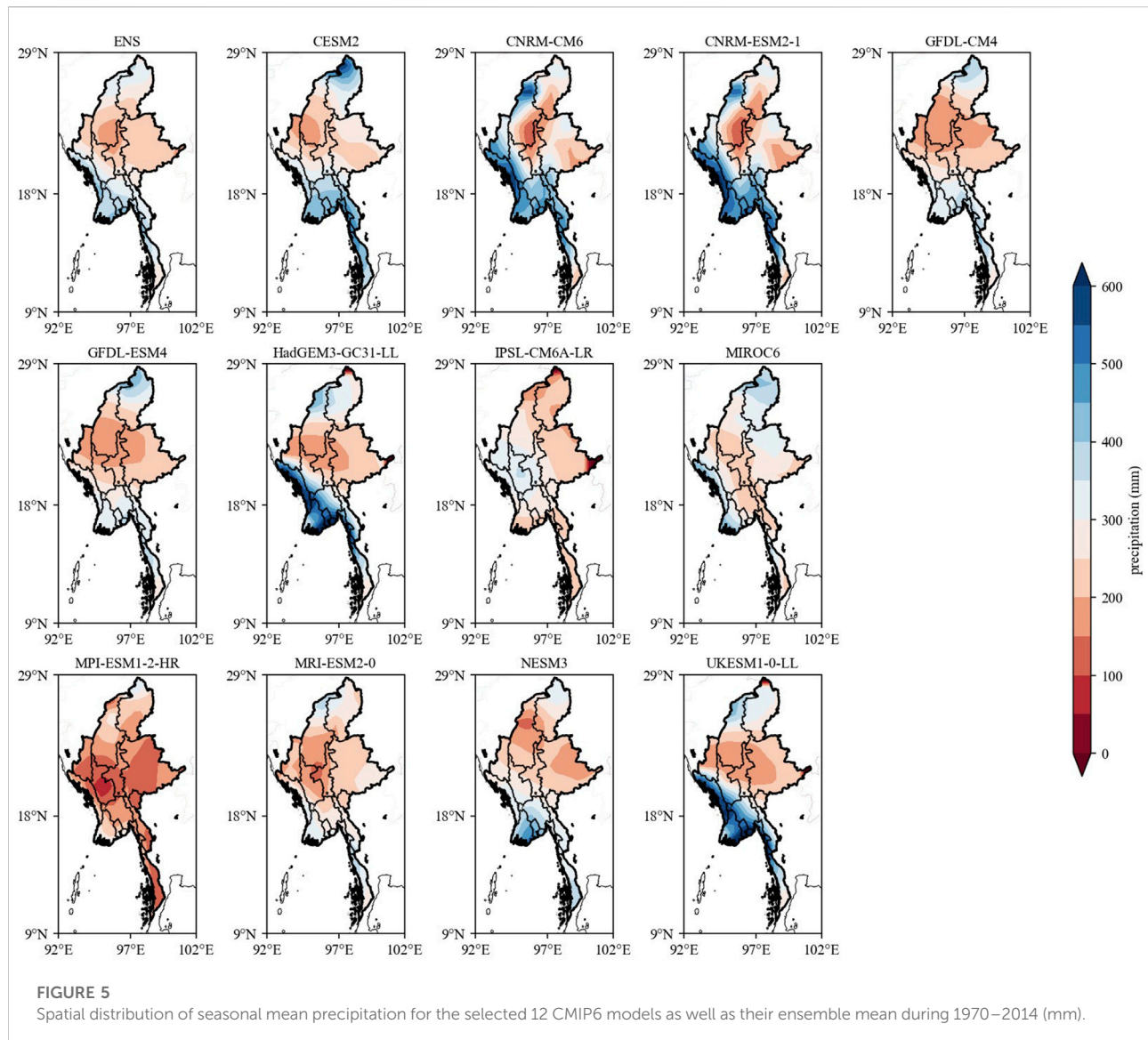
3.2 Precipitation variations in CMIP6 models

Figure 4 presents the annual and seasonal cycle of precipitation for the 12 CMIP6 models and the ENS over the region during the period 1970–2014. The ENS exhibits relatively lower precipitation in the western and southern coastal regions but relatively higher precipitation in central and northern regions. The ENS shows higher precipitation over the central region (i.e., Mandalay, lower Sagaing, and Magway) and lower

precipitation along the coast (i.e., Rakhine and Mon, Kayin and Tanintharyi). The results of CESM2, CNRM-CM6, MRI-ESM2-0, and IPSL-CM6A-LR relative to the ENS produces highest precipitation values. The study observed that many of the CMIP6 models are similar—namely, CNRM-ESM2-1, CNRM-CM6, HadGEM3-GC31-LL, MIROC6, CESM2, MRI-ESM2-0, and UKESM1-0-LL—but all except MRI-ESM2-0 also show high precipitation in north and northeast regions. Moreover, similar spatial patterns are observed in GFDL-CM4 and GFDL-ESM4 but with low precipitation occurring in the northwest. MPI-ESM1-2-HR yields low precipitation over the entire region except in the north and deltaic regions.

Figure 5 presents the seasonal cycle of precipitation for 12 CMIP6 models and the ENS during the period 1970–2014. The ENS reveals low precipitation in the central region but high precipitation along the western and southern coastlines and over





the Gulf of Martaban. The results of some of the CMIP6 models, such as CNRM-ESM2-1, CNRM-CM6, HadGEM3-GC31-LL and UKESM1-0-LL, presents low precipitation in the central region and high precipitation along the west and south coasts and in the northwest. Meanwhile, GFDL-CM4 and GFDL-ESM4 show low precipitation in the central and northwestern regions but high precipitation in the south and at the northern tip. IPSL-CM6A-LR produces high precipitation in central and western regions but low precipitation in the northwest. MIROC6 shows low precipitation in central and northwestern regions but high precipitation in the west, deltaic and northern tip areas. CESM2 presents low (high) precipitation in the central and northwest (north and south) regions. MPI-ESM1-2-HR produces low precipitation in central, eastern and southern areas but high precipitation in the deltaic and northern

regions. MRI-ESM2-0 produces low precipitation in the center of the country but high precipitation along the western and southern coasts and in the Andaman Sea. NESM3 shows low (high) precipitation in the east and northwest (deltaic region).

3.2.1 Trends in annual and seasonal CMIP6 precipitation

CNRM-ESM2-1 shows a significant positive precipitation trend over the northwest but a significant negative trend at the northern tip and in the south. GFDL-CM4 presents a significant negative trend in the north, northwest and south. CNRM-CM6 shows a significant negative trend in the center of the country, in the east, in the deltaic region, and in the south. Moreover, GFDL-ESM4 and IPSL-CM6A-LR show a significant negative trend in the south. HadGEM3-GC31-LL produces a significant positive

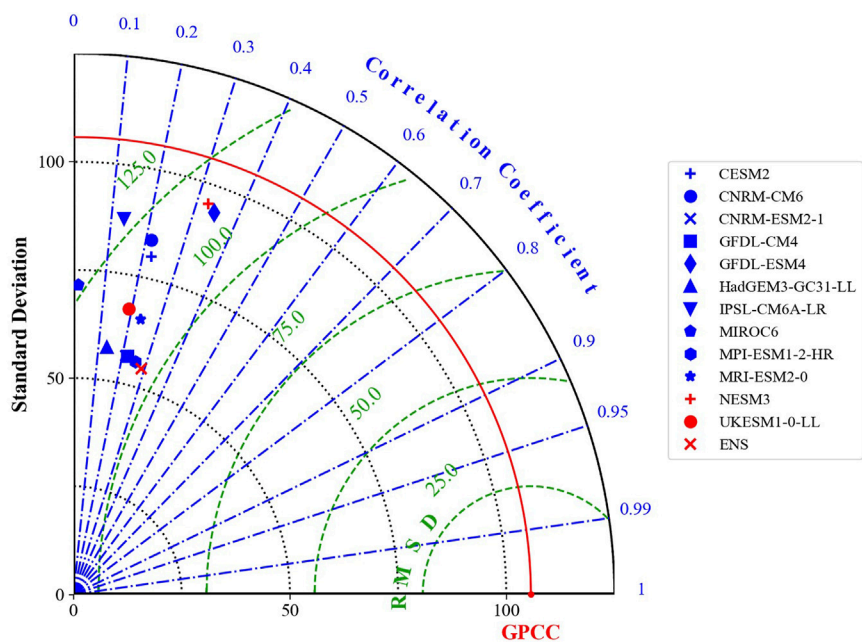


FIGURE 6
Taylor diagram comparing annual (January-December) PRE observation (GPCC) with models (CMIP6).

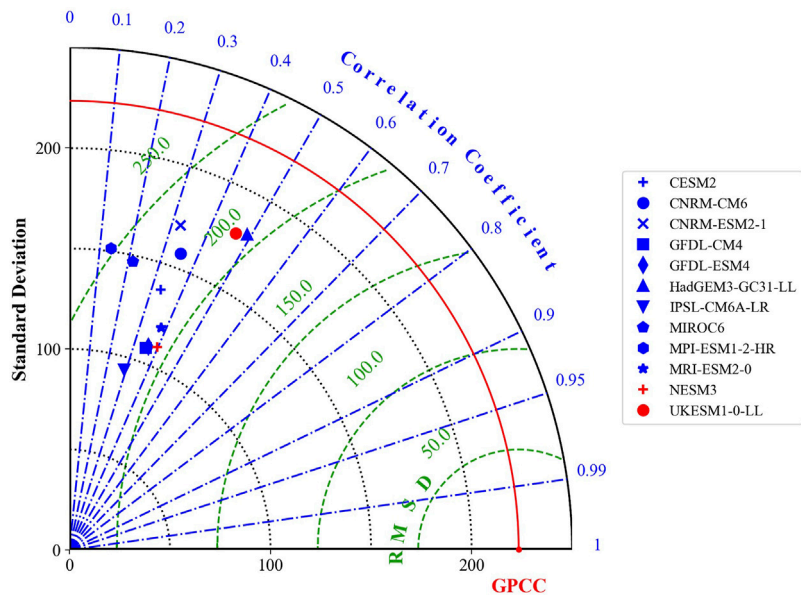


FIGURE 7
Taylor diagram comparing seasonal (MJJASO) PRE observation (GPCC) with models (CMIP6).

TABLE 2 Root mean square error (RMSE, mm) and relative bias (RBIAS, %) for seasonal (May–October, MJJASO) and annual precipitation in Myanmar during 1970–2014.

Model	Seasonal (MJJASO)		Annual	
	RMSE (mm)	RBIAS (%)	RMSE (mm)	RBIAS (%)
CESM2	63.51	−5.09	48.48	−4.32
CNRM-CM6	54.52	−18.06	41.23	−16.24
CNRM-ESM2-1	45.73	−14.36	34.62	−13.36
GFDL-CM4	67.75	−20.62	51.11	−21.98
GFDL-ESM4	72.58	−20.47	54.73	−22.15
HadGEM3-GC31-LL	69.59	−17.57	51.48	−11.87
IPSL-CM6A-LR	137.00	−43.94	98.20	−41.86
MIROC6	36.24	−3.27	26.96	−2.46
MPI-ESM1-2-HR	79.48	−26.74	59.08	−27.94
MRI-ESM2-0	93.01	−29.34	67.59	−28.80
NESM3	57.90	−17.78	41.27	−14.13
UKESM1-0-LL	74.79	−17.97	55.39	−12.92
ENS	63.13	−19.60	46.50	−18.17

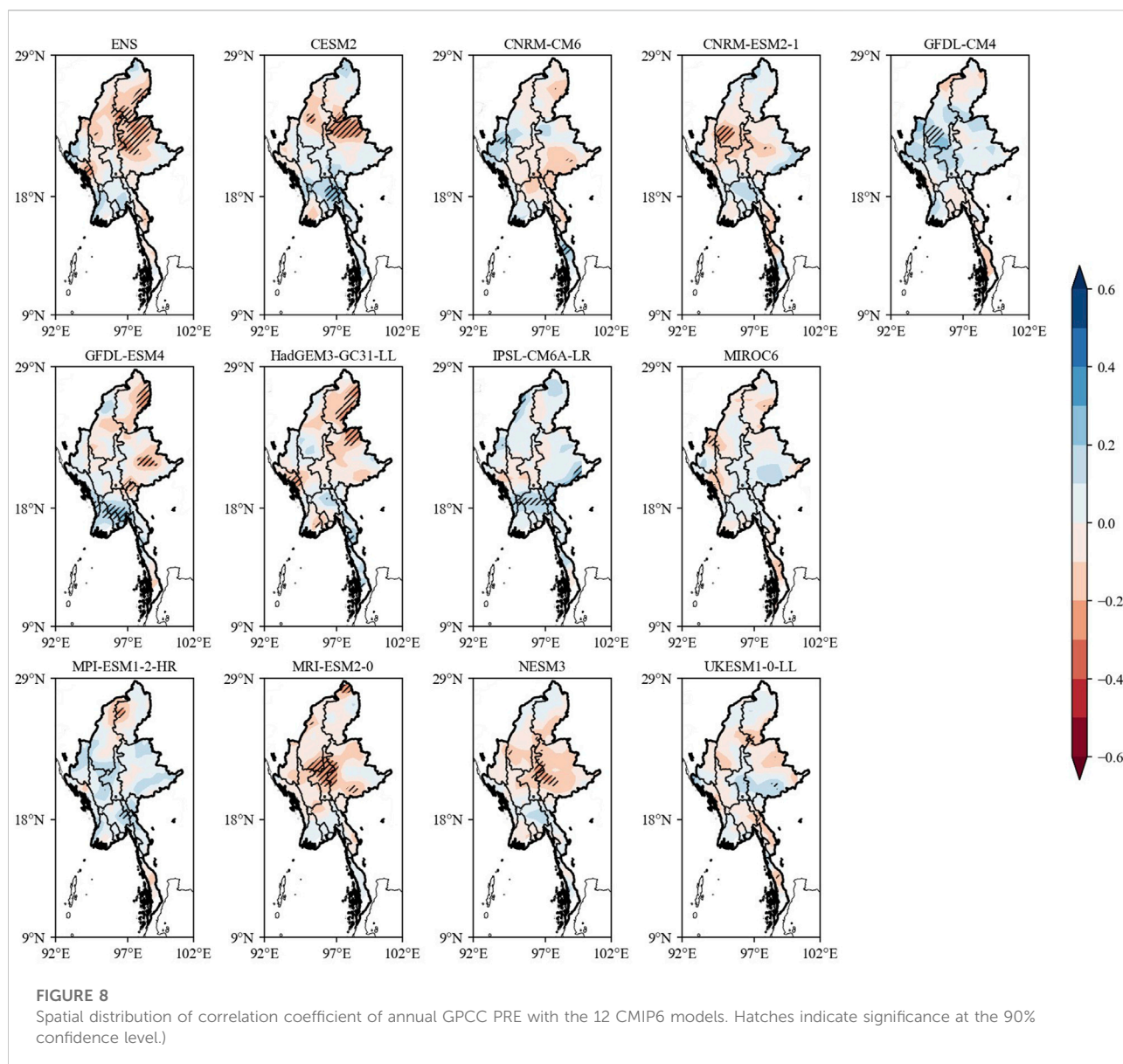
trend in the Bay of Bengal and Gulf of Martaban but a negative trend in the northeast. MIROC6 shows a significant negative trend in the south and in the deltaic region but a significant positive trend in the north. CESM2 produces a significant negative trend in the deltaic region but a significant positive trend in the central part of the country. MPI-ESM1-2-HR presents a significant negative trend in central, eastern, northwestern and southern Myanmar, but a significant positive trend over the Andaman Sea. MRI-ESM2-0 shows a significant negative trend over sea areas (i.e., the Andaman Sea and the eastern and central Bay of Bengal). NESM3 produces a significant positive trend over the northwest and south. UKESM1-0-LL shows a significant positive trend over the west but a negative trend in the north, east and south. And finally, ENS shows a significant positive trend in the northwest but a negative trend in the deltaic, eastern and southern regions.

Similarly, the MK test was also applied to investigate the linear trends in the seasonal (MJJASO) variation of precipitation, based on both the observational data (from GPCC) and the 12 CMIP6 models and their ENS at the 90% confidence level. The results help us to further understand how the different GCMs and observational data capture the precipitation seasonality over this period in Myanmar. The GPCC results show a positive (negative) trend in the west and Gulf of Martaban (northwest). CNRM-ESM2-1 produces a significant positive (negative) trend in the north (south). However, negative trend values can be observed at the northern tip of the country. GFDL-CM4 presents a negative trend in the north and south. CNRM-CM6 (GFDL-ESM4) shows a negative trend over part of the country, mainly in the central, eastern, deltaic and southern regions (west, northwest and south). HadGEM3-GC31-LL shows a negative (positive)

trend in the north (east and deltaic area). IPSL-CM6A-LR generates a significant negative trend in southern areas. MIROC6 shows a significant negative trend in the deltaic region and in the south but a significant positive trend in the north. CESM2 yields a significant negative (positive) trend in the west and deltaic (central and northern) regions. MPI-ESM1-2-HR presents a significant negative trend in the eastern, northeastern, central and southern regions, as does MRI-ESM2-0 but only in the eastern region. NESM3 produces a significant positive trend in the north and northwest, and UKESM1-0-LL presents a significant positive (negative) trend in the west (north, east and southern tip) regions.

3.3 Evaluation of CMIP6 performance against observations

Figure 6 is a Taylor diagram of the annual precipitation over the region simulated by the 12 CMIP6 models relative to the GPCC observations. The simulated pattern of each model is marked with symbols (red and blue). GPCC lies on the positive x-axis, which indicates the reference precipitation data. ENS presents a better correlation coefficient than the other models, with a CC (root-mean-square difference, RMSD) of 0.29 (104 mm). MRI-ESM2-0's correlation (RMSD) is found to be 0.24 (110 mm), and HadGEM3-GC31-LL's is 0.13 (113 mm). MPI-ESM1-2-HR shows a CC of 0.26 and RMSD of 106 mm, while CESM2 produces values of 0.23 with 117 mm, respectively. UKESM1-0-LL, CNRM-ESM2-1, GFDL-CM4 and GFDL-ESM4 show CCs of 0.19 (113 mm), 0.21 (108 mm), 0.22 (108 mm), and 0.35 (114 mm). In addition, MIROC6, CNRM-CM6 and

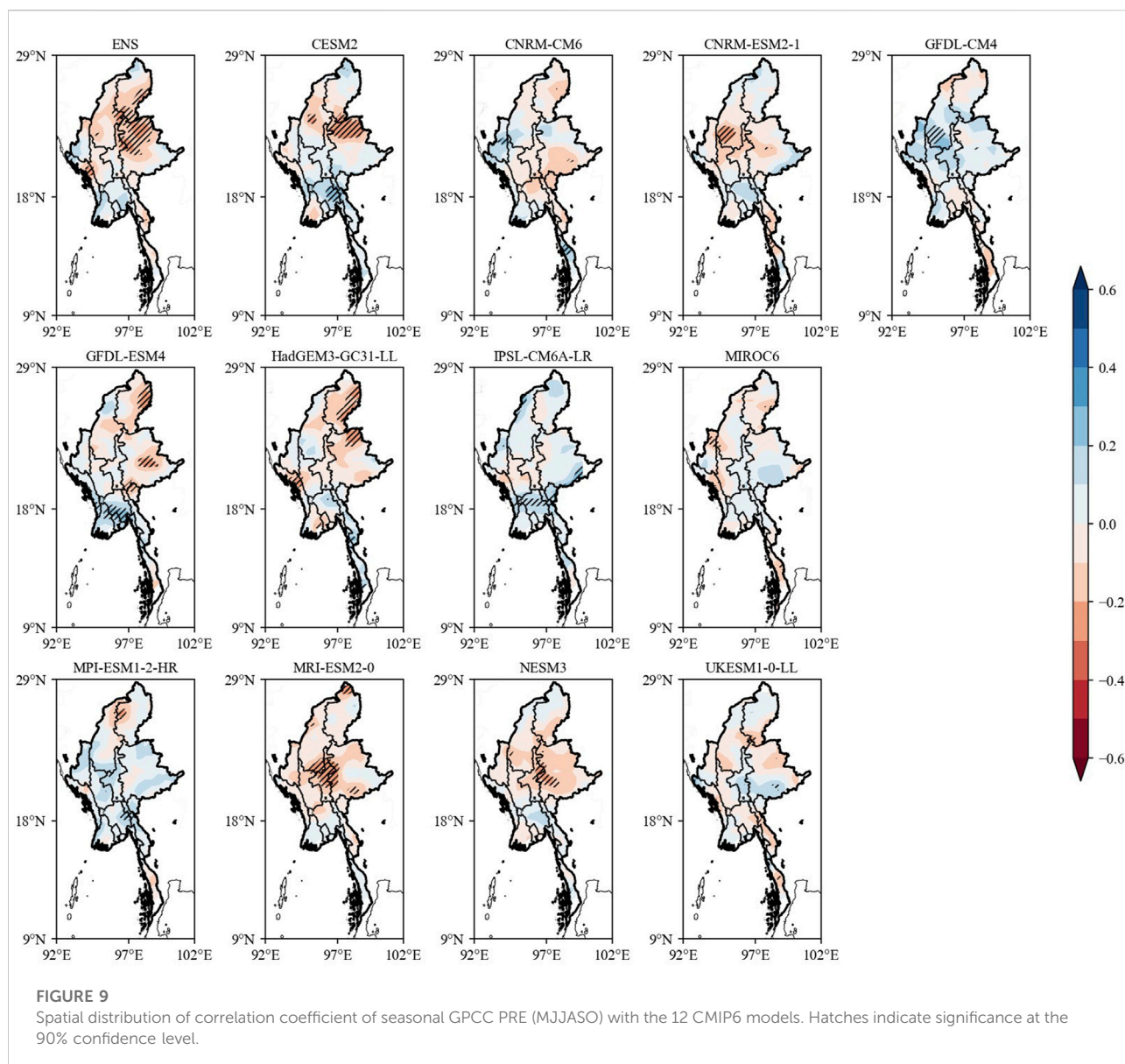


NESM3 present a CC (RMSD) of 0.02 (126 mm), 0.21 (120 mm), and 0.33 (117 mm), respectively.

To evaluate the models' performances in terms of the mean annual cycle (January–December) of precipitation in Myanmar, as well as that of ENS, we employed some metrics parameters. From the whole models, the RMSEs range from 26.96 to 98.2 mm. The results of the individual models' RMSE (PCC) are as follows: MIROC6, 26.96 mm (0.93); CNRM-ESM2-1, 34.62 mm (0.97); CNRM-CM6, 41.23 mm (0.98); NESM3, 41.27 mm (0.97); CESM2, 48.48 mm (0.84); GFDL-CM4, 51.11 mm (0.95); HadGEM3-CC31-LL, 51.48 mm (0.85); GFDL-ESM4, 54.73 mm (0.89); UKESM1-0-LL, 55.39 mm

(0.80); MPI-ESM1-2-HR, 59.08 mm (0.97); MRI-ESM2-0, 67.59 mm (0.92); IPSL-CM6A-LR, 98.2 mm (0.92). Meanwhile, ENS produces an RMSE of 46.50 mm.

Figure 7 presents the seasonal (MJJASO) precipitation over Myanmar simulated by the CMIP6 models relative to GPCC observations. The ENS shows low RMSD (201 mm) and CC (0.43), indicating the ENS correlation is among the best models that are strongly interconnected with GPCC precipitation. In general, most of the models simulated with good correlation coefficients. For instance, the correlation coefficient along with root mean square deviation is 0.33 (220 mm), 0.35 (223 mm), 0.32 (233 mm), 0.35 (210 mm), 0.36 (210 mm), 0.49 (207 mm), 0.38 (209 mm), 0.40 (206 mm) and 0.47 (211 mm) for CESM2,



CNRM-CM6, CNRM-ESM2-1, GFDL-CM4, GFDL-ESM4, HadGEM3-GC3, MRI-ESM2-O-L, NESM3, and UKESM-O-LL, respectively. Meanwhile, three models such as IPSL-CM6, MIROC6 and MPI-ESM1 presented low correlations along with relatively high deviations from the reference with the values of 0.29 (215 mm), 0.22 (239 mm) and 0.14 (252 mm), respectively; in representing the seasonal precipitation over the region of study. Based on correlation coefficient, the preferred model is HadGEM3 while the ENS presents the lowest deviation from the mean of the reference. The model showing the lowest standard deviation is IPSL-CM followed by the ENS. The low standard deviation indicates the low variability in the model to simulate the observation GPCP precipitation.

Overall, MIROC6, CNRM-ESM2-1, CNRM-CM6, and NESM3 reveal lower RMSEs and higher PCCs. Table 2 lists the RMSE (mm) and RBIAS (%) values for annual rainfall during 1970–2014.

Further analysis of the spatial distribution of the CCs of GPCP precipitation and that of the 12 individual CMIP6 models at the annual scale is shown in Figure 8. The results indicate significant negative (positive) correlation for CESM2-G in the east (south) of the region, for GFDL-ESM4-G in the north and east (deltaic region); for HadGEM3-GC31-LL-G in the west (central and southern regions); and for MPI-ESM1-2-HR-G in the north (central, northwestern and eastern regions). Meanwhile, there is significant positive correlation for CNRM-

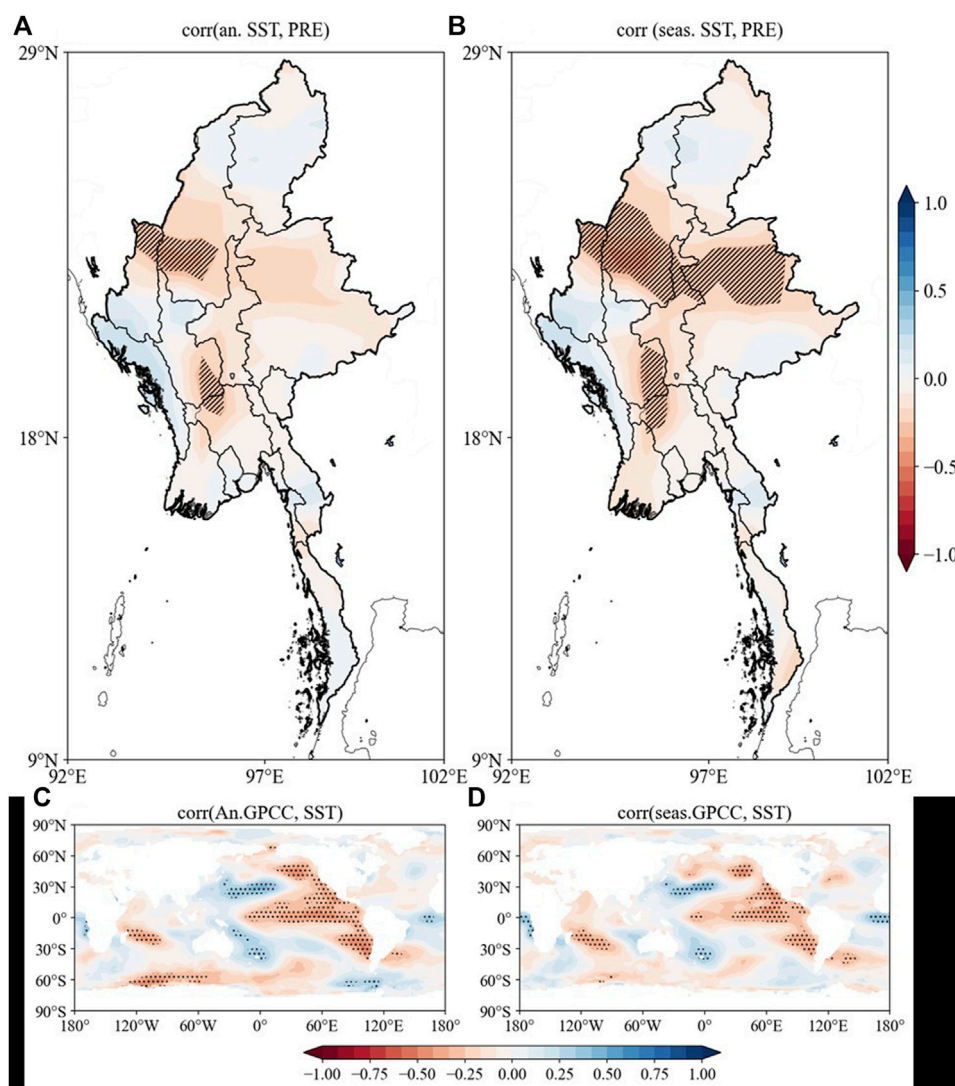


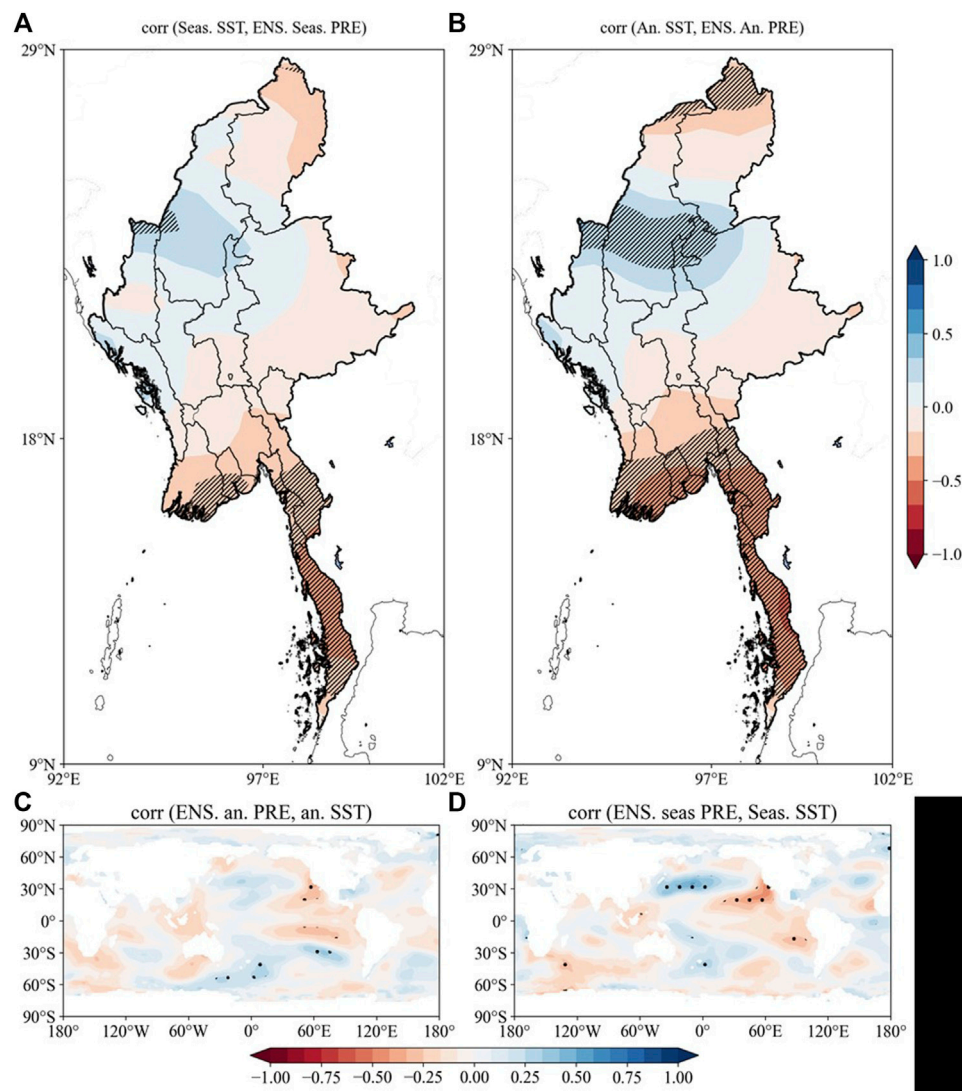
FIGURE 10

Spatial distributions of (A,C) correlation coefficients of GPCC PRE (i.e., annual and seasonal) and SST during 1970–2014). (A) GPCC-annual (B) Region GPCC-annual (C) GPCC -seasonal and (D) Region GPCC -seasonal. Hatched area indicates 95% confidence level.

CM6-G in the south; for GFDL-CM4-G in the central part of the region; for IPSL-CM6A-LR-G in the north, northwest and east; for MIROC6-G in the north and northwest; and for UKESM1-0-LL-G in the north. In addition, there is significant negative correlation for CNRM-ESM2-1-G and MRI-ESM2-0-G in central areas; for NESM3-G in the north and east; and for ENS in the eastern, central and western regions.

Figure 9 shows the spatial distribution of the CCs between the seasonal (MJJASO) observed (GPCC) precipitation and that of the 12 CMIP6 models. There are negative (positive) CCs for CESM2-G in the east (south); for GFDL-CM4-G in the south (central region); for GFDL-ESM4-G in the north

and east (deltaic region); and for MPI-ESM1-2-HR-G in the north (south). Meanwhile, there are positive CCs for CNRM-CM6-G in the south and northwest; for IPSL-CM6A-LR-G in the east and south; and for UKESM1-0-LL-G in the west and east. Moreover, there are negative CCs for CNRM-ESM2-LG in central and southern areas; for HadGEM3-GC31-LL-G in the north, east and west; for MIROC6-G in the northwest and south; for MRI-ESM2-0-G at the northern tip of the country and in central and eastern regions; for NESM3-G in the east; and for ENS in the northeastern, central and western areas. All the results are significant at the 90% confidence level.

**FIGURE 11**

Spatial distribution of the correlation coefficients between ENS PRE (annual and seasonal) and SST during 1970–2014. (A) ENS-annual (B) Region ENS-annual (C) ENS-seasonal and (D) Region ENS-seasonal. Hatched area indicates 95% confidence level.

3.4 Relationship between SST and precipitation

The correlation was computed to examine the underlying atmospheric circulation factors (i.e., SST) that influence precipitation variations over the monsoon corridor of Southeast Asia. Specifically, we computed the relationship using simple correlation analysis at the 95% significance level, and the results in terms of the relationship between precipitation (GPCC and ENS) and SST anomalies, globally and in the Myanmar region, are shown in Figure 10 (for GPCC) and Figure 10 (for ENS) at the annual and seasonal scales.

Figure 10A shows negative (low) correlation between annual observed (GPCC) precipitation and SST over the northeastern, central and southeastern Pacific Ocean but positive (high) correlation over the northwestern and southwestern Pacific Ocean. Moreover, the Indian Ocean shows negative (low) correlation east of Africa extending north and east of Madagascar. In Myanmar, there is negative (low) correlation in central, northwestern and eastern areas (Figure 10B). For seasonal (MJJASO) GPCC precipitation and SST, the annual spatial pattern of their correlation is similar, but with weaker negative correlation over the central Pacific Ocean than at the annual scale (Figure 10C). In addition, negative (low) correlation over central and northwest Myanmar is shown in Figure 10D.

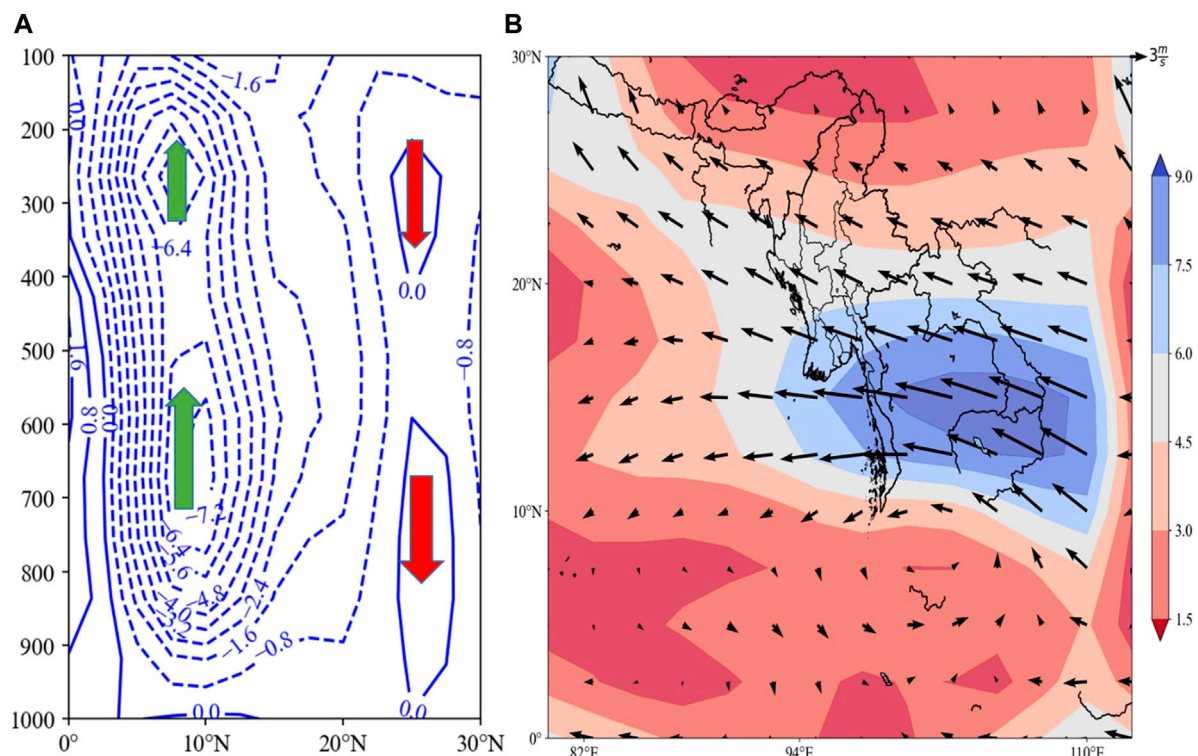


FIGURE 12

Mean of (A) pressure vertical velocity and (B) winds circulation for the period from 1970 to 2014. Arrows in green and pointing up indicates rising motion and arrows in red pointing down indicates descending motion while the shaded represents the wind speed.

Figure 11A shows negative correlation between annual simulated (ENS) precipitation and SST over the northeastern and southeastern Pacific Ocean but positive correlation over the northwestern, southwest and southeastern Pacific Ocean. However, the spatial distribution in the Indian Ocean does not show any significant correlation. In Myanmar, there is significant negative (positive) correlation in the south (northwest) of the region (Figure 11B). Seasonally (MJJASO), Figure 11C shows positive (negative) CCs in the northwest (northeast) Pacific Ocean, but weaker than at the annual scale. Regionally (i.e., in Myanmar), positive (negative) CCs are apparent in the northwest (south and at the northern tip) of the country (Figure 11D).

Overall, the GPCC and ENS results show negative (positive) correlation in the northeastern, central and southeastern (northwestern and southwestern) Pacific Ocean, with ENS showing a similar spatial pattern of CCs to GPCC, albeit with weaker negative (positive) correlation in the central (southern) Pacific Ocean in ENS. In addition, ENS does not perform well in the Indian Ocean. In Myanmar, at the annual scale, GPCC shows negative correlation over central, eastern and northwestern parts, while at the seasonal (MJJASO) scale it is in only in the central and northwestern areas (Figure 11). Meanwhile, ENS, both at

the annual and seasonal (MJJASO) scale, shows negative (positive) correlation in the south (northwest), but negative correlation over the northern tip of the region at the seasonal scale only (Figure 11).

Circulations of two atmospheric variables over Myanmar for the period of study are depicted by Figure 12. A low large center (negative pressure vertical velocity) is developed between 950 hPa and 100 hPa within about 5°N–10°N. Meanwhile, two high centers (positive pressure vertical velocity) are found at upper and lower atmosphere around 25°N as shown by the red arrows pointing down (Figure 12A). The negative center indicates a rising motion (i.e., green arrows pointing up), which favors the precipitation, whereas the positive center corresponds with descending motion that involves the dry period. The climatology of wind circulations over Myanmar is featured by southwesterly with a high center found in southern part of the country (Figure 12B).

4 Discussion

This study uses 12 state-of-the-art GCMs from CMIP6 to investigate the precipitation patterns across Myanmar at

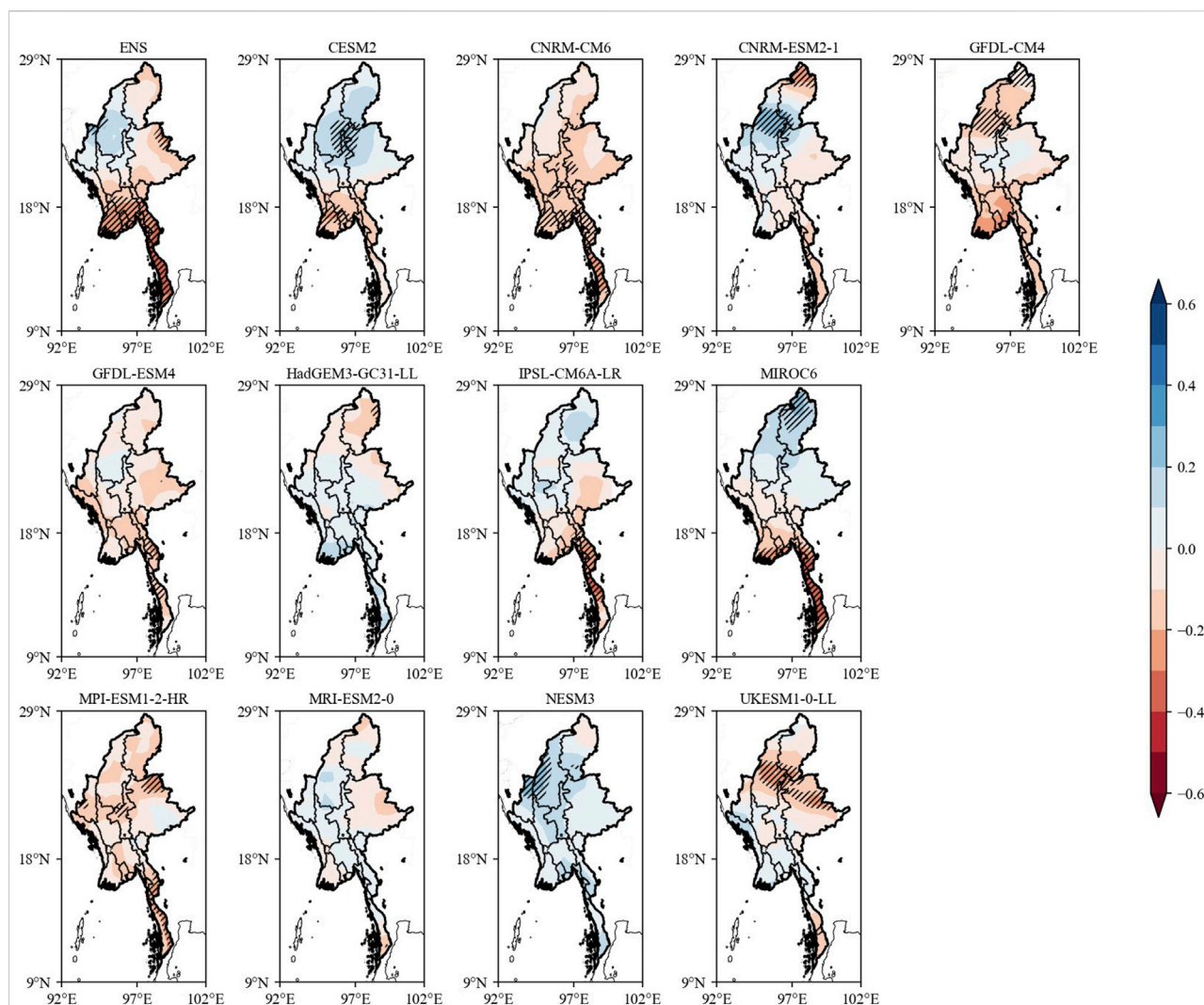


FIGURE 13

MK trend test of annual precipitation for the selected 12 CMIP6 models, and ENS. Hatches indicate significance at the 90% confidence level.

different spatial and temporal scales during the period 1970–2014, as well as the trends and potential drivers. The performances of the 12 individual models and their ENS in reproducing the historical precipitation is evaluated against GPCC observations. Overall, at the annual scale, IPSL-CM6A-LR, MRI-ESM2-0 and HadGEM3-GC31-LL present high correlation and relatively lower RMSDs (Figure 2). In contrast, CESM2, UKESM1-0-LL, CNRM-ESM2-1 and GFDL-CM4 show low to no correlation and relatively higher RMSE. Meanwhile, MIROC6, CNRM-CM6 and NESM3 perform poorly over the region, with negative correlation (Figure 2). The PCCs of the individual models and their ENS range from 0.8 to 0.97, and the RMSE from 26.96 to 98.2 mm (Figure 3). The seasonal (MJJASO) results of the CMIP6 models relative to GPCC observations were also investigated, revealing that IPSL-

CM6A-LR performs better than GFDL-CM4, MPI-ESM1-2-HR, NESM3, MRI-ESM2-0, CNRM-CM6, and HadGEM3-GC31-LL. Meanwhile, CESM2 shows no correlation, and GFDL-ESM4, CNRM-ESM2-1 and MIROC6 show negative and low correlation values (Figure 4). The seasonal precipitation analysis showed that IPSL-CM6A-LR produces a lower RMSE (9.0 mm) and CC (0.3) than the rest of the individual models (Figure 5).

The performances of the models in terms of the mean annual cycle of precipitation were also evaluated, using PCCs, with all models showing high PCC values of >0.80. ENS outperforms the individual models, except for MIROC6, CNRM-ESM2-1, and CNRM-CM6. Similar results were found in the seasonal analysis (Figures 4, 5). The RMSEs of the CMIP6 models and their ENS (Figures 4, 5) reflect the

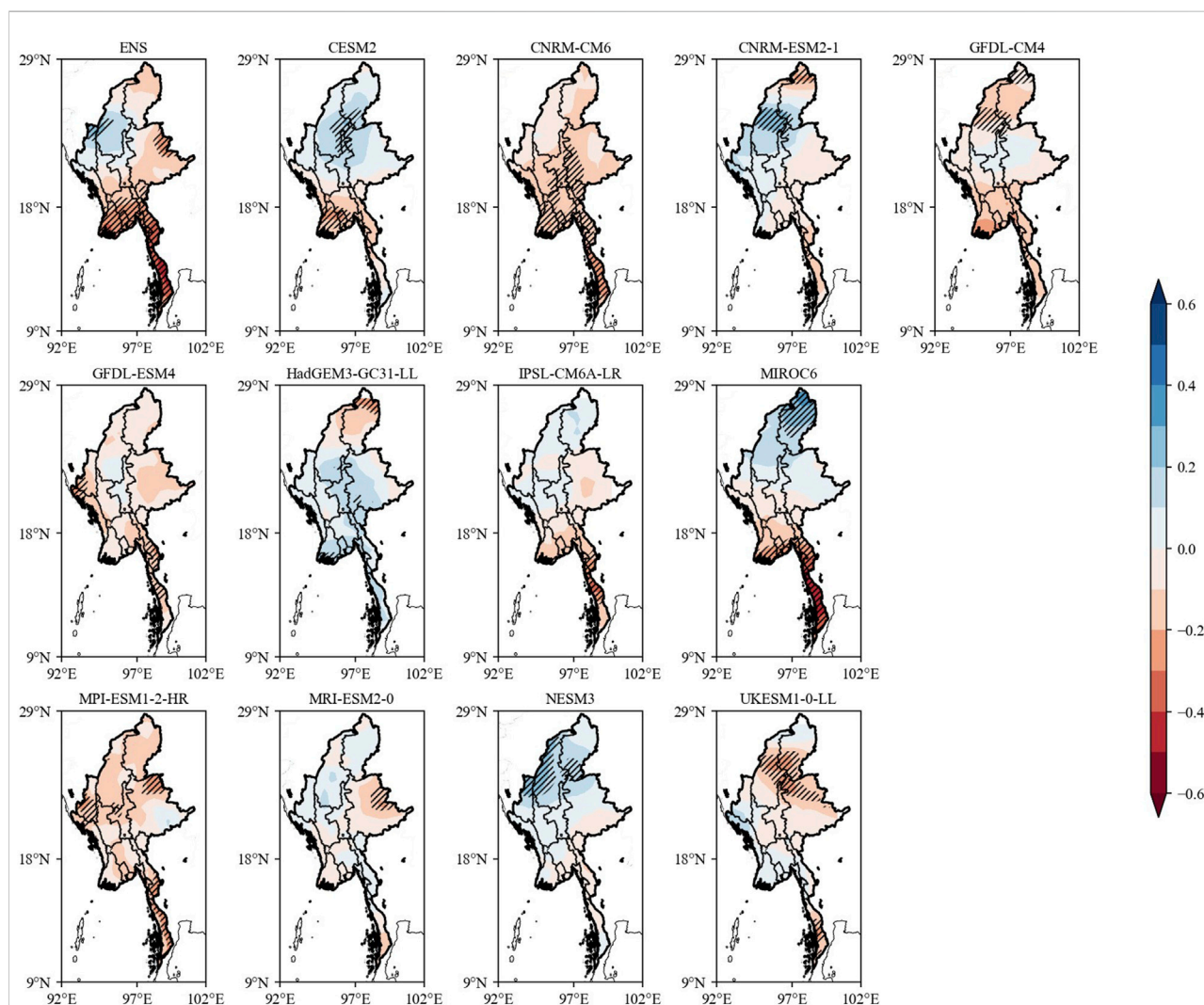


FIGURE 14

MK trend test of seasonal (MJJASO) precipitation for the selected 12 CMIP6 models and ENS. Hatches indicate significance at the 90% confidence level.

differences between them and the GPCC observations. The four (“best”) models with RMSEs lower than the ENS value of 46.50 mm/yr were chosen, and these four best models at the annual scale were MIROC6, CNRM-ESM2-1, CNRM-CM6, and NESM3. The remaining models—CESM2, GFDL-CM4, HadGEM3-CC31-LL, GFDL-ESM4, UKESM1-0-LL, MPI-ESM1-2-HR, MRI-ESM2-0, and IPSL-CM6A-LR—show slightly higher RMSE. Similarly, the same models were selected for seasonal values (Figure 5) based on the RMSEs of individual models being lower than the ENS value of 63.13 mm. The differences in the results of individual models might be related to the uncertainty in their simulations, which may stem from inherent model biases and other sources, as stipulated by (Taylor et al., 2012; Eyring et al., 2016).

The climatological results in Figure 13 show that the 12 CMIP6 models and their ENS present similar spatial and temporal patterns of annual precipitation over Myanmar to those of GPCC. The results show that the western and southern coastal regions receive the most precipitation, with central areas receiving the least (Sein et al., 2015; Sein et al., 2021a; Sein et al., 2022). In terms of the interannual and seasonal variations in Myanmar, GPCC and the individual models (except for MRI-ESM2-0) show similarity insofar as they both present high precipitation in the north and northeast regions. MPI-ESM1-2-HR reveals low precipitation in the entire region, except in the north and deltaic area. IPSL-CM6A-LR shows an opposite pattern to the precipitation gradient of GPCC, and ENS exhibits

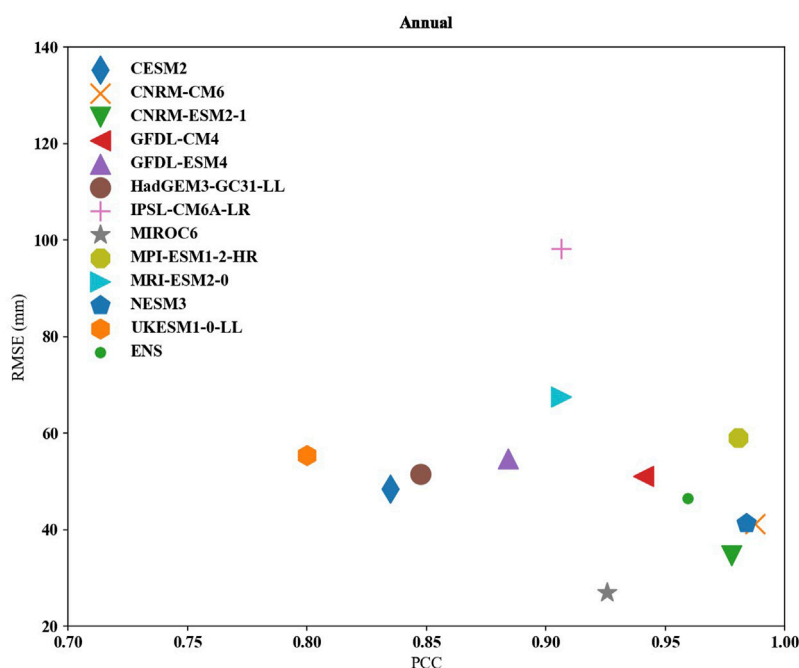


FIGURE 15

Performance of mean annual cycle PRE (mm) for CMIP6 models and their multimodal ensemble mean (ENS) on PRE climatology (1970-2014). The abscissa and ordinates are pattern correlation coefficient (PCC) and root mean square error (RMSE), respectively.

relatively low (high) precipitation in the central (coastal and northern) regions.

The annual mean precipitation climatology over Myanmar was also investigated (Figure 14), revealing a strong temporal variability over the region. The low precipitation in February and peak in July, captured by both GPCC and the GCMs, is consistent with the climatology of the region. The highest (lowest) precipitation is recorded by CESM2 (IPSL-CM6A-LR) (Figure 14). Meanwhile, CNRM-CM6, MRI-ESM2-0, IPSL-CM6A-LR, GPCC and ENS show a higher precipitation peak in July (Figure 14) than the rest of the models. The ENS results reproduce the region's climatology well, and better than the individual models. The performance of ENS over individual models in terms of precipitation simulation is consistent with a previous study (Xu and Xu 2012).

Using linear trend analysis to assess the 12 CMIP6 models, five models were selected for Myanmar to show the significant trend in precipitation in northern Myanmar, including the northeast and northwest (Figure 15)—namely, CNRM-ESM2-1, GFDL-CM4, CNRM-CM6, GFDL-ESM4, and IPSL-CM6A-LR. The west, center and east of Myanmar are shown in HadGEM3-GC31-LL, MIROC6, CESM2, MPI-ESM1-2-HR, MRI-ESM2-0, NESM3, and UKESM1-0-LL to have low but significant trends. These results suggest that these models capture the precipitation seasonality over the study period in

Myanmar consistently with previous studies in the Southeast Asian region (Kumar et al., 2013).

The relationship between precipitation and SST investigated the link between summer monsoon precipitation and global-scale SST. A simple correlation was performed for the ENS and global SST, and the annual ENS precipitation and SST were analyzed over the Pacific Ocean. Significant negative correlation was found across the northeast and southeast parts of the Pacific Ocean, while positive correlation was found across the northwest, southwest and southeast parts. Similarly, the seasonal (MJJASO) ENS precipitation and SST showed positive (negative) CCs in the northwest (northeast) Pacific Ocean, but weaker than at the annual scale in the southern Pacific. No significant correlation was recorded for the Indian Ocean. Generally, for ENS, the annual and seasonal correlation between SST and precipitation was found to be negative (positive) in the south (northwest), but ENS shows negative seasonal correlation in the northern tip of the region (Figure 11). The circulation results of the two atmospheric variables (Figure 12) shown low large center (negative pressure vertical velocity) is developed between 950 hpa and 100 hpa within about 5°N to 10°N. Two high centers (positive pressure vertical velocity) are found at upper and lower atmosphere around 25°N as shown by the red arrows pointing down (Figure 12A). The negative center indicates a rising motion (i.e., green arrows pointing up), which favors the precipitation, whereas the

positive center corresponds with descending motion that involve the dry period. The climatology of winds circulations over is featured by southwesterly with a high center found in southern part of the country (Figure 12B). In summary, the use of the latest GPCC observations and CMIP6 model data shows the ability of GCMs to reproduce well the patterns of seasonal precipitation in Myanmar, consistent with previous studies across the region, with high PCCs and lower RMSE.

5 Conclusion

In the present study, the individual and collective (i.e., ENS) performances of 12 GCMs from CMIP6 in capturing the precipitation pattern over Myanmar for the period 1970–2014 were analyzed. More specifically, the GCM precipitation was compared with that of observations from GPCC through displaying the climatology at annual and seasonal scales and the interannual variability. In addition, skill scores were used for statistical evaluation. Moreover, the relationship between the time series of GPCC and ENS was examined to uncover how the precipitation is controlled by the variability of SST over Myanmar through the tele-connectivity of atmospheric parameters. The main conclusions can be summarized as follows:

- 1) Among the 12 CMIP6 models, only MPI-ESM1-2-HR is able to roughly reproduce the GPCC precipitation pattern over Myanmar during 1970–2014 at both annual and seasonal scales. Meanwhile, at the interannual scale, most models underestimate the monthly precipitation, except CESM2, which overestimates that of GPCC from July to December. Furthermore, 3 out of the 12 models fail to capture the peak precipitation in July.
- 2) The RMSE of ENS produces an annual value of 46.50 mm and seasonal value of 63.13 mm. The RBIAS is −18.17 and −19.60 at the annual and seasonal scale over Myanmar, respectively.
- 3) MIROC6, CNRM-ESM2-1, CNRM-CM6, and NESM3 show lower RMSEs than the ENS value. The remaining models (CESM2, GFDL-CM4, HadGEM3-CC31-LL, GFDL-ESM4, UKESM1-0-LL, MPI-ESM1-2-HR, MRI-ESM2-0, and IPSL-CM6A-LR) show slightly higher RMSE.
- 4) Linear trend analysis shows that CNRM-CM6, GFDL-ESM4, GFDL-CM4, IPSL-CM6A-LR, and CNRM-ESM2-1 produce a significant positive trend in capturing the precipitation seasonality over the study period in Myanmar. HadGEM3-CC31-LL, MIROC6, CESM2, MPI-ESM1-2-HR, MRI-ESM2-0, NESM3, and UKESM1-0-LL show significant negative trends.
- 5) The ENS (annual and seasonal) correlation between precipitation and SST is negative (positive) in the south

(northwest), but the ENS seasonal correlation is negative over the northern tip of the region.

Based on these results, we recommend further studies consider simulating the precipitation changes over Myanmar to provide more information toward a better understanding and ability to project future precipitation changes in this region.

Data availability statement

The original contributions presented in the study are included in the article/Supplementary Material, further inquiries can be directed to the corresponding author.

Author contributions

ZS and XZ: conceptualization, methodology, investigation, writing-original draft, writing-review and editing, resources, supervision. FO, IN, and KP: conceptualization, data curation, writing-review and editing. ZS, XZ, FO, IN, and KP were all involved in the scientific interpretation and discussion. All authors provided commentary on the paper.

Funding

This work was jointly supported by the National Key Research and Development Program of China (2017YFC1502000) and the National Basic Research Program of China (2012CB955204).

Acknowledgments

We are grateful to the Collaborative Innovation Centre on the Forecast and Evaluation of Meteorological Disasters, Key Laboratory of Meteorological Disasters, Ministry of Education, Nanjing University of Information Science and Technology, Nanjing, China. Special appreciation goes to the World Climate Research Programme (WCRP) for the provision of the datasets used in the study.

Conflict of interest

The authors declare that the research was conducted in the absence of any commercial or financial relationships that could be construed as a potential conflict of interest.

Publisher's note

All claims expressed in this article are solely those of the authors and do not necessarily represent those of their affiliated

References

- Alexander, L. V. (2016). Global observed long-term changes in temperature and precipitation extremes: A review of progress and limitations in IPCC assessments and beyond. *Weather Clim. Extrem.* 11, 4–16. doi:10.1016/j.wace.2015.10.007
- Amato, R., Steptoe, H., Buonomo, E., and Jones, R. (2019). High-resolution history: Downscaling China's climate from the 20CRv2c reanalysis. *J. Appl. Meteorol. Climatol.* 58, 2141–2157. doi:10.1175/jamc-d-19-0083.1
- Ashok, K., Behera, S. K., Rao, S. A., Weng, H., and Yamagata, T. (2007). El niño modoki and its possible teleconnection. *J. Geophys. Res.* 112 (C11), C11007. doi:10.1029/2006jc003798
- Babar, Z. A., Zhi, X., and Fei, G. (2014). Precipitation assessment of Indian summer monsoon based on CMIP5 climate simulations. *Arab. J. Geosci.* 8, 4379–4392. doi:10.1007/s12517-014-1518-4
- Bayen, A. M., and Siauw, T. (2015). "An introduction to MATLAB® programming and numerical methods for engineers," in *An introduction to MATLAB® programming and numerical methods for engineers* (Boston: Academic Press).
- Department of Disaster Management (2020). Country report 2020. Available At: https://www.adrc.asia/countryreport/MMR/2020/MMR_CR2020.pdf.
- Dong, T.-Y., Dong, W.-J., Guo, Y., Chou, J.-M., Yang, S.-L., Tian, D., et al. (2018). Future temperature changes over the critical Belt and Road region based on CMIP5 models. *Adv. Clim. Change Res.* 9 (1), 57–65. doi:10.1016/j.accre.2018.01.003
- Eckstein, D., Künzel, V., and Schäfer, L. (2020). *Global climate risk index 2021. Who suffers most from extreme weather events?*. Bonn, Germany: Think Tank & Research.
- Eyring, V., Bony, S., Meehl, G. A., Senior, C. A., Stevens, B., Stouffer, R. J., et al. (2016). Overview of the coupled model Intercomparison project Phase 6 (CMIP6) experimental design and organization. *Geosci. Model. Dev.* 9 (5), 1937–1958. doi:10.5194/gmd-9-1937-2016
- Fremme, A., and Sodemann, H. (2019). The role of land and ocean evaporation on the variability of precipitation in the Yangtze River valley. *Hydrol. Earth Syst. Sci.* 23 (6), 2525–2540. doi:10.5194/hess-23-2525-2019
- Ge, F., Zhu, S., Luo, H., Zhi, X., and Wang, H. (2021). Future changes in precipitation extremes over southeast Asia: Insights from CMIP6 multi-model ensemble. *Environ. Res. Lett.* 16, 024013. doi:10.1088/1748-9326/abd7ad
- Ge, F., Zhu, S., Peng, T., Zhao, Y., Sielmann, F., Fraedrich, K., et al. (2019). Risks of precipitation extremes over southeast Asia: Does 1.5 °C or 2 °C global warming make a difference? *Environ. Res. Lett.* 14, 044015. doi:10.1088/1748-9326/aaff7e
- GPCC (2021). Global precipitation climatology Centre) datasets version 7. Available At: https://opendata.dwd.de/climate_environment/GPCC/html/fulldata_v7 doi download.html.
- He, W.-p., and Zhao, S.-s. (2018). Assessment of the quality of NCEP-2 and CFSR reanalysis daily temperature in China based on long-range correlation. *Clim. Dyn.* 50 (1), 493–505. doi:10.1007/s00382-017-3622-0
- Horton, R., De Mel, M., Peters, D., Lesk, C., Bartlett, R., Helsing, H., et al. (2017). *Assessing climate risk in Myanmar: Summary for policymakers and planners*. New York, NY, USA: Center for Climate Systems Research at Columbia University.
- Huang, B., Thorne, P. W., Banxon, V. F., Boyer, T., Chepurin, G., Lawrimore, J. H., et al. (2017). Extended reconstructed Sea surface temperature version 5 (ERSSTv5), upgrades, validations, and intercomparisons. *J. Clim.* 30, 8179–8205. doi:10.1175/JCLI-D-16-0836.1
- IPCC (2021). "Summary for policymakers," in *Climate change 2021, the physical science basis contribution of working group I to the sixth assessment report of the intergovernmental panel on climate change* (Cambridge, UK: Cambridge University Press).
- Iqbal, Z., Shahid, S., Ahmed, K., Ismail, T., and Nawaz, N. (2019). Spatial distribution of the trends in precipitation and precipitation extremes in the sub-Himalayan region of Pakistan. *Theor. Appl. Climatol.* 137 (3), 2755–2769. doi:10.1007/s00704-019-02773-4
- Iqbal, Z., Shahid, S., Ahmed, K., Ismail, T., Ziarh, G. F., Chung, E.-S., et al. (2021). Evaluation of CMIP6 GCM rainfall in mainland Southeast Asia. *Atmos. Res.* 254, 105525. doi:10.1016/j.atmosres.2021.105525
- Jiang, Z. H., Ding, Y. G., and Chen, W. L. (2007). Projection of precipitation extremes for the 21st Century over China. *Adv. Clim. Chang. Res.* 3, 202–207.
- Jiang, Z. H., Song, J., Li, L., Chen, W. L., Wang, Z. F., and Wang, J. (2012). Extreme climate events in China: IPCC-AR4 model evaluation and projection. *Clim. Change* 110, 385–401. doi:10.1007/s10584-011-0090-0
- Kitoh, A., Endo, H., Krishna Kumar, K., Cavalcanti, I. F. A., Goswami, P., and Zhou, T. (2013). Monsoons in a changing world: A regional perspective in a global context. *J. Geophys. Res. Atmos.* 118, 3053–3065. doi:10.1002/jgrd.50258
- Kumar, S., Merwade, V., Kinter, J. L., and Niyogi, D. (2013). Evaluation of temperature and precipitation trends and long-term persistence in CMIP5 twentieth century climate simulations. *J. Clim.* 26, 4168–4185. doi:10.1175/jcli-d-12-00259.1
- Mann, H. B. (1945). Nonparametric tests against trend. *Econometrica* 13, 245. doi:10.2307/1907187
- Meehl, G. A., Moss, R., Taylor, K. E., Eyring, V., Stouffer, R. J., Bony, S., et al. (2014). Climate model intercomparisons: Preparing for the next Phase. *Eos Trans. AGU.* 95 (9), 77–78. doi:10.1002/2014eo090001
- NECC (2012). *MECF Myanmar's national adaptation Programme of action (NAPA) to climate change*. Haverhill, MA, USA: NECC.
- O'Neill, B. C., Tebaldi, C., van Vuuren, D. P., Eyring, V., Friedlingstein, P., Hurtt, G., et al. (2016). The scenario model Intercomparison project (ScenarioMIP) for CMIP6. *Geosci. Model. Dev.* 9 (9), 3461–3482. doi:10.5194/gmd-9-3461-2016
- OCHA (2021). Myanmar humanitarian. Available At: <https://reliefweb.int/report/myanmar/myanmar-humanitarian-update-no-9-30-july-2021>.
- Oo, S. S., Hmwe, K. M., Aung, N. N., Su, A. A., Soe, K. K., Mon, T. L., et al. (2020). Diversity of insect pest and predator species in monsoon and summer rice fields of taungoo environs, Myanmar. *Adv. Entomol.* 03, 117–129. doi:10.4236/ae.2020.83009
- Ren, Y.-Y., Ren, G., Sun, X., Shrestha, A., Zhan, Y., Rajbhandari, R., et al. (2017). Observed changes in surface air temperature and precipitation in the Hindu Kush Himalayan region over the last 100-plus years. *Adv. Clim. Change Res.* 8, 148–156. doi:10.1016/j.accre.2017.08.001
- Schneider, U., Becker, A., Finger, P., Meyer-Christoffer, A., Rudolf, B., and Ziese, M. (2015). GPCC full data monthly product version 7.0 at 0.5°: Monthly land-surface precipitation from rain-gauges built on GTS-based and historic data. *Earth Syst. Sci. Data* 6, 49–60. doi:10.5194/essd-6-49-2014
- Sein, Z., Olgwang, B., Ongoma, V., Ogou, F., and Batebana, K. (2015). Inter-annual variability of summer monsoon rainfall over Myanmar in relation to IOD and ENSO. *J. Environ. Agric. Sci.* 2313–8629 4, 28–36.
- Sein, Z. M. M., Ullah, I., Saleem, F., Zhi, X., Syed, S., and Azam, K. (2021a). Interdecadal variability in Myanmar rainfall in the monsoon season (May–October) using eigen methods. *Water* 13, 729. doi:10.3390/w13050729
- Sein, Z. M. M., Zhi, X., Ullah, I., Azam, K., Ngoma, H., Saleem, F., et al. (2022). Recent variability of sub-seasonal monsoon precipitation and its potential drivers in Myanmar using *in-situ* observation during 1981–2020. *Int. J. Climatol.* 42 (6), 3341–3359. doi:10.1002/joc.7419
- Stouffer, R. J., Eyring, V., Meehl, G. A., Bony, S., Senior, C., Stevens, B., et al. (2017). CMIP5 scientific gaps and recommendations for CMIP6. *Bull. Am. Meteorological Soc.* 98 (1), 95–105. doi:10.1175/bams-d-15-00013.1
- Taylor, K. E., Stouffer, R. J., and Meehl, G. A. (2012). An overview of CMIP5 and the experiment design. *Bull. Am. Meteorol. Soc.* 93, 485–498. doi:10.1175/bams-d-11-00094.1
- Vinayachandran, P. N., Francis, P. A., and Rao, S. A. (2009). Indian ocean dipole: Processes and impacts. *Curr. Trends Sci.* 46 (10), 569–589.
- Wang, N., Zeng, X.-M., Guo, W.-D., Chen, C., You, W., Zheng, Y., et al. (2018). Quantitative diagnosis of moisture sources and transport pathways for summer precipitation over the mid-lower Yangtze River Basin. *J. Hydrology* 559, 252–265. doi:10.1016/j.jhydrol.2018.02.003
- WMO (2021). *State of the global climate 2020*. Geneva, Switzerland: WMO.
- Xu, C. H., and Xu, Y. (2012). The projection of temperature and precipitation over China under RCP scenarios using a CMIP5 multi-model ensemble. *Atmos. Ocean. Sci. Lett.* 5, 527–533. doi:10.1080/16742834.2012.11447042



OPEN ACCESS

EDITED BY

Junyu Qi,
University of Maryland, College Park,
United States

REVIEWED BY

T. P. Sabin,
Indian Institute of Tropical Meteorology
(IITM), India
Hewen Niu,
Northwest Institute of Eco-
Environment and Resources (CAS),
China

*CORRESPONDENCE

Xiuyang Jiang,
✉ xyjiang@fjnu.edu.cn

SPECIALTY SECTION

This article was submitted to
Atmosphere and Climate,
a section of the journal
Frontiers in Environmental Science

RECEIVED 05 October 2022

ACCEPTED 30 November 2022

PUBLISHED 12 December 2022

CITATION

Cai J, Yang Y, Yang Z, Qiu W and Jiang X
(2022), Isotope composition of daily
precipitation from 2019 to 2020 in
Sanming, southeastern China.
Front. Environ. Sci. 10:1061882.
doi: 10.3389/fenvs.2022.1061882

COPYRIGHT

© 2022 Cai, Yang, Yang, Qiu and Jiang.
This is an open-access article
distributed under the terms of the
Creative Commons Attribution License
(CC BY). The use, distribution or
reproduction in other forums is
permitted, provided the original
author(s) and the copyright owner(s) are
credited and that the original
publication in this journal is cited, in
accordance with accepted academic
practice. No use, distribution or
reproduction is permitted which does
not comply with these terms.

Isotope composition of daily precipitation from 2019 to 2020 in Sanming, southeastern China

Jianrong Cai^{1,2}, Yunyue Yang^{1,2}, Zhijie Yang^{1,2,3}, Wanyin Qiu^{1,2}
and Xiuyang Jiang^{1,2*}

¹Key Laboratory for Humid Subtropical Ecogeographical Processes of the Ministry of Education, Fujian Normal University, Fuzhou, China, ²School of Geographical Sciences, Fujian Normal University, Fuzhou, China, ³Sanming Forest Ecosystem and Global Change National Observation and Research Station, Sanming, China

Introduction: Many studies in southeastern China (SEC) have used stable isotope (δD and $\delta^{18}O$) records from natural archives (e.g., stalagmites, tree-ring cellulose, sediments) to reconstruct past East Asian Summer Monsoon (EASM) climate. However, the interpretation of the meanings of isotope variation in these records has not been fully resolved, and the key to solve this problem is to clarify the referential meaning of modern precipitation isotopes.

Methods: In this study, we collected daily precipitation from January 2019 to December 2020 in Sanming to clarify the characteristics of isotope variations and their controlling factors during different seasonal periods [e.g., non-summer monsoon (NSM) and summer monsoon (SM)] in SEC.

Results and Discussion: Our results show that the precipitation $\delta^{18}O$ ($\delta^{18}O_p$) and d -excess values in the SM season (-12.94‰ – 0.15‰ , -4.05‰ – 21.01‰) were more light than those in the NSM season (-6.91‰ – 4.37‰ , 0.85‰ – 30.38‰). Combining the findings of backward trajectory and averaged outgoing longwave radiation analyses, the seasonal variation of precipitation isotopes is believed to be determined by a shift in water vapor sources and the intensity of upstream atmospheric convection during water vapor transportation. The consistent variation between the isotope values and convective intensity over the South China Sea in the dragon boat rainy period highlights that $\delta^{18}O_p$ has the potential to respond rapidly to the upstream convective intensity and can serve as a substitute method for investigating the complicated East Asian summer monsoon system. Therefore, the results of this study imply that the stable isotopes in precipitation and related paleoclimate proxies may not reflect the signal of temperature or precipitation alone but rather reflect changes in moisture sources and upstream convective intensity.

KEYWORDS

precipitation, stable isotopes, seasonal variation, upstream convective intensity, southeastern China

1 Introduction

Stable isotope signals in modern precipitation are valuable for interpreting paleo-isotope records preserved in natural archives, such as stalagmites (Wang et al., 2001; Cheng et al., 2016; Zhang et al., 2021), tree-ring cellulose (Xu et al., 2016; Liu et al., 2017), and plant cellulose in peat bogs (Xu et al., 2002; Hong et al., 2009), which are essential for the reconstruction of past climate and hydrological cycles (Yao et al., 2013). In southeastern China (SEC), stalagmite oxygen isotope ($\delta^{18}\text{O}_c$) records from the E'mei and Shennong caves suggest that the regional $\delta^{18}\text{O}_c$ record is mainly regulated by precipitation seasonality (the mean percentage of summer monsoon precipitation to non-summer precipitation) (Zhang et al., 2018a; Zhang et al., 2018b). This is mainly controlled by the El Niño–Southern Oscillation (Zhang et al., 2020). Shi et al. (2020) suggest that tree-ring cellulose $\delta^{18}\text{O}$ records in the southeastern region can be referred to as monsoon precipitation. However, owing to the shortage of long-term observation records of modern precipitation isotopes in this region, these studies can only use monthly precipitation isotope observations from Changsha (Central China) or Hong Kong (Southern China) for comparison. Therefore, to determine stable isotope records derived from natural archives and to complement previous studies, it is necessary to study regional atmospheric precipitation isotopes and clarify the control factors.

Sanming lies in SEC and experiences first-hand the monsoon onset signal, being in the frontal region of the East Asian summer monsoon (EASM). The beginning of the EASM season is marked by the outbreak and evolution of the South China Sea summer monsoon (SCSSM), which also represents the beginning of the rainy season (Tao and Chen, 1987; Wang et al., 2004). Bounded by the onset of SCSSM, Sanming has two rainy seasons: spring persistent rain (SPR) and the dragon boat rainy (DBR) season (Liang and Wang, 1997). In spring, owing to the mechanical forcing and thermal effects of the plateau, there is a continuous precipitation period in this area (Wan et al., 2008a; Wan and Wu, 2008b). SPR amounts in this region can reach 348 mm, accounting for 21% of the total annual precipitation (Li, 2006). Zhang et al. (2020) proposed that SPR has an important effect on annual precipitation $\delta^{18}\text{O}$ ($\delta^{18}\text{O}_p$). However, due to the absence of long-term precipitation isotope observation records in SEC, the data are based on the monthly scale of the Changsha Global Network of Isotopes in Precipitation (GNIP) site data in central China with low resolution (Zhang et al., 2020). The use of such data to study the isotope characteristics and influencing factors during the SPR period in SEC is limited. Thus, improved knowledge of the daily $\delta^{18}\text{O}_p$ in this region is vital for a thorough interpretation of the $\delta^{18}\text{O}_c$ record of stalagmites from SEC. With the onset of the SCSSM, this

region enters a period of the SM rainy season called DBR, where rainfall can reach 527 mm, accounting for 31.8% of the total annual precipitation (Li, 2006). A better comprehension of the isotope composition of these periods of high precipitation ratios will help interpret the long-term records in this region. Therefore, standardized continuous multi-year monitoring on a daily scale is essential to gain a comprehensive understanding of the interannual and seasonal changes in precipitation stabilization isotopes in this region.

Here, we present a daily scale record of the precipitation isotope composition from 2019 to 2020 from Sanming, SEC. The purposes of this study were 1) to clarify the characteristics and seasonal changes of precipitation isotopes in Sanming, and 2) to identify the controlling factors in different periods (such as SM, NSM, SPR, and DBR) for the year. The isotope variation characteristics of precipitation, monitored here for 2 years, can aid in a better understanding of the importance of the oxygen isotope record in the paleoclimate reconstruction in SEC.

2 Material and methods

2.1 Geographical location

Sanming (25°30'–27°07'N, 116°22'–118°39'E) is located in the mid-west of Fujian Province in coastal SEC in the frontal area of the EASM region (Figure 1). The study area has a typically humid subtropical monsoon climate. According to historical meteorological data from 1980 to 2000, the mean annual air temperature and precipitation in Sanming are 19.5°C and 1,560 mm, respectively. As shown in Figure 1, the uneven precipitation in this area is mainly concentrated from March to June, accounting for more than 57% of the annual precipitation. Due to the absence of long-term precipitation observations in Sanming, monthly precipitation data from 1951 to 2012 at the nearest meteorological station at Yong'an, 27 km from Sanming, were used to study the regional representativeness of the annual variation characteristics of precipitation at the sampling sites. We analyzed the correlation between the monthly precipitation data in Yong'an and in other regions, which suggests that precipitation over Sanming is highly representative of the southeastern region in China (Figure 1).

2.2 Sampling and measurement

Precipitation samples were collected from a bare area in the Sanming Forest Ecosystem and Global Change Observation and Research Station (26°9'N, 117°28'E, altitude: 134 m a.s.l.), from January 2019 to December 2020. Each precipitation event was sampled for isotope analysis using a ZJC-V Intelligent rainfall sampler (Supplementary Figure S1) which senses rainfall and

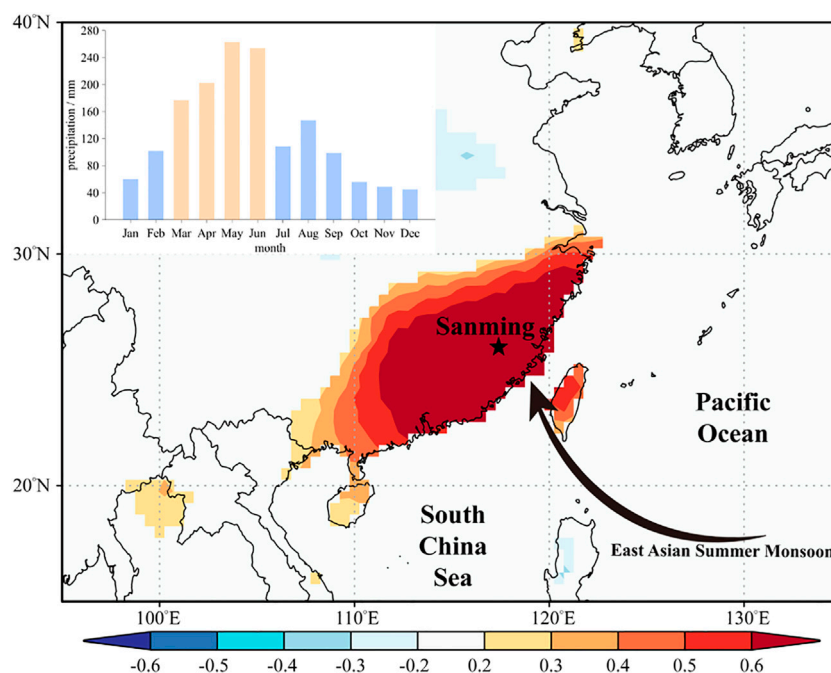


FIGURE 1

Study area and sampling stations in the SEC region. The upper left is the average monthly precipitation at Yong'an station from 1951 to 2012; the black star represents the sampling site in Sanming; background colors represent the whole year spatial correlations between the precipitation in Yong'an station and CRU TS4.05 precipitation (from 1951 to 2012, $p < 0.1$).

opens a lid for collection. Rainwater flows directly into a refrigerated bottle through a water pipe, effectively preventing the evaporation of samples. After collection, each sample was poured into 20 ml and 2 ml polypropylene colorless plastic bottles with no space. These bottles were sealed with Parafilm sealing film to prevent evaporation and chilled at 4°C to prevent isotope fractionation. A total of 209 samples were collected on rainy days from 2019 to 2020.

Stable isotope composition ($\delta^2\text{H}$ and $\delta^{18}\text{O}$) analyses were performed at the Stable Isotope Laboratory, School of Geographical Sciences, Fujian Normal University. The samples were analyzed using Picarro-L2140i cavity ring-down spectroscopy (CRDS). Three isotope standards and seven samples were examined as a group in this study. Seven samples were measured after the three standards, and each of the samples or standards was measured separately with seven injections. Taking into account the memory effect and stability of the instrument, only the final three injections were averaged and calibrated. The test findings were based on the samples' calibrated values. Measurement calibration utilized three internal standards ($\delta^{18}\text{O}$: 19.13‰, -8.61‰, and -0.15‰; $\delta^2\text{H}$: 144‰, -63.4‰, and -1.7‰). The results were presented as δ -values relative to the standard Vienna Standard Mean Ocean Water (V-SMOW). The measurement accuracies were typically better than $\pm 0.1\text{‰}$ for $\delta^{18}\text{O}$ and $\pm 0.5\text{‰}$ for $\delta^2\text{H}$.

2.3 $\delta^{18}\text{O}$ data from IsoGSM simulations

IsoGSM is a general circulation model based on water isotope (Yoshimura et al., 2008), which is used to fill in missing data (June to July 2020) and explore the control of atmospheric processes on $\delta^{18}\text{O}$ variability (Supplementary Table S1). IsoGSM has a time resolution of 6 h, and a horizontal resolution of 200 km, 28 vertical levels. Detailed descriptions of the model setup are available in previous studies (Yoshimura et al., 2008; Yoshimura et al., 2014; Yang et al., 2016). The monthly variations in precipitation and water vapor isotope compositions linked to synoptic weather cycles may be reasonably replicated by the IsoGSM. We first cross-compared the data from IsoGSM with observed data from Sanming station from 2019 to 2020 to confirm the reliability of the data from IsoGSM (Supplementary Figure S2). Result showed that the observed $\delta^{18}\text{O}_p$ data are consistent with the simulated $\delta^{18}\text{O}_p$ data from IsoGSM, which is a sign of good replication.

2.4 Hybrid single-particle lagrangian integrated trajectory (HYSPLIT) model

HYSPLIT was applied to locate and distinguish potential air mass source regions during the sampled rain episodes (Draxler

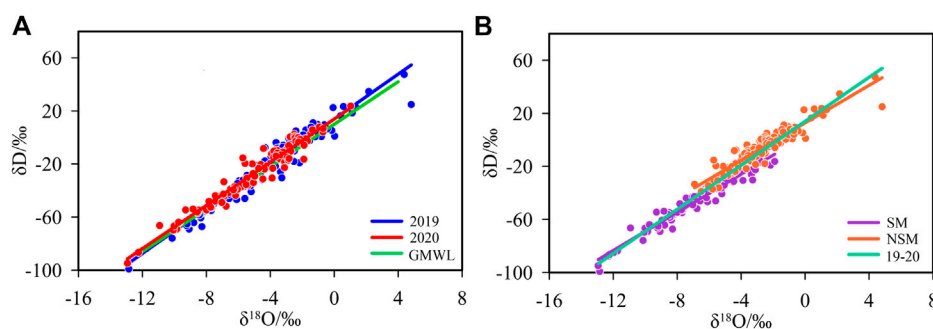


FIGURE 2

$\delta^2\text{H}$ and $\delta^{18}\text{O}_\text{p}$ relationships during the daily precipitation from 2019 to 2020, (A) in different years, (B) in different seasons.

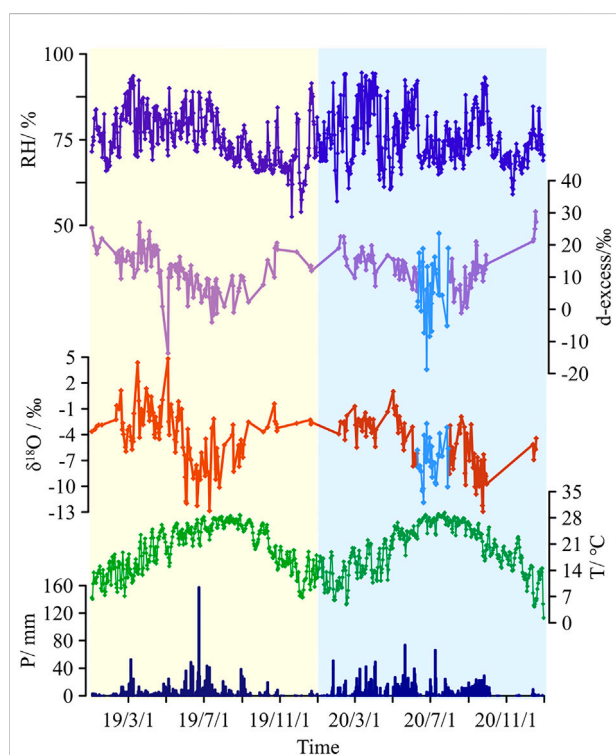


FIGURE 3

Seasonal variations of the precipitation amount, air temperature, relative humidity, $\delta^{18}\text{O}$, and d -excess from January 2019 to December 2020. The data for Jun–July 2020 are from IsoGSM simulations data.

and Hess, 1998). The model is obtained from the National Oceanic and Atmospheric Administration (NOAA) at the Air Resources Laboratory (<https://ready.arl.noaa.gov/HYSPLIT.php>). We set the end height for the backward trajectory model at 1500 m a.g.l. At the sampling site. The height is generally considered to be the largest water vapor transport volume and the precipitation is most likely to start (Aggarwal

et al., 2004; Breitenbach et al., 2010; Wei et al., 2018). In addition, we computed the trajectories for 120 h back in time to reconstruct the original transport trajectory because it is sufficient to identify the air mass backward trajectories at the regional scale (Tao et al., 2021).

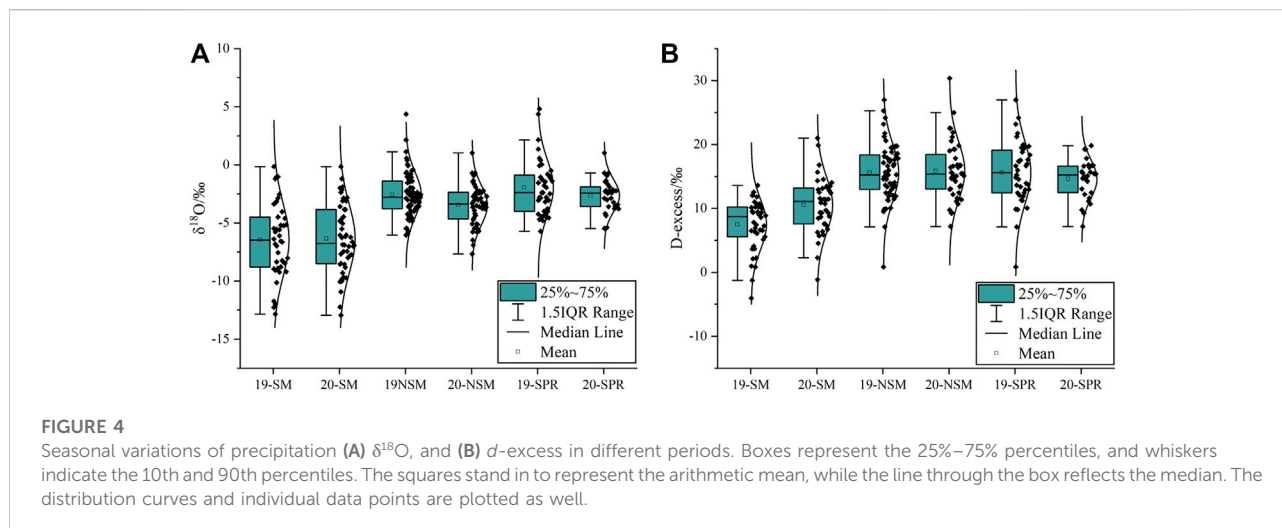
2.5 Meteorological and reanalysis data

The associated meteorological data (precipitation amount, air temperature, and relative humidity) were monitored using an automatic HOBO rain gauge and a wireless temperature and humidity data logger next to the rainfall sampler, from January 2019 to December 2020. The National Climate Center provided monthly instrumental data for the Yong'an meteorological station from 1951 to 2010 (<https://ncc-cma.net/cn/>). To calculate the water vapor flux and analyze the relationships between regional integrated convective activity and daily precipitation stable isotope composition during the observation period, we obtained 850 hPa zonal and meridional wind components, specific humidity, and outgoing longwave radiation (OLR) data from the NOAA Physical Sciences Laboratory (<https://psl.noaa.gov>). KNMI Climate Explorer (<https://www.knmi.nl>), a web-based tool for high-resolution paleoclimatology, was used to conduct a spatial correlation test for the regional representation of the Sanming area (Trouet and Oldenborgh, 2013).

3 Results

3.1 Local meteoric water line (LMWL)

Craig (1961) first reported the regression line $\delta^2\text{H} = 8 * \delta^{18}\text{O} + 10$ as the global meteoric water line (GMWL) based on the positive connection between $\delta^2\text{H}$ and $\delta^{18}\text{O}$ found in natural meteoric waters throughout the world. With the increased



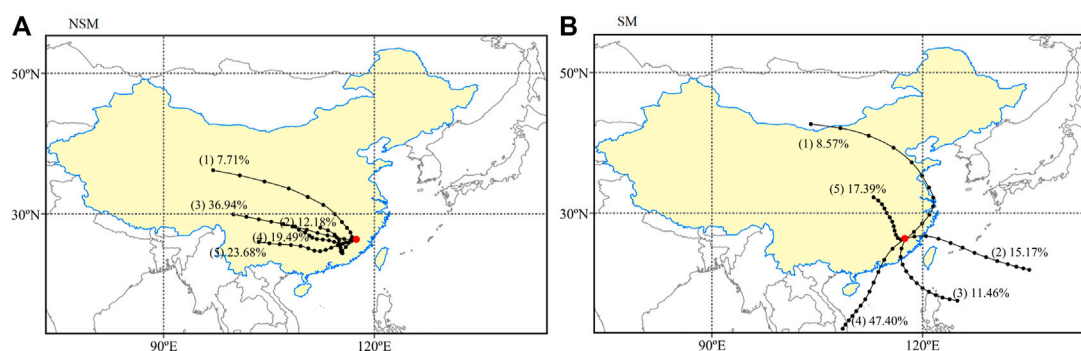
establishment of GNIP program stations, numerous LMWLs have been built (Merlivat and Jouzel, 1979; Araguás-Araguás et al., 1998; Zhang et al., 2016; Wu et al., 2022). Although there are considerable geographical differences in climatic characteristics and sources of water vapor, the slope of the LMWL and GMWL are still in agreement. The correlation between daily stable precipitation isotope data at the Sanming station is defined here as the LMWL: $\delta^2\text{H} = 8.29 * \delta^{18}\text{O} + 13.93$ ($R^2 = 0.95$, $p < 0.0001$, $n = 209$). Compared to the GMWL and the meteoric water line of China (CMWL) ($\delta^2\text{H} = 7.9 * \delta^{18}\text{O} + 8.2$, $R^2 = 0.98$) (Zheng et al., 1983), the slope and intercept of Sanming LMWL were both higher. This is because GMWL and CMWL combine data from global or national studies that include several places with radically differing climates. The Sanming station, on the other hand, is located in a monsoon region and has a humid environment that results in a large slope and intercept. The correlation for the yearly precipitation isotopes in 2019 and 2020 was defined as $\delta^2\text{H} = 8.44 * \delta^{18}\text{O} + 13.93$ ($R^2 = 0.95$, $p < 0.0001$, $n = 117$) and $\delta^2\text{H} = 8.14 * \delta^{18}\text{O} + 13.94$ ($R^2 = 0.95$, $p < 0.0001$, $n = 92$), respectively (Figure 2A). The intercepts of the LMWL in 2019 and 2020 were almost consistent; however, the slope in 2020 was lower than that in 2019 which may have been due to the relative dryness and high evaporation in 2019.

The $\delta^{18}\text{O}_p$ and $\delta^2\text{H}$ data for the SM and NSM periods are shown in Figure 2B to demonstrate how the EASM affected the LMWL. The scatters are located above or near the GMWL in the SM (May–September). The NSM (October to April of the following year) scatters distribute below the GMWL. The slopes in both periods were smaller than those of the GMWL and LMWL. The slope of the LMWL in the NSM period was lower than the slope of 7.70 in the SM period, but its intercept of 14.98 was considerably higher than the intercept of 7.53 in the SM period, showing seasonal differences in the precipitation water vapor sources in this regional. Typically, the intercept and slope of the meteoric water line are positively related (Yao et al.,

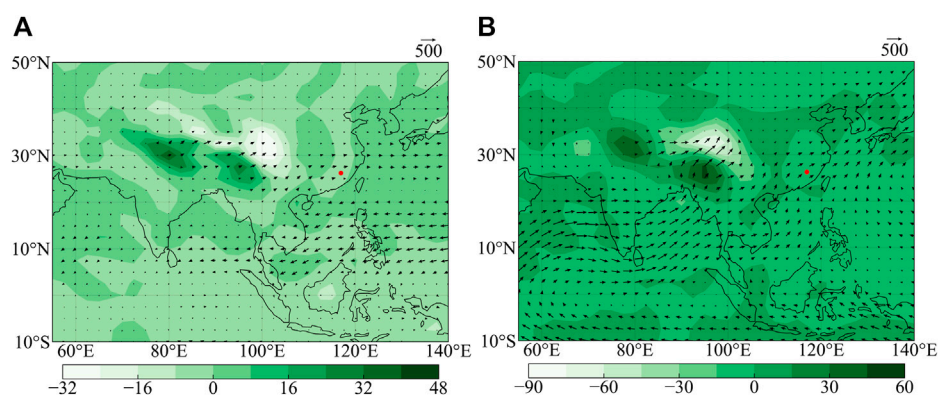
2018). However, in the monsoon region, because the average stable isotope value of the NSM period is more positive than that of the SM period, the scatter in the NSM waterline chart deviates from the upper right relative to the SM, resulting in a larger intercept of the LMWL during the NSM period than that during the SM period.

3.2 Meteorological and isotope temporal characteristics

Figure 3 shows the temporal characteristics of daily $\delta^{18}\text{O}_p$ and d -excess ($d = \delta^2\text{H} - 8 * \delta^{18}\text{O}$, a parameter associated with the meteorological conditions of the source region (Dansgaard, 1964; Breitenbach et al., 2010) and corresponding meteorological factors, i.e., surface air temperature, relative humidity, local precipitation amount) in Sanming from 2019 to 2020. As shown in Figure 3, the daily mean temperature exhibited cyclical variations ranging from 1.3°C to 29.4°C, with an average air temperature of 19.5°C and the maximum temperature occurring in July. Relative humidity in Sanming ranged from 52.6% to 94.5%, with an average relative humidity of 75%. The daily precipitation in Sanming ranged from 0 to 157.4 mm, with the maximum and minimum monthly precipitation occurring in May or June, and November, respectively. Notably, the region receives the most abundant precipitation from March to May, accounting for 25%–50% of the annual precipitation. During the observation period, $\delta^2\text{H}$, $\delta^{18}\text{O}_p$, and d -excess values ranged from -99.07‰ to 47.39‰ , -12.94‰ – 4.37‰ , and -4.05‰ – 30.38‰ , with quantity-weighted means of -33.96‰ , -5.72‰ ($\delta^{18}\text{O}_w$), and 11.77‰ (d_w), respectively. We performed a correlation analysis between environmental parameters and $\delta^{18}\text{O}_p$ to explore the impact of environmental factors on precipitation isotopes. Poor correlations were found between the daily scale

**FIGURE 5**

HYSPLIT4 moisture back-trajectory at Sanming from 2019 to 2020, (A) in NSM and (B) in SM. The number in parentheses represents the cluster number and the percentage of this trajectory. The red dots represent the sampling points.

**FIGURE 6**

Vertically integrated mean water vapor transport from 2019 to 2020, (A) in NSM and (B) in SM. The red dots represent the sampling points.

precipitation $\delta^{18}\text{O}_p$ and precipitation ($R^2 = 0.085$, $p < 0.0001$, $n = 209$), temperature ($R^2 = 0.09$, $p < 0.0001$, $n = 209$), and relative humidity ($R^2 = 0.02$, $p = 0.07$, $n = 209$) (Supplementary Figure S3). The findings showed that on a daily scale, local environmental parameters had less impact on the seasonal variations in precipitation isotopes.

The Sanming stable precipitation isotope data showed a clear seasonal variation (Figure 4A), similar to other reports globally (e.g., Xie et al., 2011; Zhou et al., 2019; Bedaso and Wu, 2020). To determine the seasonal variations in $\delta^{18}\text{O}_p$, the year was subdivided into SM and NSM periods. The SPR period was also included in the comparison owing to its high precipitation. Specifically, the $\delta^{18}\text{O}_p$ values ranged from -12.94‰ to -0.15‰ with an average value of -7.41‰ in the SM period. In the NSM period, $\delta^{18}\text{O}_p$ values ranged from -6.91‰ to 4.37‰ with an average value of -3.50‰ . In the SPR period, $\delta^{18}\text{O}_p$ values ranged from -5.72‰ to 4.37‰ with an average value of -2.08‰ . In

general, the $\delta^{18}\text{O}_p$ values in the SM period were lower than those in the NSM period and fluctuated widely. For both the SM and NSM periods, the $\delta^{18}\text{O}_p$ values in 2020 were lower than those in 2019, and the degree of fluctuation was relatively consistent (Figure 4A). The data distribution for the SPR period was similar to that of the NSM period, but the average value was slightly higher. Although the SPR period had higher precipitation, its $\delta^{18}\text{O}_p$ average value was still higher than that of the SM and NSM periods, which is different from the “amount effect” (Dansgaard, 1964).

The d -excess of precipitation had also been used to explore the seasonal variations in precipitation caused by the shift of water vapor sources in different seasons. For the d -excess value, the variation ranged from -4.05‰ to 21.01‰ with a d_w value of 9.70‰ in the SM and from 0.85‰ to 30.38‰ with a d_w value of 14.47‰ in the NSM. The d -excess values in the SM season were more negative than those in the NSM season, which can be

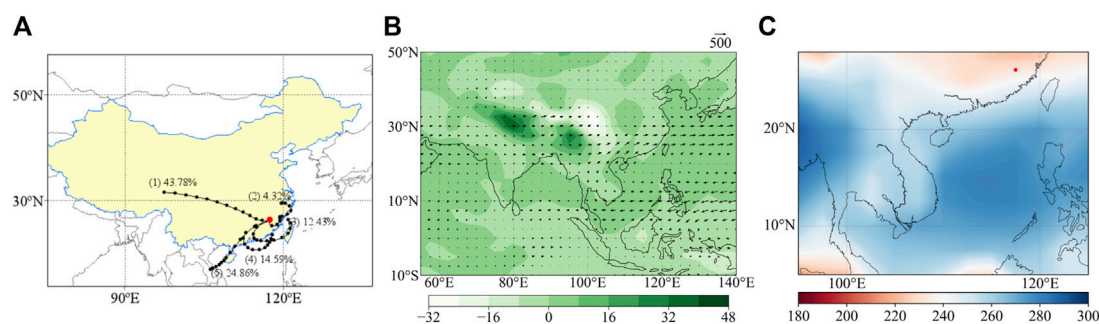


FIGURE 7
HYSPLIT4 moisture back-trajectory (A), vertically integrated mean water vapor transport (B), and averaged OLR (C) in SPR during 2019–2020. The red dots represent the sampling points.

attributed to the regional climatic feature. During the SM period, it is dominated by the EASM, resulting in light precipitation and negative d -excess values. While in NSM, the regional climate is controlled by westerlies and inshore air mass, the d -excess values are more positive. This finding is consistent with the results of Zhang et al. (2009), who observed that in southwest China, the water vapor generating precipitation from low-latitude oceans with high humidity has small d -excess values, whereas that from westerly or inland recirculation with low humidity has large d -values. During the SPR period, the d -excess values varied from 0.85‰ to 26.99‰ with a d_w value of 8.41‰ (Figure 4B), similar to the NSM period. This similarity suggests that the source of water vapor that caused more precipitation during the SPR period was similar to the source of water vapor during the NSM period.

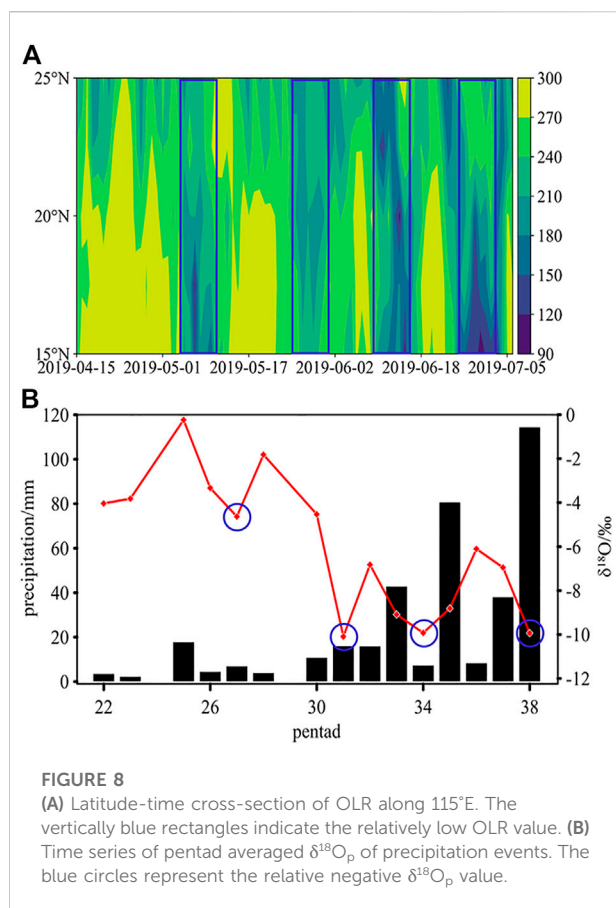
4 Discussion

4.1 Seasonal variation of precipitation isotopes

Sanming has a typical subtropical monsoon climate, with obvious seasonal variation in precipitation. The precipitation isotope results also showed marked seasonal variation (Figure 4). We calculated the d -excess values based on isotope data which reflected meteorological indicators in the moisture source area are less influenced by the local environment and can be used to identify the precipitation moisture sources (Dansgaard, 1964; Breitenbach et al., 2010). The consistent interannual fluctuation of the $\delta^{18}\text{O}_p$ and d -excess values during the 2-year monitoring period reveals that they are likely to be governed by transitions in water vapor sources and atmospheric circulation (Figure 3). Therefore, we used the HYSPLIT backward trajectory model to track water vapor during the SM and NSM periods. To exclude the possible influence of moisture transport on the results obtained on non-precipitation days, we excluded the trajectory

and only selected water vapor on precipitation days during the study period for the simulation analysis. In addition, we calculated the water vapor flux during the observation period to compensate for the fact that HYSPLIT can only reflect the frequency of water vapor sources.

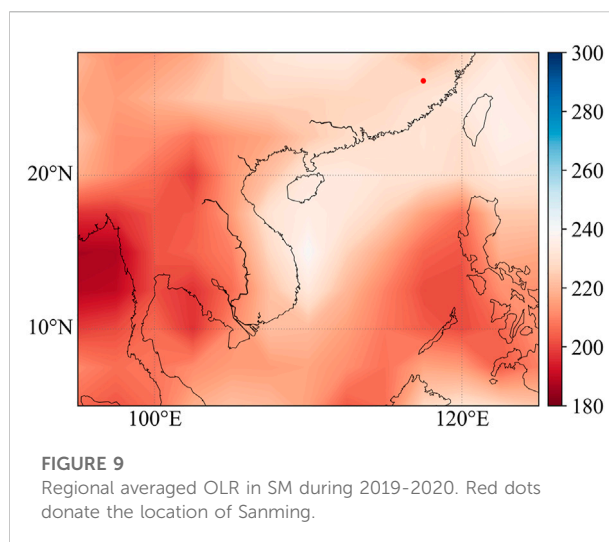
The cluster analysis results based on all backward trajectories for the SM/NSM seasons and the vertically integrated mean water vapor transport during the observation period are presented in Figures 5, 6. On a seasonal scale, water vapor flux dispersion was generally low and precipitation amounts were small during the NSM season. Moisture is usually transported by westerly winds and most of it is inland water vapor, with positive $\delta^{18}\text{O}_p$ and d -excess values. During the SM season, the amount of water vapor transported from the ocean increased, and the overall water vapor flux dispersion was more marked than that during the NSM season. The SM brings a large amount of low-latitude tropical oceanic water vapor (73.38% in total) to the Sanming region, mainly transported by the southwest water vapor channel, the SCS channel, and the northwest Pacific channel (Figure 5B). Consistent with the results in Figure 3, moisture derived from oceanic sources is relatively depleted, while the moisture associated with continental or local sources is more enriched. The $\delta^{18}\text{O}_w$ (−3.50‰) and d_w (14.47‰) values for NSM were positive, reflecting relatively short transport pathways and possible sub-cloud evaporation effects during the precipitation process (local sources) or long-distance transport associated with less pronounced rainout process (continental sources) (Figures 5A, 6A). SM has negative $\delta^{18}\text{O}_w$ (−7.41‰) and d_w (14.47‰) values, indicating that progressive rainout along long-distance transport pathways of air masses should be considered (Figures 5B, 6B). Previous studies have also found that the negative d -excess values during the summer season are associated with weak kinetic isotope fractionation over the oceanic source with warm and humid conditions, whereas the cold and dry air masses from both continental and local sources cause high d -excess values in autumn and winter (Liu et al., 2008; Li et al., 2020). Our results (Figures 3, 5, 6) are consistent with these findings and suggest



that moisture sources play a significant role in explaining the observed seasonal variation in $\delta^{18}\text{O}_p$. Notably, there is no single source of water vapor on a seasonal scale, with various water vapor mixing and dominating by turns occurring at different periods (Li et al., 2020; Guo et al., 2021). Therefore, due to the seasonal variation in precipitation isotopes in the region, the paleoclimate $\delta^{18}\text{O}$ records of this region may be able to reflect the strength of EASM in the region.

4.2 Characteristics and influencing factors of $\delta^{18}\text{O}$ in SPR

SPR is the “early summer rainy season” that occurs from SEC (south of 30°N and east of 110°E) to southern Japan from 13 to 27 pentad (early March to mid-May) (Ding, 1992; Tian and Yasunari, 1998; Wan and Wu, 2008b). To further investigate the main controlling factors of precipitation stable isotopes during the SPR period, we show the backward trajectory analysis, water vapor flux field, and average OLR during the SPR period in Figure 7. In terms of backward trajectory analysis, water vapor sources are mainly divided into two categories: inland and offshore



water vapor (Figures 7A, B). Although the precipitation amount was large during the SPR period, the $\delta^{18}\text{O}_p$ value was still relatively positive and different from that in the SM season (Figure 4). Evidently, the shift in moisture sources is not the dominant factor in the precipitation isotope composition change during the SPR period. As shown in Figure 7C, the relatively high average OLR values in the surrounding ocean indicate weaker convection activity and shorter water vapor transport pathways during this period. Suppressed convective activity at the water vapor source and transport trajectory weaken the rain rainout effect of water vapor (Cai and Tian, 2016), which leads to positive $\delta^{18}\text{O}_p$ values at the sampling site. Whether the SPR period represents the onset of the EASM has long been debated. Previous studies have found that SPR is a portion of the summer monsoon rainfall, which is a signal of the establishment of the East Asian subtropical monsoon (i.e., a part of the EASM) (Ding et al., 1994; He et al., 2008). Other studies have argued that SPR is an extension of winter atmospheric circulation caused by increased southwest wind speed on the southern side of the Tibetan Plateau (Tian and Yasunari, 1998; Wan et al., 2008a). Combined with the previous results, we suggest that SPR should be considered as part of the NSM season based on the positive value of $\delta^{18}\text{O}_p$.

4.3 Monsoon onset process revealed from daily $\delta^{18}\text{O}_p$

As shown in Figure 3, there is a dramatic and sustained depletion of $\delta^{18}\text{O}_p$ from May to June, which coincides with the dates of DBR precipitation (i.e., a time that occurs during the dragon boat race from late May to mid-June). DBR is associated with the alternation of winter and summer monsoons (Wu et al.,

2017) and is usually considered the beginning of the SCSSM, which always accompanies the end of the SPR period. Therefore, to explore the possible relationship between the SCSSM and $\delta^{18}\text{O}_p$ in DBR precipitation in Sanming, a comparative analysis of the OLR [suggestive of strong convection (Yang et al., 2017)] was conducted in the SCS from mid-April to early June (Figure 8).

As shown in Figure 8, the bias of $\delta^{18}\text{O}_p$ was not steep and had many fluctuations, and the OLR had multiple variations during the DBR period. According to Yang et al. (2017) observed that the summer monsoon is featured by intermittent activity on the synoptic scale. In addition, previous studies have reported a negative correlation between $\delta^{18}\text{O}_p$ and monsoon intensity (Tian et al., 2001; Vuille et al., 2005). It is worth noting that the small decreases in each fluctuation correspond roughly to the occurrence of low OLR values, whereas the timing of the slight decrease does not coincide with the timing of the OLR lows (Figure 8). More specifically, there are four decreases in $\delta^{18}\text{O}_p$ in the 26th, 30th, 33rd, and 38th pentads, while the OLR lows occurred on May 7 (26th pentad), 26 (30th pentad), June 8 (32nd pentad), and June 29 (36th pentad). This consistent lag further indicated that the $\delta^{18}\text{O}_p$ values in the Sanming region reflect the convection situation in the SCS promptly and can provide a good indication of the timing and process of SM onset. This result also highlights the potential of the precipitation isotope composition to capture atmospheric circulation signals.

4.4 Characteristics and influencing factors of $\delta^{18}\text{O}$ in SM

With the gradual onset of the SCSSM, the isotope values gradually become negative and maintain this level with an average $\delta^{18}\text{O}_w$ value of -7.41‰ (Figure 3). During the SM period, water vapor from the ocean is the primary source of SM precipitation in the Sanming area, which causes negative precipitation $\delta^{18}\text{O}_p$ values. Recently, many studies have emphasized the critical role of large-scale deep convective activity in the upstream regions. More specifically, the upstream rainout and convection activities along air mass trajectories can deplete the heavy isotopes in water vapor, which explains the isotope seasonal variability at downstream sites (Risi et al., 2008; Crawford et al., 2013; Aggarwal et al., 2016; Zwart et al., 2016; Ansari et al., 2020). Therefore, we analyzed the large-scale atmospheric convection intensity, as measured by the average OLR in the SM (Figure 9). The relatively low average OLR values around the water vapor source during the SM period indicated that the atmospheric convective intensity along the water vapor transport path was frequent and intense (Figure 9). Therefore, the strong convective activity of water vapor increases the depleting effect in the moisture source and along the transport pathway, resulting in negative $\delta^{18}\text{O}_p$ values in the Sanming area (Lee and Fung, 2008; Risi et al., 2008; Cai et al., 2017;

Ruan et al., 2019; Zhou et al., 2019), which is similar to the results shown in Figure 3. These observations further verify that, although the transfer of moisture sources has a non-negligible effect on the precipitation isotope composition in the SM and NSM seasons, the convective processes on the water vapor sources and transport pathways also play an essential role in the changes in precipitation isotope composition.

5 Conclusion

In this study, we exhibit a 2-year detailed description of the precipitation isotope characteristics from 2019 to 2020 in Sanming, SEC. The HYSPLIT backward trajectory model and OLR analysis were used to clarify the basic features and seasonal variability in precipitation isotopes in Sanming. The LMWL was developed as $\delta^2\text{H} = 8.29 * \delta^{18}\text{O} + 13.93$ ($R^2 = 0.95$, $p < 0.0001$, $n = 209$), and seasonal changes in $\delta^{18}\text{O}_p$ and d -excess in this study area were observed. The $\delta^{18}\text{O}_p$ and d -excess values in the SM season (-12.94‰ – 0.15‰ , -4.05‰ – 21.01‰) were more negative than those in the NSM season (-6.91‰ – 4.37‰ , 0.85‰ – 30.38‰). The backward trajectory and OLR analyses also show seasonal variations, with moisture during the SM period mainly coming from remote seas with high convective activity, while westerly and inland local water vapor with weak convective activity contributes to the NSM period. The above results suggest that the seasonal variation in precipitation isotopes is related to the conversion of water vapor sources and the intensity of convective activity in the process of water vapor transportation. SPR is a particular period of the NSM season with higher precipitation, and the primary water vapor sources are the western and offshore oceans. More importantly, owing to the high percentage of precipitation throughout the year, the SPR influence should be considered more in the annual isotope composition. The isotope values showed a sharp decreasing pattern during the DBR period and corresponded well to the convective intensity over the SCS, highlighting the potential of $\delta^{18}\text{O}_p$ as a substitute method for investigating the complicated Asian monsoon system. Our results highlight that the stable isotopes in precipitation and related paleoclimate proxies are primarily influenced by moisture sources and large-scale upstream convective activities, rather than local environmental factors.

Data availability statement

The original contributions presented in the study are included in the article/Supplementary Material, further inquiries can be directed to the corresponding author.

Author contributions

All authors listed have made a substantial, direct, and intellectual contribution to the work and approved it for publication.

Funding

This study was jointly supported by grants of the National Natural Science Foundation of China (42071106).

Conflict of interest

The authors declare that the research was conducted in the absence of any commercial or financial relationships that could be construed as a potential conflict of interest.

References

- Aggarwal, P. K., Fröhlich, K., Kulkarni, K. M., and Gourcy, L. L. (2004). Stable isotope evidence for moisture sources in the Asian summer monsoon under present and past climate regimes. *Geophys. Res. Lett.* 31 (8), L08203. doi:10.1029/2004GL019911
- Aggarwal, P. K., Romatschke, U., Araguas-Araguas, L., Belachew, D., Longstaffe, F. J., Berg, P., et al. (2016). Proportions of convective and stratiform precipitation revealed in water isotope ratios. *Nat. Geosci.* 9 (8), 624–629. doi:10.1038/ngeo2739
- Ansari, M. A., Noble, J., Deodhar, A., and Saravana Kumar, U. (2020). Atmospheric factors controlling the stable isotopes ($\delta^{18}\text{O}$ and $\delta^2\text{H}$) of the Indian summer monsoon precipitation in a drying region of Eastern India. *J. Hydrol. X* 584, 124636. doi:10.1016/j.jhydrol.2020.124636
- Araguás-Araguás, L., Fröhlich, K., and Rozanski, K. (1998). Stable isotope composition of precipitation over southeast Asia. *J. Geophys. Res.* 103 (D22), 28721–28742. doi:10.1029/98jd02582
- Bedaso, Z., and Wu, S. (2020). Daily precipitation isotope variation in Midwestern United States: Implication for hydroclimate and moisture source. *Sci. Total Environ.* 713, 136631. doi:10.1016/j.scitotenv.2020.136631
- Breitenbach, S. F. M., Adkins, J. F., Meyer, H., Marwan, N., Kumar, K. K., and Haug, G. H. (2010). Strong influence of water vapor source dynamics on stable isotopes in precipitation observed in Southern Meghalaya, NE India. *Earth Planet. Sci. Lett.* 292 (1), 212–220. doi:10.1016/j.epsl.2010.01.038
- Cai, Z., and Tian, L. (2016). Atmospheric controls on seasonal and interannual variations in the precipitation isotope in the East Asian monsoon region. *J. Clim.* 29 (4), 1339–1352. doi:10.1175/jcli-d-15-0363.1
- Cai, Z., Tian, L., and Bowen, G. J. (2017). ENSO variability reflected in precipitation oxygen isotopes across the Asian Summer Monsoon region. *Earth Planet. Sci. Lett.* 475, 25–33. doi:10.1016/j.epsl.2017.06.035
- Cheng, H., Edwards, R. L., Sinha, A., Spötl, C., Yi, L., Chen, S., et al. (2016). The Asian monsoon over the past 640,000 years and ice age terminations. *Nature* 534 (7609), 640–646. doi:10.1038/nature18591
- Craig, H. (1961). Isotopic variations in meteoric waters. *Science* 133 (3465), 1702–1703. doi:10.1126/science.133.3465.1702
- Crawford, J., Hughes, C. E., and Parkes, S. D. (2013). Is the isotopic composition of event based precipitation driven by moisture source or synoptic scale weather in the Sydney Basin, Australia? *J. Hydrol. X* 507, 213–226. doi:10.1016/j.jhydrol.2013.10.031
- Dansgaard, W. (1964). Stable isotopes in precipitation. *Tellus* 16 (4), 436–468. doi:10.3402/tellusa.v16i4.8993
- Ding, Y., Chen, L., and Murakami, M. (1994). *The East asian monsoon*. Beijing: China Meteorological Press.
- Ding, Y. (1992). Summer monsoon rainfalls in China. *J. Meteorological Soc. Jpn.* 70 (1B), 373–396. doi:10.2151/jmsj.1965.70.1B_373
- Draxler, R., and Hess, G. (1998). An overview of the HYSPLIT_4 modeling system for trajectories, dispersion, and deposition. *Aust. Meteorol. Mag.* 47, 295–308.
- Guo, X., Gong, X., Shi, J., Guo, J., Domínguez-Villar, D., Lin, Y., et al. (2021). Temporal variations and evaporation control effect of the stable isotope composition of precipitation in the subtropical monsoon climate region, Southwest China. *J. Hydrol. X* 599, 126278. doi:10.1016/j.jhydrol.2021.126278
- He, J., Zhao, P., Zhu, C., Zhang, R., Tang, X., Chen, L., et al. (2008). Discussion of some problems as to the East Asian subtropical monsoon. *J. Meteorol. Res.-PRC.* 22, 419–434.
- Hong, B., Liu, C., Lin, Q., Yasuyuki, S., Leng, X., Wang, Y., et al. (2009). Temperature evolution from the $\delta^{18}\text{O}$ record of Hani peat, Northeast China, in the last 14000 years. *Sci. China Ser. D-Earth. Sci.* 52 (7), 952–964. doi:10.1007/s11430-009-0086-z
- Lee, J.-E., and Fung, I. (2008). Amount effect of water isotopes and quantitative analysis of post-condensation processes. *Hydrol. Process.* 22 (1), 1–8. doi:10.1002/hyp.6637
- Li, L. (2006). *Preliminary analysis on the regularity and cause of precipitation anomaly in rainy season in Fujian province (in Chinese)*. Nanjing, China: Nanjing University of Information Science and Technology. doi:10.7666/d.y868475
- Li, Y., An, W., Pang, H., Wu, S., Tang, Y., Zhang, W., et al. (2020). Variations of stable isotopic composition in atmospheric water vapor and their controlling factors—a 6-year continuous sampling study in nanjing, eastern China. *J. Geophys. Res. Atmos.* 125 (22), doi:10.1029/2019jd031697
- Liang, J., and Wang, Y. (1997). Characters of precipitation change in rainy seasons (May–June) in the last hundred years in coastal Fujian (in Chinese). *J. Oceanography Taiwan Strait* 16 (04), 415–419.
- Liu, Y., Cobb, K. M., Song, H., Li, Q., Li, C., Nakatsuka, T., et al. (2017). Recent enhancement of central Pacific El Niño variability relative to last eight centuries. *Nat. Commun.* 8, 15386. doi:10.1038/ncomms15386
- Liu, Z., Tian, L., Yao, T., and Yu, W. (2008). Seasonal deuterium excess in nagqu precipitation: Influence of moisture transport and recycling in the middle of Tibetan plateau. *Environ. Geol.* 55 (7), 1501–1506. doi:10.1007/s00254-007-1100-4
- Merlivat, L., and Jouzel, J. (1979). Global climatic interpretation of the deuterium-oxygen 18 relationship for precipitation. *J. Geophys. Res.* 84 (C8), 5029–5033. doi:10.1029/JC084iC08p05029
- Risi, C., Bony, S., and Vimeux, F. (2008). Influence of convective processes on the isotopic composition ($\delta^{18}\text{O}$ and δD) of precipitation and water vapor in the tropics: 2. Physical interpretation of the amount effect. *J. Geophys. Res.* 113 (D19), D19306. doi:10.1029/2008jd009943
- Ruan, J., Zhang, H., Cai, Z., Yang, X., and Yin, J. (2019). Regional controls on daily to interannual variations of precipitation isotope ratios in Southeast China: Implications for paleomonsoon reconstruction. *Earth Planet. Sci. Lett.* 527, 115794. doi:10.1016/j.epsl.2019.115794

Publisher's note

All claims expressed in this article are solely those of the authors and do not necessarily represent those of their affiliated organizations, or those of the publisher, the editors and the reviewers. Any product that may be evaluated in this article, or claim that may be made by its manufacturer, is not guaranteed or endorsed by the publisher.

Supplementary material

The Supplementary Material for this article can be found online at: <https://www.frontiersin.org/articles/10.3389/fenvs.2022.1061882/full#supplementary-material>

- Shi, S., Shi, J., Xu, C., Leavitt, S. W., Wright, W. E., Cai, Z., et al. (2020). Tree-ring $\delta^{18}\text{O}$ from Southeast China reveals monsoon precipitation and ENSO variability. *Palaeogeogr. Palaeoclimatol. Palaeoecol.* 558, 109954. doi:10.1016/j.palaeo.2020.109954
- Tao, S., and Chen, L. (1987). "A review of recent research on the East Asian summer monsoon in China," in *Monsoon Meteorology*. Editors C.-P. Chang and T. N. Krishnamurti (Oxford University Press), 60–92.
- Tao, S., Zhang, X., Pan, G., Xu, J., and Zeng, Z. (2021). Moisture source identification based on the seasonal isotope variation of precipitation in the Poyang Lake Wetland, China. *J. Hydrology Regional Stud.* 37, 100892. doi:10.1016/j.ejrh.2021.100892
- Tian, L., Masson-Delmotte, V., Stievenard, M., Yao, T., and Jouzel, J. (2001). Tibetan Plateau summer monsoon northward extent revealed by measurements of water stable isotopes. *J. Geophys. Res.* 106 (D22), 28081–28088. doi:10.1029/2001JD900186
- Tian, S.-F., and Yasunari, T. (1998). Climatological aspects and mechanism of spring persistent rains over central China. *J. Meteorological Soc. Jpn.* 76 (1), 57–71. doi:10.2151/jmsj.1965.76.1_57
- Trouet, V., and Oldenborgh, G. J. (2013). KNMI climate explorer: A web-based research tool for high-resolution paleoclimatology. *Tree. Ring. Res.* 69 (1), 3–13. doi:10.3959/1536-1098-69.1.3
- Vuille, M., Werner, M., Bradley, R. S., and Keimig, F. (2005). Stable isotopes in precipitation in the Asian monsoon region. *J. Geophys. Res.* 110 (D23), D23108. doi:10.1029/2005JD006022
- Wan, R., Wang, T., and Wu, G. (2008a). Temporal variations of the spring persistent rains and SCS subtropical high and their correlations to the circulation and precipitation of the East Asia summer monsoon (in Chinese). *Acta. Meteorol. Sin.* 66 (05), 800–807. doi:10.11676/qxxb2008.073
- Wan, R., and Wu, G. (2008b). Temporal and spatial distribution of the spring persistent rains over southeastern China (in Chinese). *Acta. Meteorol. Sin.* 66 (03), 310–319. doi:10.11676/qxxb2008.029
- Wang, B., LinHoZhang, Y., and Lu, M. (2004). Definition of south China Sea Monsoon onset and commencement of the East asia summer monsoon. *J. Clim.* 17 (4), 699–710. doi:10.1175/2932.1
- Wang, Y., Cheng, H., Edwards, R. L., An, Z., Wu, J., Shen, C. C., et al. (2001). A high-resolution absolute-dated late pleistocene monsoon record from hulu cave, China. *Science* 294 (5550), 2345–2348. doi:10.1126/science.1064618
- Wei, Z., Lee, X., Liu, Z., Seeboonruang, U., Koike, M., and Yoshimura, K. (2018). Influences of large-scale convection and moisture source on monthly precipitation isotope ratios observed in Thailand, Southeast Asia. *Earth Planet. Sci. Lett.* 488, 181–192. doi:10.1016/j.epsl.2018.02.015
- Wu, H., Fu, C., Zhang, C., Zhang, J., Wei, Z., and Zhang, X. (2022). Temporal variations of stable isotopes in precipitation from Yungui Plateau: Insights from moisture source and rainout effect. *J. Hydrometeorol.* 23 (1), 39–51. doi:10.1175/JHM-D-21-0098.1
- Wu, H., Li, C., and Wang, D. (2017). Analysis on characteristics and abnormal causes of Dragon-Boat precipitation in Guangdong in the past 55 years (in Chinese). *J. Trop. Meteorology* 33 (5), 608–616. doi:10.16032/j.issn.1004-4965.2017.05.004
- Xie, L., Wei, G., Deng, W., and Zhao, X. (2011). Daily $\delta^{18}\text{O}$ and δD of precipitations from 2007 to 2009 in Guangzhou, South China: Implications for changes of moisture sources. *J. Hydrol. X.* 400 (3–4), 477–489. doi:10.1016/j.jhydrol.2011.02.002
- Xu, C., Ge, J., Nakatsuka, T., Yi, L., Zheng, H., and Sano, M. (2016). Potential utility of tree ring $\delta^{18}\text{O}$ series for reconstructing precipitation records from the lower reaches of the Yangtze River, southeast China. *J. Geophys. Res. Atmos.* 121 (8), 3954–3968. doi:10.1002/2015JD023610
- Xu, H., Hong, Y., Lin, Q., Hong, B., Jiang, H., and Zhu, Y. (2002). Temperature variations in the past 6000 years inferred from $\delta^{18}\text{O}$ of peat cellulose from Hongyuan, China. *Chin. Sci. Bull.* 47 (15), 1578–1584. doi:10.1360/02tb9347
- Yang, H., Johnson, K. R., Griffiths, M. L., and Yoshimura, K. (2016). Interannual controls on oxygen isotope variability in Asian monsoon precipitation and implications for paleoclimate reconstructions. *J. Geophys. Res. Atmos.* 121 (14), 8410–8428. doi:10.1002/2015JD024683
- Yang, X., Davis, M. E., Acharya, S., and Yao, T. (2017). Asian monsoon variations revealed from stable isotopes in precipitation. *Clim. Dyn.* 51 (5–6), 2267–2283. doi:10.1007/s00382-017-4011-4
- Yao, T., Masson-Delmotte, V., Gao, J., Yu, W., Yang, X., Risi, C., et al. (2013). A review of climatic controls on $\delta^{18}\text{O}$ in precipitation over the Tibetan Plateau: Observations and simulations. *Rev. Geophys.* 51 (4), 525–548. doi:10.1002/rog.20023
- Yao, T., Zhang, X., Guan, H., Zhou, H., Hua, M., and Wang, X. (2018). Climatic and environmental controls on stable isotopes in atmospheric water vapor near the surface observed in Changsha, China. *Atmos. Environ. X.* 189, 252–263. doi:10.1016/j.atmosenv.2018.07.008
- Yoshimura, K., Kanamitsu, M., Noone, D., and Oki, T. (2008). Historical isotope simulation using Reanalysis atmospheric data. *J. Geophys. Res.* 113 (D19), D19108. doi:10.1029/2008JD010074
- Yoshimura, K., Miyoshi, T., and Kanamitsu, M. (2014). Observation system simulation experiments using water vapor isotope information. *J. Geophys. Res. Atmos.* 119 (13), 7842–7862. doi:10.1002/2014JD021662
- Zhang, H., Cheng, H., Cai, Y., Spötl, C., Kathayat, G., Sinha, A., et al. (2018a). Hydroclimatic variations in southeastern China during the 4.2 ka event reflected by stalagmite records. *Clim. Past.* 14 (11), 1805–1817. doi:10.5194/cp-14-1805-2018
- Zhang, H., Cheng, H., Cai, Y., Spötl, C., Sinha, A., Kathayat, G., et al. (2020). Effect of precipitation seasonality on annual oxygen isotopic composition in the area of spring persistent rain in southeastern China and its paleoclimatic implication. *Clim. Past.* 16 (1), 211–225. doi:10.5194/cp-16-211-2020
- Zhang, H., Cheng, H., Spötl, C., Cai, Y., Sinha, A., Tan, L., et al. (2018b). A 200-year annually laminated stalagmite record of precipitation seasonality in southeastern China and its linkages to ENSO and PDO. *Sci. Rep.* 8 (1), 12344. doi:10.1038/s41598-018-30112-6
- Zhang, X., Guan, H., Zhang, X., Zhang, W., and Yao, T. (2016). Numerical experiments on the impacts of surface evaporation and fractionation factors on stable isotopes in precipitation. *Asia. Pac. J. Atmos. Sci.* 52 (3), 327–339. doi:10.1007/s13143-016-0008-x
- Zhang, X., Liu, J., Kazuki, M., Xie, Z., Chen, S., Song, Z., et al. (2009). Ras dependent paracrine secretion of osteopontin by Nf1+/- osteoblasts promote osteoclast activation in a neurofibromatosis type I murine model. *Pediatr. Res.* 31 (04), 613–618. doi:10.1203/PDR.0b013e3181a1c607
- Zhang, X., Qiu, W., Jiang, X., Hu, H.-M., Xiao, H., Cai, B., et al. (2021). Three-phase structure of the East asia summer monsoon during heinrich stadial 4 recorded in xianyun cave, southeastern China. *Quat. Sci. Rev.* 274, 107267. doi:10.1016/j.quascirev.2021.107267
- Zheng, S., Hou, F., and Ni, B. (1983). The investigation of hydrogen and oxygen isotopes of precipitation in China (in Chinese). *Chin. Sci. Bull.* 28 (3), 801–806. doi:10.1360/csb1983-28-13-801
- Zhou, H., Zhang, X., Yao, T., Hua, M., Wang, X., Rao, Z., et al. (2019). Variation of $\delta^{18}\text{O}$ in precipitation and its response to upstream atmospheric convection and rainout: A case study of Changsha station, south-central China. *Sci. Total Environ.* 659, 1199–1208. doi:10.1016/j.scitotenv.2018.12.396
- Zwart, C., Munksgaard, N. C., Kurita, N., and Bird, M. I. (2016). Stable isotopic signature of Australian monsoon controlled by regional convection. *Quat. Sci. Rev.* 151, 228–235. doi:10.1016/j.quascirev.2016.09.010



OPEN ACCESS

EDITED BY
Wei Shui,
Fuzhou University, China

REVIEWED BY
Guolin Feng,
National Climate Center, China
Qianrong Ma,
Yangzhou University, China

*CORRESPONDENCE
Yanling Chen,
✉ chenyn@ms.xjb.ac.cn
Junqiang Yao,
✉ yaojq1987@126.com

SPECIALTY SECTION
This article was submitted to
Interdisciplinary Climate Studies,
a section of the journal
Frontiers in Environmental Science

RECEIVED 28 October 2022
ACCEPTED 08 December 2022
PUBLISHED 04 January 2023

CITATION
Zhou G, Chen Y and Yao J (2023),
Variations in precipitation and
temperature in Xinjiang (Northwest
China) and their connection to
atmospheric circulation.
Front. Environ. Sci. 10:1082713.
doi: 10.3389/fenvs.2022.1082713

COPYRIGHT
© 2023 Zhou, Chen and Yao. This is an
open-access article distributed under
the terms of the [Creative Commons
Attribution License \(CC BY\)](https://creativecommons.org/licenses/by/4.0/). The use,
distribution or reproduction in other
forums is permitted, provided the
original author(s) and the copyright
owner(s) are credited and that the
original publication in this journal is
cited, in accordance with accepted
academic practice. No use, distribution
or reproduction is permitted which does
not comply with these terms.

Variations in precipitation and temperature in Xinjiang (Northwest China) and their connection to atmospheric circulation

Guixiang Zhou^{1,2,3}, Yanling Chen^{2*} and Junqiang Yao^{3,4,5,6*}

¹College of Geographic Science and Tourism, Xinjiang Normal University, Urumqi, China, ²State Key Laboratory of Desert and Oasis Ecology, Xinjiang Institute of Ecology and Geography, Chinese Academy of Sciences, Urumqi, China, ³Institute of Desert Meteorology, China Meteorological Administration, Urumqi, China, ⁴Key Laboratory of Tree-ring Physical and Chemical Research, China Meteorological Administration, Urumqi, China, ⁵National Observation and Research Station of Desert Meteorology, Taklimakan Desert of Xinjiang, Urumqi, China, ⁶Xinjiang Key Laboratory of Desert Meteorology and Sandstorm, Urumqi, China

As one of the most vulnerable types of global ecosystems and water resource systems, arid regions are most sensitive to climate change. The Xinjiang (XJ) region is an important part of the arid region in Central Asia and is representative of global arid regions. The complex topography and underlying surface result in distinct climate change characteristics in XJ. In this study, XJ was divided into five sub-regions: the Irtys River Basin (IRB), the economic belt on the northern slope of the Tianshan Mountains (NSTM), the Ili River Basin (ILRB), the Turpan-Hami Basin (THB), and the Tarim River Basin (TRB). The change in temperature and precipitation over XJ and its sub-regions were investigated from 1960 to 2019 using the Mann-Kendall method and cross-wavelet analysis. Moreover, the multi-timescale correlations between the variations in temperature and precipitation and the atmospheric circulation indices were explored. The results show significant warming and wetting trends in XJ from 1960 to 2019. The warming rate was 0.32°C/10 a ($p < 0.01$), with an abrupt change during the mid-1990s. The increasing rate of precipitation was 9.24 mm/10 a ($p < 0.01$), with an abrupt change during the middle to late 1990s. In terms of seasonal variation, the greatest warming rate was during winter (0.37°C/10 a), whereas the precipitation increase was concentrated in summer (3.48 mm/10 a). In terms of spatial variation, a significant warming trend was observed in THB, IRB, ILRB, and NSTM, and precipitation increased significantly in ILRB, NSTM, and the western TRB in southern XJ. The Hurst index analysis indicated that the warming and wetting trends in XJ will slow in the future. Climate change in XJ was closely related to atmospheric circulation at multiple timescales. The subtropical high, Northern-Hemisphere polar vortex activities and the Tibetan Plateau have a significant impact on climate change in XJ. The annual mean temperature in XJ was positively correlated with the area and intensity index of the subtropical high over North Africa, Atlantic, and North America, and negatively correlated with the area and intensity index of the Asia polar vortex. The XJ annual precipitation was positively correlated with the index of the Tibet Plateau Region one and negatively correlated with the intensity index of the Atlantic

and European polar vortex, and the area and intensity index of the Northern Hemisphere polar vortex. The results of this study can provide some references for the scientific assessment and accurate prediction of climate change in XJ.

KEYWORDS

temperature, Xinjiang, atmospheric circulation indices, cross-wavelet analysis, precipitation

Introduction

The sixth assessment report of the Intergovernmental Panel on Climate Change (IPCC) suggested that the global average surface temperature during 2011–2020 had increased by 1.09°C from that in 1850–1900 (IPCC, 2022). Various hazards associated with global warming are increasing. Only when global warming is maintained within 1.5°C can the losses and damages to natural and human systems caused by the climate change can be reduced (Jiang et al., 2022). As the area with the most vulnerable ecosystem and water resource system, the arid region is the most sensitive area to global climate change.

The Xinjiang Uyghur Autonomous Region is located in the western arid region of Northwest China and the hinterland of the Eurasian continent. It is an essential part of the Central Asian arid region with little precipitation and a fragile ecological environment (Yao et al., 2020; Yao et al., 2022a). Its sensitivity to climate change increases with global warming (Chen et al., 2014; Yao et al., 2021), and it is a remarkable representative of the global arid region (Chen et al., 2015). Numerous studies have demonstrated “warming and wetting” trends during the past decades in Xinjiang (XJ) region (Yao et al., 2022b). A previous study found that both daytime and nocturnal precipitation increased in western China from 1990 to 2019 (Deng et al., 2022). Some studies have found a slightly decreasing trend in warming and wetting rates in XJ after 1997 (Yao et al., 2018). In combination with analysis of the standardized precipitation evapotranspiration index (SPEI), the transition from “warming and wetting” to “aridification” has been observed since 1997 (Yao et al., 2021). The interannual temperature and humidity configuration in XJ was mainly “warm-wet” and “warm-dry” during 1961–2019, but the “warm-dry” configuration will be more prominent in the future (Yao et al., 2022b). The climate in Central Asia tends to be wetter during the wet season and drier during the dry season (Ren et al., 2022). The trend of “warming and wetting” in XJ is projected to become more obvious in the future, but its arid and semi-arid characteristics will be maintained, and the frequency of hydrological droughts will relatively increase (Wang et al., 2021). Subtropical highs are also known as subtropical anticyclones (Li et al., 2012). The Northern Hemisphere subtropical high is usually divided into five parts: the Indian, Western Pacific, Eastern Pacific, and North African Atlantic Subtropical highs (Zhang et al., 2008). A polar vortex is a large vortex system located in the middle and upper polar troposphere and above the stratosphere. It can extend horizontally over middle and high latitudes (Liu L. et al., 2020).

The high-latitude circulation system and atmospheric circulation in the Northern Hemisphere are strongly affected by changes in the polar vortex intensity and area (Li et al., 2017). The Tibetan Plateau is a large highland in the mid-latitude region of the Northern Hemisphere, which influences regional and global circulation and climate through mechanical and thermal effects (Duan et al., 2012; Liu Y. J. et al., 2020). The above studies mainly focused on the changes in temperature and precipitation over XJ, whereas information regarding atmospheric circulation indices affecting climate change remains scarce.

Based on the temperature and precipitation datasets of XJ from 1960 to 2019 and the atmospheric circulation indices, this study investigated the latest changes in temperature and precipitation in five sub-regions of XJ based on the expedition zones of the Third XJ Scientific Expedition and Research Program. The multi-timescale correlations between the temperature and precipitation, and the atmospheric circulation indices were also explored in this study. This study can provide some references for the construction of an ecological civilization in XJ and to improve its ability to deal with various climate hazards caused by future climate change.

The remainder of this paper is organized as follows: Section 2 introduces the data and methods. Section 3 shows the variation trends in temperature and precipitation in XJ over the past 60 years and predicts future trends. In addition, the correlations between climate change in XJ and atmospheric circulation factors are also analyzed in Section 3. Discussions are presented in Section 4, and the conclusions are presented in Section 5.

Data and methods

Study area

XJ is located in the arid region of Northwest China. The basins and mountains are distributed alternately in XJ, forming a unique and complex topographic structure. XJ has an arid climate with an average annual temperature of 10°C–15°C and an average annual precipitation of less than 150 mm (Li et al., 2011). It is highly sensitive to global warming and the ecological environment in this region is very fragile.

According to topography, XJ is divided by the Tianshan Mountains into northern and southern XJ, resulting in three major sub-regions: northern XJ, Tianshan Mountains, and southern XJ

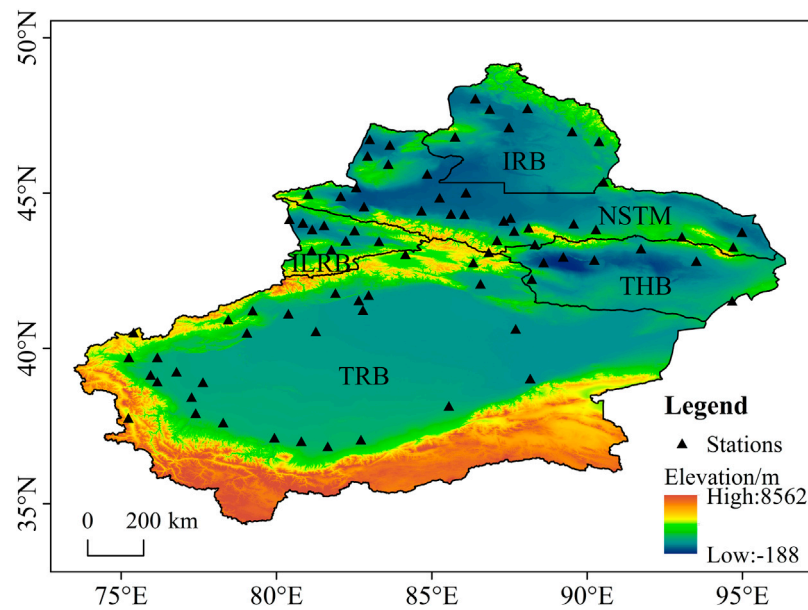


FIGURE 1

Study area and the distribution of meteorological stations. (The Irtys River Basin, the economic belt on the northern slope of the Tianshan Mountains, the Ili River Basin, the Turpan-Hami Basin, and the Tarim River Basin are marked as IRB, NSTM, ILRB, THB, and TRB, respectively).

(Reziwanguli et al., 2016; Kang et al., 2018; Wu et al., 2020). Several studies have divided XJ into mountainous, oasis, and desert areas (Chen et al., 2005; Zhang et al., 2021), and obtained some beneficial conclusions about the climate of XJ. For extremely arid XJ, water is a fundamental natural and strategic economic resource, and it is also the lifeblood of XJ's high-quality social and economic development. The watershed, as the main carrier of water resources in XJ, connects the natural elements in the watershed into a whole river. Human activities are primarily performed in watersheds. However, few studies have considered the watershed as a unit for conducting research on climate change in XJ. Based on the distribution of major watersheds and water systems in XJ, and also in terms of the expedition zones of the Third XJ Scientific Expedition and Research Program, we divided XJ into five sub-regions: the Irtys River Basin (IRB), the economic belt on the northern slope of the Tianshan Mountains (NSTM), the Ili River Basin (ILRB), the Turpan-Hami Basin (THB), and the Tarim River Basin (TRB) (Figure 1). Within the IRB, the Irtys River is the only river in China that flows into the Arctic Ocean. It originates from the southwestern slope of the Altai Mountains in China, and its water volume ranks second in XJ following the Ili River (Liu et al., 2017; Wang et al., 2022). The NSTM consists of small- and medium-sized rivers and is the most economically developed area in XJ, with the sharpest contradiction between the supply and demand of water resources (Sun et al., 2022). In the ILRB, the Ili River originates in the Tianshan Mountains and eventually joins Balkhash Lake, and is the river with the largest water volume in XJ (Liu et al., 2022). The THB is among the most arid basins in XJ and is rich in wind and solar energy but extremely limited in water resources (Fang et al., 2010). The TRB

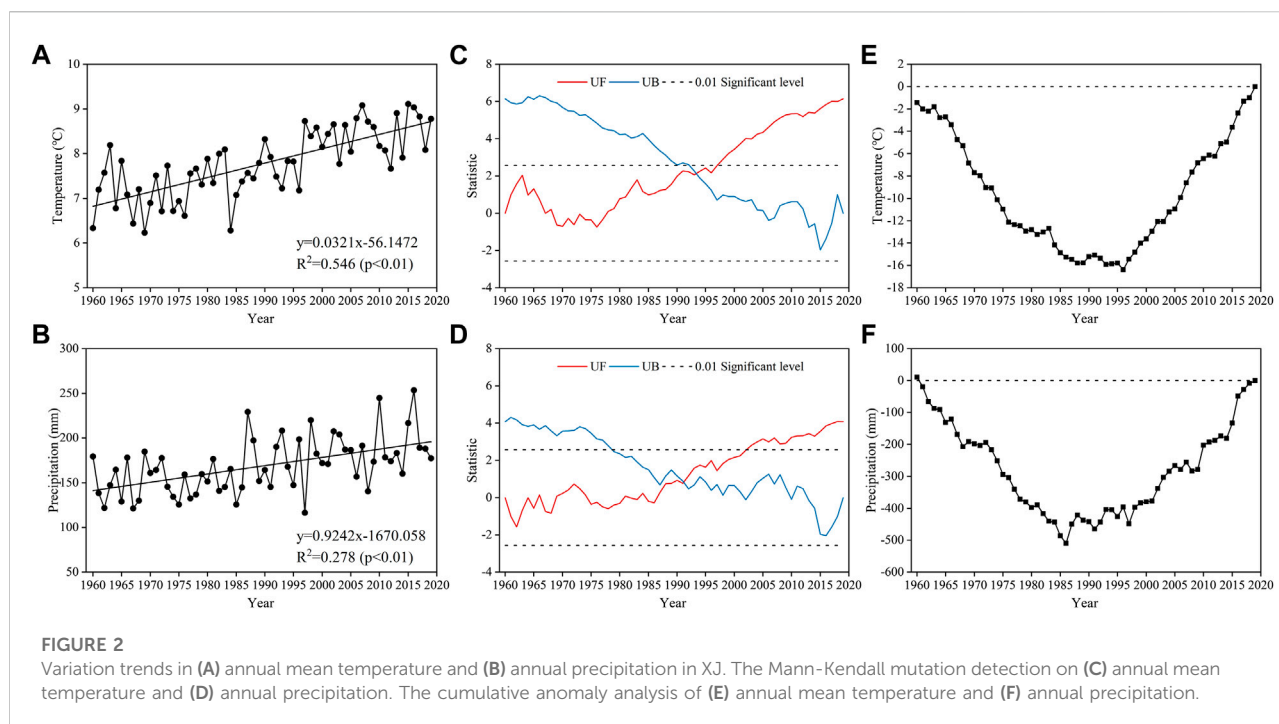
is located in southern XJ, between the Tianshan and Kunlun Mountains, and is the largest inland river basin in China (Xue et al., 2022).

Data sources

The daily average temperature and precipitation data in XJ from 1960 to 2019 were provided by the China Meteorological Administration (CMA, <http://data.cma.cn/en>). To ensure the continuity of data, some meteorological stations with missing data on temperature and precipitation were excluded, and 80 meteorological stations were finally selected for the analysis in this study (Figure 1). Seventy-four atmospheric circulation indices were obtained from the National Climate Center of China Meteorological Administration (<https://cmdp.ncc-cma.net/cn>), with seven indices excluded from practical use due to missing data from June to September.

Methodology

In this study, the variation trends in temperature and precipitation in XJ and its subregions over the past 60 years were analyzed using the linear regression method. The Mann-Kendall method was used to detect abrupt change years and tendencies of climate sequences, and R/S analysis was applied to predict future variations in temperature and precipitation (Ding et al., 2018; Fang



et al., 2022). The Pearson correlation analysis method was used to analyze the correlation between the atmospheric circulation index and climate factors in XJ, and the atmospheric circulation index with strong positive and negative correlations was selected. Cross-wavelet analysis was used to analyze the periodic characteristics of the climate factors and atmospheric circulation indices.

The cross wavelet transform (XWT) highlights the interrelationship among temperature, precipitation, and atmospheric circulation indices in high-energy regions (Grinsted et al., 2004; Hu et al., 2021). Wavelet transform coherence (WTC) shows this interrelationship in the low-energy region. The thin black arcs in XWT and WTC indicate the cone of influence of the wavelet boundary effect, and the thick black solid line indicates a significant correlation between the two, which passed the red noise test with a confidence level of 95%. The symbol “←” (“→”) indicates that the climate and atmospheric circulation factors are negatively (positively) correlated. The symbol “↓” (“↑”) denotes that the climate factor is 90° ahead of (behind) the variations in the atmospheric circulation factor (Liu et al., 2021).

Results

Trends of temperature and precipitation in XJ

The annual mean temperature in XJ during 1960–2019 showed a significant increasing trend with a warming rate of 0.32°C/10 a ($p < 0.01$), which is higher than

the average in China (Zhao et al., 2020) (Figure 2A). The results of the Mann-Kendall test showed that the temperature changed abruptly in 1994 (Figure 2C). After the abrupt change, the multi-year average temperature increased by 1.08°C. The cumulative anomaly analysis showed that the annual mean temperature experienced a decreasing trend from 1960 to 1996 and an increasing trend from 1997 to 2019, with 1996 being the turning point (Figure 2E). Considering the results of the two methods, the annual mean temperature in XJ was concluded to have changed abruptly in the mid-1990s.

The annual precipitation in XJ shows a significant increasing trend from 1960 to 2019 with a wetting rate of 9.24 mm/10 a ($p < 0.01$), which is slightly lower than the average in China (Zhao et al., 2020) (Figure 2B). The results of Mann-Kendall showed that an abrupt change in precipitation occurred in 1991 (Figure 2D). After the sudden change, the multi-year average annual precipitation increased by 29.48 mm. The cumulative anomaly analysis showed that the annual precipitation in XJ experienced a decreasing trend from 1960 to 1986 and an increasing trend from 1987 to 2019, with 1986 being the turning point (Figure 2F). Considering the results of the two methods, the annual precipitation was concluded to have changed abruptly in the mid-late 1980s.

Temperature and precipitation in XJ showed significant increasing trends in all seasons. The warming rates for the four seasons were 0.36°C/10 a, 0.24°C/10 a, 0.32°C/10 a and 0.37°C/10 a, respectively, all of which have passed the significance test at the 99% significance level (Table 1). The most significant warming trend in XJ occurred in winter.

TABLE 1 Variation trends of annual and seasonal temperature in XJ and its sub-regions (°C/10 a), and the results of significance tests.

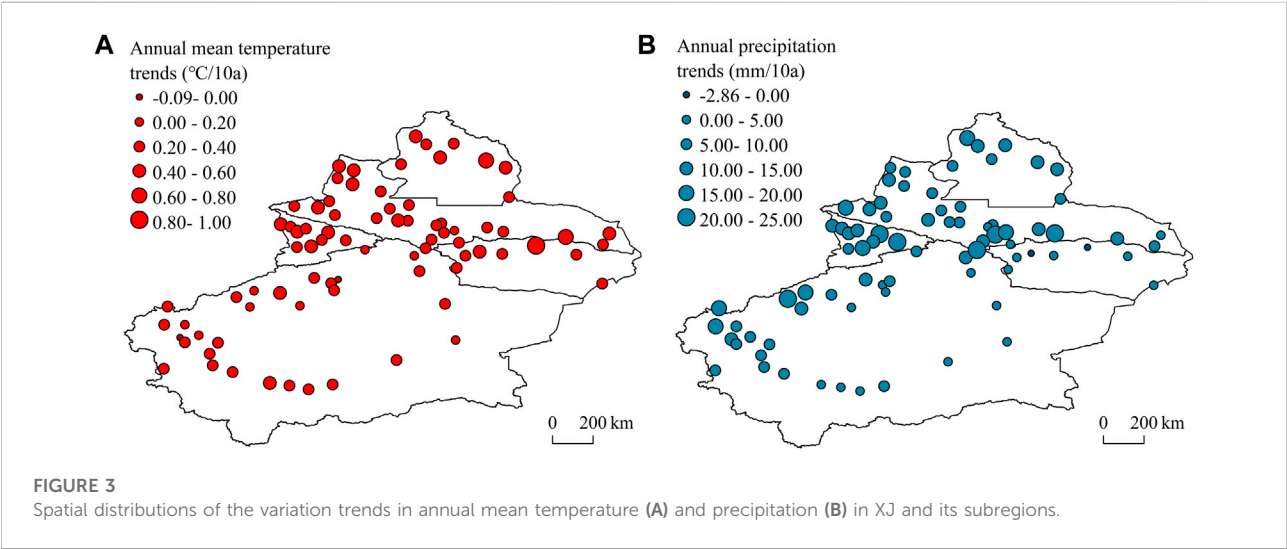
Name	Annual		Spring		Summer		Autumn		Winter	
	a	r	a	r	a	r	a	r	a	r
XJ	0.32	0.74**	0.36	0.53**	0.24	0.70**	0.32	0.57**	0.37	0.41**
IRB	0.41	0.64**	0.45	0.43**	0.31	0.61**	0.39	0.46**	0.51	0.39**
NSTM	0.33	0.66**	0.38	0.44**	0.26	0.64**	0.35	0.50**	0.32	0.31*
ILRB	0.41	0.73**	0.43	0.53**	0.35	0.74**	0.34	0.53**	0.50	0.43**
THB	0.42	0.81**	0.43	0.59**	0.35	0.68**	0.43	0.65**	0.47	0.54**
TRB	0.24	0.71**	0.29	0.56**	0.14	0.42**	0.24	0.58**	0.31	0.41**

*Significant at $p < 0.05$; **significant at $p < 0.01$.

TABLE 2 Variation trends of annual and seasonal precipitation in XJ and its sub-regions (mm/10 a), and the results of significance tests.

Name	Annual		Spring		Summer		Autumn		Winter	
	a	r	a	r	a	r	a	r	a	r
XJ	9.24	0.53**	1.82	0.28*	3.48	0.41**	2.11	0.41**	1.84	0.51**
IRB	10.51	0.44**	2.25	0.28*	2.53	0.20	2.68	0.35**	3.05	0.35**
NSTM	10.81	0.46**	3.03	0.31*	2.96	0.26*	2.40	0.34**	2.50	0.50**
ILRB	14.03	0.34**	1.94	0.11	3.78	0.21	3.44	0.25	4.45	0.45**
THB	1.11	0.20	0.49	0.22	0.29	0.08	0.15	0.07	0.18	0.18
TRB	8.00	0.53**	0.90	0.17	4.76	0.48**	1.77	0.34**	0.57	0.24

*Significant at $p < 0.05$; **significant at $p < 0.01$.



Among the subregions, the most significant warming trend was observed in the THB. In spring, the most significant warming occurred in the IRB; in summer, it was in the

ILRB and THB; in autumn, it was in the THB; and in winter, it was in the IRB. The wetting rates in XJ in the four seasons were 1.82, 3.48, 2.11, and 1.84 mm/10 a,

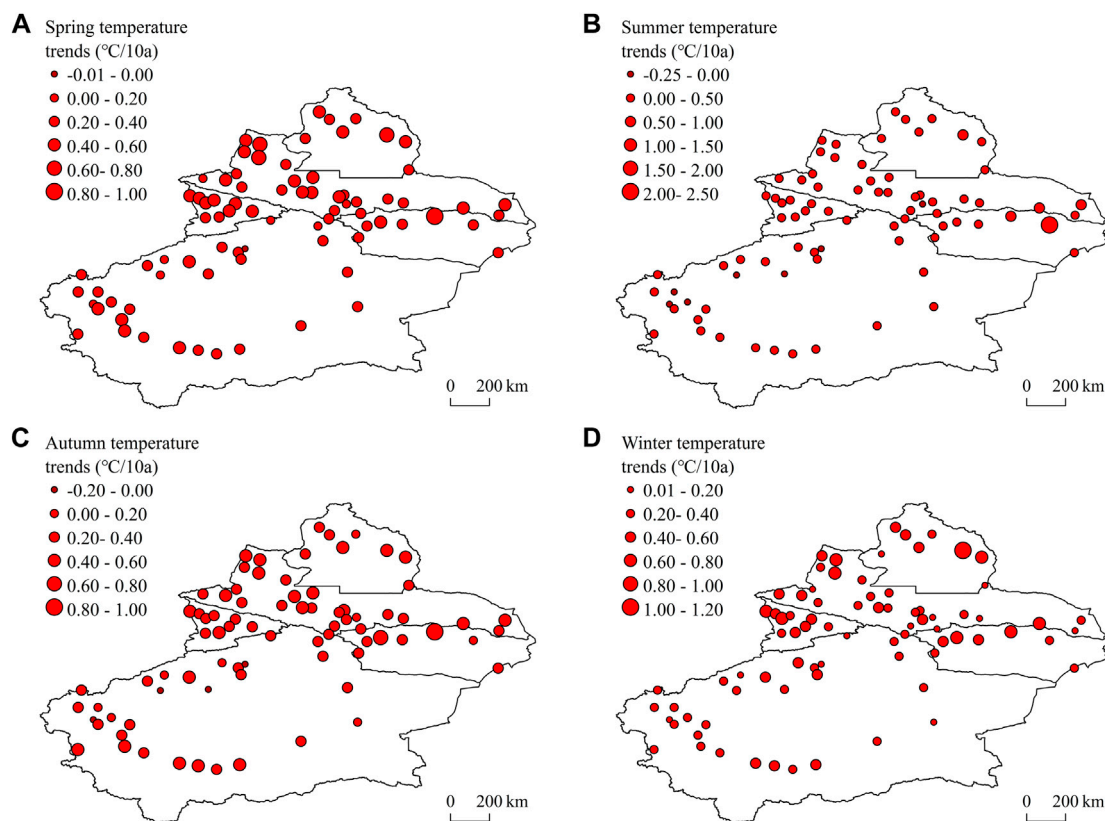


FIGURE 4
Variation trends in temperature during different seasons (A–D) in XJ and its subregions.

respectively. The wetting trends of all seasons passed the significance test at the 99% significance level (Table 2). The maximum increase in precipitation in XJ occurred in the summer. The subregion with the most significant increasing trend in annual precipitation was IRB. The increasing trend of precipitation was remarkable in the NSTM during spring, TRB during summer, and IRB during autumn and winter.

Spatial distributions of the variation trends in temperature and precipitation in XJ

More than 98% of the stations in XJ showed warming and wetting trends from 1960 to 2019. The subregions with significant warming were concentrated in IRB, NSTM, ILRB, and THB (Figure 3A). The warming trend was most pronounced at the Shisanjianfang station of the THB, with a warming rate of $0.82^{\circ}\text{C}/10\text{ a}$. The Kuqa and Aketao stations in the TRB showed a decreasing trend in temperature with variation rates of $-0.09^{\circ}\text{C}/10\text{ a}$ and $-0.03^{\circ}\text{C}/10\text{ a}$, respectively. The increase in precipitation was more pronounced in the IRB, NSTM, ILRB, and western

regions of the TRB (Figure 3B). The most significant precipitation increase was observed in Urumqi on the NSTM, with a wetting rate of $24.95\text{ mm}/10\text{ a}$. The precipitation in Shisanjianfang and Turpan stations in THB showed a decreasing trend, with variation rates of -2.86 and $-0.31\text{ mm}/10\text{ a}$, respectively.

Obvious regional differences were observed in seasonal warming in the sub-regions of XJ. In spring, summer, and autumn, the warming rate was the highest in the IRB. In winter, the greatest warming occurred mainly in the ILRB and THB. In terms of spatial differences, the most significantly warmed areas were mainly in the THB. The greatest warming rates were recorded at Shisanjianfang station in the THB ($0.84^{\circ}\text{C}/10\text{ a}$ and $0.90^{\circ}\text{C}/10\text{ a}$, respectively) in spring and autumn (Figure 4A,C); Hami ($2.26^{\circ}\text{C}/10\text{ a}$) in summer (Figure 4B); and Fuyun station in the IRB ($1.11^{\circ}\text{C}/10\text{ a}$) in winter (Figure 4D).

Regional differences in precipitation were also noted among the sub-regions of XJ. In summer, autumn, and winter, the largest wetting rates were observed in the ILRB. In summer, the subregions with the greatest precipitation increase were mainly in the ILRB and western TRB. In terms of stations, the most

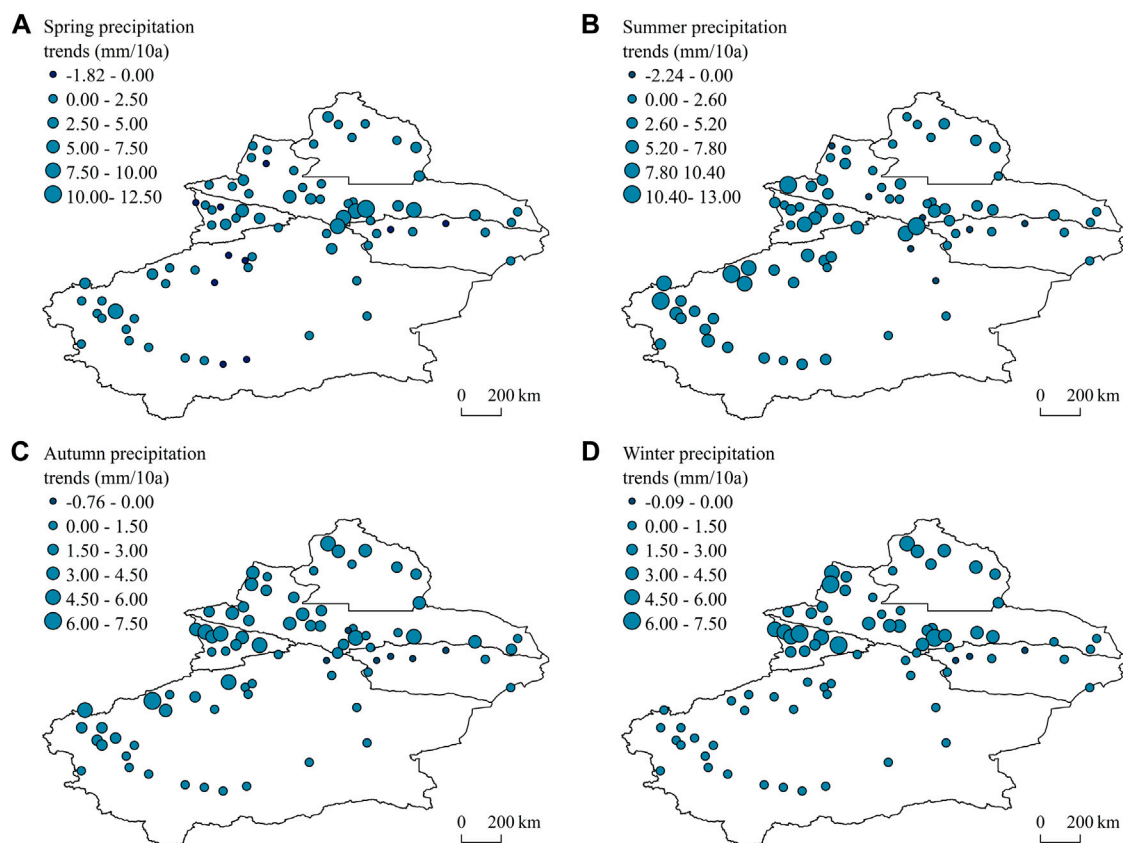


FIGURE 5

Variation trends in precipitation during different seasons (A–D) in XJ and its subregions.

significant precipitation increase was mainly in the NSTM. In summer (Figure 5B), the largest wetting rate was observed at Daxigou station (12.89 mm/10 a); in spring (Figure 5A), at Tianchi station (10.75 mm/10 a); in autumn (Figure 5C), at Aheqi station (7.16 mm/10 a) in the TRB; and in winter (Figure 5D), at Yining (6.84 mm/10 a) in the ILRB.

Trend prediction of potential climate change in XJ

The aforementioned analysis shows significant increasing trends of both annual mean temperature and annual precipitation in XJ and its subregions over the last 60 years. The results of the R/S analysis indicate that the Hurst indices of the annual mean temperature and precipitation in XJ and the subregions are both <0.5 , presenting a decreasing trend in the future (Table 3). In the five subregions of XJ, the most significant decrease in annual mean temperature is predicted in the TRB, and the most significant decrease in annual precipitation is predicted in the THB. Analysis of the Hurst index indicates that warming and wetting in XJ will slow down in the future.

Cross-wavelet analysis of the climate change and atmospheric circulation indices

The key atmospheric circulation indices affecting climate change in XJ were selected by analyzing the correlations of temperature and precipitation with the atmospheric circulation indices (Table 4). The results showed that the subtropical high, polar vortex, Tibetan Plateau index, and other related circulation indices had significant effects on climate change in XJ. The indices with the most significant correlation and physical significance were selected. Temperature showed a significant and positive correlation with the area index of the subtropical high over North Africa, Atlantic, and North America (AISHNA) and its intensity index (IISHNA) (Figure 6A), whereas it was significantly and negatively correlated with the area index of the Asia polar vortex (AIAPV) and its intensity index (IIAPV) (Figure 6B). The annual precipitation showed a significant and positive correlation with the index of the Tibetan Plateau Region 1 (ITPR 1) (Figure 6C), and a significant and negative

TABLE 3 Hurst indexes of climate change in XJ.

Name	Annual average temperature			Annual precipitation		
	Hurst index	Anti-persistence	Future trends	Hurst index	Anti-persistence	Future trends
XJ	0.36	weak	decrease	0.30	weak	decrease
IRB	0.33	weak	decrease	0.29	strong	decrease
NSTM	0.36	weak	decrease	0.28	strong	decrease
ILRB	0.34	weak	decrease	0.28	strong	decrease
THB	0.41	weak	decrease	0.15	strong	decrease
TRB	0.29	strong	decrease	0.30	weak	decrease

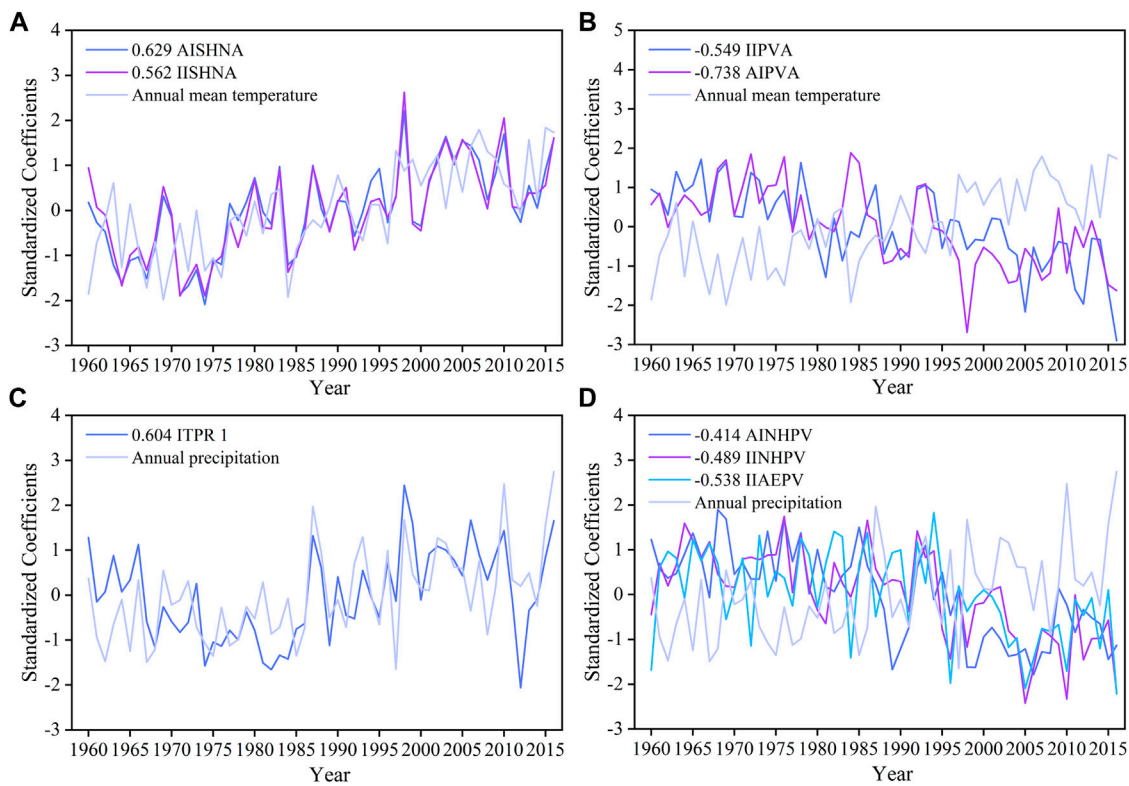


FIGURE 6 Time series of the key atmospheric circulation indices and annual mean temperature (A,B) and precipitation (C,D) in XJ.

correlation with the intensity index of the Atlantic-European Polar Vortex (IIAEPV), the area index of the Northern Hemisphere Polar Vortex (AINHPV) and its intensity index (IINHPV) (Figure 6D).

Cross-wavelet analysis was performed to reveal the relationships between temperature/precipitation variations and key atmospheric circulation indices, such as subtropical high,

polar vortex, and Tibet Plateau. Moreover, multi-timescale correlations between climate change and contemporaneous atmospheric circulation are discussed. The XWTs of temperature to AISHNA and IISHNA were consistent, both showing a significant resonance period at 1.5–4 a, which passed the significance test in 1980–1999 (Figures 7A, C). The WTC revealed that the significance of the two is greater in the

TABLE 4 Correlation coefficients of the climate change in XJ to atmospheric circulation factors.

Atmospheric circulation factors		Temperature	Atmospheric circulation factors	Precipitation
the area index of the subtropical high over North Africa, Atlantic, and North America (AISHNA)		0.629	the index of the Tibet Plateau Region 1 (ITPR 1)	0.604
the intensity index of the subtropical high over North Africa, Atlantic, and North America (IISHNA)		0.562	the intensity index of the Northern Hemisphere Subtropical High (IINHSH)	0.588
the index of the Tibet Plateau Region 2 (ITPR 2)		0.530	the intensity index of the India-Burma trough (IIBT)	0.582
the index of the Atlantic and Europe pattern C (IAEP C)		0.502	the area index of the Northern Hemisphere Subtropical High (AINHSH)	0.570
the intensity index of the India-Burma trough (IIBT)		0.478	the index of the Atlantic and Europe pattern E (IAEP E)	0.413
the index of the Eurasian Zonal Circulation (IEZC)		0.393	the area index of the Northern Hemisphere Polar Vortex (AINHPV)	−0.414
the intensity index of the Asia polar vortex (IAPV)		−0.549	the intensity index of the Northern Hemisphere Polar Vortex (IINHPV)	−0.489
the area index of the Asia polar vortex (AIAPV)		−0.738	the intensity index of the Atlantic-European Polar Vortex (IAEPV)	−0.538

low-energy region than in the high-energy region, and the coherence in 1981–2002 was extremely strong at the quasi-4a scale (Figures 7B, D). The XWT of temperature to IIPVA showed that they have a significant resonance period at the quasi-2a scale and have passed the significance test in 1964–1969 and 1981–1985 (Figure 7E). The XWT of temperature to AIPVA demonstrated a significant resonance period at 8–10 a scale, and they have a significant negative correlation. The WCT of the two showed extremely strong correlations at the 3–5 a scale for 1978–1988 and 1990–2001, and at the 6.5–14 a scale for 1978–2003 (Figures 7G, H).

A positive-phase quasi-2a resonance period existed in the high-energy region of the XWT between the precipitation variations in the XJ and ITPR 1 (Figure 8A). The XWT of the precipitation variation in XJ to AINHPV had resonance periods of 2–3 and 1–2.5 a in the high-energy region (Figure 8C) and 1–3 and 6–7 a in the low-energy region (Figure 8D). In addition, the XWT of the precipitation variation in XJ to IIPVNH had negative-phase resonance periods at 2.5–4 and 1–3 a in the high-energy region (Figure 8E) and at 1–3 a resonance period in the low-energy region (Figure 8F). The XWT of the precipitation variation in XJ to IIAEPV had negative-phase resonance periods at 2–4 and 1–3 a (Figure 8G). The above analysis further confirmed that the variations in temperature and precipitation in XJ were closely related to the anomalies of key circulation indices such as the subtropical high, polar vortex, and Tibet Plateau. These results could provide an important reference for the prediction of climate change in XJ.

Discussions

This study further confirms the warming and wetting trends in XJ (Reziwanguli et al., 2016; Kang et al., 2018; Wu et al., 2020) and its subregions according to the watersheds. These subregions are consistent with the expedition zones of the Third XJ Scientific Expedition and Research Program implemented by the Ministry of Science and Technology of China in 2021. The climate change characteristics of each subregion are presented in detail in this study. The results revealed significant warming trends in the THB, IRB, ILRB, and NSTM, whereas the precipitation increased significantly in the ILRB, NSTM, and western TRB in southern XJ. The Hurst index analysis indicated that both temperature and precipitation will decrease in XJ in the future, and the decreasing rate of precipitation would be more pronounced. A warm-dry trend is speculated to appear in XJ in the future. It is consistent with the “wet–dry transition” of XJ proposed by Yao et al. (2018); Yao et al. (2022a), but not completely consistent with the

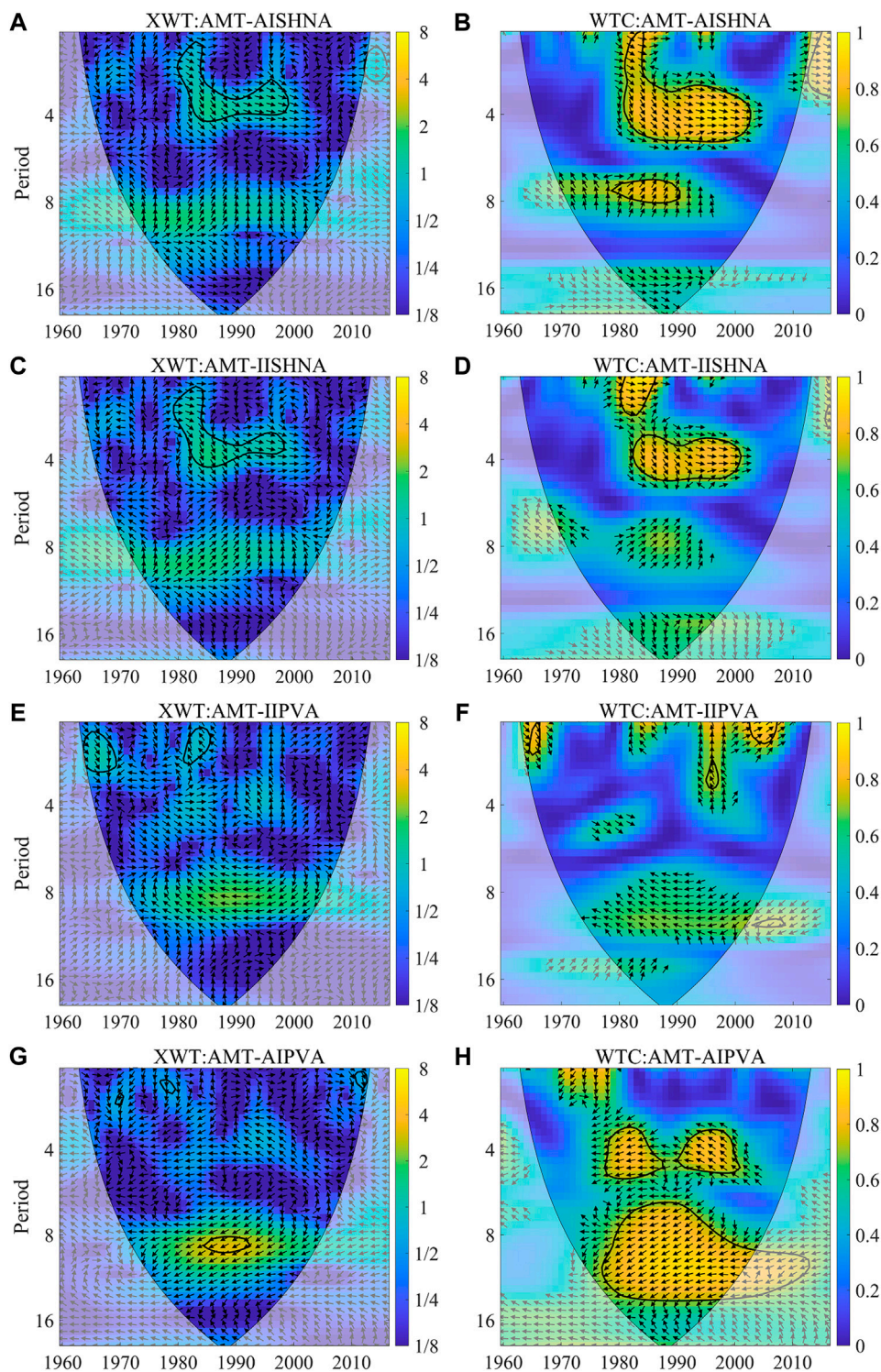


FIGURE 7
XWT and WTC of the annual mean temperature (A–H) in XJ to the area index of the subtropical high over North Africa, Atlantic, and North America (AISHNA), the intensity index of the subtropical high over North Africa, Atlantic, and North America (IISHNA), the intensity index of the polar vortex in Asia (IIPVA), and the index area of Asia polar vortex (AIPVA).

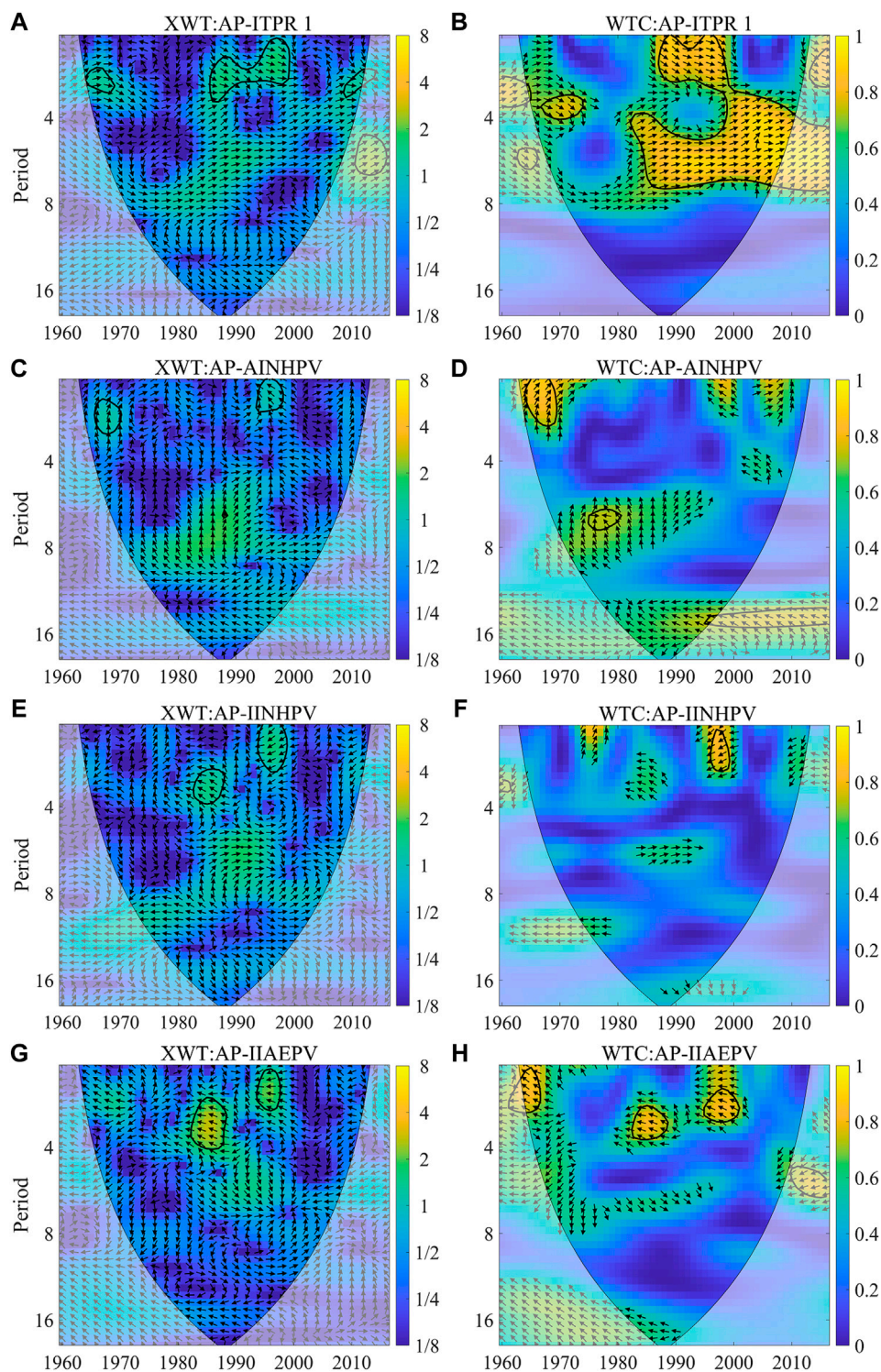


FIGURE 8
XWT and WTC of the annual precipitation (A–H) in XJ to the index of the Tibet Plateau Region 1 (ITPR 1), the area index of the Northern Hemisphere Polar Vortex (AINHPV), the intensity index of the Northern Hemisphere Polar Vortex (IINHPV), and the intensity index of the Atlantic-European PolarVortex (IIAEPV).

results reported by Guan et al. (2022), which were projected using CMIP6. Their results suggested that the extreme climate change in the 21st century will continue the change trend from 1961 to 2014, that is, both extreme warm and precipitation events will increase (Guan et al., 2022). The uncertainty of future climate change remains owing to anomalous changes in future atmospheric circulation indices.

XJ is in the mid-latitude region of the Northern Hemisphere and is mainly influenced by changes in mid-high latitude atmospheric circulation systems (Yao et al., 2022a). The polar vortex is the main atmospheric circulation system that dominates the Northern Hemisphere in winter. In last 60 years, the interdecadal variation in the polar vortex has been evident, and it has significantly decreased in size and intensity since the 1980s. The area and intensity index of the Asia polar vortex are closely related to the temperature in Central Asia, and the weakening of the Asian polar vortex and the reduction in its area are among the reasons for the changes in temperature in Central Asia (Yao et al., 2014). The polar vortex in the Northern Hemisphere also has a strong correlation with winter temperature in XJ. The winter temperature is high when the polar vortex index is low (Shen et al., 2012; Zhang et al., 2020). The strong westerly winds in the Northern Hemisphere are accompanied by a decrease in the meridional degree of mid- and high-latitude circulations, which may lead to high average winter temperatures in XJ (Chen et al., 2019). The increase in winter temperature contributes to warming in XJ. The IRB is in a high-latitude area and is close to the influence area of polar vortex activity, which leads to fast winter warming in the IRB. The findings of this study further confirm the periodic correlation between the polar vortex and temperature in XJ at multiple timescales, which can provide a reference for temperature forecasting and prediction in XJ.

The atmospheric circulation indices affecting the precipitation change in XJ and the physical mechanisms involved are complex. The precipitation change in XJ is not only influenced by the polar vortex activities at high latitudes but is also related to the low latitude circulation and the thermal-dynamical effects of the Tibetan Plateau (Zhao et al., 2018). A significant negative correlation was found between the Atlantic–European polar vortex area and summer precipitation in the TRB. When the polar vortex is small, the westerly jet weakens in central and western Asia, and the TRB experiences more summer precipitation (Li et al., 2017). The West Asia westerly jet connects the high-, mid-, and low-latitude circulation systems. summer precipitation in XJ is influenced by the North Atlantic oscillation and Indian monsoons. When the West Asia westerly jet weakens, summer precipitation in XJ tends to increase (Yang et al., 2018). The TPI is large in May, and the

low-latitude circulation configuration and water vapor transport favor precipitation in northern XJ (Zhou et al., 2018).

Based on an analysis of climate change characteristics and future trends in XJ, this study investigated the correlation between atmospheric circulation indices and climate factors. However, the multi-model ensembles in CMIP6 should be used in future studies to predict future climate change under the scenarios of human socio-economic changes and to analyze the hazard risks arising from future climate change. Atmospheric circulation indices have complex effects on climate change. Therefore, future climate change in XJ will have different responses to global warming. The formation and evolution mechanisms and degree of impact of extreme climate events caused by atmospheric circulation anomalies need to be further studied.

Conclusion

Based on the observation data from 80 meteorological stations in XJ, this study analyzed the climate change in XJ and its five subregions and explored the relationships between climate change in XJ and atmospheric circulation indices. The main results are as follows: The annual mean temperature in XJ showed an increasing trend from 1960 to 2019, with a warming rate of $0.32^{\circ}\text{C}/10\text{ a}$, and an abrupt change occurring in 1994–1996. The temperature also increased during all seasons, with the greatest warming occurring in winter. Significant warming trends were recorded in the THB, IRB, ILRB, and NSTM. The Hurst Index indicated that the annual mean temperature in XJ will show a weak decreasing trend in the future.

The precipitation in XJ showed an increasing trend from 1960 to 2019, with a wetting rate of $9.24\text{ mm}/10\text{ a}$, and an abrupt change occurring in 1986–1991. The precipitation in XJ also showed an increasing trend in all four seasons, with the greatest increase in summer. Precipitation increased significantly in the ILRB, NSTM, and the western side of the TRB in southern XJ. Analysis of the Hurst Index indicated a strong decreasing trend in annual precipitation, with the greatest decrease in the THB.

The subtropical high, Northern Hemisphere polar vortex activities, and the Tibetan Plateau have a significant impact on climate change in XJ. The annual mean temperature in XJ was positively correlated with AISHNA and IISHNA, and negatively correlated with AIPVA and IIPVA. Moreover, their resonance periods were 1.5–4, 1.5–4, 1–2.5, and 8–10 a, respectively. The XJ annual precipitation was positively correlated with the ITPR 1, and negatively correlated with the IIAEPV, IINHPV, and AINHPV, with the resonance periods at 1–3.5, 1–2.5, 2.5–4, and 2–4 a, respectively.

Data availability statement

The original contributions presented in the study are included in the article/supplementary material, further inquiries can be directed to the corresponding authors.

Author contributions

GZ performed the analysis and wrote the manuscript. YC reviewed and edited the manuscript. JY contributed to the conception and design of the study, visualization and reviewed the manuscript.

Funding

This work was funded by the National Natural Science Foundation of China (U1903113, 42171038); and the Third

Xinjiang Scientific Expedition Program (Grant No. 2022xjkk0101).

Conflict of interest

The authors declare that the research was conducted in the absence of any commercial or financial relationships that could be construed as a potential conflict of interest.

Publisher's note

All claims expressed in this article are solely those of the authors and do not necessarily represent those of their affiliated organizations, or those of the publisher, the editors and the reviewers. Any product that may be evaluated in this article, or claim that may be made by its manufacturer, is not guaranteed or endorsed by the publisher.

References

- Chen, X., Luo, G. P., Xia, J., Zhou, K. F., Lou, S. P., and Ye, M. Q. (2005). Ecological response to the climate change on the northern slope of the Tianshan Mountains in Xinjiang. *Sci. China Ser. D-Earth Sci.* 48, 765–777. doi:10.1360/04yd0050
- Chen, Y., and Jiazila, B. (2019). Annual variation of winter temperature and its causes in Xinjiang. *Arid. Land Geo* 42 (2), 223–231. doi:10.12118/j.issn.1000-6060.2019.02.01
- Chen, Y. N., Li, Z., Fan, Y. T., Wang, H. J., and Fang, G. H. (2014). Research progress on the impact of climate change on water resources in the arid region of Northwest China. *Acta. Geogr. Sin.* 69 (9), 1295–1304. doi:10.11821/dlxb201409005
- Chen, Y. N., Li, Zhi., Fan, Y. T., Wang, H. J., and Deng, H. J. (2015). Progress and prospects of climate change impacts on hydrology in the arid region of northwest China. *Environ. Res.* 139, 11–19. doi:10.1016/j.envres.2014.12.029
- Deng, H., Pepin, N. C., Chen, Y., Guo, B., Zhang, S., Zhang, Y., et al. (2022). Dynamics of diurnal precipitation differences and their spatial variations in China. *J. Appl. Meteorol. Clim.* 61 (8), 1015–1027. doi:10.1175/JAMC-D-21-0232.1
- Ding, Z. Y., Lu, R. J., Liu, C., and Duan, C. X. (2018). Temporal change characteristics of climatic and its relationships with atmospheric circulation patterns in Qinghai Lake Basin. *Adv. Earth Sci.* 33 (3), 281–292. doi:10.11867/j.issn.1001-8166.2018.03.0281
- Duan, A. M., Wu, G. X., Liu, Y. M., Ma, Y. M., and Zhao, P. (2012). Weather and climate effects of the Tibetan plateau. *Adv. Atmos. Sci.* 29 (5), 978–992. doi:10.1007/s00376-012-1220-y
- Fang, S., Pei, H., Liu, Z. H., Keith, B., and Wei, Z. C. (2010). Water resources assessment and regional virtual water potential in the turpan basin, China. *Water Resour. Manage* 24, 3321–3332. doi:10.1007/s11269-010-9608-x
- Fang, X., Liu, X. K., and Yue, D. P. (2022). Analysis of climate change characteristics and influencing factors in Mu Us sandy land from the 1960–2018. *Res. Soil Water Conserv.* 29 (2), 163–169.
- Grinsted, A., Moore, J. C., and Jevrejeva, S. (2004). Application of the cross wavelet transform and wavelet coherence to geophysical time series. *Nonlinear Proc. Geoph.* 11 (5/6), 561–566. doi:10.5194/npg-11-561-2004
- Guan, J., Yao, J., Li, M., Li, D., and Zheng, J. (2022). Historical changes and projected trends of extreme climate events in Xinjiang, China. *China. Clim. dynam.* 59 (5–6), 1753–1774. doi:10.1007/s00382-021-06067-2
- Hu, W., Yao, J., He, Q., and Chen, J. (2021). Changes in precipitation amounts and extremes across Xinjiang (northwest China) and their connection to climate indices. *PeerJ* 9, e10792. doi:10.7717/peerj.10792
- IPCC (2022). *Climate change 2022: Impacts, adaptation and vulnerability. Summary for policymakers*. Cambridge, UK: Cambridge University Press.
- Jiang, T., Zhai, J. Q., Luo, Y., Su, B. D., Chao, Q. C., Wang, Y. J., et al. (2022). Understandings of assessment reports on climate change impacts, adaptation and vulnerability: Progress from IPCC AR5 to IPCC AR6. *Trans. Atmos. Sci.* 45 (4), 502–511. doi:10.13878/j.cnki.dqkxb.20220529013
- Kang, L. J., Batur, B., Luo, N. N., Xue, Y. R., and Wang, M. H. (2018). Spatial-temporal variations of temperature and precipitation in Xinjiang from 1961 to 2013. *Xinjiang Agric. Sci.* 55 (1), 123–133. doi:10.6048/j.issn.1001-4330.2018.01.014
- Li, H. J., and Ma, Y. F. (2017). Impacts of the regional north polar vortex anomalies on summer precipitation of the Tarim river basin. *J. Appl. Meteor. Sci.* 28 (05), 589–599. doi:10.11898/1001-7313.20170507
- Li, Q. H., Chen Y. N., Shen, Y. J., Li, X. G., and Xu, J. H. (2011). Spatial and temporal trends of climate change in Xinjiang, China. *J. Geogr. Sci.* 21 (6), 1007–1018. doi:10.1007/s11442-011-0896-8
- Li, W. H., Li, L. F., Ting, M. F., and Li, Y. M. (2012). Intensification of Northern Hemisphere subtropical highs in a warming climate. *Nat. Geosci.* 5, 830–834. doi:10.1038/ngeo1590
- Liu, J. Q., and Wu, S. L. (2017). Variation characteristics of diurnal temperature and influence factor of Irtysh river in Xinjiang. *J. Soil Water Conserv.* 31 (4), 351–356. doi:10.13870/j.cnki.stbcb.2017.04.055
- Liu, L., Guan, J. Y., Mu, C., Han, W. Q., Qiao, X. L., and Zheng, J. H. (2022). Spatio-temporal characteristics of vegetation net primary productivity in the Ili River Basin from 2008 to 2018. *Acta Ecol. Sin.* 42 (12), 4861–4871. doi:10.5846/stxb202104251084
- Liu, L., Zhang, W. J., Lu, Q. F., and Wang, G. X. (2020a). Variations in the sensible heating of Tibetan plateau and related effects on atmospheric circulation over south Asia. *Asia-Pac. J. Atmos. Sci.* 57 (3), 499–510. doi:10.1007/s13143-020-00207-0
- Liu, Y. J., Wei, Z. G., Chen, G. Y., Liu, Y. J., Zhu, X., and Zheng, Z. Y. (2020b). Shift of the Arctic polar vortex in recent decades and its simulation by the NCEP CFSv2. *Phys. Chem. Earth.* 115, 102823. doi:10.1016/j.pce.2019.102823
- Liu, Y. T., Xue, G. L., Yang, Z., Ren, X. Z., Yang, X. C., and Li, A. J. (2021). Variation of extreme temperature and its association with climate indices in Anhui province during the past 56 year. *Res. Soil Water Conserv.* 28 (2), 248–255. doi:10.13869/j.cnki.rswc.2021.02.035
- Ren, Y., Yu, H., Liu, C., He, Y., Huang, J., Zhang, L., et al. (2022). Attribution of dry and wet climatic changes over central Asia. *J. Clim.* 35 (5), 1399–1421. doi:10.1175/JCLI-D-21-0329.1
- Reziwanguli, M., Yang, J. J., Liu, Y. Q., Guo, Y. C., and He, X. M. (2016). Characteristics of changes in temperature and precipitation in Xinjiang in recent 54 years. *Res. Soil Water Conserv.* 23 (2), 128–133. doi:10.13869/j.cnki.rswc.2016.02.024

- Shen, B. Z., Lian, Y., Zhang, S. X., and Li, S. F. (2012). Impacts of arctic oscillation and polar vortex anomalies on winter temperature over Eurasian continent. *Adv. Clim. Change Res.* 8 (6), 434–439. doi:10.3969/j.issn.1673-1719.2012.06.007
- Sun, G. L., Lu, H. Y., Yu, M. Z., Yan, X. R., Zhen, X., and Zhang, Y. M. (2022). Ecological vulnerability spatial-time distribution and driving forces analysis in the economic belt on the northern slope of Tianshan Mountains. *Southwest China J. Agric. Sci.* 1–12. [2022-10-20].
- Wang, D., Zhang, S., Wang, G., Liu, Y., Wang, H., and Gu, J. (2022). Reservoir regulation for ecological protection and remediation: A case study of the Irtysh River Basin, China. *Int. J. Environ. Res. Public Health*. 19, 11582. doi:10.3390/ijerph191811582
- Wang, Z. Q., Gao, X. J., Tong, Y., Han, Z. Y., and Xu, Y. (2021). Future climate change projection over Xinjiang based on an ensemble of regional climate model simulations. *Chin. J. Atmos. Sci.* 45 (2), 407–423. doi:10.3878/j.issn.1006-9895.2006.20108
- Wu, X. L., Zhang, T. X., Wang, H., Yu, X. J., Zheng, X. N., and Li, H. Y. (2020). Characteristics of temperature and precipitation change in Xinjiang during 1961–2017. *Desert Oasis Meteor* 14 (4), 27–34. (in Chinese). doi:10.12057/j.issn.1002-0799.2020.04.004
- Xue, L. Q., Bai, Q. Y., and Lui, Y. H. (2022). Study on the Propagation of meteorological-hydrological drought in Tarim River Basin under the impact of human activities. *Water Resour. Prof.* 1–10. [2022-10-22].
- Yang, L. M., Guan, X. F., and Zhang, Y. X. (2018). Atmospheric circulation characteristics of precipitation anomaly in arid regions in central Asia. *Arid. Zone Res.* 35 (2), 249–259. doi:10.13866/j.azr.2018.02.01
- Yao, J. Q., Chen, Y. N., Guan, X. F., Zhao, Y., Chen, J., and Mao, W. Y. (2022a). Recent climate and hydrological changes in a mountain-basin system in Xinjiang, China. *Earth-sci Rev.* 226, 103957. doi:10.1016/j.earscirev.2022.103957
- Yao, J. Q., Chen, Y. N., Zhao, Y., Guan, X. F., Mao, W. Y., and Yang, L. M. (2020). Climatic and associated atmospheric water cycle changes over the Xinjiang, China. *J. Hydrol.* 585, 124823. doi:10.1016/j.jhydrol.2020.124823
- Yao, J. Q., Li, M. Y., Tuoliewubieke, D., Chen, J., and Mao, W. Y. (2022b). The assessment on "warming-wetting" trend in Xinjiang at multi-scale during 1961–2019. *Arid. Zone Res.* 39 (2), 333–346. doi:10.13866/j.azr.2022.02.01
- Yao, J. Q., Liu, Z. H., Yang, Q., Liu, Y., Li, C. Z., and Hu, W. F. (2014). Temperature variability and its possible causes in the typical basins of the arid Central Asia in recent 130 years. *Acta. Geogr. Sin.* 69 (3), 291–302. doi:10.11821/dlxb201403001
- Yao, J. Q., Mao, W. Y., Chen, J., and Tuoliewubieke, D. (2021). Signal and impact of wet-to-dry shift over Xinjiang, China. *Acta. Geogr. Sin.* 76 (1), 57–72. doi:10.11821/dlxb202101005
- Yao, J., Zhao, Y., Chen, Y., Yu, X., and Zhang, R. (2018). Multi-scale assessments of droughts: A case study in Xinjiang, China. *Sci. Total Environ.* 630, 444–452. doi:10.1016/j.scitotenv.2018.02.200
- Zhang, H. D., Jin, R. H., and Zhang, Y. S. (2008). Relationships between summer northern polar vortex with sub-tropical high and their influence on precipitation in north China. *J. Trop. Meteorol.* 4, 417–422.
- Zhang, T. X., Jiang, Y. A., Fan, J., Liu, J., and Yu, X. J. (2020). Analysis of cold air process activity in northern Xinjiang during 1961–2016 and the atmospheric circulation index. *Desert Oasis Meteor* 14 (5), 107–114. doi:10.12057/j.issn.1002-0799.2020.05.014
- Zhang, Y., An, C. B., Liu, L. Y., Zhang, Y. Z., Lu, C., and Zhang, W. S. (2021). High mountains becoming wetter while deserts getting drier in Xinjiang, China since the 1980s. *Land* 10 (11), 1131. doi:10.3390/land10111131
- Zhao, D. S., Gao, X., Wu, S. H., and Zheng, D. (2020). Trend of climate variation in China from 1960 to 2018 based on natural regionalization. *Adv. Earth Sci.* 35 (7), 750–760. doi:10.11867/j.issn.1001-8166.2020.056
- Zhao, Y., Wang, Q., and Huang, A. N. (2018). Relationship between Iran high pattern of south Asia high and summer precipitation in Xinjiang. *Plateau Meteor* 37 (3), 651–661. doi:10.7522/j.issn.1000-0534.2017.00049
- Zhou, Y. M., Li, N., Ma, C., An, D. W., and Shi, J. J. (2018). The relationship between circulation over Tibetan plateau in May with summer precipitation over northern Xinjiang. *Desert Oasis Meteor* 12 (5), 39–45. doi:10.12057/j.issn.1002-0799.2018.05.006



OPEN ACCESS

EDITED BY
Shaoquan Liu,
Institute of Mountain Hazards and
Environment (CAS), China

REVIEWED BY
Daniel Fiifi Tawia Hagan,
Nanjing University of Information Science
and Technology, China
Lei Zhang,
South China Sea Institute of Oceanology
(CAS), China

*CORRESPONDENCE
Mohammad Kamruzzaman,
✉ milonbri@gmail.com
Abu Reza Md. Towfiqul Islam,
✉ towfiq_dm@brur.ac.bd

[†]These authors contributed equally to this
work and share first authorship

SPECIALTY SECTION
This article was submitted
to Atmosphere and Climate,
a section of the journal
Frontiers in Environmental Science

RECEIVED 20 October 2022
ACCEPTED 19 December 2022
PUBLISHED 06 January 2023

CITATION
Islam HMT, Kamruzzaman M, Shahid S,
Mainuddin M, Alam E, Islam ARMT,
Biswas JC and Islam MA (2023),
Spatiotemporal changes in temperature
projections over Bangladesh using multi-
model ensemble data.
Front. Environ. Sci. 10:1074974.
doi: 10.3389/fenvs.2022.1074974

COPYRIGHT
© 2023 Islam, Kamruzzaman, Shahid,
Mainuddin, Alam, Islam, Biswas and Islam.
This is an open-access article distributed
under the terms of the [Creative Commons
Attribution License \(CC BY\)](#). The use,
distribution or reproduction in other
forums is permitted, provided the original
author(s) and the copyright owner(s) are
credited and that the original publication in
this journal is cited, in accordance with
accepted academic practice. No use,
distribution or reproduction is permitted
which does not comply with these terms.

Spatiotemporal changes in temperature projections over Bangladesh using multi-model ensemble data

H. M. Touhidul Islam^{1†}, Mohammad Kamruzzaman ^{2*†},
Shamsuddin Shahid³, Mohammed Mainuddin⁴, Edris Alam^{5,6},
Abu Reza Md. Towfiqul Islam^{1*}, Jatish Chandra Biswas⁷ and
Md. Azharul Islam⁸

¹Department of Disaster Management, Begum Rokeya University, Rangpur, Bangladesh, ²Farm Machinery and Postharvest Technology Division, Bangladesh Rice Research Institute, Gazipur, Bangladesh, ³School of Civil Engineering, Universiti Teknologi Malaysia (UTM), Johor, Malaysia, ⁴CSIRO Land and Water, Canberra, ACT, Australia, ⁵Faculty of Resilience, Rabdan Academy, Abu Dhabi, United Arab Emirates, ⁶Department of Geography and Environmental Studies, University of Chittagong, Chittagong, Bangladesh, ⁷Krishi Gobeshona Foundation (KGF), Bhabha Atomic Research Centre, Dhaka, Bangladesh, ⁸Department of Environmental Science, Bangladesh Agricultural University, Mymensingh, Bangladesh

Temperature rise is a concern for future agriculture in different regions of the globe. This study aimed to reveal the future changes and variabilities in minimum temperature (Tmin) and maximum temperature (Tmax) in the monthly, seasonal, and annual scale over Bangladesh using 40 General Circulation Models (GCMs) of Coupled Model Intercomparison Project Phase 5 (CMIP5) for two radiative concentration pathways (RCPs, RCP4.5 and RCP8.5). The statistical downscaling climate model (SimCLIM) was used for downscaling and to ensemble temperature projections (Tmax and Tmin) for the near (2021–2060) and far (2071–2100) periods compared to the base period (1986–2005). Multi-model ensemble (MME) exhibited increasing Tmax and Tmin for all the timescales for all future periods and RCPs. Sen's slope (SS) analysis showed the highest increase in Tmax and Tmin in February and relatively less increase in July and August. The mean annual Tmax over Bangladesh would increase by 0.61°C and 1.75°C in the near future and 0.91°C and 3.85°C in the far future, while the mean annual Tmin would rise by 0.65°C and 1.85°C in the near future and 0.96°C and 4.07°C in the far future, for RCP4.5 and RCP8.5, respectively. The northern and northwestern parts of the country would experience the highest rise in Tmax and Tmin, which have traditionally been exposed to temperature extremes. In contrast, the southeastern coastal region would experience the least rise in temperature. A higher increase in Tmin than Tmax was detected for all timescales, signifying a future decrease in the diurnal temperature range (DTR). The highest increase in Tmax and Tmin will be in winter compared to other seasons for both the periods and RCPs. The spatial variability of Tmax and Tmin changes can be useful for the long-term planning of the country.

KEYWORDS

temperature projection, minimum and maximum temperature, Bangladesh, statistical downscaling, SimCLIM

1 Introduction

Temperature is an important factor in determining the effects of climate change (CC) on the globe or on the region of interest (Almazroui et al., 2020b). Since 1850, the earth's temperature has risen significantly (Ozturk et al., 2018; Wang et al., 2021). This has altered the frequency, severity, duration, timing, and spatial variability of temperature extremes (Islam A. R. M. T. et al., 2021; Pérez et al., 2021; Mallick et al., 2022a), and significantly impacted ecological instability, public health, agricultural production, water supplies, and socioeconomic progress (Allen et al., 2010; Islam H. M. T. et al., 2021; Mallick et al., 2022b). Even if all countries reduce greenhouse gas (GHG) emissions committed in the Paris Agreement, the earth's average temperature will increase by 2.6°C–4.8°C in 2100 (Wang et al., 2021). Hence, it is of absolute necessity to examine future temperature projections to reduce global warming consequences and for strategic planning of CC adaptations.

GCMs are used to project temperature globally. Different Coupled Model Intercomparison Projects (CMIPs) introduced many GCMs to examine future climate patterns. The CC assessment models have been updated significantly since CMIP3 (Song et al., 2021). The RCPs have lately been developed in CMIP5 to provide projections for different radiative forcings (Rahman and Rob, 2019). CMIP5 models have thoroughly outlined the earth system with high geospatial resolution and integrated physics (Almazroui et al., 2020a) and, therefore, shown better skill in climate projections than CMIP3 models (Song et al., 2021; Islam et al., 2022). GCMs have been extensively used for climate modeling (IPCC, 2014). However, they still cannot fully describe many regional climate dynamics because of their coarser resolution (Ali et al., 2021; Wang et al., 2021). Downscaling strategies, which can retrieve higher resolution data from coarse resolution datasets, are crucial for addressing this difficulty for regional or local scale climate modeling (Kamruzzaman et al., 2019b; Kamruzzaman et al., 2021a; Kamruzzaman et al., 2021b; Das et al., 2022a; Das et al., 2022b). Statistical Downscaling (SD) and Dynamic Downscaling (DD) are the two main approaches used for climate downscaling. The SD is frequently preferred because of its simplicity, cost, quick computations, and lower computational requirements (Rashid et al., 2015).

GCM projections are inherently coupled with uncertainty due to the modeling approach, initial condition, and future scenarios (Katzenberger et al., 2021). Moreover, an individual GCM cannot model all atmospheric processes and identify every climatic variation at a smaller scale with greater accuracy (Almazroui et al., 2020b; Ali et al., 2021). Therefore, multi-model ensembles (MME) of GCMs are usually suggested for climate modeling to address uncertainty and improve projection performance (Xu and Xu, 2012; Wang et al., 2021). A large number of studies have projected temperature based on MME of CMIP5 models at various scales (Almazroui et al., 2016; 2020a; Pattanayak et al., 2017; Amin et al., 2018a; Kumar and Sarthi, 2019; Ali et al., 2021). They found that the future temperature will increase, which might be attributed mostly to climatic diversity, geographical factors, and societal context (King et al., 2018). Hence, further research, particularly at the regional or national level, is required to assess the suitability of GCMs in temperature projection and provide ample and precise supplementation for the sensitivity of local or regional temperature variability to climatic changes.

Bangladesh is extremely vulnerable to CC due to its unique geographical location, poor infrastructure, low-lying topography,

and high population density (Huq, 2001). Understanding potential climatic change is essential for creating adaptation strategies and increasing resilience to CC. However, a few studies used CMIP5 models to assess future changes in temperature in Bangladesh for various CC scenarios (Alamgir et al., 2015; Hasan et al., 2018; Rahman and Rob, 2019; Bosu et al., 2021). Alamgir et al. (2019) projected Tmax and Tmin over Bangladesh using MME of eight CMIP5 GCMs. They projected an increase in Tmax by 1.3°C–4.3°C and Tmin by 1.8°C–5.1°C for different RCPs. They also projected the highest rise in Tmax and Tmin in the northern region and the lowest in the southeastern coastal region of Bangladesh. Hasan et al. (2018) utilized MME of five bias-correction CMIP5 regional climate models to project the climate extremes. They reported a higher increase in Tmax and Tmin in the southwest region than in other parts of Bangladesh. Earlier research was mostly concentrated on a limited number of GCMs or RCMs for monthly or annual Tmax and Tmin projections at the regional or national scale. Unfortunately, understanding the spatiotemporal trends and variations of future temperature changes at monthly, seasonal, and annual timescales is limited. Moreover, no extensive study has been conducted for temperature projections employing all existing CMIP5 GCMs at various time scales over Bangladesh. This study is expected to fill this gap.

This study used CMIP5 GCM temperature simulation to investigate probable temperature changes across Bangladesh. The main objectives of this research are i) to investigate the monthly, seasonal, and annual future Tmax and Tmin trends across Bangladesh for the near (2021–2060) and the far (2061–2100) periods based on the MME of 40 CMIP5 GCMs; ii) to examine the spatiotemporal variability and changes in future Tmax and Tmin over the country. The novelty of this study is that this is the first study using all available CMIP5 models to project temperature over Bangladesh. Furthermore, a pattern-scaling bias-correction technique based on the SimCLIM climate model has been adopted for the first time for temperature downscaling and projection in Bangladesh. The findings of this study will help design and develop targeted CC adaptation or mitigation strategies in Bangladesh.

2 Methods

2.1 Study area

Bangladesh is a flat topographical country in Southeast Asia, consisting of low-lying alluvial plains in the deltas of Asia's three largest rivers known as the Ganges-Brahmaputra-Meghna. It has a tropical monsoon climate distinguished by considerable seasonal rainfall variation, moderate hot temperature, and high humidity (Islam H. M. T. et al., 2021). The four main seasons of Bangladesh can be categorized as pre-monsoon (March to May), monsoon (June to September), post-monsoon (October to November), and winter (December to February) (Kamruzzaman et al., 2019a; Jerin et al., 2021). The country's mean temperature varies from 26.9°C to 31.1°C in pre-monsoon, while in winter, it ranges from 17.0°C to 20.6°C. January is the coldest month, with a mean temperature of 20.6°C in the coastal zone and 17°C in the northwestern and northeastern regions. May is the warmest month when the average temperature varies from 27°C in the eastern and southern parts to 31°C in the western-central region. The northwestern region of Bangladesh has the highest temperature

TABLE 1 The CMIP5 40 GCMs used in SimCLIM4.0 (Yin et al., 2013).

No	Model	Developed	No	Model	Developed
1	ACCESS1.3	Australia	21	GISS-E2-H-CC	United States
2	ACCESS1.0	Australia	22	GISS-E2-R	United States
3	BCC-CSM1-1	China	23	GISS-E2-R-CC	United States
4	BCC-CSM1-1-m	China	24	HADCM3	United Kingdom
5	BNU-ESM	China	25	HadGEM2-AO	United Kingdom
6	CanESM2	Canada	26	HadGEM2-CC	United Kingdom
7	CCSM4	United States	27	HadGEM2-ES	United Kingdom
8	CESM1-BGC	United States	28	INMCM4	Russia
9	CESM1-CAM5	United States	29	IPSL-CM5A-LR	France
10	CMCC-CM	Italy	30	IPSL-CM5A-MR	France
11	CMCC-CMS	Italy	31	IPSL-CM5B-LR	France
12	CNRM-CM5	France	32	MIROC4H	Japan
13	CSIRO-Mk3-6-0	Australia	33	MIROC5	Japan
14	EC-EARTH	Netherlands	34	MIROC-ESM	Japan
15	FGOALS-g2	China	35	MIROC-ESM-CHEM	Japan
16	FGOALS-s2	China	36	MPI-ESM-LR	Germany
17	GFDL-CM3	United States	37	MPI-ESM-MR	Norway
18	GFDL-ESM2G	United States	38	MRI-CGCM3	Japan
19	GFDL-ESM2M	United States	39	NorESM1-M	Norway
20	GISS-E2-H	United States	40	NorESM1-ME	Norway

extremes. In some pre-monsoon summer months, the temperature can rise over 42°C, while in winter, the nighttime temperature can fall below 5°C (Shahid et al., 2012; Alamgir et al., 2019).

2.2 Data sources

In this study, downscaled data for two time slices, i.e. near (2021–2060) and far (2061–2100), was used to assess the future changes of Tmax and Tmin for two different periods based on the reference period (1986–2005). SimCLIM 4.0 was employed to anticipate future Tmax and Tmin using the MME of 40 GCMs, presented in Table 1. The earth System Grid (ESG) was used to collect CMIP5 GCMs temperature projection data (Taylor et al., 2012; Islam et al., 2022). CMIP5 models included multiple emission scenarios, namely RCP2.6, 4.5, 6.0, and 8.5 (IPCC, 2014). RCP4.5 represents moderate greenhouse gas (GHG) emissions and, thus, provides a median projection of global climate. In contrast, RCP8.5 represents high GHG emissions in the future like the present and, therefore, provides a higher range of projections. This study used the GCM simulations for RCP4.5 and RCP8.5.

For downscaling and projection of GCM temperature, monthly Tmax and Tmin data of 30 meteorological stations (Figure 1) were used as reference (1986–2005) datasets. The data were collected from the Bangladesh Metrological Department (BMD). The recommended method by World Meteorological Organization (WMO) was used for

the homogeneity test of the collected data at all meteorological stations. In Bangladesh, BMD now runs 39 weather stations to monitor the country's weather (BMD, 2020). Some stations were set up after 1990, so no long-term data are available at those sites. The meteorological stations were selected based on their location, data availability (less than 3% of data is missing) and homogeneity, allowing these data to cover all over Bangladesh. Inverse Distance Weighting (IDW) Interpolation of the neighboring stations' temperatures was used to fill up the missing data of the chosen stations. The IDW was also used for visualizing the spatial changes in future Tmax and Tmin. Despite some limitations, such as the bull's-eye effect around data points, consider only distance effect, and the inability to measure prediction errors (Tobin et al., 2011; Daly, 2006), it is one of the most popular interpolation techniques in the world, including Bangladesh. The land of Bangladesh is very flat, as mentioned in the study area description. The influence of each station in such topography predominantly varies with distance, as assumed in the IDW method.

2.2.1 SimCLIM 4.0

SimCLIM 4.0 (<https://www.climsystems.com/simclim>) is a user-friendly application for climate data processing that facilitates access to critical climatic information for determining climate risk and response. SimCLIM 4.0 for Desktop can handle both spatial and site data. It includes several tools, such as spatial scenario generation and impact models, to provide meaningful and

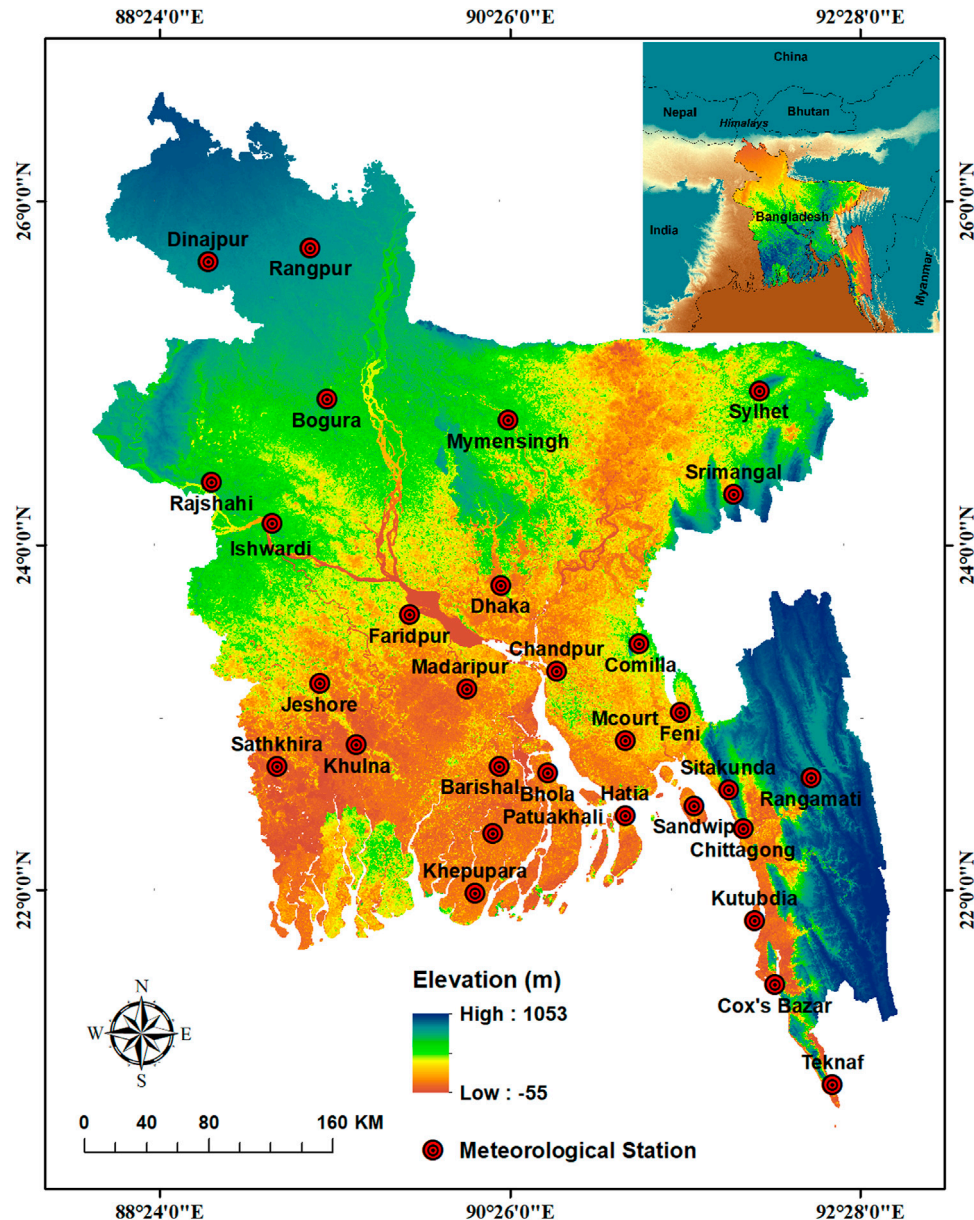


FIGURE 1
Geographical position of the study area and the sites of the meteorological stations.

comfortable information retrieval on historical, present, and future climate extremes (Warrick et al., 2012; Islam et al., 2022). SimCLIM, first utilized in New Zealand, was primarily inspired by CLIMPACTS (Warrick, 2009). It now covers many other countries and regions worldwide, including Bangladesh, to create climate datasets (Amin et al., 2018a; b; Rahman and Rob, 2019; Zheng et al., 2020; Islam et al., 2022). This study used SimCLIM 4.0 to generate climate projections for RCP4.5 and RCP8.5.

SimCLIM downscales and projects climatic parameters using a pattern scaling bias correction technique. Local differences between two specified periods are estimated first and then adjusted using global mean Tmin and Tmax variations (Rogelj et al., 2012; Yin et al., 2013). This enables downscaling GCMs considering the geographical,

temporal, and multivariable climatic structure. V^* can be defined as the anomaly of a climatic variable V like maximum or minimum temperatures, in a certain i (grid cell), j (month) and y (period) for an RCP can be calculated using the yearly global average temperature, T following subsequent formula:

$$\Delta V_{yij}^* = \Delta T_y \cdot \Delta V_{ij} \quad (1)$$

Then the local variation (ΔV_{ij}) is computed employing linear regression of GCM simulated anomaly (V_{yij}). The regression line slope can be calculated as,

$$\Delta V_{ij} = \frac{\sum_{y=1}^m \Delta T_y \cdot \Delta V_{ij}}{\sum_{y=1}^m (\Delta T_y)^2} \quad (2)$$

where m is the future sample periods number in any 5-year average between 2021 and 2100.

Pattern-scaling downscaling enables SimCLIM 4.0 to anticipate multiple climatic parameters at fine accuracy and resolution for diverse spatiotemporal scales (Amin et al., 2018a; Amin et al., 2018b; Islam et al., 2022). It has easily configurable downscaling capabilities for downscaling GCMs to the geographic resolution necessary for the CC impact evaluation (Yin et al., 2013).

Some climate processes are not fully understood or cannot be resolved due to computational constraints, leading to uncertainty in initial conditions, boundary conditions (such as a radiative forcing scenario), parameterization, and, eventually, climate simulations. Multi-model ensemble (MME) approaches, in which the results of selected GCMs are combined for climate projections, are frequently employed to reduce the uncertainties associated with GCMs. Moreover, the MME performs well in comparison with the performance of individual models, as the MME GCMs compensate for each other's computational errors.

SimCLIM can also produce an “ensemble” model from the user-selected GCM outputs with lower, upper, and median projections (Amin et al., 2018b). This study used the MME median of the 40 GCMs to reduce the influence of individual GCMs.

2.3 Statistical analyses

2.3.1 Mann-kendall test (MK)

The non-parametric Mann-Kendall (MK) test, suggested by the World Meteorological Organization (WMO) to examine the trends in hydro-meteorological time series, was employed for identifying projected temperature trends (Mann, 1945; Kendall, 1975). The MK test null hypothesis (H_0) implies the existence of no monotonic trend in the time series, whereas the alternative hypothesis (H_a) states the existence of a monotonic trend. The MK test statistic S can be expressed as:

$$S = \sum_{k=1}^{n-1} \sum_{j=k+1}^n \text{sign}(x_j - x_k) \quad (3)$$

where $j > k$ and n indicates data point. x_j and x_k signify the data point at j and K time, respectively.

$$\text{sign}(x_j - x_k) = \begin{cases} 1 & \text{if } (x_j - x_k) > 0 \\ 0 & \text{if } (x_j - x_k) = 0 \\ -1 & \text{if } (x_j - x_k) < 0 \end{cases} \quad (4)$$

The S value is assumed to be identical to the normal distribution with an average of zero, and the statistical discrepancy of S can be estimated by Eq. (5):

$$\text{VAR}(S) = \left[\frac{n(n-1)(2n+5) - \sum_{y=1}^x t_y(t_y-1)(2t_y+5)}{18} \right] \quad (5)$$

The Z value is used to determine whether or not a significant trend exists in the time-series data. The normalized Z value can be calculated by Eq. (6):

$$Z = \begin{cases} \frac{S-1}{\sqrt{\text{VAR}(S)}} & \text{if } S > 0 \\ 0 & \text{if } S = 0 \\ \frac{S+1}{\sqrt{\text{VAR}(S)}} & \text{if } S < 0 \end{cases} \quad (6)$$

In a Z statistic, the positive value represents increasing and the negative value represents a decreasing trend. The null hypothesis (H_0) of no trend is rejected at the 99%, 95%, and 90% significance levels if Z value is greater than or equal to 2.58, 1.96, and 1.65, respectively. This study used a 95% confidence level for recognizing a positive or negative significant trend.

2.3.2 Sen's slope estimator

Sen's slope (SS) estimator, a non-parametric method introduced by Sen (1968), was used to analyze the trend magnitude in projected temperature. The main advantage of this strategy over other techniques is that the outlier has less impact on the computed slope (Novotny and Stefan, 2007). It is computed as follows:

$$\beta = \text{Median} \left[\frac{x_j - x_i}{j - i} \right] \text{ all } j > i \quad (7)$$

where x_j and x_i denote the j th and i th values, respectively, in the time series. A positive or negative value of β suggests an increasing or decreasing rate of changes, respectively.

3 Results

3.1 Reproducibility of climate models

The simulated Tmax and Tmin of MME of 40 CMIP5 GCMs are compared with the observed Tmax and Tmin and presented using the line graph of average (Figures 2A, C) and standard deviations (STD) for the period 1986–2005 (Figures 2B, D). The line graph of monthly mean Tmax and Tmin provides an overall view of the models' reliability, whereas STD shows variability in temperature. The simulated historical MME Tmax and Tmin showed good performance, with $R^2 \Rightarrow 0.80$, thus regarded to be in accordance with the observed temperature.

The MME temperature reproduced the observed temperature with a little underestimation or overestimation in different months. The MME underestimated observed Tmax by about 1.81°C–3.73°C during winter months (Dec–Feb), while it overestimated Tmin by 0.14–3.03°C. Similar underestimation and overestimation of Tmax and Tmin were also observed in pre-monsoon months in a range of 1.16°C–2.89°C and 1.36°C–2.89°C, respectively. The underestimation and overestimation of Tmax were also noticed in monsoon and post-monsoon months. In contrast, Tmin was underestimated in monsoon and post-monsoon months at a range of 0.04–2.09°C and 0.31–1.29°C, respectively. The results showed the ability of the downscaling method to reproduce the observed temperature at the stations reliably.

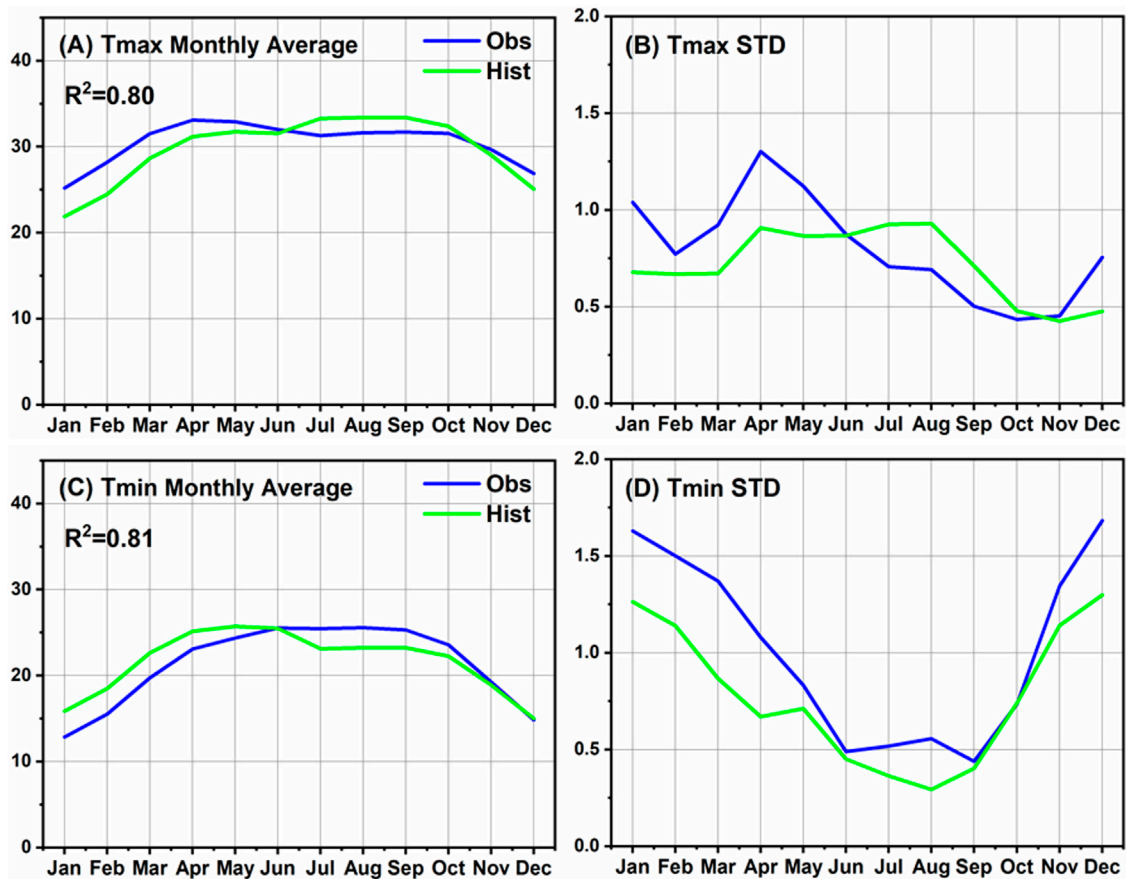


FIGURE 2
Comparison of observed and historical GCM of maximum temperature (Tmax) and minimum temperature (Tmin) for the period 1986–2005. (A,C) Monthly average, (B,D) Standard deviation.

3.2 Spatiotemporal Tmax trends for the future periods

The monthly Tmax trends (SS) for future periods considering RCP4.5 and RCP8.5 are exhibited in Figures 3, 4, respectively. The figures show the spatial distribution of Tmax trends for the near (2021–2060) and far (2061–2100) futures over Bangladesh, providing a glimpse into the future Tmax. The SS analysis revealed that the greatest Tmax increases were in January, February and December at a rate of 0.03–0.16°C/decade for RCP4.5 and 0.35–0.81°C/decade for RCP8.5 (Figures 3, 4). The highest increase in these months was projected at Rangpur, Mymensingh, and Sylhet stations in northern Bangladesh. A similar spatial trend was observed in March and April, where the highest increase was observed in Rangpur. The greatest increases in August, October, and November Tmax were also noticed at this station. For May–July, the greater Tmax increase was in the western region (the greatest is in Rajshahi) and the lower in the northeastern region (the lowest was in Sylhet). The results indicate a higher Tmax rise in the near and lower in the far period for RCP4.5. In contrast, a higher Tmax trend was observed in the far future than near future for RCP8.5.

Figure 5 presents the annual and seasonal change (SS) in Tmax for the near and far future periods at 30 stations across Bangladesh for RCP4.5 and RCP8.5. The highest annual Tmax increase was by 0.13°C/decade in near and 0.03°C/decade in far futures for RCP4.5. The

projected increases for RCP8.5 were 0.51°C/decade in the near and 0.66°C/decade in the far period. Among the seasons, winter exhibited the highest increase at a rate of 0.16°C/decade in near and 0.04°C/decade in far futures for RCP4.5. For RCP8.5, increases were 0.62°C/decade in the near and 0.80°C/decade in the far periods. SS analysis of annual and seasonal Tmax indicated the highest trend in Rangpur, Rajshahi, Bogura, Sylhet, and Mymensingh in northern and northwestern Bangladesh (Figure 5).

Table 2 presents the areal average Tmax trends of Bangladesh in monthly, seasonal and annual scales for both RCPs. Like Figures 3, 4, the greatest Tmax increases were also found in December–January, similar to the results presented in Table 2. The mean annual Tmax was projected to increase by 0.12°C/decade in the near and 0.03°C/decade in the far future for RCP4.5. The changes would be 0.46°C/decade and 0.59°C/decade for RCP8.5 in the near and far future, respectively. The highest increase in Tmax in Bangladesh will be in winter than in other seasons.

3.3 Spatiotemporal Tmin trends for the future periods

The spatial distribution of Tmin trends (SS) for the near (2021–2060) and far (2061–2100) futures for RCP4.5 and

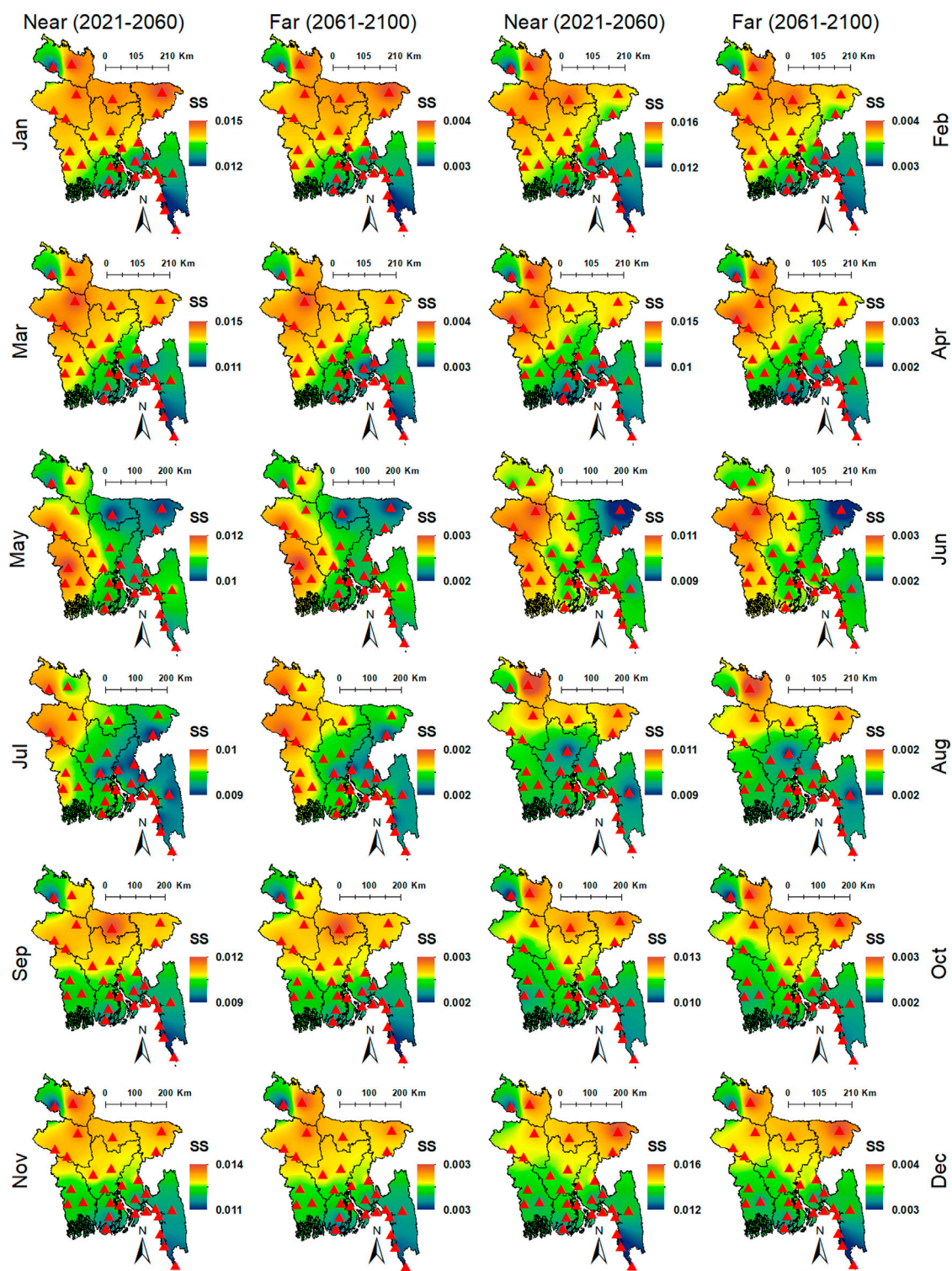


FIGURE 3

Spatial distribution of monthly (Jan-Dec) T_{max} ($^{\circ}\text{C}$) trends (SS) for near (2021–2060) and far (2061–2100) futures periods over Bangladesh considering 30 meteorological stations for RCP4.5.

RCP8.5 are presented in Figure 6, 7, respectively. The MK test revealed a significant trend in T_{min} at all 30 stations in both future periods and RCPs. SS revealed the highest T_{min} rise in February at a rate of 0.03–0.17 $^{\circ}\text{C}/\text{decade}$ for RCP4.5 and 0.48–0.85 $^{\circ}\text{C}/\text{decade}$ for RCP8.5 in

both futures. The lowest T_{min} rise was projected in July and August for both RCPs. The highest rise was for January–April at Srimangal, Sylhet, and Mymensingh, in the northern or northeastern region, and for May–June at Ishwardi and Rajshahi stations, in the western region,

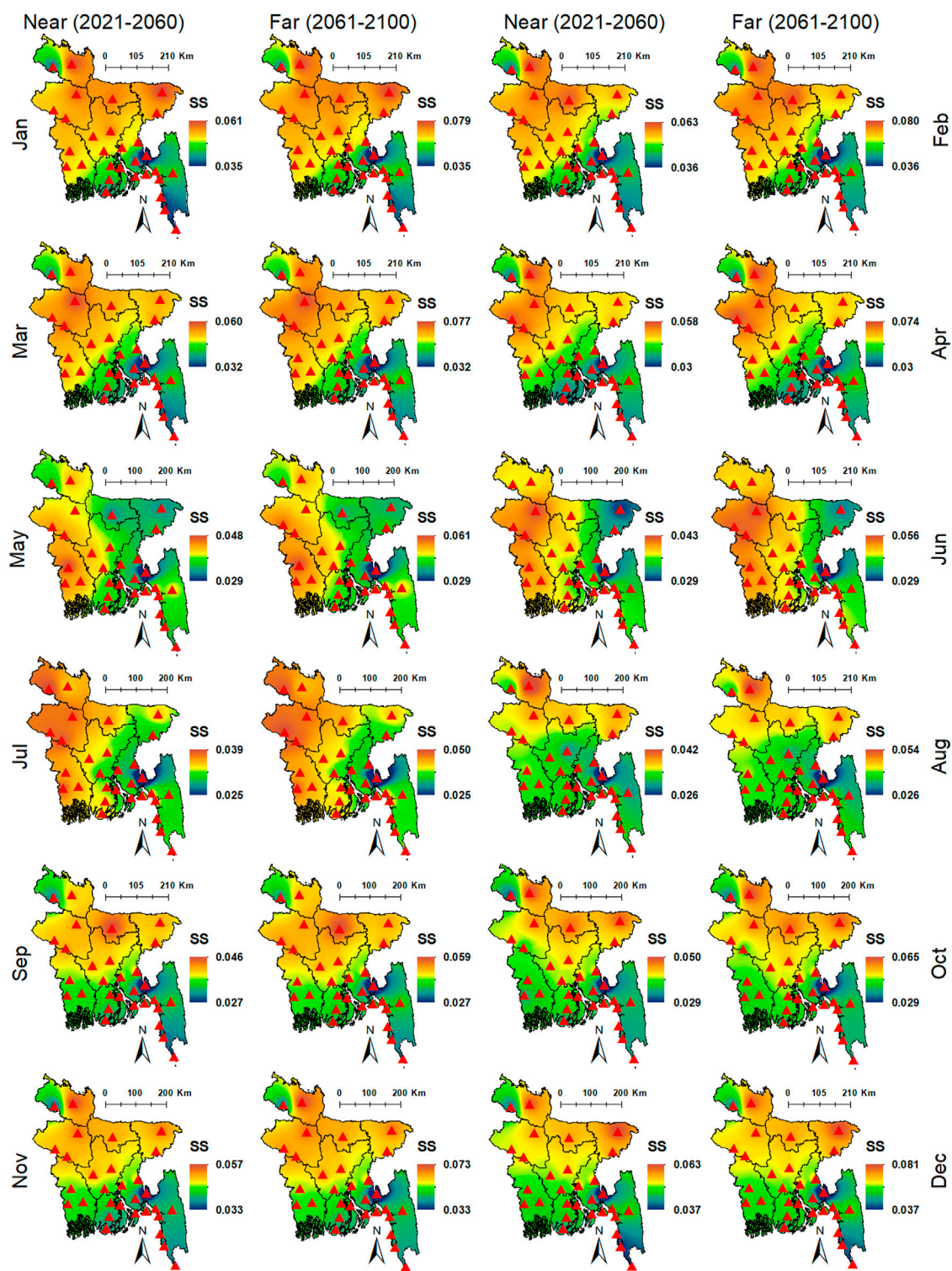


FIGURE 4
Same as Figure 3 but for the RCP8.5.

for both RCPs. Moreover, a higher rise in T_{min} was observed in the northern region in September–December, like January–April (Figures 6, 7).

Figure 8 depicts the annual and seasonal changes (SS) in T_{min} for the near and far future periods at 30 sites across Bangladesh for

RCP4.5 and RCP8.5. For RCP4.5, the projected highest annual T_{min} rise was $0.13^{\circ}\text{C}/\text{decade}$ in near futures and $0.03^{\circ}\text{C}/\text{decade}$ in far futures. The increases for RCP8.5 were $0.53^{\circ}\text{C}/\text{decade}$ in the near and $0.68^{\circ}\text{C}/\text{decade}$ in the far future. winter would experience the greatest increase among the seasons, by $0.16^{\circ}\text{C}/\text{decade}$ in near and

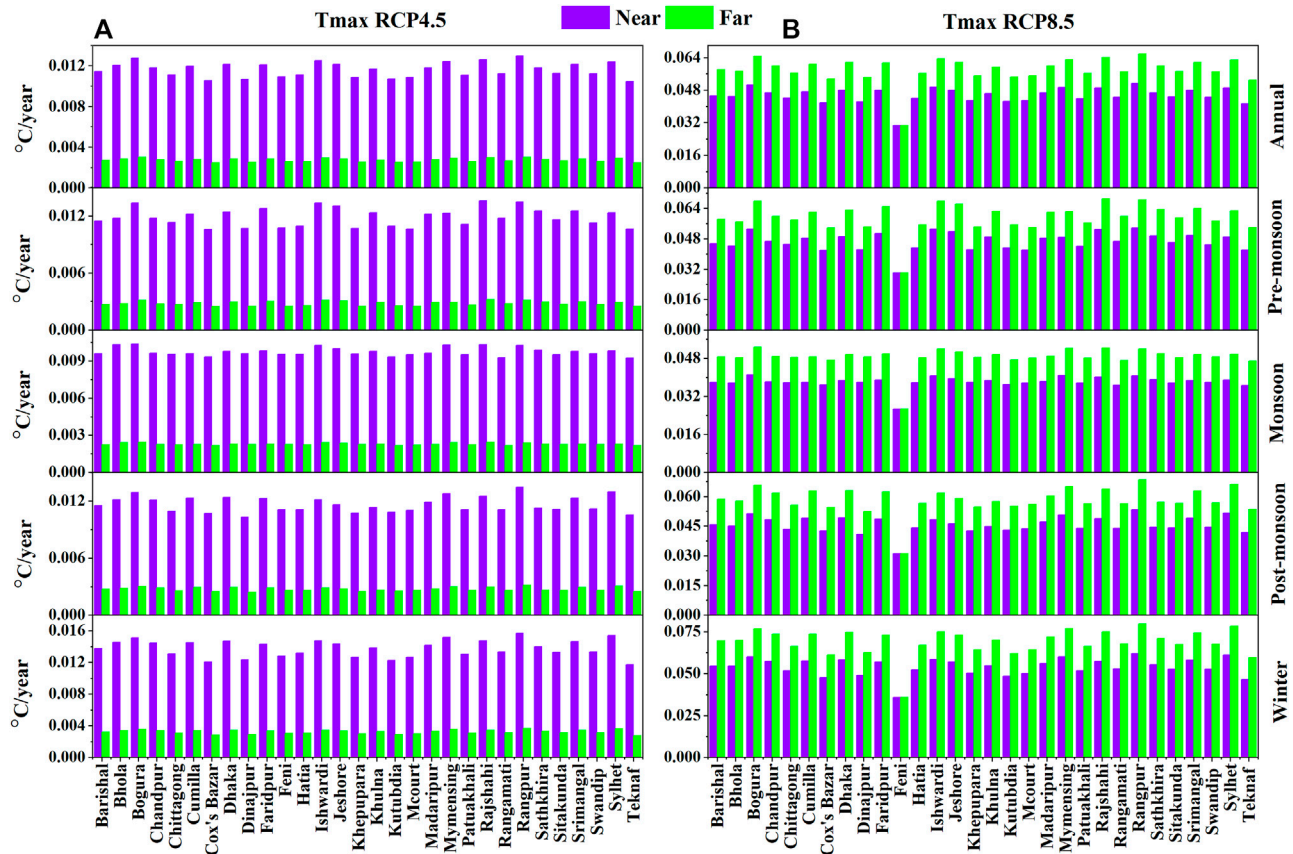


FIGURE 5

Sen's slope estimator for annual and seasonal Tmax (°C) trend (SS) analysis for near (2021–2060) and far (2061–2100) periods over Bangladesh considering 30 meteorological stations under (A) RCP4.5 and (B) RCP8.5.

0.04°C/decade in far futures for RCP4.5. However, RCP8.5 showed to rise of 0.64°C/decade in the near period and 0.83°C/decade in the far period. The SS revealed the highest increase in annual Tmin in the eastern, central, northern, and western regions. The highest increase in Tmin during pre-monsoon, post-monsoon, and winter was found in central to eastern, northeastern, and northwestern Bangladesh (Figure 8).

Table 2 shows the Tmin trends at monthly, yearly, and seasonal timeframes for both RCPs over the whole of Bangladesh. The mean annual Tmin for RCP4.5 showed an increase of 0.12°C/decade and 0.03°C/decade in the near and far future, respectively. In comparison, the trends for RCP8.5 were 0.49°C/decade and 0.62°C/decade in the near and far future, respectively. Nevertheless, the seasonal Tmin trend analysis showed the highest increase in winter for both the periods and RCPs (Table 2).

3.4 Future projected Tmax variability and change

Figure 9 illustrates the monthly and seasonal MME Tmax variability over Bangladesh for the near and far periods for RCP4.5 and RCP8.5. The Tmax variability for RCP4.5 and RCP8.5 is shown using black and red lines, respectively. Figures 9A, B, L shows that Tmax in January, February, and December

would differ from 22°C to 27°C for RCP4.5 and 22.5°C–31.5°C for RCP8.5 in the near and far periods. This projected Tmax range would reach 31.5°C–34.5°C for RCP4.5 while 32°C–38°C for RCP8.5 in May–September (Figures 9E–I). Tmax would range from 29°C to 33.5°C for RCP4.5 and 29.5°C–37.5°C for RCP8.5 throughout the transitional months of March–April and October–November (Figures 9C, D, J, K).

The projected annual Tmax was in the range of 30.05°C–30.62°C for RCP4.5, while between 30.57°C and 34.71°C for RCP8.5 in both periods (Figure 9M). The projected Tmax variability was very much identical during pre-monsoon and post-monsoon seasons, extending from 30.5°C to 32°C for RCP4.5 and 31°C–36°C for RCP8.5 for both periods (Figures 9N, P). However, a higher Tmax variability was projected during monsoon, 33°C–37°C for RCP4.5 and RCP8.5 (Figure 9O), and the lower variability in the winter, 24°C–25°C for RCP4.5 and 24.5°C–30°C for RCP8.5 (Figure 9Q). The results revealed a higher deviation in the warming signal for different months and seasons for both RCPs. Higher future warming is likely for RCP8.5 than RCP4.5 because of the higher radiative forcing for RCP8.5.

The projected change in mean monthly Tmax for near and far futures for RCP4.5 and RCP8.5 is illustrated in Figures 10A,B, respectively. The results showed an increase in Tmax in all months for both futures and scenarios. The greatest increase in Tmax would be in February by 0.64–0.83°C (1.84–2.39°C) in the near and 0.96–1.24°C

TABLE 2 Monthly and seasonal mean Tmax (°C) and Tmin (°C) and its changes in overall Bangladesh during near and far future periods for RCP4.5 and RCP8.5.

Tmax	Hist. Period	Mean (RCP4.5)		Mean (RCP8.5)		Trend (RCP4.5)		Trend (RCP8.5)		Change (RCP4.5)		Change (RCP8.5)	
		Near	Far	Near	Far	Near	Far	Near	Far	Near	Far	Near	Far
Jan	21.87	22.59	22.95	23.94	26.42	0.14	0.03	0.54	0.69	0.72	1.08	2.07	4.55
Feb	24.49	25.22	25.58	26.59	29.11	0.14	0.03	0.55	0.70	0.73	1.09	2.10	4.62
Mar	28.65	29.34	29.67	30.62	32.98	0.13	0.03	0.52	0.66	0.69	1.02	1.97	4.34
Apr	31.18	31.80	32.11	32.97	35.11	0.12	0.03	0.47	0.60	0.62	0.93	1.79	3.93
May	31.76	32.33	32.60	33.38	35.33	0.11	0.02	0.43	0.54	0.57	0.84	1.62	3.57
Jun	31.56	32.10	32.36	33.10	34.94	0.10	0.02	0.40	0.52	0.54	0.80	1.54	3.38
Jul	33.29	33.79	34.03	34.71	36.40	0.09	0.02	0.37	0.47	0.49	0.73	1.41	3.11
Aug	33.41	33.89	34.13	34.80	36.48	0.09	0.02	0.37	0.47	0.49	0.73	1.40	3.07
Sep	33.40	33.93	34.19	34.92	36.76	0.10	0.02	0.40	0.51	0.53	0.79	1.53	3.36
Oct	32.40	32.98	33.26	34.06	36.05	0.11	0.02	0.43	0.56	0.58	0.86	1.66	3.65
Nov	29.03	29.68	30.00	30.89	33.12	0.12	0.03	0.49	0.62	0.65	0.97	1.86	4.09
Dec	25.10	25.82	26.18	27.18	29.67	0.14	0.03	0.54	0.70	0.72	1.08	2.08	4.57
Annual	29.68	30.29	30.59	31.43	33.53	0.12	0.03	0.46	0.59	0.61	0.91	1.75	3.85
Pre-monsoon	30.53	31.16	31.46	32.32	34.47	0.12	0.03	0.47	0.60	0.63	0.93	1.79	3.95
Monsoon	32.92	33.43	33.68	34.38	36.14	0.10	0.02	0.38	0.49	0.51	0.76	1.47	3.23
Post-monsoon	30.72	31.33	31.63	32.47	34.59	0.12	0.03	0.46	0.59	0.61	0.91	1.76	3.87
winter	23.82	24.55	24.90	25.90	28.40	0.14	0.03	0.55	0.70	0.73	1.08	2.08	4.58
Tmin													
Jan	15.88	16.63	16.99	18.02	20.59	0.14	0.03	0.56	0.72	0.75	1.11	2.14	4.71
Feb	18.50	19.28	19.66	20.73	23.42	0.15	0.03	0.59	0.75	0.78	1.16	2.24	4.92
Mar	22.64	23.36	23.72	24.71	27.19	0.14	0.03	0.54	0.69	0.72	1.07	2.07	4.55
Apr	25.15	25.81	26.13	27.04	29.30	0.12	0.03	0.49	0.63	0.66	0.98	1.89	4.15
May	25.73	26.32	26.62	27.44	29.49	0.11	0.03	0.45	0.57	0.60	0.89	1.71	3.76
Jun	25.52	26.08	26.36	27.14	29.08	0.11	0.02	0.42	0.54	0.57	0.84	1.62	3.56
Jul	23.13	23.65	23.91	24.62	26.41	0.10	0.02	0.39	0.50	0.52	0.77	1.49	3.28
Aug	23.24	23.76	24.01	24.72	26.50	0.10	0.02	0.39	0.50	0.52	0.77	1.48	3.26
Sep	23.23	23.80	24.08	24.86	26.82	0.11	0.02	0.43	0.55	0.57	0.85	1.63	3.59
Oct	22.27	22.90	23.21	24.08	26.25	0.12	0.03	0.47	0.61	0.63	0.94	1.81	3.98
Nov	18.93	19.61	19.95	20.88	23.23	0.13	0.03	0.51	0.65	0.68	1.01	1.95	4.29
Dec	14.99	15.75	16.13	17.17	19.79	0.14	0.03	0.57	0.73	0.76	1.13	2.18	4.80
Annual	21.60	22.25	22.56	23.45	25.67	0.12	0.03	0.49	0.62	0.65	0.96	1.85	4.07
Pre-monsoon	24.51	25.17	25.49	26.39	28.66	0.12	0.03	0.49	0.63	0.66	0.98	1.89	4.15
Monsoon	23.78	24.32	24.59	25.34	27.20	0.10	0.02	0.41	0.52	0.54	0.81	1.56	3.42
Post-monsoon	20.60	21.26	21.58	22.48	24.74	0.12	0.03	0.49	0.63	0.66	0.98	1.88	4.14
winter	16.46	17.22	17.59	18.64	21.27	0.14	0.03	0.57	0.73	0.76	1.14	2.19	4.81

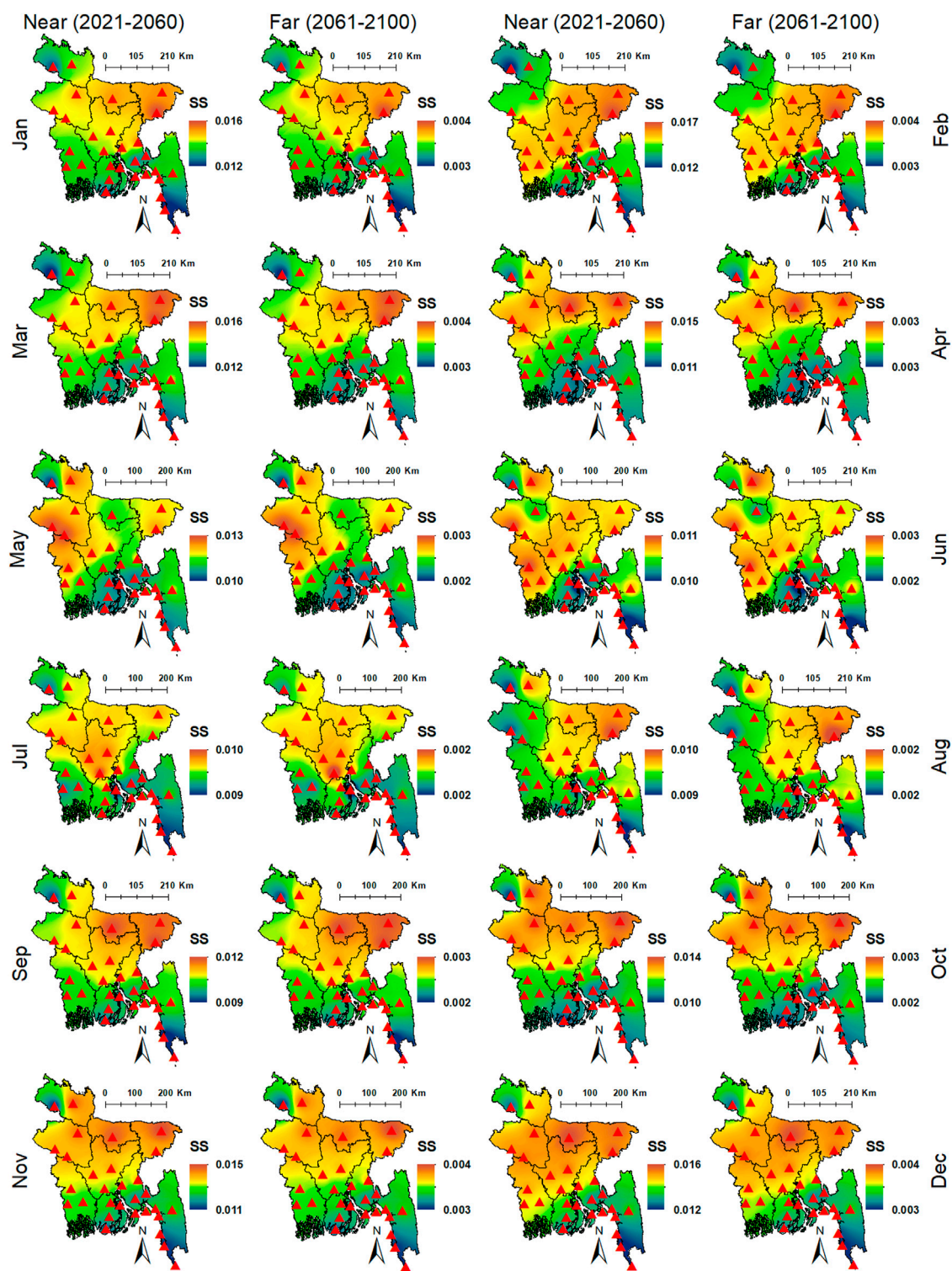


FIGURE 6

Spatial distribution of monthly (Jan–Dec) Tmin (°C) trends (SS) for near (2021–2060) and far (2061–2100) futures over Bangladesh considering 30 meteorological stations for RCP4.5.

(4.05–5.26°C) in the far future for RCP4.5 (RCP8.5), while relatively less increase in the June–August (Figures 10A,B). However, a higher increase in Tmax will be in the far period than in the near for both RCPs.

The annual Tmax over Bangladesh was predicted to rise under RCP4.5 by 0.55–0.68°C (1.58–1.98°C) in the near future with an average of 0.61°C (1.75°C) and 0.81–1.02°C (3.47–4.31°C) in the far future with an average of 0.91°C (3.85°C) (RCP8.5) (Figures 11A,B;

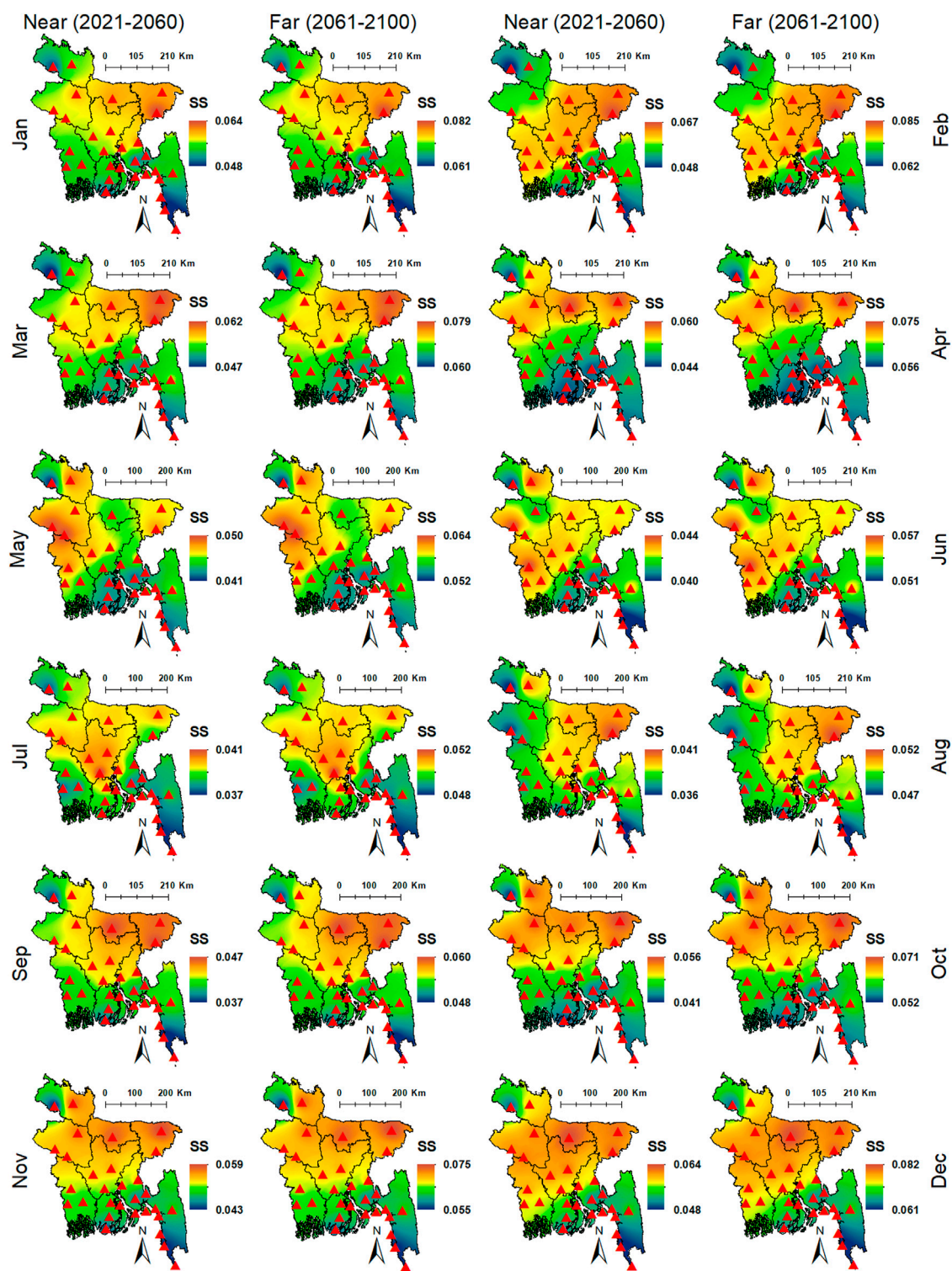


FIGURE 7
Same as Figure 6 but for the RCP8.5.

Table 2). However, on a seasonal timescale, winter displayed the greatest rise in projected T_{max} and monsoon showed the least for both periods and RCPs. The highest increase in T_{max} was projected in winter, $0.62\text{--}0.83^{\circ}\text{C}$ ($1.78\text{--}2.37^{\circ}\text{C}$) with an average of 0.73°C (2.08°C) in the near period and $0.92\text{--}1.23^{\circ}\text{C}$ ($3.90^{\circ}\text{C}\text{--}5.21^{\circ}\text{C}$) with an average

of 1.08°C (4.58°C) in far future for RCP4.5 (RCP8.5). In contrast, the least increase in T_{max} was projected in monsoon, $0.49\text{--}0.55^{\circ}\text{C}$ ($1.40^{\circ}\text{C}\text{--}1.57^{\circ}\text{C}$) in the near future with a mean of 0.51°C (1.47°C) and $0.73\text{--}0.82^{\circ}\text{C}$ ($3.07\text{--}3.45^{\circ}\text{C}$) with a mean of 0.76°C (3.23°C) in far future for RCP4.5 (RCP8.5) (Figures 11A,B; Table 2).

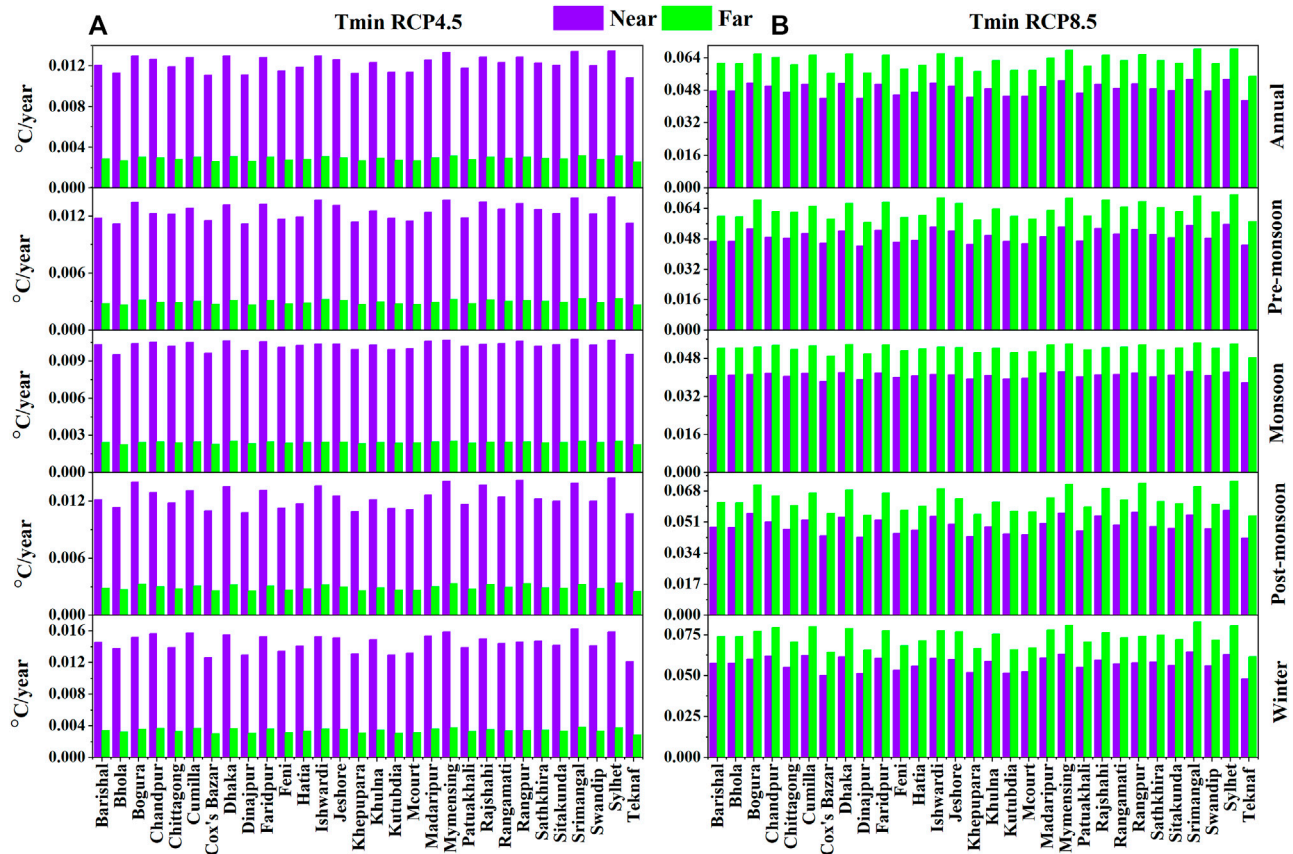


FIGURE 8

Sen's slope estimator for annual and seasonal Tmin (°C) trend (SS) analysis for near (2021–2060) and far (2061–2100) periods over Bangladesh at 30 meteorological stations under (A) RCP4.5 and (B) RCP8.5.

The spatial distribution of projected annual and seasonal Tmax changes is exhibited in Figure 12. It shows the degree of the Tmax change varies greatly across Bangladesh for both futures and RCPs. A noticeable increase in annual Tmax was detected at the Rangpur, in the north, for RCP4.5. In contrast, the rising Tmax area was extended from the central, northern, and western regions except for Dinajpur (extreme northwestern part) for RCP8.5. An analogous to the annual spatial pattern was observed for the monsoon season for both periods and RCPs. The pre-monsoon season showed a higher increase at the Rajshahi, Rangpur, Bogura, Ishwardi, and Jessore stations in northwestern and western regions. Overall, the winter exhibited the highest Tmax increase for both periods and RCPs. A higher increase in winter Tmax was also observed over the whole of Bangladesh, except in the extreme northwest and some parts of the south and southeast. The projected changes in annual and seasonal Tmax were higher in the central, northern, and western regions and lesser in the extreme northwest (Dinajpur) and some parts in the south and southeast.

3.5 Future projected Tmin variability and change

Figure 13 exhibits the average monthly and seasonal Tmin variability across Bangladesh for the near and far futures for

RCP4.5 (black) and RCP8.5 (red). The figure shows that the projected Tmin in January, February, and December vary from 15°C to 20°C for RCP4.5 while 16°C–25°C for RCP8.5 in both periods (Figures 13A, B, L). The projected Tmin would be higher during May–September and reach 23°C–27°C for RCP4.5 while 24°C–31°C for RCP8.5 (Figures 13E–I). During the seasonal transitional months of March–April and October–November, the Tmin would fluctuate from 19°C to 24.5°C for RCP4.5, while it will remain between 20°C and 31°C for RCP8.5 (Figures 13C,D,J,K).

The projected mean annual Tmin ranges from 22°C to 22.60°C for RCP4.5, while between 22.5°C and 27°C for RCP8.5 for both periods (Figure 13M). The variability of Tmin showed a gradual decrease from the pre-monsoon to the winter season (Figures 13N–Q). The projected Tmin in the pre-monsoon was 24.5°C–30°C. It would decrease to 24°C–28.5°C and 21°C–26°C in monsoon and post-monsoon, respectively, for both periods and RCPs. The projected Tmin in winter was between 16.5°C and 23°C for both periods and RCPs. The results revealed higher deviation in monthly, annual, and seasonal Tmin than Tmax between RCPs.

The projected changes in average monthly Tmin for the near and far future for RCP4.5 and RCP8.5 are demonstrated in Figures 10C,D, respectively. The projected monthly Tmin showed a rise in all months for both periods and RCPs. The highest rise in Tmin was projected for February by 0.64–0.89°C (1.84°C–2.55°C) in the near future, with a

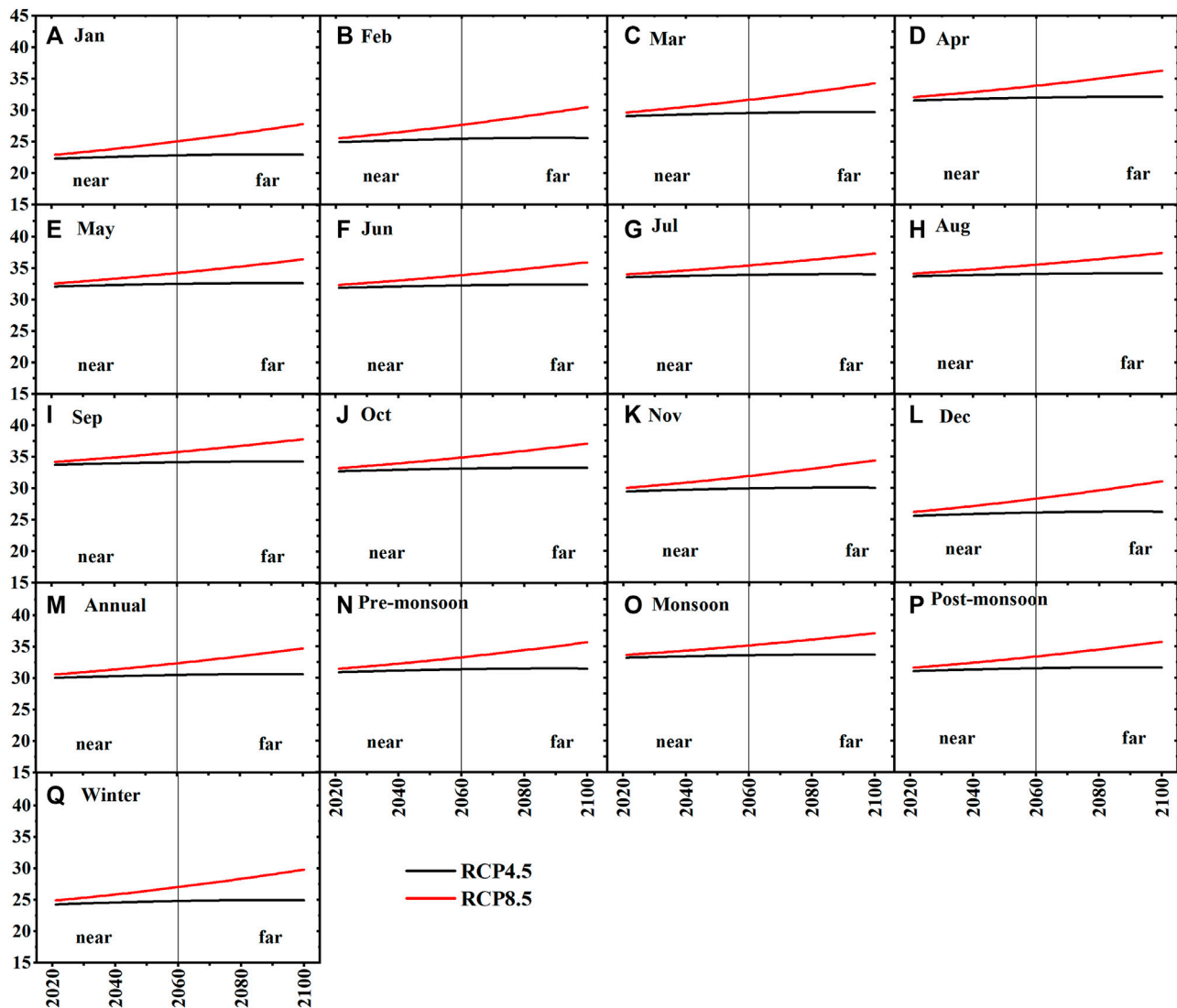


FIGURE 9

Monthly, Annual and Seasonal Tmax (°C) variability of multi-model ensemble (MME) of CMIP5 datasets under RCP4.5 and RCP8.5 for the near and far periods in Bangladesh. (A) January, (B) February, (C) March, (D) April, (E) May, (F) June, (G) July, (H) August, (I) September, (J) October, (K) November, (L) December, (M) Annual, (N) Pre-monsoon, (O) Monsoon, (P) Post-monsoon, and (Q) Winter.

mean of 0.78°C (2.24°C) and 0.96°C – 1.32°C (4.05°C – 5.60°C) in far future, with a mean of 1.16°C (4.92°C) for RCP4.5 (RCP8.5). In contrast, a relatively less increase in Tmin was projected for June–August (Figures 10C,D; Table 2). Nevertheless, Tmin was projected to rise higher in the far future than near future for both RCPs.

RCP4.5 projected an increase in annual Tmin over Bangladesh by 0.57 – 0.71°C (1.63°C – 2.03°C), with an average of 0.65°C (1.85°C), in the near future, and by 0.85 – 1.06°C (3.59°C – 4.46°C), with an average of 0.96°C (4.07°C), in the far future (RCP8.5) (Figures 11C,D; Table 2). Nevertheless, on a seasonal timescale, winter exhibited the highest increase in Tmin and monsoon revealed the lowest for both periods and RCPs. The projected increase in winter Tmin was 0.64 – 0.86°C (1.83°C – 2.46°C) with an average of 0.76°C (2.19°C) in the near period, and 0.95°C – 1.28°C (4.02°C – 5.41°C) with an average of 1.14°C (4.781°C) in the far

future for RCP4.5 (RCP8.5). Conversely, the monsoon Tmin was projected to rise the least, 0.50 – 0.56°C (1.44°C – 1.62°C) with a mean of 0.54°C (1.56°C) in the near future and 0.75 – 0.84°C (3.17°C – 3.56°C) with a mean of 0.81°C (3.42°C) in far future for RCP4.5 (RCP8.5) (Figures 11C,D; Table 2).

The spatial patterns of projected changes in annual and seasonal Tmin are presented in Figure 14. For both periods and scenarios, an increase in Tmin was observed for all annual and seasonal timescales over Bangladesh. The higher annual Tmin rise was projected in northeastern, northern, and northwestern parts of Bangladesh for both periods and RCPs. The higher increase in pre-monsoon and post-monsoon Tmin was projected in Srirangal, Sylhet, Mymensingh Bogura, and Rajshahi in northeastern, northern, and northwestern Bangladesh. The higher rise in winter Tmin was projected in Dhaka, Faridpur, Madaripur, Srirangal, Sylhet, Mymensingh, and Rangpur in the central,

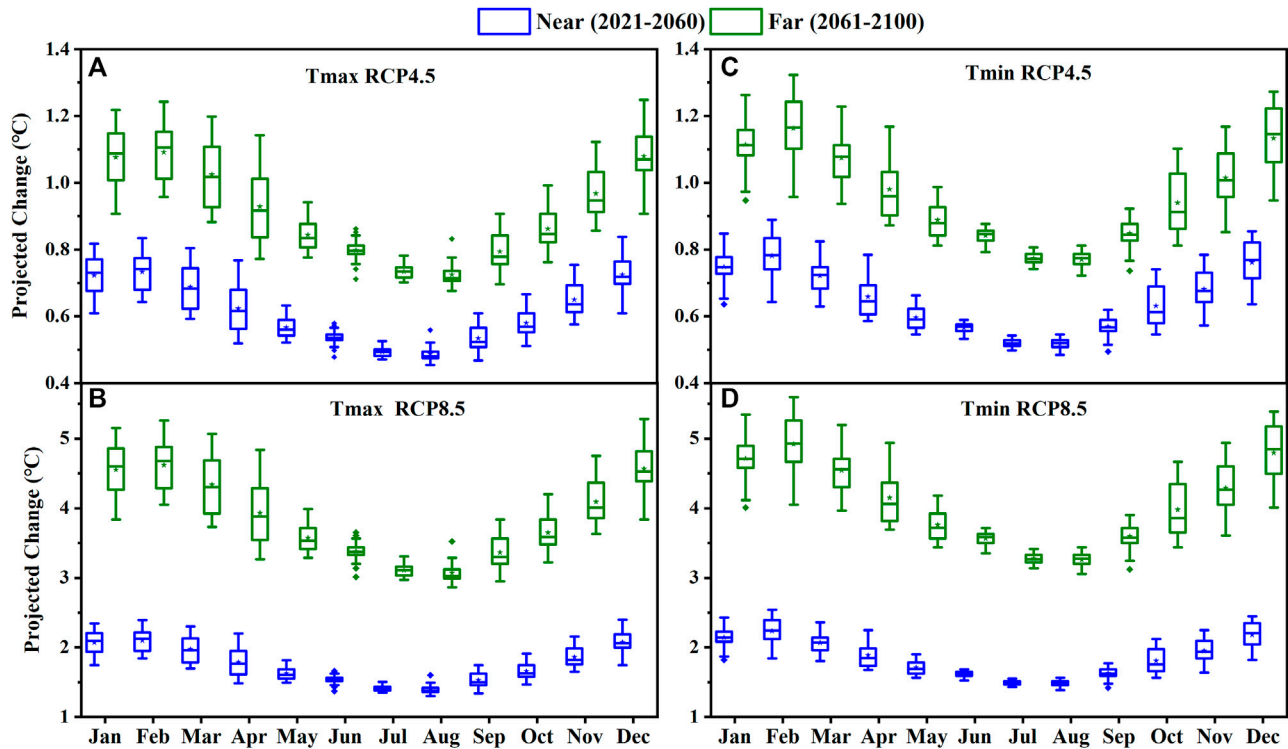


FIGURE 10

Projected change in average monthly Tmax (°C) and Tmin (°C) for near (2021–2060) and far (2061–2100) future periods over Bangladesh for RCP4.5 and RCP8.5. (A) Tmax RCP4.5, (B) Tmax RCP8.5, (C) Tmin RCP4.5, and (D) Tmin RCP8.5.

northern, and northeastern regions of Bangladesh. Among the seasons, the winter exhibited the highest increase in Tmin, particularly in the region extending from the west to north and northeast. The study also showed a relatively lower increase in Tmin in the extreme northwest, middle south, and southeast while higher in the middle, north, and west of Bangladesh.

4 Discussion

4.1 Reproducibility of CMIP5 models

The ability of models to generate the “present climate” is a critical aspect of GCM projections (Yang et al., 2019). This study used SimCLIM 4.0 for Tmax and Tmin projection of Bangladesh for two RCPs using MME of 40 GCMs (4.5 and 8.5). SimCLIM has been widely used for temperature projection at higher resolution and better accuracy in various temporal and geographical scales around the world, including Bangladesh (Amin et al., 2018a; b; Rahman and Rob, 2019; Zheng et al., 2020; Wang et al., 2021). Though some underestimations and overestimations of CMIP5 MME were observed in this study, overall, it showed satisfactory performance in reproducing observed Tmax and Tmin. In this study, SimCLIM model projection showed a cold bias in Tmax, but a warm bias in Tmin. Tmax seems to have a greater cold bias in the winter and pre-monsoon months than in monsoon or post-monsoon months, whereas Tmin has a warm bias in the winter and pre-monsoon months than in monsoon or

post-monsoon months. This finding almost coincided with the results of Chotamonsak et al. (2011) in Southeast Asia employed a WRF RCM (regional climate model). They found a higher cold bias in the cool-dry season (Nov–Feb) than the hot-dry (Mar–Apr) and rainy seasons (May–Oct), where Tmin showed a weaker warm bias in the cool-dry season (Nov–Feb) than the hot-dry (Mar–Apr) and rainy seasons (May–Oct). Some studies also identified cold bias for Tmax or annual mean temperature in Bangladesh using CMIP5 MME (Pattnayak et al., 2017; Kamruzzaman et al., 2021a). Moreover, biases in GCMs are primarily attributed to the global energy balance amongst different physical mechanisms or processes used for modeling, such as radiative mechanisms like cloud and surface albedo effect as well as non-radiative mechanisms like surface turbulent fluxes and large-scale atmospheric oscillation (IPCC 2007; Yang and Rong-Cai, 2015; Pattnayak et al., 2017). However, the origins of biases are not the goal of this research and, therefore, not investigated.

4.2 Spatiotemporal trends in temperature (Tmax and Tmin) projection

The present study showed increasing trends in monthly, annual and seasonal Tmax and Tmin in both the future periods and scenarios. The study revealed that Bangladesh’s seasonal warming is substantially quicker than the global average, nearly 2–3 times higher in hot and humid summer seasons. Even seasonal

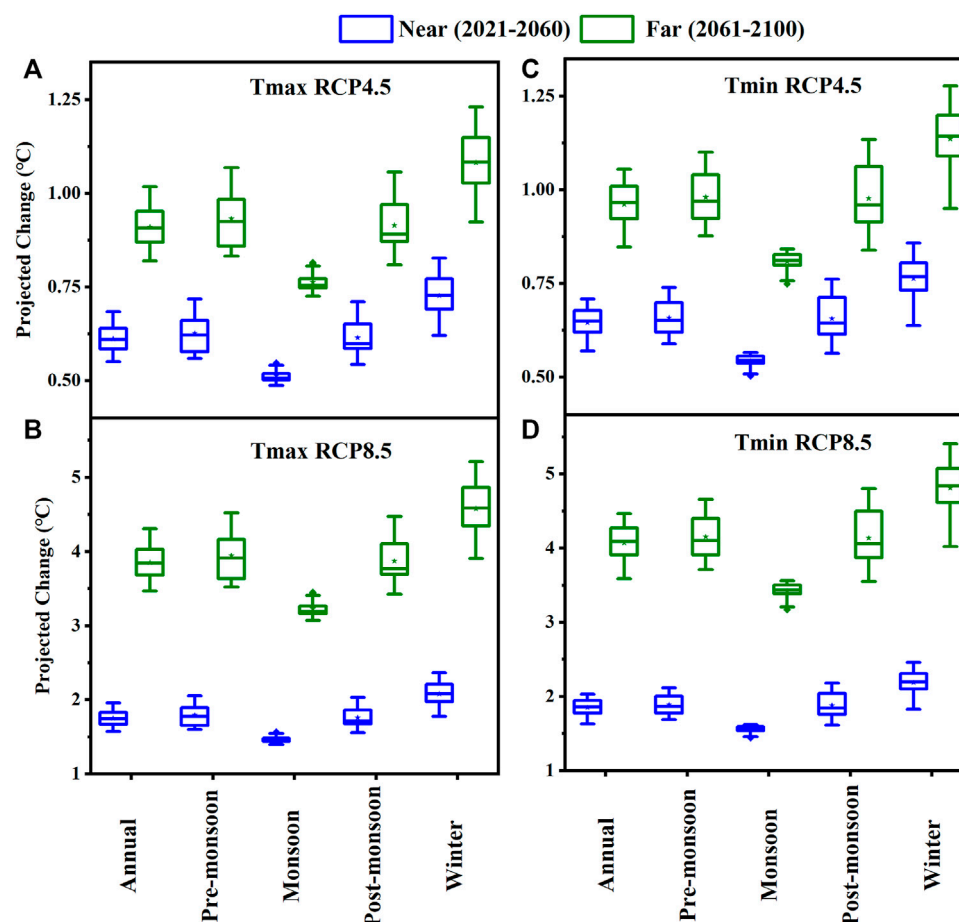


FIGURE 11

Projected change in annual and seasonal temperature for near (2021–2060) and far (2061–2100) future periods in Bangladesh for RCP4.5 and RCP8.5. (A) Tmax RCP4.5, (B) Tmax RCP8.5, (C) Tmin RCP4.5, and (D) Tmin RCP8.5.

warming in Bangladesh is much quicker than in India (Kothawale et al., 2010; Rahman and Lateh, 2016). The study indicates that the country may experience higher annual and seasonal temperature trends in the future. A sharp rise in Tmax and Tmin may negatively influence irrigation timing and planning, evapotranspiration, soil moisture availability and mineralization. As a result, higher irrigation rates will be needed in future, causing greater groundwater level depletion in many areas of the country (Mainuddin et al., 2022). Higher temperatures will cause increased carbon loss from soil (Hossain et al., 2017) and, thus, depletion of soil organic matter. As soil organic matter is soil's bloodline, its depletion will reduce soil productivity if corrective measures are not taken. Besides, high temperature is most likely to reduce rice production, the dominant food crop in Bangladesh, yield by 0%–61% depending on the country's seasonal temperature rise and locations (Hossain et al., 2021). To counter the deleterious effects, integrated nutrient management (Naher et al., 2020) and the use of recalcitrant organic material (Hossain et al., 2017) and efficient water management (Hossain et al., 2021) will be needed. It might ultimately raise agricultural production costs and impede the government's poverty reduction goal.

4.3 Spatiotemporal temperature (Tmax and Tmin) variability and change

The projected Tmax and Tmin temperature variability is a useful indicator of providing information on how much temperature will rise in future. The mean annual Tmax and Tmin range estimated in this study are similar to other studies (Hasan et al., 2013; 2018; Alamgir et al., 2019). Hasan et al. (2018) reported an increase in average annual Tmax from 31.5°C to 32°C for RCP4.5 and 32.5°C–34°C for RCP8.5 over Bangladesh, which is slightly higher or lower than that found in this study. They also reported a rise in mean Tmin above 23°C in 2100 for RCP4.5 and 24.5°C–26.5°C during the 2080s for RCP8.5 using five bias-corrected CMIP5 models. It is nearly analogous to the finding of the present study.

This study projected an increase in mean annual Tmax in Bangladesh by 0.61°C (1.75°C) in the near period and 0.91°C (3.85°C) in the far for RCP4.5 (RCP8.5). The mean annual Tmin is projected to rise by 0.65°C (1.85°C) in the near period while 0.96°C (4.07°C) in the far future for RCP4.5 (RCP8.5). A greater increase in Tmax and Tmin is found in the far future, coinciding with the findings of Alamgir et al. (2019). They reported the highest temperature increase (Tmax and Tmin) in northern and the lowest in the

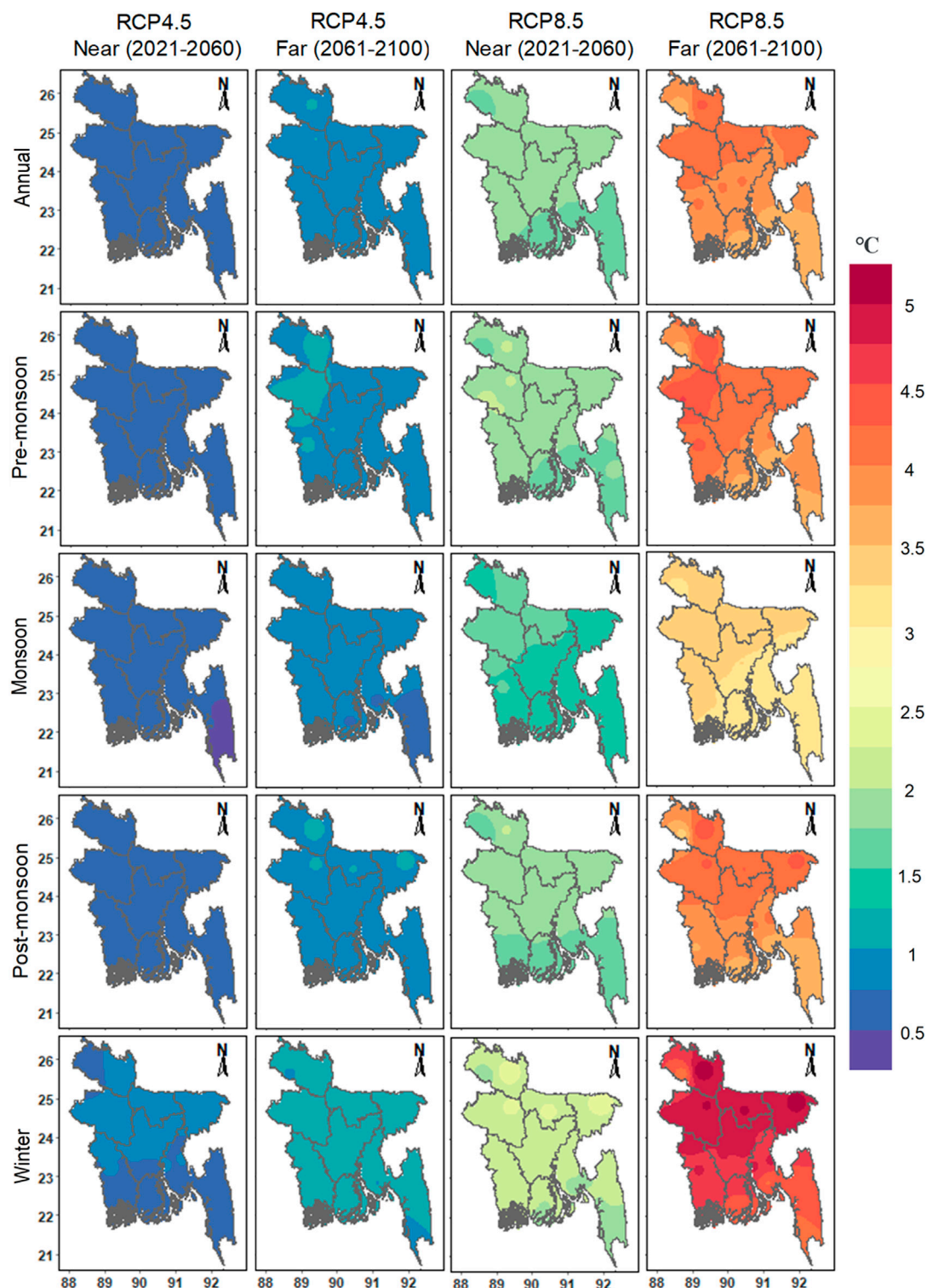


FIGURE 12

Spatial distribution of projected change in annual and seasonal Tmax (°C) for near (2021–2060) and far (2061–2100) future periods in Bangladesh for RCP4.5.

southeastern coastal part of Bangladesh using MME of eight CMIP5 models. It differs slightly from this study as this study found higher increases in the western and central regions. One of the key findings of this study was that Tmin changes were greater than

Tmax changes, a finding validated by prior research using CMIP5 models (Hasan et al., 2018; Alamgir et al., 2019; Rahman and Rob, 2019). Therefore, it indicates that nighttime temperatures (Tmin) will rise faster than daytime temperatures (Tmax), and

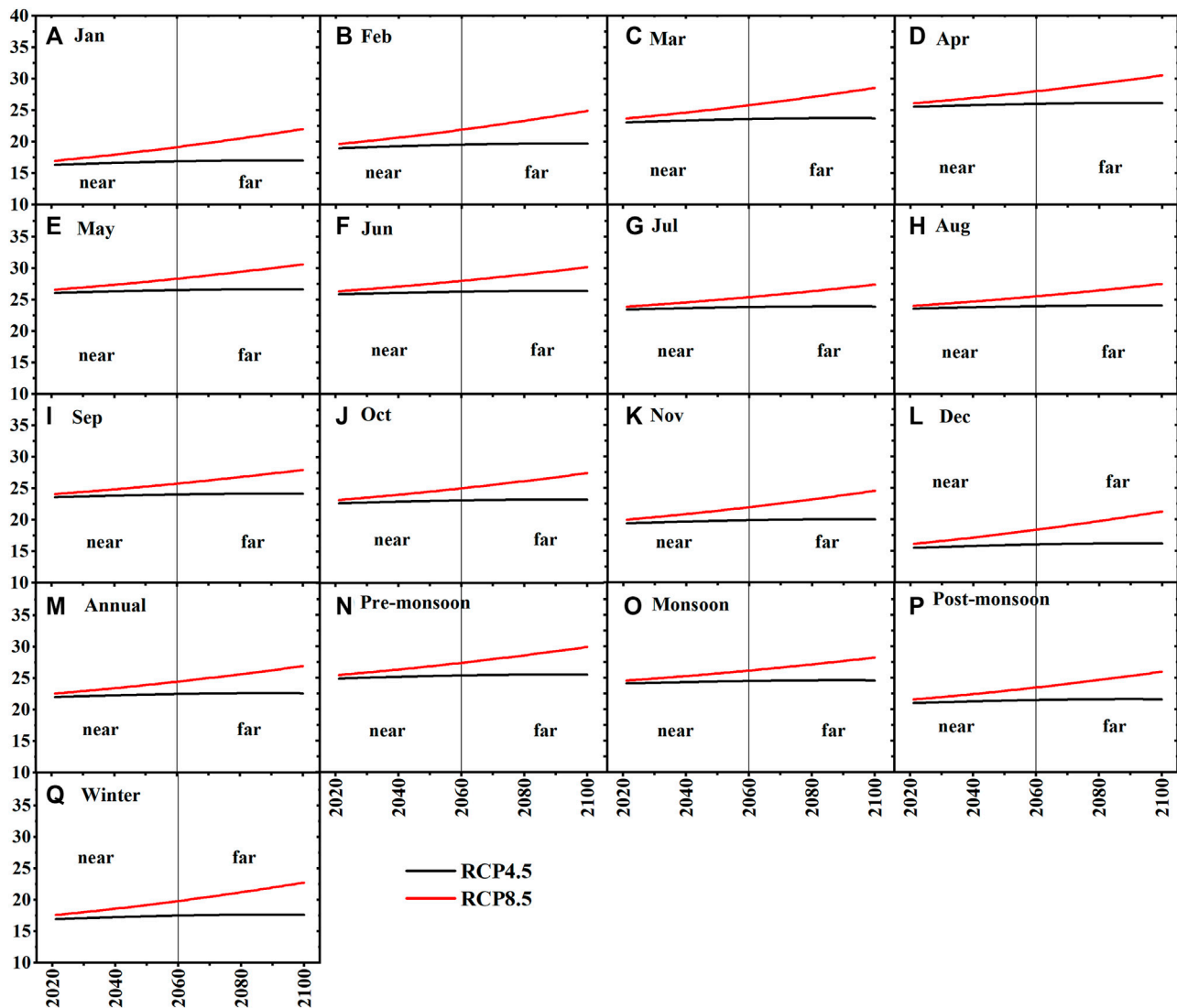


FIGURE 13

Monthly, Annual and Seasonal Tmin (°C) variability of multi-model ensemble (MME) of CMIP5 dataset under RCP4.5 and RCP8.5 for the near and far periods in Bangladesh. (A) January, (B) February, (C) March, (D) April, (E) May, (F) June, (G) July, (H) August, (I) September, (J) October, (K) November, (L) December, (M) Annual, (N) Pre-monsoon, (O) Monsoon, (P) Post-monsoon, and (Q) Winter.

eventually, the diurnal temperature range (DTR) will fall. Studies showed that the worldwide average DTR decreased significantly between 1950 and 1990 (Karl et al., 1991; Easterling et al., 1997). DTR decreases have also been documented in Bangladesh (Shahid et al., 2012; Abdullah et al., 2022) and neighboring India (Roy and Balling, 2005; Jhaharia and Singh 2011). DTR would decline by the existence of urban heat islands, land use changes owing to overpopulation and increased economic activities, and expansion in agricultural areas because of deforestation (Gallo et al., 1996; Bonan, 2001; Abdullah et al., 2022). Alternations in DTR can affect agricultural productivity and human health (Lobell, 2007; Shahid et al., 2012; Peng et al., 2013). Bangladesh might experience reduced rice yields in future as the investigation found that greater nighttime temperatures or lower DTR negatively impact rice yield (Peng et al., 2004). A decline in DTR would also increase human discomfort as greater summer Tmin will not permit the required

nocturnal cooling to offset the high Tmax throughout a heatwave period (De et al., 2005; Tam et al., 2009).

The maximum increase in temperature in February and minimum in July and August are not consistent with the findings of Alamgir et al. (2019). The present study revealed that winter will experience the highest increase in Tmax and Tmin, indicating that crops grown in winter will suffer from increased respiratory losses, thus, a reduction in yields is obvious. For example, dry season irrigated rice yield would be decreased by 13%–23% if the temperature rises by 4°C (Maniruzzaman et al., 2018). However, the result of this study agrees with several other studies (Manabe et al., 1991; Chowdhury and Ndiaye, 2017; Rahman and Rob, 2019). Chowdhury and Ndiaye (2017) also reported that the winter temperature (Tmax and Tmin) would increase faster in northern and central regions, which is mostly similar to our study.

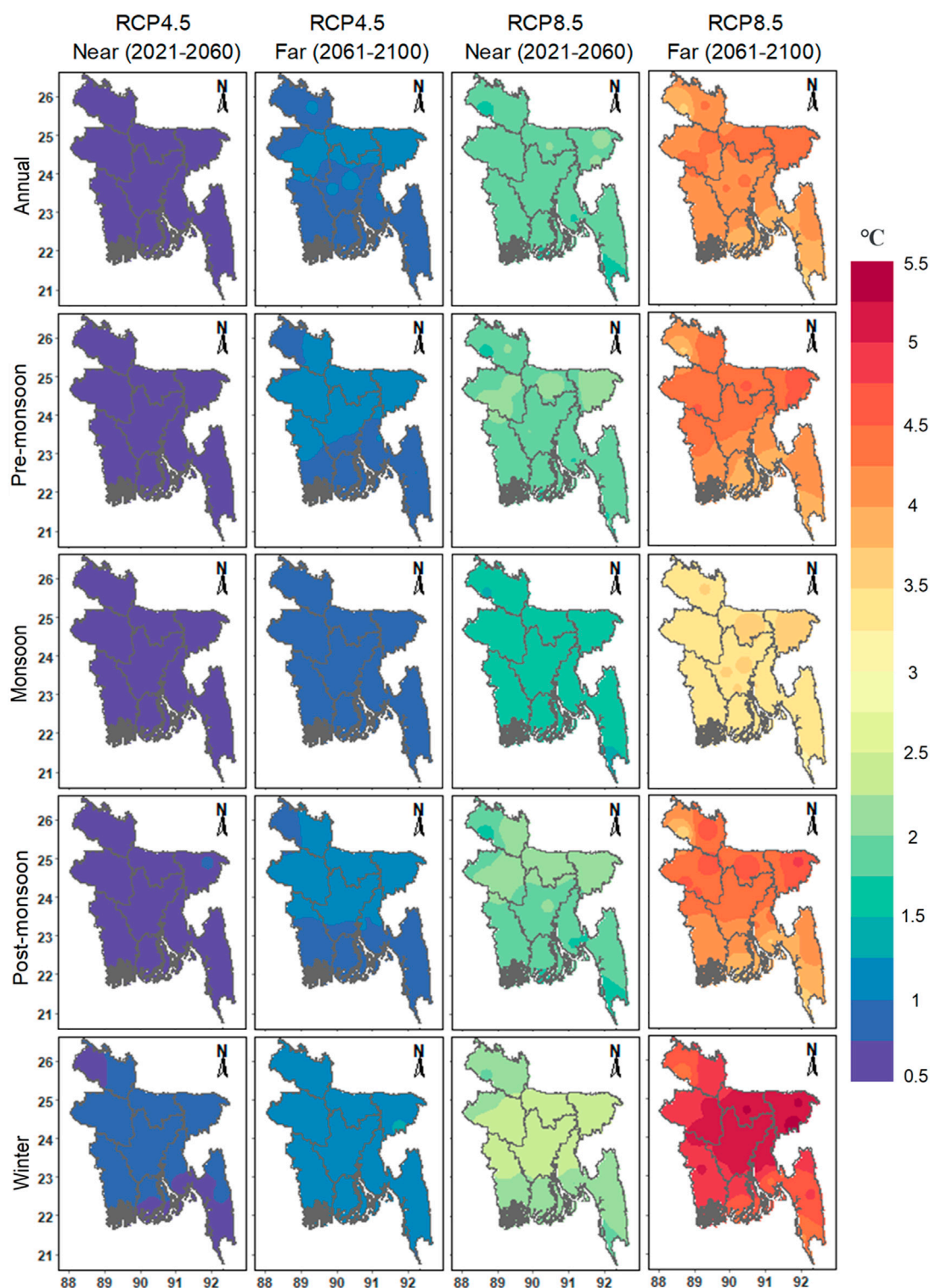


FIGURE 14

Spatial distribution of projected change in annual and seasonal T_{min} ($^{\circ}\text{C}$) for near (2021–2060) and far (2061–2100) future periods in Bangladesh for RCP8.5.

The projected monsoon T_{max} and T_{min} showed a relatively lower increase than in other seasons. Similar to annual and winter, the pre-monsoon and post-monsoon season exhibits greater changes in T_{max} and T_{min} . Central and northwestern regions were predicted to have the most significant annual and seasonal temperature

changes. The northwestern portion of Bangladesh, particularly the Barind region, is considered a drought-prone zone. The annual average rainfall over the region is about 1,400 and 1,550 mm (national average 2,200 mm), with an uneven distribution within the seasons (Shahid and Khairulmaini 2009). Due to the effects of

climate change, the spatial distribution of changes in drought characteristics shows that drought-vulnerable areas will expand in the future in the central and southern regions under both RCP4.5 and RCP8.5 scenarios (Kamruzzaman et al., 2019b; 2022). The highest increase in Tmax and Tmin in these regions may be attributable to land use and land cover (LULC) changes, less evaporative cooling and other factors (Shahid, 2011; Islam H. M. T. et al., 2021). Available soil moisture can remove surface heat through evaporation, but if the land is dry, there is no opportunity to transport it away, which increases the local temperature. However, a large increase in temperature might lead to an increase in rainfall through more evaporation. A number of studies also reported increasing rainfall in these regions (Fahad et al., 2018; Pour et al., 2018; Kamruzzaman et al., 2019b; Karim et al., 2020; Das et al., 2022b; Islam et al., 2022). Extreme rainfall events may increase with the increase in mean rainfall. This might result in higher flood risks, soil erosion, and crop loss (IPCC, 2014).

The MME projected a sharp temperature increase in all timescales over Bangladesh. It is very crucial to be aware of anthropogenic impacts on CC for sustainable development. Population growth, uncontrolled energy consumption, unplanned industrialization and urbanization, growing transportation, and LULC changes might increase GHG emissions in Bangladesh in the future. It eventually may cause a further rise in temperature. Therefore, it is required to investigate the variability and change in the driving factors of GHG emissions and temperature increase in Bangladesh to understand future temperature rise-induced consequences in Bangladesh. This will contribute to developing effective financial, environmental, and CC adaptation planning and mitigation strategies at the local and national levels.

Future studies should consider climatic hot spot areas of Bangladesh in the near future. Besides, future studies should consider high-resolution CMIP6 climate methods. The direct utilization of the climate model outputs is not suggested for decision-making research at a finer scale. Thus, the scientific community depends on multi-ensemble downscaling tools (e.g., SimCLIM model), which could further include uncertainty under specific scenarios. With the introduction of CMIP6 GCMs, an analogous evaluation can be done to obtain a better insight into the temperature projections of Bangladesh. Higher-resolution projections of temperature would also help to understand the complicated atmospheric processes.

5 Conclusion

The spatiotemporal patterns in future temperature (Tmax and Tmin) variabilities over Bangladesh in monthly, seasonal and yearly scales were examined in this study. A single GCM is insufficient for understanding CC in any region. Hence, multi-model ensembles (MME) were employed in this study to better assess temperature changes. In contrast to early studies, the present study adopted the median of 40-model CMIP5 GCMs to generate an MME. The key findings can be outlined as.

- Temperature for all timescales exhibited increasing trends in both future periods and RCPs. The SS estimator revealed a greater Tmax and Tmin rise in the near future than in the far future for RCP4.5, while the opposite for RCP8.5.

- The projected Tmax and Tmin revealed a higher increase in February and a lower increase in July and August.
- winter would experience the highest increase in Tmax and Tmin among the seasons for both future periods and RCPs.
- A higher increase in Tmin than Tmax for all timescales would cause a decrease in DTR in future, indicating a faster rise in nighttime temperature (Tmin) than the daytime temperature (Tmax).

The results of this study can support determining CC adaptation or mitigation strategies in Bangladesh. The study can be repeated with recently released CMIP6 GCMs to update the projections for the new scenarios. Besides, the projected changes in temperature extremes can be evaluated in a future study.

Data availability statement

The raw data supporting the conclusions of this article will be made available by the authors, without undue reservation.

Author contributions

HI: Formal analysis; visualization; writing—original draft. MK: Data curation; software; supervision; writing—review and editing. SS: Writing—review and editing. MM: Writing—review and editing. EA: writing—review and editing; AI: Supervision; JB: Writing—review, and editing. MI—review and editing.

Funding

The research was supported by a research grant from the Bangladesh Rice Research Institute (BRRI) under the project name: “Strengthening Farm Machinery Research Activity for Mechanized Rice Cultivation”; Project Code: 224298400, Ministry of Agriculture, Bangladesh. This study was undertaken with the financial help from a research project (CRP-II, 2ndPhase) of Krishi Gobeshona Foundation (KGF). The authors gratefully appreciate KGF for the help.

Conflict of interest

The authors declare that the research was conducted in the absence of any commercial or financial relationships that could be construed as a potential conflict of interest.

Publisher’s note

All claims expressed in this article are solely those of the authors and do not necessarily represent those of their affiliated organizations, or those of the publisher, the editors and the reviewers. Any product that may be evaluated in this article, or claim that may be made by its manufacturer, is not guaranteed or endorsed by the publisher.

References

- Abdullah, A. Y. M., Bhuiyan, M. H., Kiselev, G., Dewan, A., Hassan, Q. K., and Rafiuddin, M. (2022). Extreme temperature and rainfall events in Bangladesh: A comparison between coastal and inland areas. *Int. J. Climatol.* 42, 3253–3273. doi:10.1002/joc.6911
- Alamgir, M., Ahmed, K., Homs, R., Dewan, A., Wang, J. J., and Shahid, S. (2019). Downscaling and projection of spatiotemporal changes in temperature of Bangladesh. *Earth Syst. Environ.* 3, 381–398. doi:10.1007/s41748-019-00121-0
- Alamgir, M., Shahid, S., Hazarika, M. K., Nashrullah, S., Harun, S. B., Shamsudin, S., et al. (2015). Analysis of meteorological drought pattern during different climatic and cropping seasons in Bangladesh. *J. Amer. Water Resour. Assoc.* 51, 794–806. doi:10.1111/jawr.12276
- Ali, S., Kiani, R. S., Reboita, M. S., Dan, L., Eum, H., Cho, J., et al. (2021). Identifying hotspots cities vulnerable to climate change in Pakistan under CMIP5 climate projections. *Int. J. Climatol.* 41, 559–581. doi:10.1002/joc.6638
- Allen, C. D., Macalady, A. K., Chenchouni, H., Bachelet, D., McDowell, N., Vennetier, M., et al. (2010). A global overview of drought and heat-induced tree mortality reveals emerging climate change risks for forests. *For. Ecol. Manage.* 259, 660–684. doi:10.1016/j.foreco.2009.09.001
- Almazroui, M., Islam, M. N., Alkhalaf, A. K., Saeed, F., Dambul, R., and Rahman, M. A. (2016). Simulation of temperature and precipitation climatology for the CORDEX-MENA/Arab domain using RegCM4. *Arabian J. Geosciences* 9, 13. doi:10.1007/s12517-015-2045-7
- Almazroui, M., Khalid, M. S., Islam, M. N., and Saeed, S. (2020a). Seasonal and regional changes in temperature projections over the Arabian Peninsula based on the CMIP5 multi-model ensemble dataset. *Atmos. Res.* 239, 104913. doi:10.1016/j.atmosres.2020.104913
- Almazroui, M., Saeed, S., Saeed, F., Islam, M. N., and Ismail, M. (2020b). Projections of precipitation and temperature over the south asian countries in CMIP6. *Earth Syst. Environ.* 4, 297–320. doi:10.1007/s41748-020-00157-7
- Amin, A., Nasim, W., Fahad, S., Ali, S., Ahmad, S., Rasool, A., et al. (2018a). Evaluation and analysis of temperature for historical (1996–2015) and projected (2030–2060) climates in Pakistan using SimCLIM climate model: Ensemble application. *Atmos. Res.* 213, 422–436. doi:10.1016/j.atmosres.2018.06.021
- Amin, A., Nasim, W., Mubeen, M., Sarwar, S., Urich, P., Ahmad, A., et al. (2018b). Regional climate assessment of precipitation and temperature in Southern Punjab (Pakistan) using SimCLIM climate model for different temporal scales. *Theor. Appl. Climatol.* 131, 121–131. doi:10.1007/s00704-016-1960-1
- BMD (2020). Bangladesh climate data portal. Agargoan, Dhaka: Government of Bangladesh. Available at: <http://bmd.wowspace.org/team/homex.php> (Accessed January 10, 2021).
- Bonan, G. B. (2001). Observational evidence for reduction of daily maximum temperature by Croplands in the Midwest United States. *J. Clim.* 14, 2430–2442. doi:10.1175/1520-0442(2001)014<2430:oeofdr>2.0.co;2
- Bosu, H., Rashid, T., Mannan, A., and Meandad, J. (2021). Climate change analysis for Bangladesh using CMIP5 models. *Dhaka Univ. J. Earth Environ. Sci.* 9, 1–12. doi:10.3329/duees.v9i1.54856
- Chotamonsak, C., Salathé, E. P., Kresuwan, J., Chantara, S., and Siriwitayakorn, K. (2011). Projected climate change over Southeast Asia simulated using a WRF regional climate model. *Atmos. Sci. Lett.* 12, 213–219. doi:10.1002/asl.313
- Chowdhury, M. R., and Ndiaye, O. (2017). Climate change and variability impacts on the forests of Bangladesh—a diagnostic discussion based on CMIP5 GCMs and ENSO. *Int. J. Climatol.* 37, 4768–4782. doi:10.1002/joc.5120
- Daly, C. (2006). Guidelines for assessing the suitability of spatial climate data sets. *Int. J. Climatol.* 26 (6), 707–721. doi:10.1002/joc.1322
- Das, S., Islam, A., and Kamruzzaman, M. (2022a). Assessment of climate change impact on temperature extremes in a tropical region with the climate projections from CMIP6 model. *Clim. Dyn.* doi:10.1007/S00382-022-06416-9
- Das, S., Kamruzzaman, M., and Islam, A. (2022b). Assessment of characteristic changes of regional estimation of extreme rainfall under climate change: A case study in a tropical monsoon region with the climate projections from CMIP6 model. *J. Hydrol. (Amst)* 610, 128002. doi:10.1016/j.jhydrol.2022.128002
- De, U. S., Dube, R. K., Rao, G. S. P., and Easterling, D. R. (2005). Extreme weather events over India in the last 100 years. *J. Indian Geophys. Union* 9, 277.
- Easterling, D. R., Horton, B., Jones, P. D., Peterson, T. C., Karl, T. R., Parker, D. E., et al. (1997). Maximum and minimum temperature trends for the globe. *Science* 277 (5324), 364–367. doi:10.1126/science.277.5324.364
- Fahad, M. G. R., Saiful Islam, A. K. M., Nazari, R., Alfi Hasan, M., Tarekul Islam, G. M., and Bala, S. K. (2018). Regional changes of precipitation and temperature over Bangladesh using bias-corrected multi-model ensemble projections considering high-emission pathways. *Int. J. Climatol.* 38, 1634–1648. doi:10.1002/joc.5284
- Gallo, K. P., Easterling, D. R., and Peterson, T. C. (1996). The influence of land use/land cover on climatological values of the diurnal temperature range. *J. Clim.* 9, 2941–2944. doi:10.1175/1520-0442(1996)009<2941:tioluc>2.0.co;2
- Hasan, M. A., Hasan, M. A., and Islam, A. K. M. S. (2013). “Changes of seasonal temperature extremes in future over Bangladesh using projections by a regional climate model high end climate impact and extremes (HELIX) view project STARS project view project changes of seasonal temperature extremes in future over Bangladesh using projections by a regional climate model,” in Proceeding of the National Seminar on Climate Change Impact and Adaptation Center for Climate Change and Sustainability Research (3CSR).
- Hasan, M. A., Islam, A. K. M. S., and Akanda, A. S. (2018). Climate projections and extremes in dynamically downscaled CMIP5 model outputs over the bengal delta: A quartile based bias-correction approach with new gridded data. *Clim. Dyn.* 51, 2169–2190. doi:10.1007/s00382-017-4006-1
- Hossain, M. B., Rahman, M. M., Biswas, J. C., Miah, M. M. U., Akhter, S., Maniruzzaman, M., et al. (2017). Carbon mineralization and carbon dioxide emission from organic matter added soil under different temperature regimes. *Int. J. Recycl. Waste Agric.* 6, 311–319. doi:10.1007/s40093-017-0179-1
- Hossain, M. B., Roy, D., Maniruzzaman, M., Biswas, J. C., Naher, U. A., Haque, M. M., et al. (2021). Response of crop water requirement and yield of irrigated rice to elevated temperature in Bangladesh. *Int. J. Agron.* 2021, 1–11. doi:10.1155/2021/9963201
- Huq, S. (2001). Climate change and Bangladesh. *Science* 294, 1617. doi:10.1126/science.294.5547.1617
- IPCC (2007). “Technical summary of climate change 2007: The physical science basis,” in *Contribution of working group I to the fourth assessment report of the intergovernmental panel on climate change*.
- IPCC (2014). *IPCC, 2014: Climate change 2014: Mitigation of climate change. Contribution of working group III to the fifth assessment report of the intergovernmental panel on climate change*.
- Islam, A. R. M. T., Islam, H. M. T., Shahid, S., Khatun, M. K., Ali, M. M., Rahman, M., et al. (2021). Spatiotemporal nexus between vegetation change and extreme climatic indices and their possible causes of change. *J. Environ. Manage.* 289, 112505. doi:10.1016/j.jenvman.2021.112505
- Islam, H. M. T., Islam, A., Abdullah-Al-Mahbub, M., Shahid, S., Tasnuva, A., Kamruzzaman, M., et al. (2021). Spatiotemporal changes and modulations of extreme climatic indices in monsoon-dominated climate region linkage with large-scale atmospheric oscillation. *Atmos. Res.* 264, 105840. doi:10.1016/j.atmosres.2021.105840
- Islam, H. M. T., Islam, A. R. M. T., Shahid, S., Alam, G. M. M., Biswas, J. C., Rahman, M. M., et al. (2022). Future precipitation projection in Bangladesh using SimCLIM climate model: A multi-model ensemble approach. *Int. J. Climatol.* 42, 6716–6740. doi:10.1002/joc.7605
- Jerin, J. N., Islam, H. M. T., Islam, A. M. R. T., Shahid, S., Hu, Z., Badhan, M. A., et al. (2021). Spatiotemporal trends in reference evapotranspiration and its driving factors in Bangladesh. *Theor. Appl. Climatol.* 144, 793–808. doi:10.1007/s00704-021-03566-4
- Jhajharia, D., and Singh, V. P. (2011). Trends in temperature, diurnal temperature range and sunshine duration in Northeast India. *Int. J. Climatol.* 31, 1353–1367. doi:10.1002/joc.2164
- Kamruzzaman, M., Almazroui, M., Salam, M. A., Mondol, M. A. H., Rahman, M. M., Deb, L., et al. (2022). Spatiotemporal drought analysis in Bangladesh using the standardized precipitation index (SPI) and standardized precipitation evapotranspiration index (SPEI). *Sci. Rep.* 12, 20694. doi:10.1038/s41598-022-24146-0
- Kamruzzaman, M., Hwang, S., Cho, J., Jang, M. W., and Jeong, H. (2019a). Evaluating the spatiotemporal characteristics of agricultural drought in Bangladesh using effective drought index. *WaterSwitzerl.* 11, 2437. doi:10.3390/w11122437
- Kamruzzaman, M., Jang, M.-W. W., Cho, J., and Hwang, S. (2019b). Future changes in precipitation and drought characteristics over Bangladesh under CMIP5 climatological projections. *Water* 11, 2219. doi:10.3390/w11112219
- Kamruzzaman, M., Shahid, S., Islam, A. T., Hwang, S., Cho, J., et al. (2021a). Comparison of CMIP6 and CMIP5 model performance in simulating historical precipitation and temperature in Bangladesh: A preliminary study. *Theor. Appl. Climatol.* 145, 1385–1406. doi:10.1007/s00704-021-03691-0
- Kamruzzaman, M., Shahid, S., Roy, D. K., Islam, A. R. M. T., Hwang, S., Cho, J., et al. (2021b). Assessment of CMIP6 global climate models in reconstructing rainfall climatology of Bangladesh. *Int. J. Climatol.* n/a 42, 3928–3953. doi:10.1002/joc.7452
- Karim, F., Mainuddin, M., Hasan, M., and Kirby, M. (2020). Assessing the potential impacts of climate changes on rainfall and evapotranspiration in the northwest region of Bangladesh. *Climate* 8, 94. doi:10.3390/CLI8080094
- Karl, T. R., Kukla, G., Razuvayev, V. N., Changery, M. J., Quayle, R. G., Heim, R. R., et al. (1991). Global warming: Evidence for asymmetric diurnal temperature change. *Geophys. Res. Lett.* 18, 2253–2256. doi:10.1029/91GL02900
- Katzenberger, A., Schewe, J., Pongratz, J., and Levermann, A. (2021). Robust increase of Indian monsoon rainfall and its variability under future warming in CMIP6 models. *Earth Syst. Dyn.* 12, 367–386. doi:10.5194/esd-12-367-2021
- Kendall, M. G. (1975). *Rank Correlation measures* (London: Charles Griffin), 25–55.
- King, A. D., Knutti, R., Uhe, P., Mitchell, D. M., Lewis, S. C., Arblaster, J. M., et al. (2018). On the linearity of local and regional temperature changes from 1.5°C to 2°C of global warming. *J. Clim.* 31, 7495–7514. doi:10.1175/JCLI-D-17-0649.1
- Kothawale, D. R., Munot, A. A., and Kumar, K. K. (2010). Surface air temperature variability over India during 1901–2007, and its association with ENSO. *Clim. Res.* 42, 89–104. doi:10.3354/cr00857

- Kumar, P., and Sarthi, P. P. (2019). Surface temperature evaluation and future projections over India using CMIP5 models. *Pure Appl. Geophys.* 176, 5177–5201. doi:10.1007/s00024-019-02203-6
- Lobell, D. B. (2007). Changes in diurnal temperature range and national cereal yields. *Agric. For. Meteorol.* 145, 229–238. doi:10.1016/j.agrformet.2007.05.002
- Mainuddin, M., Peña-Arancibia, J. L., Karim, F., Hasan, M. M., Mojid, M. A., and Kirby, J. M. (2022). Long-term spatio-temporal variability and trends in rainfall and temperature extremes and their potential risk to rice production in Bangladesh. *PLOS Clim.* 1, e0000009. doi:10.1371/journal.pclm.0000009
- Mallick, J., Islam, A. R. M. T., Ghose, B., Islam, H. M. T., Rana, Y., Hu, Z., et al. (2022a). Spatiotemporal trends of temperature extremes in Bangladesh under changing climate using multi-statistical techniques. *Theor. Appl. Climatol.* 147, 307–324. doi:10.1007/s00704-021-03828-1
- Mallick, J., Salam, R., Islam, H. M. T., Shahid, S., Kamruzzaman, M., Pal, S. C., et al. (2022b). Recent changes in temperature extremes in subtropical climate region and the role of large-scale atmospheric oscillation patterns. *Theor. Appl. Climatol.* 148, 329–347. doi:10.1007/s00704-021-03914-4
- Manabe, S., Stouffer, R. J., Spelman, M. J., and Bryan, K. (1991). Transient responses of a coupled ocean-atmosphere model to gradual changes of atmospheric CO₂. Part I. Annual mean response. *J. Clim.* 4, 785–818. doi:10.1175/1520-0442(1991)004<0785:troaco>2.0.co;2
- Maniruzzaman, M., Biswas, J. C., Hossain, M. B., Haque, M. M., Naher, U. A., Choudhury, A. K., et al. (2018). Effect of elevated air temperature and carbon dioxide levels on dry season irrigated rice productivity in Bangladesh. *Am. J. Plant Sci.* 09, 1557–1576. doi:10.4236/ajps.2018.97114
- Mann, H. B. (1945). Nonparametric tests against trend. *Econometrica* 13 (3), 245–259. doi:10.2307/1907187
- Naher, U. A., Hossain, M. B., Haque, M. M., Maniruzzaman, M., Choudhury, A. K., and Biswas, J. C. (2020). Effect of long-term nutrient management on soil organic carbon sequestration in rice-rice-fallow rotation. *Curr. Sci.* 118, 587. doi:10.18520/cs/v118/i4/587-592
- Novotny, E. V., and Stefan, H. G. (2007). Stream flow in Minnesota: Indicator of climate change. *J. Hydrol. (Amst)* 334, 319–333. doi:10.1016/j.jhydrol.2006.10.011
- Ozturk, T., Turp, M. T., Türkeş, M., and Kurnaz, M. L. (2018). Future projections of temperature and precipitation climatology for CORDEX-MENA domain using RegCM4.4. *Atmos. Res.* 206, 87–107. doi:10.1016/j.atmosres.2018.02.009
- Pattnayak, K. C., Kar, S. C., Dalal, M., and Pattnayak, R. K. (2017). Projections of annual rainfall and surface temperature from CMIP5 models over the BIMSTEC countries. *Glob. Planet. Change* 152, 152–166. doi:10.1016/j.gloplacha.2017.03.005
- Peng, S., Huang, J., Sheehy, J. E., Laza, R. C., Visperas, R. M., Zhong, X., et al. (2004). Rice yields decline with higher night temperature from global warming. *Proc. Natl. Acad. Sci. U. S. A.* 101, 9971–9975. doi:10.1073/pnas.0403720101
- Peng, S., Piao, S., Ciais, P., Myneni, R. B., Chen, A., Chevallier, F., et al. (2013). Asymmetric effects of daytime and night-time warming on Northern Hemisphere vegetation. *Nature* 501, 88–92. doi:10.1038/nature12434
- Pérez, J., Correa-Araneda, F., López-Rojó, N., Basaguren, A., and Boyero, L. (2021). Extreme temperature events alter stream ecosystem functioning. *Ecol. Indic.* 121, 106984. doi:10.1016/j.ecolind.2020.106984
- Pour, S. H., Shahid, S., Chung, E. S., and Wang, X. J. (2018). Model output statistics downscaling using support vector machine for the projection of spatial and temporal changes in rainfall of Bangladesh. *Atmos. Res.* 213, 149–162. doi:10.1016/j.atmosres.2018.06.006
- Rahman, M. M., and Rob, M. A. (2019). The use of a CMIP5 climate model to assess regional temperature and precipitation variation due to climate change: A case study of Dhaka megacity, Bangladesh. *Earth Syst. Environ.* 3, 399–417. doi:10.1007/s41748-019-00117-w
- Rahman, M. R., and Lateh, H. (2016). Meteorological drought in Bangladesh: Assessing, analysing and hazard mapping using SPI, GIS and monthly rainfall data. *Environ. Earth Sci.* 75, 1026. doi:10.1007/s12665-016-5829-5
- Rashid, M. M., Beecham, S., and Chowdhury, R. K. (2015). Statistical downscaling of CMIP5 outputs for projecting future changes in rainfall in the Onkaparinga catchment. *Sci. Total Environ.* 530–531, 171–182. doi:10.1016/j.scitotenv.2015.05.024
- Rogelj, J., Meinshausen, M., and Knutti, R. (2012). Global warming under old and new scenarios using IPCC climate sensitivity range estimates. *Nat. Clim. Chang.* 2, 248–253. doi:10.1038/nclimate1385
- Roy, S. S., and Balling, R. C. (2005). Analysis of trends in maximum and minimum temperature, diurnal temperature range, and cloud cover over India. *Geophys. Res. Lett.* 32 (12). doi:10.1029/2004GL022201
- Sen, P. K. (1968). Estimates of the regression coefficient based on Kendall's tau. *J. Am. Stat. Assoc.* 63, 1379–1389. doi:10.1080/01621459.1968.10480934
- Shahid, S., Harun, S. B., and Katimon, A. (2012). Changes in diurnal temperature range in Bangladesh during the time period 1961–2008. *Atmos. Res.* 118, 260–270. doi:10.1016/j.atmosres.2012.07.008
- Shahid, S. (2011). Impact of climate change on irrigation water demand of dry season Boro rice in northwest Bangladesh. *Clim. Change* 105, 433–453. doi:10.1007/s10584-010-9895-5
- Shahid, S., and Khairulmaini, O. S. (2009). Spatio-temporal variability of rainfall over Bangladesh during the time period 1969–2003. *Asia. Pac. J. Atmos. Sci.* 43 (3), 375–389.
- Song, Y. H., Chung, E. S., and Shahid, S. (2021). Spatiotemporal differences and uncertainties in projections of precipitation and temperature in South Korea from CMIP6 and CMIP5 general circulation models. *Int. J. Climatol.* 41, 5899–5919. doi:10.1002/joc.7159
- Tam, W. W. S., Wong, T. W., Chair, S. Y., and Wong, A. H. S. (2009). Diurnal temperature range and daily cardiovascular mortalities among the elderly in Hong Kong. *Arch. Environ. Occup. Health* 64, 202–206. doi:10.1080/19338240903241192
- Taylor, K. E., Stouffer, R. J., and Meehl, G. A. (2012). An overview of CMIP5 and the experiment design. *Bull. Amer. Meteor. Soc.* 93 (4), 485–498. doi:10.1175/BAMS-D-11-00094.1
- Tobin, C., Nicotina, L., Parlange, M. B., Berne, A., and Rinaldo, A. (2011). Improved interpolation of meteorological forcings for hydrologic applications in a Swiss Alpine region. *J. Hydrol.* 401 (1–2), 77–89. doi:10.1016/j.jhydrol.2011.02.010
- Wang, X., Hou, X., Piao, Y., Feng, A., and Li, Y. (2021). Climate change projections of temperature over the coastal area of China using SimCLIM. *Front. Environ. Sci.* 9. doi:10.3389/fenvs.2021.782259
- Warrick, R. A., Ashford, G., Kouwenhoven, P., Li, Y., Urlich, P., and Ye, W. (2012). Spatial risk-based assessments for climate adaptation using the SimCLIM modelling system: A case study of domestic rainwater harvesting as the sole source of water. *J. Water Clim. Change* 3, 257–265. doi:10.2166/wcc.2012.003
- Warrick, R. A. (2009). “Using SimCLIM for modelling the impacts of climate extremes in a changing climate: A preliminary case study of household water harvesting in Southeast Queensland,” in *Proceeding of the 18th World IMACS Congress and MODSIM 2009 - International Congress on Modelling and Simulation: Interfacing Modelling and Simulation with Mathematical and Computational Sciences*.
- Xu, C., and Xu, Y. (2012). The projection of temperature and precipitation over China under RCP scenarios using a CMIP5 multi-model ensemble. *Atmos. Oceanic Sci. Lett.* 5 (6), 527–533. doi:10.1080/16742834.2012.11447042
- Yang, Y., and Rong-Cai, R. (2015). Understanding the global surface-atmosphere energy balance in FGOALS-s2 through an attribution analysis of the global temperature biases. *Atmos. Ocean. Sci. Lett.* 8, 107–112. doi:10.1080/16742834.2015.11447246
- Yang, Y., Bai, L., Wang, B., Wu, J., and Fu, S. (2019). Reliability of the global climate models during 1961–1999 in arid and semiarid regions of China. *Sci. Tot. Environ.* 667, 271–286. doi:10.1016/j.scitotenv.2019.02.188
- Yin, C., Li, C., and Clim, P. U. (2013). *SimCLIM 2013 data manual*.
- Zheng, Z., Hoogenboom, G., Cai, H., and Wang, Z. (2020). Winter wheat production on the Guanzhong Plain of Northwest China under projected future climate with SimCLIM. *Agric. Water Manag.* 239, 106233. doi:10.1016/j.agwat.2020.106233



OPEN ACCESS

EDITED BY

Shaoquan Liu,
Institute of Mountain Hazards and
Environment (CAS), China

REVIEWED BY

Suhong Zhou,
Sun Yat-sen University, China
Tayierjiang Aishan,
Xinjiang University,
China
Dong Dong,
Institute of Geographic Sciences and
Natural Resources Research (CAS),
China

*CORRESPONDENCE

Xianhui Feng
✉ xhfeng@scut.edu.cn

SPECIALTY SECTION

This article was submitted to
Interdisciplinary Climate Studies,
a section of the journal
Frontiers in Ecology and Evolution

RECEIVED 26 October 2022

ACCEPTED 08 December 2022

PUBLISHED 09 January 2023

CITATION

Feng X, Zeng Z and He M (2023) A 20-year
vegetation cover change and its response
to climate factors in the Guangdong-Hong
Kong-Macao Greater Bay Area under the
background of climate change.
Front. Ecol. Evol. 10:1080734.
doi: 10.3389/fevo.2022.1080734

COPYRIGHT

© 2023 Feng, Zeng and He. This is an
open-access article distributed under the
terms of the [Creative Commons Attribution
License \(CC BY\)](#). The use, distribution or
reproduction in other forums is permitted,
provided the original author(s) and the
copyright owner(s) are credited and that
the original publication in this journal is
cited, in accordance with accepted
academic practice. No use, distribution or
reproduction is permitted which does not
comply with these terms.

A 20-year vegetation cover change and its response to climate factors in the Guangdong-Hong Kong-Macao Greater Bay Area under the background of climate change

Xianhui Feng^{1*}, Zhilin Zeng² and Mu He¹

¹School of Architecture, South China University of Technology, Guangzhou, China, ²Health Science Center, Yangtze University, Jingzhou, Hubei, China

Introduction: The Guangdong-Hong Kong-Macao Greater Bay Area (GBA) is located in the south subtropical area along the southeast coast of China, which is one of the world-class urban agglomerations and an important part for economic development. In order to investigate the change of vegetation indexes and its response to climate factors in such circumstance of climate change, this study is an important component in the protection and establishment of the ecological environment in the GBA.

Methods: The Moderate Resolution Imaging Spectroradiometer-Enhanced Vegetation Index (MODIS-EVI) and climate data were recorded from National Aeronautics and Space Administration (NASA) and Resource and Environment Science Data Center of the Chinese Academy of Sciences. Trend analysis, Mann-Kendall (MK) Test and rescaled range analysis (R/S Analysis) offer an effective way of analyzing the correlation between the vegetation cover change and climate factors.

Results: The results provide important insights into the following aspects: (1) The changes of climate factors (temperature, precipitation, wind speed, humidity, and sunshine radiation) are fluctuated in GBA, with no obvious increasing or decreasing trend. It comprehensively exhibited an extremely slow development of humidify and warming. (2) It presents an increasing trend of EVI in GBA, with the rate of 0.0045/a. The range of increase is in the middle level ($0.4 \leq \text{EVI} < 0.6$) based on the EVI. The vegetation cover in GBA is improved comprehensively, the area of vegetation improvement is larger than the area of vegetation degression, with the extremely improved vegetation cover area (66.98%) and the extremely degraded vegetation cover area (5.70%). There are obvious differences and agglomerations in the distribution of the EVI trends. (3) In future, the changing trends will be combinedly affected by various factors, and there is no obvious factor temporarily. The improved vegetation cover area (over 80%) are predicted. (4) There are significant spatiotemporal differences in the annual effects of EVI on various climate factors comprehensively. Wind speed and relative humidity have the strongest correlations with EVI; the area of significant correlation is more than 40% of the pixels. The correlation between temperature and EVI is second, with the area of significant correlation over 20% of the pixels. The precipitation

and sunshine radiation weakly correlated with EVI, with the area of significant correlation is less than 5% of the pixels.

Discussion: The result of this study indicated that the EVI changing trend in the future by R/S analysis method is affected by climate and human factors together and there are no significant factors. The result indicated precipitation has no significant correlation with EVI trends in the Hot and humid area with mean precipitation of 1800mm. However, there is a significant positive correlation between the EVI trend and two climate factors (relative humidity and wind speed). In the terms of spatial distribution, the influence of temperature to EVI is complex in GBA, the spatial distribution of correlation is scattered.

KEYWORDS

EVI, spatiotemporal characteristics, climate factors, climate factors change, Guangdong-Hong Kong-Macao Greater Bay Area

1. Introduction

Vegetation is the fundamental component of terrestrial ecosystems, which plays vital roles in material cycling and energy conversion. Furthermore, evidence suggests that vegetation cover is among the most irreplaceable factors for water and soil conservation, climate mitigation, and global carbon balance (Piao et al., 2011, 2020). Fractional vegetation cover (FVC) is an important indicator of vegetation cover, which comprehensively indicates the growth of vegetation communities, and is monitored as a vital indicator of ecosystem (Gitelson et al., 2002; Wang et al., 2003). The existing body of research on large-scale remote sensing suggests that it is difficult to investigate the change in vegetation cover through ground-based observations. Instead, the Vegetation Index (VI) is currently the most popular index for investigating vegetation cover by remote sensing. The Moderate Resolution Imaging Spectroradiometer was equipped on the Terra and Aqua satellites, with 36 bands, collected the normalized difference vegetation index (NDVI) and enhanced vegetation index (EVI), both of which indicate the change of vegetation cover accurately (Xiao and Moody, 2005; Cheng et al., 2008; Pei et al., 2015). EVI, an improved version of NDVI can elucidate the impact of saturation of vegetation growth (Wang et al., 2006; Li et al., 2007; Chen et al., 2014; Zhang et al., 2021).

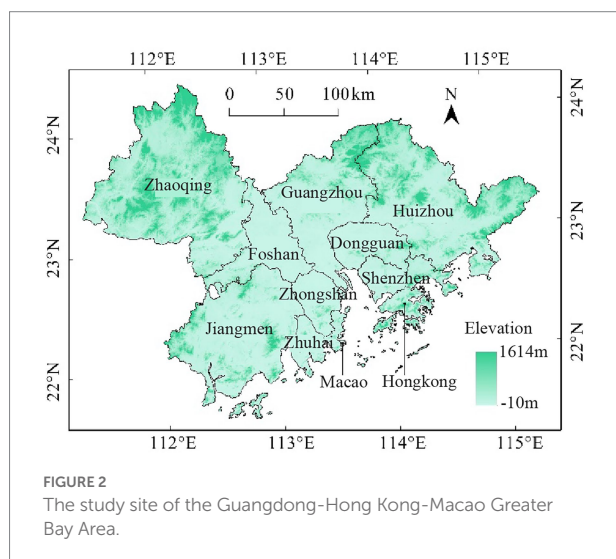
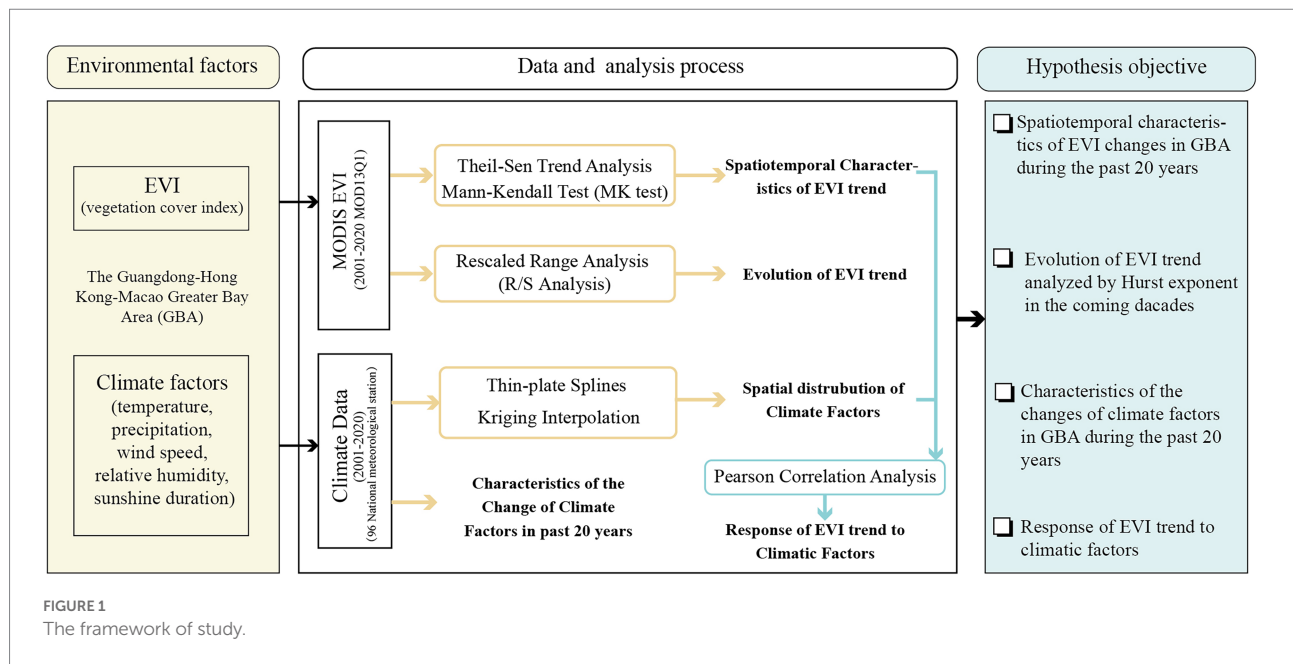
The influence of climate change on vegetation cover has long been a question of great interest in a wide range of fields. The change of vegetation cover *via* impacting the characteristics of the vegetation growth, and further impact the structure and capability of ecosystem. Vegetation cover change, which enlarge the carbon pool of terrestrial ecosystems through the plant growth, influence the climate by change the bio-geophysical properties of organisms on the earth (Xia et al., 2013; Jiang et al., 2017; Liu et al., 2019).

A considerable amount of literature has been investigated that the most significant phenomenon of climate change is that changes in vegetation growth are impacted by the climate change in the long time series and large spatial scale. These studies revealed that vegetation cover represents the conditions of ecosystems objectively (Myneni et al., 1997; Tucker et al., 2001; Parmesan, 2006; Fensholt et al., 2012). Much of the literature since the last 20 years emphasizes

the vegetation cover change and its influential factors in different climate zones by using VI. Because of the differences in various climate zones, there are obvious gaps among these results. Collectively, these studies outline a critical role for identifying the main factors of vegetation cover change that are human activities and climate factors. On the contrary, the relationship between vegetation cover change and its influential factors in different climate zone is extremely complex. There are linear correlations in some sites and non-linear in others. Additionally, the range of influence of different climate factors is distinct relatively (Gan et al., 2011; Mu et al., 2012; Liu et al., 2013, 2021; Li et al., 2017; de la Barrera and Henríquez, 2017; Zhang et al., 2019; He et al., 2020), while the utilization of different VI lead to dissimilar results (Li et al., 2007; Ye et al., 2012; Xie et al., 2022).

The Guangdong-Hong Kong-Macao Greater Bay Area (GBA) is the largest alluvial plain in subtropical zone of China. There is a long coastline and a dense river network around the GBA. In terms of climate characteristic, GBA is in the south subtropical humid monsoon climate zone, with hot summer and warm winter in the Hot and humid area. Furthermore, a major characteristic of the climate of GBA is that high temperature throughout the year, adequate sunshine radiation, and abundant precipitation. The existing literature on the vegetation cover change in GBA is extensive and focuses particularly on the NDVI and its influential mechanisms (He, 2019; Hu and Xia, 2019; Deng et al., 2021; Feng et al., 2022; Zhao et al., 2022). The GBA is in the climate of high temperature and relative humidity, with the growth of lush plants. Under such circumstance, the NDVI tends to be saturated, since it is unsensitive to the lush vegetation. Not only do the EVI elucidate the disruption of atmosphere and the saturation, but, in the same spatial resolution, also indicate the differences in spatial distribution of the high-saturated vegetation cover better.

Together, this study gathered and analyzed the EVI and climate data from 2001 to 2020 in GBA. We indicated the characteristics of vegetation cover *via* EVI and its changing trend by using Theil-Sen approach, Mann-Kendall (MK) test and Rescaled range analysis (R/S analysis). The characteristics of climate change for 20 years were analyzed. The correlation between the EVI changing trends and the change of climate factors was analyzed, which revealed the



spatiotemporal characteristics of the EVI changes and its internal mechanism by the influence of climate change (Figure 1).

2. Materials and methods

2.1. Study area

The Greater Bay Area (GBA) is located in the central part of Guangdong Province (21° 26'N–24° 28' N, 111° 14'E–115° 24'E), covers $5.6 \times 10^4 \text{ km}^2$, including the nine municipalities: Guangzhou (GZ), Shenzhen (SZ), Zhuhai (ZH), Foshan (FS), Huizhou (HZ), Dongguan (DG), Zhongshan (ZS), Jiangmen (JM), Zhaoqing (ZQ) and the two Special Administrative Region: Hong Kong (HK) and Macao (MC; Figure 2). GBA is a world-class urban agglomeration, an important engine of economic growth, and a spatial carrier to

participate in global competition. GBA in the south-subtropical monsoon climate zone, with an annual mean temperature of 21–23°C and an annual mean precipitation of 1,300–2,400 mm. It is surrounded by mountains and hills on three sides (east, west, and north), plains in the middle, and borders the South China Sea. The main types of land use in GBA are forest, agricultural, and residential and constructional. Forest area is mainly distributed in the mountainous areas in the east, west, and north, such as ZQ, JM, HZ, and northern GZ, while residential land and construction land is mainly distributed in the center of urban agglomeration, such as southern GZ, FS, DG, SZ, HK, ZS, ZH, and MC. The vegetation in the study area is dominated by evergreen broadleaf forests in south-subtropical zone, rainforest forests in the subtropics, and mangroves.

2.2. Data sources and pre-processing

The vegetation cover in the study area grew lushly, and to eradicate the influence of saturated VI. Therefore, Enhanced Vegetation Index (EVI) selected for analyzing the trend of vegetation changes.

The MODIS Land Cover Type Product (MOD13Q1) supplies global maps of land cover at annual time steps and 250-m spatial resolution from 2001 to 2020 (23 images per year). After downloaded the data, we used MODIS Reprojection Tools (MRT) to reproject the images, with the Projection coordinate system named Albers Equal Area, and regard the boundary as mask to clip the raster. The annual maximum of EVI in GBA is combined from annual images by the method of maximum value composite (MVC). Finally, we reconstruct the annual maximum of EVI in time series by the Savitzky–Golay filter (S-G filter).

The data of climate factors (temperature, precipitation, wind speed, relative humidity, and sunshine duration) was provided by Resource and Environment Science Data Center of the Chinese

TABLE 1 Climate data source.

Data source	Site level	Data type	Time series range	Number of sites
Resource and Environment Science and Data Center, CAS	National Ground-Level Meteorological Observation Station	Daily data	2001–2020	95
Hong Kong Observatory	Hong Kong Reference Weather Station	Annual data	2001–2020	1

Academy of Sciences, with the time span from 2001 to 2020 (Table 1). Using linear interpolation, we were able to fill in missing data and combine the annual data per station. The climate data were interpolated using Thin-plate Splines and Kriging Interpolation, which recorded by 96 national climate stations around study area. According to the obvious influence of elevation on temperature and precipitation, utilizing thin-plate splines to interpolate the temperature and precipitation, with the elevation as covariate. While using Kriging Interpolation to interpolate other climate data, with the resolution of 250-m.

2.3. Methods

2.3.1. Theil-Sen approach and Mann-Kendall test

Theil-Sen median trend analysis and Mann-Kendall trend test are both non-parametric estimation methods, and do not assume a normal distribution, which also effectively avoid errors and is suitable for dealing with the long-time series climate data. To estimate every pixel of the EVI changing trends from 2001 to 2020, we used the nonparametric Theil-Sen estimator. This estimate, known as Theil-Sen Slope, which is not sensitive to potential outliers. Mann-Kendall (MK) test were performed for EVI time series and each of the climate-impacted EVI's time series for the study period from 2001 to 2020.

The Sen slope's formula is as follows.

$$\beta = \text{Median} \left(\frac{x_j - x_i}{j - i} \right), 1 < i < j < n$$

Where β is the slope of EVI interannual change, the x_i and x_j are represent annual EVI in years i and j . n is the length of the time series. If $\beta > 0$, EVI indicates an increasing trend, and if $\beta < 0$, EVI indicate a decreasing trend.e.

In Mann-Kendall (MK) test, the cumulative score of all pairs is used to calculate S :

$$S = \sum_{i=1}^{n-1} \sum_{j=i+1}^n \text{sgn}(x_j - x_i)$$

where, $\text{sgn}(x_j - x_i)$ is the Sign function.

$$\text{sgn}(x_j - x_i) = \begin{cases} 1, & x_j - x_i > 0 \\ 0, & x_j - x_i = 0 \\ -1, & x_j - x_i < 0 \end{cases}$$

When $n > 8$, the S follow an approximately normal distribution, and its variance of the S stat ($\text{Var}(S)$) as follows.

$$\text{Var}(S) = \frac{n(n-1)(2n+5) - \sum_{i=1}^n t_i(i-1)(2i+5)}{18}$$

The standardized Z score is defined as follows.

$$Z = \begin{cases} \frac{S-1}{\sqrt{\text{Var}(S)}}, & S > 0 \\ 0, & S = 0 \\ \frac{S+1}{\sqrt{\text{Var}(S)}}, & S < 0 \end{cases}$$

When $|Z| > u_{1-\alpha/2}$, it indicates that there is a significant change at the α level.

Since there no exist of the result that $\beta = 0$ in the Theil-Sen slope, when $-0.0005 \leq \beta \leq 0.0005$ is indicated as stable area; when $\beta > 0.0005$ is indicated as the vegetation improvement area, and when $\beta < -0.0005$ is indicated as the degradation vegetation area. The results of the Mann-Kendall test were classified as an obvious significant change ($|Z| > 2.58$), a significant change ($1.96 < |Z| \leq 2.58$), and a insignificant change ($|Z| \leq 1.96$) based on the confidence intervals of $\alpha = 0.01$ and $\alpha = 0.05$. The β and Z values were combined for classification, thus classifying the EVI trend seven types (Table 2).

2.3.2. Continuity analysis

Rescaled range analysis (R/S Analysis) describe the autocorrelation of long-term change in time-series data. It has been widely applied in Economics, Meteorology, and Hydrology. The Hurst exponent is a quantitative method and indicated the reliance of long-time series by utilizing R/S Analysis (Hurst, 1951; Mandelbrot and Wallis, 1969). The R/S Analysis has advantages in investigating the trend of vegetation cover, which is affected by climate factors, in future. What we know about R/S Analysis is largely based upon empirical studies that investigate the trend of vegetation cover in long-time series in the center of Asia (Jiang et al., 2017), Qinghai-Tibet Plateau (Peng et al., 2012), Beijing-Tianjin-Hebei metropolitan regions (Li et al., 2017), the middle reaches of the Yangtze River (Yi et al., 2021, 2022) and the GBA (Zhao et al., 2022). The methods contain these following steps:

Define the long-time sequence $\{\xi(t)\}$, $t = 1, 2, \dots$ for an integer $\tau \geq 1$. Defining the time series mean $\langle \xi \rangle_\tau$:

TABLE 2 The proportion of EVI trend classified as seven levels.

β EVI	Z score	EVI trend	Proportion (%)
$S > 0.0005$	> 2.58	Extremely significant improvement	66.98
$S > 0.0005$	$1.96 < Z \leq 2.58$	Significant improvement	6.83
$S > 0.0005$	$ Z \leq 1.96$	Slight improvement	9.91
$-0.0005 \leq S \leq 0.0005$	-	Stable	4.14
$S < -0.0005$	$ Z \leq 1.96$	Slight degradation	4.73
$S < -0.0005$	$1.96 < Z \leq 2.58$	Significant degradation	1.73
$S < -0.0005$	$ Z > 2.58$	Extremely significant degradation	5.70

$$\langle \xi \rangle_{\tau} = \frac{1}{\tau} \sum_{t=1}^{\tau} \xi(t), \tau = 1, 2, \dots, n$$

Calculating the accumulated deviation of $X(t, \tau)$.

$$X(t, \tau) = \sum_{u=1}^t (\xi(u) - \langle \xi \rangle_{\tau}), 1 \leq t \leq \tau$$

Calculating the rescaled range of RS.

$$\frac{\left(\max_{1 \leq t \leq \tau} X(t, \tau) - \min_{1 \leq t \leq \tau} X(t, \tau) \right)}{\left(\frac{1}{\tau} \sum_{t=1}^{\tau} (\xi(t) - \langle \xi \rangle_{\tau})^2 \right)^{\frac{1}{2}}} = (c\tau)^H,$$

c is a constant.

H is the Hurst exponent. In the R/S analysis of FVC (EVI) sequences, the significance of the Hurst exponent is as follows.

If $H = 0.5$, the changes in the FVC (EVI) time series are unrelated and random.

If $0 < H < 0.5$, it indicates that the FVC (EVI) time series changes have non-persistence. The closer to 0 the Hurst is, the stronger the non-persistence is.

If $0.5 < H < 1$, it indicates that the FVC (EVI) time series of FVC (EVI) have persistence. The closer to 1, the stronger the persistence is.

2.3.3. Pearson correlation analysis

To study the correlations between the variables, Pearson correlation analyses were calculated. The calculation equation is as follows.

$$r_{XY} = \frac{\sum_{i=1}^n (X_i - \bar{X})(Y_i - \bar{Y})}{\sqrt{\sum_{i=1}^n (X_i - \bar{X})^2 \cdot \sum_{i=1}^n (Y_i - \bar{Y})^2}}$$

Where r_{XY} is the correlation between variables X and Y , n is the sample size determination, \bar{X} is the mean of X , and \bar{Y} is the mean of Y . The range of r_{XY} is $[-1, 1]$. When $r_{XY} > 0$, it means that

the two variables are positively linearly correlated; when $r_{XY} < 0$, it means that the two variables are negatively linearly correlated.

Using MATLAB to calculate the Pearson correlation between the annual maximum FVC (EVI) and the annual temperature, precipitation, wind speed, relative humidity, and sunshine duration, respectively.

Then we test for significance using t test. The significance of correlation was divided into four grades by combining confidence: significant negative correlation ($r_{XY} < 0$, $p < 0.05$), insignificant negative correlation ($r_{XY} < 0$, $p \geq 0.05$), insignificant positive correlation ($r_{XY} > 0$, $p \geq 0.05$) and significant positive correlation ($r_{XY} > 0$, $p < 0.05$).

3. Results

3.1. Characteristics of the interannual change of climate factors in Guangdong-Hong Kong-Macao Greater Bay Area

The interannual change of climate factors, such as temperature, precipitation, wind speed, humidity and sunshine radiation in the GBA during 2001–2020, generally indicated a fluctuation, with no obvious increase or decrease tendency. Differences in the variability of climate factors. The temperature decreased and then increased, with a mean of 22.17°C , the highest in 2019 (22.66°C), and the lowest in 2011 (21.56°C). The relative humidity has a trend of insignificant increasing trend, with the mean of 77.33%, the highest in 2016 (81.52%), and the lowest in 2011 (72.39%). GBA is predicted to severely slow the warming and humidify. The precipitation, sunshine radiation, and wind speed have interannual fluctuations; however, the 20-year time series change indicated a insignificant trend. Precipitation fluctuated between 1,500–2,500 mm in the last 20 years, with the mean of 1,913 mm, the highest in 2016 (2,466 mm) and the lowest in 2011 (1,426 mm). The wind speed fluctuated steadily with a mean of 2.07 m/s, with the highest in 2011 (2.16 m/s) and the lowest in 2001 (1.85 m/s). Sunshine duration fluctuated steadily, with the mean of 1,696 h, the highest in 2003 (1,989 h), and the lowest in 2012 (1,494 h) (Figure 3).

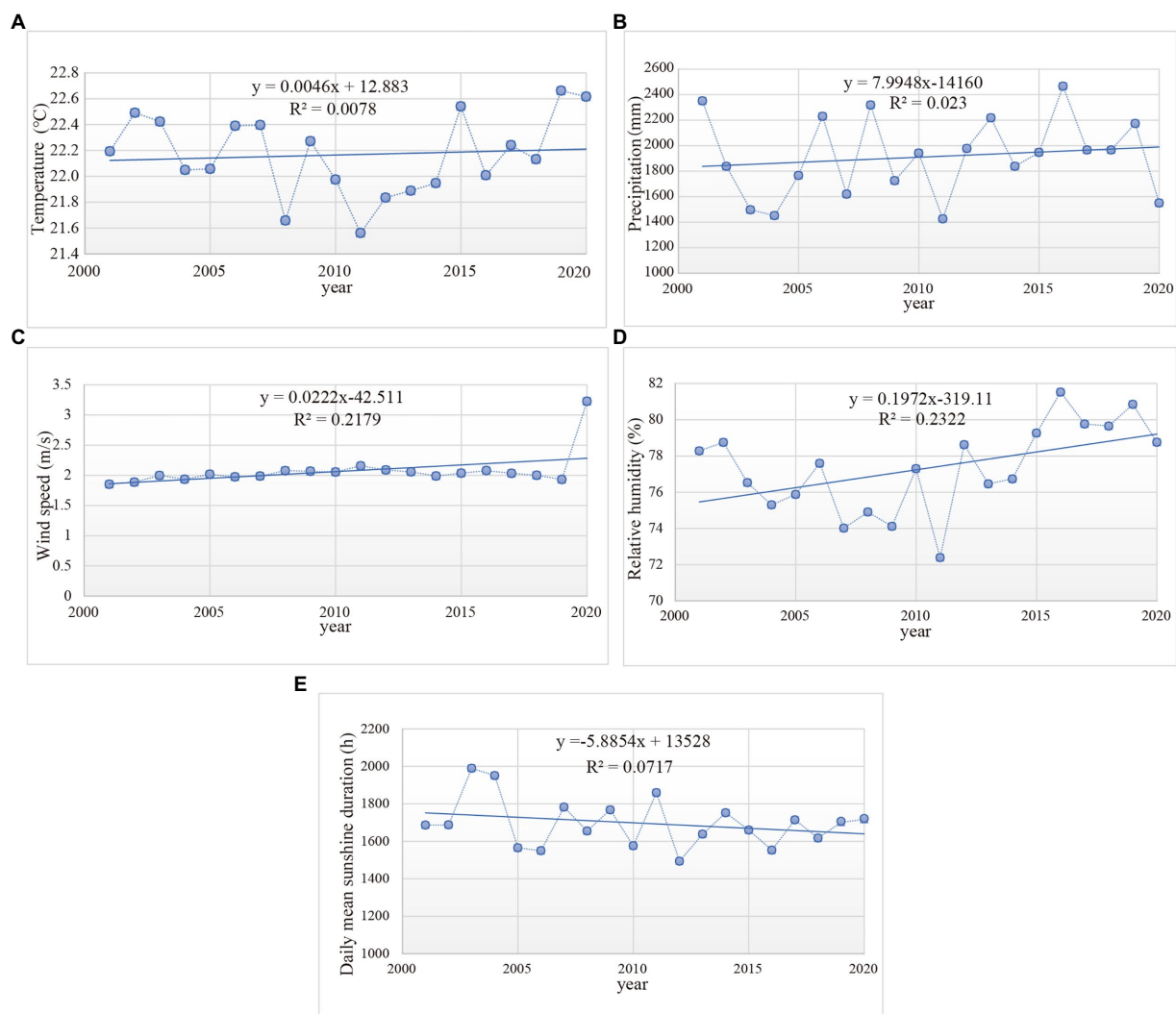


FIGURE 3 Interannual change of climate factors. (A) Temperature. (B) Precipitation. (C) Wind speed. (D) Relative humidity. (E) Daily mean sunshine duration.

3.2. Spatiotemporal change characteristics of enhanced vegetation index in the Guangdong-Hong Kong-Macao Greater Bay Area

The mean EVI were calculated based on the annual maximum EVI from 2001 to 2020 in GBA. We divided the mean EVI into the five grades according to the condition of vegetation cover by the equal intervals: low ($\text{EVI} < 0.2$), relatively low ($0.2 < \text{EVI} < 0.4$), medium ($0.4 < \text{EVI} < 0.6$), relatively high ($0.6 < \text{EVI} < 0.8$), and high ($\text{EVI} \geq 0.8$) (Figure 4). There are obvious spatial differences in the distribution of EVI in GBA. The middle and relatively high EVI are distributed in the northern, western and eastern of GBA, with an area of 78.09%, while the minimum and relatively low EVI are mainly distributed in the center of GBA, with the area of 21.89%.

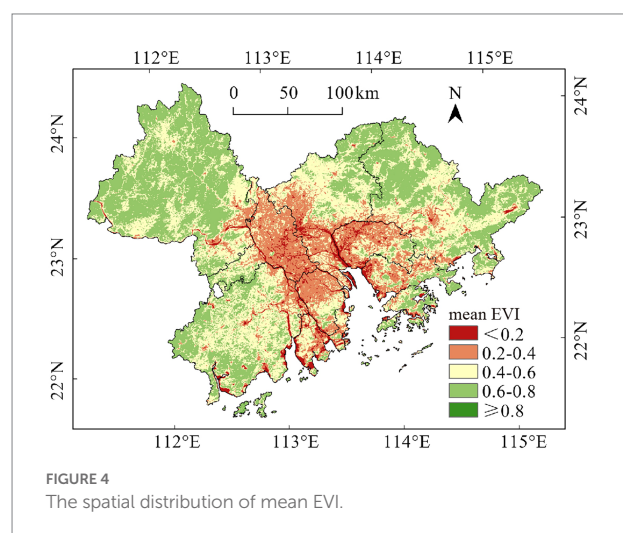


FIGURE 4 The spatial distribution of mean EVI.

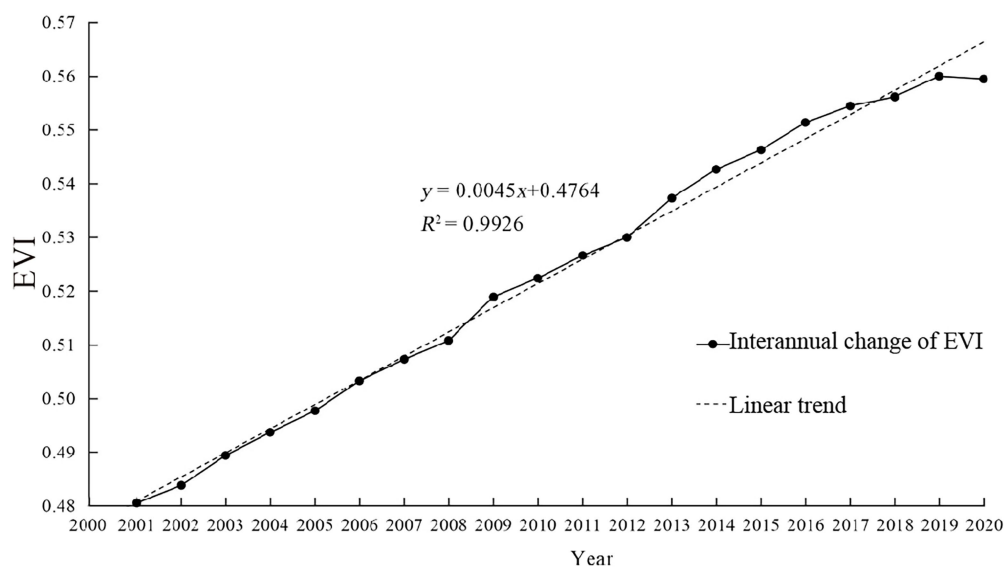


FIGURE 5
The interannual change of EVI in the Guangdong-Hong Kong-Macao Greater Bay Area.

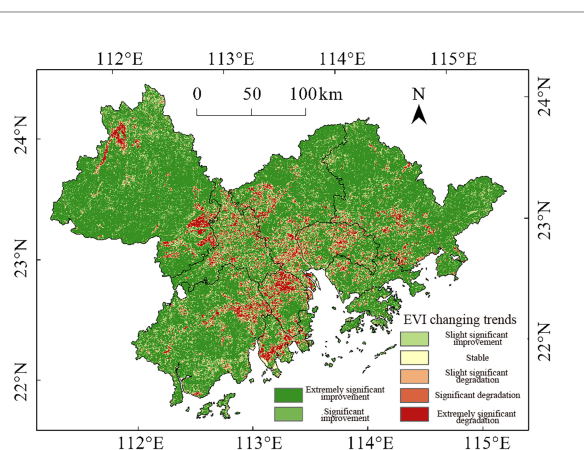


FIGURE 6
The EVI spatial changing trend.

Based on the maximum annual EVI, we analysis the characteristics of the annual time series change (Figure 5). The EVI exhibited an increasing trend (with growth rate of 0.0045/a) comprehensively in the time series. The range of EVI change is from 0.48 to 0.56 and the mean is 0.52. In summary, for the informants in this analysis, the vegetation is well-protected in GBA in past 20 years, along with improving the condition of plant growth.

According to the distribution of maximum annual EVI, the Theil-Sen trend analysis and Mann-Kendall (MK) test were carried out, to indicate the spatial distribution of the EVI changing trends in GBA during the past 20 years (Figure 6). In accordance with the present results, it has demonstrated that the vegetation cover has increased in a comprehensive trend in the past 20 years,

the area of vegetation improvement is larger than the area of vegetation degradation, with the extremely significant vegetation improvement area of 66.98% and the extremely significant vegetation degradation area of 5.70% (Table 2).

There are obvious differences and agglomerations in the distribution of the EVI trends. The significant vegetation improvement area exhibited obvious agglomerated, and mainly distributed in northern, western, and eastern parts of GBA. The significant vegetation degradation area scattered and had obvious differences in the distribution, which mainly distributed in southern part of GZ, western part of FS, southern parts of ZH, northern part of ZS, and central part of DG. In summary, these results show that vegetation degradation areas are distributed around the peripheral area of urban agglomeration. The extremely significant vegetation improvement area mainly distrusted in eastern, western, and northern part of GBA, which has a relative distance away from the urban agglomeration, therefore, are less disrupted by human activities.

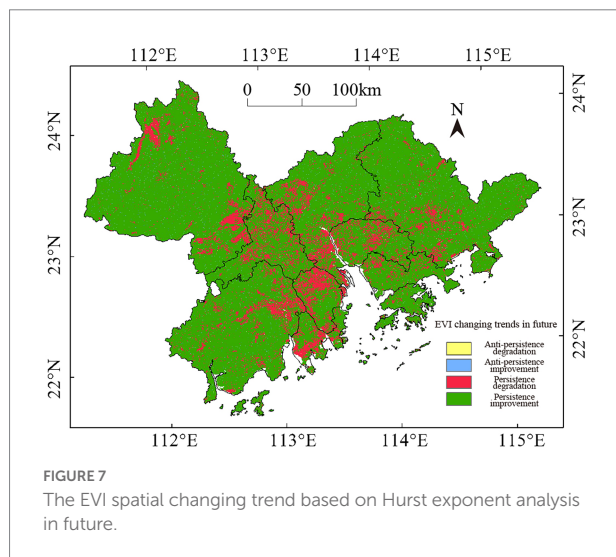
The R/S analysis predicted the EVI changing trend in the future, according to the persistence in long-term change of vegetation cover in GBA in the past 20 years. The analysis was based on the classification of the Hurst exponent proposed by Peng et al. (2012) and Li et al. (2017), which is showed in Figure 7 and Table 3. The pixels of the mean Hurst exponent area of 98.84%, which indicated persistence ($H \geq 0.50$), while the anti-persistence ($H < 0.50$) pixels are account the area of 1.16%. Both persistence and anti-persistence area are distributed scattered. The evolution degradation of area is 14.77%, with insignificant agglomerations in spatial distribution. The evolution improvement area is of 85.23%.

There are several possible explanations for this result. The appearance of significant persistence is mainly impacted by natural factors or human activities, such as deforestation,

afforestation, and auto-restoration after disasters. On the other hand, the weakened persistence indicated that the vegetation cover are influenced combinedly by natural factors and human activities, with insignificant differences in the influence degree. In this study, the combined influence of various factors in EVI trend were predicted by the considering the regular pattern of the past 20 years. Combining the result of Theil-Sen slope and Hurst exponent, the prediction of the EVI trends is exhibited as Figure 7. The EVI tends to improve in the future, since more than 80% of the area showed improvement, while 13.72% of the area showed degradation vegetation, mainly distributed in the central and northwestern part of the GBA. Additionally, we investigate little area of the non-persistence degradation and non-persistence improvement.

3.3. Analysis of the response of enhanced vegetation index trends to climatic factors

The Pearson correlation coefficient between maximum annual EVI and five climate factors (Temperature, precipitation, wind speed, relative humidity and sunshine duration) has been calculated, and the significances are tested by using *t*-test. The result indicated that there are significant spatiotemporal differences in the correlation between annual EVI changing trend and climate factors.



There are 49.16% of the area had positive correlation between the change of EVI trend and temperature. However, there are 7.15% of the area had significant positive correlation, and 21.55% of the area had significant correlation. In terms of the spatial distribution, the EVI, with significant correlation with temperature, distributed scattered and mainly indicated around the urban agglomeration, which is the southern coastal area of GBA (the center of HZ). The 14.40% of significant negative area mainly distributed in ZQ, the northern part of GZ, the northern and eastern part of HZ (Figure 8).

There are only 3.22% of the area had significant correlation between precipitation and EVI trends, and 2.51% of the area had significant positive correlation, with a scattered distribution. Additionally, 0.71% of the area had significant negative correlation. The observed correlation between precipitation and the EVI trends could be explained in this way: there are weakened correlation between precipitation and the EVI trend, and more than 90% of the area had insignificant correlation (Figure 9).

There are 42.19% of the area had significant correlation between wind speed and EVI trends, with 32.99% of the significant positive correlated area. The distribution of the correlated area exhibited agglomerated in the northeastern and northwestern part of GBA, which mainly had forest land and far away from urban agglomeration. The significantly positive correlated area was mainly distributed in the most part of ZQ, the western part of FS, the northern part of JM and the northeastern part of HZ. The significantly negative correlated area (9.20%) mainly distributed in SZ, HK and the northern part of HZ (Figure 10).

Approximately 80.23% of the area had a significant positive correlation between relative humidity and the trends of EVI, 43.51% of the area had a significant correlation and 37.74% had a significant positive correlation ($r > 0$, $p < 0.05$). The correlated area distributed widely and agglomerated in the northern, western, and eastern part of the GBA (the western, central, and southern parts of ZQ, the northwestern part of FS, the center of GZ, the central and eastern part of HZ, DG, the northern part of HK and the western part of JM). The significant correlated area (5.77%) is distributed in the northern and southeastern part of ZQ, the northern part of ZS and the eastern part of JM (Figure 11).

There is weak correlation between EVI trends and sunshine radiation and no significant correlation. There are 68.22% of the area insignificantly negative correlated ($r > 0$, $p < 0.05$) with sunshine radiation and 3.53% of the area significant correlated. There are 0.44% of the area had significant positive correlation between EVI trends and 3.09% of the area had significant negative

TABLE 3 The proportion of EVI changing trends classified as four levels.

Slope	Hurst	Type	Proportion (%)
<0	<0.5	Anti-persistence degradation	0.11
>0	<0.5	Anti-persistence improvement	1.05
<0	>0.5	Persistence degradation	13.72
>0	>0.5	Persistence Improvement	85.12

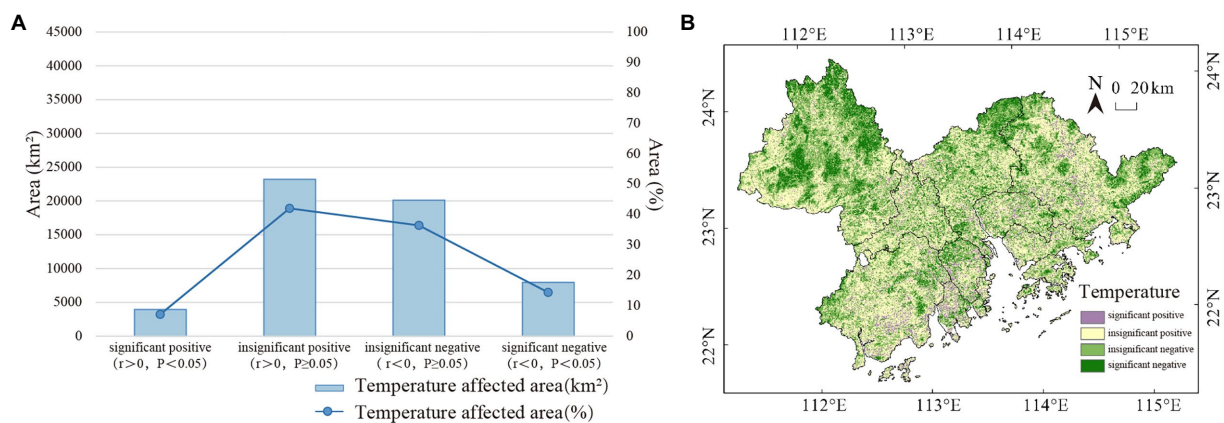


FIGURE 8

The coefficients between the changing trend of EVI and temperature in GBA. (A) Area (%) correlated with the temperature. (B) Correlation of changes in vegetation cover changes influenced by the temperature.

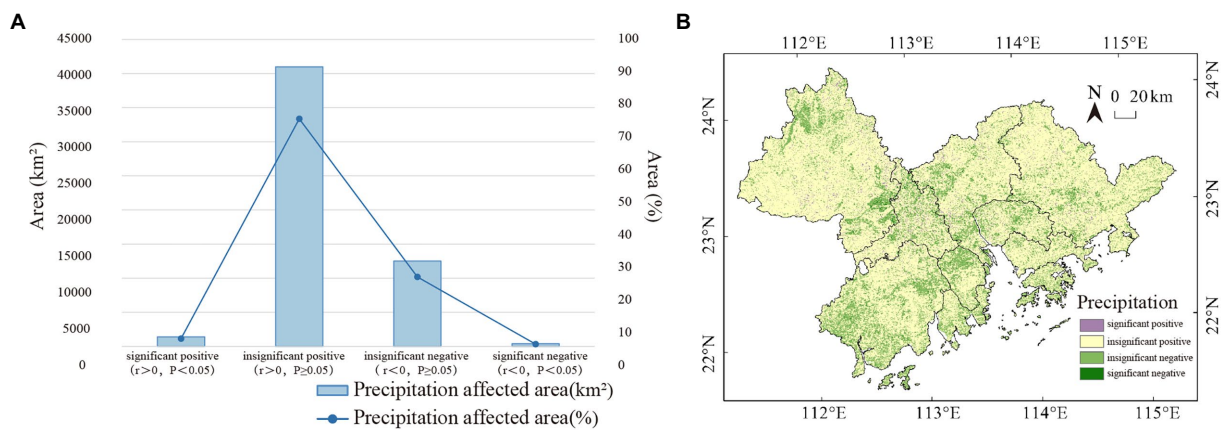


FIGURE 9

The coefficients between the changing trend of EVI and precipitation in GBA. (A) Area (%) correlated with precipitation. (B) Correlation of changes in vegetation cover changes influenced by precipitation.

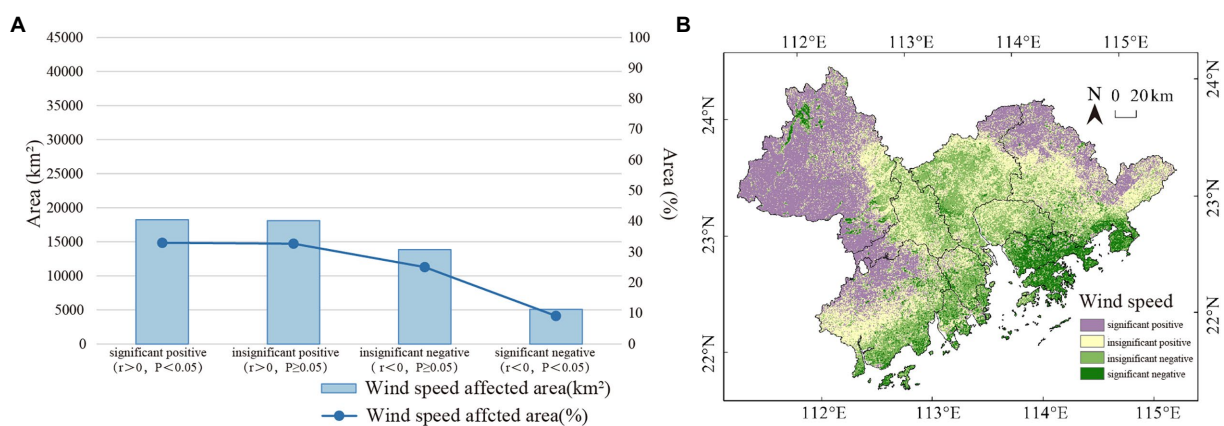


FIGURE 10

The coefficients between the changing trend of EVI and wind speed in GBA. (A) Area (%) correlated with wind speed. (B) Correlation of changes in vegetation cover changes influenced by wind speed.

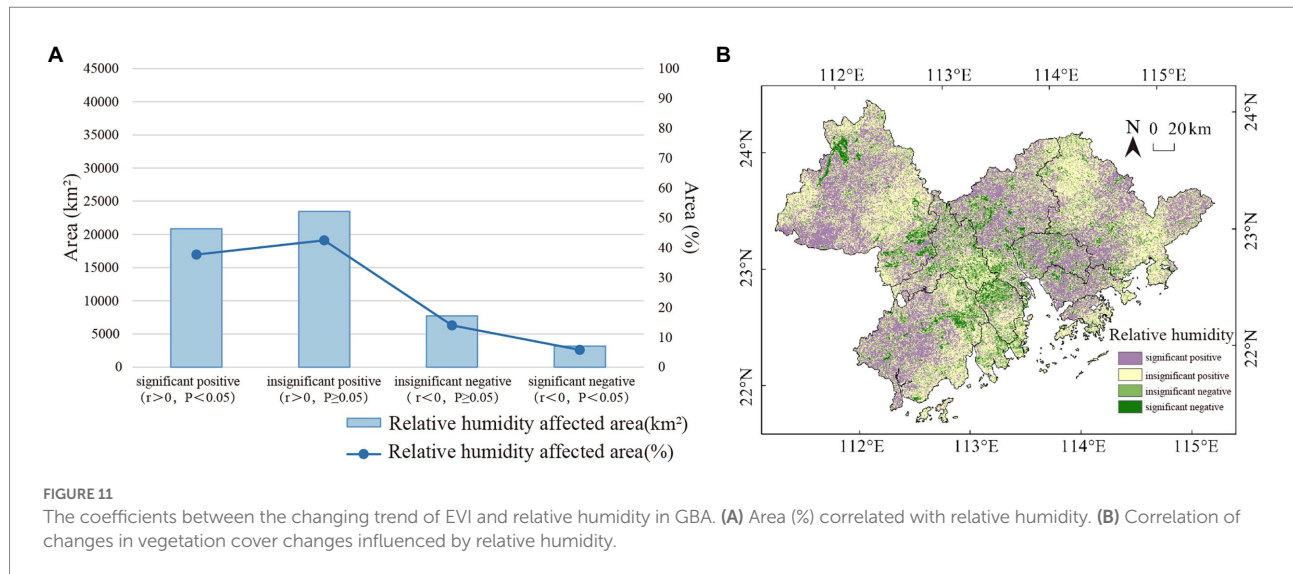


FIGURE 11

The coefficients between the changing trend of EVI and relative humidity in GBA. (A) Area (%) correlated with relative humidity. (B) Correlation of changes in vegetation cover changes influenced by relative humidity.

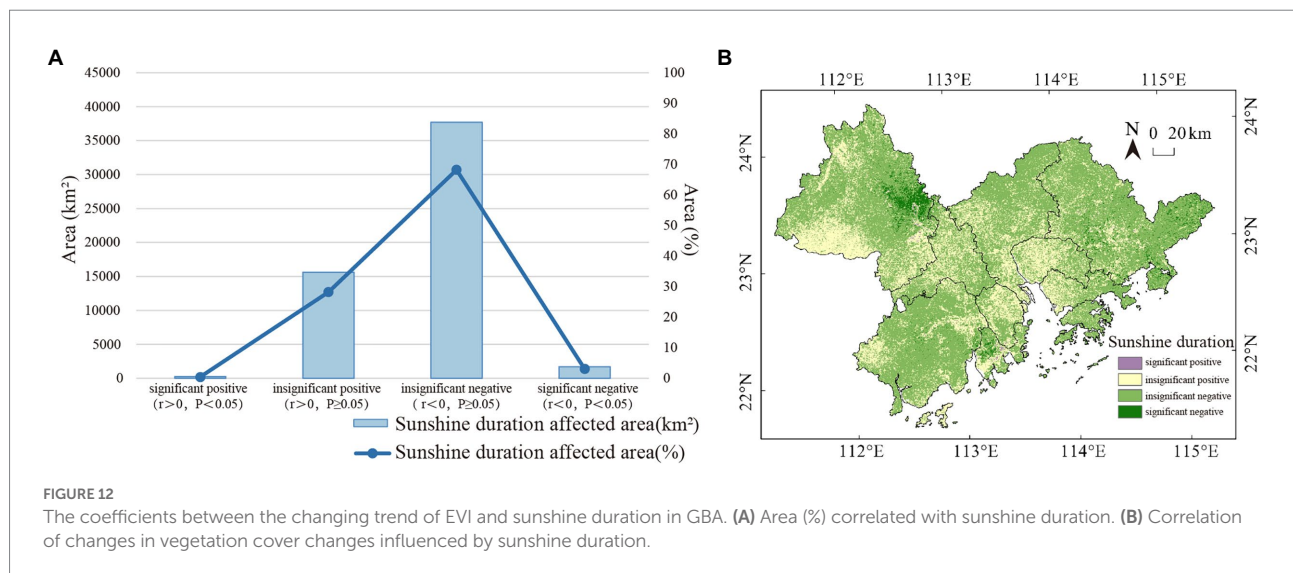


FIGURE 12

The coefficients between the changing trend of EVI and sunshine duration in GBA. (A) Area (%) correlated with sunshine duration. (B) Correlation of changes in vegetation cover changes influenced by sunshine duration.

correlation, which mainly distributed in the eastern part of ZQ (Figure 12).

4. Discussion

During the past 20 years from 2001 to 2020, according to the mean of the EVI trends, the vegetation cover comprehensively exhibited a significant improvement in GBA. There are similarities between the result expressed by EVI trend in this study and the NDVI trends described by Deng et al. (2021) in Guangdong province. However, the rate of EVI trend is lower than the NDVI trends in Guangdong province. And from 2000 to 2020, the vegetation NPP increased trend about $0.001 \text{ kgC/m}^2 \cdot \text{a}$ (Zhao et al., 2022). This study corroborates the conclusions of Chen et al. (2019) and Yuan et al. (2018), who suggested that the vegetation changing

trend of China and the global vegetation changing trend are improved similarly. The vegetation improvements are shown in the eastern part of China (Zhejiang province) (He et al., 2020), the western part of China (Guizhou province) (Xu et al., 2020), the Beijing-Tianjin-Hebei metropolitan regions (Li et al., 2017), the Yellow River Basin (Xie et al., 2022) and the western part of the Jinsha River Basin (Zhang et al., 2021). The previous results are different in the trend of vegetation change. For example, the rate of EVI trends is $0.045/10\text{a}$ in the Hot and humid area, as the result indicated in the present study. While the rate of EVI trend is $0.038/10\text{a}$ in the arid and semi-arid area of China (Yellow River Basin) (Xie et al., 2022). Additionally, conclusion such as that conducted by Zhang et al. (2021) have shown that the rate of EVI trend ($0.011/10\text{a}$) is slower in the western part of the Jinsha River Basin.

In terms of the spatial distribution of EVI trend, there are comprehensive vegetation improvement in GBA, and the area of

vegetation improvement is larger than the area of vegetation degradation. The spatial distribution of EVI trend exhibited obvious differences and agglomeration. According to spatial distribution, it is significant vegetation degradation around urban agglomerations, since a few studies considered that human activities are the main reason (Qi et al., 2019; Zhao et al., 2022). The result of this study indicated that the EVI changing trend in the future by R/S analysis method is affected by climate and human factors together and there are no significant factors. The improvement of vegetation is predicted in the future by comprehensive analysis of the Theil-Sen slope and Hurst exponent, with the vegetation improvement area of 80% and an extremely significant vegetation degradation area of 5.7%. Based on this analysis, we can infer that both ecological environment protection and economic development can be simultaneously achieved in GBA.

Much of the literature emphasizes the vegetation growth had obvious response to climate factors. To date, several studies have investigated the precipitation and temperature is the main factors of vegetation change in the arid and semi-arid area and the region in the climate zone that plants both have growth and deciduous seasons (Gan et al., 2011; Mu et al., 2012; He et al., 2020). While there are differences in the results by using various VI (Xie et al., 2022). However, it has been suggested that the influence of precipitation is more obvious (Xie et al., 2016; Liu et al., 2021; Zhang et al., 2021). This does not appear to be the case in other regions. This finding is different from other studies that have suggested that temperature had more obvious effects (Hua et al., 2017; Deng et al., 2021; Zhao et al., 2022). There is mainly south-subtropical ever-green broad leaf forest and in the GBA, with sufficient sunshine radiation and abundant rainfall. And the climate change in GBA is stable. However, in this study, precipitation and sunshine had no effect on EVI trend.

The correlation between EVI and five climate factors (Temperature, precipitation, wind speed, relative humidity and sunshine duration) has been calculated, and the significances are tested by using *t*-test. The result indicated precipitation has no significant correlation with EVI trends in the Hot and humid area with mean precipitation of 1,800 mm. In contrast to the findings in arid and semi-arid area, however, significant correlation between precipitation and vegetation change was detected. Our results corroborate the findings of the previous work in the insignificant correlation between precipitation and NDVI trends (Zhang et al., 2021). The previous studies demonstrated that the vegetation cover is significantly positively correlated with temperature both in humid area and GBA by using the NDVI. This study seems to be consistent with other research which found there are correlation between temperature and vegetation cover, but it's insignificant. In the terms of spatial distribution, the influence of temperature to EVI is complex in GBA, the spatial distribution of correlation is scattered.

Although extensive research has been conducted on vegetation change and climate factors, few studies have identified the correlation between vegetation change and two climate factors

(relative humidity and wind speed). In this study, not only the three factors (temperature, precipitation and sunshine duration) that have been analyzed, but also relative humidity and wind speed. There is a significant positive correlation between the EVI trend and two climate factors (relative humidity and wind speed). An issue that was not addressed in this study was what is the internal mechanisms of these influences. The relevance of EVI and climate factors analyzed by annual data is clearly supported by current findings. The wind speed and relative humidity correlated with EVI significantly. An additional uncontrolled factor is the possibility that there are differences in the climate factors of various seasons. These differences make these findings less generalizable to enhance the correlation of EVI and some climate factors in annual scale. More information on month or seasonal scale would help us establish a greater degree of accuracy in this matter and to analysis the hysteresis of the influences.

5. Conclusion

The MODIS-EVI and climate data were analyzed from the National Aeronautics and Space Administration (NASA) and the Resource and Environment Science Data Center of the Chinese Academy of Sciences. This paper elucidated the characteristics of spatiotemporal change of EVI and its trend in the future by using Theil-Sen trends analysis, Mann-Kendall Test and R/S Analysis, basing on the MODIS-EVI and climate data from 2001 to 2020. The paper indicated the correlation between EVI trend and the change of climate factors by using Pearson correlation analysis.

The study highlighted the change of climate factors (temperature, precipitation, wind speed, relative humidity, and sunshine duration) has relatively stable and slightly fluctuated in the past 20 years. Temperature, precipitation, and humidity exhibited an extremely slow and insignificant increasing trend, and the sunshine duration showed an insignificant decreasing trend. The temperature fluctuates from 22.1°C to 22.2°C and the mean precipitation are fluctuated from 1800 mm–2000 mm. Relative humidity increased from 75 to 79%. Taken together, the result identified an extremely slowly warming and humidify of GBA, and a relatively stable climate change.

In this condition of climate change, the result showed the mean EVI increased in GBA, and the rate of increase is 0.045/10a in the past 20 years. The area of extremely significant vegetation improvement is approximately 70% and the area of significant and extremely significant vegetation degradation is 7.43%, which mainly distributed in the central of GBA. In the prediction, more than 80% of the area showed an increasing trend of EVI. There are obvious differences in the spatial distribution of vegetation. The middle and relatively high EVI distributed in the northern, western, and eastern part of GBA, with an area of 80% approximately. The relatively low value mainly distributed in the central of GBA, with the area of 20% approximately. The EVI increasing from the 2001 to 2020, while the area of extremely vegetation improvement is larger than the area of vegetation degradation. The result indicated the positive

improvement of vegetation in GBA. Therefore, the trends of EVI that we have identified assists in our understanding of the contribution of environmental protection in GBA during the past 20 years.

There are spatiotemporal differences in the influence of EVI trend to five climate factors (temperature, precipitation, wind speed, relative humidity, and sunshine duration). One of the more significant findings to emerge from this study is that wind speed, relative humidity relatively obviously significant correlated with EVI trend, the area of significant correlation is over than 40%. Temperature correlated with EVI weaker; the area of significant correlation is more than 20%. Precipitation and sunshine duration had the least correlation with EVI, and the area of significant correlation are less than 5%. Therefore, in the south-subtropical Hot and humid area, precipitation and sunshine duration have weak influence on the vegetation. On the contrary, relative humidity and wind speed have more significant influence on the vegetation.

Data availability statement

Publicly available datasets were analyzed in this study. This data can be found here: National Aeronautics and Space Administration, National Ground-Level Meteorological Observation Station, and Hong Kong Reference Weather Station.

Author contributions

XF and ZZ completed the data collection and methodological construction of this study, and wrote the first draft of the

manuscript. ZZ analyzed the feasibility of the study data, collected the data, and calculated the results. XF and MH wrote parts of the manuscript. All authors participated in the revision of the manuscript, read and approved the submitted version.

Funding

This study was supported by National Natural Science Foundation of China (NSFC) (No. 51978276), The interactive influence mechanism of urban green space, local wind climate, and residents' health based on the multi-spatial scale in Guangdong-Hong Kong-Macao Greater Bay Area.

Conflict of interest

The authors declare that the research was conducted in the absence of any commercial or financial relationships that could be construed as a potential conflict of interest.

Publisher's note

All claims expressed in this article are solely those of the authors and do not necessarily represent those of their affiliated organizations, or those of the publisher, the editors and the reviewers. Any product that may be evaluated in this article, or claim that may be made by its manufacturer, is not guaranteed or endorsed by the publisher.

References

- Chen, Y. L., Luo, Y. M., Mo, W. H., Mo, J. F., Huang, Y. L., and Ding, M. H. (2014). Differences between MODIS NDVI and MODIS EVI in response to climatic factors. *J. Nat. Resour.* 29, 1802–1812. doi: 10.11849/zrzyxb.2014.10.015
- Chen, C., Park, T., Wang, X., Piao, S., Xu, B., Chaturvedi, R. K., et al. (2019). China and India lead in greening of the world through land-use management. *Nat. Sustain.* 2, 122–129. doi: 10.1038/s41893-019-0220-7
- Cheng, H. F., Zhang, W. B., and Chen, F. (2008). Advances in researches on application of remote sensing method to estimating vegetation coverage. *Rem. Sens. Land Res.* 20, 13–18.
- De la Barrera, F., and Henriquez, C. (2017). Vegetation cover change in growing urban agglomerations in Chile. *Ecol. Indic.* 81, 265–273. doi: 10.1016/j.ecolind.2017.05.067
- Deng, Y. J., Wang, J. C., Xu, J., Du, Y. D., Chen, J. Y., and Chen, D. C. (2021). Spatiotemporal variation of NDVI and its response to climatic factors in Guangdong Province. *Ecol. Environ. Sci.* 30, 37–43. doi: 10.16258/j.cnki.1674-5906.2022.09.001
- Feng, X. H., Zeng, Z. L., and Zhang, D. S. (2022). Temporal-spatial evolution of vegetation coverage in the Guangdong-Hong Kong-Macao Greater Bay Area on MODIS NDVI data. *J. Chin. Urban Forest.* 20, 1–28. doi: 10.16258/j.cnki.1674-5906.2022.09.001
- Fensholt, R., Langanke, T., Rasmussen, K., Reenberg, A., Prince, S. D., Tucker, C., et al. (2012). Greenness in semi-arid areas across the globe 1981–2007 — an earth observing satellite based analysis of trends and drivers. *Remote Sens. Environ.* 121, 144–158. doi: 10.1016/j.rse.2012.01.017
- Gan, C. Y., Wang, X. Z., Li, B. S., Liang, Z. X., Li, Z. W., and Wen, X. H. (2011). Changes of vegetation coverage during recent 18 years in Lianjiang River watershed. *Scientia Geographica Sinica/Dili Kexue.* 31, 1019–1024. doi: 10.13249/j.cnki.sgs.2011.08.013
- Gitelson, A. A., Kaufman, Y. J., Stark, R., and Rundquist, D. (2002). Novel algorithms for remote estimation of vegetation fraction. *Remote Sens. Environ.* 80, 76–87. doi: 10.1016/S0034-4257(01)00289-9
- He, Q. J. (2019). Spatio-temporal variation of NDVI and its response to meteorological factors in Pearl River Delta based on MODIS data. *Ecol. Environ. Sci.* 28, 1722–1730. doi: 10.16258/j.cnki.1674-5906.2019.09.002
- He, Z. H., Zhang, Y. H., He, Y., Zhang, X. W., Cai, J. Z., and Lei, L. P. (2020). Trends of vegetation change and driving factor analysis in recent 20 years over Zhejiang Province. *Ecol. Environ. Sci.* 29, 1530–1539. doi: 10.16258/j.cnki.1674-5906.2020.08.004
- Hu, M., and Xia, B. (2019). A significant increase in the normalized difference vegetation index during the rapid economic development in the Pearl River Delta of China. *Land Degrad. Dev.* 30, 359–370. doi: 10.1002/ldr.3221
- Hua, W., Chen, H., Zhou, L., Xie, Z., Qin, M., Li, X., et al. (2017). Observational quantification of climatic and human influences on vegetation greening in China. *Remote Sens.* 9:425. doi: 10.3390/rs9050425
- Hurst, F. B. (1951). Climates prevailing in the yellow-gray earth and yellow-brown earth zone in New Zealand. *Soil Sci.* 72, 1–20. doi: 10.1097/00010694-195107000-00001
- Jiang, L., Bao, A., Guo, H., and Ndayisaba, F. (2017). Vegetation dynamics and responses to climate change and human activities in Central Asia. *Sci. Total Environ.* 599–600, 967–980. doi: 10.1016/j.scitotenv.2017.05.012
- Li, Z., Sun, R., Zhang, J. C., and Zhang, C. (2017). Temporal-spatial analysis of vegetation coverage dynamics in Beijing-Tianjin-Hebei metropolitan regions. *Acta Ecol. Sin.* 37, 7418–7426. doi: 10.5846/stxb201609231919
- Li, H., Zheng, L., Lei, Y., Li, C. Q., and Zhou, K. (2007). Comparison of NDVI and EVI based on EOS/MODIS data. *Prog. Geogr.* 26, 26–32. doi: 10.3969/j.issn.1007-6301.2007.01.003

- Liu, H., Liu, F., and Zhen, L. (2021). Effects of climate change and human activities on vegetation cover change in the Yellow River basin. *J. Soil Water Conserv.* 35, 143–151. doi: 10.13870/j.cnki.stbxb.2021.04.020
- Liu, Q., Piao, S., Fu, Y. H., Gao, M., Peñuelas, J., and Janssens, I. A. (2019). Climatic warming increases spatial synchrony in spring vegetation phenology across the northern hemisphere. *Geophys. Res. Lett.* 46, 1641–1650. doi: 10.1029/2018GL081370
- Liu, X. F., Yang, Y., Ren, Z. Y., and Lin, Z. H. (2013). Changes of vegetation coverage in the loess plateau in 2000–2009. *J. Desert Res.* 33, 1244–1249. doi: 10.7522/j.issn.1000-694X.2013.00175
- Mandelbrot, B. B., and Wallis, J. R. (1969). Some long-run properties of geophysical records. *Water Resour. Res.* 5, 321–340. doi: 10.1029/WR005i002p00321
- Mu, S. J., Li, J. L., Chen, Y. Z., Gang, C., Zhou, W., and Ju, W. M. (2012). Spatial differences of variations of vegetation coverage in Inner Mongolia during 2001–2010. *Acta Ecol. Sin.* 67, 1255–1268.
- Myneni, R. B., Keeling, C. D., Tucker, C. J., Asrar, G., and Nemani, R. R. (1997). Increased plant growth in the northern high latitudes from 1981 to 1991. *Nature* 386, 698–702. doi: 10.1038/386698a0
- Parmesan, C. (2006). Ecological and evolutionary responses to recent climate change. *Annual review of ecology. Evol. Syst.* 37, 637–669. doi: 10.1146/annurev.ecolsys.37.091305.110100
- Pei, F., Xia, L. I., Liu, X., and Xia, G. (2015). Dynamic simulation of urban expansion and their effects on net primary productivity: a scenario analysis of Guangdong province in China. *J. Geo-Inf. Sci.* 17, 469–477. doi: 10.3724/SPJ.1047.2015.00469
- Peng, J., Liu, Z., Liu, Y., Wu, J., and Han, Y. (2012). Trend analysis of vegetation dynamics in Qinghai–Tibet plateau using Hurst exponent. *Ecol. Indic.* 14, 28–39. doi: 10.1016/j.ecolind.2011.08.011
- Piao, S., Wang, X., Ciais, P., Zhu, B., Wang, T., and Liu, J. (2011). Changes in satellite-derived vegetation growth trend in temperate and boreal Eurasia from 1982 to 2006. *Glob. Chang. Biol.* 17, 3228–3239. doi: 10.1111/j.1365-2486.2011.02419.x
- Piao, S., Wang, X., Park, T., Chen, C., Lian, X., He, Y., et al. (2020). Characteristics, drivers and feedbacks of global greening. *Nat. Rev. Earth Environ.* 1, 14–27. doi: 10.1038/s43017-019-0001-x
- Qi, X., Jia, J., Liu, H., and Lin, Z. (2019). Relative importance of climate change and human activities for vegetation changes on China's silk road economic belt over multiple timescales. *Catena* 180, 224–237. doi: 10.1016/j.catena.2019.04.027
- Tucker, C. J., Slayback, D. A., Pinzon, J. E., Los, S. O., Myneni, R. B., and Taylor, M. G. (2001). Higher northern latitude normalized difference vegetation index and growing season trends from 1982 to 1999. *Int. J. Biometeorol.* 45, 184–190. doi: 10.1007/s00484-001-0109-8
- Wang, Z. X., Liu, C., and Alfredo, H. (2003). From AVHRR-NDVI to MODIS-EVI: advances in vegetation index research. *Acta Ecol. Sin.* 05, 979–987. doi: 10.3321/j.issn:1000-0933.2003.05.020
- Wang, Z., Liu, C., Chen, W., and Lin, X. V. (2006). Preliminary comparison of MODIS-NDVI and MODIS-EVI in eastern Asia. *Geomat. Inform. Sci. Wuhan Univ.* 31, 407–410. doi: 10.3969/j.issn.1671-8860.2006.05.008
- Xia, C., Li, J., and Liu, Q. (2013). Review of advances in vegetation phenology monitoring by remote sensing Yaogan Xuebao. *J. Rem. Sens.* 17, 1–16.
- Xiao, J., and Moody, A. (2005). A comparison of methods for estimating fractional green vegetation cover within a desert-to-upland transition zone in Central New Mexico, United States. *Remote Sens. Environ.* 98, 237–250. doi: 10.1016/j.rse.2005.07.011
- Xie, B., Jia, X., Qin, Z., Shen, J., and Chang, Q. (2016). Vegetation dynamics and climate change on the loess plateau, China: 1982–2011. *Reg. Environ. Chang.* 16, 1583–1594. doi: 10.1007/s10113-015-0881-3
- Xie, H., Tong, X. J., Li, J., Zhang, J. R., Liu, P. R., and Yu, P. Y. (2022). Changes of NDVI and EVI and their responses to climate variables in the Yellow River Basin during the growing season of 2000–2018. *Acta Ecol. Sin.* 42, 4536–4549. doi: 10.584/stxb202104271108
- Xu, Y. F., Pan, W. S., and Zhang, Y. L. (2020). Vegetation NDVI change and its response to climate change in Guizhou plateau. *Ecol. Environ. Sci.* 29, 1507–1518. doi: 10.16258/j.cnki.1674-5906.2020.08.002
- Ye, Q., Zhao, P., and Sun, J. (2012). Comparative analysis of vegetation coverage along the Yangtze River in Anhui Province based on MODIS/NDVI and EVI. *Res. Environ. Yangtze Basin* 21, 361–368.
- Yi, Y., Hu, X. L., Shi, M. C., Kang, H. Z., Wang, B., Zhang, C., et al. (2021). Vegetation dynamics and its relationship with climate factors in the middle reaches of the Yangtze River based on MODIS NDVI. *Acta Ecol. Sin.* 41, 7796–7807. doi: 10.5846/stxb202007251953
- Yi, Y., Shi, M., Yi, X., Liu, J., Shen, G., Yang, N., et al. (2022). Dynamic changes of plantations and natural forests in the middle reaches of the Yangtze River and their relationship with climatic factors. *Forests* 13:1224. doi: 10.3390/f13081224
- Yuan, W., Piao, S., Qin, D., Dong, W., Xia, J., Lin, H., et al. (2018). Influence of vegetation growth on the enhanced seasonality of atmospheric CO₂. *Glob. Biogeochem. Cycles* 32, 32–41. doi: 10.1002/2017GB005802
- Zhang, G. P., Chen, G. M., Shao, H. Y., and Xian, W. (2021). Spatial-temporal characteristics of vegetation coverage and its response to climate from 2000 to 2015 in Jinsha River basin, China. *Res. Environ. Yangtze Basin* 30, 1638–1648.
- Zhang, K. X., Fan, P. P., Wang, J. B., and Ye, H. (2019). Study on vegetation changes and climate factors in a karst region of Southwest China. *Ecol. Environ.* 28, 1080–1091. doi: 10.16258/j.cnki.1674-5906.2019.06.002
- Zhao, J. C., Zhang, S. H., Yin, X. X., Zhu, Y. P., and Duan, G. H. (2022). Changes in vegetation coverage and its influencing factors across the Guangdong-Hong Kong-Macao Bay Area. *Sci. Surv. Map.* 47, 75–84. doi: 10.16251/j.cnki.1009-2307.2022.03.011



OPEN ACCESS

EDITED BY
Shaoquan Liu,
Institute of Mountain Hazards and
Environment, CAS, China

REVIEWED BY
Britt Kniesel,
Technical University Dresden, Germany
Guoyin Wang,
Fudan University, China

*CORRESPONDENCE
Xianhui Feng,
✉ xhfeng@scut.edu.cn

SPECIALTY SECTION
This article was submitted to Atmosphere
and Climate,
a section of the journal
Frontiers in Environmental Science

RECEIVED 25 November 2022
ACCEPTED 27 January 2023
PUBLISHED 16 February 2023

CITATION
Feng X, Wen H, He M and Xiao Y (2023),
Microclimate effects and influential
mechanisms of four urban tree species
underneath the canopy in hot and
humid areas.
Front. Environ. Sci. 11:1108002.
doi: 10.3389/fenvs.2023.1108002

COPYRIGHT
© 2023 Feng, Wen, He and Xiao. This is an
open-access article distributed under the
terms of the [Creative Commons
Attribution License \(CC BY\)](https://creativecommons.org/licenses/by/4.0/). The use,
distribution or reproduction in other
forums is permitted, provided the original
author(s) and the copyright owner(s) are
credited and that the original publication in
this journal is cited, in accordance with
accepted academic practice. No use,
distribution or reproduction is permitted
which does not comply with these terms.

Microclimate effects and influential mechanisms of four urban tree species underneath the canopy in hot and humid areas

Xianhui Feng^{1,2*}, Huan Wen¹, Mu He¹ and Yiqiang Xiao^{1,2}

¹School of Architecture, South China University of Technology, Guangzhou, China, ²State Key Laboratory of Subtropical Building Science, South China University of Technology, Guangzhou, Guangdong, China

Purpose: Urban trees play a key role in ameliorating extreme urban climates in cities. At the micro-level, it is crucial to investigate the variations in microclimates affected by the canopies of different tree species. The significance of this research is to provide scientific evidence for the selection of tree species in urban planning that can improve the local microclimate. This study examines the factors of microclimate (air temperature, relative humidity, wind environment, and solar radiation) underneath the canopy of four different evergreen tree species in hot and humid areas. Furthermore, the correlation between the physiological characteristics of these tree species and microclimate was statistically analyzed using data on the physiological parameters of the trees and microclimate factors.

Methods: In this study, four tree species were selected for field measurements: *Ficus microcarpa* L. f., *Ficus virens* Aiton, *Bauhinia x blakeana* Dunn, and *Cinnamomum camphora* (L.) Presl. We used the HOBE (H21-0024, onset) to measure three climatic parameters (Temperature, Relative Humidity, and Instantaneous Wind Speed), and the Li-6400 Portable Photosynthesis System to measure five plant physiological parameters: Stomatal Conductance (Gs), Leaf Temperature (Tleaf), Leaf Surface Relative Humidity (RHsfc), Photosynthetically Active Radiation (PAR), and Leaf-level Vapor Pressure Deficit (Vpdl). The observations were conducted during winter (January 16 - January 22) and summer (August 7 - August 22). The investigation periods were 9:00–11:00, 12:00–14:00, and 16:00–18:00, and data were recorded at 15-min intervals. The observational data obtained were analyzed using statistical methods, including one-way analysis of variance, Pearson correlation coefficient, and multiple regression analysis.

Results: The results of this study indicated that the four tree species being measured had different effects on the microclimate at the sites in both the winter and summer seasons. During the 7-day observation in the summer, the cooling effect of the four tree species was significant. The relative humidity underneath the canopies was 3%–11% higher than that of weather stations. The instantaneous wind speed in the afternoon was relatively higher than at other times. The solar radiation intensity was dramatically reduced by 85%–95%. During the 7-day observation in the winter, the trees had a warming effect in the morning. The relative humidity underneath the canopies was 10%–20% higher than that of the weather stations. The areas underneath the canopies were windless in the afternoon. The solar radiation intensity was reduced by 78%–95%. *Ficus microcarpa* was found to be one of the most effective tree species for increasing the relative humidity and reducing solar radiation intensity in hot and humid areas. Additionally, the highest instantaneous wind speed was observed in the areas underneath the canopies of *F. virens* and *C. camphora*.

Statistical tests revealed that the air temperature and the instantaneous wind were extremely significantly correlated with Tleaf and RHsfc.

Conclusion: The four urban tree species studied had varying degrees of effect on air temperature, relative humidity, wind speed, and reducing solar radiation intensity in the areas underneath their canopies. Furthermore, these trees demonstrated varying abilities to improve microclimate conditions in different seasons. The four trees had a cooling effect in the summer. The instantaneous wind speed was calm in the afternoons during the winter in contrast to being relatively high speed in the afternoons during the summer. This characteristic is beneficial to warmth in winter and coolness in summer. In terms of the internal influence mechanisms, the results of the analysis indicated that microclimate factors were significantly correlated with the physiological parameters of the trees. Tleaf, RHsfc, and Vpdl were significant physiological parameters and had different contribution rates to microclimate factors.

KEYWORDS

urban tree, microclimate, hot and humid area, *Ficus microcarpa*, *Cinnamomum camphora*, *Ficus virens*, *Bauhinia x blakeana*

1 Introduction

Green spaces are one of the major types of urban land development. Trees in urban green spaces have positive effects and cool urban temperatures. There is considerable research demonstrating their cooling effect on temperatures and their effect on increasing the air humidity, which improves the local urban microclimate through trees in greenspaces (Bao et al., 2001; Guo et al., 2008; Li et al., 2011; Zhu et al., 2011).

The influence effect of urban trees on local urban climatic environments is a complex natural phenomenon. First, recent studies have shown urban trees have varying degrees of capability to mitigate high temperatures in cities under different climate contexts. The cooling efficiency of urban trees under different climatic conditions was shown to have significant differences in 510 cities, and the influence of mitigating temperature was particularly notable in arid cities (Cheng et al., 2022). Studies in two coastal cities with different climatic contexts, Seattle, Washington, and Baltimore, Maryland, USA, showed that the compactness of canopy cover was not significant in reducing land surface temperature (Jung et al., 2021). Secondly, trees have different local microclimate influence effects compared to shrubs and grasses, and the ecological effects of various species of trees are different. Using analysis of high-resolution land surface temperature (LSTs) and land-cover data from 293 European cities, it was found that the cooling effect of spaces without trees was approximately 2–4 times higher than that of green space (Schwaab et al., 2021). It has been shown in Jinan city that the taller the trees, the more effective they are in reducing the temperature of surrounding areas. (Xia et al., 2013). It has been confirmed that tree greenbelts have the best cooling and humidifying effects in Shenzhen, as compared to the microclimate effects of other landscape types, such as lawns, and waterscapes, as determined by ENVI-met (Wu et al., 2016). Due to the different efficiencies of the internal mechanisms of trees, such as photosynthesis and evapotranspiration, different tree species have varying effects on microclimate conditions. (Yang et al., 2022). Research has established that there is a non-linear threshold relationship between the area underneath the canopy and the decrease in land surface temperature, and compactness of the canopy cover was found to have no significant impact on reducing the land surface temperature (Jung et al., 2021). It

is hypothesized that microclimate conditions at a site can be influenced by different tree species through their photosynthesis or evapotranspiration processes. A study in northern China has shown that there are differences in the cooling and humidifying effects of *Pinus densiflora* forests and mixed *Quercus acutissima*/*Pinus massoniana* forests (Dong et al., 2017). The arborous layer has a significant impact on ecosystems, particularly on soil runoff. In forest tree species, spruce forests had the driest environmental conditions, which was also confirmed at the Soil Experiment Station of Moscow State University during 60 years of observations of ecosystems (Matyshak et al., 2021).

In terms of methodology, recently, software simulation techniques, such as FLUENT and ENVI-met, have been used frequently. FLUENT was used to simulate air turbulence in an ideal urban green space condition in Guangzhou (Feng and Chu, 2017). Previous studies using ENVI-met have found that outdoor thermal improvements in campus areas are related to the effects of different levels of tree canopy closure in Nigeria (Abdulkarim et al., 2021). Liu et al. (2018) set up simulation experiments using ENVI-met. The simulated experiments are accurately calculated based on the field-measured physiological parameters data of *Ficus microcarpa*, thus proving the physiological and microclimate performance of *Ficus microcarpa* in hot and humid areas. But the simulation method is limited by its algorithms and the lack of perception of complex real environmental conditions; the selection of representative real sites for field observation is still the most accurate method of microclimate research.

Previous studies have established that trees can affect the microclimate. This study selected four urban tree species, *F. microcarpa*, *Ficus virens*, *Bauhinia x blakeana*, and *Cinnamomum camphora*, all of them growing in Guangzhou city parks. The main purpose was to research the different impact effects of a variety of tree species on a site's microclimate environment. Thus, the research hypothesis propose to investigate the following questions: 1) What are the conditions of the temperature, relative humidity, wind speed, and solar radiation intensity underneath the canopy of these tree species in a hot and humid area of southern subtropical region? 2) How different is the influence of these trees on the microclimate underneath their canopies compared with the observation results from weather stations? 3) Which physiological parameters of the trees affect

TABLE 1 The range of mean extrema values of climate factors in Guangzhou during the 30-year period (1991–2020).

Climate factor	Temperature (°C)	Precipitation (mm)	Relative humidity (%)	Wind speed (m/s)	Wind direction frequency
Range					
The range of monthly mean extrema values in winter half-year	11.0–30.7	34.5–101.0	48.7–68.3	0.6–1.8	North and northeast
The range of monthly mean extrema values in summer half-year	19.6–33.5	193.8–364.9	56.5–84.1	1.1–1.6	South and southwest
The range of daily mean extrema values in January	10.6–18.7	–	34.6–71.3	0.4–1.9	North and northeast
The range of daily mean extrema values in August	25.5–33.2	–	53.5–88.3	0.6–1.7	South and southwest

January is the representative month of winter and the month of observation; August is the representative month of summer and the month of observation.

the temperature, relative humidity, wind environment, and solar radiation intensity underneath the canopy, and what is the underlying correlation? The purpose of this study is to investigate the above assumptions through actual measurements of four tree species.

2 Materials and methods

2.1 Study area

Guangzhou is a southern, subtropical city characterized by a hot and humid climate, and is a typically static wind city (Table 1). According to the 2021 Guangzhou Climate Bulletin, the annual average temperature is 24.0°C, and has increased at a rate of 0.3°C/10 years since 1961. The average wind speed is 1.9 m/s. Since 1961, the annual average wind speed has shown a significant decrease at a rate of 0.07 m/s per 10 years. According to meteorological data from the National Station in Guangzhou (59287), in the past 10 years (2009–2018), the annual average relative humidity was 71.1%. The area experiences its highest annual precipitation from May to June, with an annual mean precipitation of 1,695.9 mm and a maximum daily precipitation of 214.7 mm. Guangzhou vegetation consists of southern subtropical evergreen broad-leaved forests, and the trees are evergreen during four seasons.

The field of observation was Dongshan Lake Park, covering 31.7 ha, and with one of the four major artificial lakes in Guangzhou. In addition, Dongshan Lake Park is one of the most comprehensive city parks in Guangzhou, designated as a protected cultural heritage site in Guangzhou. Due to the well-protected tree species growing in the park and the characteristics of the Canton landscape, it has become a hotspot for nearby residents to rest. The areas underneath the tree canopies are some of the residents' favorite activity spaces in the park.

2.2 Tree selection and observation sites

According to the authoritative green space survey report of Guangzhou, we planned to select the trees with the largest number of plantings and the most widely used for research. The report was compiled by the Guangzhou Institute of Forestry and Landscape Architecture (GZ-IFLA). From 2011 to 2016, institute staff

investigated all ten districts within the metropolitan area of Guangzhou, including 313 parks, 12,868 residential green spaces, 88 forest parks and nature reserves, 365 flyover green areas, and 600,000 street trees, in order to gather information about the planted tree species in urban green spaces. The survey reported that the three top trees, *Bauhinia x blakeana*, *Ficus microcarpa* (*F. microcarpa*), and *Ficus virens* (*F. virens*) are the most widely used, and the survey also reported on the planting numbers of these top three trees. The most widely used non-native tree species is *Cinnamomum camphora* (*C. camphora*). Therefore, in this study, four tree species were selected in total as research objects: *Bauhinia x blakeana*, *F. microcarpa*, *F. virens*, and *C. camphora*.

Site microclimate is influenced by a variety of factors. To the extent possible, to eliminate other factors affecting the site, all observation sites were required to have convergent features or a similar environment in this study. The distribution of the four observation sites is shown in Figure 1.

The selected observation sites meet the following requirements: 1) the sites were all located next to Dongshan Lake (distance < 5 m), and the distance between each site was approximately 500 m to eliminate the local climate differences caused by significant distance differences; 2) the trees of each observation site were of the same species, and all the sites had the same kind of pavement; 3) the ages of the trees in the four observation sites was older than 50 years, with crown base heights of over 2 m; 4) the observation sites did not have shrubs or grasses, to eliminate other plants influences; 5) the planting areas of the four observation sites were the same size; 6) the closure canopy of all trees was above 70% in summer. Details and real conditions of the observation sites are shown in Figure 1 and Table 2.

We measured the closure canopy of the trees by using fish-eye photographs at the observation sites. Both values of Sky View Factor (SVF) and closure canopy were analyzed by Rayman software (Matzarakis et al., 2007; Matzarakis et al., 2010), as shown in Table 3.

2.3 Observation instruments and measurement parameters

This study used Onset HOBO equipment to measure three climatic parameters, including air temperature (Temp/°C), relative humidity (RH/%), and wind speed (WS/m/s); an Li-6400 Portable Photosynthesis System instrument to measure five physiological parameters, including Gs (mol/H₂O/(m²·s)), Tleaf (°C), RHsc (%),

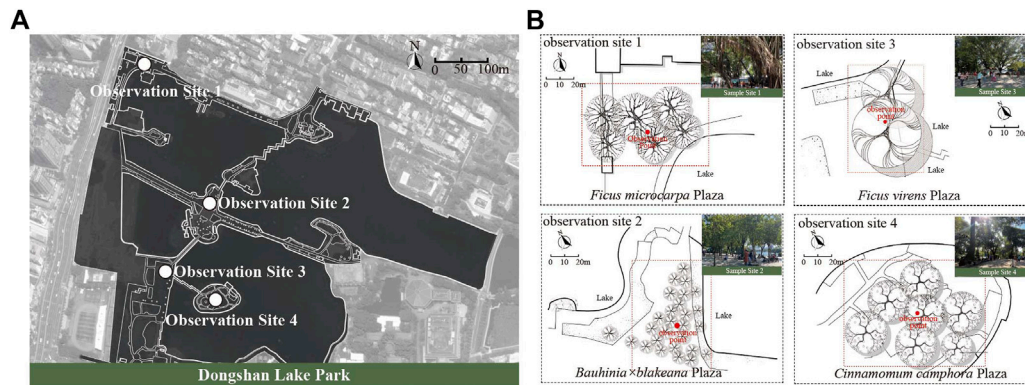


FIGURE 1

Study site (A) distribution map of the four measurement sites (B) sample site plan and field photos.

PAR(KPa), and V_{pdl} ($\mu\text{mol}/(\text{m}^2\cdot\text{s})$). The intensity of solar radiation (SR, w/m^2) was measured by LPPYRA06 albedo measuring instrument produced by Delta OHM in Italy.

The instrument properties, parameters, and observational times are shown in Table 4.

The V_{pdl} was calculated by the equation:

$$V_{pdl} = SVT_{leaf} - V_{p_{kpa}} = 0.61365 \times e^{\frac{17.502 \times T_{leaf}}{240.97 + T_{leaf}}} - H_2O \times \frac{Press}{1000}$$

Where: T_{leaf} = leaf temperature; $V_{p_{kpa}}$ = vapor pressure chamber air; SVT_{leaf} = SatVap (The saturation vapor pressure is calculated based on the temperature of the leaf.); H_2O = concentration of sample cell H_2O ; Press = atmospheric pressure.

2.4 Experimental design

According to the Guangzhou weather website, for 30 years (1991–2020), generally, the weather in Guangzhou has been divided into two typical seasons: the winter half-year, which is the period from October to March, and the summer half-year, which is the period from April to September. The lowest monthly mean temperature occurs in December, during the winter season. The highest monthly mean temperature occurs in June, during the summer.

To avoid the impact of extreme temperatures, this study selected January in the winter half-year and August in the summer half-year as the representative months for the winter and summer observation. January is third on the rank of monthly mean temperature from the lowest to the highest in winter; August is the same for summer. The general climate data of the weather stations are shown in Table 1.

In the winter season, the observation times were from 16th to 22 January 2021, with continuous observation for a week. The observation times in the summer were from 7th to 22 August 2021, excluding rainy days by selecting 7 days of clear and cloudless weather. The observation periods were 9:00–11:00, 12:00–14:00, and 16:00–18:00, recorded at 15-min intervals, and the mean values of the data were stored.

The data were calculated by Excel 2016, SPSS software, and illustrated by Origin 2021. In terms of data statistical methods, one-way analysis of variance, Pearson correlation coefficient analysis, and multiple regression analysis were used. One-way

analysis of variance was used to compare the significance levels of air temperature and relative humidity between the different trees and the weather stations. Pearson correlation analyzed the correlation between the physiological parameters of the trees and the microclimatic factors. The multiple regression further analyzed the contribution rate of physiological parameters to microclimatic factors.

3 Result and analysis

3.1 Effects of different trees on air temperature and relative humidity

In the winter, the effects on temperature were more complex. Due to the heat storage and insulation capacity of plants, the air temperatures of the areas underneath the canopies of the four species were significantly higher than that of weather stations from 8:00–9:00. Before 12:00, the temperature underneath the canopy of *F. microcarpa* was warmer than the weather stations. Among the four tree species, *F. microcarpa* had the strongest warming effect. The trees increased the air temperature in the morning, but the temperature underneath the canopy was lower than that of the weather stations after 12:00, except for *F. microcarpa*, which was close to that of the weather stations (Figure 2A Above).

The results indicated that during the summer, the four analyzed species demonstrated significant cooling effects during the daytime. However, there were notable variations in the cooling effect among the tree species after 10:00. The minimum temperature was observed underneath the canopy of *C. camphora*, and the maximum temperature was observed underneath the canopy of *Bauhinia x blakeana* (Figure 2A Below).

During observation times in January, the diurnal variation of air temperature underneath the canopies also increased gradually, but the warming effect was relatively slow, resulting in lower air temperature after 12:00, and the diurnal variation curve of air temperature underneath the canopies were gentler than that of the weather stations. Similarly, during observation time in August, because the temperatures underneath the canopies rose slowly, the temperatures were significantly lower than that at the weather stations, and the diurnal variation curve was smoother, as shown in Figure 2A.

TABLE 2 Description of the conditions of the sample sites.

Site	Tree species	Area underneath the canopy (m ²)	Quantity	Diameter at breast height (cm)	Average branching point height(m)	Average crown (m)	Density (ind 100m ⁻²)	Closure canopy (%)	Underpad surface	Growth status
1	<i>Ficus microcarpa</i> L. f	500	6	42.4	4.4	4.3 m × 5.7 m	1.2	90.42	concrete blocks	Good
2	<i>Bauhinia x blakeana</i> Dunn	500	27	6.6	2.7	2.1 m × 2.5 m	5.4	70.92	concrete blocks	Good
3	<i>Ficus virens</i> Alton	500	2	39.3	3.8	4.8 m × 5.3 m	0.4	91.92	concrete blocks	Good
4	<i>Cinnamomum camphora</i> (L.) Presl	500	7	23.7	7.2	4 m × 4.6 m	1.4	83.21	concrete blocks	Good

Taking the data from the weather stations as the control group, we analyzed the differences in temperature of the areas underneath the canopies of the four tree species using a one-way analysis of variance. During the winter, the results of the analysis of variance for the four tree species during three periods were as follows: $F = 0.058$, $p = 0.981$ (9:00–11:00); $F = 0.005$, $p = 0.999$ (12:00–14:00); $F = 0.021$, $p = 0.996$ (16:00–18:00), respectively. The values of the analysis of variance for the four tree species in summer were as follows: $F = 5.440$, $p = 0.005$ (9:00–11:00); $F = 5.318$, $p = 0.006$ (12:00–14:00); $F = 1.993$, $p = 0.151$ (16:00–18:00). As the results showed, in winter, the fitting degree of diurnal air temperature variation underneath the canopies among the four tree species was low. On the contrary, it was high in summer. Furthermore, the difference in the diurnal air temperature variation range was not relatively significant, but the difference in degree was higher in the summer than that in winter.

During the 7-day observation in the winter, the air temperature change range of the areas underneath the canopies of *F. microcarpa*, *F. virens*, *Bauhinia x blakeana*, and *C. camphora* was 14.86°C–20.26°C, 14.41°C–20.01°C, 14.24°C–21.39°C, and 14.41°C–21.89°C, respectively. The maximum temperature occurred between 12:00–14:00 or 16:00–18:00. The maximum temperature of *F. virens* occurred at noon (12:00–14:00) and *C. camphora* in the afternoon (16:00–18:00) (Figure 3A). The diurnal mean temperatures underneath the canopies of *F. microcarpa*, *Bauhinia x blakeana*, *F. virens*, and *C. camphora* were 17.96°C, 18.17°C, 18.33°C, and 18.20°C, respectively. During the 7-day observation in the summer, the air temperature change range of the areas underneath the canopies of *F. macrocarpa*, *F. virens*, *Bauhinia x blakeana*, and *C. camphora* was 30.31°C–34.65°C, 30.47°C–36.09°C, 31.02°C–35.50°C, and 31.28°C–34.73°C, respectively (Figure 3B). The diurnal mean temperature underneath the canopies of *F. microcarpa*, *Bauhinia x blakeana*, *F. virens*, and *C. camphora* were 32.60°C, 33.30°C, 32.96°C and 32.70°C, respectively. *F. microcarpa* exhibited the strongest cooling effect among the four tree species and the cooling effect of *Bauhinia x blakeana* was the weakest.

As shown in Figure 2B, the results showed that, compared with the weather stations, the trees had a significant effect on increasing humidity both in winter and summer. The relative humidity underneath the canopies of the four tree species exhibited a slow decrease from morning to noon, but an increase in the afternoon both in the winter and summer. However, there were differences in the humidifying effect of different tree species in different seasons.

In the winter, the relative humidity of the area underneath the canopies was significantly higher than that of the weather stations. The daily mean relative humidity at the weather stations was 40.02%, while the area underneath of *F. microcarpa*, *Bauhinia x blakeana*, *F. virens*, and *C. camphora*, it was 53.55%, 50.60%, 50.72%, and 50.50%, respectively. Of these, the highest relative humidity was found underneath the canopy of *F. microcarpa*, which was 13.53% higher than that at the weather stations. The diurnal change curve of relative humidity of these four tree species revealed that the curve of *F. microcarpa* was the flattest (Figure 2B Above). During the summer, the relative humidity underneath the canopy of all tree species was higher than that at the weather stations (57.12%). Specifically, the relative humidity beneath *F. microcarpa*, *F. virens*, *Bauhinia x blakeana*, and *C. camphora* was 64.85%, 62.76%, 61.31%, and 64.58%, respectively (Figure 2B Below). The average daily humidity beneath *F. microcarpa* was the highest among the four trees.

TABLE 3 Closure of the canopy of the four tree species.

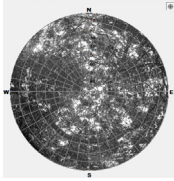
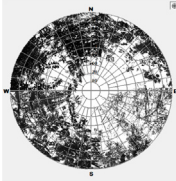
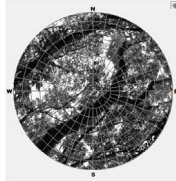
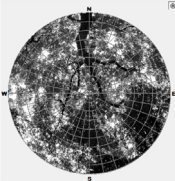
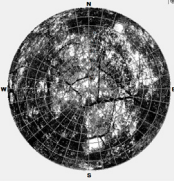
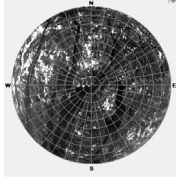
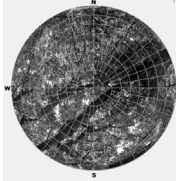
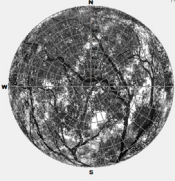
Observation point	No.1	No.2	No.3	No.4
Sky View Factor (SFV) of the Observation point in winter				
Visibility (%)	6.65	50.80	10.89	10.65
Closure canopy (%)	93.35	49.20	89.11	89.35
Sky View Factor (SFV) of the Observation point in the summer				
Visibility (%)	12.51	7.36	5.27	22.94
Closure canopy (%)	87.49	92.64	94.73	77.06

TABLE 4 The information of observation.

Measurement parameters	Instrument type	Photograph of instrument	Manufacturer	Measurement range	Observation time (min)
Temperature (Temp)	HOBO Climate monitoring (H21-0024)		Onset Computer Corporation	−40°C–70°C	15
Relative Humidity (RH)				0%–100%	15
Instantaneous Wind Speed (IWS)				0–40 m/s	15
Solar Radiation (SR)	LPPYRA06 Spectrally Flat Class C (Second Class) albedometer		Delta OHM Srl	0–2000 W/m2	5
Stomatal Conductance (Gs)	Li-6400 Portable Photosynthesis System		LI-COR Biosciences GmbH	0.005–1.2 mol H2Om-2 s-1	5
Leaf Temperature (Tleaf)				−200°C–260°C	5
Leaf Surface Relative Humidity (RHsf)				0–100%	5
Photosynthetically Active Radiation (PAR)				0–1500 μmol m-2s-1	5
Leaf-level Vapor Pressure Deficit (Vpdl)				0–20 kPa	5

As shown in [Figure 4](#), in general, the relative humidity underneath the canopies in the summer was higher than that in the winter. At noon, the relative humidity was the lowest during the daytime.

During the 7 days of observation in the winter, the range of relative humidity change for *F. microcarpa*, *Bauhinia x blakeana*, *F. virens*, and *C. camphora* was 43.40%–66.92%, 39.55%–62.38%, 39.48%–64.77%, and 43.74%–62.51%, respectively. The differences in change of magnitude were 23.52%, 22.83%, 25.29%, and 18.77%, respectively

([Figure 4A](#)). During the 7-day observation in the summer, the range of *F. microcarpa*, *F. virens*, *Bauhinia x blakeana*, and *C. camphora* was 51.60%–76.02%, 55.36%–72.37%, 56.69%–73.83%, and 53.55%–72.40%, respectively, and the change of magnitude was 24.42%, 17.01%, 17.14%, and 18.85%, respectively ([Figure 4B](#)).

A one-way analysis of variance was used to analyze the differences in relative humidity of the four tree species. In the summer, the results of the analysis of variance were as follows: $F = 2.469$, $p = 0.086$

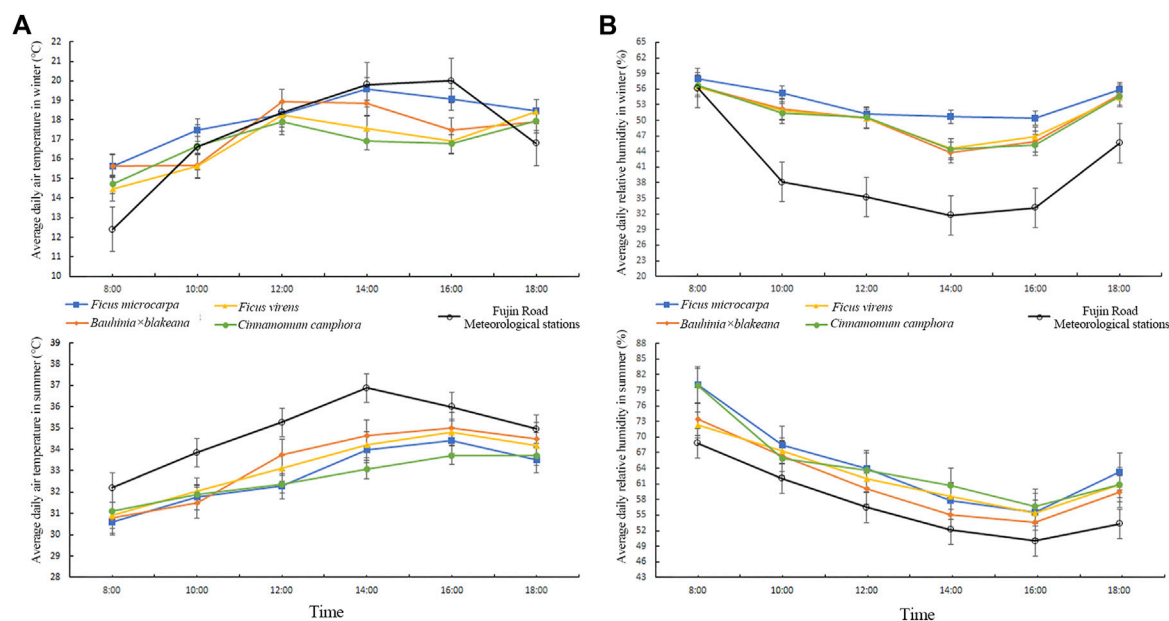


FIGURE 2 Diurnal change of air temperature and relative humidity of the four tree species in winter and summer community weather stations (A) air temperature (B) relative humidity.

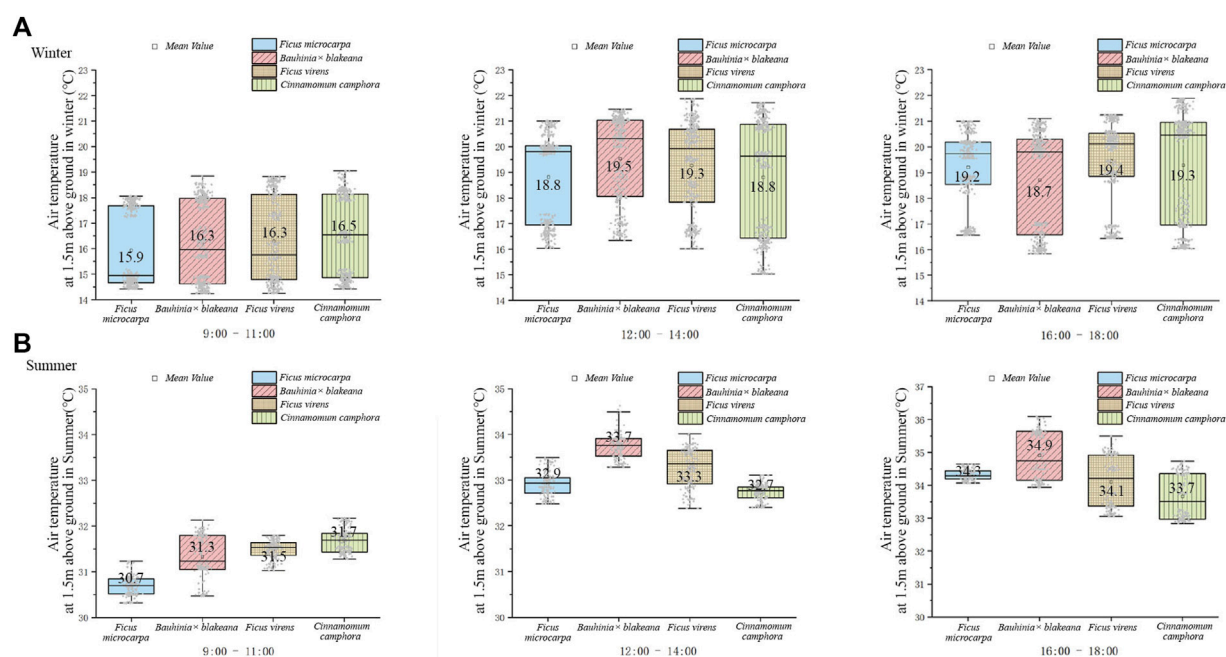


FIGURE 3 Temperatures underneath the canopy of the four tree species in winter (A) and summer (B).

(9:00–11:00); $F = 16.05$, $p = 0.000$ (12:00–14:00); $F = 5.289$, $p = 0.006$ (16:00–18:00). In the winter, the values were as follows: $F = 0.133$, $p = 0.939$ (9:00–11:00); $F = 0.129$, $p = 0.942$ (12:00–14:00); $F = 0.187$, $p = 0.904$ (16:00–18:00). As the results showed, in summer, the fitting degree of diurnal relative humidity variation underneath the canopies among the four tree species was high. Furthermore, the difference in the diurnal relative humidity variation range was not relatively significant.

3.2 Effects of different trees on wind environment

Guangzhou is a city with typically calm wind, characterized by low wind speeds at the near-ground layer and poor ventilation. Therefore, the wind environment in Guangzhou is dominated by near-ground turbulence (Feng and Wei, 2011). As shown in Figure 5, the wind

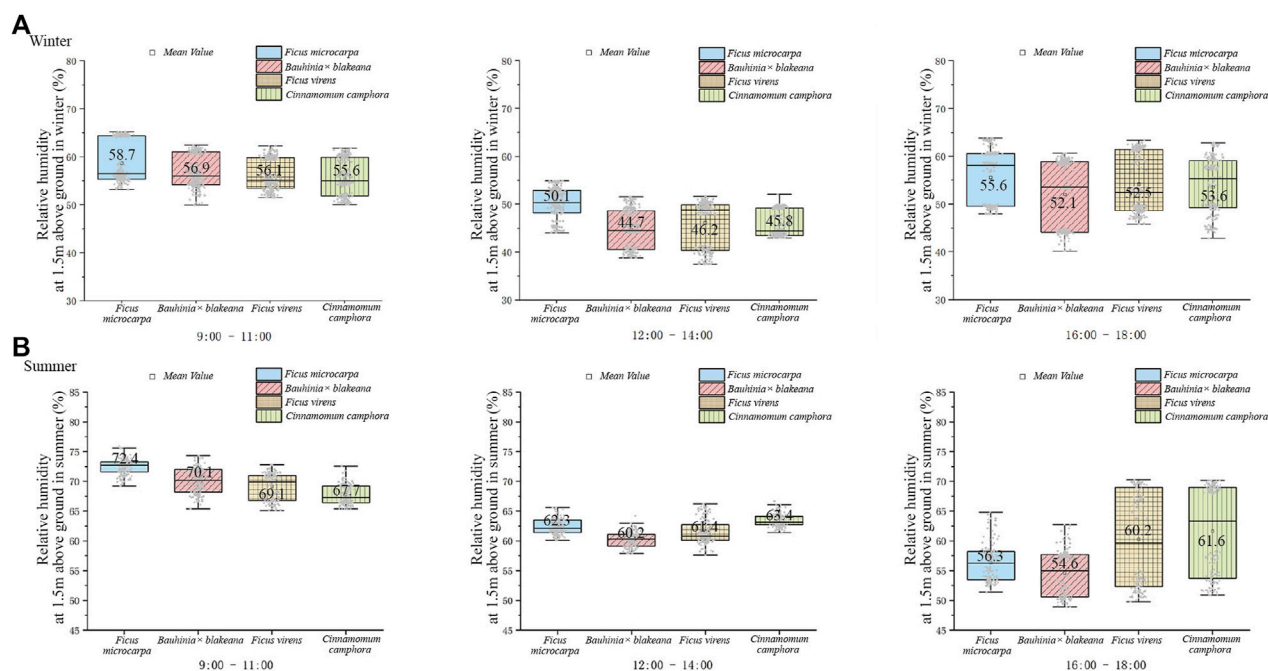


FIGURE 4
Relative humidity underneath the canopy of the four tree species in winter (A) and summer (B).

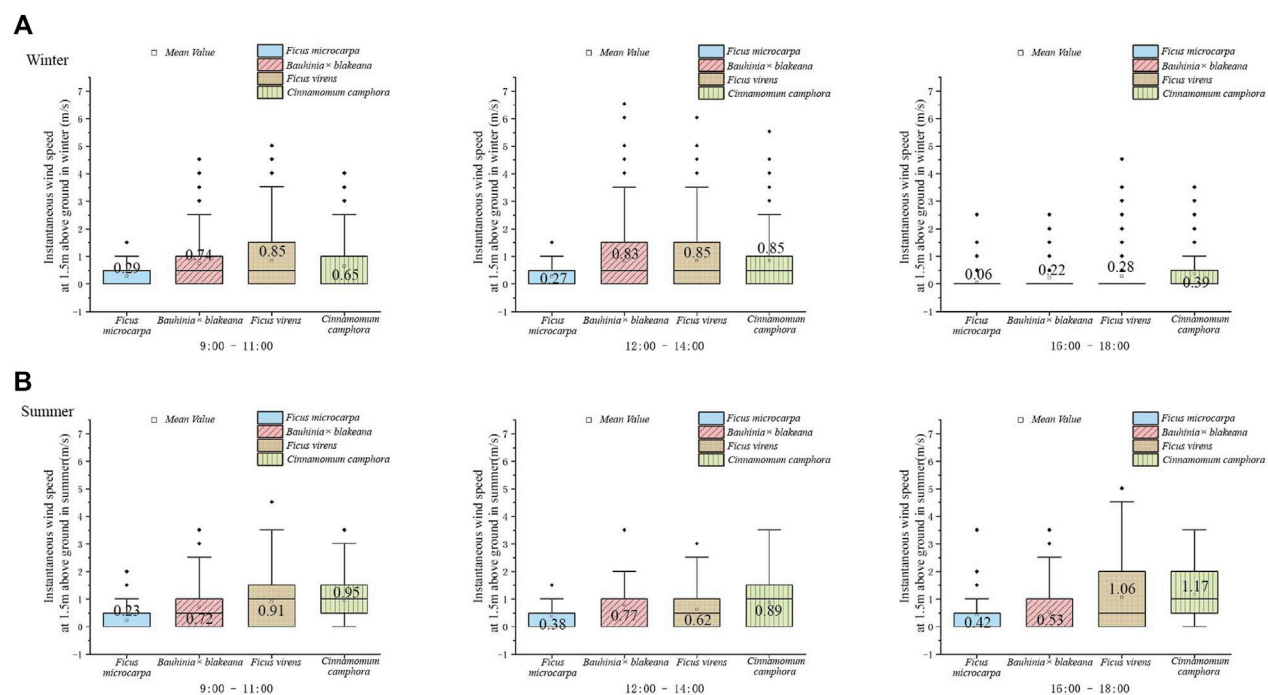
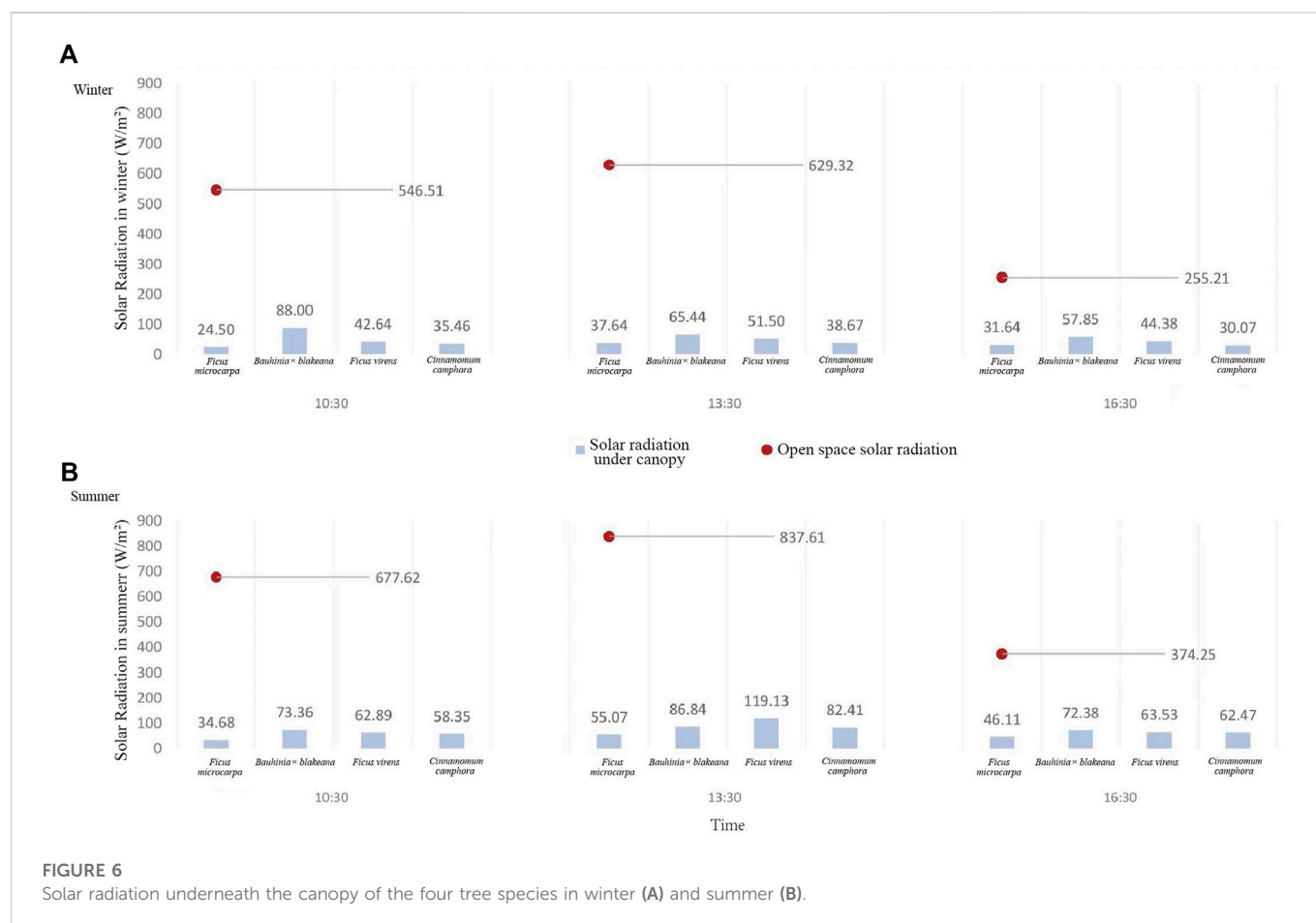


FIGURE 5
Instantaneous wind speed underneath the canopy of the four tree species in winter (A) and summer (B).

speed data observed beneath the tree canopies showed that there was no continuous or persistent wind flow, and just instantaneous winds speed were observed. There were differences in the instantaneous wind speed and frequency underneath the canopies of different trees.

During the 7-day observation period in the winter, the daily average instantaneous wind speed of *F. microcarpa* was 0.21 m/s. A range of change was observed from 0.00 to 0.77 m/s in the daytime. *Bauhinia x blakeana*, *F. virens*, and *C. camphora* were observed to have daily average instantaneous wind speeds of 0.59 m/s, 0.66 m/s, and



0.63 m/s, with a range of wind speed change from 0.01 to 2.34 m/s, 0.02–2.32 m/s, and 0.01–2.69 m/s, respectively. The regulation of daily change showed that the instantaneous wind speed was highest at noon (12:00–14:00), and that it was almost windless in the afternoon (16:00–18:00). The daily average instantaneous wind speed underneath the canopy of *F. microcarpa* was the lowest and the *F. virens* was highest (Figure 5A).

During the 7-day observation in the summer, the daily average instantaneous wind speeds of *F. microcarpa*, *Bauhinia x blakeana*, *F. virens*, and *C. camphora* were observed to be 0.34 m/s, 0.67 m/s, 0.86 m/s, and 1.01 m/s, and the range of wind speed change was 0.19–0.49 m/s, 0.43–1.05 m/s, 0.45–1.51 m/s, and 0.48–1.48 m/s, respectively. The result showed that the daily variation of wind speed was opposite to that in winter. The instantaneous wind speed was highest in the afternoon (16:00–18:00), except for *Bauhinia x blakeana*. The daily average instantaneous wind speed underneath the canopy of *F. microcarpa* was the lowest and the *C. camphora* was the highest (Figure 5B).

3.3 Effects of different trees on solar radiation

Generally, the canopies of trees reduces solar radiation intensity by avoiding direct exposure to sunlight. As shown in Figure 6, the trees greatly reduced solar radiation in winter and summer, especially at noon.

In the winter, the range of diurnal mean values of solar radiation intensity for the control observation point (open space) was found to

be 255.21–629.32 w/m². However, the solar radiation intensity of the areas underneath the canopies of *F. microcarpa*, *Bauhinia x blakeana*, *F. virens*, and *C. camphora* was 24.5–37.64 w/m², 57.85–88.00 w/m², 42.64–51.5 w/m², and 30.07–38.67 w/m², respectively (Figure 6A). In the summer, the solar radiation intensity of the control observation point was 374.25–837.61 w/m², and for *F. microcarpa*, *Bauhinia x blakeana*, *F. virens*, and *C. camphora* it was 34.68–55.07 w/m², 62.47–119.13 w/m², 72.38–86.84 w/m², and 58.35–82.41 w/m², respectively (Figure 6B).

The result showed *F. microcarpa* had the strongest impact on reducing solar radiation intensity. In the winter, the area underneath the canopy of *Bauhinia x blakeana* had the highest solar radiation intensity. During all the observation periods in winter and summer, it was found that the solar radiation intensity underneath the canopy of *F. microcarpa* had the smallest fluctuations, with a range of fluctuation of about 30.56 w/m²; *F. virens* had the most significant fluctuation of solar radiation, with fluctuations of about 60.49 w/m².

3.4 Correlation analysis of physiological characteristics of trees and microclimatic factors

This study used the Li-6400 Portable Photosynthesis System instrument to measure five physiological parameters of plants, including Gs, Tleaf, RHsfc, PAR, and Vpdl. The observation periods were 9:00–11:00, 12:00–14:00, and 16:00–18:00, and were recorded at 5-

TABLE 5 Correlation of physiological parameters of trees with microclimatic factors.

Tree species	Climate factors	Trees physiological parameters				
		Tleaf	RHsfc	Gs	PAR	Vpdl
<i>Ficus microcarpa</i>	Temperature (Temp)	0.991**	0.887**	0.58	0.774*	0.663
	Relative Humidity (RH)	0.351	0.652	0.123	0.174	0.389
	Instantaneous Wind Speed (IWS)	0.833**	0.684*	0.488	0.49	0.511
	Solar Radiation Under Forest (RS)	0.583	0.369	0.303	0.720*	0.509
<i>Bauhinia x blakeana</i>	Temperature (Temp)	0.984**	0.932**	0.381	0.602	0.734*
	Relative Humidity (RH)	−0.019	0.166	0.083	0.141	0.167
	Instantaneous Wind Speed (IWS)	0.798*	0.845**	0.334	0.673	0.855**
	Solar Radiation Under Forest (RS)	0.738*	0.621	0.642	0.783*	0.635
<i>Ficus virens</i>	Temperature (Temp)	0.995**	0.969**	0.679	0.633	0.837*
	Relative Humidity (RH)	0.069	0.179	0.137	0.134	−0.007
	Instantaneous Wind Speed (IWS)	0.768*	0.759*	0.14	0.149	0.553
	Solar Radiation Under Forest (RS)	0.735	0.681	0.652	0.549	0.894**
<i>Cinnamomum camphora</i>	Temperature (Temp)	0.995**	0.965**	0.773*	0.666	0.804*
	Relative Humidity (RH)	0.678	0.811*	−0.333	0.241	0.771*
	Instantaneous Wind Speed (IWS)	0.797*	0.795*	0.682	0.342	0.516
	Solar Radiation Under Forest (RS)	0.796*	0.727*	0.263	0.848**	0.303

**= Extremely Significantly correlated at the 0.01 level (bilateral); * = Significantly correlated at the 0.05 level (two-sided).

min intervals. The Pearson correlation coefficient method was adopted to calculate the correlation between the physiological parameters and the data from observational records of microclimate in the same periods.

The results of the analysis, as shown in Table 5, revealed the air temperature underneath the canopies of the four tree species was extremely significantly correlated ($p < 0.01$) with the Tleaf and RHsfc. The instantaneous wind speed was extremely significantly correlated ($p < 0.01$) with the Tleaf of *F. microcarpa* and the RHsfc of *Bauhinia x blakeana*, respectively. The relative humidity correlated significantly ($p < 0.05$) with RHsfc and Vpdl of *C. camphora* but was not found to be significantly correlated with the physiological parameters of other trees. The solar radiation intensity was extremely significantly correlated ($p < 0.01$) with the PAR of *C. camphora* and Vpdl of *F. virens*, and significantly correlated ($p < 0.05$) with the PAR of *F. microcarpa* and *Bauhinia x blakeana*.

For *F. microcarpa*, as a native plant of Canton, there was an extremely significant correlation ($p < 0.01$) between Tleaf, RHsfc, and air temperature, and also Tleaf and instantaneous wind speed. There was a significant correlation ($p < 0.05$) between PAR with air temperature, RHsfc with instantaneous wind speed, and PAR with solar radiation. The relative humidity was not found to be correlated with any physiological parameters. However, there was no correlation found between Gs, Vpdl, and the microclimate data. The Tleaf and RHsfc of *F. microcarpa* were the major parameters related to the microclimate environment, and mainly affected temperature and instantaneous wind speed.

For *Bauhinia x blakeana*, there was an extremely significant correlation ($p < 0.01$) between the Tleaf, RHsfc, and air temperature, and also RHsfc, Vpdl, and instantaneous wind speed. There were significant correlations ($p < 0.05$) between Vpdl and air

temperature, Tleaf and instantaneous wind speed, and Tleaf, PAR, and solar radiation. The change of Vpdl led to significant changes in air temperature and instantaneous wind speed. A possible explanation for this may be that *Bauhinia x blakeana* affected the microclimate by impacting its transpiration rate. The temperature and instantaneous wind speed of the area underneath the canopy had correlations with Tleaf, RHsfc, and Vpdl. The relative humidity was not found to be correlated with any physiological parameters.

For *F. virens*, there was an extremely significant correlation ($p < 0.01$) between Tleaf, RHsfc, and air temperature, and also Vpdl and solar radiation. *Ficus virens* had a significant correlation ($p < 0.05$) between Vpdl and air temperature, and Tleaf, RHsfc, and instantaneous wind speed. The air temperature and instantaneous wind speed of the area underneath the canopy had a correlation with the physiological parameters of Tleaf, RHsfc, and Vpdl. Vpdl was correlated with solar radiation and air temperature simultaneously. The relative humidity was not found to be correlated with any physiological parameters.

For *C. camphora*, the five physiological parameters all had a correlation with the four factors of microclimate. There was an extremely significant correlation ($p < 0.01$) between Tleaf, RHsfc, and air temperature, and PAR and solar radiation. The air temperature had a significant correlation ($p < 0.05$) with Gs and Vpdl. The instantaneous wind speed and solar radiation had significant correlation ($p < 0.05$) with Tleaf and RHsfc. The relative humidity had a significant correlation ($p < 0.05$) with RHsfc and Vpdl. However, except *C. camphora*, relative humidity showed no correlation with the physiological parameters of other tree species.

According to the Pearson correlation analysis, the correlation between the physiological parameters and the factors of

TABLE 6 Regression equation and contribution of physiological parameters of trees.

Tree species	Meteorological factors	Regression equation	Contribution of tree physiological parameters (%)				
			Tleaf	RHsfc	Gs	PAR	Vpdl
<i>Ficus microcarpa</i>	Temp	$Y_{Temp} = 0.860X_{Tleaf} - 0.072X_{PAR} + 0.095X_{Cond} + 0.13X_{Vpdl}$	75.1	/	8.2	6.2	11.2
	IWS	$Y_{IWS} = 0.879X_{RHleaf} - 1.493X_{Tleaf} + 0.445X_{PAR} + 0.949X_{Cond} + 0.444X_{Vpdl} + 0.612$	35.5	20.9	22.5	10.6	10.5
	RS	$Y_{RS} = -0.3X_{Tleaf} - 0.438X_{RHleaf} + 0.349X_{Cond} + 0.027X_{PAR} + 0.755X_{Vpdl}$	16.1	23.4	18.7	1.4	40.4
<i>Bauhinia x blakeana</i>	Temp	$Y_{Temp} = 1.143X_{Tleaf} - 0.492X_{RHleaf} + 0.352X_{Cond} - 0.035X_{PAR}$	56.2	24.2	17.3	1.7	0.6
	RS	$Y_{RS} = 0.399X_{Tleaf} - 0.847X_{RHleaf} + 0.664X_{Cond} + 0.512X_{PAR} + 0.261X_{Vpdl} + 0.535$	14.9	31.6	24.7	19.1	9.7
<i>Ficus virens</i>	Temp	$Y_{Temp} = 0.909X_{Tleaf} + 0.012X_{RHleaf} - 0.227X_{Cond} + 0.075X_{PAR} + 0.237X_{Vpdl}$	62.3	0.8	15.6	5	16.3
	IWS	$Y_{IWS} = -2.021X_{Tleaf} + 3.237X_{RHleaf} - 1.717X_{Cond} + 1.203X_{Vpdl} + 0.408$	24.7	39.6	21	/	14.7
	RS	$Y_{RS} = -0.033X_{Tleaf} - 0.167X_{RHleaf} + 0.145X_{Cond} + 0.12X_{PAR} + 0.894X_{Vpdl} + 0.913$	2.4	12.3	10.7	8.8	65.8
<i>Cinnamomum camphora</i>	Temp	$Y_{Temp} = 0.343X_{Tleaf} + 0.398X_{RHleaf} + 0.296X_{Cond} + 0.02X_{PAR} - 0.036X_{Vpdl} + 0.535$	31.4	36.4	27.1	1.8	3.3
	RH	$Y_{RH} = -0.571X_{Tleaf} + 1.89X_{RHleaf} - 0.551X_{Cond} - 0.235X_{PAR} + 0.129X_{Vpdl} + 0.845$	16.9	56	16.3	7	3.8
	RS	$Y_{RS} = -0.417X_{Tleaf} + 0.331X_{RHleaf} + 0.354X_{Cond} + 0.848X_{PAR}$	21.4	17	18.1	43.5	/

microclimate was significant. The physiological parameters of the four tree species had different degrees of correlation with factors of microclimate. Overall, the results of this analysis showed that the physiological parameters of native plants (*F. microcarpa*, *F. virens*, *Bauhinia x blakeana*) had significant influences on air temperature, instantaneous speed, and solar radiation, but had no significant influence on relative humidity.

3.5 Multiple regression analysis between physiological parameters of trees and microclimatic parameters

In order to statistically analyze the intrinsic correlation and valuable relationships between the five physiological parameters and four factors of microclimate, we established equations between them using multiple regression analysis and further explored the internal mechanisms between the trees and the microclimate. However, there were no mathematical characteristics of convergence of some data between the parameters and the microclimate factors, so it was impossible to establish multiple regression equations. Finally, equations were successfully established between the following microclimate factors and physiological parameters: 1) the physiological parameters of *F. microcarpa* and air temperature (Temp), instantaneous wind speed (IWS), and the solar radiation (SR); 2) the physiological parameters of *Bauhinia x blakeana* and Temp and SR; 3) the physiological parameters of *F. virens* and Temp, IWS, and SR; 4) the physiological parameters of *C. camphora* and Temp, relative humidity (RH), and SR. We established the equation to calculate the contribution of the physiological parameters of the four tree species to the microclimate factors.

As shown in Table 6, with regard to Temp, an analysis of the contributions of the physiological parameters revealed that the Tleaf of *F. microcarpa* had the highest contribution (75.10%), followed by the Tleaf of *F. virens*, which had a contribution of 62%. The Tleaf of *C. camphora* had the lowest contribution to temperature, at 31.4%.

In terms of IWS, the IWS underneath the canopy of *F. microcarpa* was found to be affected by various physiological parameters, with Tleaf, Gs, RHsfc, PAR, and Vpdl contributing 35.5%, 22.5%, 20.9%, 10.6%, and 10.5%, respectively. In the case of *F. virens*, Tleaf, RHsfc, PAR, and Vpdl were identified as the main parameters influencing wind speed, with contributions of 24.7%, 39.6%, 21%, and 14.7%, respectively. Notably, RHsfc had the highest contribution rate. In contrast, the physiological parameters of *Bauhinia x blakeana* and *C. camphora* were found to have no statistical correlation with IWS.

The various physiological parameters performed varying levels of contribution to the reduction of solar radiation intensity underneath the canopies. *Ficus microcarpa* showed a contribution rate of 16.1% for Tleaf, 23.4% for RHsfc, 18.7% for Gs, 1.4% for PAR, and 40.4% for Vpdl, with the highest contribution coming from Vpdl. On the other hand, *Bauhinia x blakeana* had a contribution of 14.9% for Tleaf, 31.6% for RHsfc, 24.7% for Gs, 19.1% for PAR, and 9.7% for Vpdl, with the highest contribution coming from RHsfc. Similarly, *F. virens* had a contribution of 2.4% for Tleaf, 12.3% for RHsfc, 10.7% for Gs, 8.8% for PAR, and 65.8% for Vpdl, with the highest contribution coming from Vpdl. Lastly, *C. camphora* had a contribution of 24.1% for Tleaf, 17.0% for RHsfc, 18.1% for Gs, and 43.5% for PAR, with the highest contribution coming from PAR.

According to the data, there appeared to be no correlation between relative humidity and the physiological parameters of the tree species with the exception of *C. camphora*. However, as a foreign species, *C. camphora* had a contribution rate to relative humidity of 16.9%, 56.0%,

16.3%, 7.0%, and 3.8% for Tleaf, RHsfc, Gs, PAR, and Vpdl, respectively. The results suggested that RHsfc had the most significant contribution (56%) to relative humidity.

4 Discussion

4.1 Effects of urban trees on microclimatic conditions

Previous studies have demonstrated the cooling and humidifying effects of urban trees. Generally, there are notable differences in terms of affecting the local microclimate between trees and shrubs, with trees being superior, particularly in their cooling and humidifying effects (Lu et al., 2006). Trees are able to enhance the local microclimate, including reducing extreme wind speeds and temperatures (Baker et al., 2021). A previous study found that the amplitude of air temperature, surface temperature, humidity, and heat stress indexes were minimized in woodlands (Fang et al., 2018). Additionally, in the forest, the cooling effect is consistent across forests of different tree species (Liu et al., 2014). In comparison to earlier studies, our observation experiment confirmed that these four tree species could increase the extremely low temperatures of winter mornings and decrease the extremely high temperatures in summer; furthermore, they could increase the humidity of the area underneath the tree canopy and significantly reduce solar radiation intensity.

Previous research has rarely involved the study of wind conditions under different trees. This study revealed that the characteristics of wind speed in the area underneath the canopy were mainly in the form of instantaneous wind. According to the instantaneous wind speeds observed, *F. microcarpa* was found to be the lowest both in winter and summer, with values of 0.21 m/s and 0.34 m/s, respectively. In comparison, the instantaneous wind speed of the areas underneath the canopies of *F. virens* and *C. camphora* were found to be higher, with values of 0.86 m/s and 101 m/s in summer and 0.66 m/s and 0.63 m/s in winter, respectively. A previous study may explain the findings of our study: Ding et al. (2022) found that a higher crown base height of *C. camphora* was associated with stronger wind speed and frequency underneath the canopy. The difference in wind speed was related to the average crown base height of the trees. This was further supported by a study conducted in Fuzhou that investigated that *C. camphora* had a strong effect on increasing wind speed by using ENVI-met (Huang et al., 2022). Specifically, in our experiment, the crown base heights of *F. microcarpa* and *C. camphora* were 4.4 m and 7.2m, respectively.

The effects of urban trees have differences in different seasons. According to Shao et al. (2015), the canopies of trees could have a significant impact on humidifying effects, with greater effects observed during the summer and autumn seasons in comparison to spring and winter. A recent study conducted by Meili et al. (2021), there are seasonal differences in four cities (Phoenix, Singapore, Melbourne and Zurich). The results of our study indicated that the microclimate regulation ability of trees has seasonal differences in winter and summer.

There are different effects produced by different types of trees on the microclimate. A previous study indicated the varying effects of three tree species on microclimate by examining the changing of sap flow, with the cooling effect order being *Populus simonii* > *Cedrus deodara* > *C. camphora*. This was attributed to the differences in the volume of the canopy transpiration cooling effect (Wang et al., 2018).

Another study found that different trees (*Sabina chinensis*, *Platycladus orientalis*, and *Populus*) had different effects in mitigating temperatures and enhancing humidity (Li et al., 2018). Our study found that the minimum temperature underneath the canopy of *F. microcarpa* was in the summer, which was also supported by a study in Shenzhen. In continuous observations of various tree species in Shenzhen, *F. microcarpa* shows the strongest potential for transpiration and cooling effect compared to other trees (Ding et al., 2022). Furthermore, *F. microcarpa* had the most effect on increasing humidity among the four tree species. It is speculated that the ability of different trees may also be related to the closure canopy. The closure canopy of *F. microcarpa* was 91.92%, and it was 90.42% for *F. virens*, both greater than 90%. Conversely, *Bauhinia x blakeana* had the lowest closure canopy both in winter (49.00%) and summer (70.92%), resulting in the fastest heat dissipation and the slowest cooling effect. This is supported by another study conducted in Shenzhen, which found that the effect of green space in mitigating temperature mainly occurred via the sheltering effects of canopies (Li et al., 2011).

The ability of trees to influence the microclimate environment must be adapted to the varying climatic conditions in different regions. In severe cold regions, planting shrubs in the gaps between trees can enhance the wind protection effect. The complex vegetation structure has a positive impact on increasing human thermal comfort by reducing wind speed. Therefore, complex plant structures are beneficial in severe cold regions (Jin et al., 2018). In arid areas, it is important to select the appropriate plant species. For example, planting *Caragana intermedia* and *Artemisia ordosica* on the dunes has been shown to significantly reduce the wind speed, soil temperature, and air temperature, and increase the relative humidity and water content of soil (Zhu et al., 2014). In semi-arid areas, due to arid and windy climate characteristics, deciduous trees are often selected for planting (Wang et al., 2020).

However, in hot and humid areas, decreasing the high temperatures in summer, improving windless conditions, and reducing solar radiation can create a comfortable microclimate environment. In this research, *F. microcarpa* was the best species for improving air temperature and increasing the relative humidity in the winter. Additionally, in terms of improving wind speed, the diurnal mean wind speed under *F. virens* and *C. camphora* was found to be relatively higher both in the winter and summer.

4.2 The internal correlation mechanisms between physiological characteristics of trees and microclimate environment

Urban trees play a crucial role in shaping the local microclimate of the areas underneath their canopy through various physiological processes, such as photosynthesis and evapotranspiration. These processes affect the circulation of thermal energy and water, thereby impacting the local microclimate environment. Such effects are not only ecologically significant but also provide valuable insights into the effects of different tree physiological characteristics on changing climate environments. For instance, the results of our research can serve as a valuable reference for selecting appropriate tree species in urban planning efforts.

Recent studies have examined the correlations between the characteristics of urban trees and the local microclimate

underneath the canopy. A major focus of this field has been the morphological characteristics of trees, such as height, crown width, and vertical structure, and their impact on the local microclimate (Wang et al., 2020). Researchers have utilized software such as ENVI-met to investigate the effects of crown structure and layout on temperature and humidity (Wei et al., 2019). Previous research conducted in Beijing Olympic Park has shown that the canopy structural characteristics (leaf area index and canopy coverage) of certain plants play a significant role in regulating microclimate factors (Yan et al., 2012).

Research on the influence of the physiological parameters of trees on the microclimate underneath the canopy is relatively scarce. However, previous research has revealed that physiological parameters have an extremely significant correlation with microclimate parameters (Shao et al., 2015). Data from one study suggested that Temp, Tleaf, and RH had a significant effect on the respiration of five tree species (*Acer buergerianum*, *Platanus acerifolia*, *Ligustrum lucidum*, *C. camphora*, and *Magnolia grandiflora*). Of these parameters, Tleaf was found to have the most significant positive influence (Gao et al., 2006). Our research also confirmed this, showing that Tleaf had an extremely significant correlation with temperature, instantaneous wind speed, and solar radiation in the microclimate underneath the canopy. Furthermore, we found that RHsfc and Vpdl were extremely significantly correlated with temperature, instantaneous wind speed, and solar radiation. These results indicated that Tleaf, RHsfc, and Vpdl were the main parameters that impacted the microclimate of the area underneath the canopy.

However, except for *C. camphora*, the physiological parameters of the other three species did not show any correlation with relative humidity. As a result, through statistical and mathematical analysis, only the physiological parameters (Tleaf, RHsfc, Gs, PAR, and Vpdl) of *C. camphora* established regression equations with relative humidity. This finding was consistent with that of Xia et al. (2021), who investigated the possibility that *C. camphora* could improve air humidity and found that *C. camphora* was sensitive to changes in water conditions.

Wang et al. (2018) investigated the effect of green spaces on mitigating temperatures through evapotranspiration during the night and providing shade during the daytime. The results showed that the contribution (60%–75%) to reducing temperatures during the daytime by providing canopy shade was significantly greater than the contribution (25%–40%) made by evapotranspiration. Furthermore, our research confirmed this finding by analyzing physiological parameters. Through the analysis of multiple regression equations, we found that the Tleaf of *F. microcarpa* and *C. camphora* contributed to mitigating temperature by 75.10% and 62.3%, respectively. In the statistical analysis of Gs and Vpdl, both of which represent evapotranspiration, *F. microcarpa* (8.2% and 11.2%) and *F. virens* (15.6% and 16.3%) contributed to the cooling effect. We also presumed that temperature was correlated with the closure canopy, which represented the parameter of shade. The canopy closure of *F. microcarpa* and *F. virens* was over 90%. This presumption could be confirmed by a study in Shandong indicating that the degree of canopy closure of trees (*S. chinensis*, *P. orientalis*, and *Populus*) could significantly affect the microclimate underneath canopy (Li et al., 2018).

5 Conclusion

The southern subtropical city of Guangzhou is known for its hot and humid climate, and characterized by the presence of evergreen trees. Our study aimed to investigate the following questions: How does the microclimate (Temp, RH, IWS, SR) vary underneath the canopy of different tree species in this area? What is the correlation between the physiological parameters of four tree species and the microclimate underneath their canopy, and what mechanisms are involved? To address these questions, we focused on the four tree species that are commonly found in hot and humid areas of Guangzhou and commonly used: *F. microcarpa*, *F. virens*, *Bauhinia x blakeana*, and *C. camphora*. To represent the typical climate characteristics of these areas, observations were conducted in January and August. Data were collected using a HOBE (H21-0024, onset), Li-6400 portable photosynthesis system, and LPPYRA06 spectrally flat class C (second class) albedometer. Pearson correlation coefficient was used to analyze the correlation between physiological and microclimate factors of the four tree species. Furthermore, through mathematical and statistical analysis, the effects of internal mechanisms between the four microclimate factors and five physiological parameters were investigated, and multiple regression equations were established to indicate the correlation between them.

1 The characteristics of the microclimate underneath the canopy

The four tree species studied showed significant cooling effects during the daytime in the summer. In winter, the Temp of the area underneath the canopy of the four tree species was found to be higher than that of the weather stations during 8:00–9:00. The Temp under *F. microcarpa* was found to be warmer than the weather stations before 12:00.

Relative humidity underneath the canopies of the four tree species was significantly higher than that of the weather stations in winter. In contrast, in summer, while the RH was still higher than that of the weather stations, the difference between the two was found to be smaller than that in winter. Furthermore, the humidifying effect of *F. microcarpa* was found to be the greatest in comparison to the other three species studied.

Regarding instantaneous wind speed underneath the canopy, *F. virens* had the highest in winter and *C. camphora* the highest in summer. Our study found that the instantaneous wind speed of the four tree species slowed down to almost no wind in the cold winter afternoons, which reduced the cooling effect in winter; however, it increased in the summer afternoons, which improved the windless conditions and heat, making it more favorable for human habitation in hot summers. The impact of the trees could improve instantaneous wind speed in summer while decreasing the cold winds in winter, thereby maintaining a comfortable local microclimate in the area underneath the canopy.

The study found that in both winter and summer, the presence of trees significantly reduced solar radiation, particularly at noon.

2 The correlation analysis between the physiological parameters of trees and microclimate

The results of the Pearson correlation coefficient analysis revealed that there was an extremely significant positive correlation between the air temperature underneath the canopy and the Tleaf of the four tree species, and a significant correlation between the instantaneous wind speed and the RHsfc of the four tree species. However, no correlation was found between the physiological parameters of the tree species with the exception of *C. camphora* and RH.

The results of the multiple regression analysis revealed that certain microclimate factors could establish correlation equations with physiological parameters, while others could not. The Tleaf of *F. microcarpa* had the highest contribution (75.10%) to the Temp, while *C. camphora* had the smallest contribution (31.4%). *Ficus microcarpa* and *F. virens* improved the wind speed via the combined impacts of Tleaf, RHsfc, Gs, PAR, and Vpdl. The RHsfc of *C. camphora* had a significant contribution (56%) to the relative humidity. Regarding reducing the solar radiation intensity, the Vpdl of *F. microcarpa* and *F. virens*, RHsfc of *Bauhinia x blakeana*, and PAR of *C. camphora* had higher contributions, comparatively.

Data availability statement

The original contributions presented in the study are included in the article/supplementary material, further inquiries can be directed to the corresponding author.

Author contributions

XF and HW contributed to conception and experimental design of the study. HW observe the data. HW and XF contributed to the statistical analysis. XF wrote the first draft of the manuscript. XF, HW, and MH wrote sections of the manuscript and edited the English

version. All authors contributed to manuscript revision, read, and approved the submitted version.

Funding

National Natural Science Foundation of China (NSFC). The interactive influence mechanism of urban green space, local wind climate and residents andapos; health Based on the multi-spatial scale in Guangdong-Hong Kong-Macao Greater Bay Area (NO.51978276). This work was supported by the National Natural Science Foundation of China (51978276).

Acknowledgments

We thank the Guangzhou Institute of Forestry and Landscape architecture for support of the observation instrument (Li-6400). This work would not have been possible without the tireless efforts of Zixuan Lian, Weisi Wang, and Biyuan Zhang, who helped with the data observation.

Conflict of interest

The authors declare that the research was conducted in the absence of any commercial or financial relationships that could be construed as a potential conflict of interest.

Publisher's note

All claims expressed in this article are solely those of the authors and do not necessarily represent those of their affiliated organizations, or those of the publisher, the editors and the reviewers. Any product that may be evaluated in this article, or claim that may be made by its manufacturer, is not guaranteed or endorsed by the publisher.

References

- Abdulkarim, K. H., Abd Ghafar, A., Lai, L. Y., and Said, I. (2021). Effects of vegetation covers for outdoor thermalimprovement: A Case Study at Abubakar Tafawa Balewa University, Bauchi, Nigeria. *JST* 29 (3), 2125–2147. doi:10.47836/pjst.29.3.43
- Baker, T. P., Marais, Z. E., Davidson, N. J., Worledge, D., and Mendham, D. S. (2021). The role of open woodland in mitigating microclimatic extremes in agricultural landscapes. *Ecol. Manag. Restor.* 22, 118–126. doi:10.1111/emr.12466
- Bao, C. S., Lou, J. H., Zhen, X. Y., and Xiang, Z. S. (2001). Effect of landscaping and greening on microclimate in Hangzhou city. *J. Zhejiang Univ. (Agric. Life Sci.)* 27 (4), 63–66.
- Cheng, X., Peng, J., Dong, J., Liu, Y., and Wang, Y. (2022). Non-linear effects of meteorological variables on cooling efficiency of African urban trees. *Environ. Int.* 169, 107489. doi:10.1016/j.envint.2022.107489
- Ding, J. J., Qin, L. J., Tan, S. L., Yu, X. H., Zhou, Z. D., Qiu, G. Y., et al. (2022). Study on characteristics of transpiration, cooling effect and carbon reduction effect of *Ficus concinna*, a native tree species in subtropical cities. *Acta Sci. Nat. Univ. Pekin.* 58, 537–545. doi:10.13209/j.0479-8023.2022.040
- Dong, J. W., Bai, S. H., Ma, F. Y., and Li, N. N. (2017). Comparative microclimate analysis of 3 types of plantation forests in Shandong Taishan. *Shandong For. Sci. Technol.* 47, 56–59+62.
- Fang, X., Sang, K. X., Huang, C., Fan, B. B., Yang, G. G., and Gou, E. H. (2018). Study on microclimatic effects of different vegetation types in yellow river wetland in zhengzhou. *Acta Agric. Jiangxi* 30, 81–85. doi:10.19386/j.cnki.jxnyxb.2018.09.18
- Feng, X. H., and Chu, Y. Y. (2017). The study of urban green space and local micro-climate effect based on air dynamics simulation. *Chin. Landsc. Archit.* 33, 29–34.
- Feng, X. H., and Wei, Q. Q. (2011). Study on the near-surface flow field in urban areas of Guangzhou. *Ecol. Environ. Sci.* 20, 1558–1561. doi:10.16258/j.cnki.1674-5906.2011.10.011
- Gao, J., Peng, Z. H., and Yu, Y. S. (2006). Transpiration rates and effects for energy absorbed and water given off through transpiration of main afforestation tree species in Hefei city. *J. Anhui Agric. Univ.* 33 (4), 445–449. doi:10.13610/j.cnki.1672-352x.2006.04.001
- Guo, W., Shen Tu, Y. J., Deng, W., and Pan, Z. J. (2008). Research advances on the effect of the urban green areas to microclimate. *Ecol. Environ. Sci.* 17, 2520–2524. doi:10.16258/j.cnki.1674-5906.2008.06.052
- Huang, Y. L., Fu, W. C., Chen, J. R., Dong, J. W., and Wang, M. H. (2022). Study on the influence of plant community characteristics on the summer microclimate of the tree-shaded space in parks. *Chin. Landsc. Archit.* 38, 118–123. doi:10.19775/j.cla.2022.03.0118
- Jin, H., Lv, H. Y., and Lin, Y. J. (2018). Influence of vegetation structures on winter and summer microclimates of urban residential areas in severe cold regions. *Landsc. Archit.* 25, 12–15. doi:10.14085/j.fjyl.2018.10.0012.04
- Jung, M. C., Dyson, K., and Alberti, M. (2021). Urban landscape heterogeneity influences the relationship between tree canopy and land surface temperature. *Urban For. Urban Green.* 57, 126930. doi:10.1016/j.ufug.2020.126930

- Li, Y. H., Wang, J. J., Chen, X., Sun, J. L., and Zeng, H. (2011). Effects of green space vegetation canopy pattern on the microclimate in residential quarters of Shenzhen City. *Chin. J. Appl. Ecol.* 22, 343–349. doi:10.13287/j.1001-9332.2011.0055
- Li, K., Li, C. R., Xu, J. W., Guo, H. L., Chen, Y., Han, B., et al. (2018). Effect of three typical road landscape forests on microclimate under summer weather in zhucheng city. *Ecol. Environ. Sci.* 27, 1060–1066. doi:10.16258/j.cnki.1674-5906.2018.06.009
- Liu, X. D., Zhou, G. Y., Chen, X. Z., Zhang, D. Q., and Zhang, Q. M. (2014). Forest microclimate change along with the succession and response to climate change in south subtropical region. *Acta Ecol. Sin.* 34, 2755–2764. doi:10.5846/stxb201307231934
- Liu, Z. X., Zhen, S. L., Fang, X. S., Lu, X. H., and Zhao, L. H. (2018). Simulating validation of ENVI-met vegetation model to Ficus microcarpa in hot-humid region of subtropical zone. *J. Beijing For. Univ.* 40, 1–12. doi:10.13332/j.1000-1522.20170396
- Lu, G. Q., Xie, Y. B., Gu, J. C., Zhang, S. C., and Bai, S. J. (2006). The analysis of reducing temperature and increasing humidity of familiar afforestation tree species in Dalian city. *J. Agric. Univ. Hebei* 29 (2), 65–67.
- Matyshak, G. V., Goncharova, O. Yu., Bogatyrev, L. G., and Riazantseva, M. I. (2021). Influence of plant cover on hydrothermal conditions in soils of large lysimeters of the MSU soil station: Results of a 60-year experiment. *Mosc. Univ. Soil Sci. Bull.* 76, 134–139. doi:10.3103/S0147687421030078
- Matzarakis, A., Rutz, F., and Mayer, H. (2007). Modelling radiation fluxes in simple and complex environments—Application of the RayMan model. *Int. J. Biometeorol.* 51, 323–334. doi:10.1007/s00484-006-0061-8
- Matzarakis, A., Rutz, F., and Mayer, H. (2010). Modelling radiation fluxes in simple and complex environments: basics of the RayMan model. *Int. J. Biometeorol.* 54, 131–139. doi:10.1007/s00484-009-0261-0
- Meili, N., Manoli, G., Burlando, P., Carmeliet, J., Chow, W. T. L., Coutts, A. M., et al. (2021). Tree effects on urban microclimate: Diurnal, seasonal, and climatic temperature differences explained by separating radiation, evapotranspiration, and roughness effects. *Urban For. Urban Green.* 58, 126970. doi:10.1016/j.ufug.2020.126970
- Schwaab, J., Meier, R., Mussetti, G., Seneviratne, S., Bürgi, C., and Davin, E. L. (2021). The role of urban trees in reducing land surface temperatures in European cities. *Nat. Commun.* 12 (1), 6763. doi:10.1038/s41467-021-26768-w
- Shao, Y. C., Zhuang, J. Y., Li, E. H., and Li, J. J. (2015). Regulating effects of urban forest canopy on microclimate. *Chin. J. Ecol.* 34, 1532–1539. doi:10.13292/j.1000-4890.2015.0133
- Wang, X. J., Kong, F. H., Ying, H. W., Xu, H. L., Li, J. S., and Pu, Y. X. (2018). Characteristics of vegetation shading and transpiration cooling effects during hot summer. *Acta Ecol. Sin.* 38, 4234–4244. doi:10.5846/stxb201712032173
- Wang, A. X., Ren, G. C., and Qin, Y. N. (2020). Research on influence of tree shape of city squares on microclimate in semiarid areas. *Landsc. Archit.* 27, 100–107. doi:10.14085/j.fjyl.2020.07.0100.08
- Wei, X., Zhou, R. M., Zhang, M. J., Shen, H. T., Qiu, Y., and Geng, H. K. (2019). Microclimate changes with simulated canopy spatial structures. *J. Zhejiang A&F Univ.* 36, 783–792. doi:10.11833/j.issn.2095-0756.2019.04.019
- Wu, C. G., Fang, Y. P., Lin, Y. Y., Ma, X. Y., Wang, Y. W., and Wang, K. H. (2016). Analysis of the effect of street greenbelt on microclimate in a hot-humid area of China using a numerical simulation method. *J. Meteorol. Environ.* 32, 99–106.
- Xia, F. M., Ji, K. S., and Yang, Y. D. (2013). The influence of different plant disposition models on temperature and humidity in the microclimate of green spaces. *J. For. Eng.* 27, 75–78. doi:10.3969/j.issn.1000-8101.2013.05.020
- Xia, Y. H., Zhang, X. P., Dai, J. J., Wang, R., and Luo, Z. D. (2021). Time-lag effects between meteorological factors and transpiration of *Cinnamomum camphora* in the subtropical monsoon region. *J. Soil Water Conserv.* 35, 194–203. doi:10.13870/j.cnki.stbcbx.2021.05.027
- Yan, H., Wang, X., and Dong, L. (2012). Microclimatic characteristics and human comfort conditions of tree communities in northern China during summer. *J. Beijing For. Univ.* 34, 57–63. doi:10.13332/j.1000-1522.2012.05.021
- Yang, Q., Huang, X., Tong, X., Xiao, C., Yang, J., Liu, Y., et al. (2022). Global assessment of urban trees' cooling efficiency based on satellite observations. *Environ. Res. Lett.* 17, 034029. doi:10.1088/1748-9326/ac4c1c
- Zhu, C. Y., Li, S. H., and Ji, P. (2011). Relationships between urban green belt structure and temperature-humidity effect. *Chin. J. Appl. Ecol.* 22, 1255–1260. doi:10.13287/j.1001-9332.2011.0172
- Zhu, Y. J., Li, H., Zhao, S. L., Jia, Z. Q., Yu, Y., and Li, Q. X. (2014). Improvement effect on microclimate in different types of shelterbelt in the gonghe basin of tibet plateau. *J. Desert Res.* 34, 841–848. doi:10.7522/j.issn.1000-694X.2013.00384

Frontiers in Environmental Science

Explores the anthropogenic impact on our natural world

An innovative journal that advances knowledge of the natural world and its intersections with human society. It supports the formulation of policies that lead to a more inhabitable and sustainable world.

Discover the latest Research Topics

[See more →](#)

Frontiers

Avenue du Tribunal-Fédéral 34
1005 Lausanne, Switzerland
frontiersin.org

Contact us

+41 (0)21 510 17 00
frontiersin.org/about/contact

